NUREG/CR-6517
SAND96-2899

Round Robin Pretest Analyses of a Steel Containment Vessel Model and Contact Structure Assembly Subject to Static Internal Pressurization

Sandia National Laboratories

U.S. Nuclear Regulatory Commission
Washington, DC 20555-0001

Nuclear Power Engineering Corporation
Tokyo, Japan

AVAILABILITY NOTICE

Availability of Reference Materials Cited in NRC Publications

NRC publications in the NUREG series, NRC regulations, and *Title 10, Energy,* of the *Code of Federal Regulations,* may be purchased from one of the following sources:

1. The Superintendent of Documents
   U.S. Government Printing Office
   P.O. Box 37082
   Washington, DC 20402–9328
   <http://www.access.gpo.gov/su_docs>
   202–512–1800
2. The National Technical Information Service
   Springfield, VA 22161–0002
   <http://www.ntis.gov>
   1–800–553–6847 or locally 703–605–6000

The NUREG series comprises (1) brochures (NUREG/BR-XXXX), (2) proceedings of conferences (NUREG/CP-XXXX), (3) reports resulting from international agreements (NUREG/IA-XXXX), (4) technical and administrative reports and books [(NUREG-XXXX) or (NUREG/CR-XXXX)], and (5) compilations of legal decisions and orders of the Commission and Atomic and Safety Licensing Boards and of Office Directors' decisions under Section 2.206 of NRC's regulations (NUREG-XXXX).

A single copy of each NRC draft report for comment is available free, to the extent of supply, upon written request as follows:

Address: Office of the Chief Information Officer
Reproduction and Distribution
Services Section
U.S. Nuclear Regulatory Commission
Washington, DC 20555–0001
E–mail: <DISTRIBUTION@nrc.gov>
Facsimile: 301–415–2289

A portion of NRC regulatory and technical information is available at NRC's World Wide Web site:

<http://www.nrc.gov>

After January 1, 2000, the public may electronically access NUREG-series publications and other NRC records in NRC's Agencywide Document Access and Management System (ADAMS), through the Public Electronic Reading Room (PERR), link <http://www.nrc.gov/NRC/ADAMS/index.html>.

Publicly released documents include, to name a few, NUREG-series reports; *Federal Register* notices; applicant, licensee, and vendor documents and correspondence; NRC correspondence and internal memoranda; bulletins and information notices; inspection and investigation reports; licensee event reports; and Commission papers and their attachments.

Documents available from public and special technical libraries include all open literature items, such as books, journal articles, and transactions, *Federal Register* notices, Federal and State legislation, and congressional reports. Such documents as theses, dissertations, foreign reports and translations, and non-NRC conference proceedings may be purchased from their sponsoring organization.

Copies of industry codes and standards used in a substantive manner in the NRC regulatory process are maintained at the NRC Library, Two White Flint North, 11545 Rockville Pike, Rockville, MD 20852–2738. These standards are available in the library for reference use by the public. Codes and standards are usually copyrighted and may be purchased from the originating organization or, if they are American National Standards, from—

American National Standards Institute
11 West 42nd Street
New York, NY 10036–8002
<http://www.ansi.org>
212–642–4900

NUREG/CR-6517
SAND96-2899

Round Robin Pretest Analyses of a Steel Containment Vessel Model and Contact Structure Assembly Subject to Static Internal Pressurization

Manuscript Completed: November 1996
Date Published: August 1998

Prepared by
V.K. Luk, E.W. Klamerus

Sandia National Laboratories
Albuquerque, NM 87185-0744

Prepared for

Systems Safety Department
Nuclear Power Engineering Corporation
Tokyo, Japan
Under Funds-in-Agreement
No. DE-F104-91AL73734

NUPEC Project Manager: M. Iriyama

Office of Nuclear Regulatory Research
U.S. Nuclear Regulatory Commission
Washington, DC 20555-0001 USA
Under Containment Integrity Under
Extreme Loads NRC Job Code A1401

NRC Project Manager: J.F. Costello

NUREG/CR-6517 has been reproduced from the best available copy.

Abstract

The Nuclear Power Engineering Corporation (NUPEC)[a] of Japan and the U.S. Nuclear Regulatory Commission (NRC), Office of Nuclear Regulatory Research, are co-sponsoring and jointly funding a Cooperative Containment Research Program at Sandia National Laboratories (SNL). As a part of this program, a steel containment vessel (SCV) model and contact structure assembly will be tested to failure at SNL in December 1996. The SCV model is representative of a steel containment for an improved Japanese Mark-II Boiling Water Reactor Plant. The geometric scale is 1:10 and the thickness scale is 1:4. The contact structure, a thick, bell-shaped steel shell separated at a nominally uniform distance from the SCV model, provides a simplified representation of some features of a reactor concrete shield building in the actual plant. The objective of the internal pressurization test is to provide measurement data of the structural response of the composite structure up to its failure in order to validate analytical modeling, to find the pressure capacity of the model, and to observe the failure mechanisms.

A pretest analysis of this structural assembly was conducted by the following organizations:

Argonne National Laboratory (ANL) [U.S.]
Agenzia Nazionale per la Protezione dell Ambienti (ANPA) [Italy]
Bhabha Atomic Research Centre (BARC) [India]
General Dynamics Electric Boat Division (GD-EB) [U.S.]
Japan Atomic Energy Research Institute (JAERI) [Japan]
Nuclear Power Engineering Corporation (NUPEC) [Japan]
Sandia National Laboratories (SNL) [U.S.]
Staatliche Material prüfungsanstalt, Universität Stuttgart (MPA Stuttgart) [Germany]

Each organization was supplied with the same basic information to use in its analyses, including design drawings of the SCV model and contact structure, as-measured material properties, and certain as-built geometrical measurements. Each organization worked independently, using its own analytical methods. The Round Robin analysis exercise provides a forum for participants to discuss pretest predictions of the deformation behavior of the SCV model at the same locations as well as to compare pretest predictions with the test data.

This report describes the analysis models and tabulates the pretest predictions submitted by each participant organization. The participants' analysis results at 43 specified locations on the SCV model were compiled to facilitate discussions at the SCV Round Robin pretest meeting on October 1–2, 1996, in Albuquerque. This report also includes a summary of participants' predictions of the failure pressure and mechanisms. All pretest predictions will be compared to the test data after the test.

[a] The work of the Nuclear Power Engineering Corporation is performed under the contract by the Ministry of International Trade and Industry, Japan.

Contents

Figures

Tables

Appendices

Acknowledgments

This report would not have been possible without the cooperation and support of many individuals and groups. The Nuclear Power Engineering Corporation (NUPEC) of Tokyo, Japan, the U.S. Nuclear Regulatory Commission (NRC), and Sandia National Laboratories (SNL) are pleased to have had the participation of the following individuals and their organizations:

Dr. Phillip Pfeiffer and Dr. Ronald Kulak: Argonne National Laboratory (ANL) [U.S.];

Mr. Giovanni Pino and Mr. Giuseppe Maresca: Agenzia Nazionale per la Protezione dell Ambienti (ANPA) [Italy];

Dr. H.S. Kushwaha: Bhabha Atomic Research Centre (BARC) [India];

Mr. Kenneth Arpin and Ms. A. Beacham: General Dynamics Electric Boat Division (GD-EB) [U.S.];

Dr. Jun Sugimoto: Japan Atomic Energy Research Institute (JAERI) [Japan];

Dr.-Ing. Ludwig Stumpfrock: Staatliche Material prüfungsanstalt, Universität Stuttgart (MPA Stuttgart) [Germany].

These organizations received no financial support from NUPEC, NRC, or SNL, and their efforts are gratefully acknowledged.

The authors also wish to acknowledge the guidance, support, and encouragement of Dr. Hideo Ogasawara, Director and General Manager, Systems Safety Department, and Mr. Tomoyuki Matsumoto, Manager, Structural Behavior Group, both of NUPEC, and Dr. James S. Costello, Structural and Geological Engineering Branch, Division of Engineering Technology, Office of Reactor Research, Nuclear Regulatory Commission.

List of Acronyms

ANL	Argonne National Laboratory
ANPA	Agenzia Nazionale per la Protezione dell Ambienti
BARC	Bhabha Atomic Research Centre
BWR	boiling water reactor
CS	contact structure
GD-EB	General Dynamics Electric Boat Division
JAERI	Japan Atomic Energy Research Institute
LWR	light water reactor
MPA Stuttgart	Staatliche Material prüfungsanstalt, Universität Stuttgart
NRC	Nuclear Regulatory Commission
NUPEC	Nuclear Power Engineering Corporation
SCV	steel containment vessel
SNL	Sandia National Laboratories

Executive Summary

For several years, Sandia National Laboratories (SNL) has tested and analyzed numerous scale models of containment vessels that have been pressurized to failure as part of the Containment Integrity Programs sponsored by the U.S. Nuclear Regulatory Commission (NRC). The overall objective of the programs has been to develop test-validated analytical methods that can be used to predict the performance of light water reactor (LWR) containment vessels subject to loads beyond the design basis. Five scale steel containment models and a scale reinforced-concrete containment model have been tested. For the static internal pressurization test of the reinforced concrete containment model, a number of organizations in the United States and Europe performed pretest and posttest analyses of predicted response and failure. This activity, referred to as a Round Robin analysis, occurred in the mid- to late-1980s.

SNL is now involved in a Cooperative Containment Research Program for LWR containments under the joint sponsorship of the Nuclear Power Engineering Corporation (NUPEC)[b] of Tokyo, Japan and the NRC. This report discusses pretest analyses of an internal pressurization test on a scale model of a steel containment vessel (SCV) that represents certain features of an improved boiling water reactor (BWR) Mark-II containment vessel in Japan. The SCV model uses a mixed-scale design: 1:10 for the geometry scale and 1:4 for the thickness scale. The objective of the test is to measure the failure pressure of the model, to observe the failure mode and mechanisms, and to provide data on the containment structural response up to failure to validate analytical models. The test assembly includes a bell-shaped steel contact structure (CS) at a nominally uniform distance from the SCV model. The uniform gap between these two structures permits the SCV model to undergo deformation well beyond the elastic range prior to its contact with the CS. The CS, a much simplified representation of a concrete shield building in a physical plant, allows an in-depth study of SCV model behavior after it makes contact with the CS. The SCV/CS structural assembly provides specific features of the interaction to be investigated, including closure of gap, progression of contact, and load sharing between the SCV and the CS.

In separate efforts, NUPEC conducted a full-scale hatch test, a biaxial tensile test, and a scaled cylindrical vessel failure test. The purpose of these tests is to provide additional information on containment vessel deformation behavior to supplement the SCV model pressure test.

Eight organizations from the U.S., Europe, and Asia have participated in a Round Robin analysis activity to conduct pretest predictions of the response of the coupled SCV/CS assembly. Their efforts will help validate analytical methods used for predicting the structural behavior of actual containments under severe accident conditions. The participating organizations are:

- Argonne National Laboratory (ANL) [U.S.]
- Agenzia Nazionale per la Protezione dell Ambienti (ANPA) [Italy]
- Bhabha Atomic Research Centre (BARC) [India]
- General Dynamics Electric Boat Division (GD-EB) [U.S.]
- Japan Atomic Energy Research Institute (JAERI) [Japan]
- Nuclear Power Engineering Corporation (NUPEC) [Japan]
- Sandia National Laboratories (SNL) [U.S.]
- Staatliche Material prüfungsanstalt, Universität Stuttgart (MPA Stuttgart) [Germany]

NUPEC and the NRC jointly invited these international organizations to participate in the pretest analyses in the spring of 1995. The analyses began in the summer of 1995 and were completed by June 1996. The Round Robin analysis activity was coordinated by SNL, which provided participants with all details necessary to perform the pretest analyses, maintained close contact with participants, prepared the Round Robin pretest analysis report, and organized the pretest meeting held October 1–2, 1996, in Albuquerque, NM. Each organization was supplied with the same basic information, including design drawings of the SCV model and the CS, as-measured material properties, and certain as-built geometrical measurements. All participants were instructed to provide pretest predictions at 43 specified standard output locations on the SCV model to facilitate comparison and discussion of analysis results and to correlate with test data after the internal pressurization test, scheduled for December 1996.

Several benefits have resulted from the Round Robin analysis exercise. First, it provides a forum for participants to discuss pretest predictions, based on different numerical codes and modeling approaches, of the deformation behavior of the SCV model at the

[b] The work of the Nuclear Power Engineering Corporation is performed under the contract by the Ministry of International Trade and Industry, Japan

same locations, as well as to compare pretest predictions to the test data. Second, when expert analysts use different finite-element codes such as ABAQUS, NEPTUNE, MARC, and TABS to solve the same problem, it is possible to advance the state-of-the-art of predictive techniques and to evaluate the suitability of these codes for the nonlinear analysis of steel structures (including contact phenomena). Finally, this exercise has led to greater recognition of the importance of containment performance and reliable prediction techniques and has facilitated the exchange of information on these and other related topics.

This report describes the pretest analyses and compiles the analysis results of the participating organizations. The background information and the description of the containment integrity program are given in Section 1. The design and material properties of the SCV model, and the design and special features of the CS are discussed in Section 2 and 3, respectively. Section 4 describes the instrumentation installed on the SCV model and the CS. The pressurization sequence of the SCV model test is summarized in Section 5. Section 6 consists of participants' predictions of failure pressure and mechanisms. Section 7 contains the conclusions. Appendices A and B contain design drawings of the SCV and CS, respectively. Appendix C presents measured material properties of the SCV. Appendix D comprises the compilation of participants' analysis results. The analysis reports and results from the participants are included in Appendix E in their entirety.

At this time, comments on the compilation of analysis results from participants are limited primarily to observations. Participants had to make strategic decisions about the features of the SCV/CS structural assembly to be represented in their analytical models such as as-built versus as-designed configurations and other structural details. As shown in Section 6, the pretest failure predictions by participants are very much dependent on their modeling approach. A true evaluation of the accuracy of the pretest predictions can be made more appropriately in light of the test data. There is no specific plan for the posttest analysis effort. After the SCV pressurization test, the pretest predictions will be compared with the test data on failure pressure, location and mechanisms, and a decision will be made at that time whether there will be a formal Round Robin posttest analysis exercise.

1. INTRODUCTION

1.1 Background

The Cooperative Containment Research Program is co-sponsored and jointly funded by the Nuclear Power Engineering Corporation (NUPEC)[c] of Japan and the US Nuclear Regulatory Commission (NRC), Office of Nuclear Regulatory Research. The purpose of the program is to investigate the response of representative scale models of nuclear containments to pressure-loading beyond the design basis accident and to compare analytical predictions to measured behavior. This is accomplished by conducting static, pneumatic overpressurization tests of scale models at ambient temperature. Prior to testing, a number of organizations are requested to conduct predictive modeling of the response of containment models to overpressurization. The containment models are being constructed by NUPEC, which is funding Sandia National Laboratories (SNL) for planning and site preparation, review of the model design and design support, instrumentation and data collection, and reporting. The NRC is funding SNL to perform analyses of the models and conduct the tests. Both sponsors are funding SNL to coordinate the Round Robin pretest analysis activities reported here.

1.2 Program Description

The first test in the Cooperative Containment Research Program consists of pressure testing a mixed-scale model of a steel containment vessel (SCV). The model is representative of a steel containment for a Japanese-improved Mark-II Boiling Water Reactor containment. The geometric scale is 1:10. However, because the same materials are being used for the model as for the actual plant, the scale on the wall thickness was set at 1:4 for manufacturability and material availability. The model was fabricated at the Hitachi Works, Japan. The model arrived at SNL on March 8, 1995, and was installed in the fragment barrier on March 22, 1995. The fragment barrier houses the SCV model during instrumentation and pressure tests. It is designed, along with its earthen cover, to contain the fragments and safely vent the overpressure from a probable catastrophic failure of the model at a maximum pressure of 12.4 MPa (1800 psig). Instrumentation of the model consists of over 800 channels of data, including strain gages, displacement transducers, and temperature sensors, as well as visual monitoring. A steel contact structure (CS) is placed over the SCV model prior to testing to represent some features of the concrete reactor shield building in the actual plant. The model should come into contact with the CS, resulting in deformation and failure modes which include the effects of contact due to a combination of pressure and thermal growth. The pressure test of the SCV model is planned to occur during December 1996.

The SCV model test is intended to accomplish the following specific objectives:

1. To provide experimental data for validating the predictive capabilities of analytical methods representing certain aspects of the static internal pressure response of a steel containment, first beyond the elastic range without consideration of contact with a surrounding shield structure or thermal effects, then after contact with a surrounding shield structure.

2. To provide experimental data for the evaluation of steel containments.

Round Robin pretest analyses of this structural assembly were conducted by the following organizations:

- Argonne National Laboratory (ANL) [U.S.]
- Agenzia Nazionale per la Protezione dell Ambienti (ANPA) [Italy]
- Bhabha Atomic Research Centre (BARC) [India]
- General Dynamics Electric Boat Division (GD-EB) [U.S.]
- Japan Atomic Energy Research Institute (JAERI) [Japan]
- Nuclear Power Engineering Corporation (NUPEC) [Japan]
- Sandia National Laboratories (SNL) [U.S.]
- Staatliche Material prüfungsanstalt, Universität Stuttgart (MPA Stuttgart) [Germany]

Each organization was supplied with the same basic information to use in its analyses, including design drawings of the SCV model and the CS, as-measured material properties, and certain as-built geometrical

[c] The work of the Nuclear Power Engineering Corporation is performed under the contract by the Ministry of International Trade and Industry, Japan.

measurements.[d,e,f] Each organization worked independently using its own analytical methods.

1.3 Organization of Report

This report presents the results of pretest predictive modeling of the effects of overpressurization on a scale SCV model at 43 selected locations. Section 2 describes the design of the SCV model and the measured properties data on the steel materials used in its construction. The contact structure which encloses the SCV model is discussed in Section 3. In Section 4, the instrumentation on the SCV model is reported. Special attention is focused on the strain gages and displacement transducers at the 43 specified locations where pretest predictions of strain and displacement were made. The procedure for pressurization of the SCV model is described in Section 5. In Section 6, the results of predictive modeling by all participants are reported. Section 7 presents the conclusions of the pretest analyses. References are given in Section 8. Appendices A and B contain design drawings of the SCV model and the CS, respectively. Appendix C presents data on measured material properties for the SCV model. A compilation of the analysis results from the participants is given in Appendix D, and the complete pretest analysis reports and results from each of the participants are found in Appendix E.

[d] Branstetter, L.J., Sandia letter to SCV Round Robin participants, July 10, 1995.

[e] Hessheimer, M.F., Sandia letter to SCV Round Robin participants, February 20, 1996.

[f] Luk, V.K., Sandia letter to SCV Round Robin participants, May 9, 1996.

2. DESIGN OF THE STEEL CONTAINMENT VESSEL MODEL

2.1 Model Design

The steel containment vessel (SCV) model is scaled 1:4 in shell thicknesses and 1:10 in overall geometry from a prototype Mark-II Boiling Water Reactor (BWR) containment structure. The model is 2.9 m in diameter and 5.9 m tall, with an enclosed volume of about 21 m^3. The model weighs 15,800 kg.

The design pressure of the prototype containment is 0.31 MPa (45 psig). The design pressure for the model is calculated as:

$$\frac{10\ \text{(geometric scale)}}{4\ \text{(thickness scale)}} \times 0.31\ MPa = 0.78\ MPa\ (113\ psig)$$

Containment details that are included in the SCV model are: the equipment hatch penetration and reinforcement plate (the hatch is not to scale, and the hatch cover is welded shut); the drywell head (also welded shut); and the SGV480/SPV490 material transition location. All other hatches, airlocks, and penetrations were omitted from the SCV model. In addition, the lower wetwell and wall-basemat junction has been replaced by a thick bottom head which is designed to ensure that failure will not occur there during testing, and that deformations in this area will be minimal. All internal structures not integral to the vessel have been omitted from the model. All thickness variations in the model occur on its outer surface; the inner surface of the model is smooth.

Figure 2.1, a diagram of the SCV model, illustrates sections and features such as a top flange, knuckle region, several stiffeners, equipment hatch with reinforcement plate, various welds, and an interface where two dissimilar steel materials come together at a butt weld. The design drawings of the SCV model are included in Appendix A.

A standard "global" coordinate system is used, corresponding to the one originally employed by Hitachi Works in describing the model. The origin of the coordinate system is on the axis of the model, at the elevation of the top surface of the ring support girder (Figure 2.1). Positive elevations are upward on the model. The global coordinate system is a *left*-handed cylindrical (r, θ, Z) system (i.e., looking *down*ward at the model, positive rotation is *clockwise*). The equipment hatch is at an angular orientation of 90°. Figure 2.2 shows angular orientations in the global system looking down at the model.

Figure 2.3 compares a cutaway view of an actual containment and the SCV model. The diagram of the actual containment includes an exterior structure that is a concrete shield building. The upper portion of the SCV model (the portion above the ring support girder) approximates the major features of an actual containment.

The outside surface of the SCV model has been covered by a layer of protective paint. The inside surface of the CS, however, is not painted. There are no plans to experimentally determine the coefficient of friction between the SCV model and the CS. The participants were asked to exercise their best modeling judgment in this regard.

2.2 Material Properties

The upper portion of the model consists of two materials: SGV480 steel and SPV490 steel. NUPEC has supplied standard properties for these materials. For any thickness of SGV480 steel, the standard properties are:

minimum yield: 265 MPa;
tensile strength: 480 to 590 MPa; and
minimum elongation after fracture: 17%.

In the NUPEC-supplied standard properties for SPV490 steel, the minimum elongation after fracture depends on thickness, but the minimum yield strength and the tensile strength do not. For SPV490 steel, the standard properties are given as:

minimum yield strength: 490 MPa;
tensile strength: 610 to 735 MPa; and
minimum elongation after fracture:
18% for 9 mm thickness
25% for 17.5 mm thickness.

NUPEC has also conducted tensile tests on samples of SGV480 steel and SPV490 steel. These samples were taken from the actual material lots used to construct the model. Tests were performed on material taken from 12 locations on the SCV model. Four tests, two in the roll direction and two in the rectangular (i.e., vertical) direction, were performed at each location for a total of 48 tests. The tests were taken to failure. The data on measured material properties are available in Appendix C.

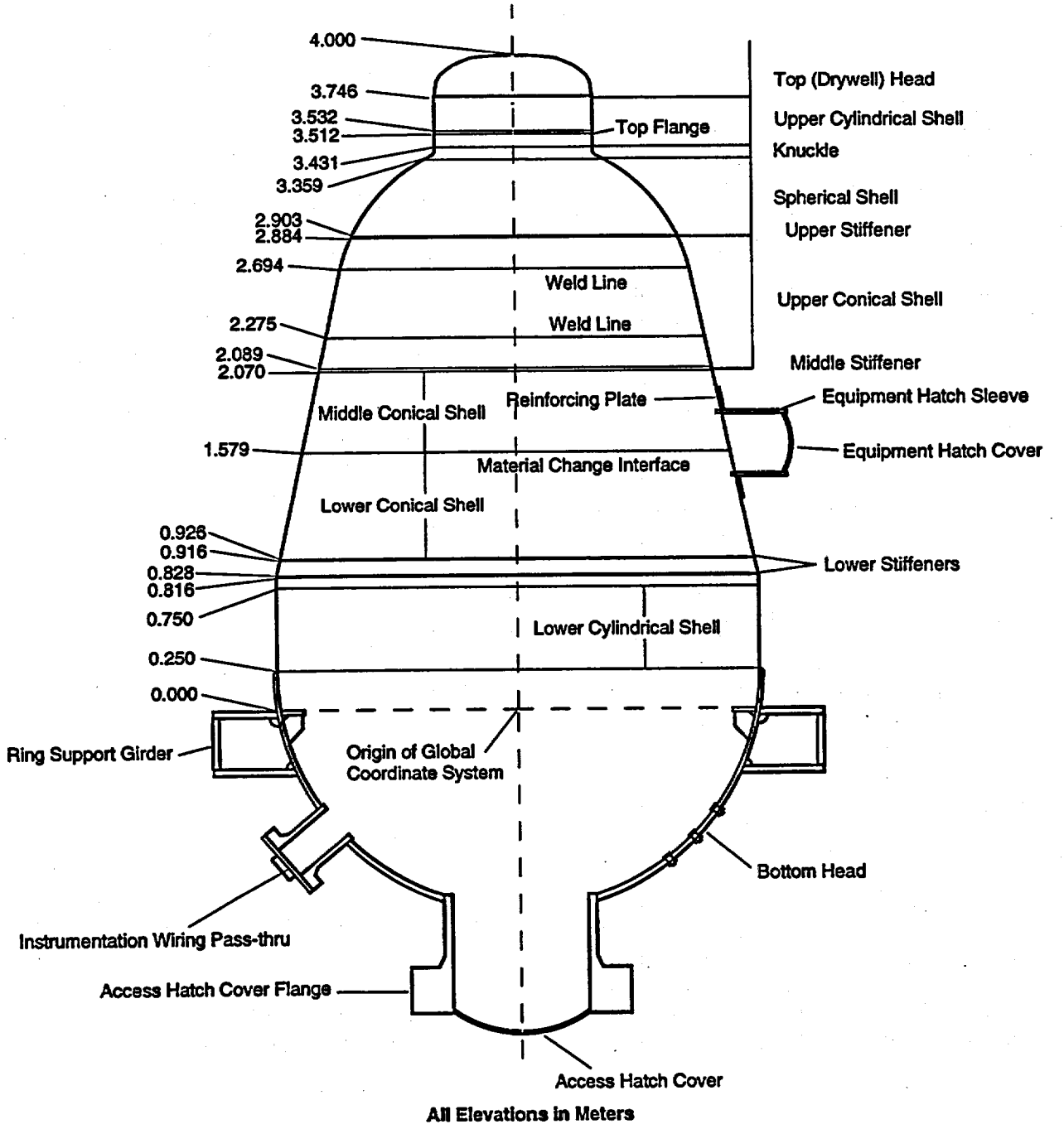

Figure 2.1. Steel containment vessel (SCV) model.

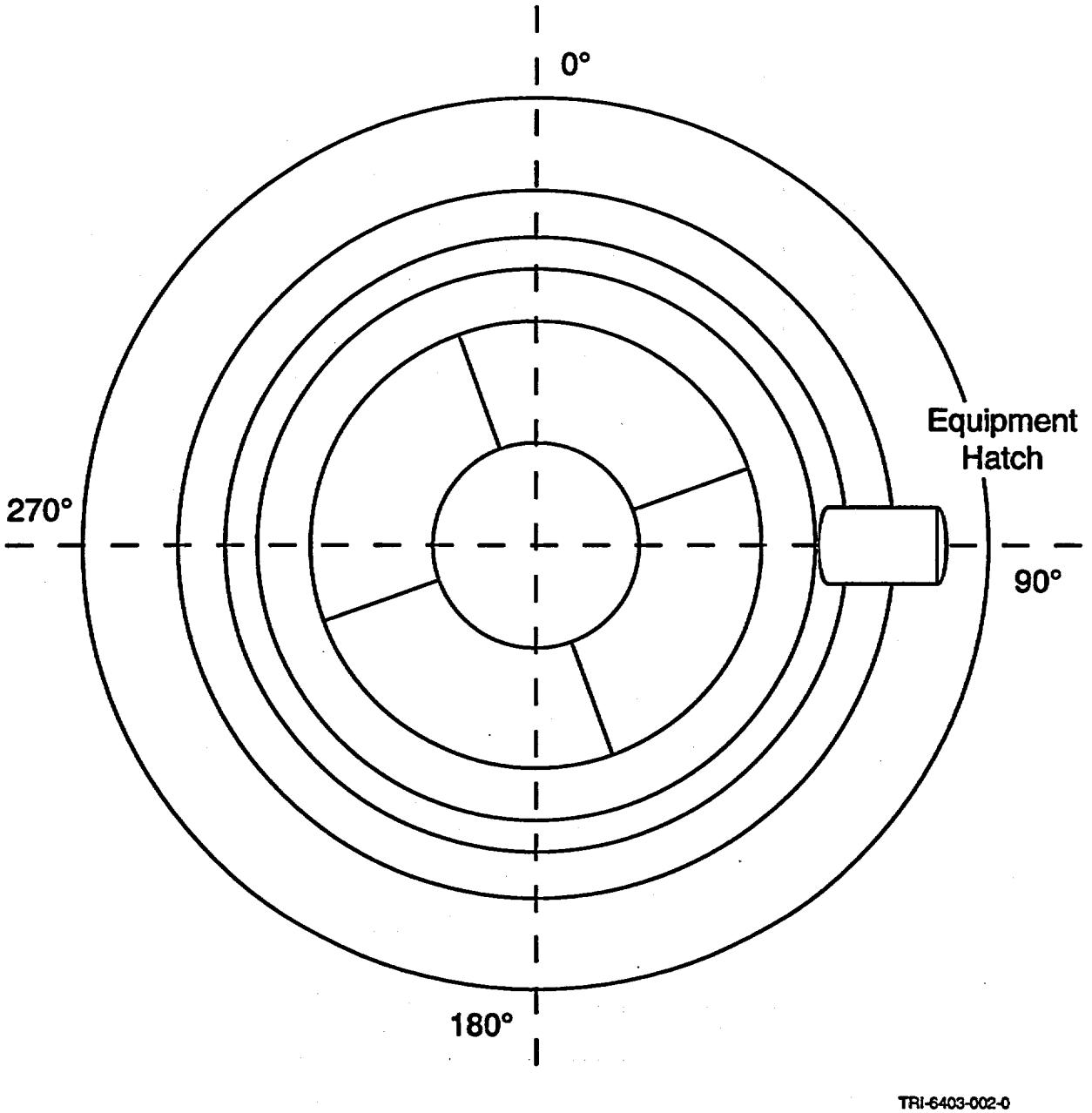

Figure 2.2. Overhead view of the SCV model.

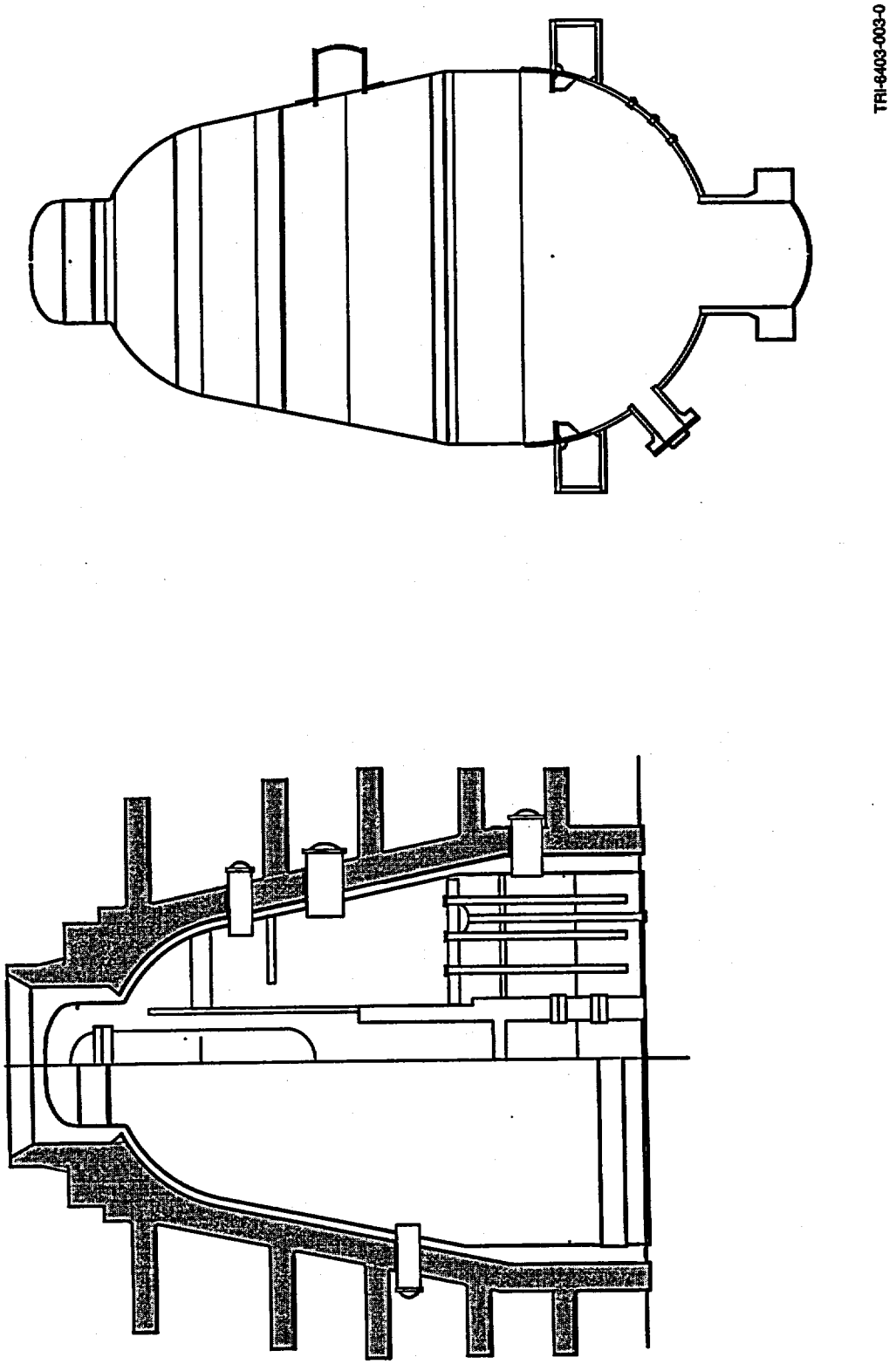

Figure 2.3. Comparison of actual containment to SCV model.

3. DESIGN OF THE CONTACT STRUCTURE

3.1 Structure and Design

The CS allows investigation of the response of the SCV model against an almost rigid surrounding shield structure during pressurization. It is not, however, intended to simulate the effects of the concrete shield building in physical plants. The CS is designed to remain essentially elastic until the SCV model reaches an internal pressure of approximately 10 P_d.

The CS is a bell-shaped structure (Figure 3.1) constructed of SA-516-70 steel with a nominal thickness of 38 mm. This material has a nominal yield strength of 258 MPa and a nominal ultimate strength of 476 MPa. The CS was welded to the top surface of the ring support girder after it was placed over the model. It does not touch the surface of the model at any point prior to the test.

Seventy holes, 12.7 mm in diameter, were drilled in the CS, both to measure the gap between the CS and the SCV model to align the CS during its installation, and later to install contact detection devices to measure gap closure during the test. In addition, four 50.8-mm depressions were counterbored into the inside of the CS to allow for continuation of strain measurements of the SCV model after it has contacted the CS during testing. Appendix B contains the design drawings for the CS.

3.2 Gap Dimensions

The minimum gap between the prototype containment and its concrete shield building is 90 mm. For geometric scaling, the gap between the SCV model and the CS should be 9 mm. However, two factors preclude using this gap. First, as noted previously, the inside of the SCV model is smooth, with material thickness differences occurring on the outside. Second, the SCV model is fabricated in sections, and during the fabrication process, the model can become out-of-round and out-of-plumb. However, the major portion of the CS, the conical section, is machined in one piece and is almost perfectly round and plumb. Therefore, to account for these possible irregularities, the scaled gap was increased by a factor of two to 18 mm.

To ensure that the internal geometry of the CS matched the external geometry of the SCV model as closely as possible, the SCV model was measured at 20 different elevations, with eight measurements (at 45° increments) taken at each elevation, for a total of 160 radial-geometry measurements. These measurements showed that the axis of the SCV model is close to vertical, and that the exterior radius of the SCV model at each location is within Hitachi fabrication tolerance (± 6 mm).

After the CS was installed over the SCV model, the gap size between the CS and the SCV model was measured at each of the 70 hole locations. By design, the gap sizes at the lowest three rows of measurement holes are much larger than the design requirement of 18 mm (see Appendix B). The majority of measured gap sizes everywhere else lie between 18 mm and 22 mm. A minimum gap size of 13.4 mm was measured at a hole location below the equipment hatch.

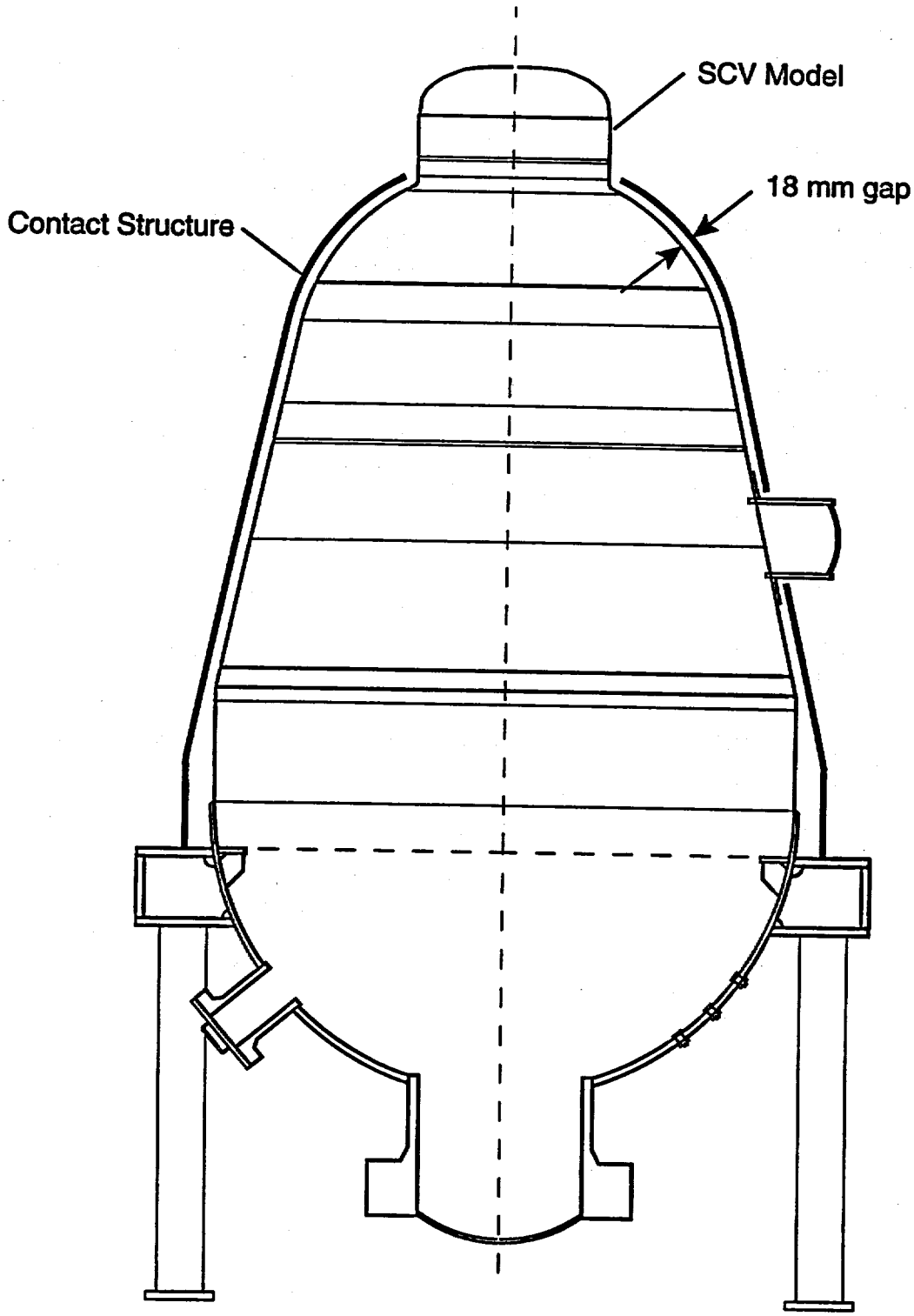

TRI-6304-004-0

Figure 3.1. Contact structure (CS) and the SCV model.

4. INSTRUMENTATION

4.1 Model Instrumentation

The complete suite of instruments that has been installed on the SCV model and the CS will:

1. measure the strain distribution, both membrane and bending components, on the model surfaces;
2. measure the displacements of the model, relative to the interior wall of the fragment barrier and to the rigid lower portion of the model;
3. measure the size of the gap between the SCV model and the CS;
4. provide information on the extent of contact between the SCV model and the CS;
5. relate all data to the internal pressure loads on the model.

The number and the locations of different types of instruments installed on the SCV model are described in detail in the SCV Instrumentation Plan[8]. The following sections describe only the strain, displacement, and pressure measurements that are related to pretest predictions.

4.1.1 Strain Measurements

The primary means of evaluating the structural behavior in this experiment is through the measurement of local strains over the surface of the SCV model. These measurements will be made using standard electrical-resistance strain gages installed in selected locations to evaluate the strain state of the model as a function of the internal pressure. Density, placement, and orientation of the gages are based on pretest analytical predictions of the model response by SNL.

Strain gages are located to provide strain information in the hoop direction (circumferential) and the meridional direction (vertical or axial). Around the equipment hatch, gages are aligned in a radial manner with respect to the hatch geometry to provide data on the complex effects the hatch creates. In addition, gages have been placed on both the inner and outer surfaces of the model to allow the total strains to be differentiated into membrane and bending components during the portion of the test before contact is made with the CS. Once contact occurs, the signals from the exterior gages will be lost due to gage or lead wire failure, but since the pretest analyses indicate that bending moment strains should become negligible after contact, this loss is not considered detrimental to the experiment. However, continuous monitoring of exterior strain gages after contact will occur at the four counterbored indentations in the CS.

Multi-element strip gages are installed in areas predicted to have relatively large strain gradients. These areas include the drywell head, in the vicinity of the knuckle, and around the equipment hatch. Bending moments will be obtained through the use of single-element gages mounted to the exterior surface adjacent to one of the strip elements. Thirty-nine strip gages have been installed on the SCV model.

Single-element strain gages are used to determine point strains on both the inner and outer surfaces of the model in areas where the strain gradient is predicted to be small or, as stated previously, to provide complementary data for evaluation of bending moments adjacent to inner-surface strip gages. These gages are oriented to monitor strains in the hoop or circumferential direction. There are 153 single-element gages on the SCV model.

Finally, in areas in which biaxial strain data are desired, three-element rosette strain gages are used. These gages provide membrane strain data for determination of the principal strains and location of the principal axes. They are installed in areas in which bending moments are considered very small throughout the entire test, such as the free fields midway between the stiffener rings. Some rosette gages are also included on the surface of the CS for membrane strain measurements after contact with the model. There are 85 rosette gages installed on the SCV model.

4.1.2 Displacement Measurements

Detailed measurements of local displacements of the SCV model and the CS are collected by displacement measuring devices. Variable resistance linear displacement transducers (also known as resistance potentiometers or rheostats) are installed to measure displacement over the expected ranges of the test.

[8] Rightley, M.J. and Lambert, L.D., "SCV Instrumentation Plan," Project Report No. R-SN-S-001, Rev. B, Sandia National Laboratories, Albuquerque, NM, September 1996.

They operate through the use of spring-loaded wire cables mounted to known reference locations.

All cable potentiometers installed inside the SCV model are mounted on the central support column that is rigidly attached to the ring support girder. The cable potentiometer measurements are taken either in the horizontal or vertical direction with respect to the central support column whose displacement is monitored by two inclinometers installed to measure its tilt along orthogonal axes. Displacement data values will be adjusted based on the output of the inclinometers. There are 60 interior and 6 exterior cable potentiometers installed on the SCV model.

4.1.3 Pressure Measurements

Two high-accuracy pressure transducers are installed in the SCV model. They will measure the internal gas pressure inside the model at all times during the test.

4.2 Standard Output Locations

The objective of the pretest analysis is to obtain predictions of the SCV model behavior to compare to data collected during the test. Forty-three locations for pretest analyses,[h,i] referred to as standard outputs, have been specified for five categories: equipment hatch area strains; top head-area strains; transition region strains; free-field strains; and displacements. The standard outputs are listed in Table 4.1 and shown in Figures 4.1 through 4.5. Many of the standard outputs correspond to pairs of measuring instruments (one on the inside surface and one on the outside surface of the SCV model) to estimate local bending within the SCV model.

Six standard outputs (1-6) were specified in the area of the equipment hatch at several angular orientations at a distance of 360 mm from the center of the hatch, 20 mm beyond the reinforcement plate. A combination of single gages, rosettes, and strip gages will monitor these areas. The angular orientations of these outputs are shown in Figure 4.1. In addition, four standard outputs (40-43) were later specified corresponding to rosette gages installed on the interior of the SCV model in an area of thinned material near the equipment hatch reinforcement plate.[j] The locations of these outputs are shown in Figure 4.1.

Four strains (7-10) in the top head area were specified. One prediction was requested at the apex of the top head, and the other three were requested at 270°, near the point of minimum radius of curvature of the top head surface. Rosette gages have been mounted on the model in each of these locations. A schematic diagram with the locations of these outputs is given as Figure 4.2.

The transition regions are locations near geometric or material changes in the model for the prediction of meridional strain. The ten predictions (11-20) consist of five pairs of values – one on the inside surface of the model and one on the outside surface. A combination of single gages, rosettes, and strip gages has been mounted on the model at these locations, all 90° counterclockwise of the equipment hatch (Figure 4.3).

Fourteen free-field strains were specified at locations away from geometric or material changes in the model. Some free-field predictions are requested in pairs, one on the inside surface of the model and one on the outside surface of the model. Four such pairs (21-28), corresponding to eight standard outputs, are requested: two for meridional strain and two for hoop strain. These pairs all correspond to measurements taken 45° counterclockwise of the equipment hatch in the global coordinate system (Figure 4.4). The remaining six free-field standard output strains (29-34) were specified at locations where gages are to be located only on the inside surface of the model (Figure 4.5). A rosette at the midheight of the spherical shell will be used to measure both meridional and hoop strain 45° counterclockwise of the equipment hatch (global coordinate system). Another rosette at the midheight of the upper conical section and directly opposite the equipment hatch (i.e., at global 270°) will measure both meridional and hoop strains at that position, and a final rosette will measure both of these quantities midway between the material change interface and the top of the lower stiffeners (also at global 270°).

The locations of the displacement standard outputs (35-39) (Figure 4.6) should be self-explanatory. The displacements specified are absolute displacements in a fixed coordinate frame. Vertical displacements of the apex of the top head and just below the knuckle are

[h] Branstetter, L.J., Sandia letter to SCV Round Robin participants, July 10, 1995.

[i] Hessheimer, M.F., Sandia letter to SCV Round Robin participants, February 20, 1996.

[j] Luk, V.K., Sandia letter to SCV Round Robin participants, May 9, 1996.

specified. Horizontal (radial) displacements are specified at three locations: just above the top flange, just below the knuckle, and at the center of the equipment hatch cover. For these measurements, positive vertical displacements are upward, and positive horizontal displacements are outward.

Table 4.1. SCV standard output list

Category	Plot ID	Instrument ID	Inst. Type	Model Surface	Coord. System	θ, X (degrees, m)	Output Quantity
Equipment Hatch Area (Strains)	1	RSG-I-EQH-12	rosette	inside	Hatch	67.5, 0.36[a]	max. prin. strain
	2	RSG-I-EQH-8	rosette	inside	Hatch	45, 0.36[a]	max. prin. strain
	3	STG-O-EQH-4c	strip	outside	Hatch	0, 0.36[a]	ext. merid. strain
	4	STG-I-EQH-2c	strip	inside	Hatch	0, 0.36[a]	int. merid. strain
	5	SSGH-O-EQH-18	single	outside	Hatch	90, 0.36[a]	ext. hoop strain
	6	STG-I-EQH-16c	strip	inside	Hatch	90, 0.36[a]	int. hoop strain
Top Head Area (Strains)	7	RSG-O-THD-1	rosette	outside	Top	-, 0.00[b]	max. prin. strain
	8	RSG-O-THD-9	rosette	outside	Top	270, 0.48[b]	ext. hoop strain
	9	RSG-O-THD-9	rosette	outside	Top	270, 0.48[b]	ext. merid. strain
	10	RSG-I-THD-10	rosette	inside	Top	270, 0.48[b]	int. merid. strain
Transition Regions (Strains)	11	STG-O-UCYS-25c	strip	outside	Global	0, 3.47[c]	ext. merid. strain
	12	SSGM-I-UCYS-27	single	inside	Global	0, 3.47[c]	int. merid. strain
	13	STG-O-KNU-1c	strip	outside	Global	0, 3.32[c]	ext. merid. strain
	14	STG-I-KNU-9c	strip	inside	Global	0, 3.32[c]	int. merid. strain
	15	SSGM-O-MST-1	single	outside	Global	0, 2.10[c]	ext. merid. strain
	16	SSGM-I-MST-7	single	inside	Global	0, 2.10[c]	int. merid. strain
	17	SSGM-O-MCI-2	single	outside	Global	0, 1.60[c]	ext. merid. strain
	18	RSG-I-MCI-1a	rosette	inside	Global	0, 1.60[c]	int. merid. strain
	19	SSGM-O-LST-17	single	outside	Global	0, 0.80[c]	ext. merid. strain
	20	SSGM-I-LST-25	single	inside	Global	0, 0.80[c]	int. merid. strain
Free Field (Strains)	21	RSG-O-UCS-17	rosette	outside	Global	45, 2.49[c]	ext. merid. strain
	22	RSG-I-UCS-18	rosette	inside	Global	45, 2.49[c]	int. merid. strain
	23	RSG-O-UCS-17	rosette	outside	Global	45, 2.49[c]	ext. hoop strain
	24	RSG-I-UCS-18	rosette	inside	Global	45, 2.49[c]	int. hoop strain
	25	RSG-O-LCS-5	rosette	outside	Global	45, 1.45[c]	ext. merid. strain
	26	RSG-I-LCS-6	rosette	inside	Global	45, 1.45[c]	int. merid. strain
	27	RSG-O-LCS-5	rosette	outside	Global	45, 1.45[c]	ext. hoop strain
	28	RSG-I-LCS-6	rosette	inside	Global	45, 1.45[c]	int. hoop strain
	29	RSG-I-SPH-2	rosette	inside	Global	45, 3.13[c]	int. merid. strain
	30	RSG-I-SPH-2	rosette	inside	Global	45, 3.13[c]	int. hoop strain
	31	RSG-I-UCS-16	rosette	inside	Global	270, 2.49[c]	int. merid. strain
	32	RSG-I-UCS-16	rosette	inside	Global	270, 2.49[c]	int. hoop strain
	33	RSG-I-LCS-11	rosette	inside	Global	270, 1.25[c]	int. merid. strain
	34	RSG-I-LCS-11	rosette	inside	Global	270, 1.25[c]	int. hoop strain
General (Disp.)	35	VCP-I-THD-11	rheostat	inside	Top	-, 0.00[b]	vertical disp.
	36	HCP-O-UCYS-43	rheostat	outside	Global	45, 3.57[c]	horizontal disp.
		HCP-I-UCYS-39	rheostat	inside	Global	45, 3.57[c]	horizontal disp.
	37	HCP-I-KNU-17	rheostat	inside	Global	0, 3.32[c]	horizontal disp.
	38	VCP-I-KNU-18	rheostat	inside	Global	0, 3.32[c]	vertical disp.
	39	HCP-I-MCI-16	rheostat	inside	Hatch	-, 0.00[a]	horizontal disp.
Equipment Hatch Area (Strains)	40	RSG-I-EQH-45	rosette	inside	Global	105.2, 1.569[c]	int. merid. strain
	41	RSG-I-EQH-45	rosette	inside	Global	105.2, 1.569[c]	int. hoop strain
	42	RSG-I-EQH-44	rosette	inside	Global	74.6, 1.569[c]	int. merid. strain
	43	RSG-I-EQH-44	rosette	inside	Global	74.6, 1.569[c]	int. hoop strain

Note: a: θ_H, R_H (H = Hatch) b: θ_T, R_T (T = Top Head) c: θ_G, Z_G (G = Global)

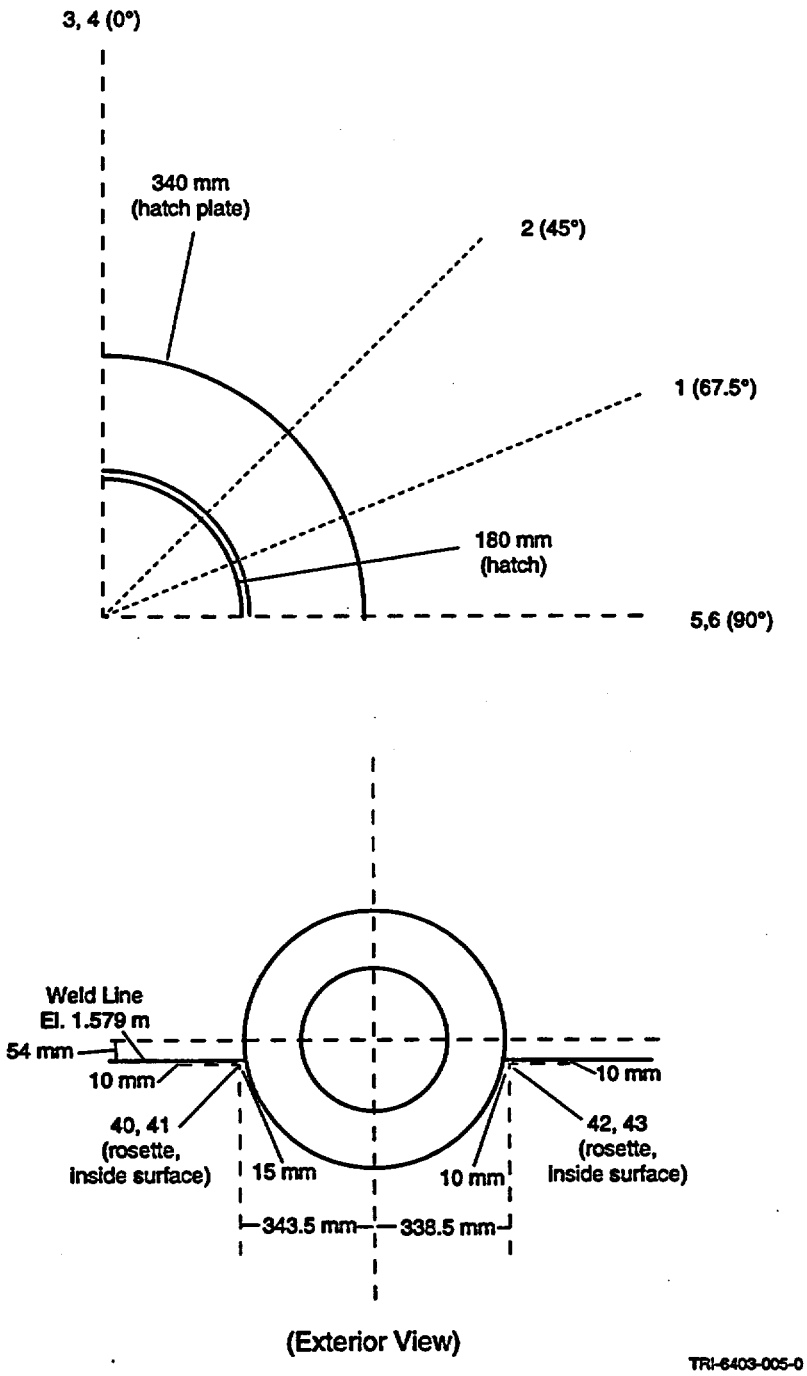

Figure 4.1. Locations of standard outputs near equipment hatch.

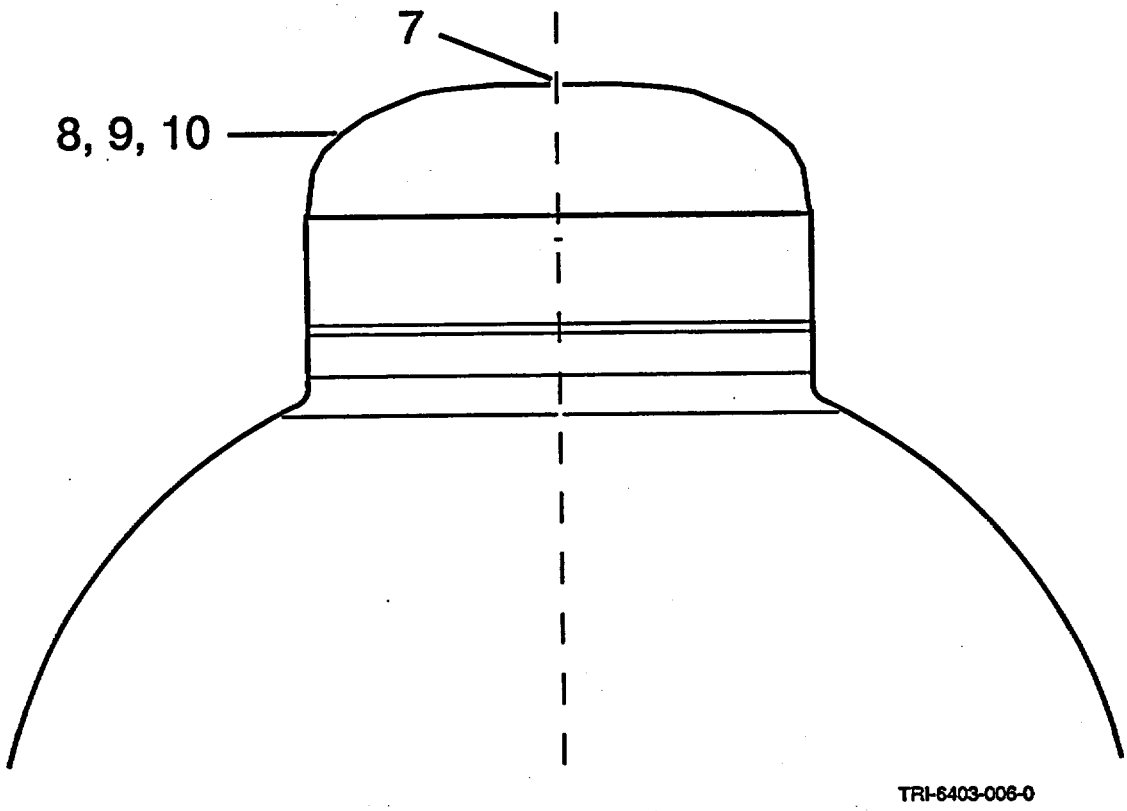

Figure 4.2. Locations of standard outputs on top head.

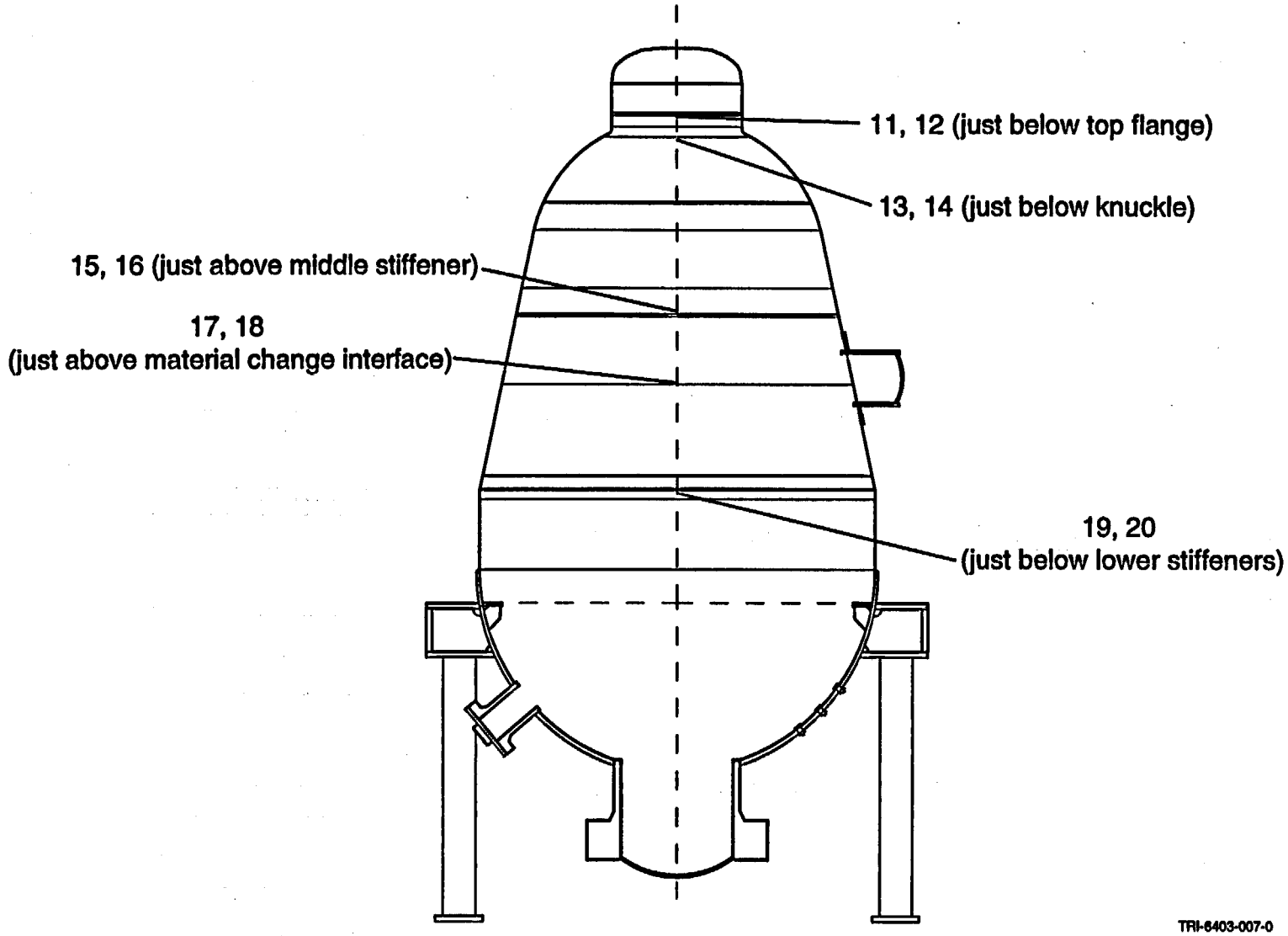

Figure 4.3. Locations of transition region standard outputs.

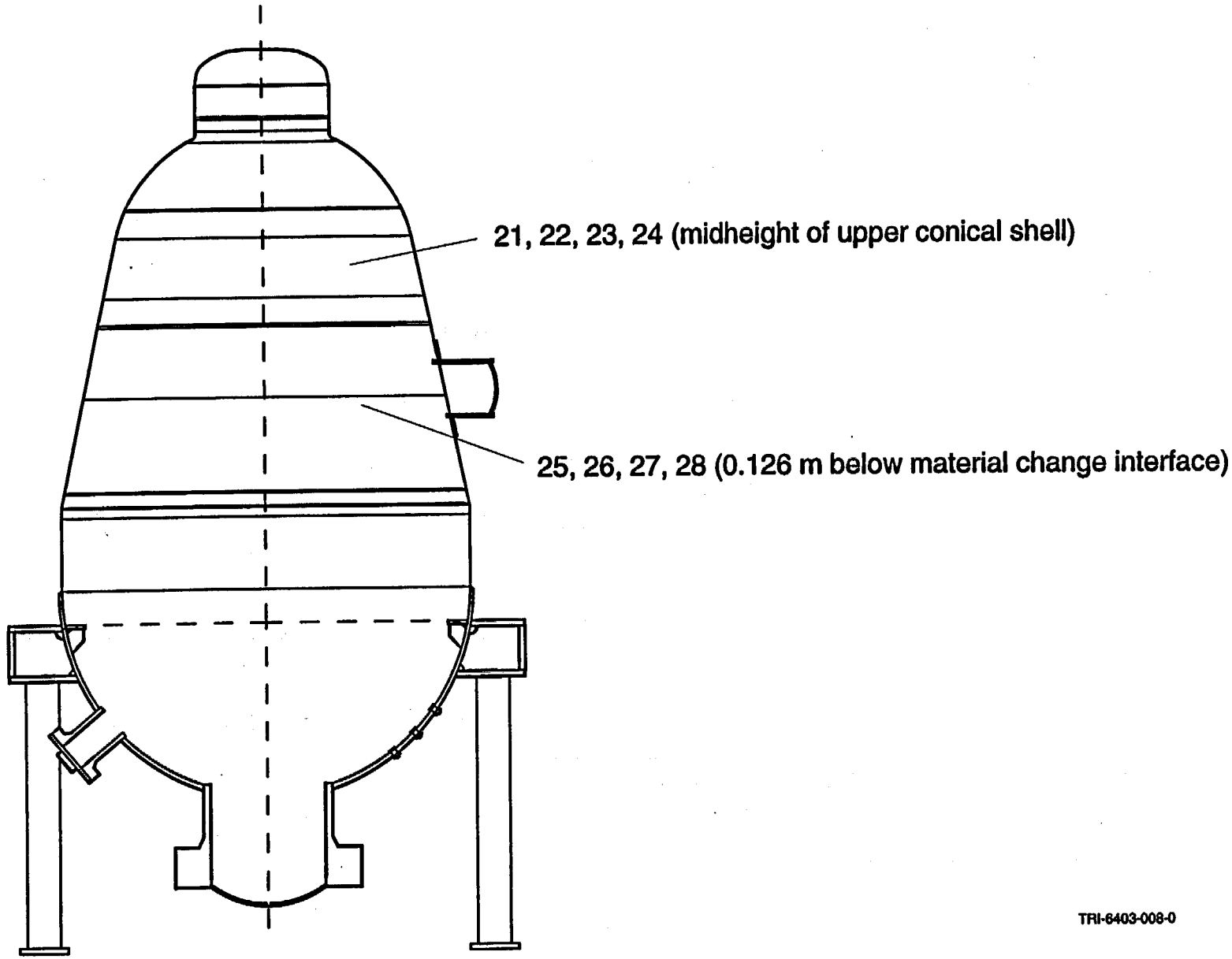

Figure 4.4. Locations of paired free-field standard outputs.

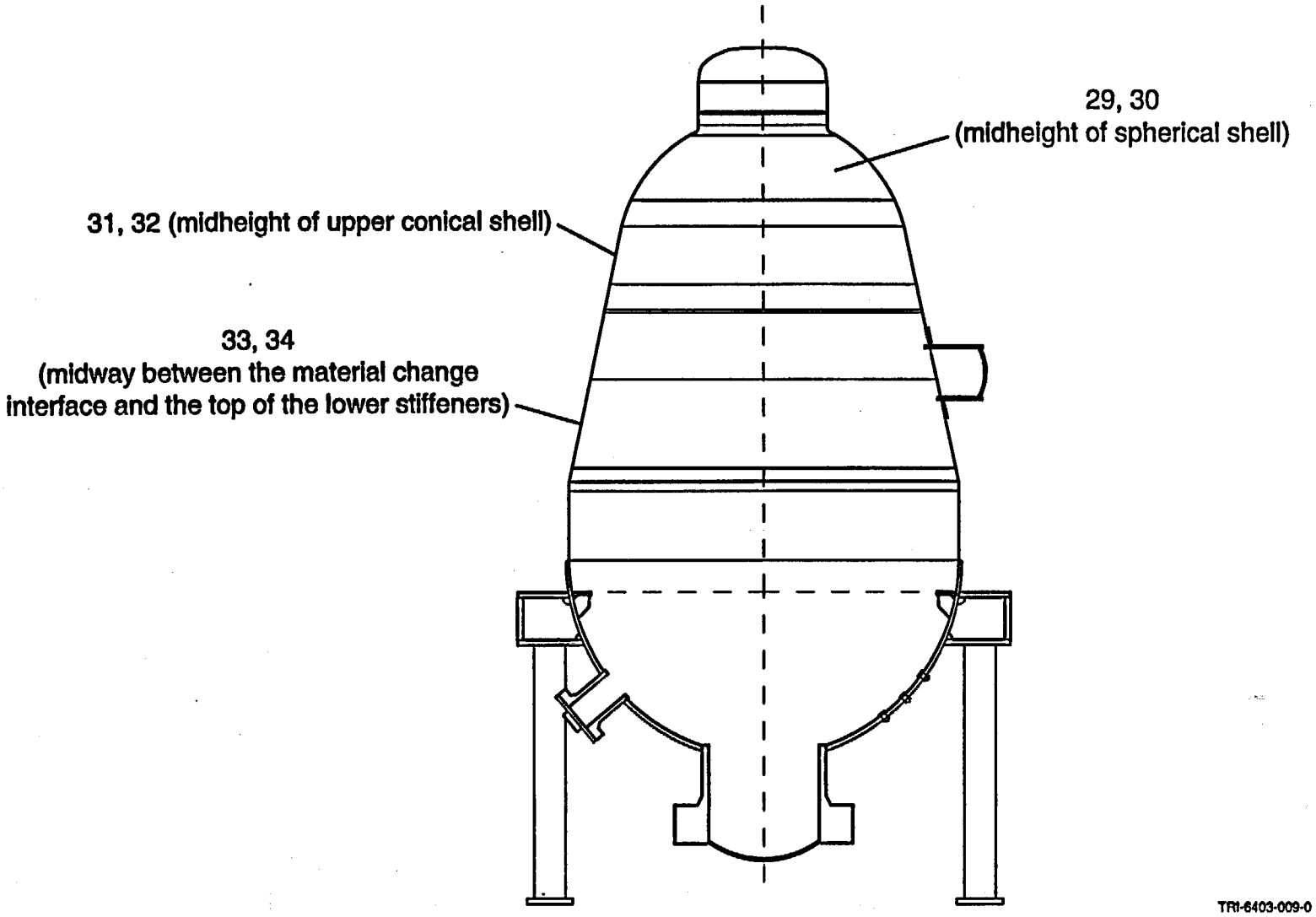

Figure 4.5. Locations of remaining free-field standard outputs.

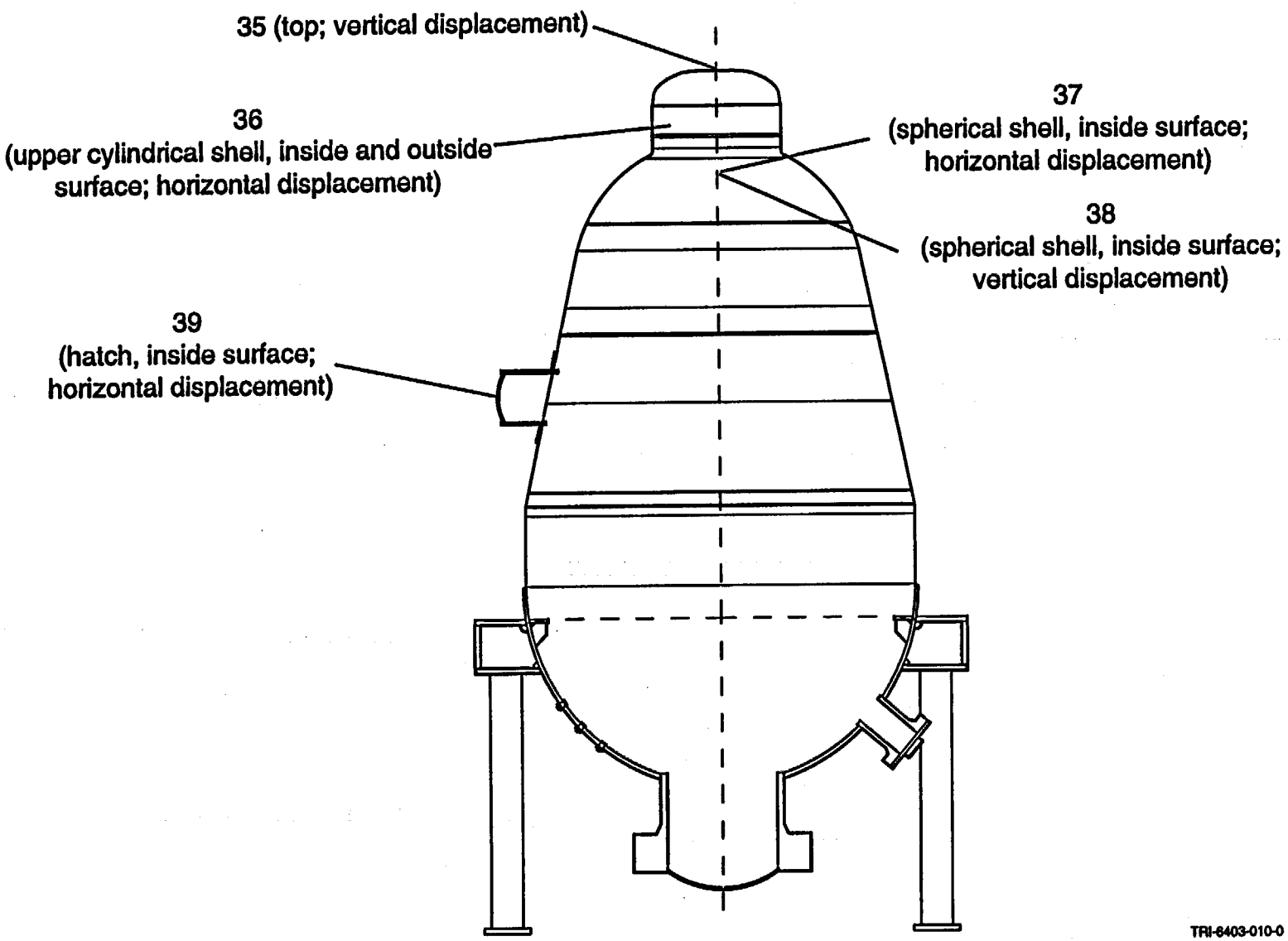

Figure 4.6. Locations of displacement standard outputs.

5. INTERNAL PRESSURIZATION TEST

5.1 Pressure Supply

For the internal pressurization test of the SCV model, the pressure source is liquid nitrogen that is gasified and regulated to a constant pressure and temperature. The pressure level and the flow rate of nitrogen gas into the SCV model is controlled by an elaborate pressurization system. The temperature of the nitrogen gas inside the SCV model is maintained to within ±3.00°C of the ambient temperature (15.00°C). This relatively constant gas temperature is achieved by first setting the temperature at the pressure source location; additional heating, if needed, is supplied by heaters before the nitrogen gas enters the model.

5.2 Pressurization Sequence

The pressurization sequence of the SCV test follows a monotonic rise of the internal pressure inside the SCV model until the model fails or the pressure level reaches 12.4 MPa (1800 psi)[k]. The pressurization test will be terminated when the SCV model experiences a structural failure in terms of a catastrophic failure or a significantly large tear. If the SCV model leaks due to the occurrence of multiple small cracks, then the pressurization system may not be able to maintain a constant pressure inside the model. At this time, the SCV model will have functionally failed, and the test will be terminated.

The internal pressurization test has three distinct stages in its test sequence:

first stage (0 - 4.6 P_d)
second stage (4.6 P_d)
third stage (4.6 P_d - model failure or 15.9 P_d)

where P_d is the scaled design pressure (0.78 MPa). The entire test sequence is shown in Figure 5.1.

5.2.1 First Stage (0 - 4.6 P_d)

According to Sandia National Laboratories' pretest analysis results[l], the conical section of the SCV model expands 9 mm at an internal pressure of 4.6 P_d, and the structure behaves essentially in the elastic domain throughout this stage.

5.2.2 Second Stage (4.6 P_d)

This pressure condition is held at a constant level for 30 minutes.

5.2.3 Third Stage (4.6 P_d - model failure or 15.9 P_d)

The SCV model behaves in the plastic domain throughout this stage. The pressure rise time is kept at a minimum of 3 minutes for each pressure step. The maximum pressure increment is maintained at 0.1 P_d for each pressure step until pressure reaches 6.0 P_d at which time the maximum pressure increment is reduced to 0.05 P_d for each pressure step.

The dwell time is expected to increase as pressure increases because the structure takes a longer time to achieve its equilibrium state in the plastic domain. The increase of strain and/or displacement as a function of pressure at certain critical locations on the model will be monitored at all times during the test to provide indications of an imminent model failure.

[k] Luk, V.K., "Steel Containment Vessel Model Test Plan," Project Report No. R-SN-S-003, Rev. B, Sandia National Laboratories, Albuquerque, NM, December 1996.

[l] Porter, V.L., Carter, P.A., and Key, S.W., "Pretest Analyses of the Steel Containment Vessel Model," NUREG/CR-6516, SAND96-2877, Sandia National Laboratories, Albuquerque, NM, November 1996 (to be published).

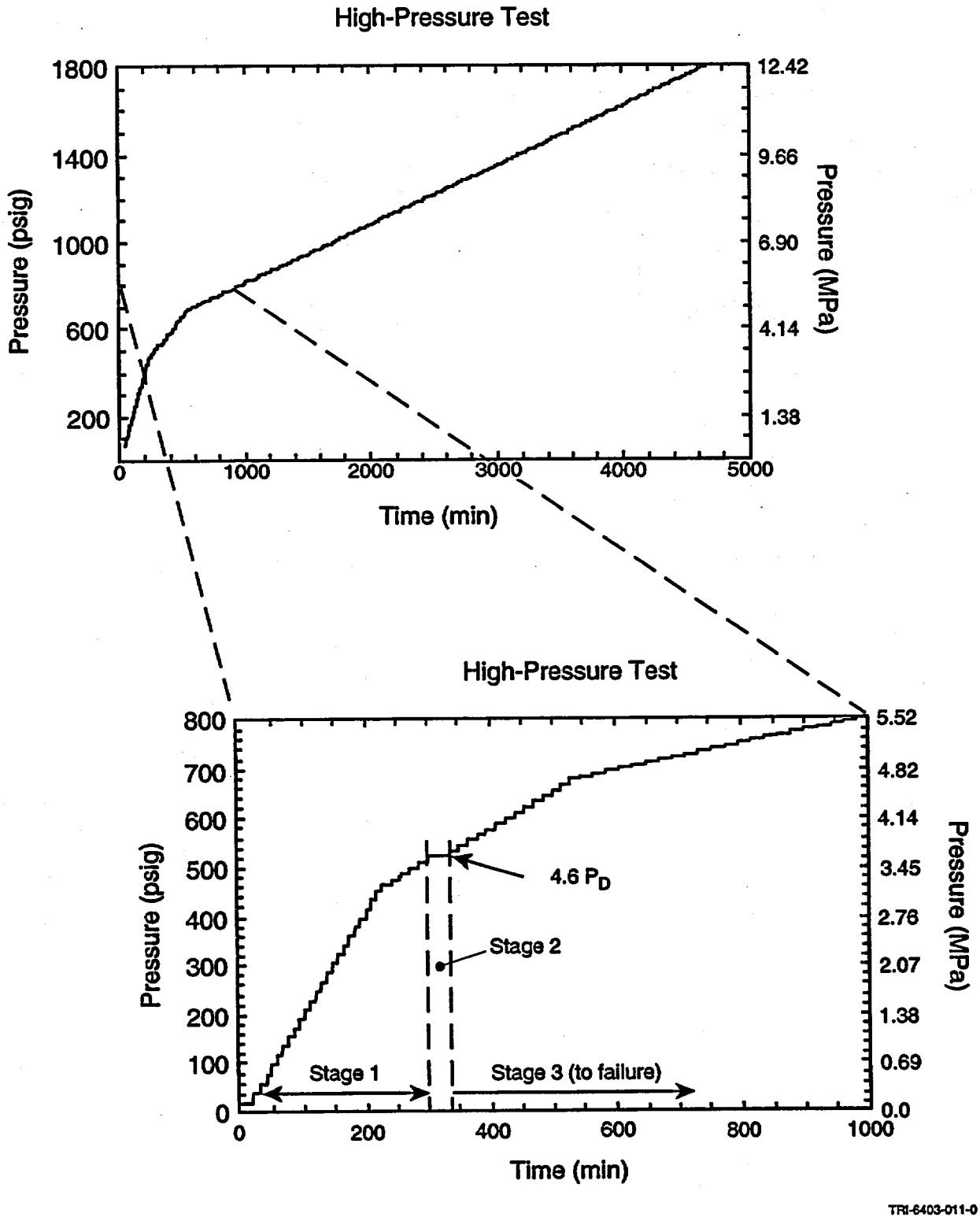

Figure 5.1. Pressurization sequence for the high-pressure test.

6. PRETEST ANALYSIS

6.1 Compilation of Analysis Results from Participants

Each organization participating in the Round Robin analysis of the SCV performed an independent analysis, using its own analytical methods. Participants were supplied with the same basic information to use in their analyses, including design drawings of SCV model and contact structure, as-measured material properties, and certain as-built geometrical measurements. All participants and the numerical codes they used are shown in Table 6.1. A detailed summary of the modeling approaches used by each participant is given in Table 6.2.

Two comparison indicators among the models that demonstrate the effects of the overall modeling approaches and inputs are the pressures and locations of the first yield of the SCV model and the first contact between the SCV model and the CS (Table 6.3). With the exception of low predicted pressures by GD-EB, the range for first yield falls between 1.78 MPa and 3.0 MPa. Predictions of the location of first yield are mostly in the knuckle region or the area of the equipment hatch. Predicted pressures for first contact between the structures range between 3.2 MPa and 4.4 MPa, with most participants predicting first contact occurring in the knuckle region or the upper and middle conical shells.

After the analysis was performed, each participant was asked to provide plots of internal gage pressure versus strain or internal gage pressure versus displacement at the 43 standard output locations on the SCV model (Table 4.1). Each of the participants submitted both hardcopy plots and electronic files of predicted results at these locations. SNL then combined these files and plotted them together in the same format (Appendix D).

Participants were given the option to perform analyses using either zero friction between the SCV and the CS, or nonzero friction, or both. The coefficient of friction between the SCV model and the contact structure was not experimentally determined. Therefore, the participants were asked to exercise their best judgment if a nonzero friction was used.

In Appendix D, two plots are given for each standard output location. The first shows all results for the participants who performed the analyses using zero friction. The second shows the results for participants using nonzero friction as well as the coefficient of friction chosen by each participant. Most of the participants chose to submit only one set of data using either zero friction or nonzero friction. However, two participants submitted plots for both zero friction and nonzero friction.

Most of the participants submitted plots for all 43 standard output locations. However, some of the participants performed only 2-D axisymmetric analysis, ignoring the equipment hatch, or they used a 3-D model but did not model the equipment hatch. These participants did not submit results for locations 1-6 and 39-43, which were measurements taken on or near the equipment hatch. The remaining locations (7-38) include results from every participant.

Table 6.1: List of participants and numerical codes

Participant [country]	Numerical Code
Argonne National Laboratory (ANL) [U.S.]	NEPTUNE
Agenzia nationale per la Protezione dell Ambienti (ANPA) [Italy]	MARC
Bhabha Atomic Research Centre (BARC) [India]	ABAQUS and TABS/NISA
Genera Dynamics Electric Boat Division (GD-EB) [U.S.]	ABAQUS
Japan Atomic Energy Research Institute (JAERI) [Japan]	ABAQUS
Nuclear Power Engineering Corporation (NUPEC) [Japan]	ABAQUS
Sandia National Laboratories (SNL) [U.S.]	ABAQUS
Staatliche Material prüfungsanstalt, Universität Stuttgart (MPA Stuttgart) [Germany]	ABAQUS

Table 6.2. Detailed description of analysis models

Participant	Type of Model Used	Post-Yield Material Model	SCV/CS Gap Dimension	Representation of CS Model at Knuckle	Model Details of Head Region	Shell Thickness of SCV Model	Local Thinning Incorporated?	Eccentricity Due to Different Shell Thicknesses of SCV Model?	Type of Contact between SCV and CS
ANL	3-D 360° shell	Isotropic/bi-linear least squares fit	As-built	As-designed; shell elements	No	Design	No	No	Elasto-plastic
ANPA	3-D 90° shell	Mean properties; high fidelity fitting total range	As-built at measurement hole #9	Per machining geometry	No fillet; continuum	Nominal	Yes	No	Rigid-deformable elastic-plastic surface
BARC ABAQUS	2-D Axisymmetric solid	Isotropic piecewise linear of minimum thickness specimen	As-designed	As-designed	No	As-built	No	No	Hard contact with opening and closing
BARC TABS/NISA	2-D Axisymmetric solid	Isotropic piecewise linear; mean values	As-built averaged over circumference	As-built	No	As-built	No	No	Hard contact with opening and closing
EB	Axisymmetric shell free field; Axisymmetric solid knuckle; 3-D shell equipment hatch	Isotropic piecewise linear	Average as-built; 21.0/25.7 mm at equipment hatch	As-built geometry	Fillet welds simulated in axisymmetric solid models	Average as-built	Yes	Only at equipment hatch	Elastic-plastic minimum properties
JAERI	3-D 180° shell	Tri-linear fit	Nominal; hard contact	Design	No	Design	No	No	Elastic
NUPEC	3-D global; 3-D equipment hatch submodel; 3-D top head submodel	Mean properties; high fidelity fitting total range	Nominal 18mm; hard contact	Design	No (shell model)	Nominal	No	Only at equipment hatch insert plate	Elasto-plastic (same as equipment hatch material)
SNL	3-D shell; Axisymmetric continuum top head; 3-D shell equipment hatch	Mean properties; high fidelity fitting total range	Nominal 18mm; ABAQUS hard contact	As-built geometry	No filled; continuum	Nominal	Yes	Only at equipment hatch insert plate	Elastic-plastic nominal properties
MPA Stuttgart	3-D 180° shell	Isotropic kinemetic hardening model	Nominal 18mm	Design	No	Nominal	No	No	ABAQUS surface interaction option

Table 6.3. Locations and pressures of first yield and first contact between the SCV model and the CS

	First Yield		First Contact between SCV Model and CS	
Participant	Pressure (MPa)	Location	Pressure (MPa)	Location
ANL	2.6	Bottom of equipment hatch and reinforcing plate	4.4	Upper conical shell
ANPA	3.0	Upper portion of spherical shell	3.5	Not stated in analysis report
BARC: ABAQUS	1.78	Below knuckle region	3.42	Knuckle region
TABS/NISA	2.0	Top spherical shell	3.5	Between knuckle region and top spherical shell
GD-EB	1.0	Knuckle region	3.2	Knuckle region
	1.1	Locally thin area around equipment hatch		
JAERI	2.8	Around knuckle region and top head	4.0	Upper and middle conical shells and around knuckle region
NUPEC	2.1	Below knuckle region	3.5	Knuckle region
SNL	2.0	Knuckle region	3.2	Knuckle region
MPA	2.5	Near equipment hatch	3.5	Upper and middle conical shells

6.2 Predictions of Failure Pressure and Mechanisms

Participants used various finite-element codes and adopted a hierarchy of modeling approaches to perform the SCV model analyses. The analyses reports of the participants (Appendix E) describe what modeling strategies were chosen and how different assumptions were made in the analysis efforts. In addition to plotting the pretest analysis results on deformation history as a function of internal pressure at the 43 specified standard output locations, participants have also provided failure predictions of the SCV model as highlights of their analyses (Table 6.4).

Table 6.4. Predicted failure pressure and mechanisms

Name of Participant Organization	Numerical Code Used	Analytical Model Used in Failure Prediction	Failure Pressure	Failure Location	Failure Mechanism/Criteria
ANL	NEPTUNE	Solid model of SCV model and CS	5.5 MPa 4.9 MPa (high confidence [>98%] that there is a low probability for failure)	Just above the knuckle region	Uniaxial ultimate strain (plastic failure strain) of 9.9%
ANPA	MARC	3-D shell model of SCV model, no CS and rigid surface for CS	No plastic instability at 10 MPa; local buckling of torospherical head at 10.87 MPa	Top head region	Local buckling
BARC	ABAQUS	3-D shell model with SCV model and CS based on as-designed configurations	11.49 MPa	Top head region	Strain at top head regions reaches ultimate strain
	TABS/NISA	2-D axisymmetrical model with SCV model and CS, based on some as-built configurations such as average thickness and average gap	11.5 – 12.0 MPa	Top head region at elevation 10 cm above the junction between the top head and the top cylinder	Imply possibility of in-plane axisymmetrical buckling
GD-EB	ABAQUS	Shell submodel to address the effect of local thinning	4.7 MPa	Local thinned section around equipment hatch	Minimum ultimate strain of 8% (reduced by a series of reduction factors to account for the variation and unknowns in the as-built SCV model)
JAERI	ABAQUS	Shell element model of SCV model and CS based on as-designed configuration	10.81 MPs	Top head region	Numerical instability due to yielding in the top head region
NUPEC	ABAQUS	Two submodel analyses - equipment hatch and knuckle region, using as-designed configuration	7.3 MPa 7.3 – 11.8 MPa 11.8 MPa	Near equipment hatch, below knuckle joint, and below top head flange joint. Top head apex	Maximum surface strain value
SNL	ABAQUS	Equipment hatch submodel with thinned section	4.5 MPa	Local thinned section next to equipment hatch reinforcement plate	Ductile rupture. SPV490 steel material reaches a plastic strain that in the uniaxial-stress tensile test led to necking
MPA	ABAQUS	3-D shell for half of SCV and CS; no failure analysis was performed	N/A	N/A	N/A

7. CONCLUSIONS

The support and continuing effort of the Round Robin participants is greatly appreciated. This work was performed on a tight schedule that limited the scope of analysis efforts, and the results included in this report reflect what could be accomplished within the limitations imposed. An important benefit of the Round Robin activity was obvious at the pretest meeting, when experts from the participating organizations who used different codes to conduct independent analyses shared their results, conclusions, and knowledge.

The pretest predictions of the behavior and failure of the SCV model are dependent on details of the features of the SCV model that were included in the analytical effort, such as the as-designed vs. the as-built configuration of the model. Results from the two organizations that incorporated the locally thinned sections around the equipment hatch into the numerical models indicate that those locally thinned areas are the most vulnerable sections for failure. Furthermore, their results indicate failure occurring at a lower pressure than shown by results based on the as-designed configuration of the SCV model. Generally, failures are predicted to take place in either the locally thinned areas around the equipment hatch, around the knuckle region, or at the top head apex.

The analysis results from the participants clearly indicate that there are differences among predictions of SCV model deformation behavior in terms of strain and displacement. However, there are striking similarities in the trends of their variation. The onset of contact between the SCV model and the CS plays a dominant role in affecting the deformation behavior of the model. Compiled analytical results indicate that the various values of friction coefficient at the interaction surface between the two structures do not affect analytical results to any great extent. There are, however, differences in results between zero friction and nonzero friction cases.

Most participants experienced numerical stability difficulties in simulating contact between the SCV model and the CS. Analysis results are sensitive to how the two structures interact at the contact interface. It will be crucial to have improved understanding and simulations on the part of numerical algorithms.

All pretest predictions should be considered in light of the design details that were incorporated in the numerical models, and the accuracy of the predictions, when compared to test data, should be evaluated in that respect.

Appendix A

SCV Model Design Drawings

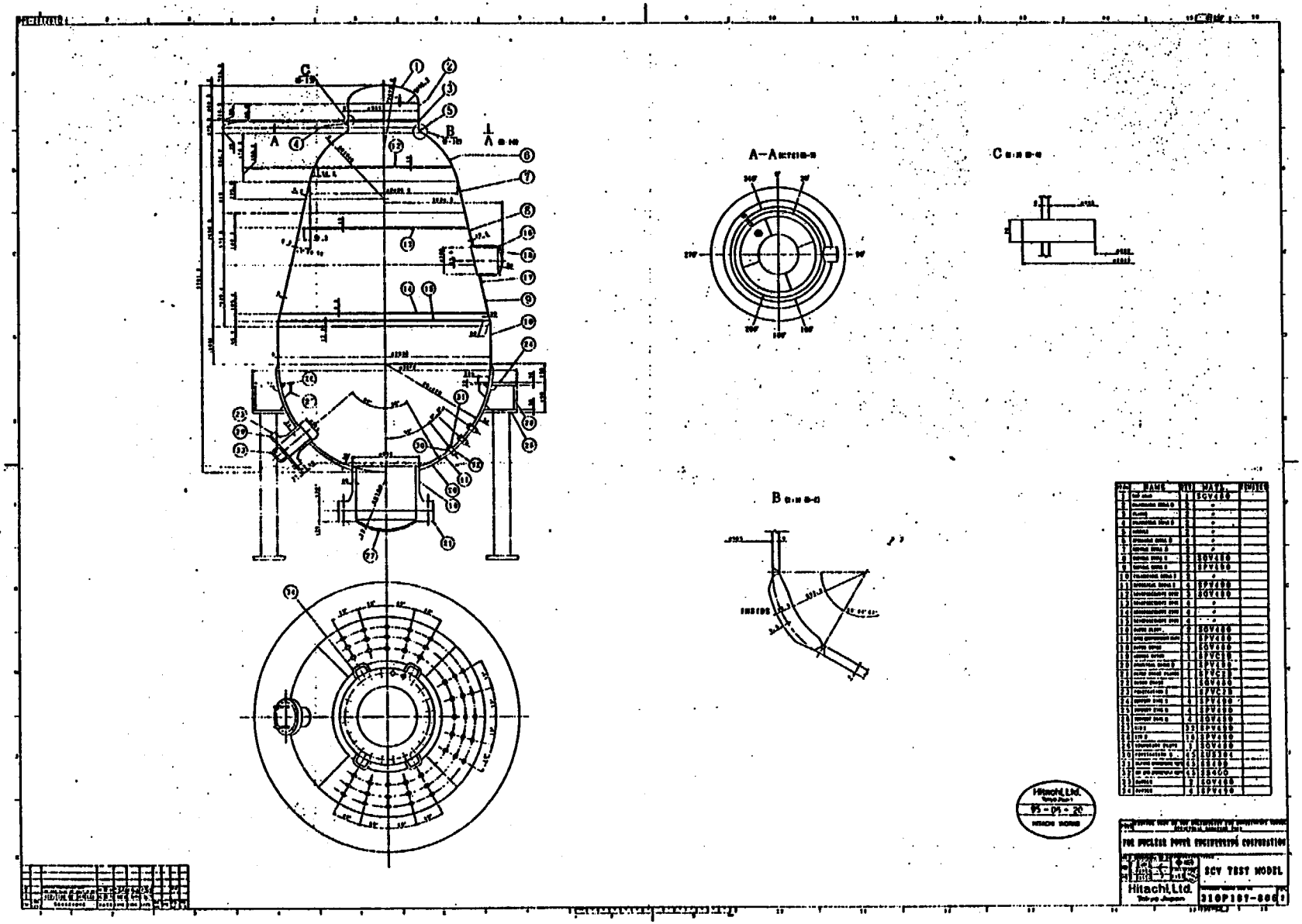
A-A
B
C
FOR NUCLEAR POWER ENGINEERING CORPORATION
SCV TEST MODEL
Hitachi,Ltd.
Tokyo Japan

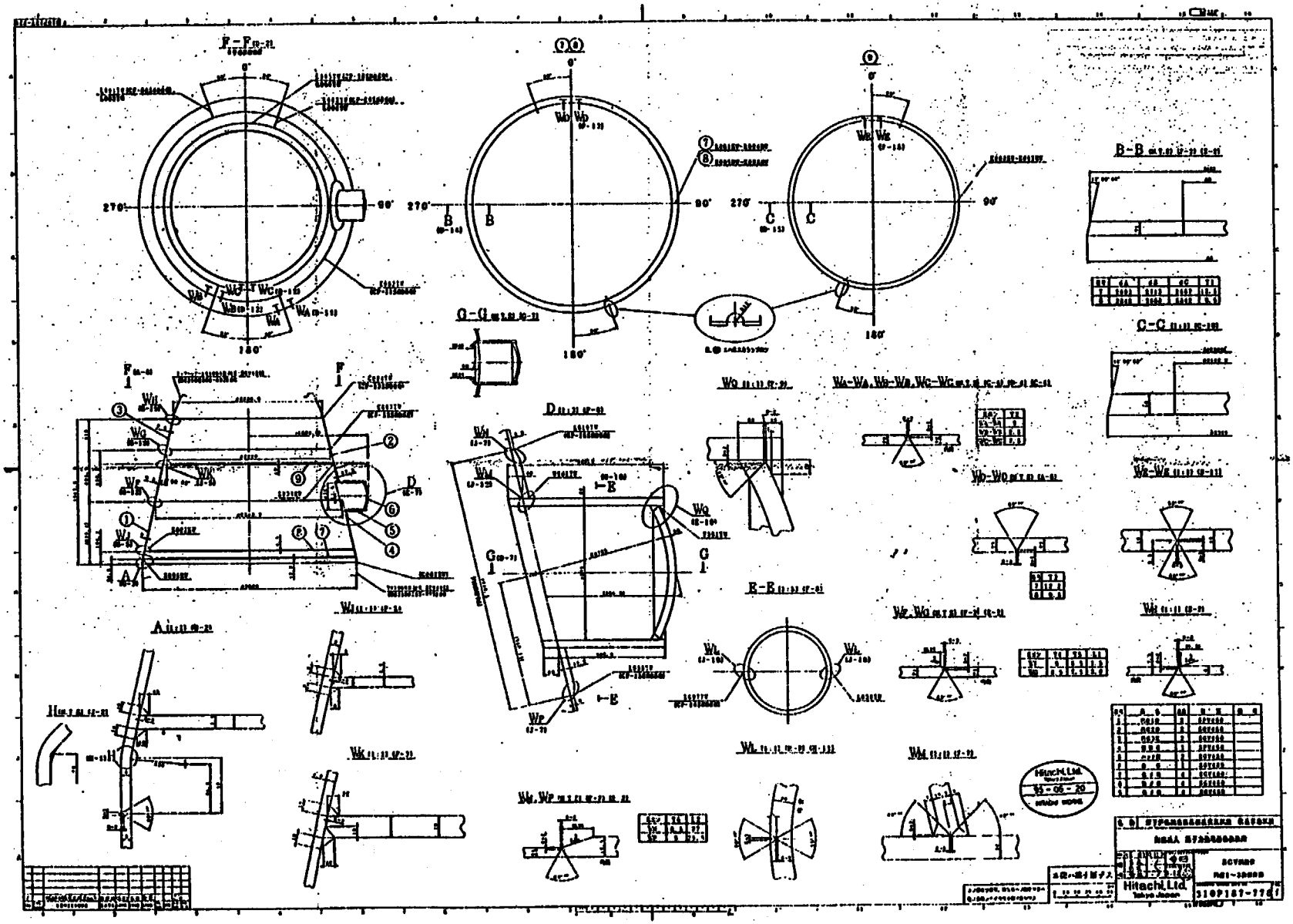
F-F
B-B
C-C
A
D
E-E
Hitachi, Ltd.
Tokyo Japan

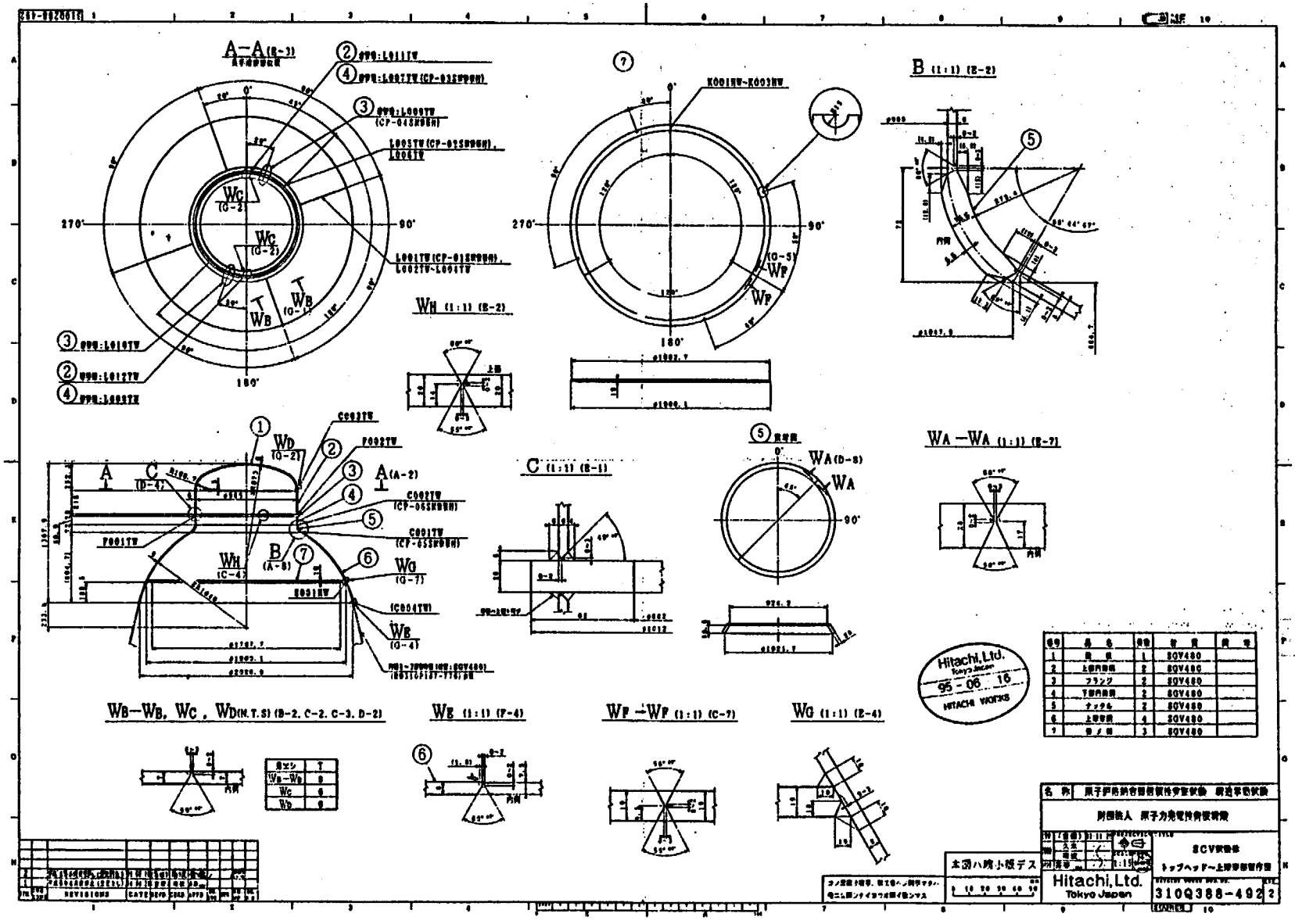
A-A (E-3)
B (1:1) (E-2)
WH (1:1) (E-2)
C (1:1) (E-1)
WA-WA (1:1) (E-7)
WB-WB, WC, WD (N.T.S) (D-2, C-2, C-3, D-2)
WE (1:1) (F-4)
WF-WF (1:1) (C-7)
WG (1:1) (E-4)
Hitachi, Ltd.
Tokyo Japan
95-06-16
HITACHI WORKS
SCV試験体
トップヘッド～上部管台溶接作業
310Q388-492

Appendix B

Contact Structure Design Drawings

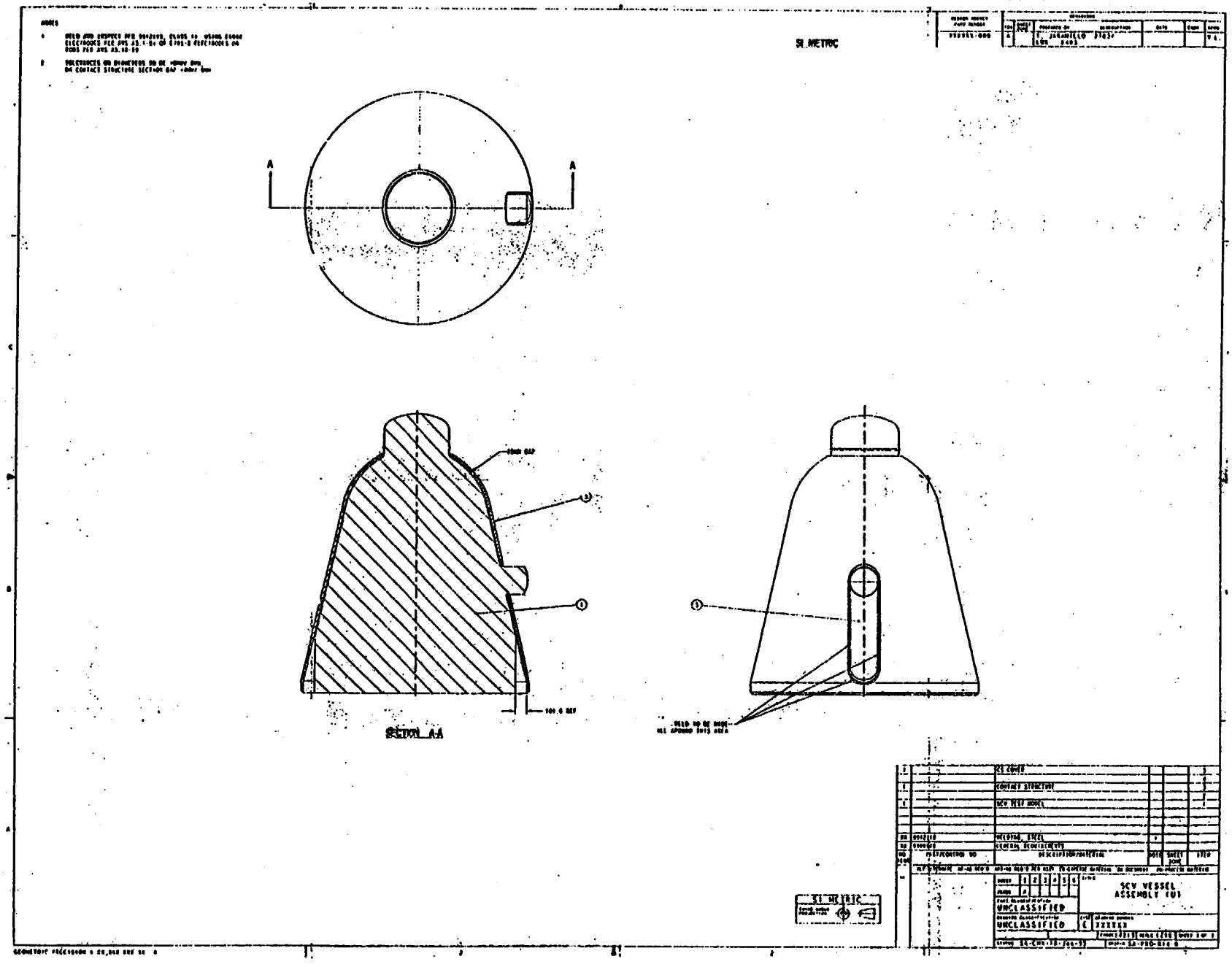
SI METRIC
A
A
SECTION A-A
SCV VESSEL
ASSEMBLY (U)
UNCLASSIFIED
UNCLASSIFIED

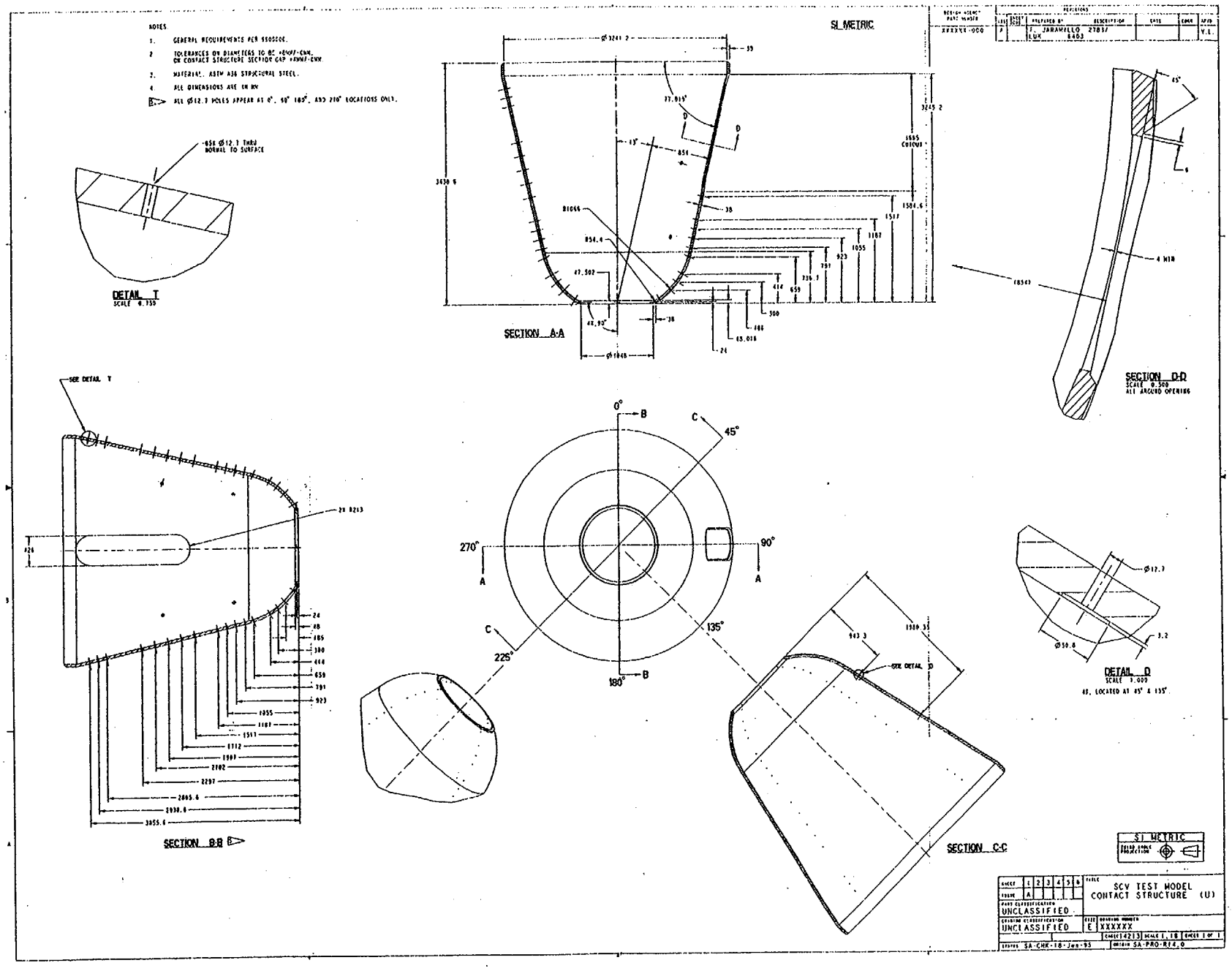
NOTES
1. GENERAL REQUIREMENTS PER 1000000.
2. TOLERANCES ON DIAMETERS TO BE +0.005/-0.000, ON CONTACT STRUCTURE SECTION GAP +0.000/-0.005
3. MATERIAL: ASTM A36 STRUCTURAL STEEL.
4. ALL DIMENSIONS ARE IN MM
5. ALL Ø12.7 HOLES APPEAR AT 0°, 90° 180°, AND 270° LOCATIONS ONLY.
SI METRIC
XXXXXX-000
REVISIONS
REV LTR | ECO NO | REPLACED BY | DESCRIPTION | DATE | CHKR | APVD
2 | | T. JARAMILLO 27837 | | | | V.L.
LUK 8403
DETAIL T
SCALE 0.750
SECTION A-A
SECTION D-D
SCALE 0.500
ALL AROUND OPENING
SEE DETAIL T
SECTION B-B
SECTION C-C
SEE DETAIL D
DETAIL D
SCALE 3.000
48, LOCATED AT 45° & 135°
SI METRIC
SCV TEST MODEL
CONTACT STRUCTURE (U)
PART CLASSIFICATION
UNCLASSIFIED
DRAWING CLASSIFICATION
UNCLASSIFIED
SIZE E
DRAWING NUMBER
XXXXXX
CHECK 4213
SCALE 1:10
SHEET 1 OF 1
STATUS SA-CHK-18-Jun-95
ORIGIN SA-PRO-R14.0

Appendix C

Measured Material Properties for the SCV Model

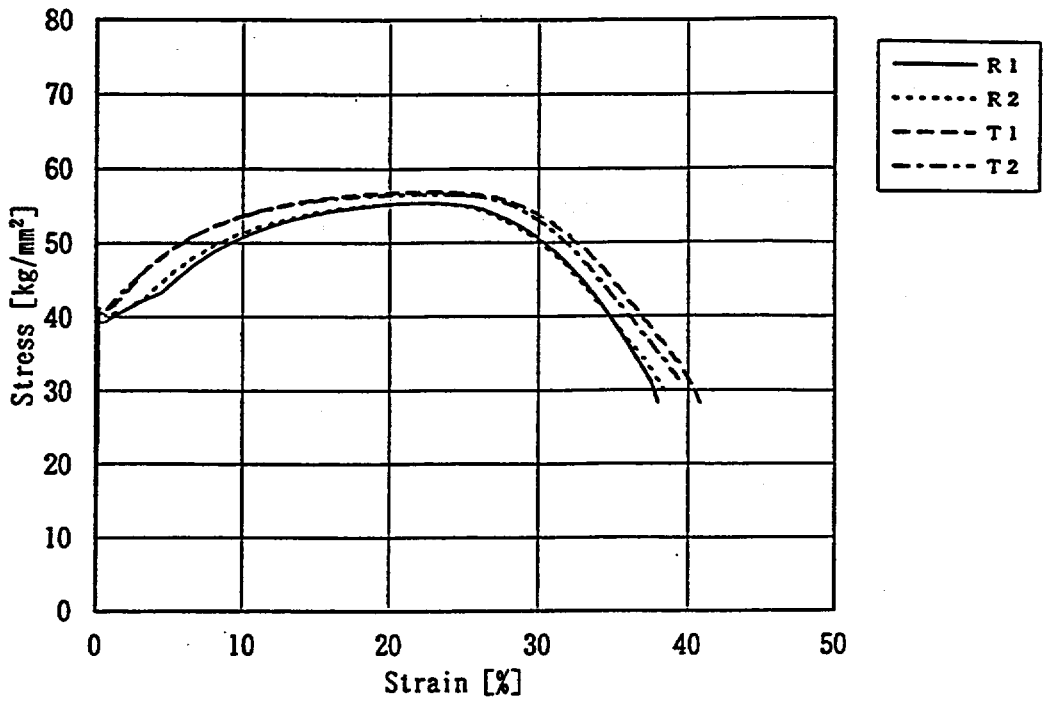

Figure C.1. Stress-strain curves for SGV480: thickness 6.0 mm plate, location 1.

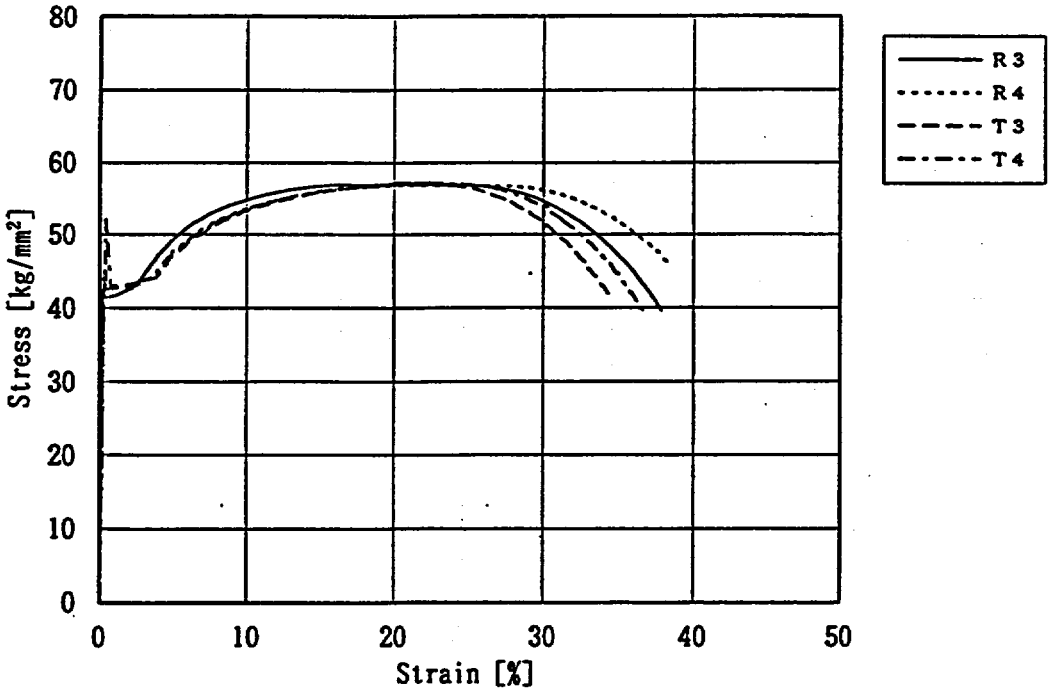

Figure C.2. Stress-strain curves for SGV480: thickness 6.0 mm plate, location 2.

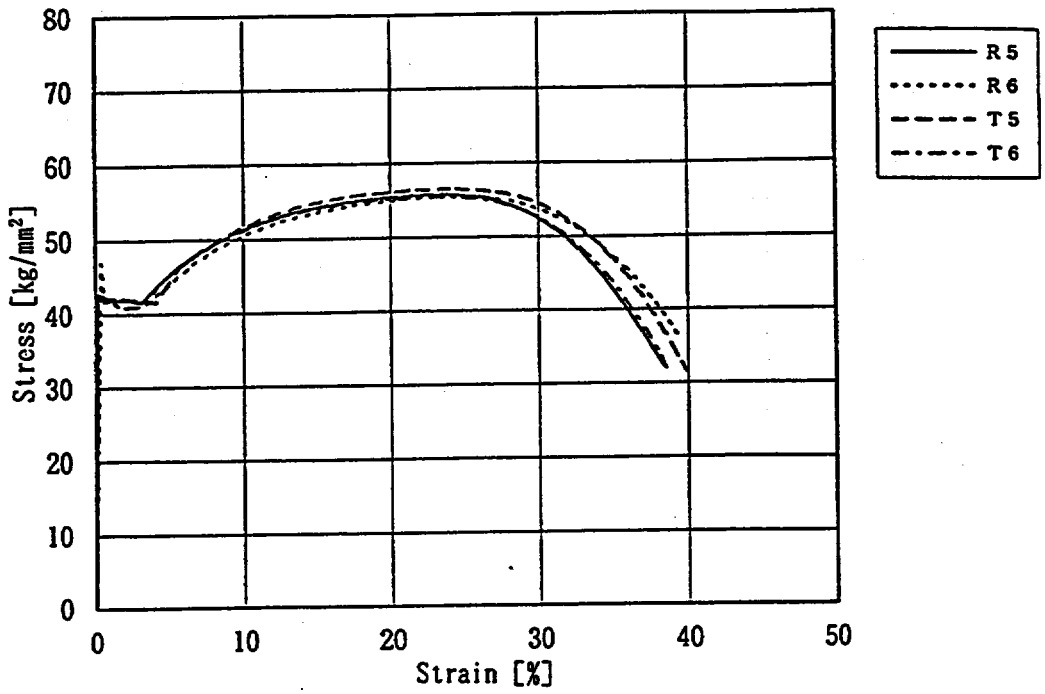

Figure C.3. Stress-strain curves for SGV480: thickness 7.5 mm plate, location 3.

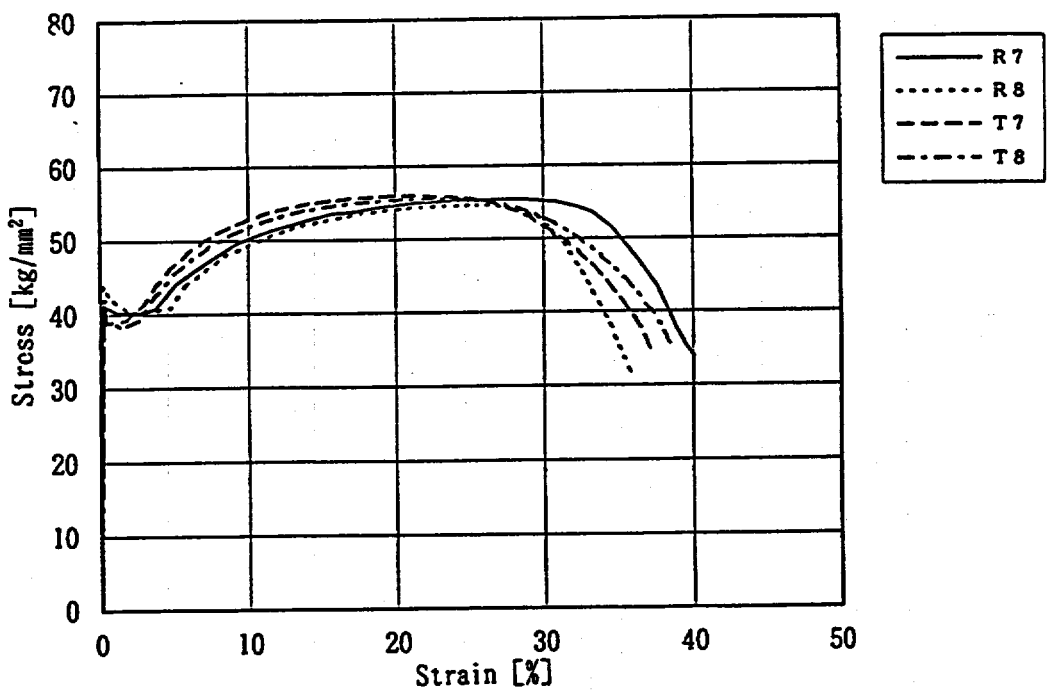

Figure C.4. Stress-strain curves for SGV480: thickness 8.0 mm plate, location 4.

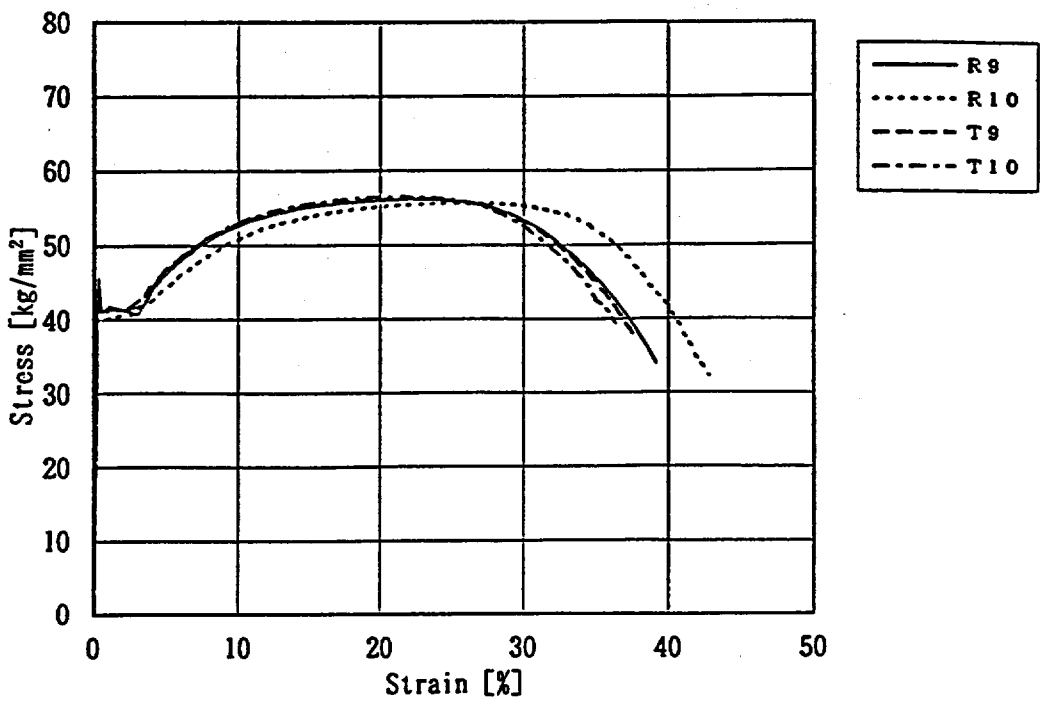

Figure C.5. Stress-strain curves for SGV480: thickness 8.5 mm plate, location 5.

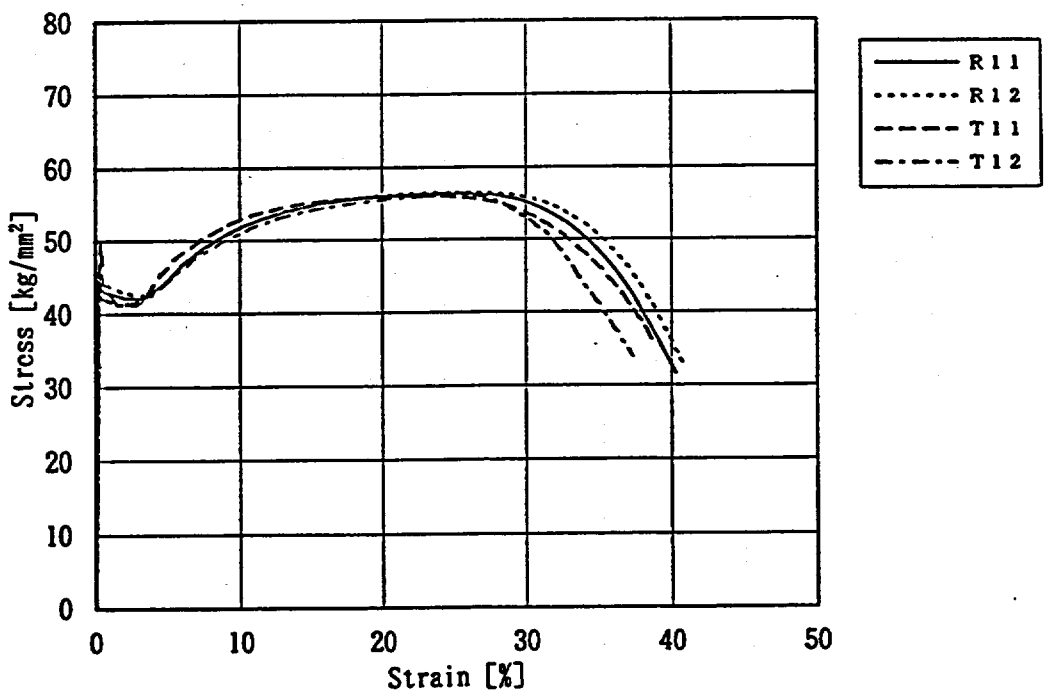

Figure C.6. Stress-strain curves for SGV480: thickness 9.5 mm plate, location 6.

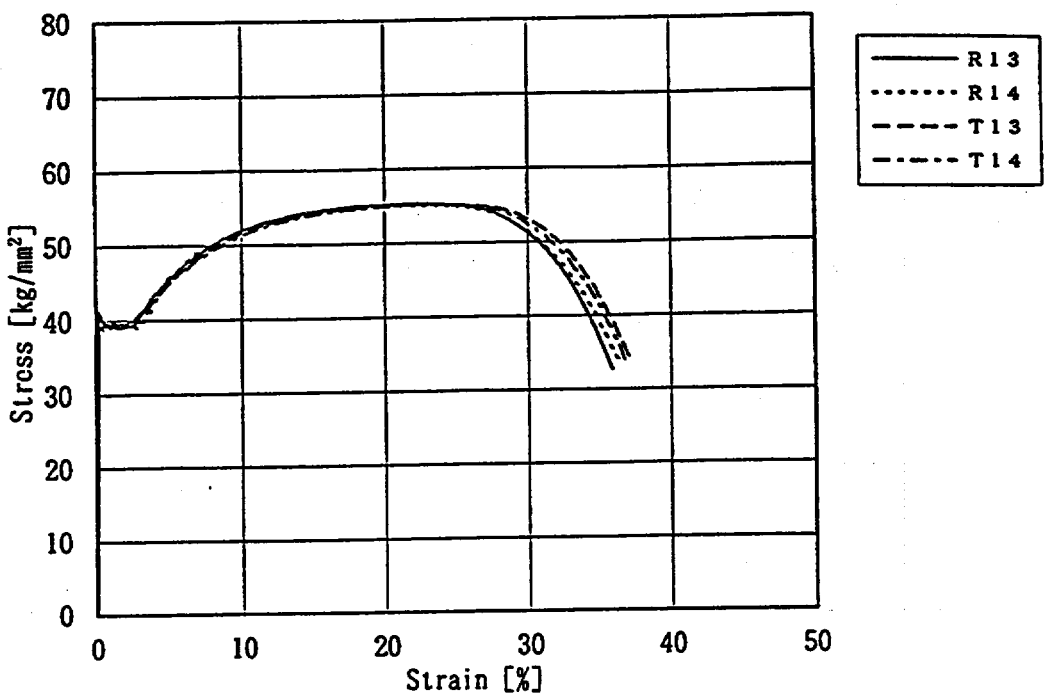

Figure C.7. Stress-strain curves for SGV480: thickness 12.5 mm plate, location 7.

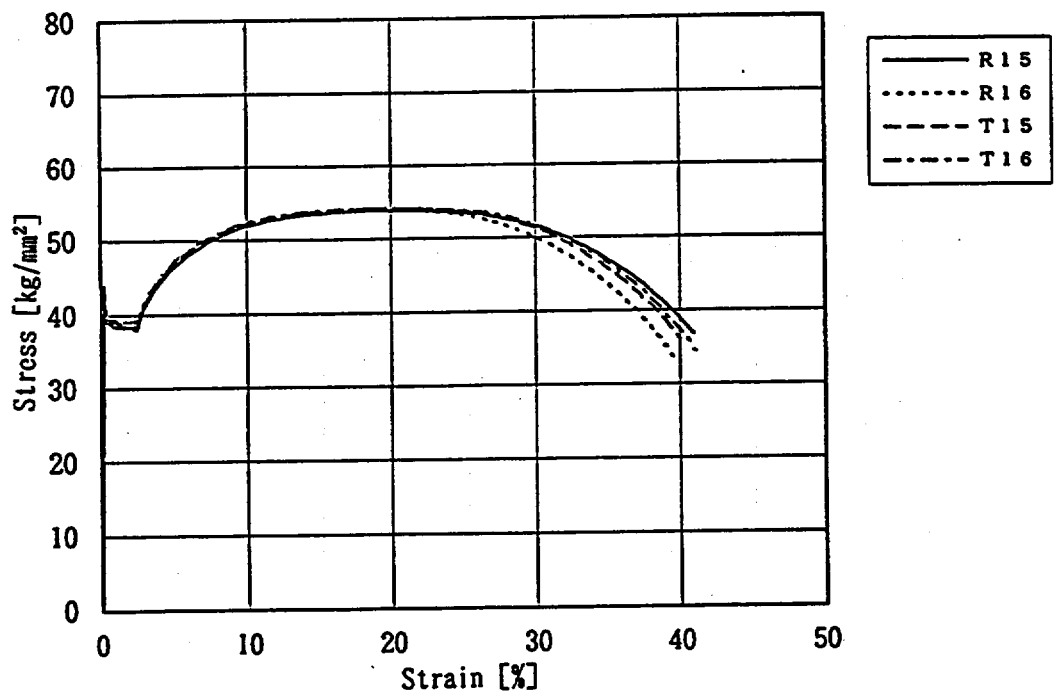

Figure C.8. Stress-strain curves for SGV480: thickness 19.0 mm plate, location 8.

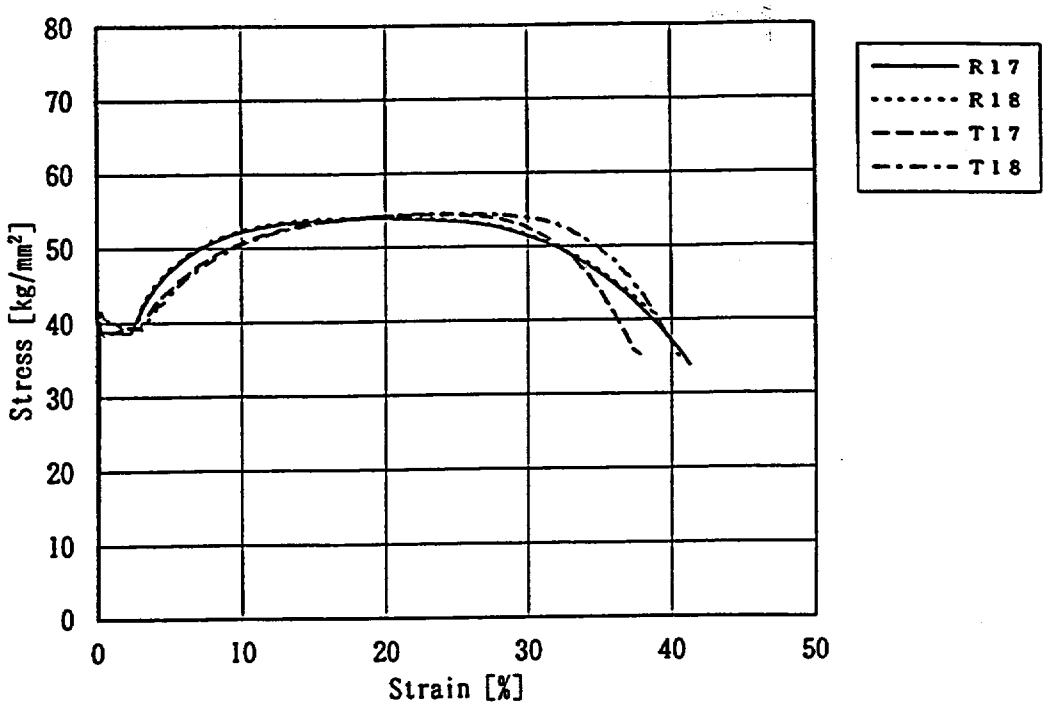

Figure C.9. Stress-strain curves for SGV480: thickness 20.0 mm plate, location 9.

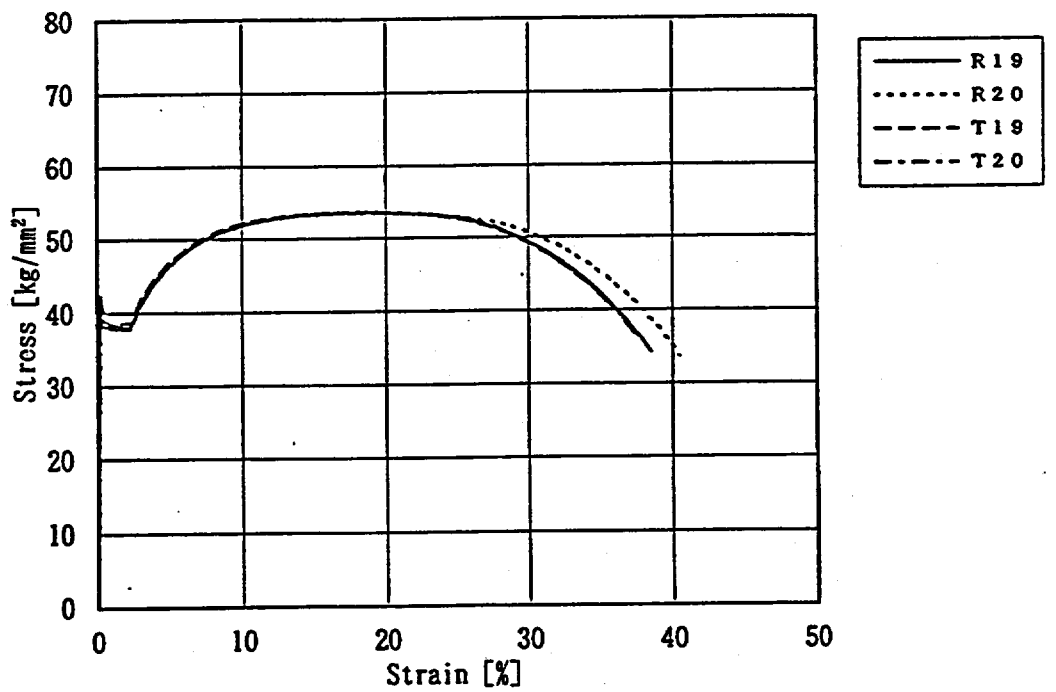

Figure C.10. Stress-strain curves for SGV480: thickness 28.0 mm plate, location 10.

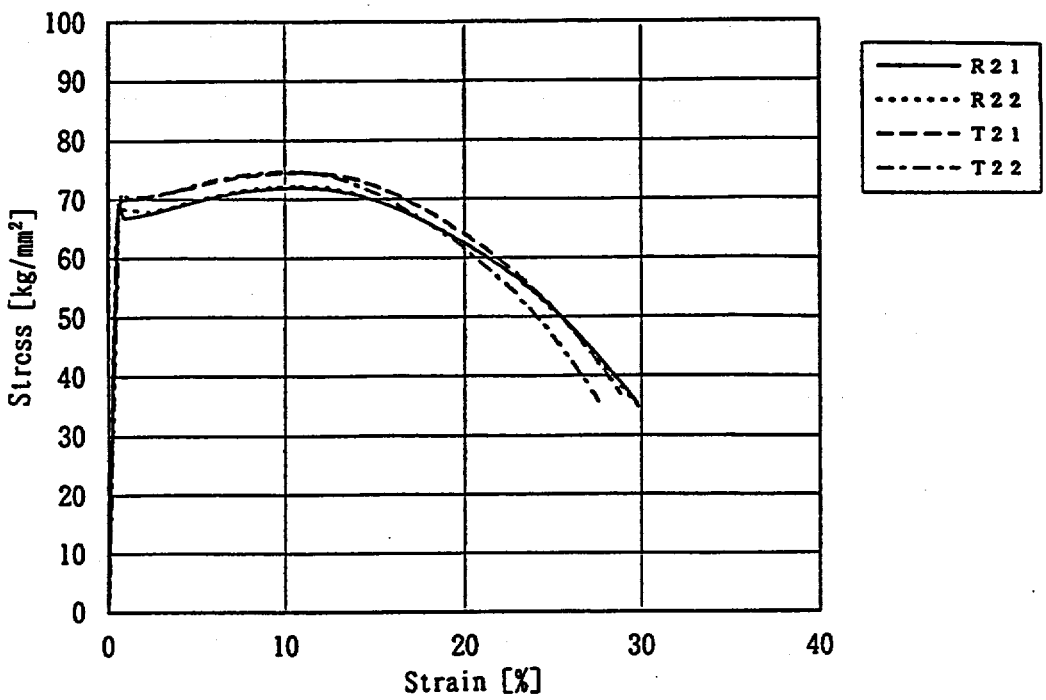

Figure C.11. Stress-strain curves for SPV490: thickness 9 mm plate, location 11.

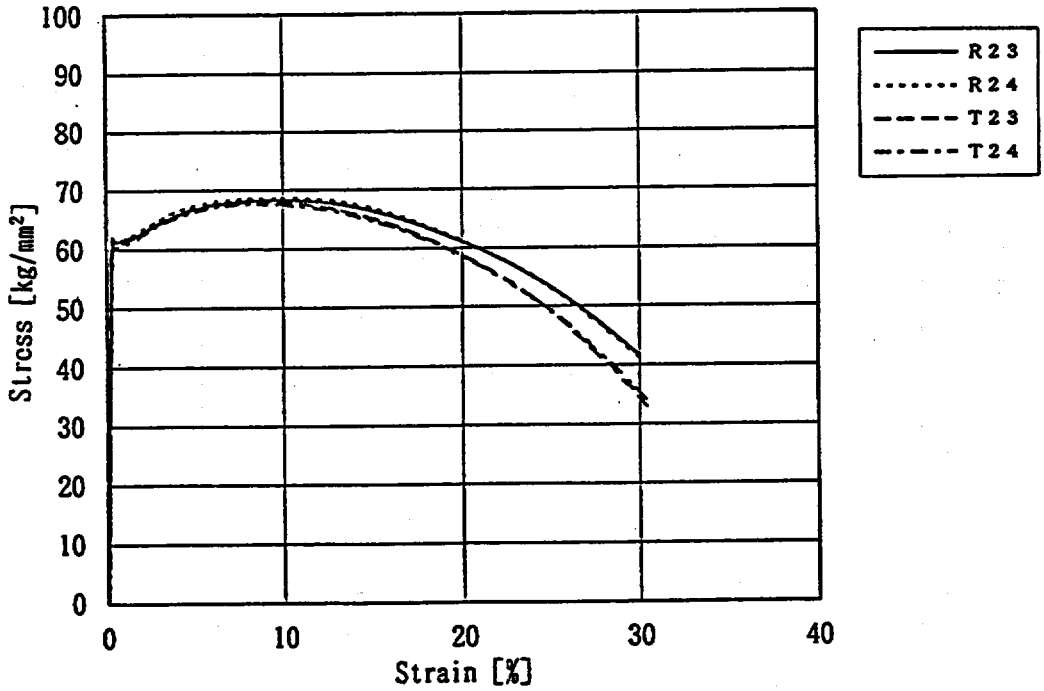

Figure C.12. Stress-strain curves for SPV490: thickness 17.5 mm plate, location 12.

Appendix D

Compilation of Analysis Results from Participants

This page intentionally
left blank.

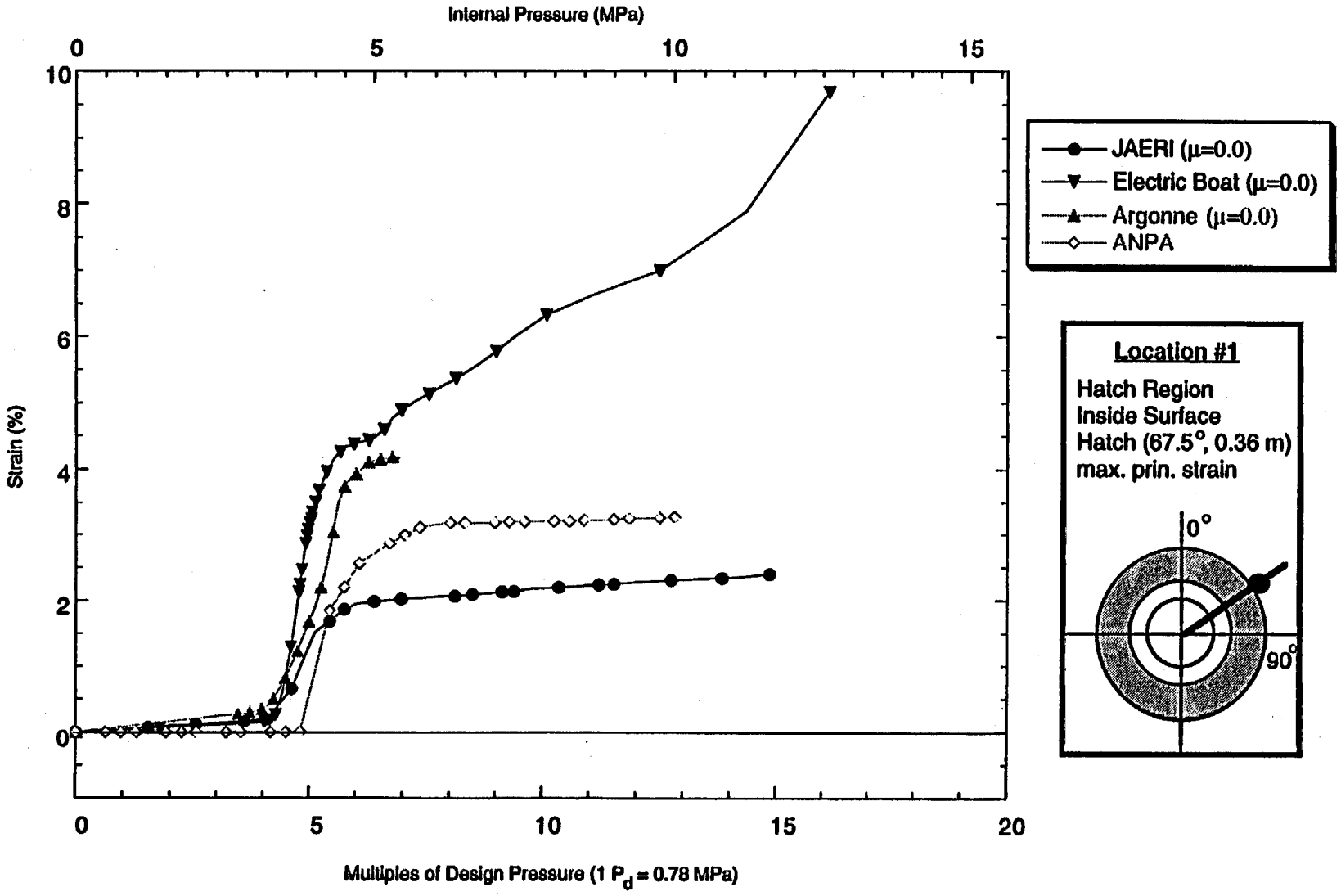

Figure D-1. Standard Output Location #1 (zero friction case)

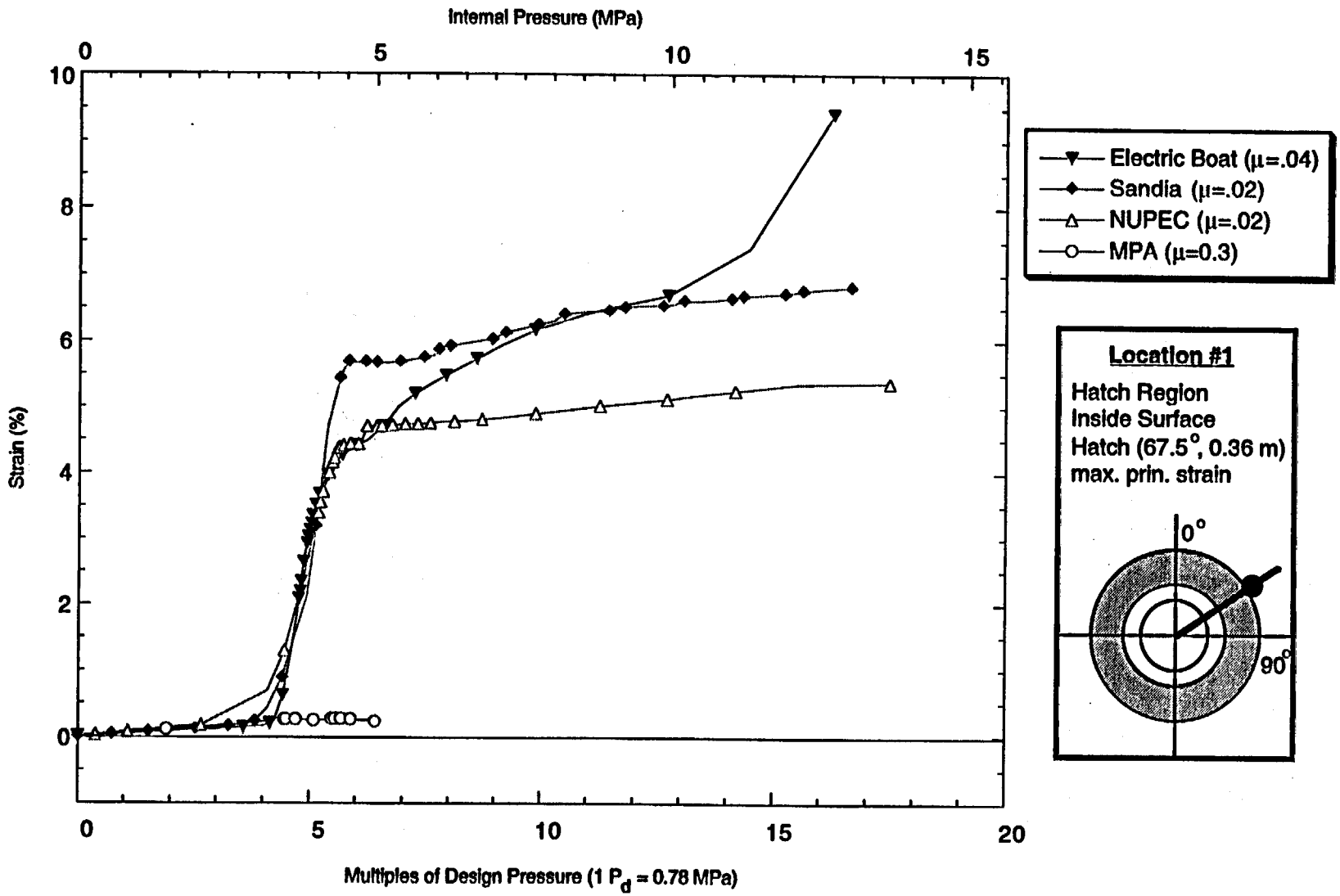

Figure D-2. Standard Output Location #1 (nonzero friction case)

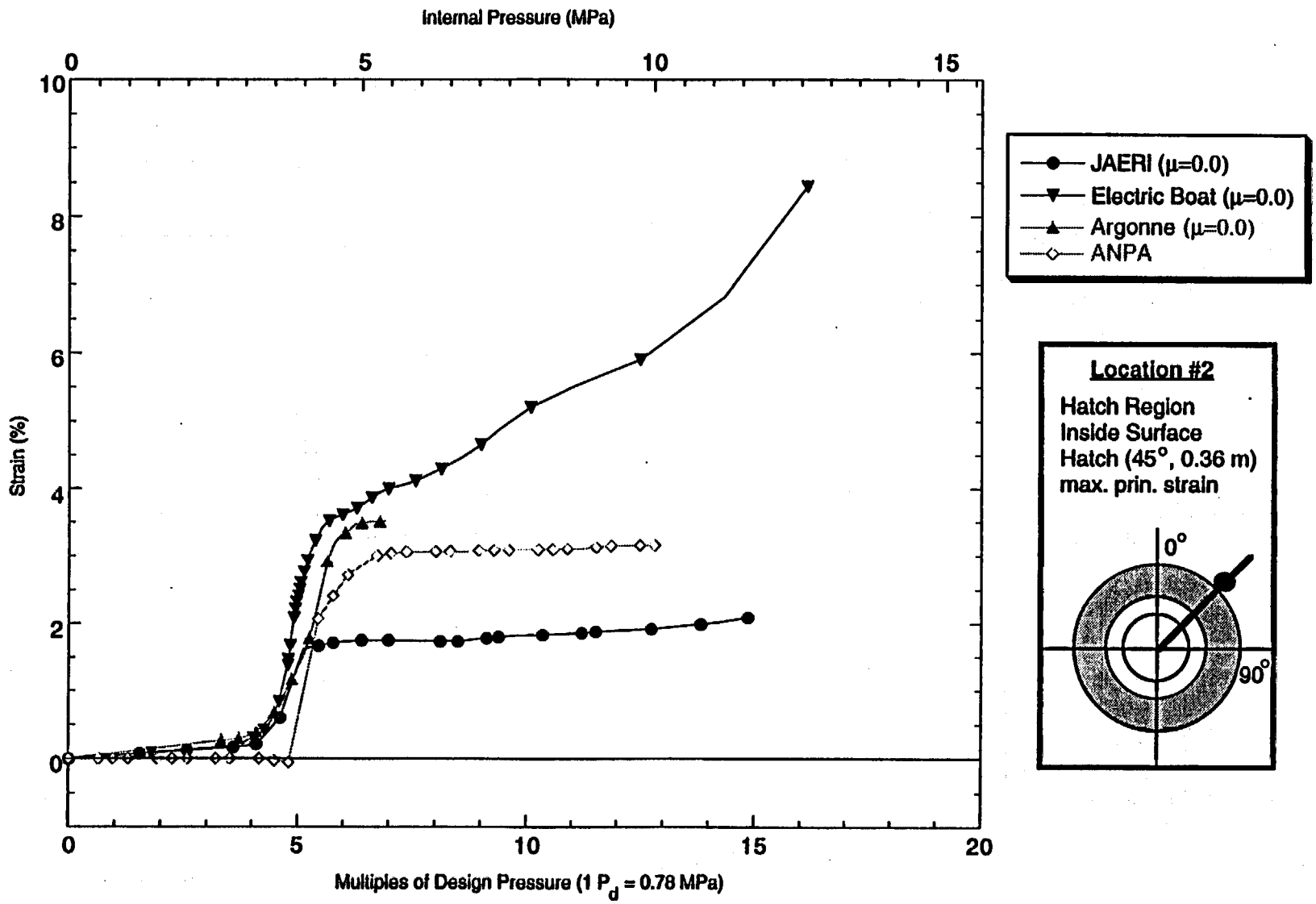

Figure D-3. Standard Output Location #2 (zero friction case)

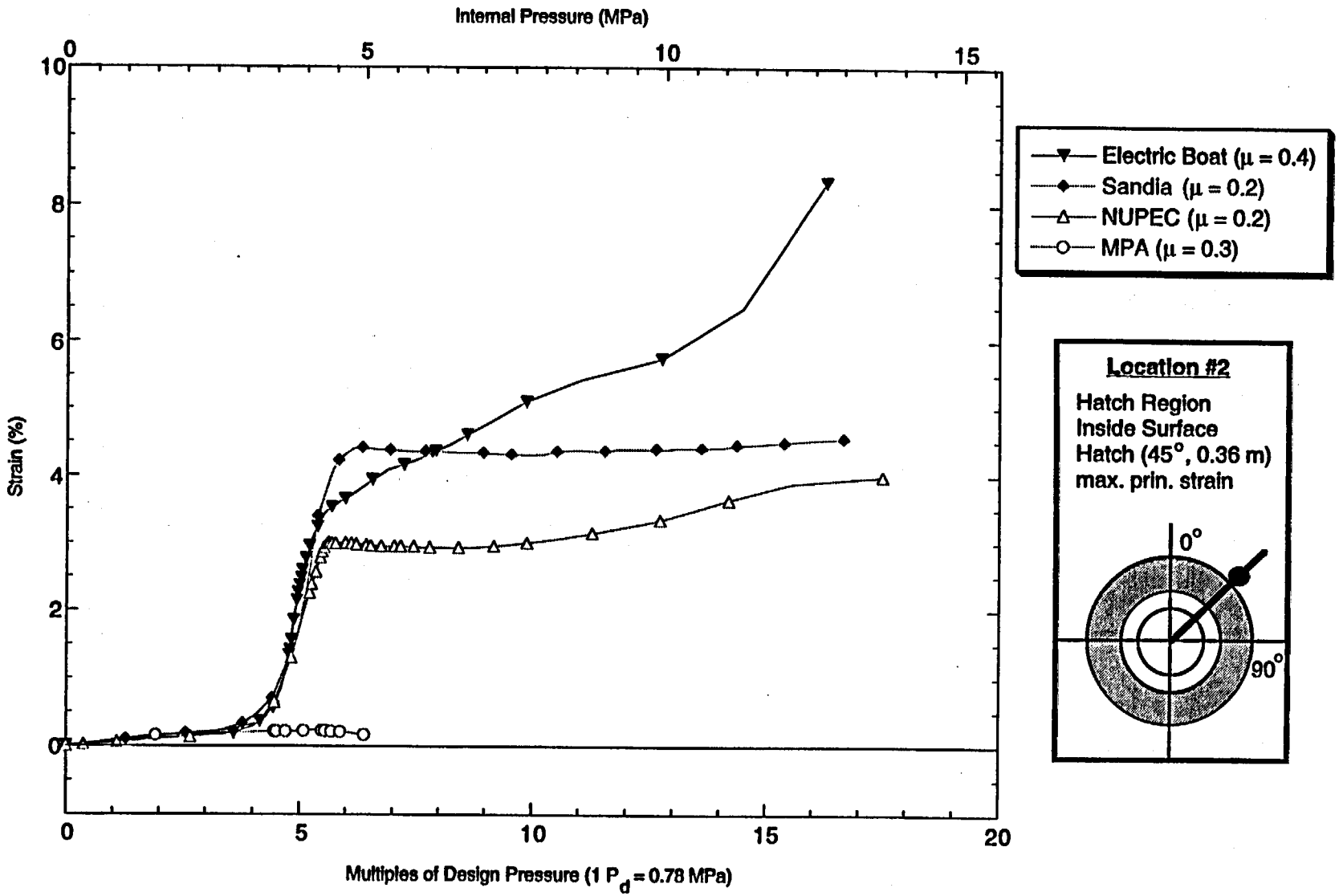

Figure D-4. Standard Output Location #2 (nonzero friction case)

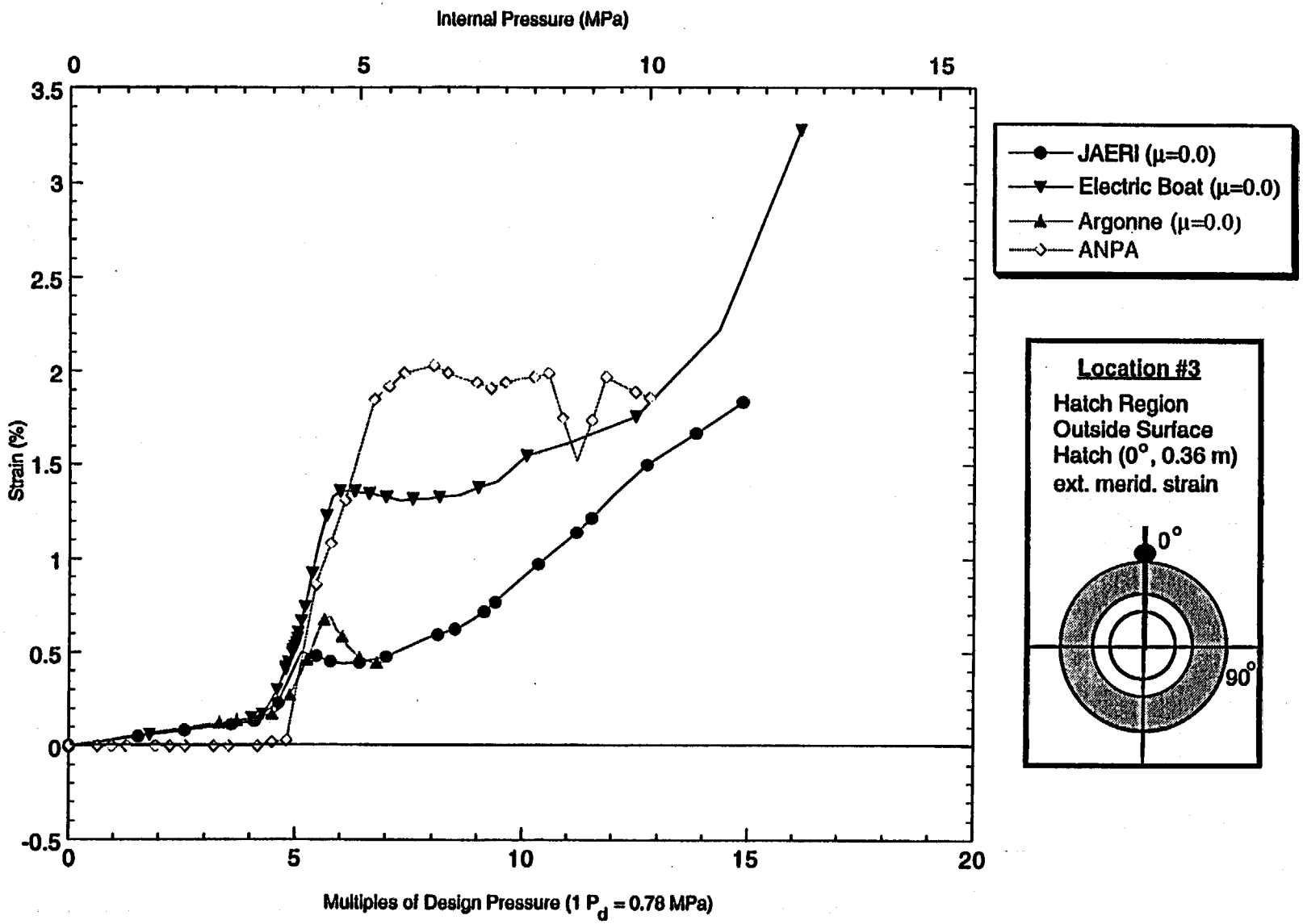

Figure D-5. Standard Output Location #3 (zero friction case)

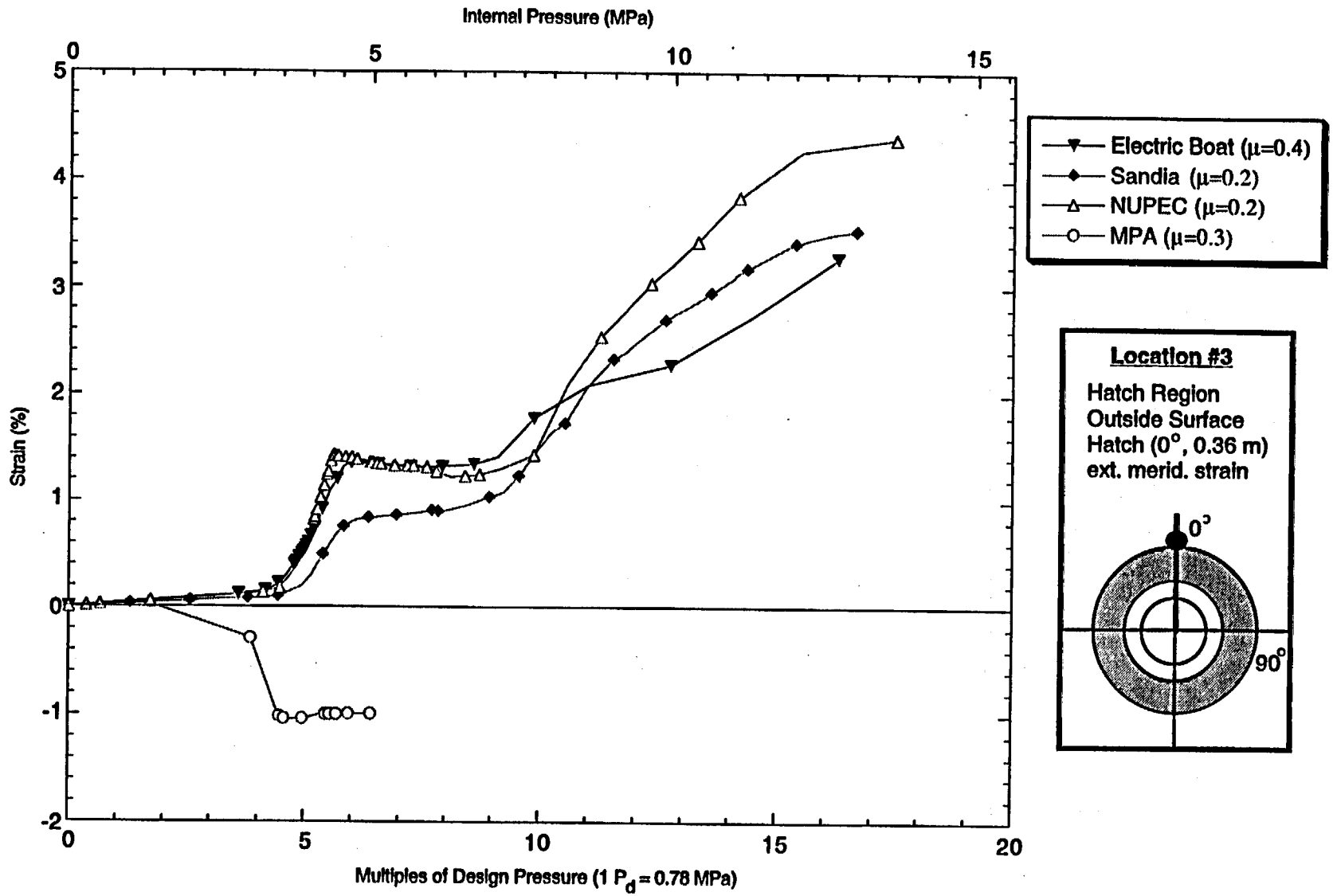

Figure D-6. Standard Output Location #3 (nonzero friction case)

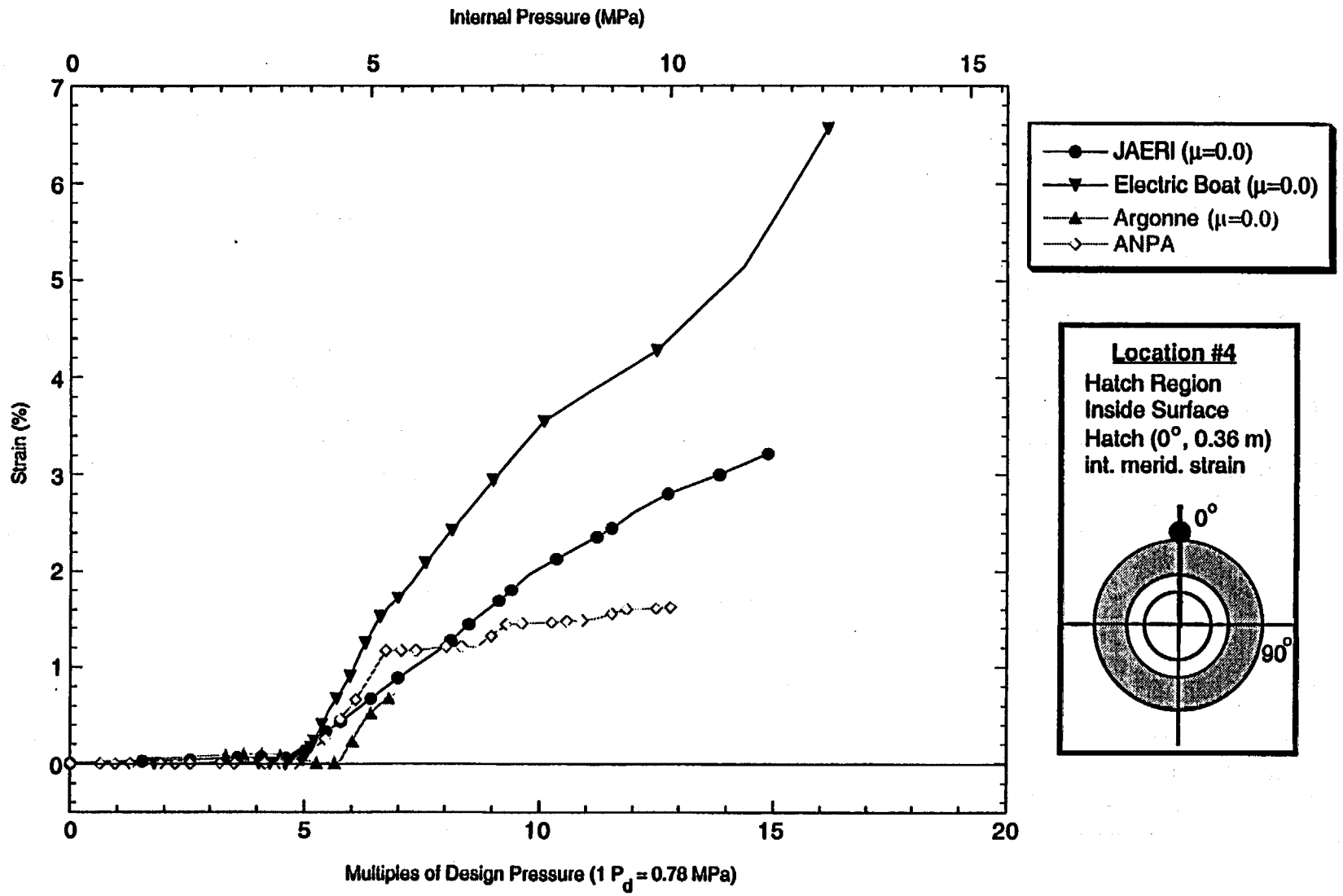

Figure D-7. Standard Output Location #4 (zero friction case)

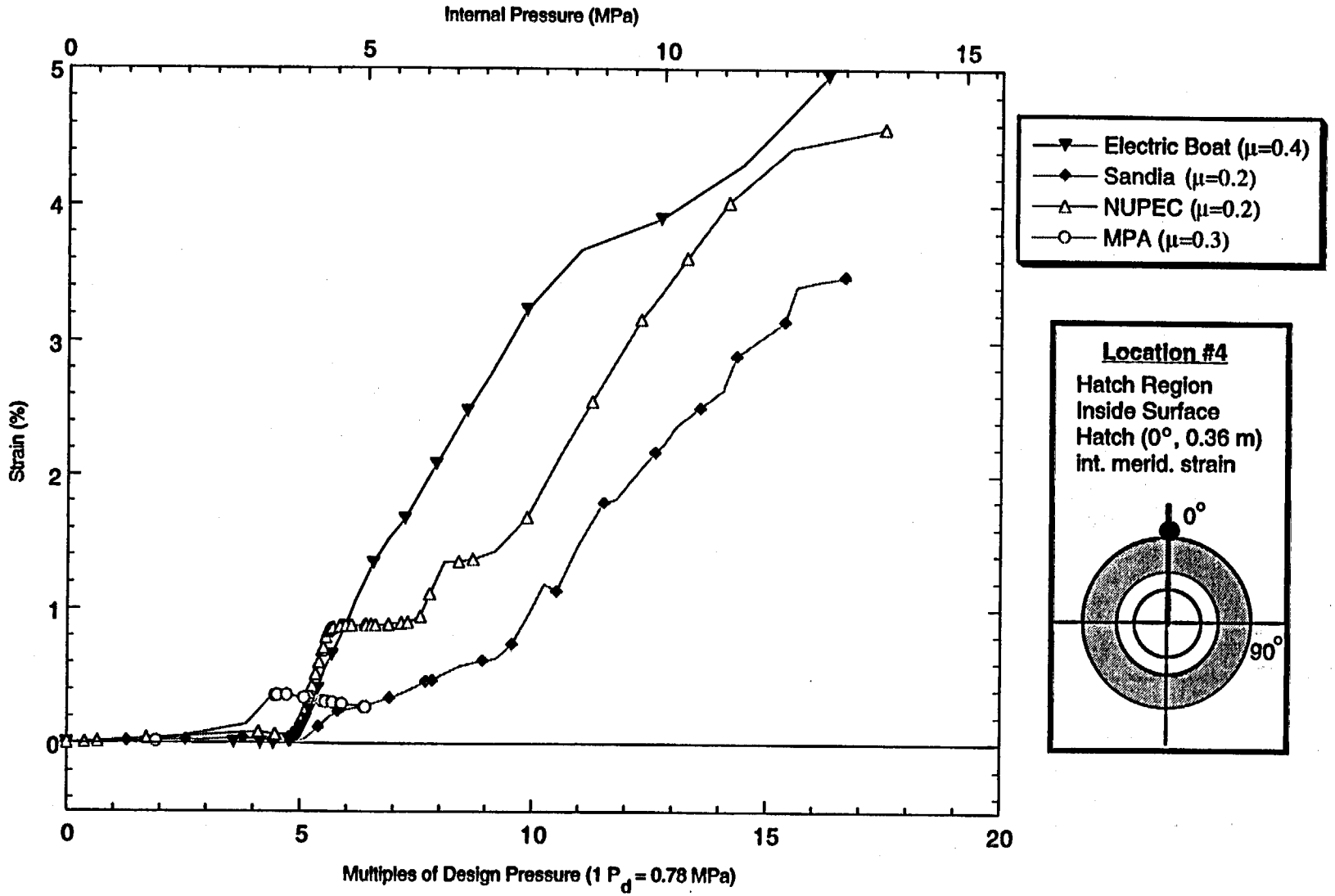

Figure D-8. Standard Output Location #4 (nonzero friction case)

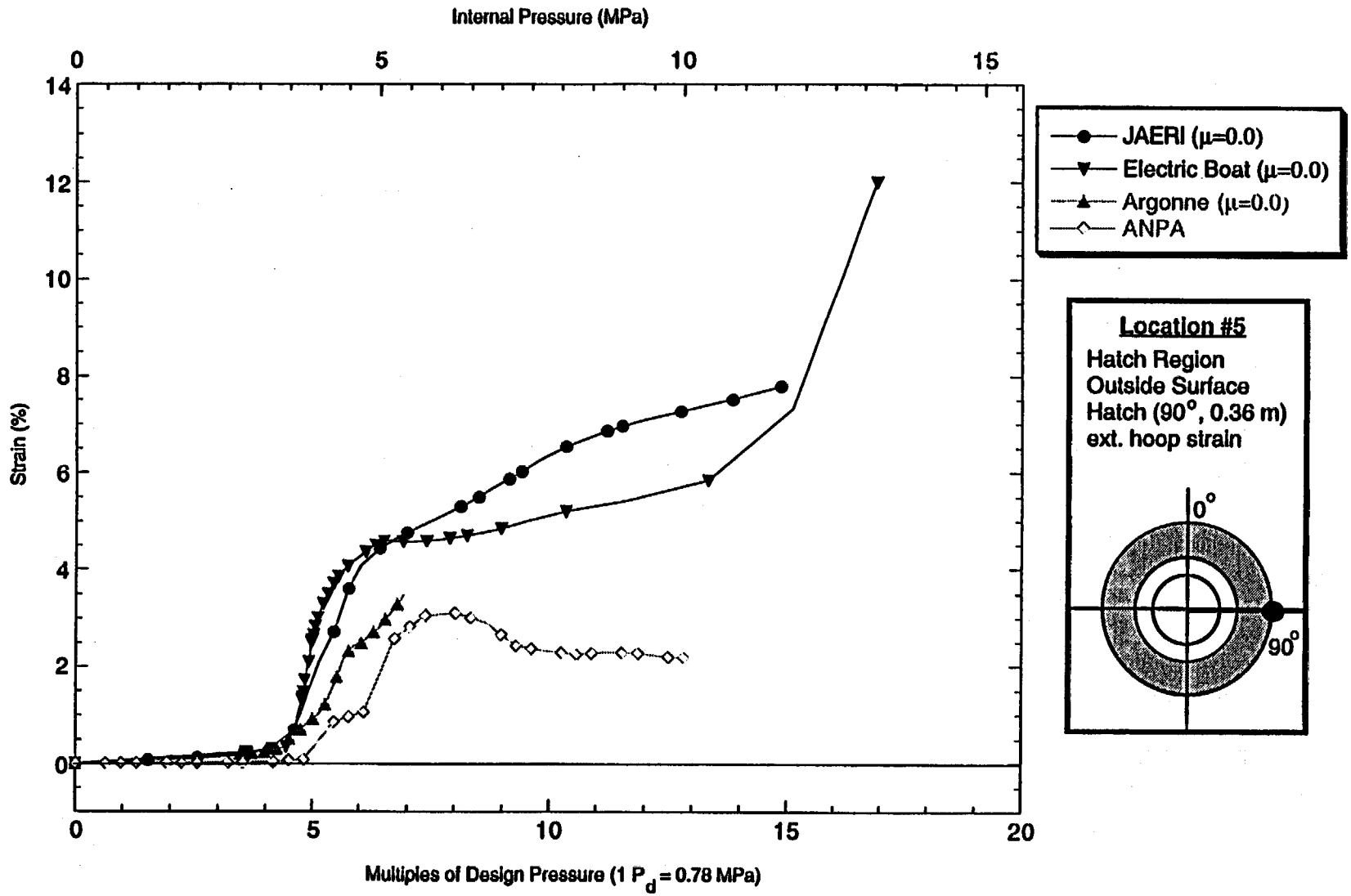

Figure D-9. Standard Output Location #5 (zero friction case)

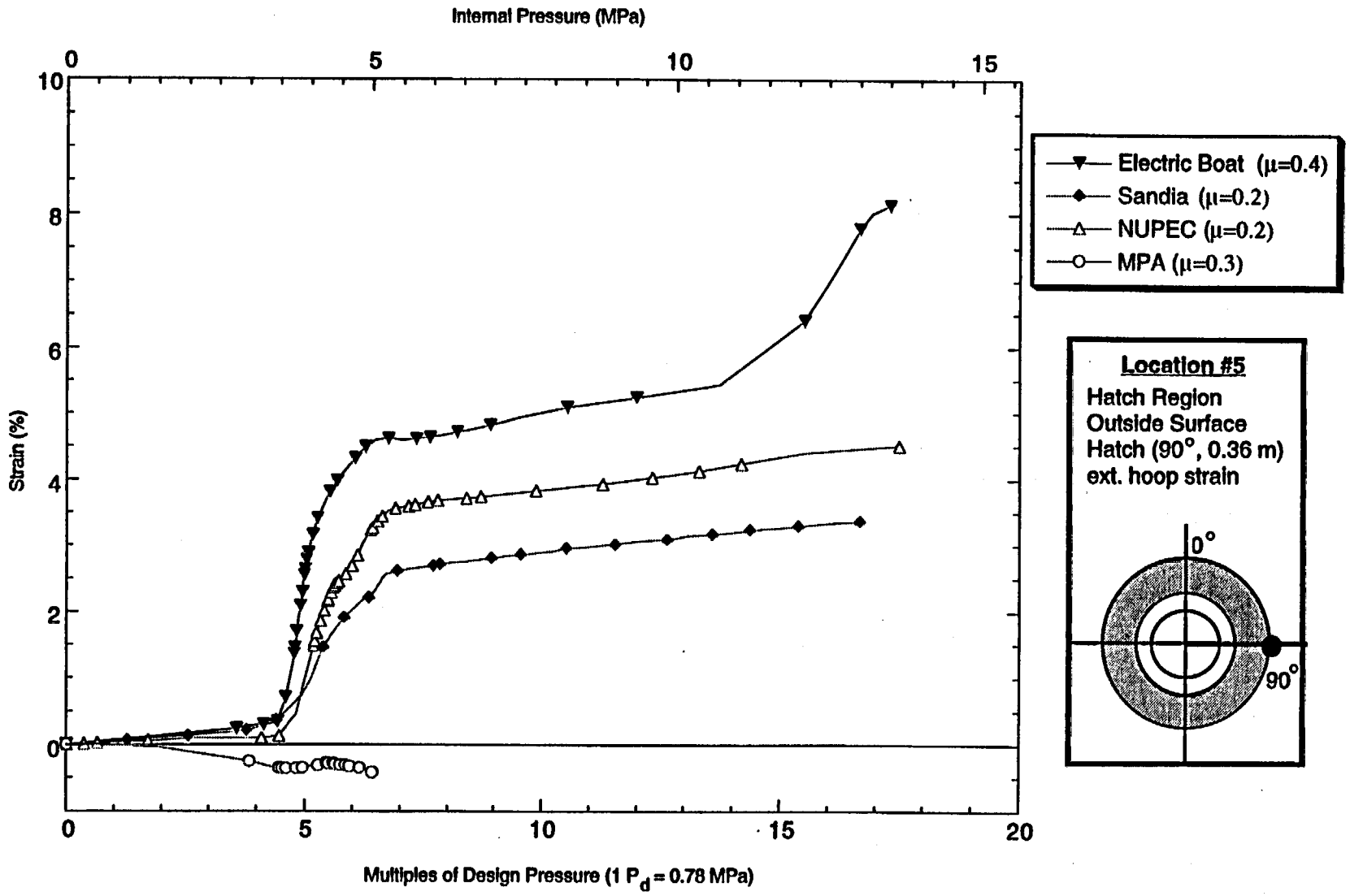

Figure D-10. Standard Output Location #5 (nonzero friction case)

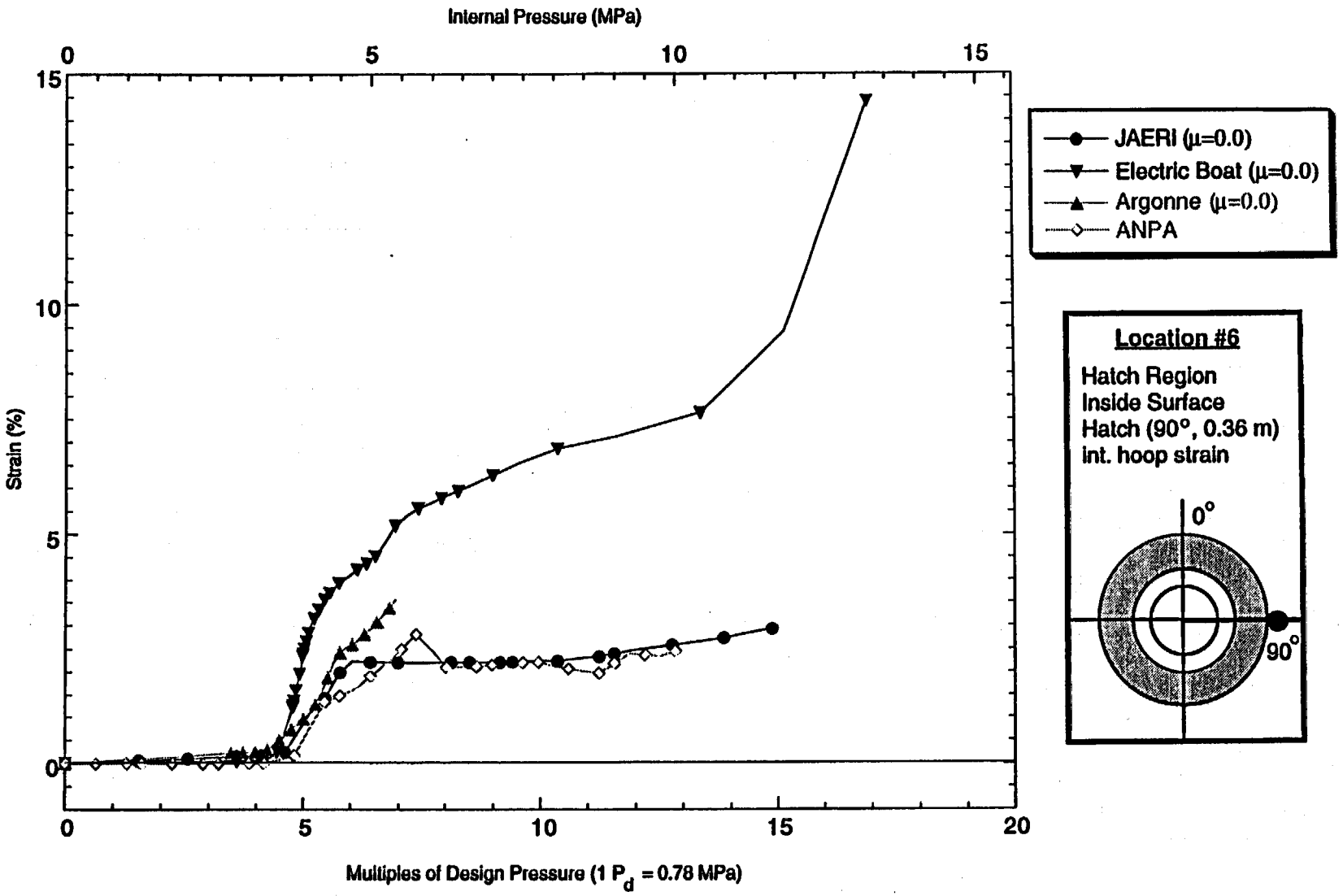

Figure D-11. Standard Output Location #6 (zero friction case)

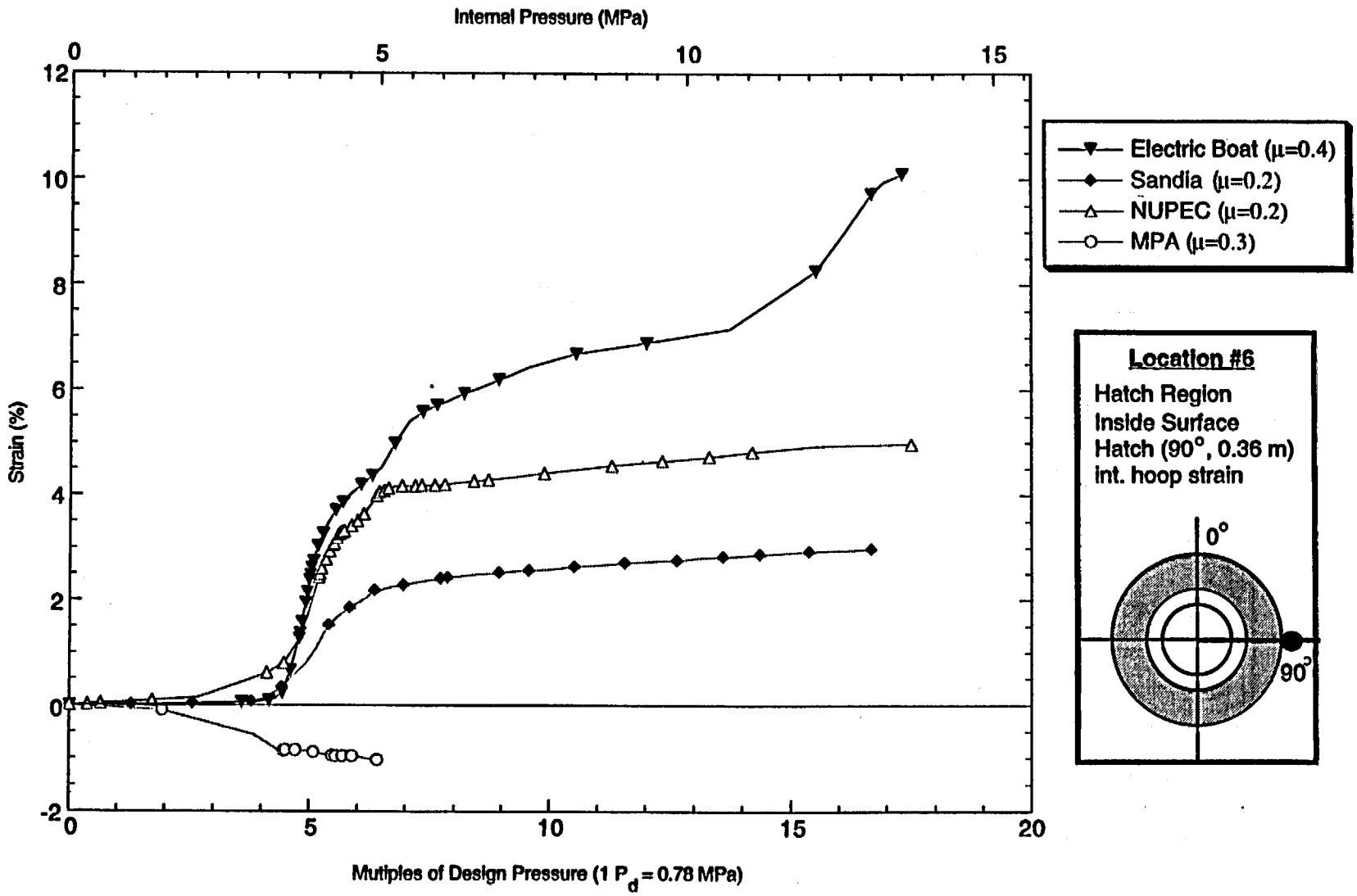

Figure D-12. Standard Output Location #6 (nonzero friction case)

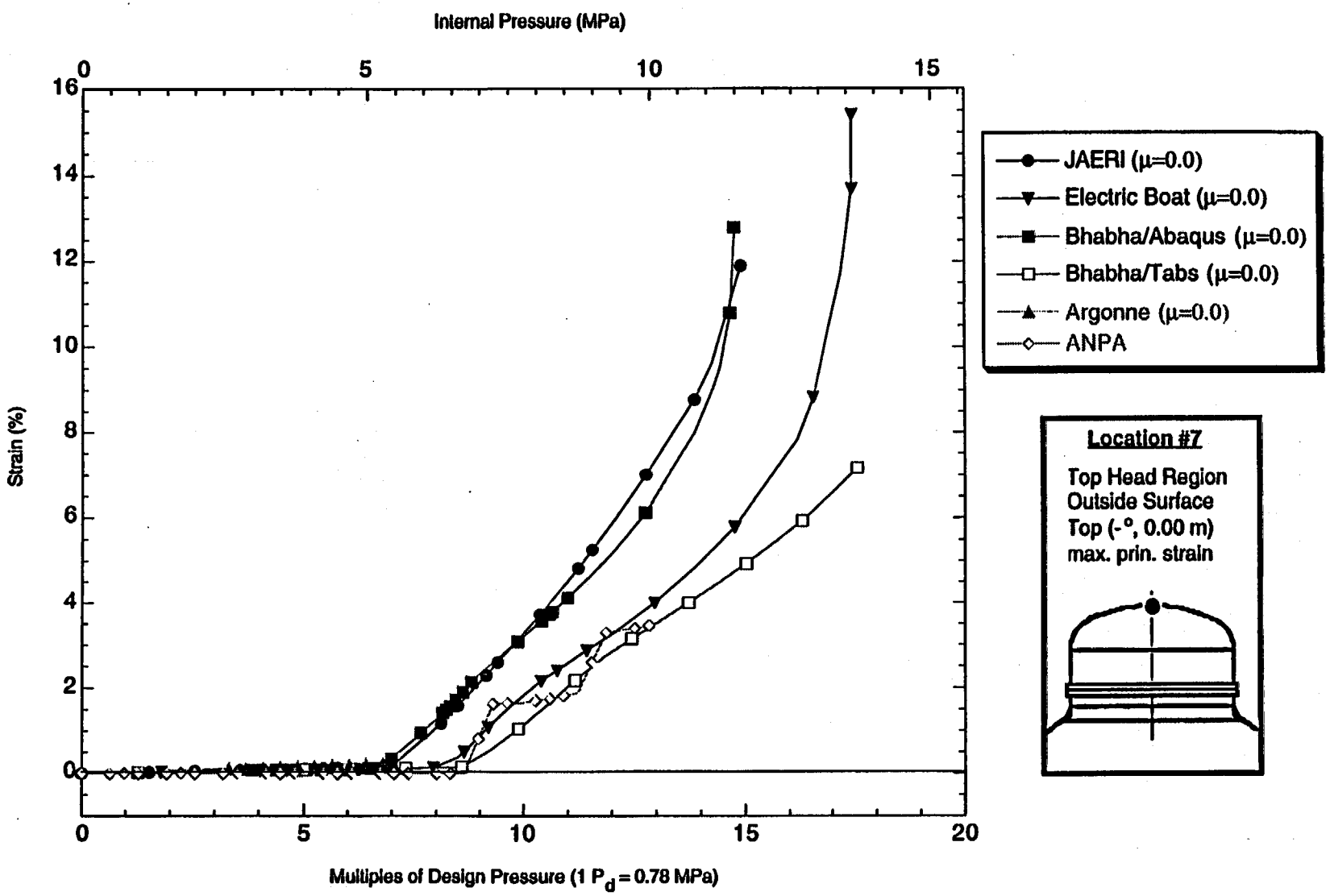

Figure D-13. Standard Output Location #7 (zero friction case)

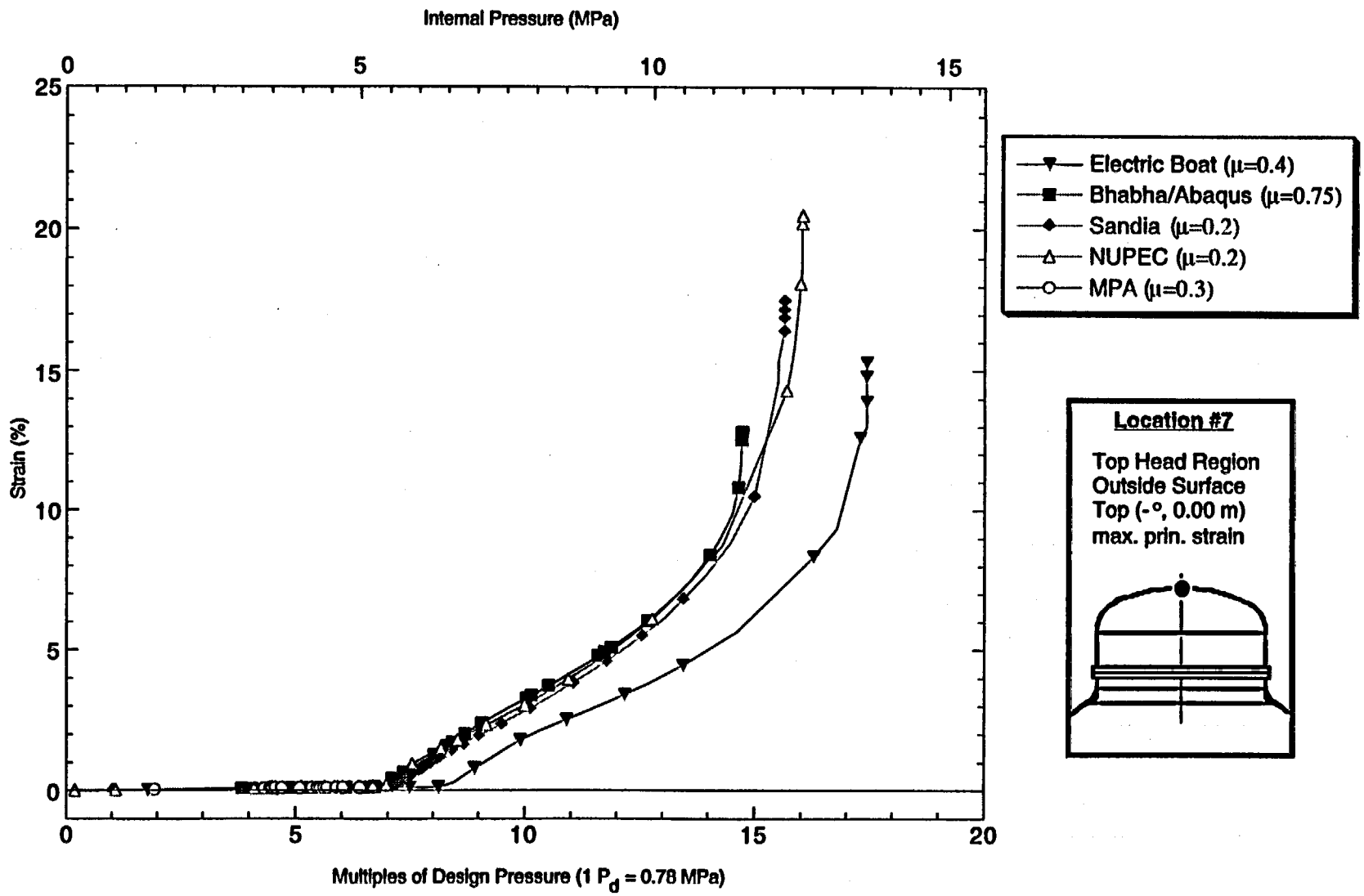

Figure D-14. Standard Output Location #7 (nonzero friction case)

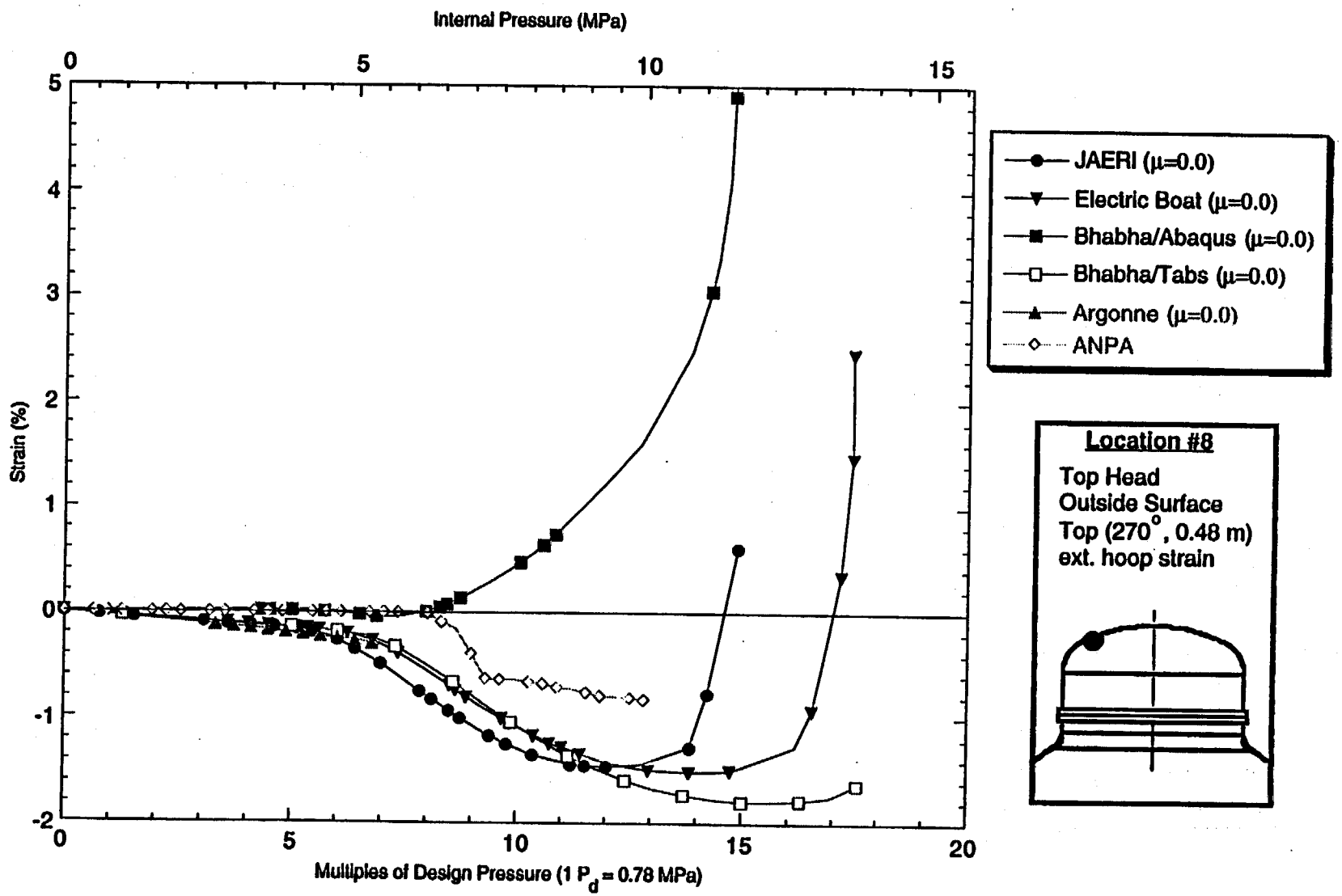

Figure D-15. Standard Output Location #8 (zero friction case)

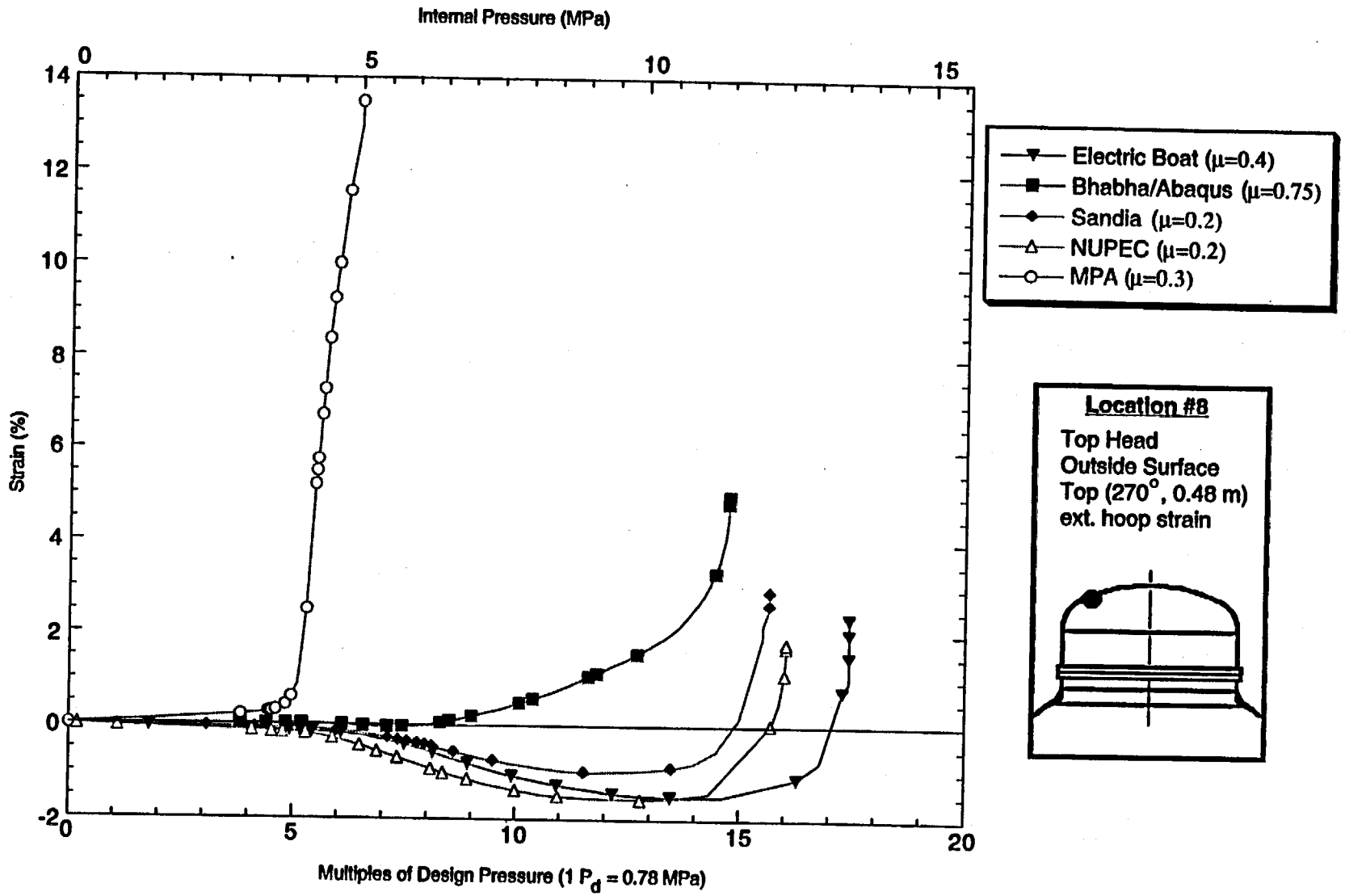

Figure D-16. Standard Output Location #8 (nonzero friction case)

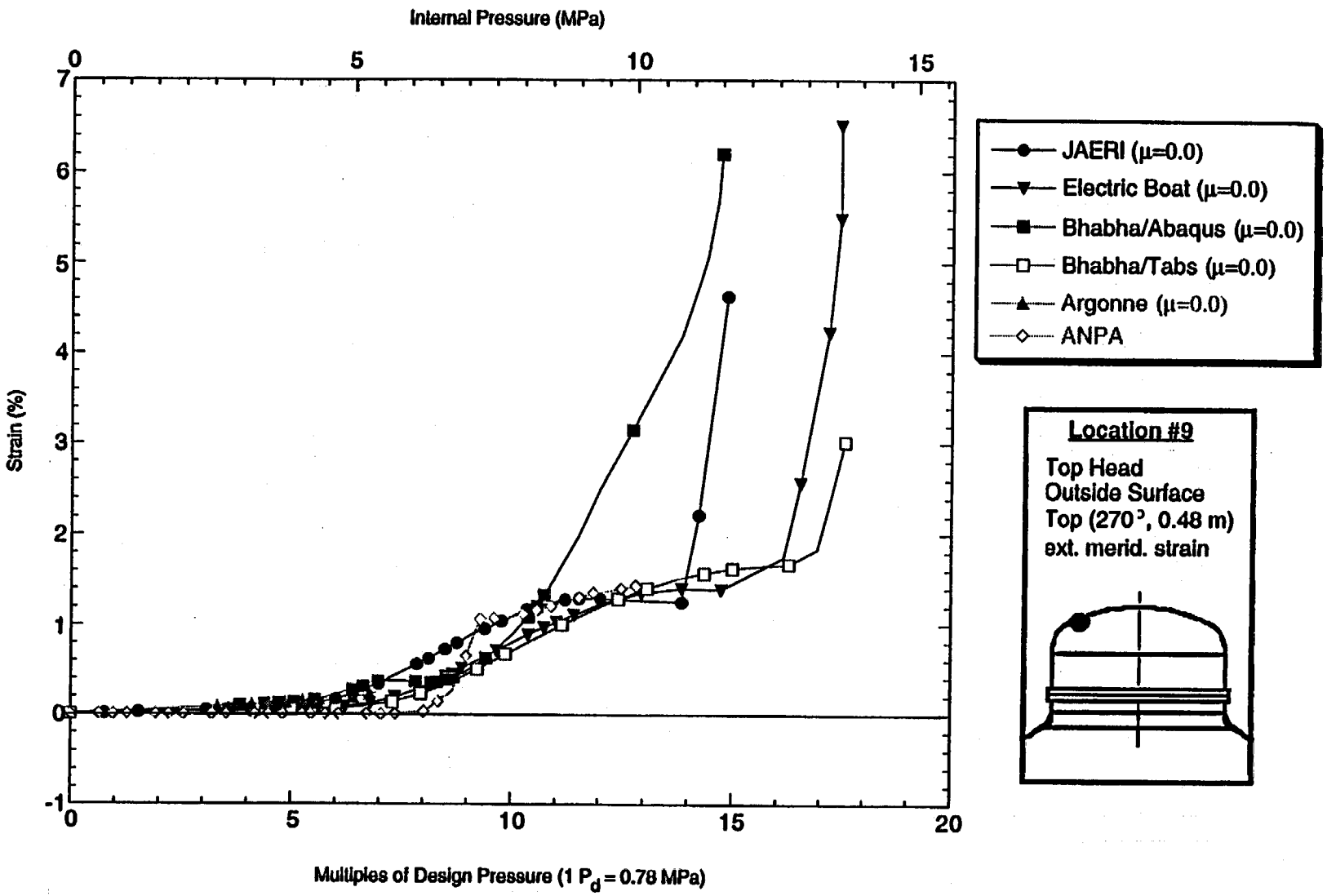

Figure D-17. Standard Output Location #9 (zero friction case)

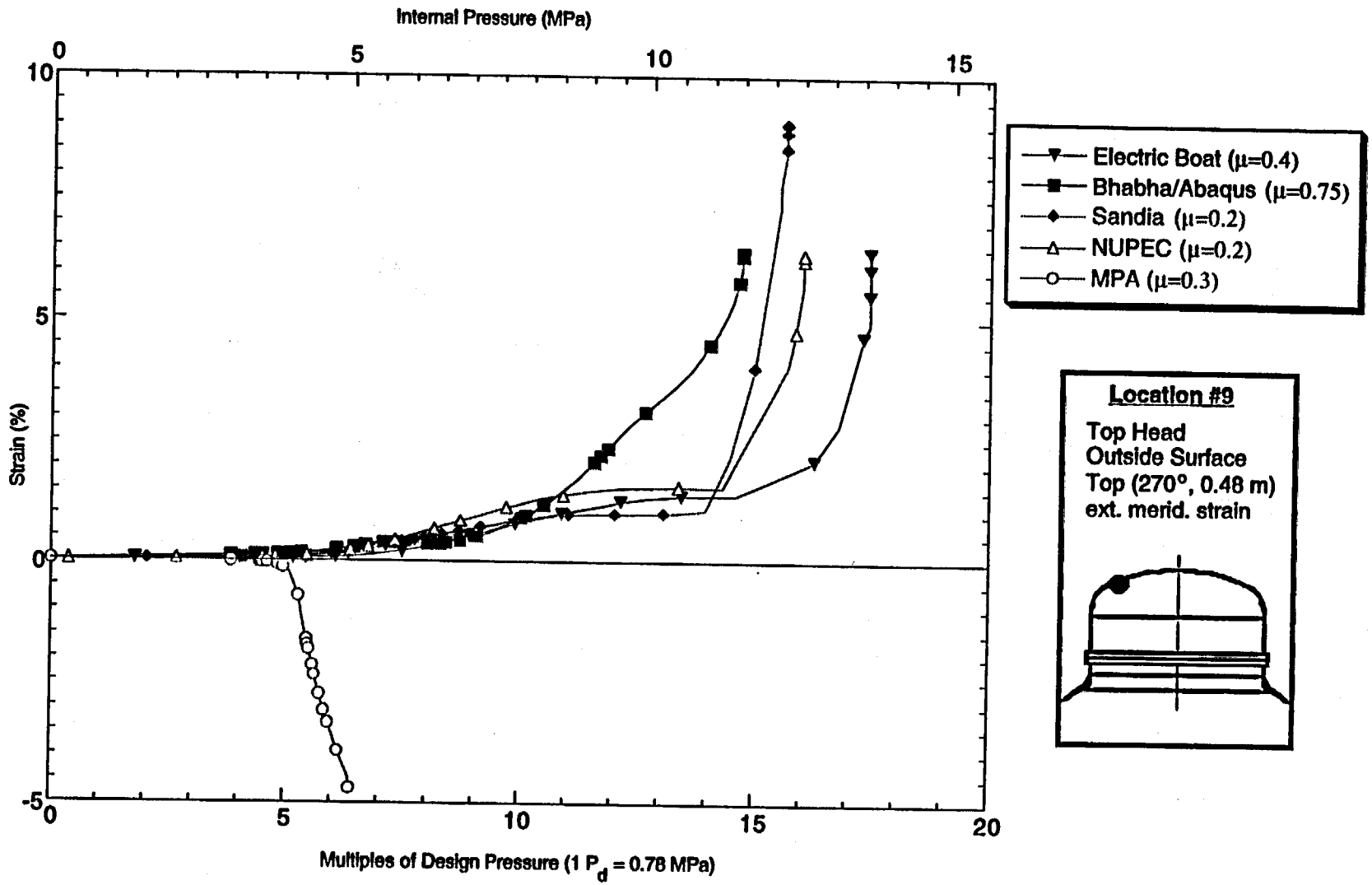

Figure D-18. Standard Output Location #9 (nonzero friction case)

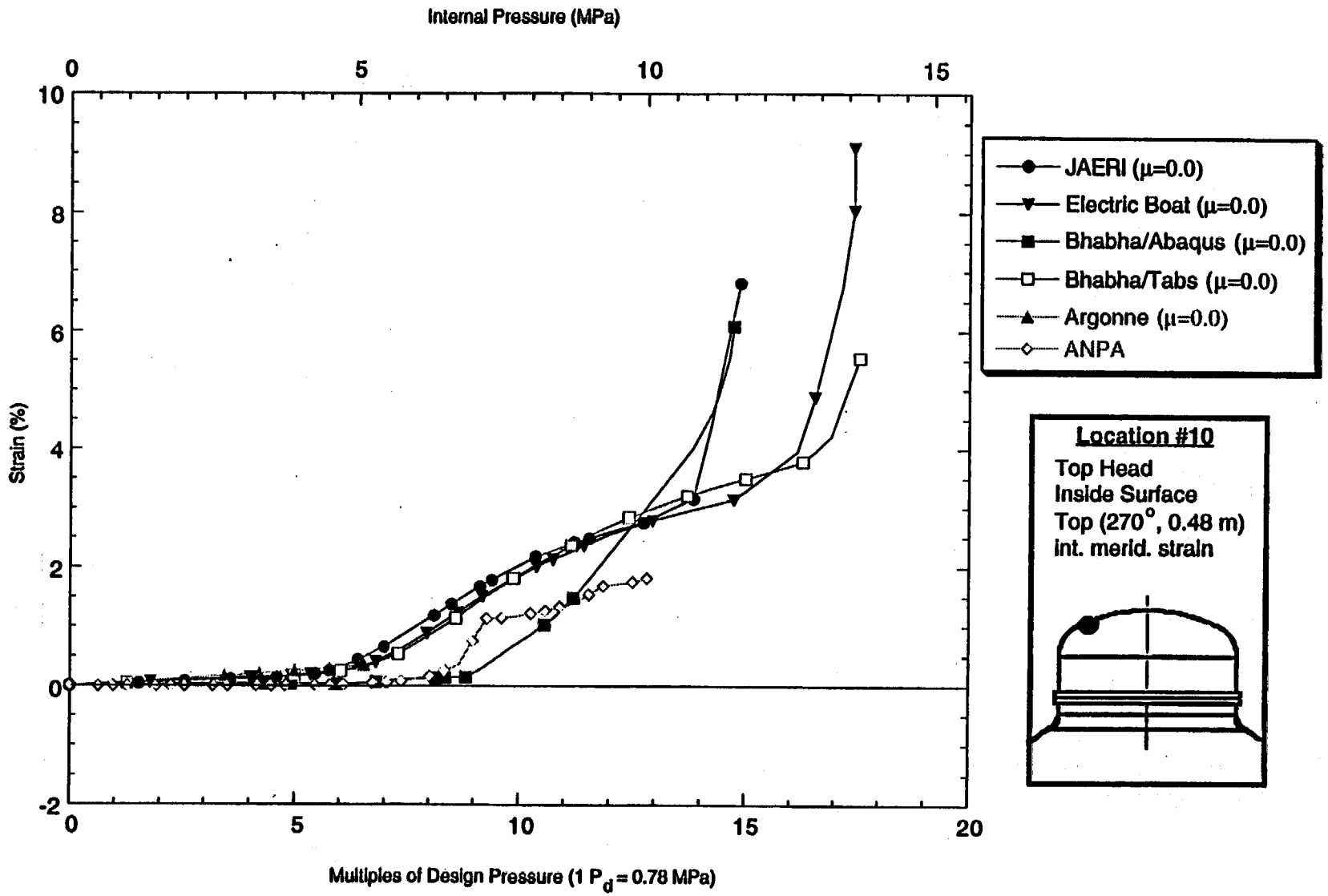

Figure D-19. Standard Output Location #10 (zero friction case)

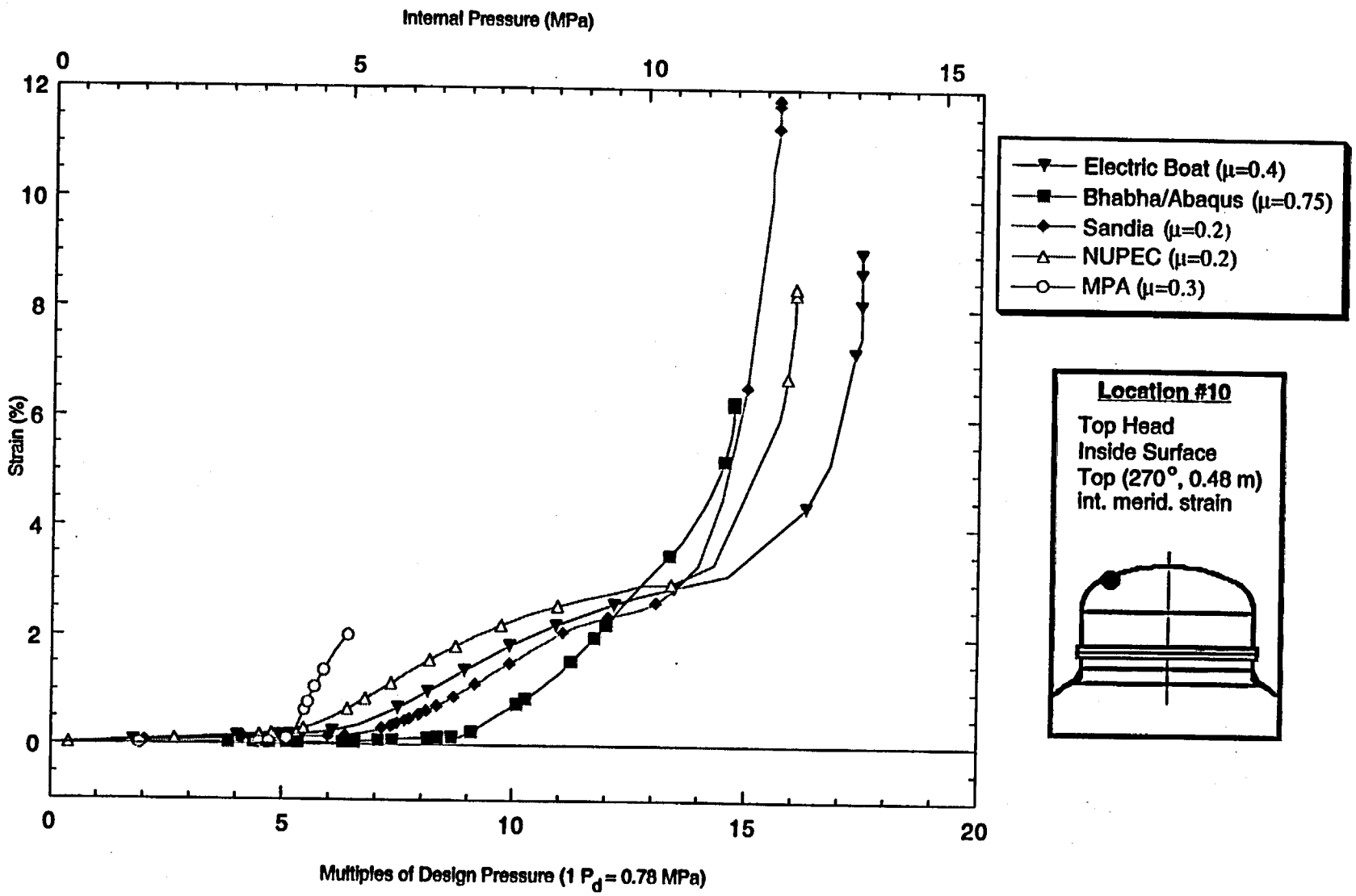

Figure D-20. Standard Output Location #10 (nonzero friction case)

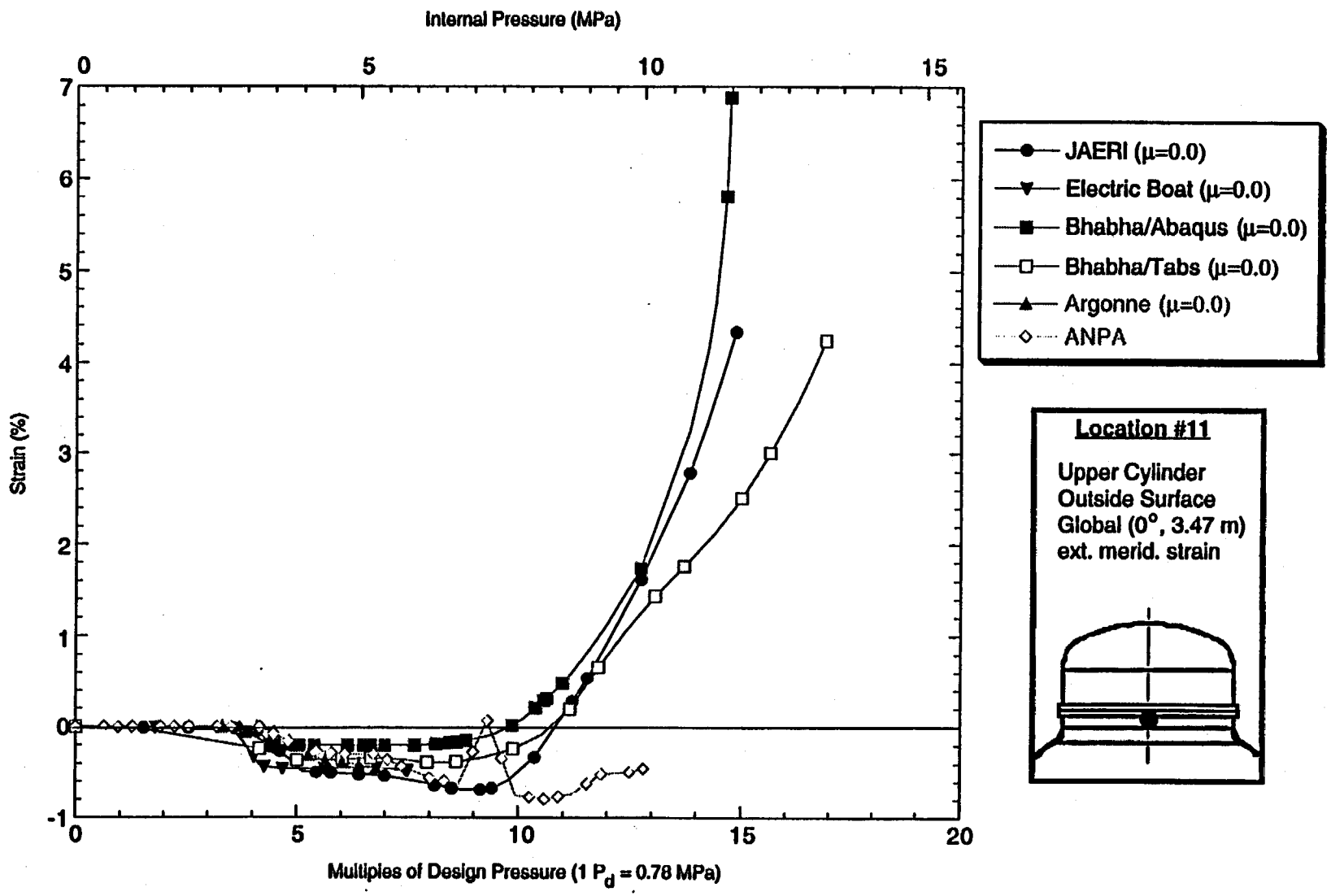

Figure D-21. Standard Output Location #11 (zero friction case)

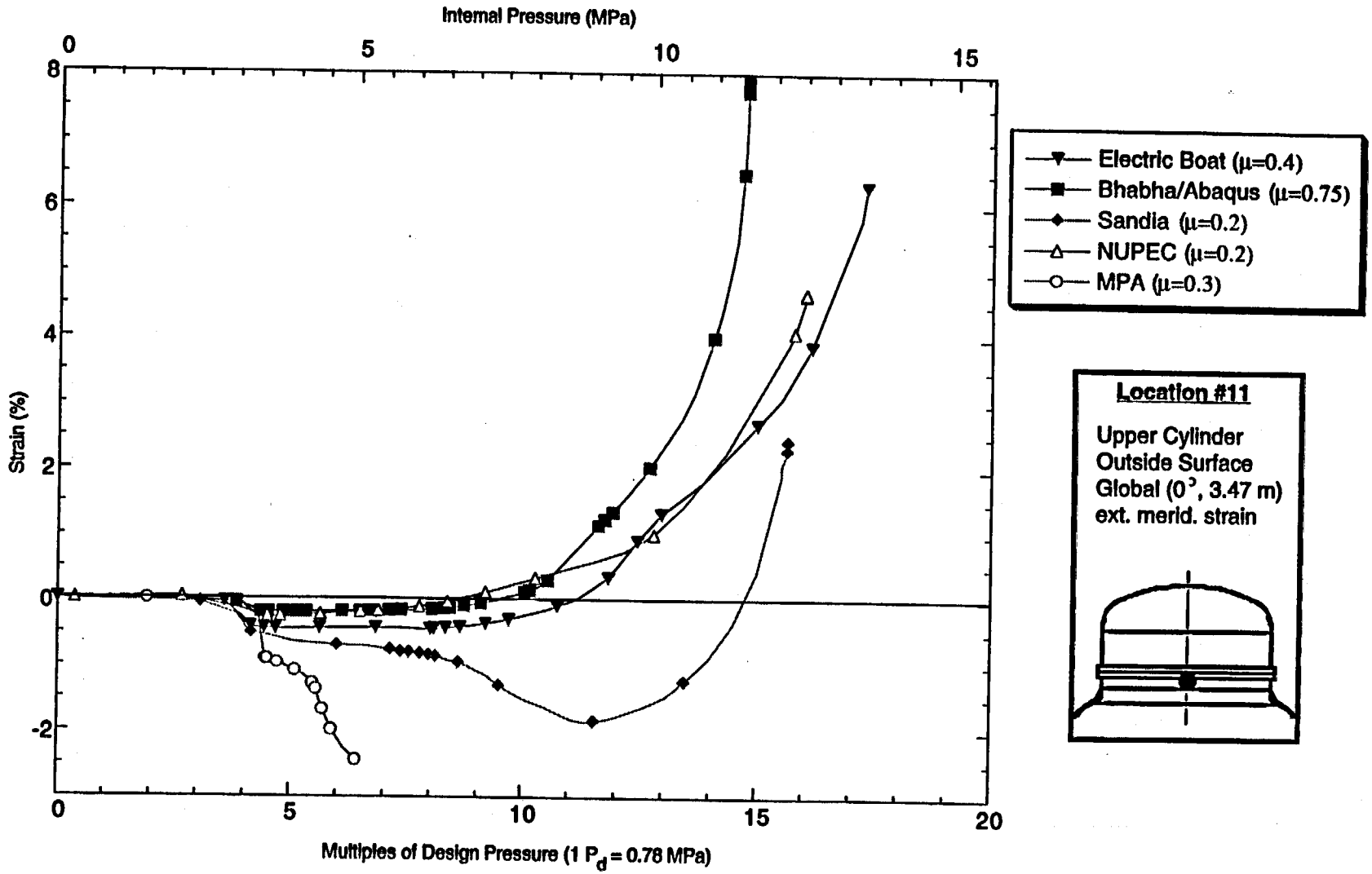

Figure D-22. Standard Output Location #11 (nonzero friction case)

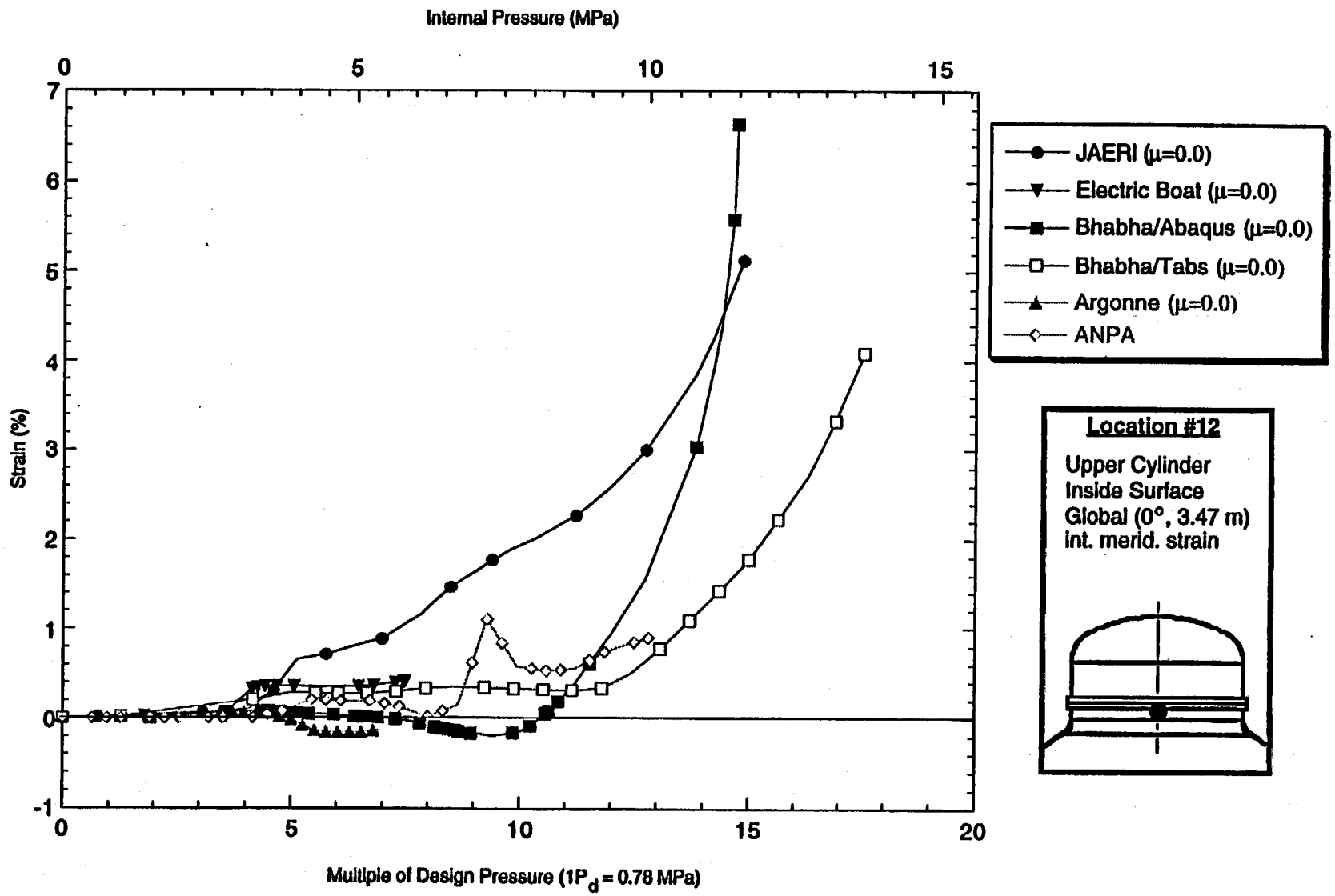

Figure D-23. Standard Output Location #12 (zero friction case)

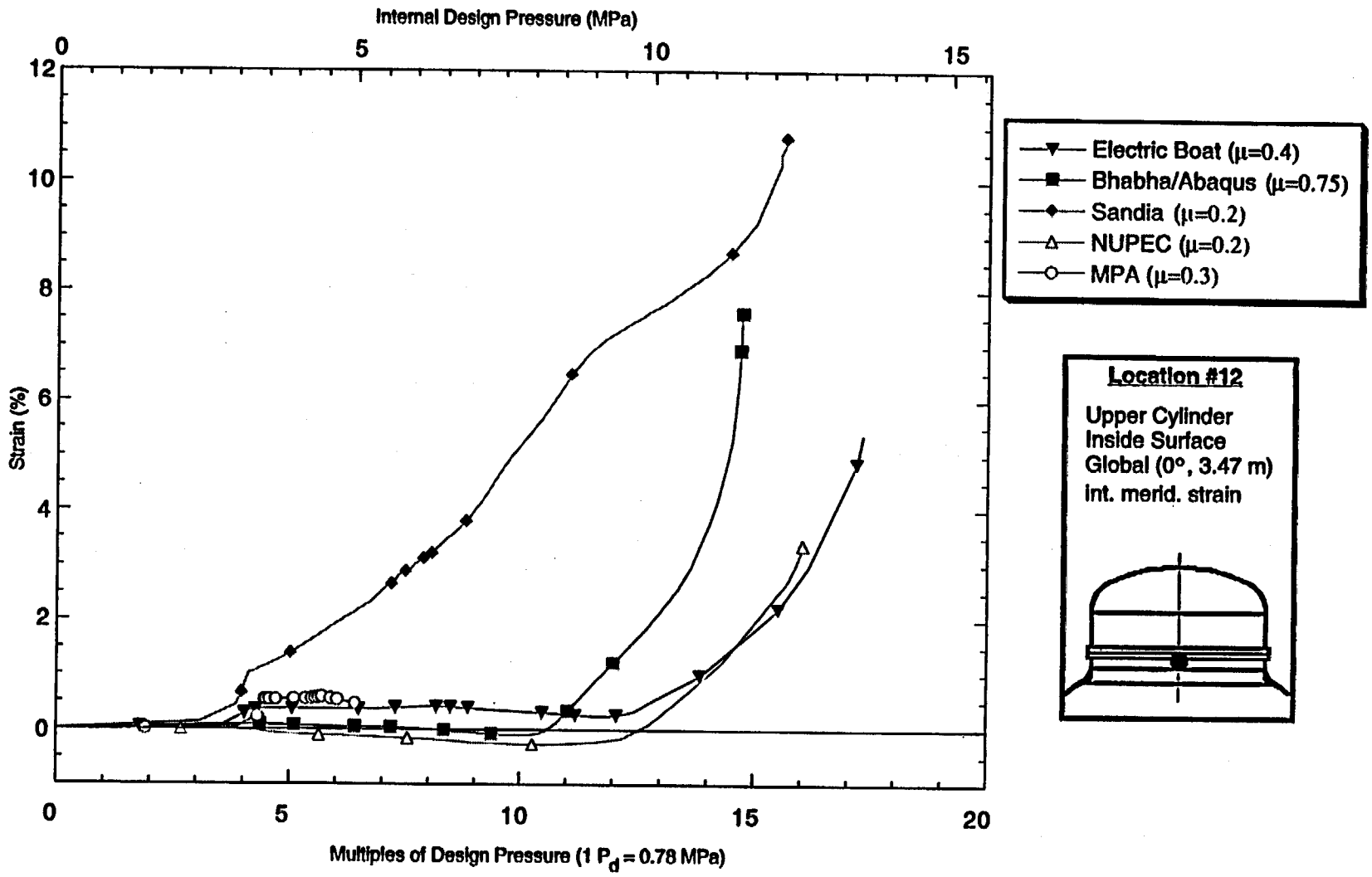

Figure D-24. Standard Output Location #12 (nonzero friction case)

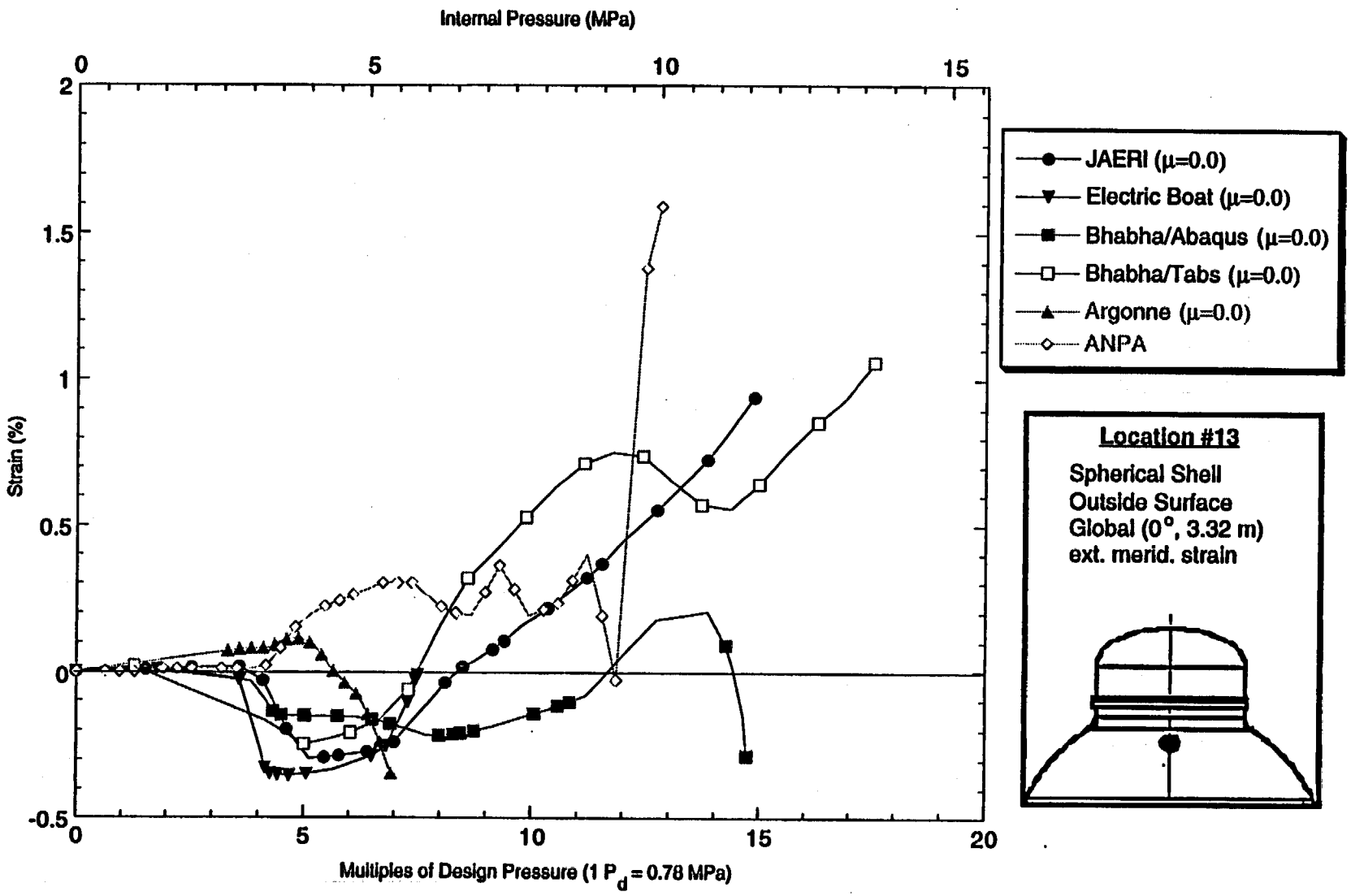

Figure D-25. Standard Output Location #13 (zero friction case)

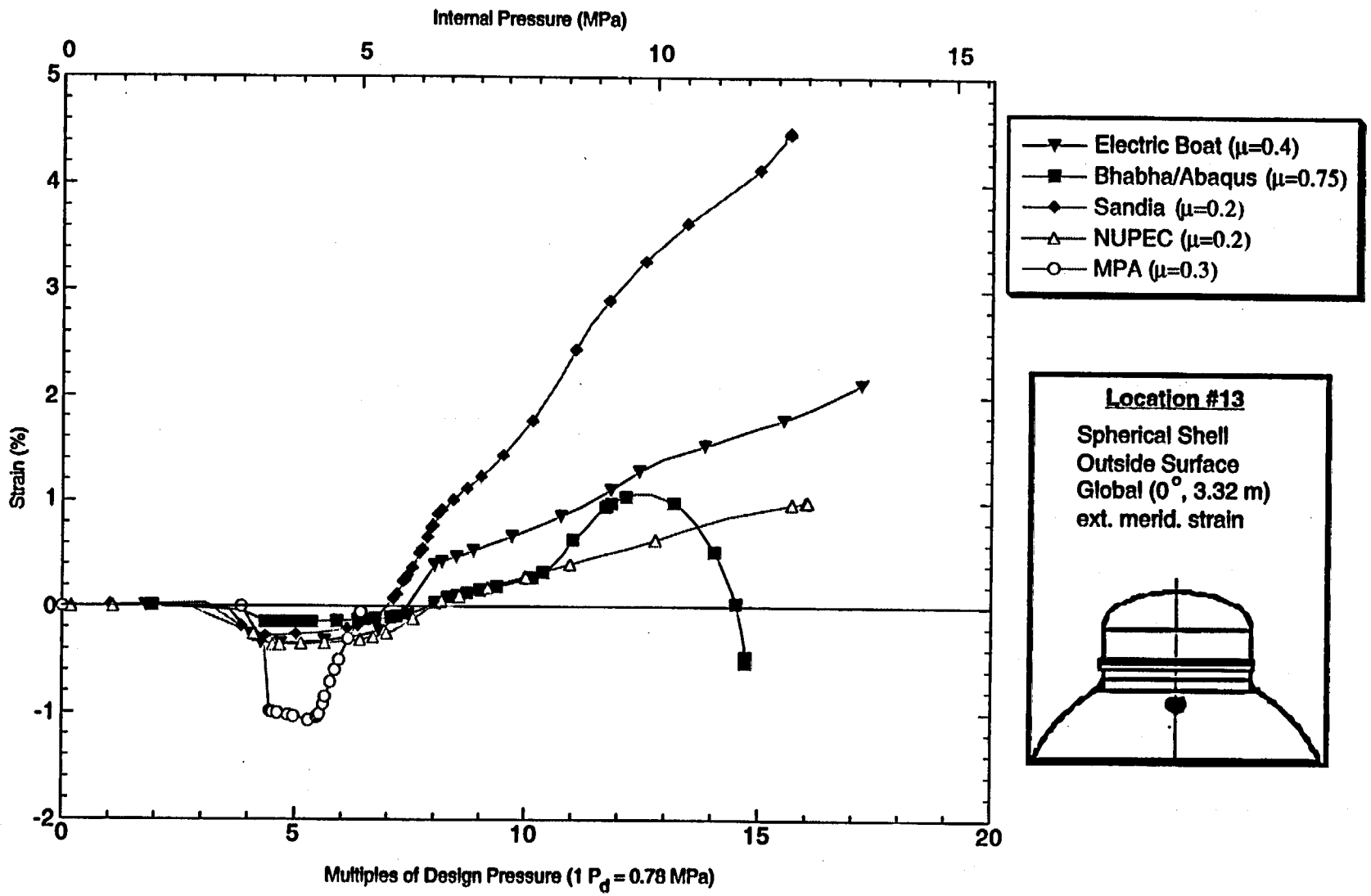

Figure D-26. Standard Output Location #13 (nonzero friction case)

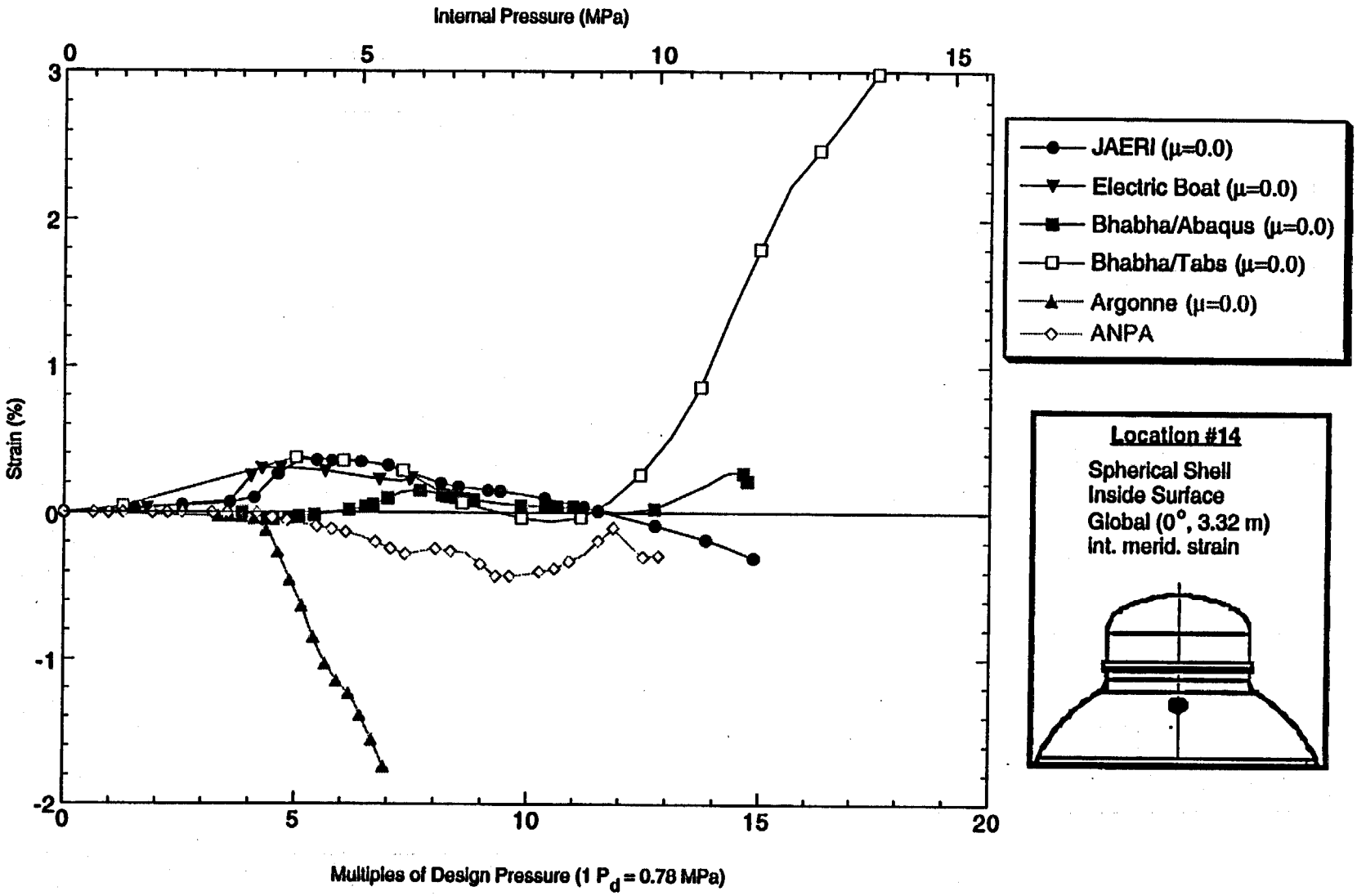

Figure D-27. Standard Output Location #14 (zero friction case)

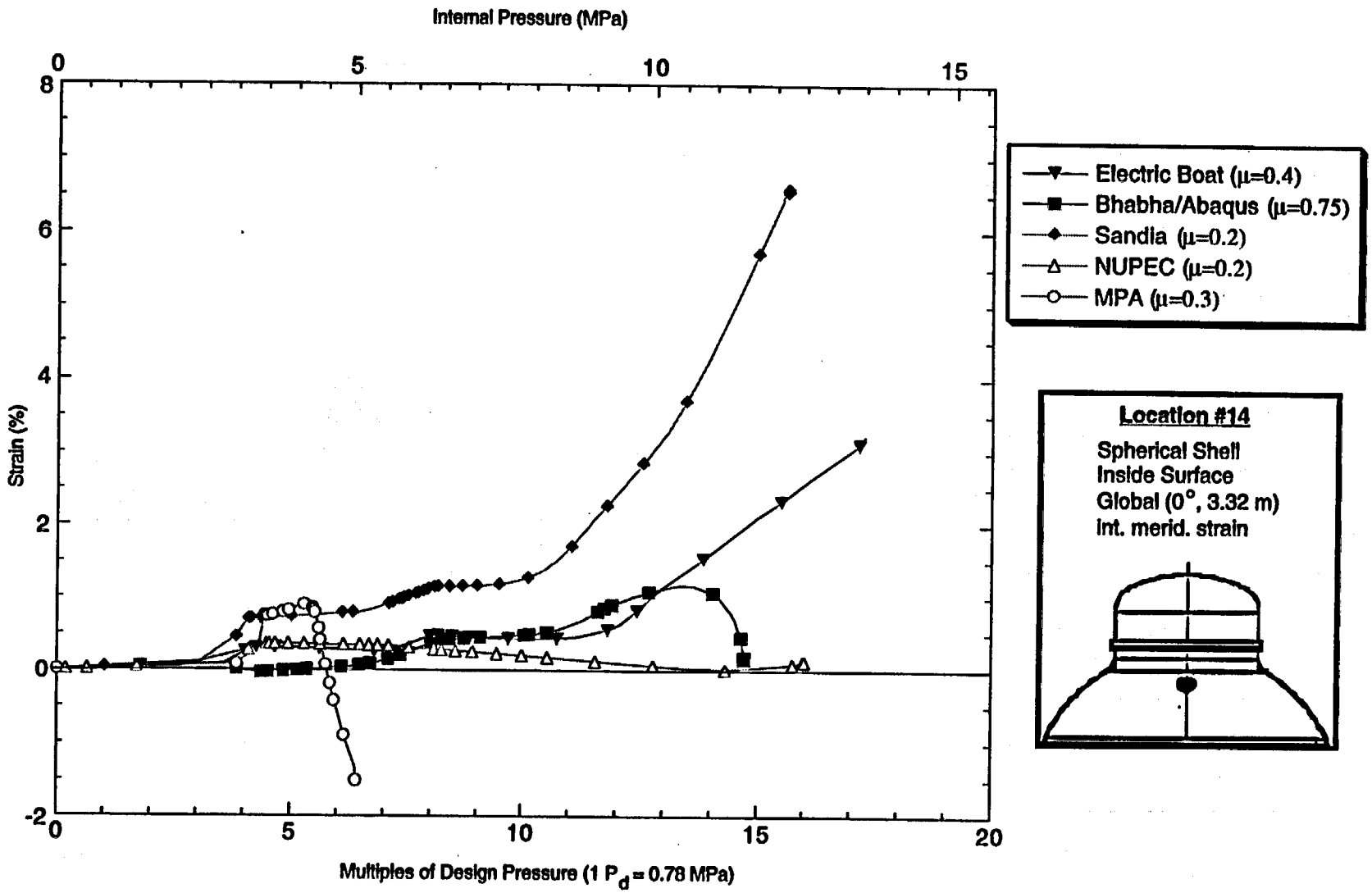

Figure D-28. Standard Output Location #14 (nonzero friction case)

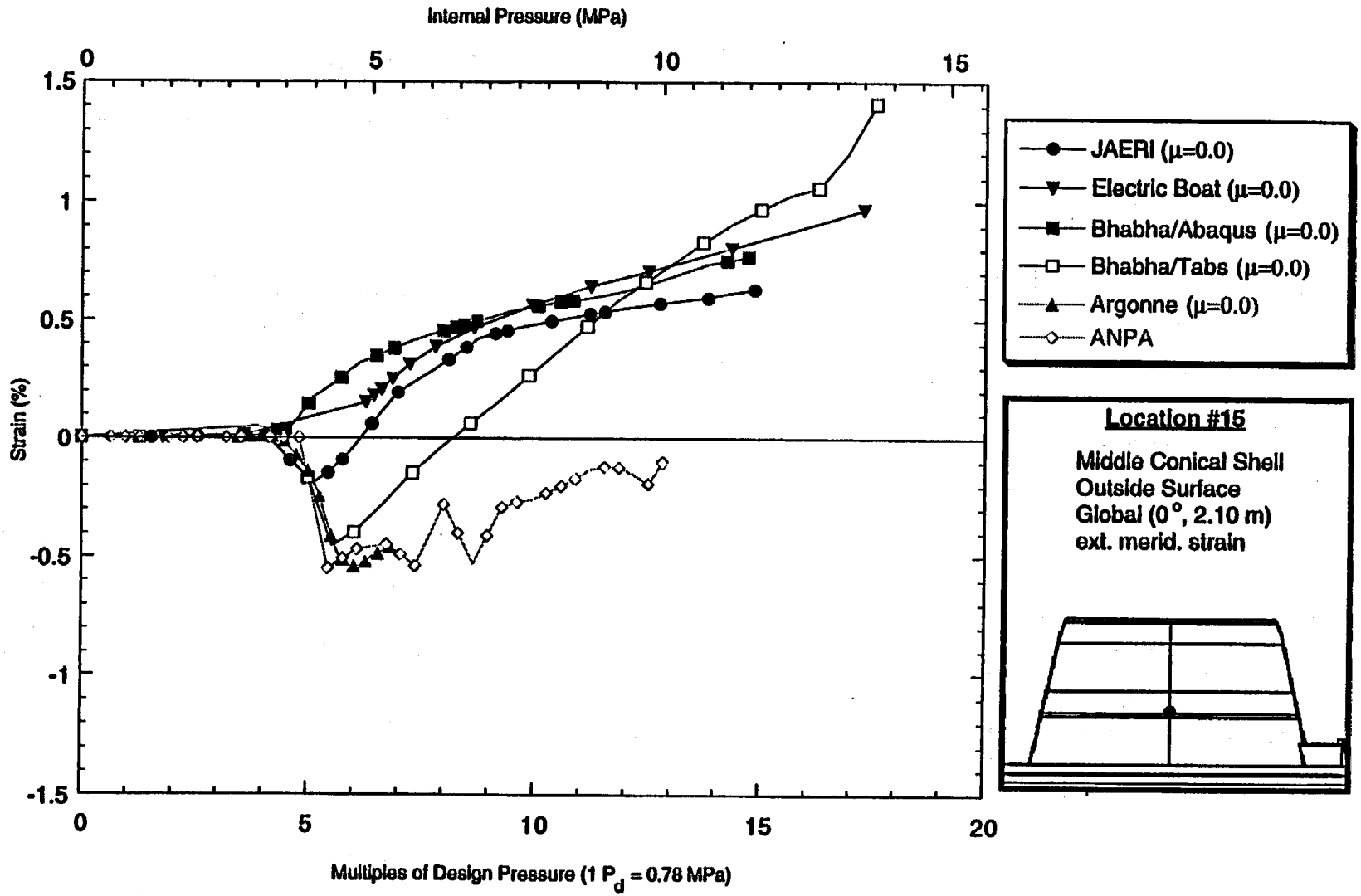

Figure D-29. Standard Output Location #15 (zero friction case)

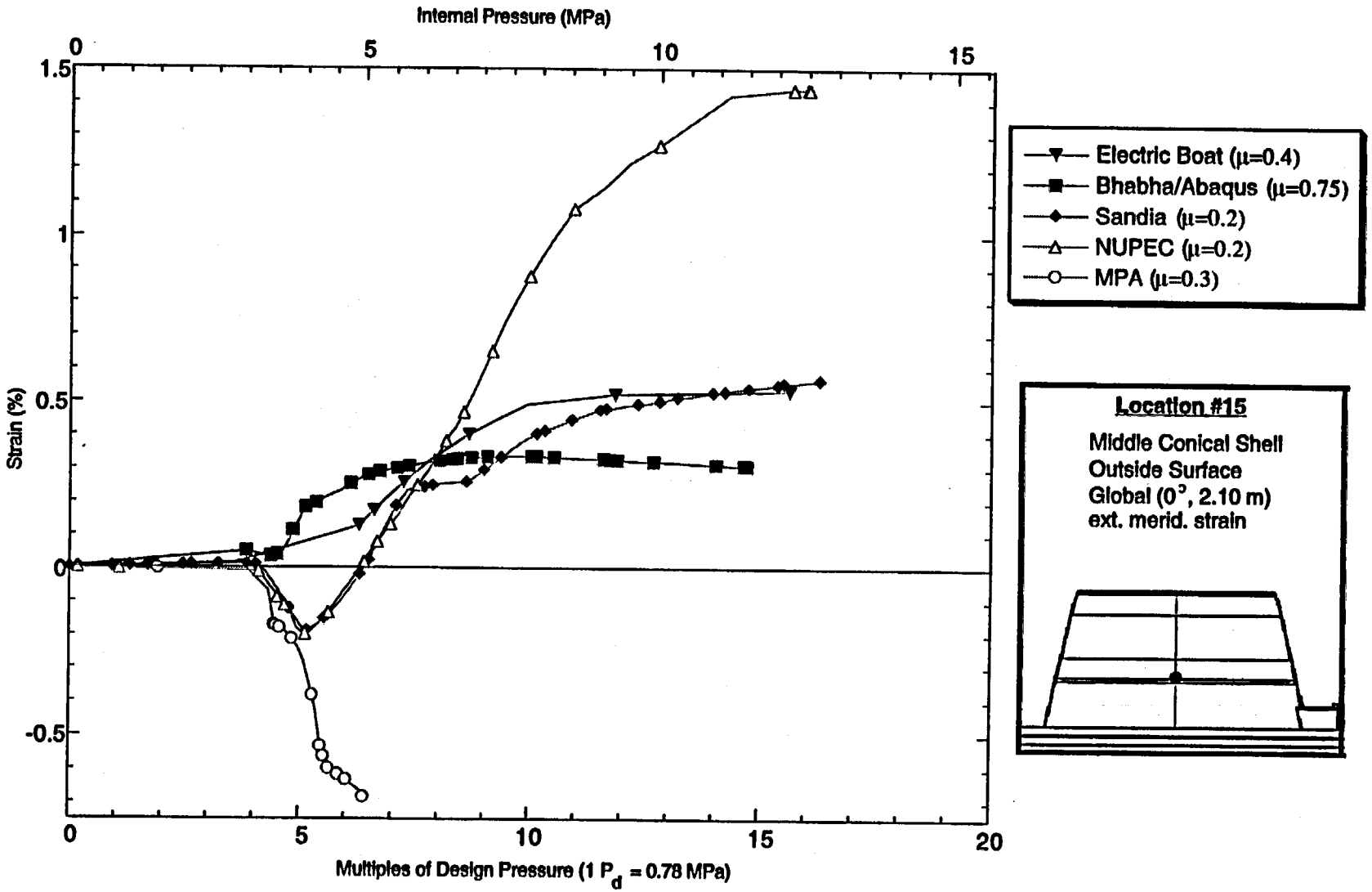

Figure D-30. Standard Output Location #15 (nonzero friction case)

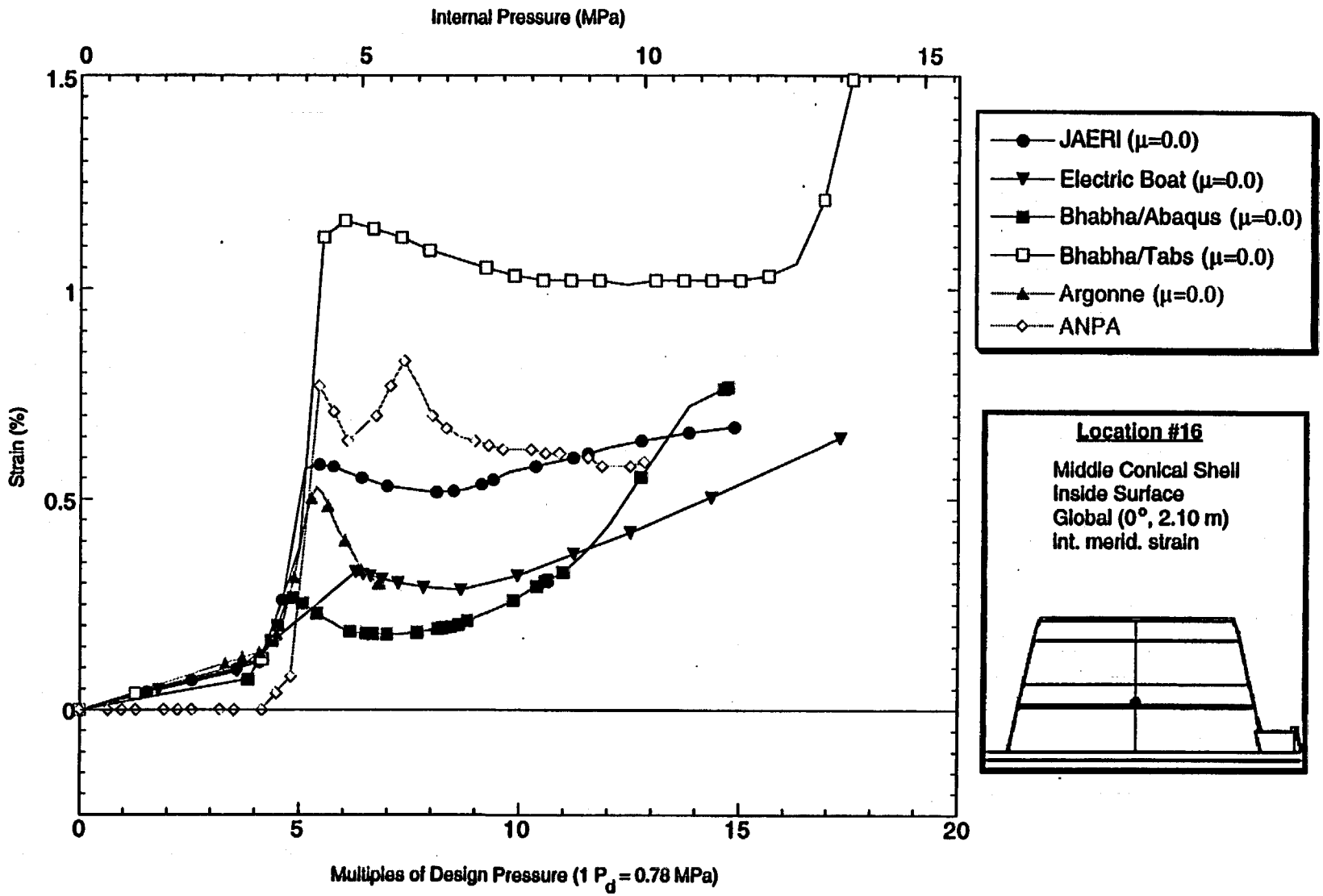

Figure D-31. Standard Output Location #16 (zero friction case)

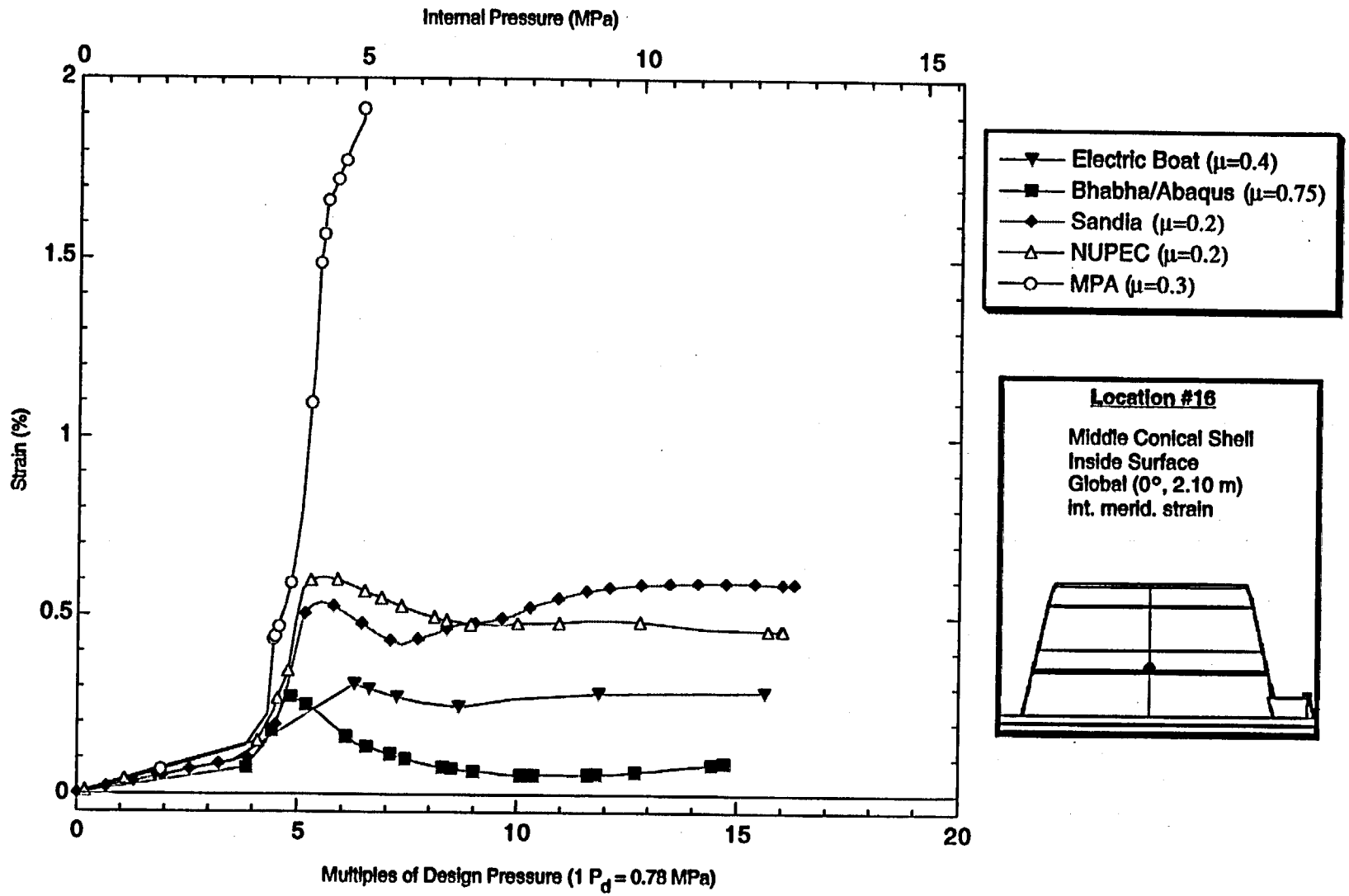

Figure D-32. Standard Output Location #16 (nonzero friction case)

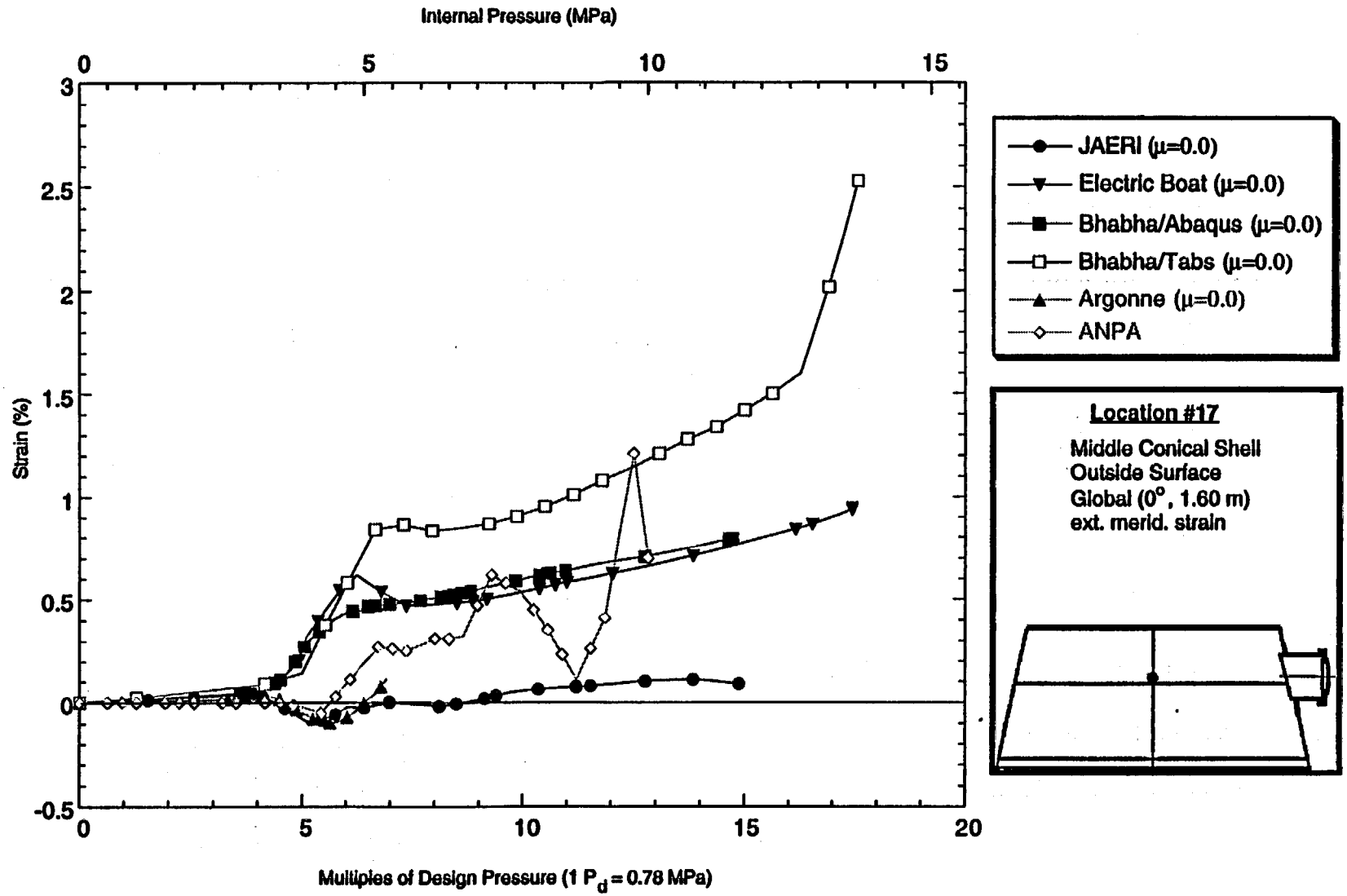

Figure D-33. Standard Output Location #17 (zero friction case)

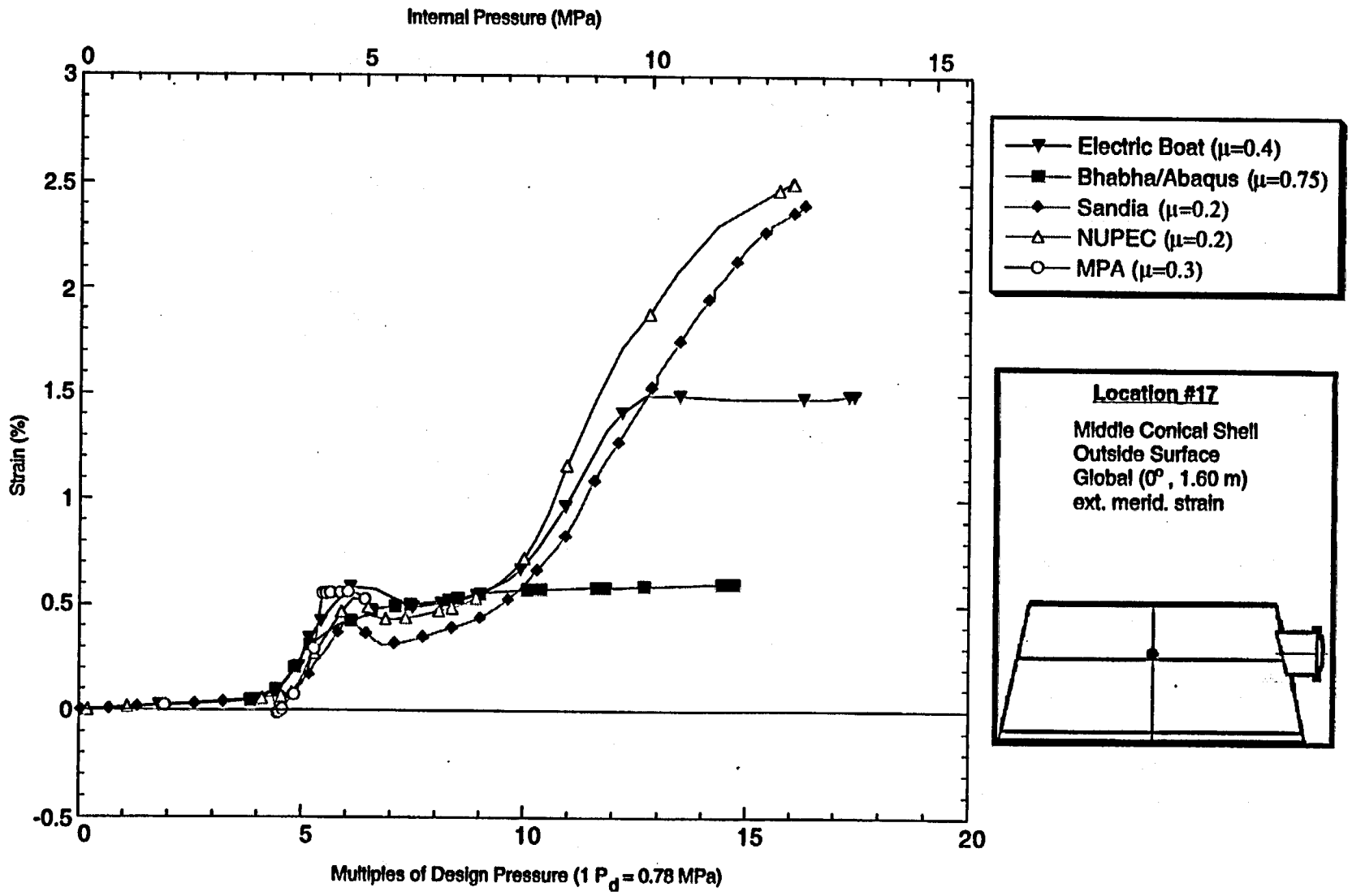

Figure D-34. Standard Output Location #17 (nonzero friction case)

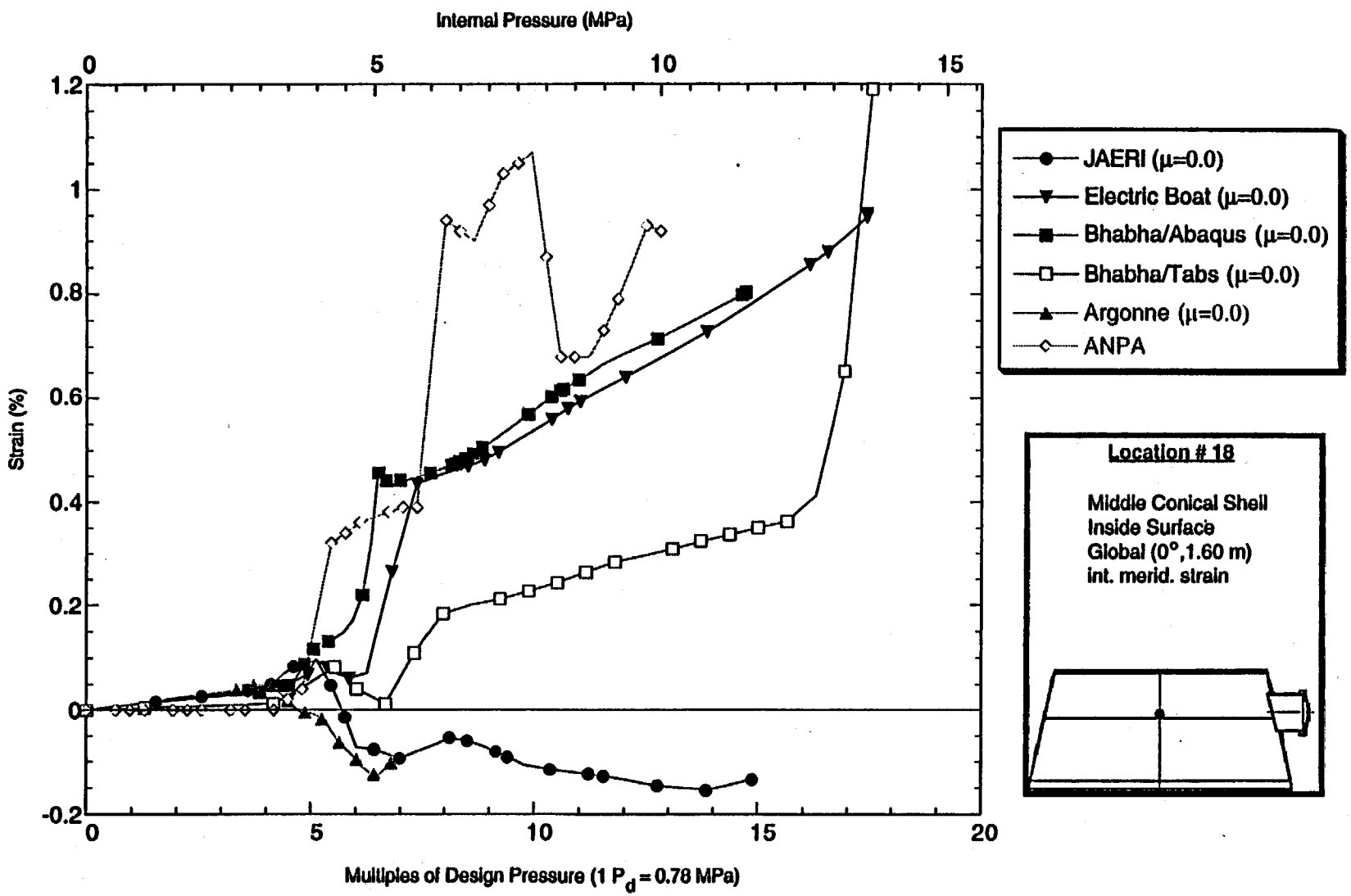

Figure D-35. Standard Output Location #18 (zero friction case)

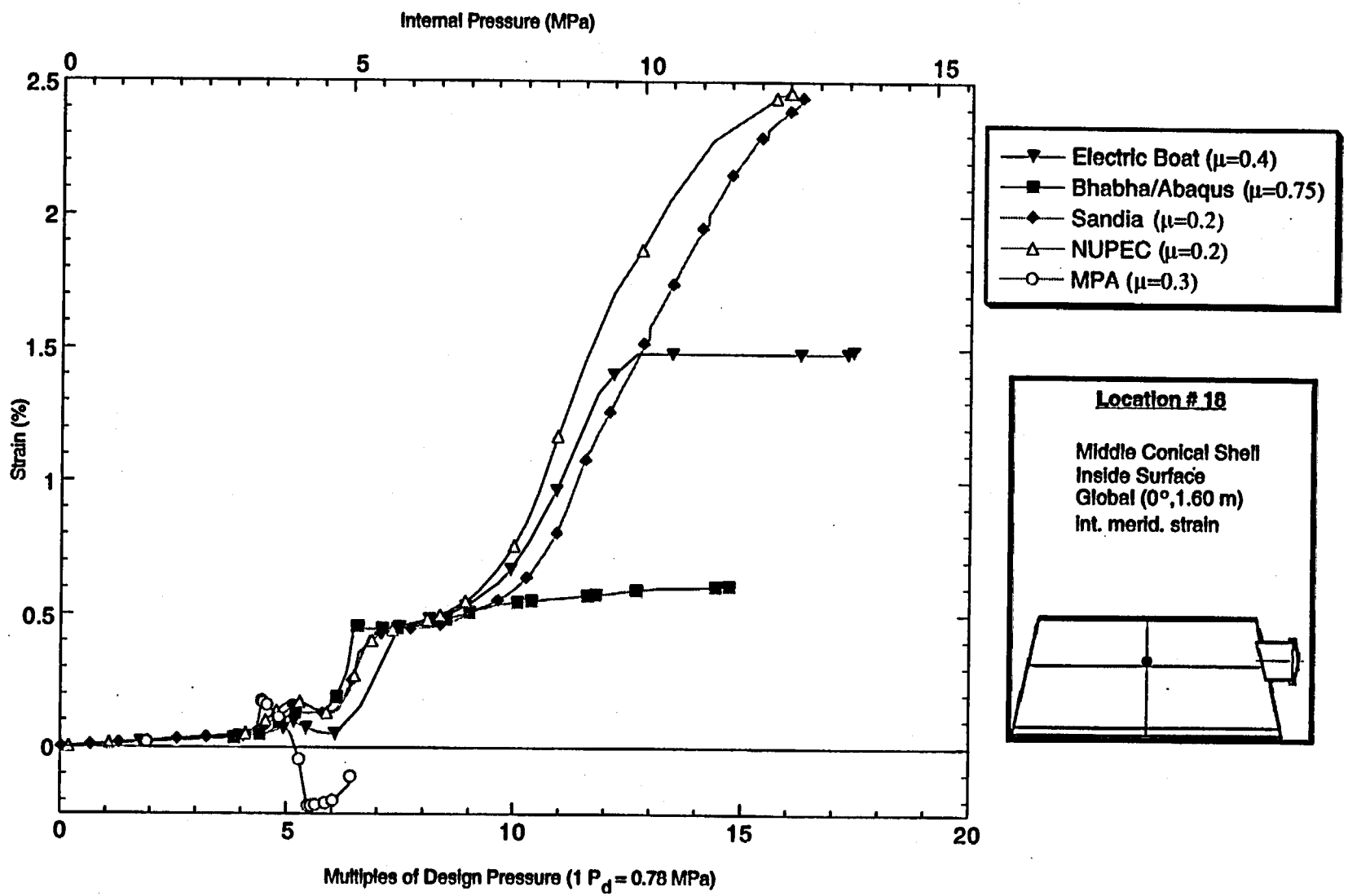

Figure D-36. Standard Output Location #18 (nonzero friction case)

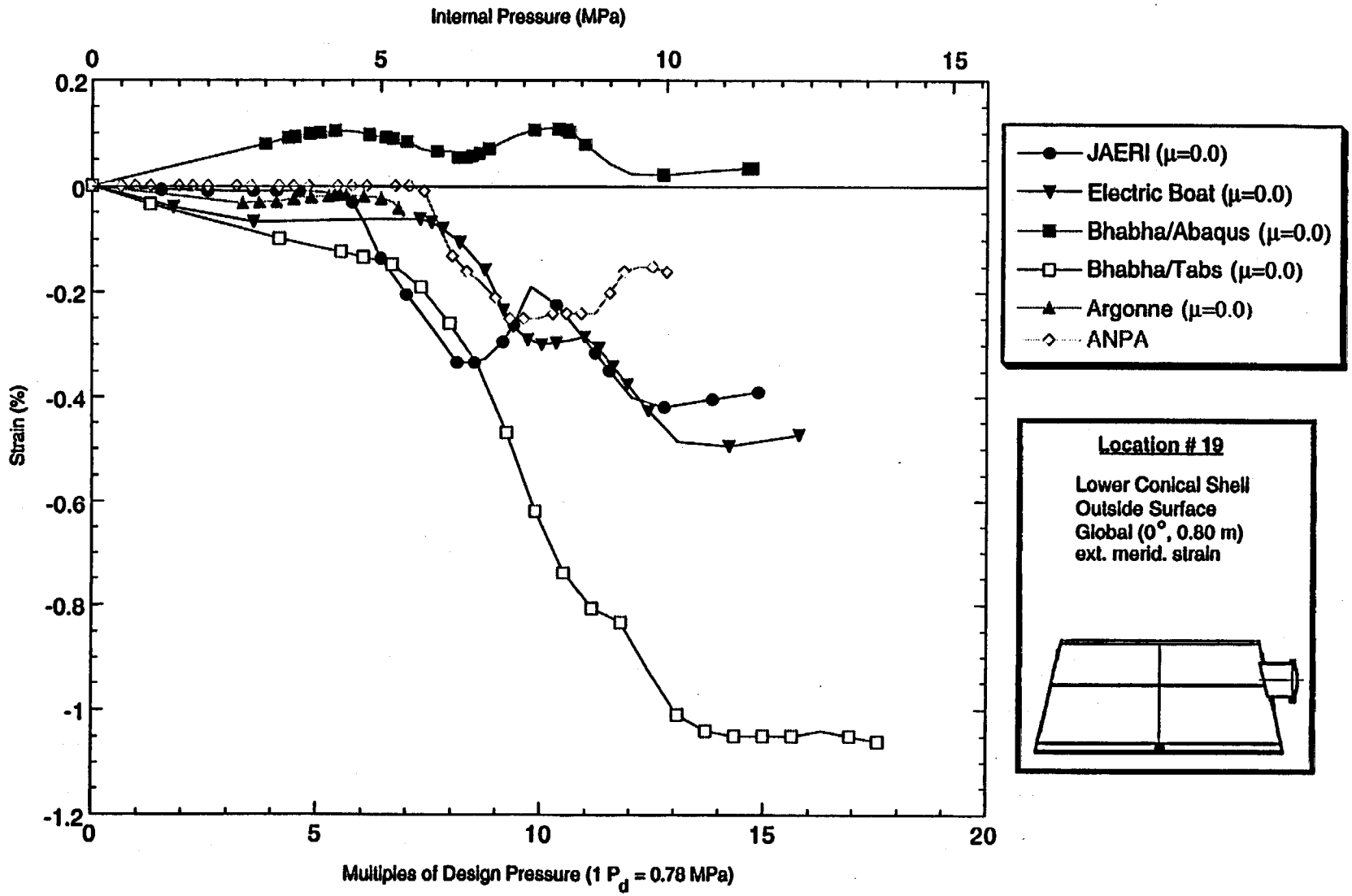

Figure D-37. Standard Output Location #19 (zero friction case)

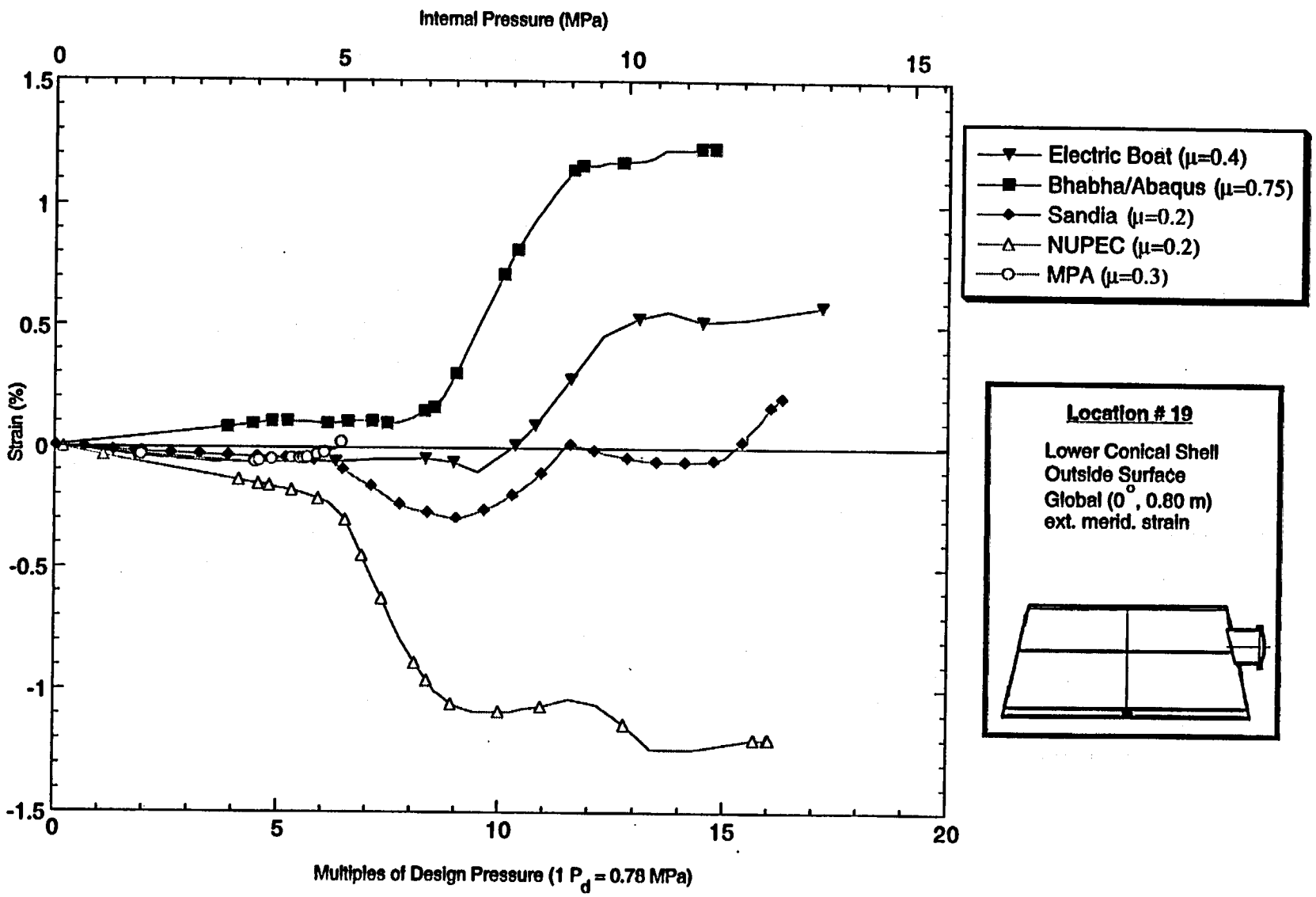

Figure D-38. Standard Output Location #19 (nonzero friction case)

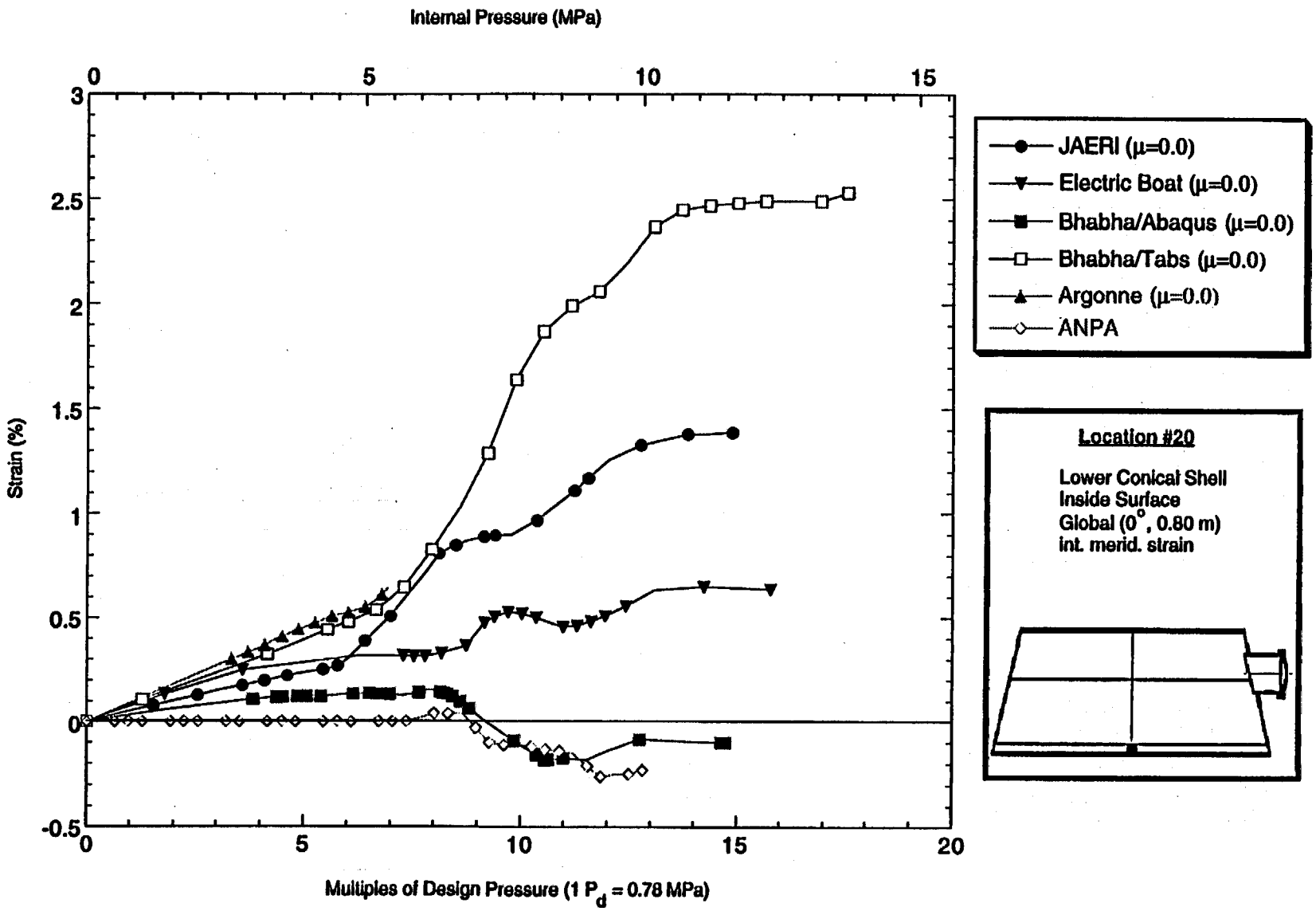

Figure D-39. Standard Output Location #20 (zero friction case)

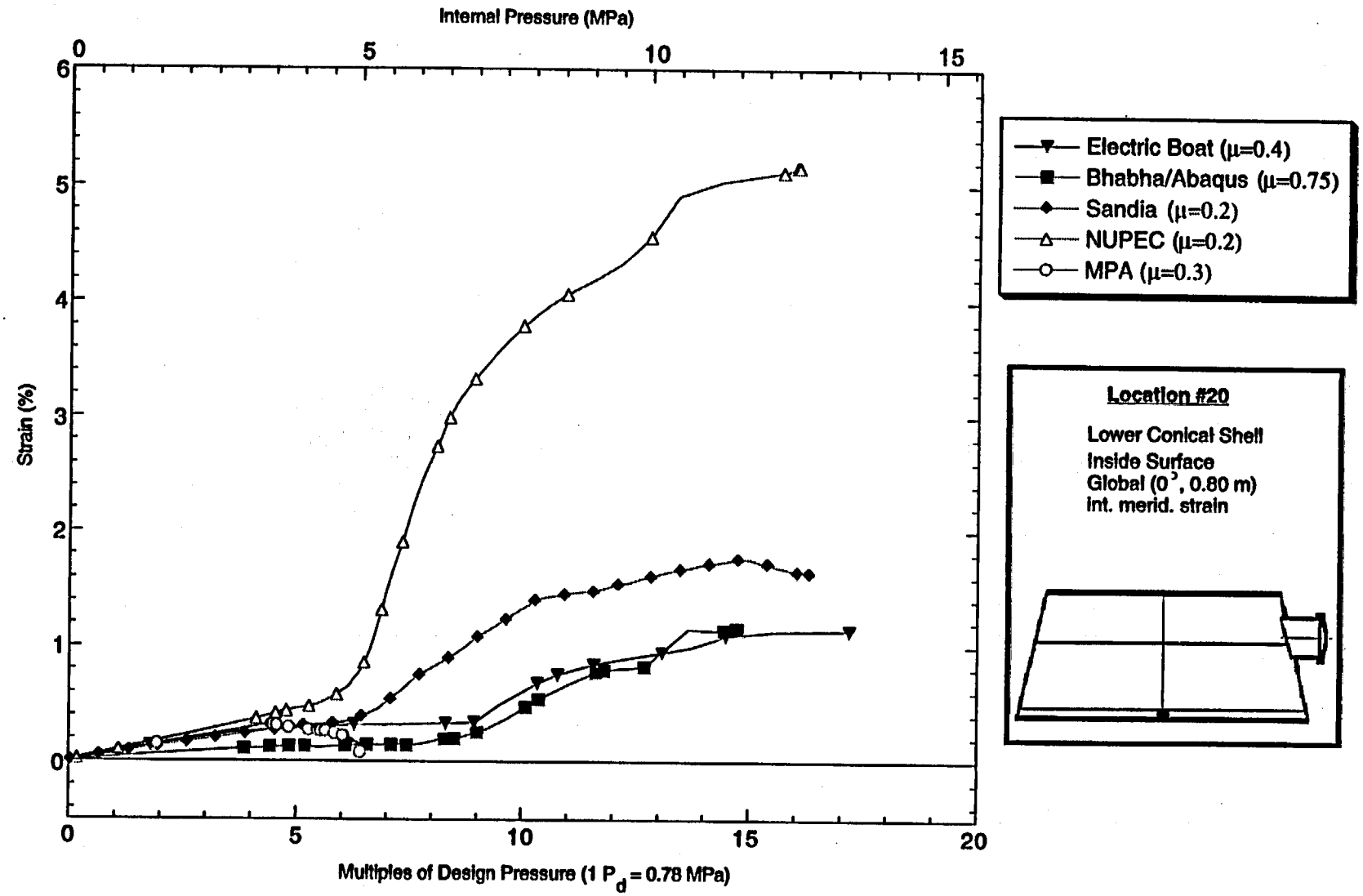

Figure D-40. Standard Output Location #20 (nonzero friction case)

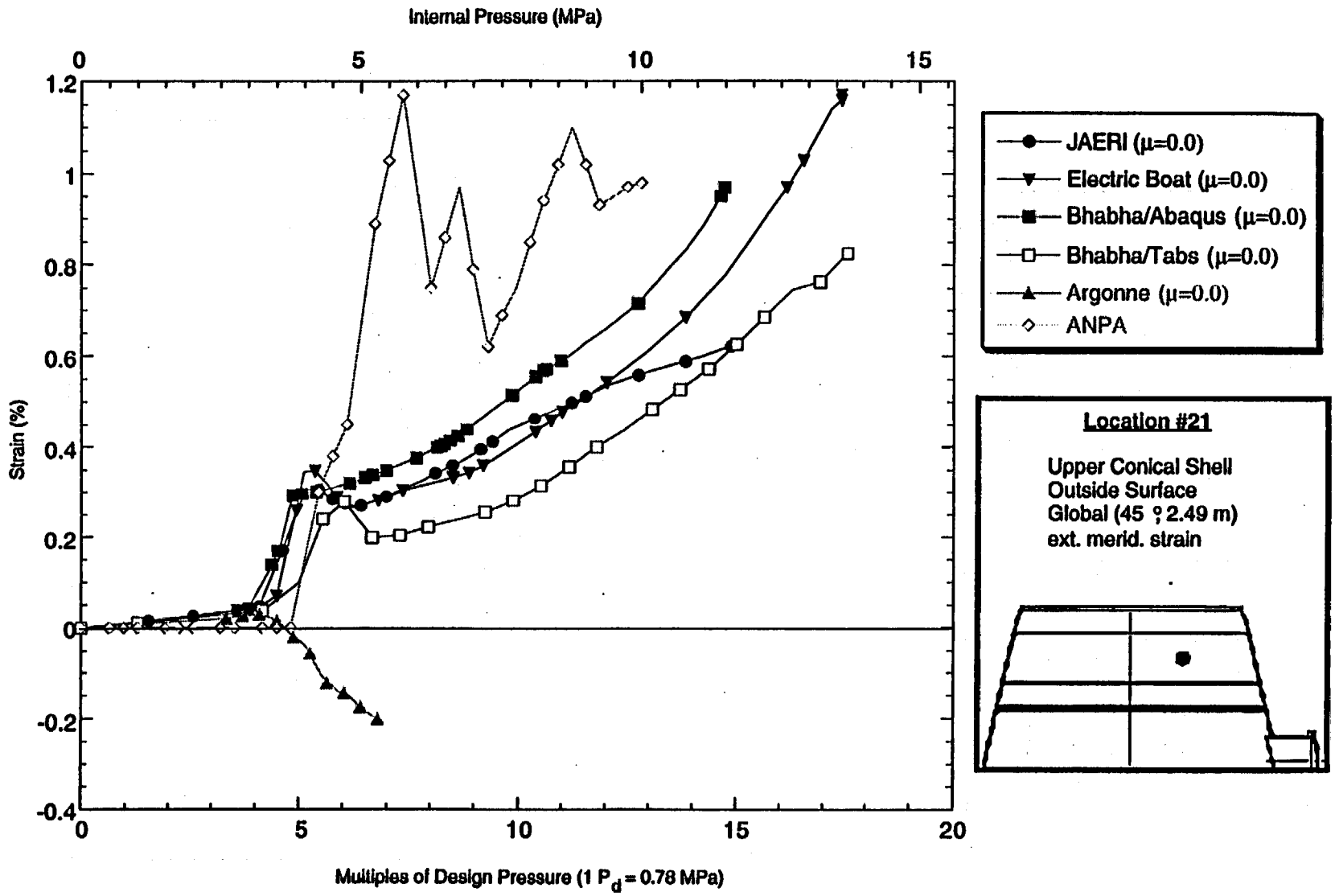

Figure D-41. Standard Output Location #21 (zero friction case)

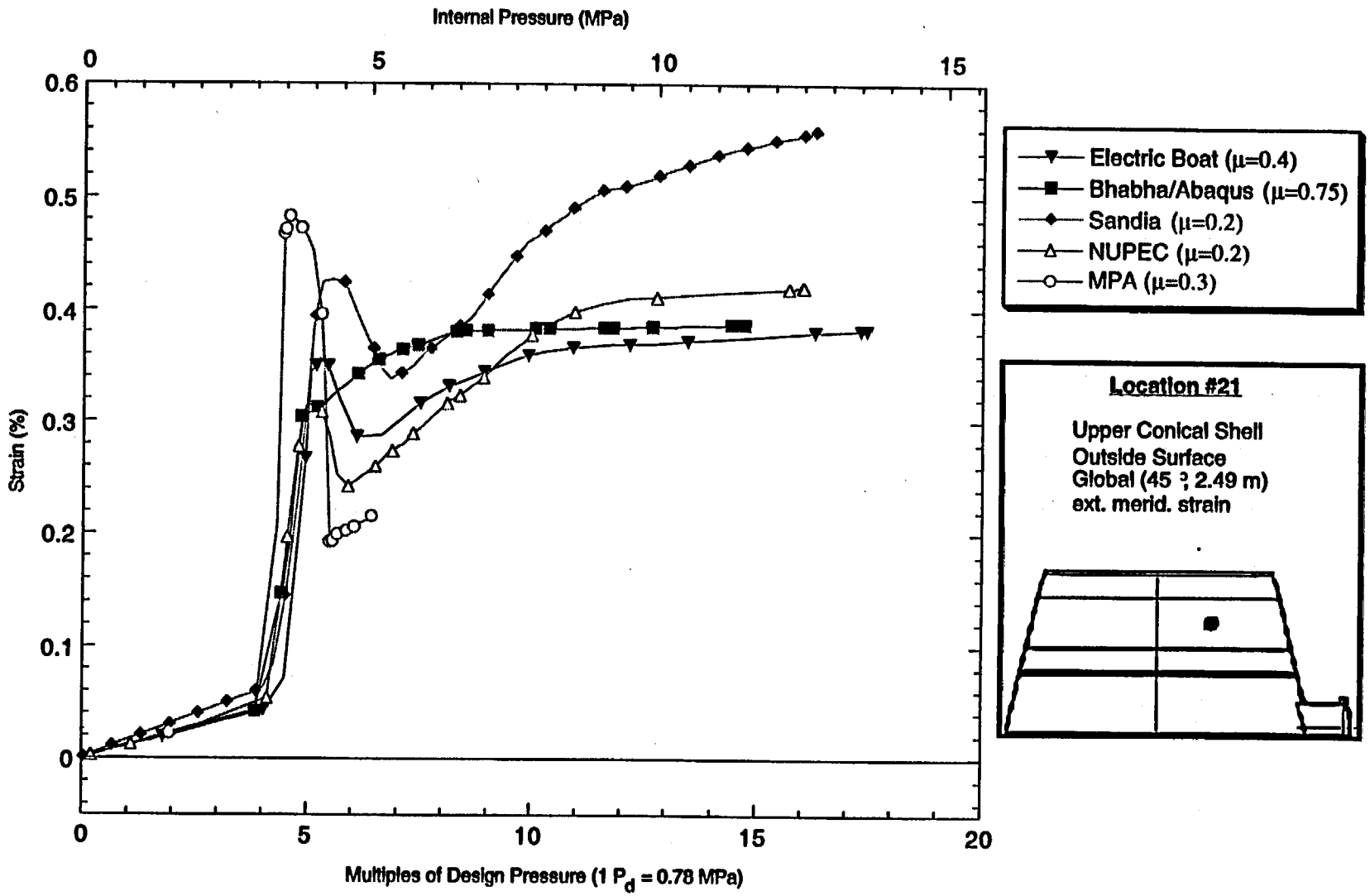

Figure D-42. Standard Output Location #21 (nonzero friction case)

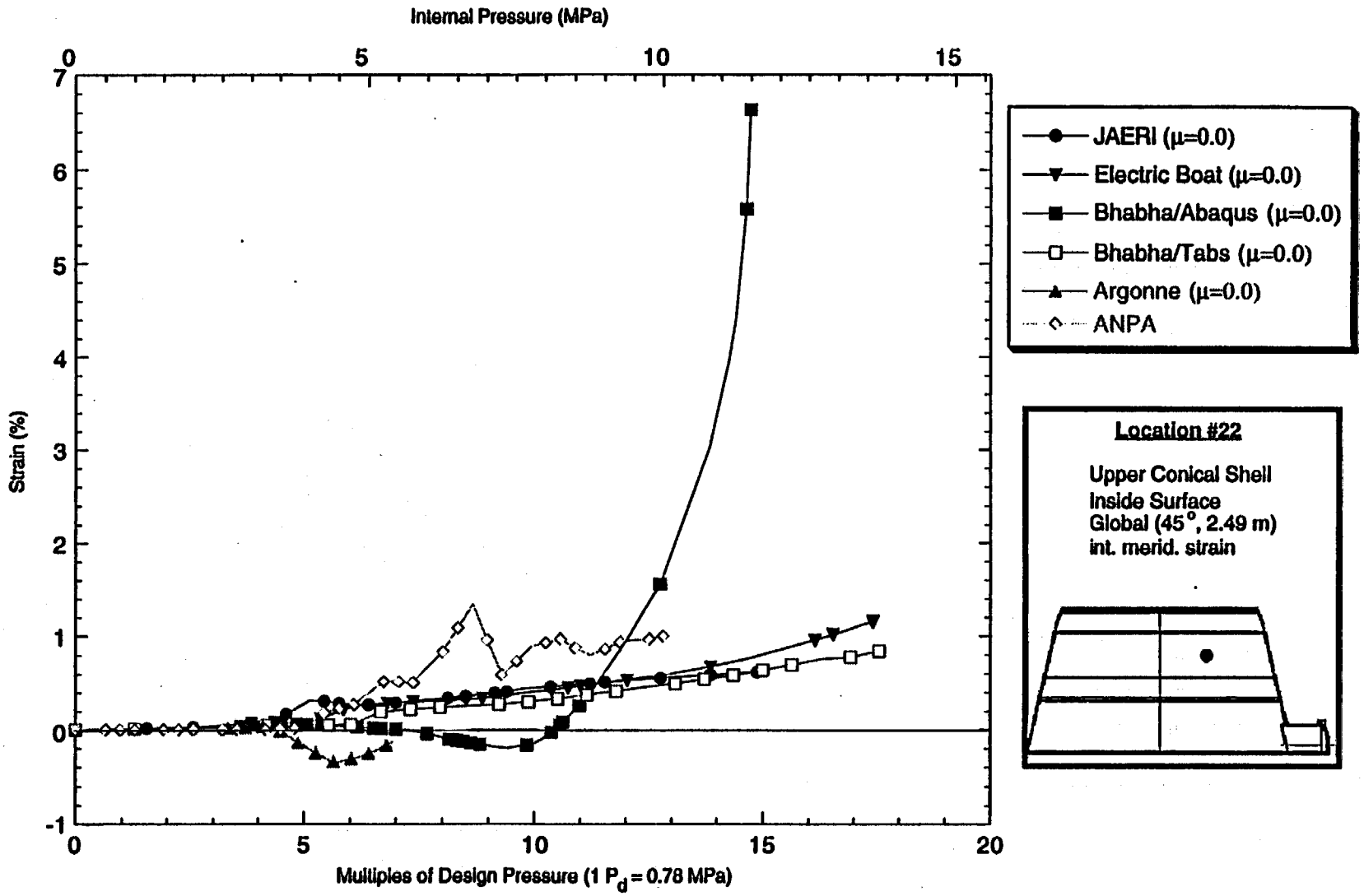

Figure D-43. Standard Output Location #22 (zero friction case)

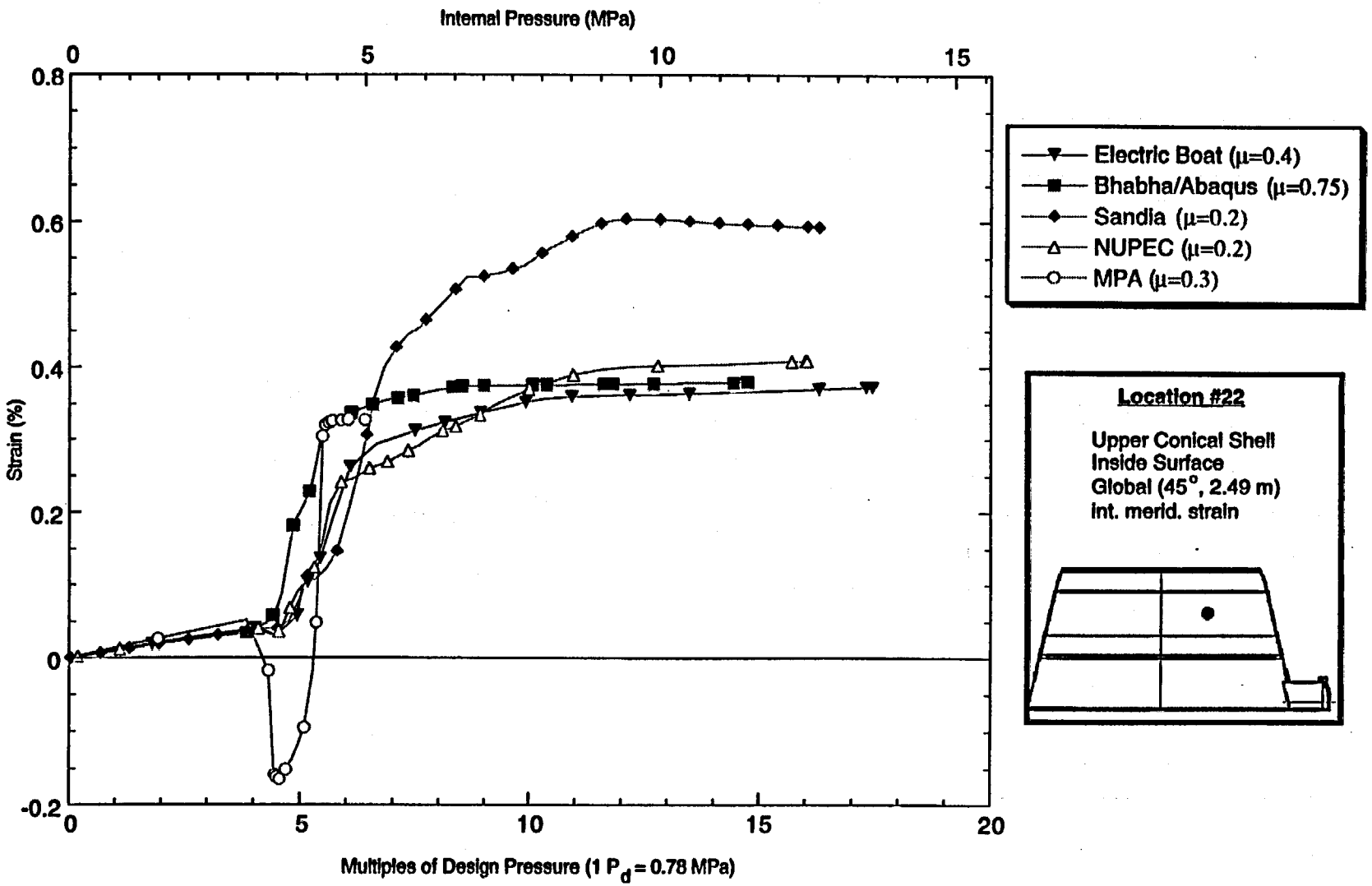

Figure D-44. Standard Output Location #22 (nonzero friction case)

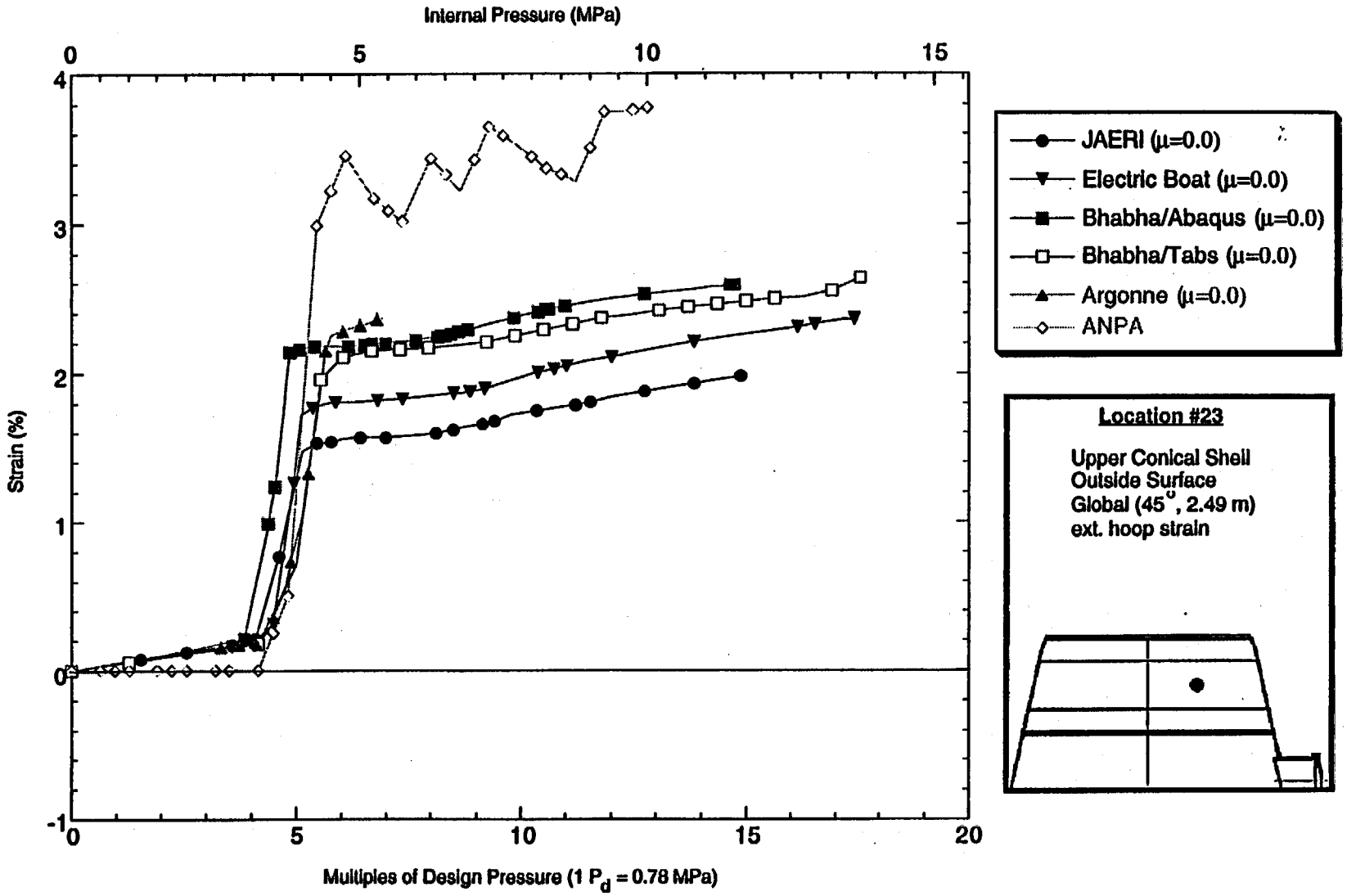

Figure D-45. Standard Output Location #23 (zero friction case)

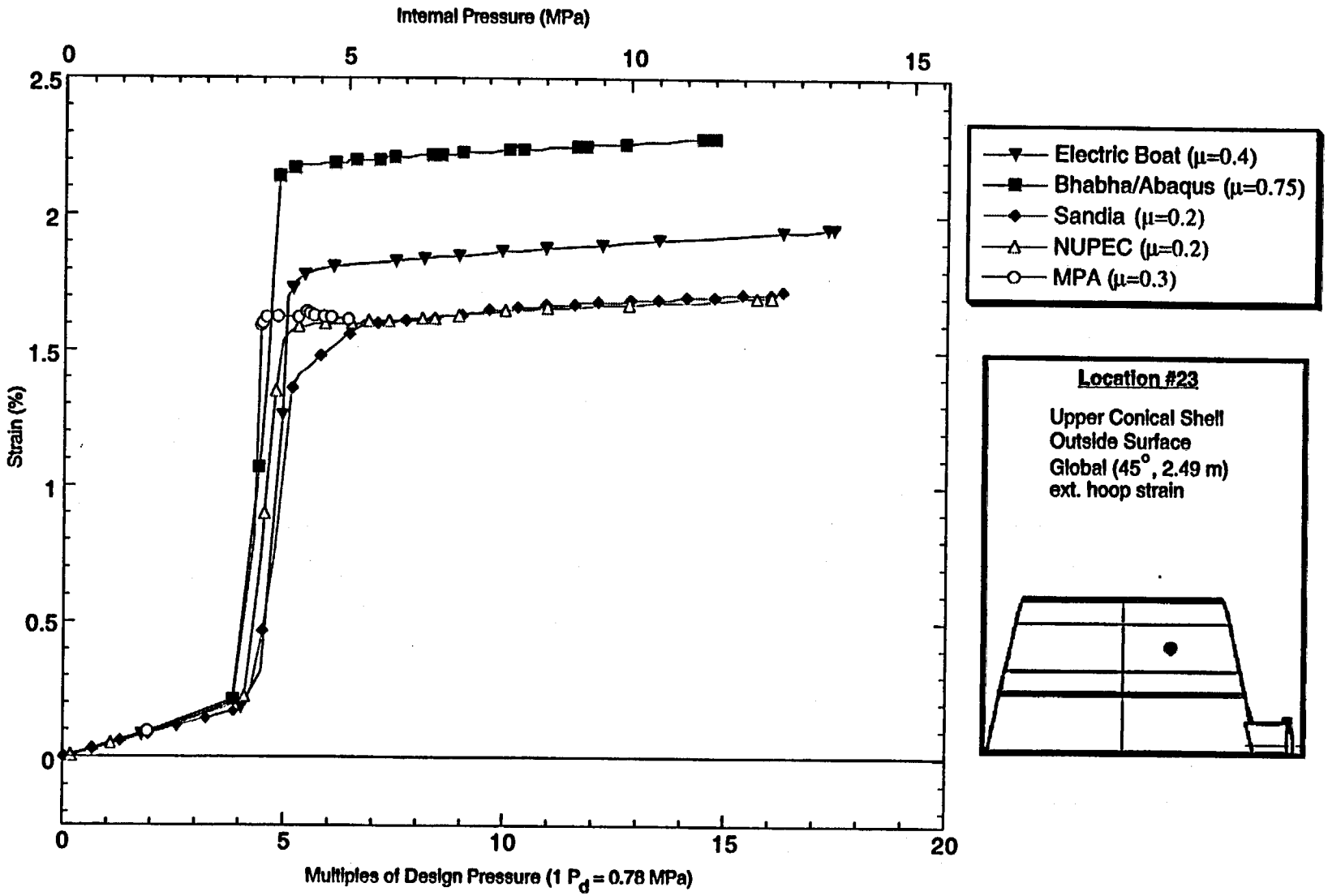

Figure D-46. Standard Output Location #23 (nonzero friction case)

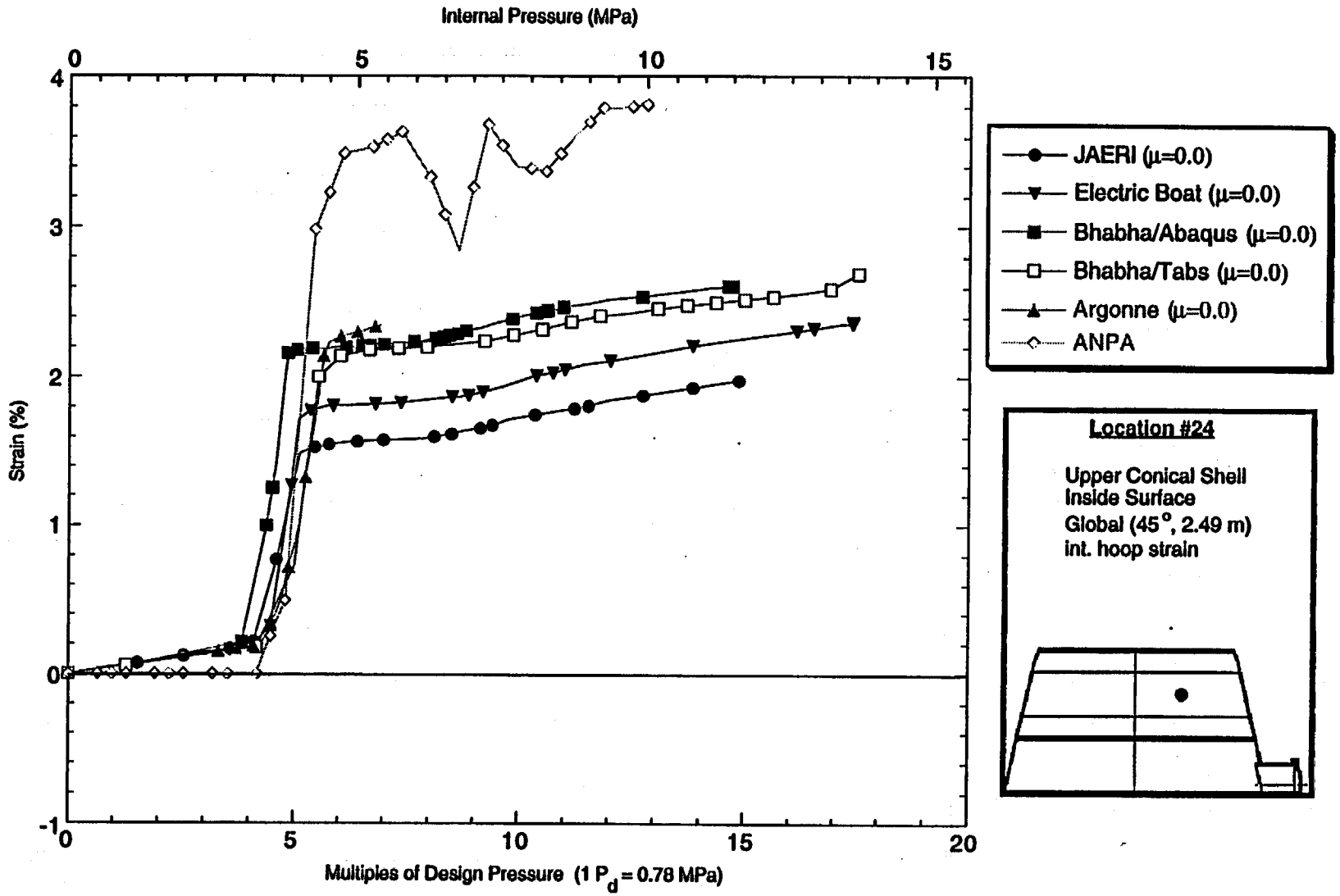

Figure D-47. Standard Output Location #24 (zero friction case)

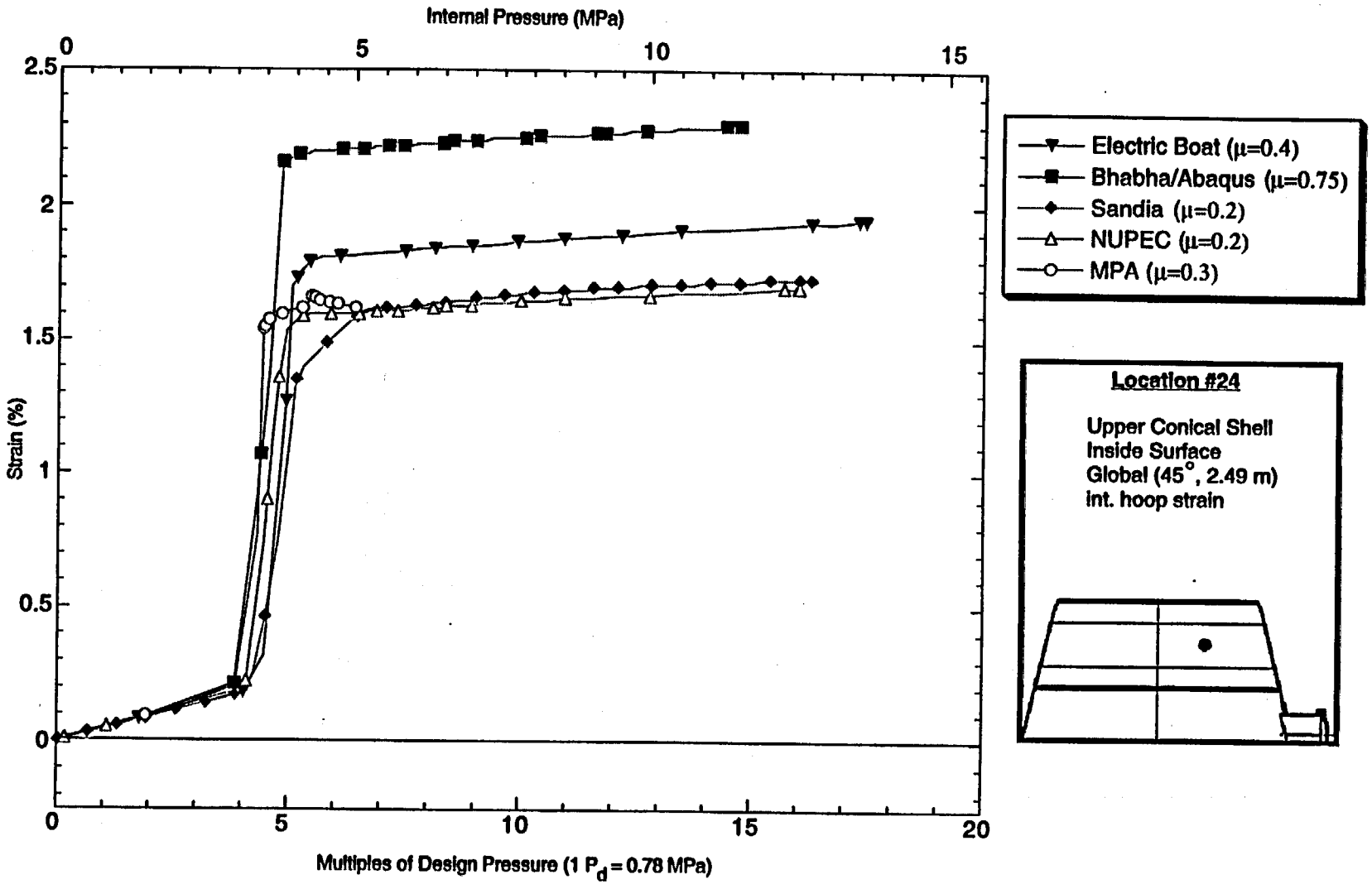

Figure D-48. Standard Output Location #24 (nonzero friction case)

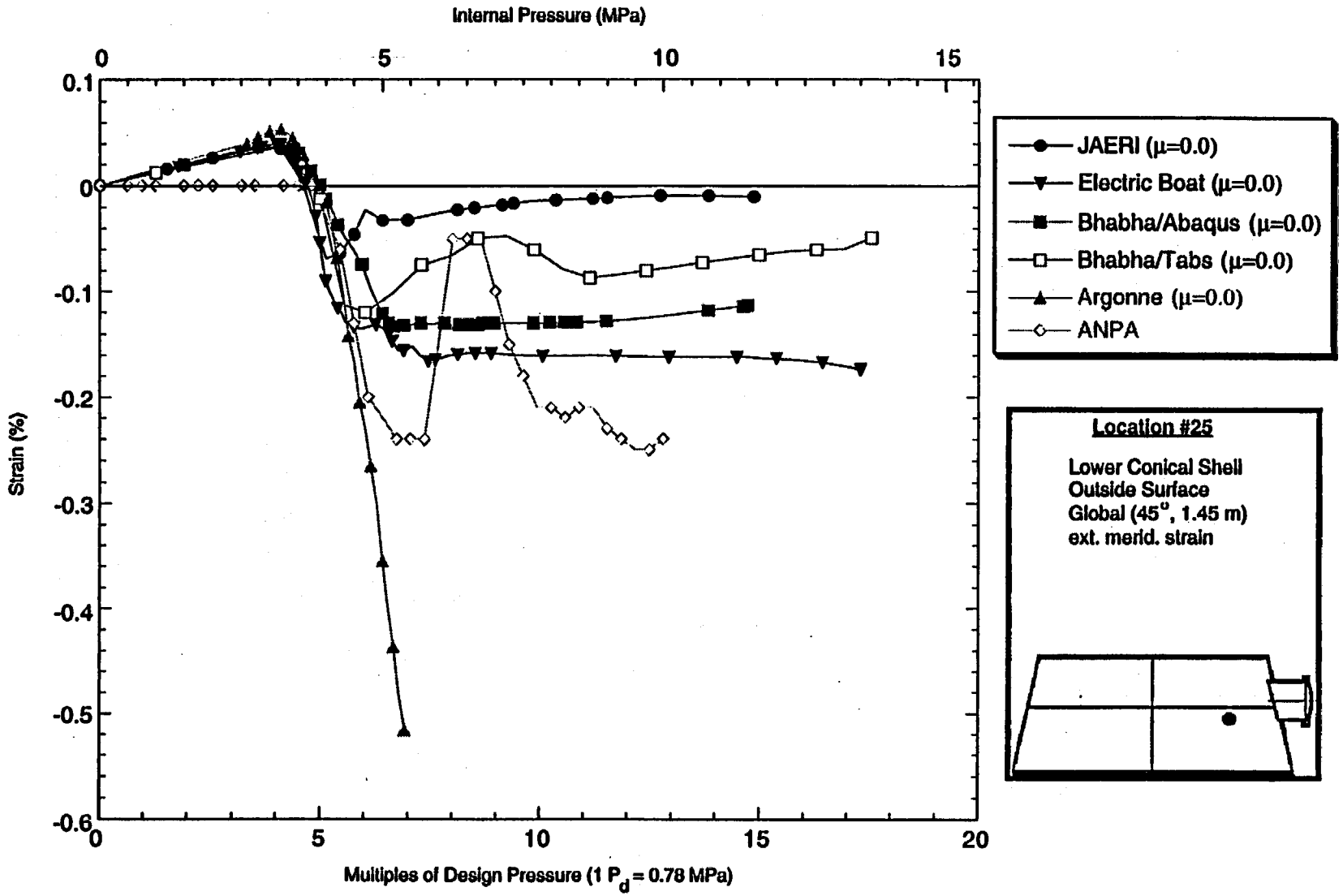

Figure D-49. Standard Output Location #25 (zero friction case)

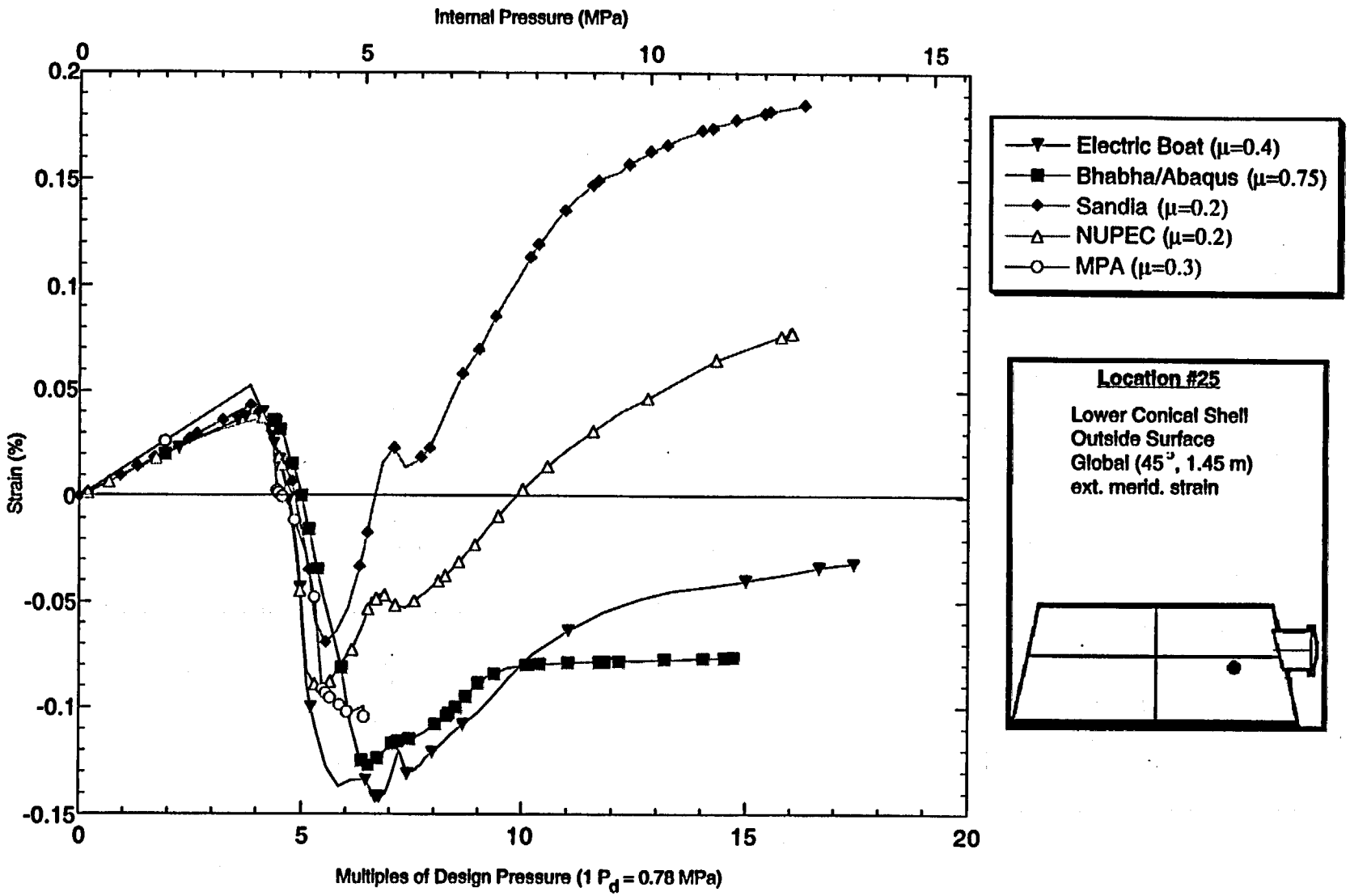

Figure D-50. Standard Output Location #25 (nonzero friction case)

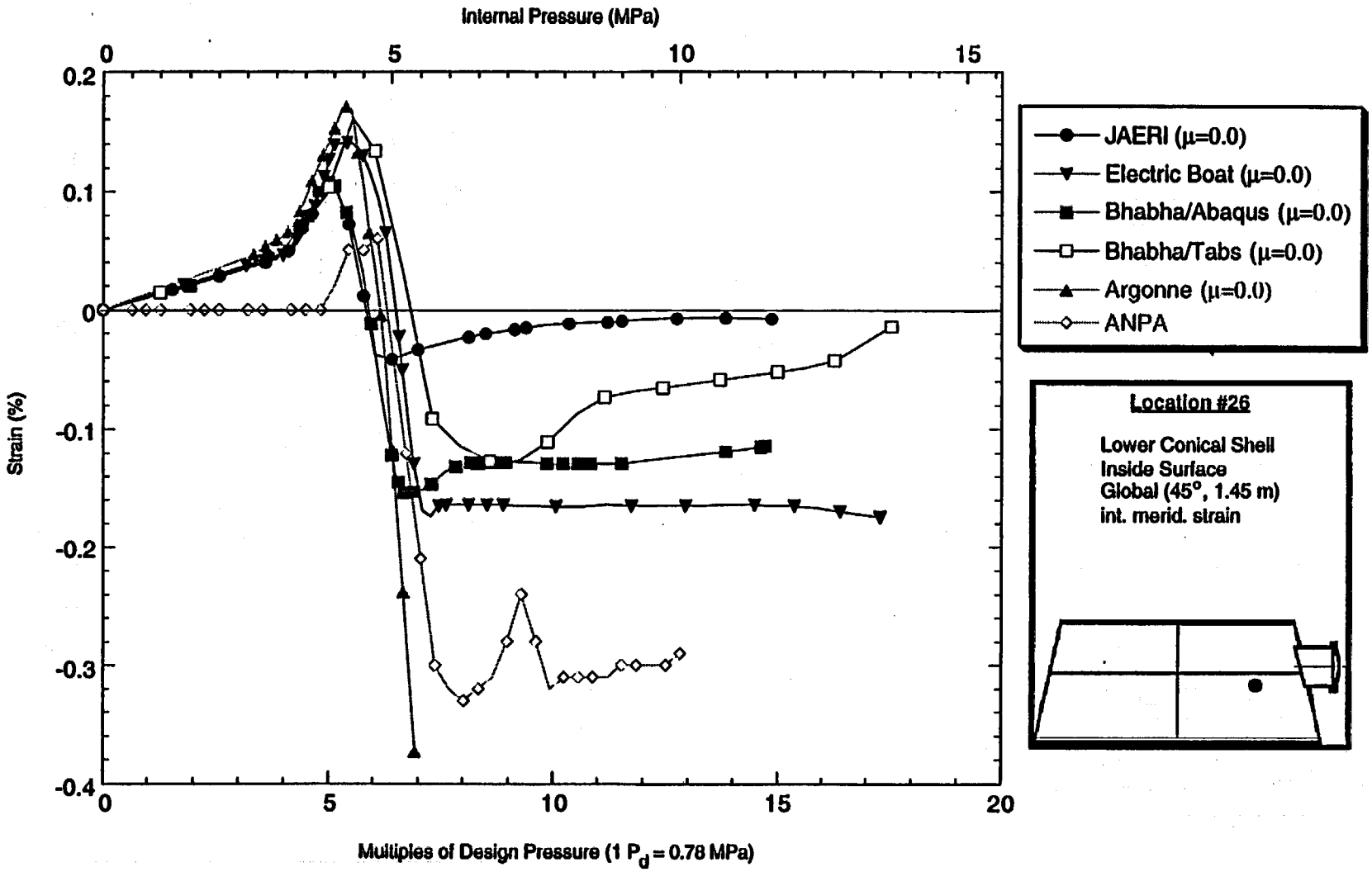

Figure D-51. Standard Output Location #26 (zero friction case)

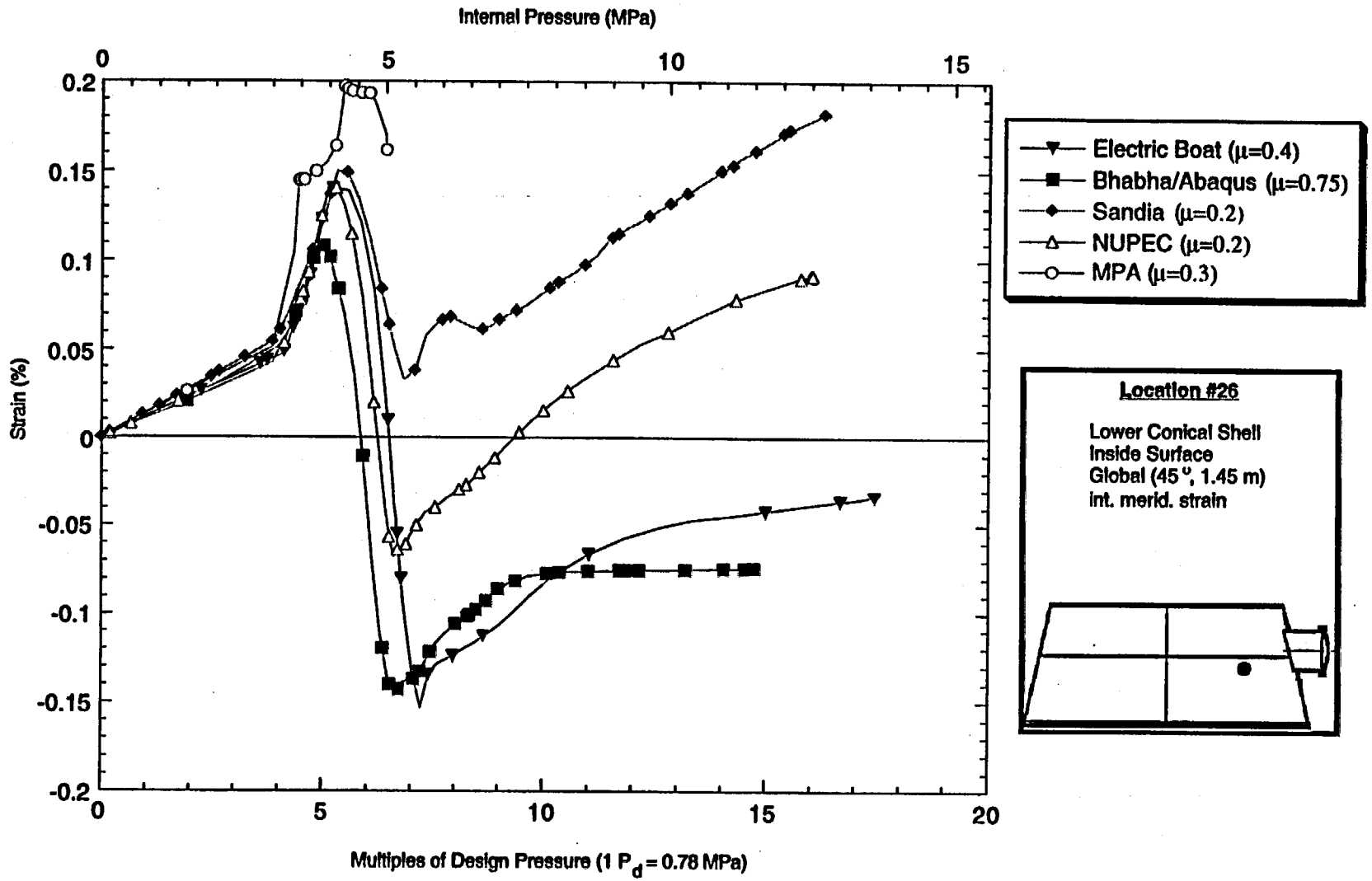

Figure D-52. Standard Output Location #26 (nonzero friction case)

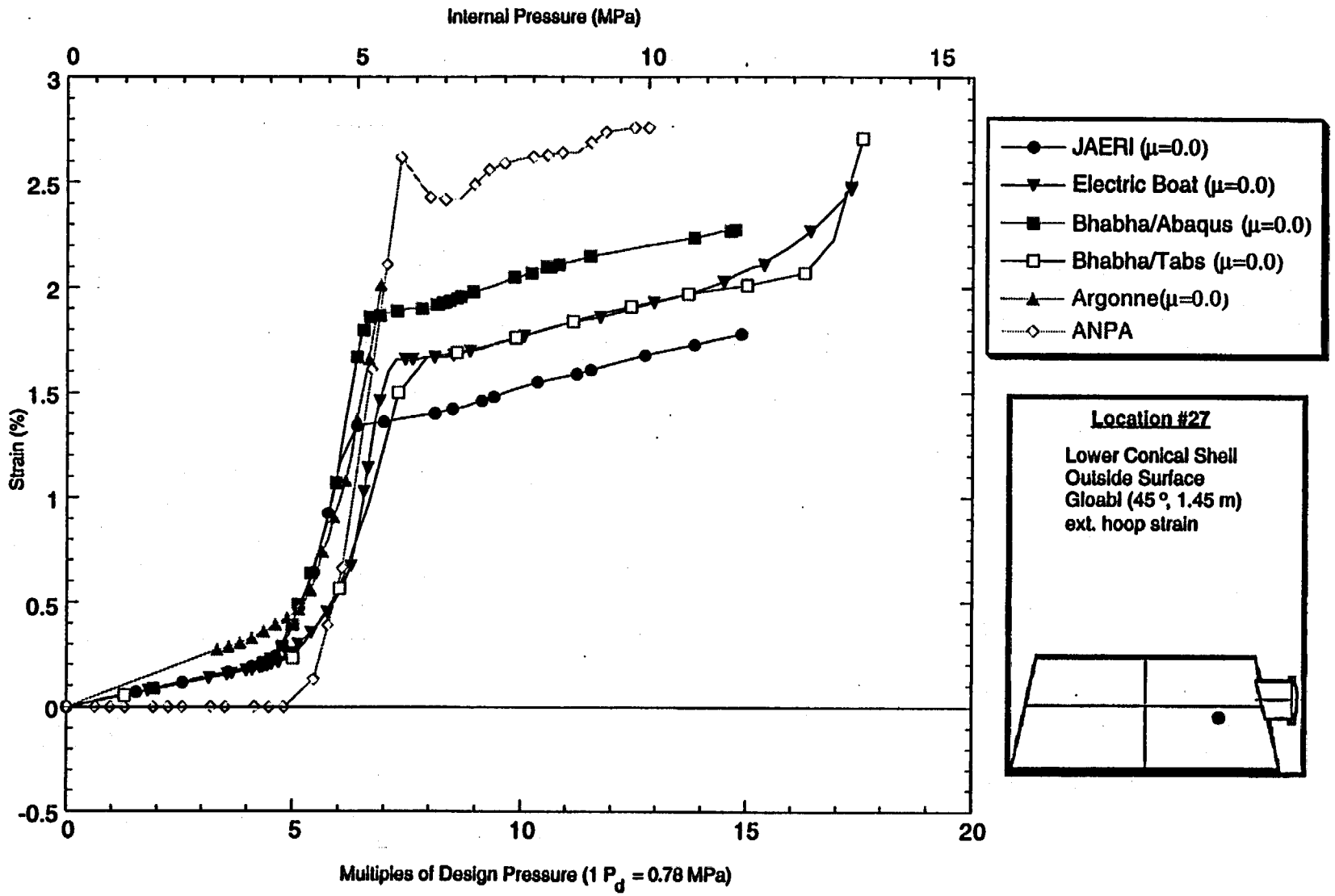

Figure D-53. Standard Output Location #27 (zero friction case)

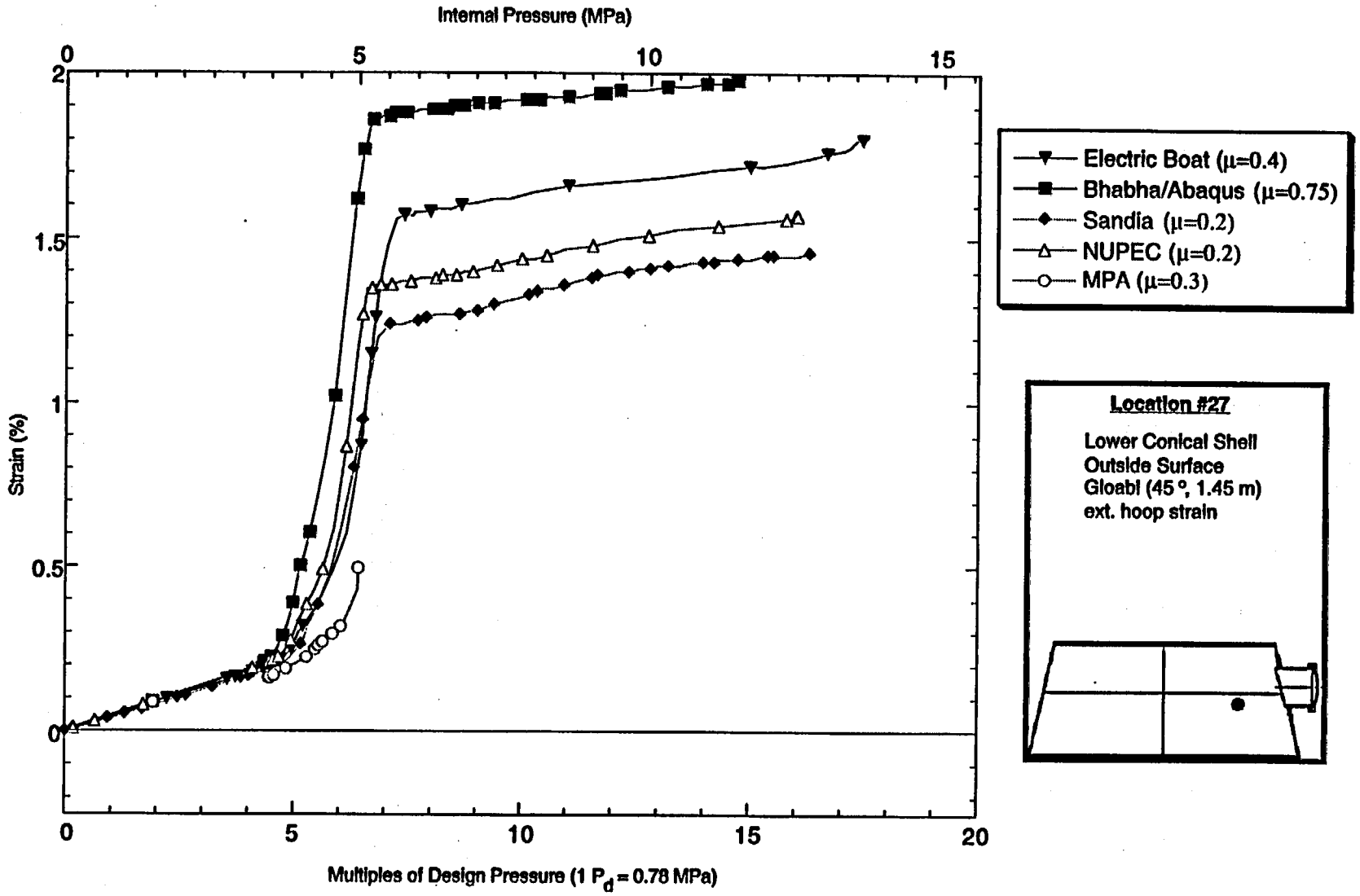

Figure D-54. Standard Output Location #27 (nonzero friction case)

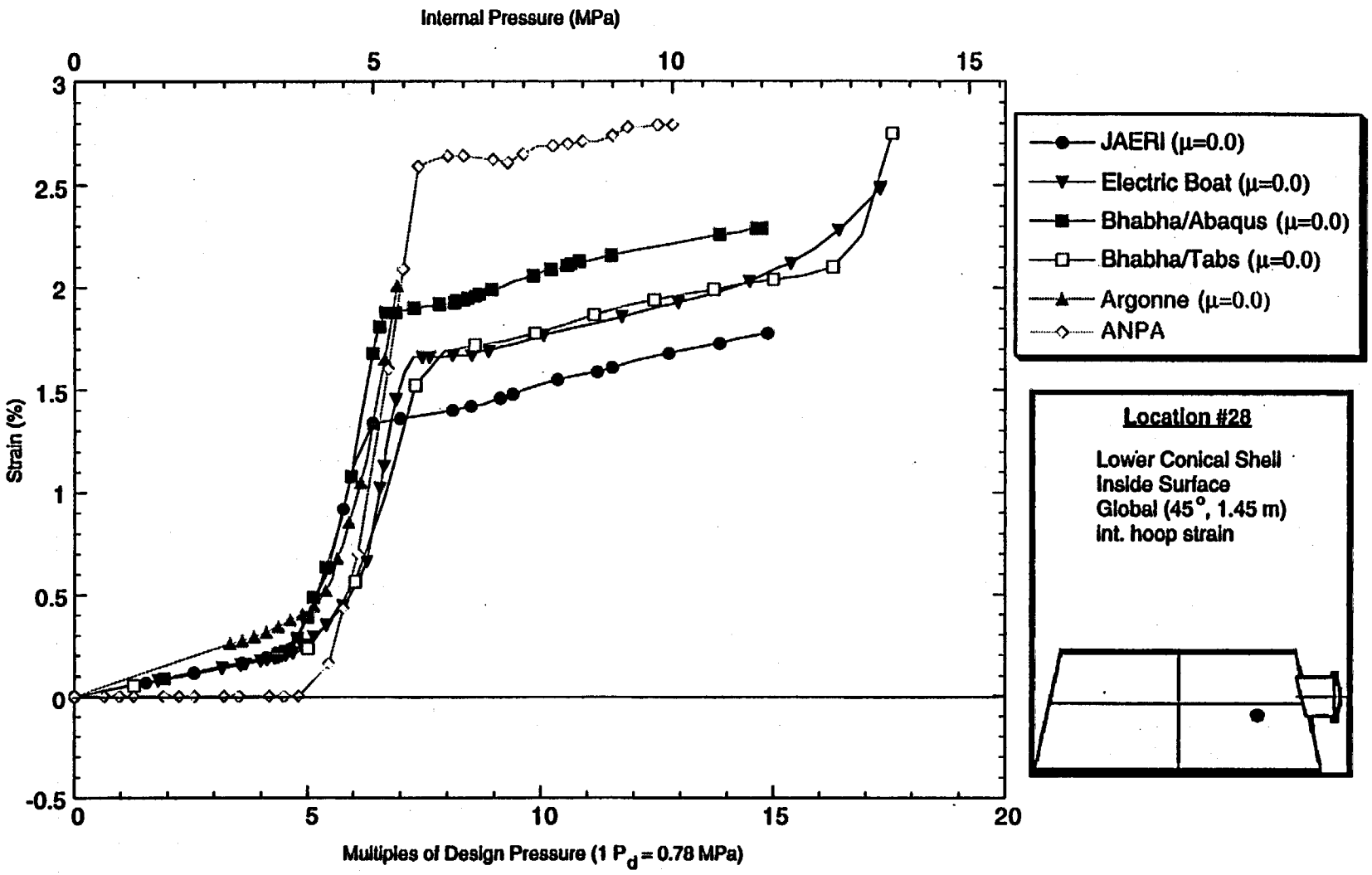

Figure D-55. Standard Output Location #28 (zero friction case)

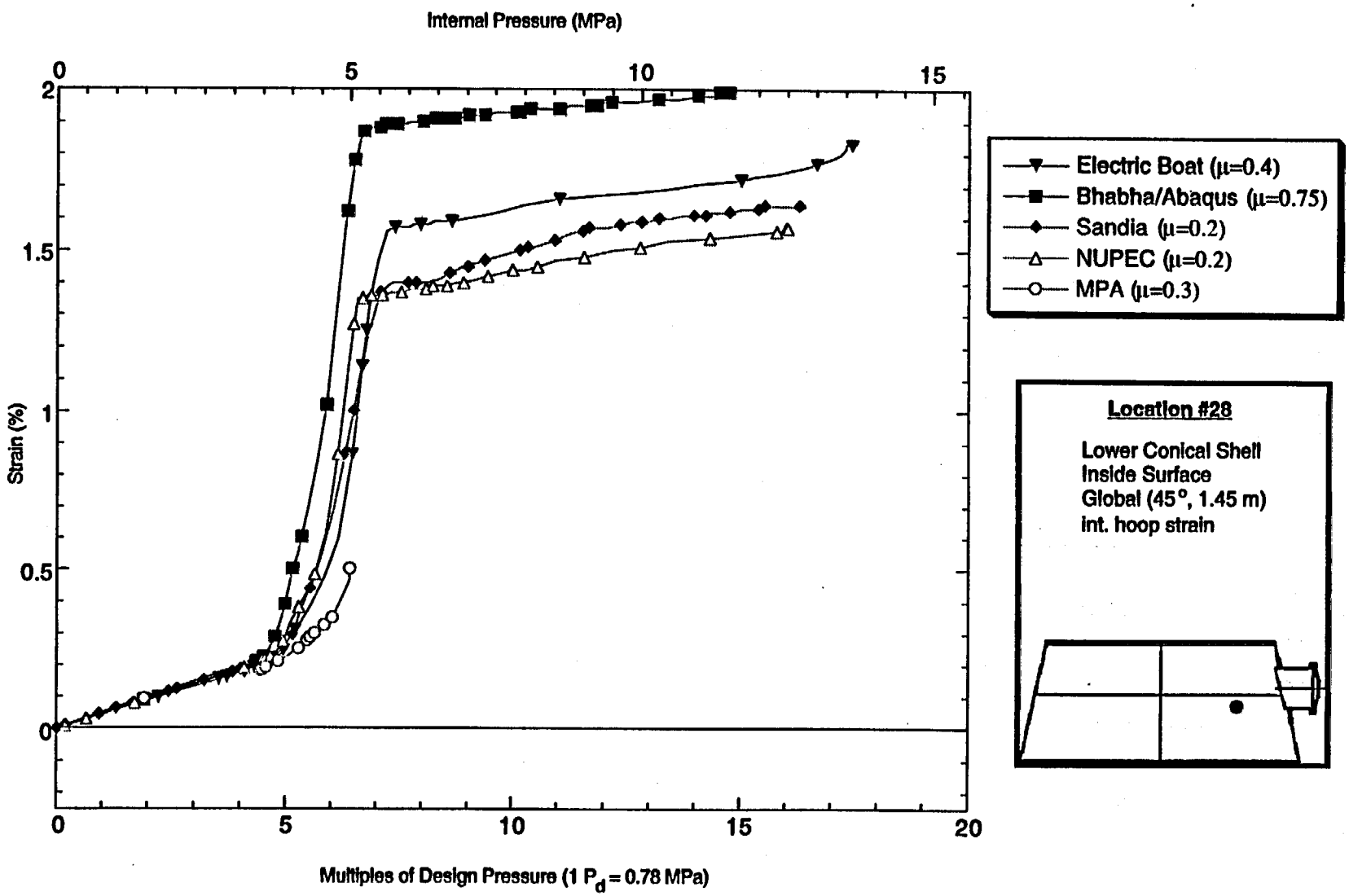

Figure D-56. Standard Output Location #28 (nonzero friction case)

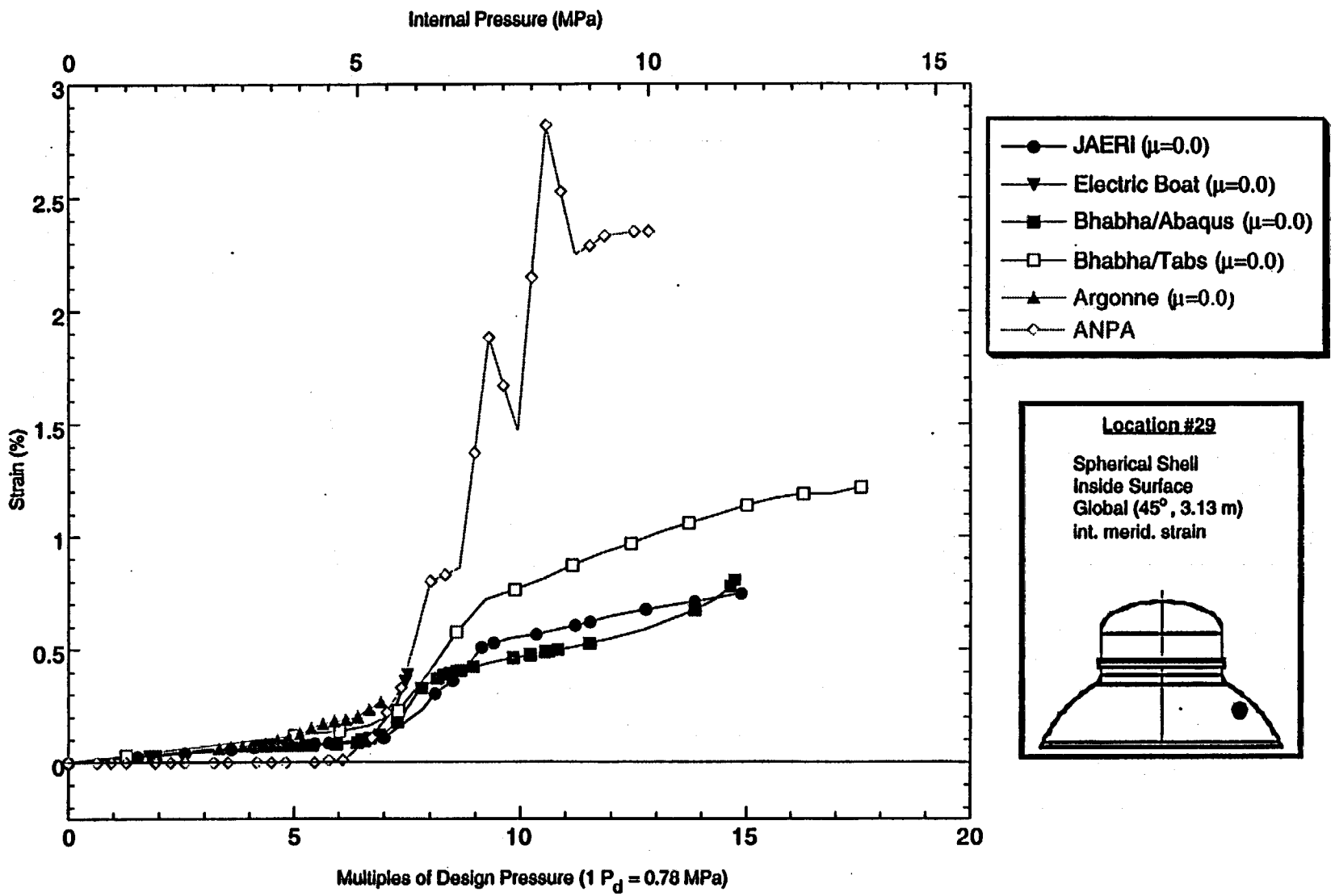

Figure D-57. Standard Output Location #29 (zero friction case)

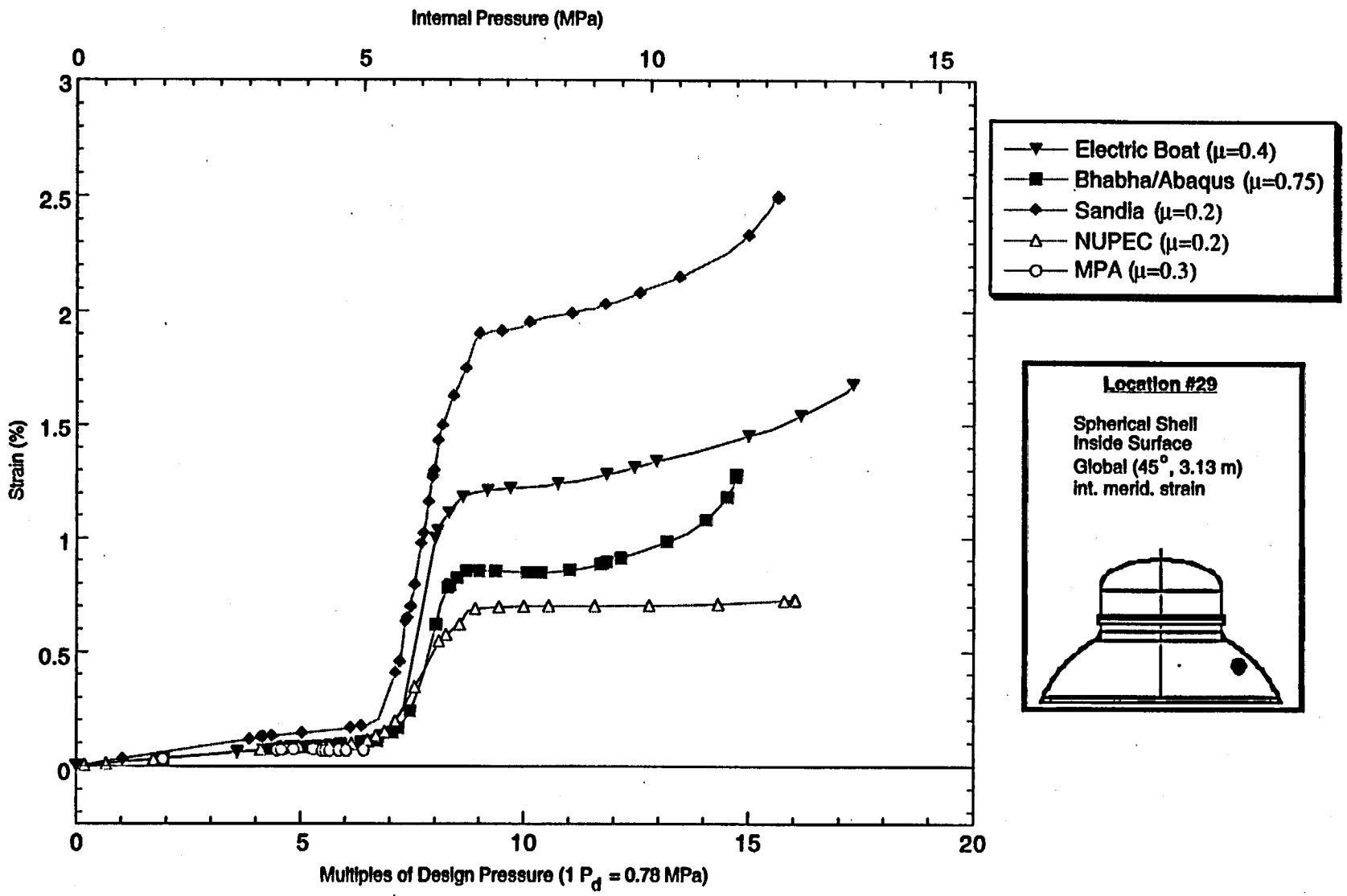

Figure D-58. Standard Output Location #29 (nonzero friction case)

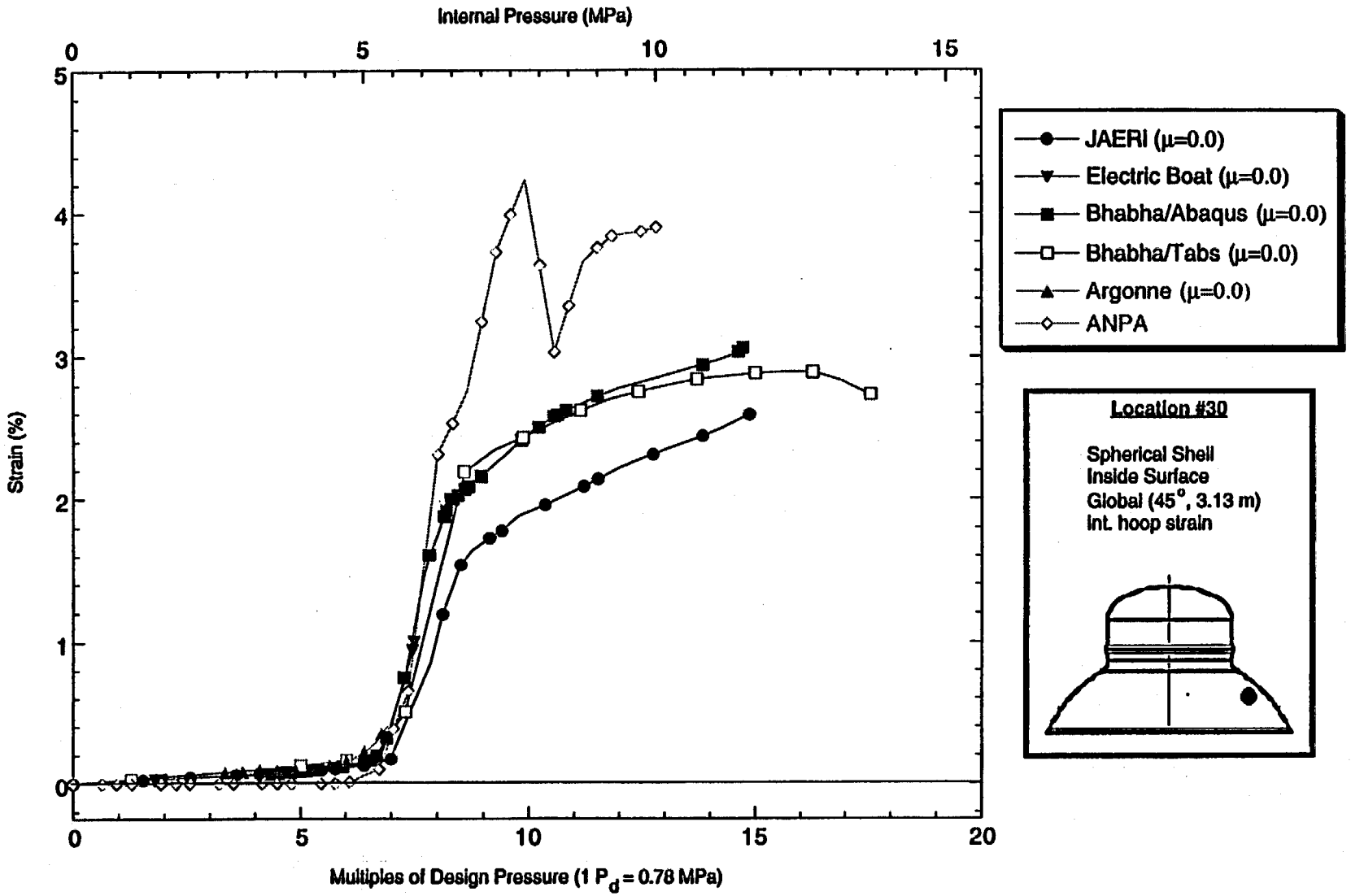

Figure D-59. Standard Output Location #30 (zero friction case)

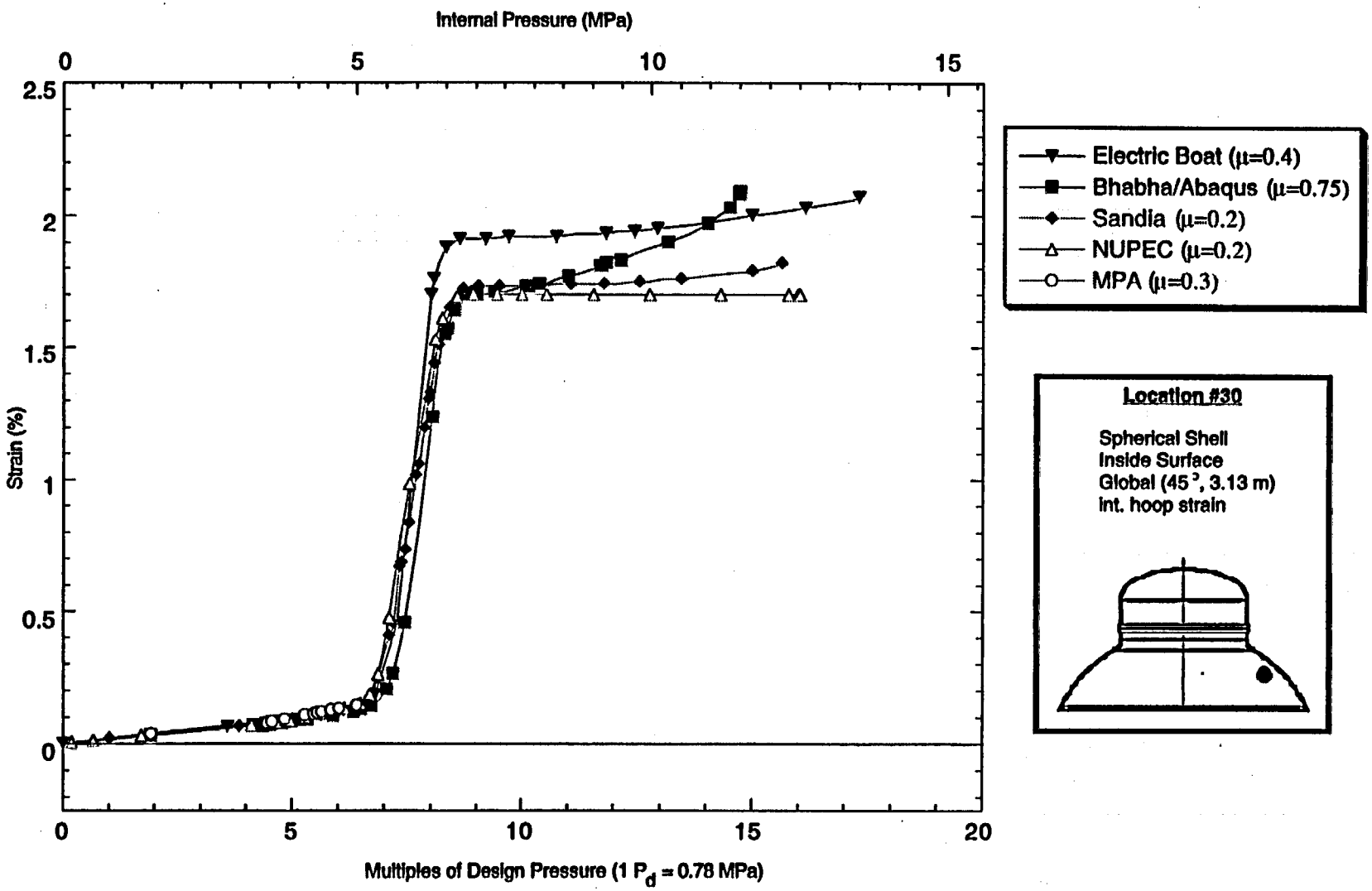

Figure D-60. Standard Output Location #30 (nonzero friction case)

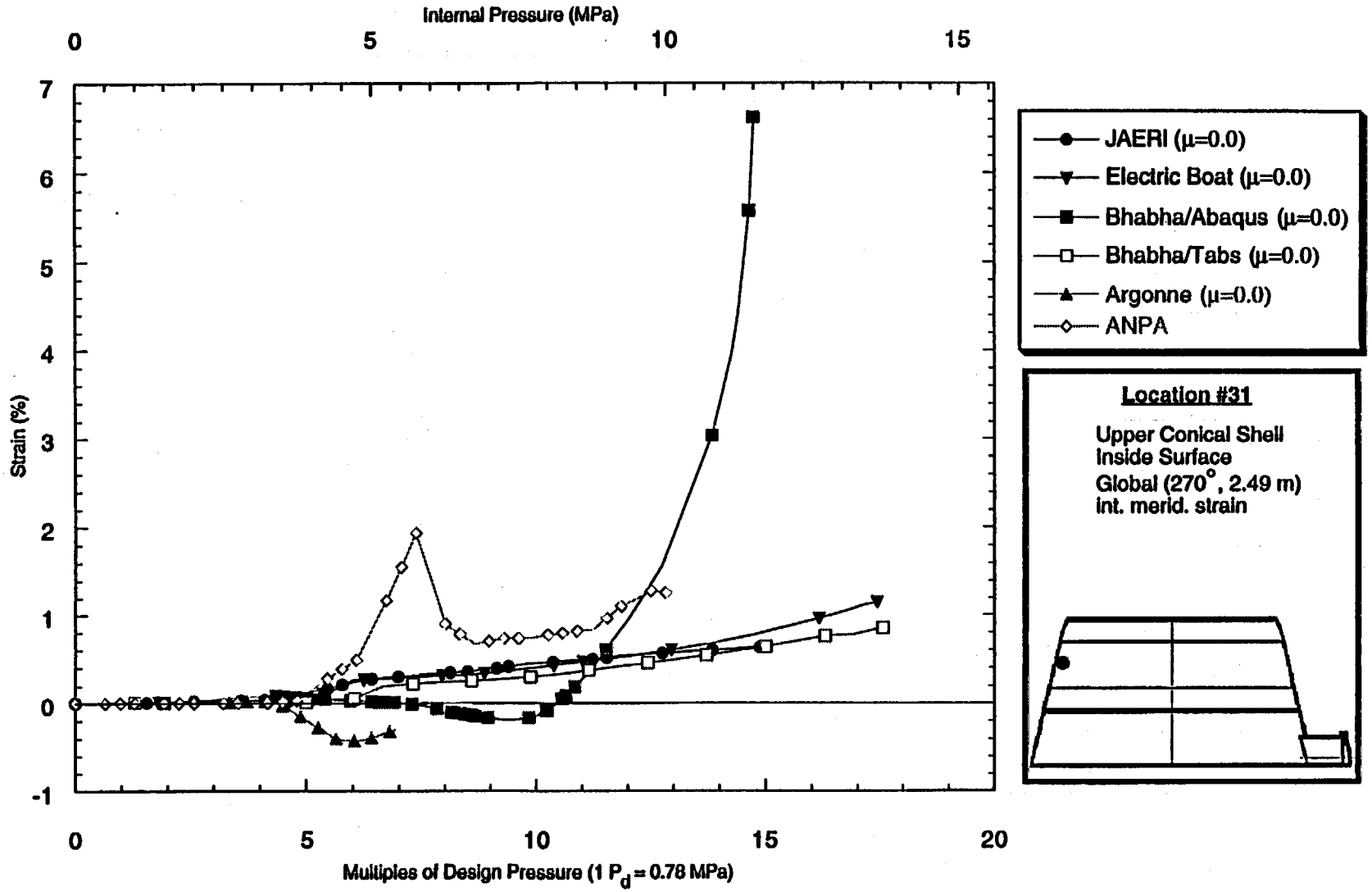

Figure D-61. Standard Output Location #31 (zero friction case)

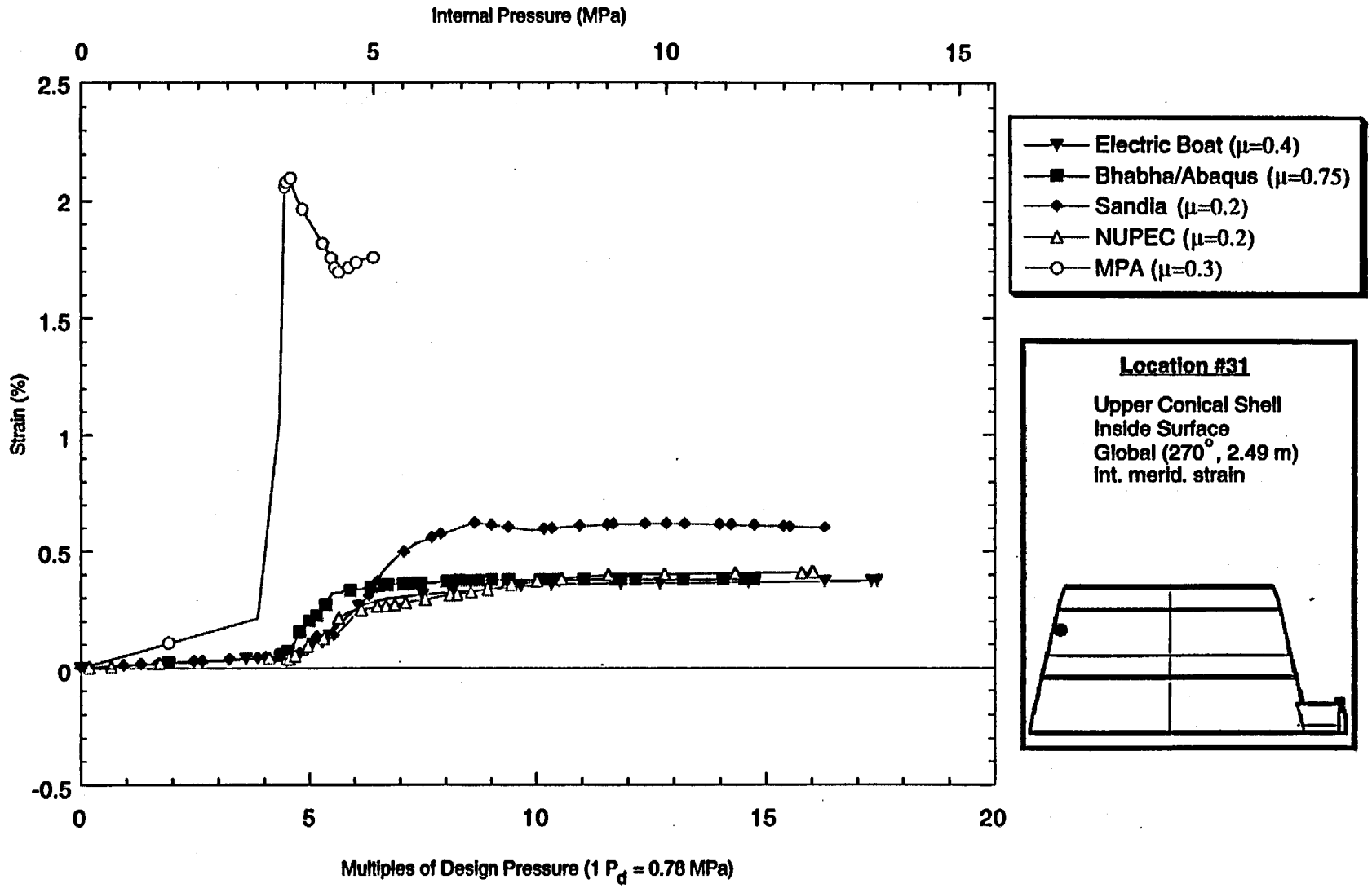

Figure D-62. Standard Output Location #31 (nonzero friction case)

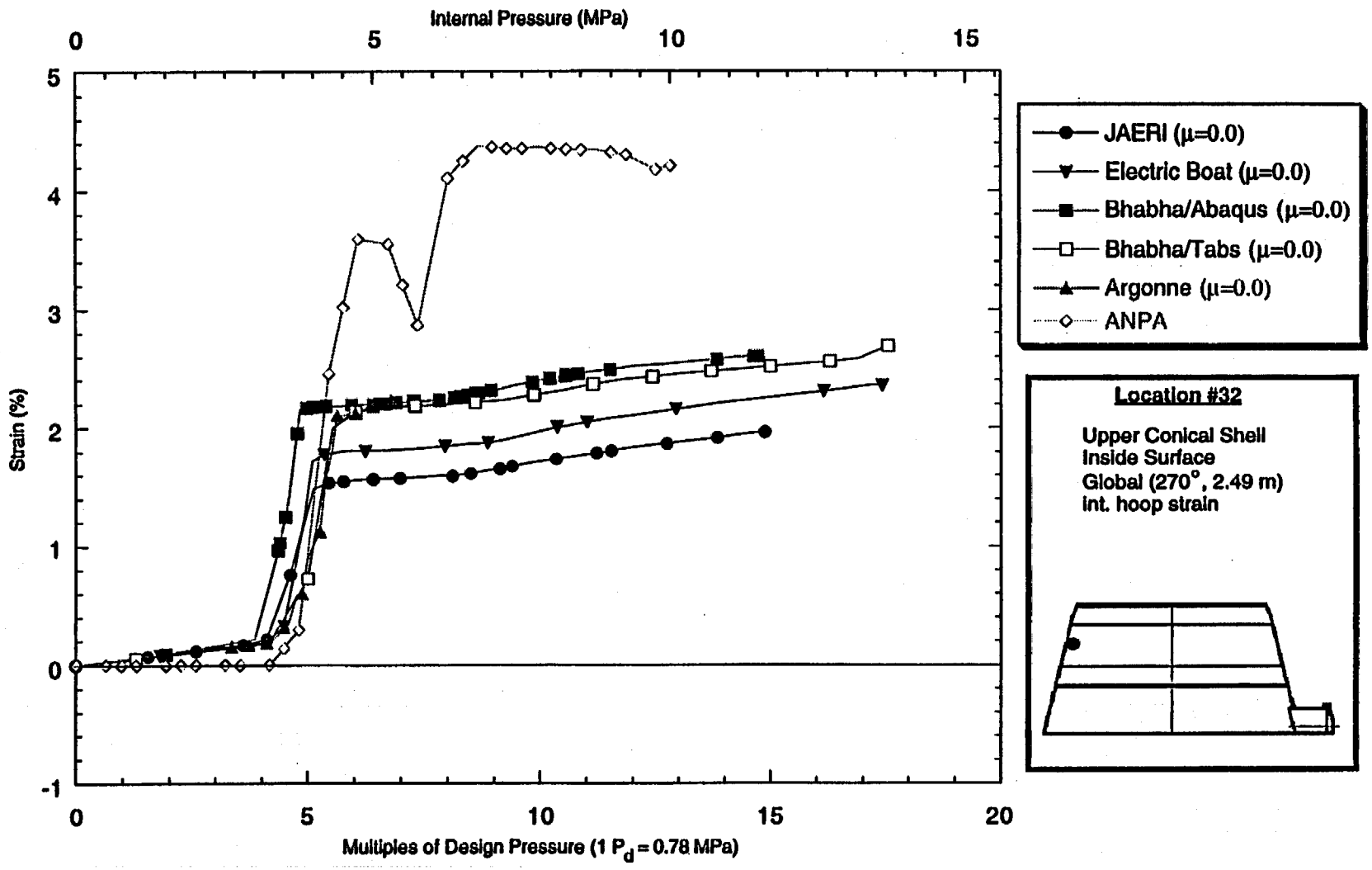

Figure D-63. Standard Output Location #32 (zero friction case)

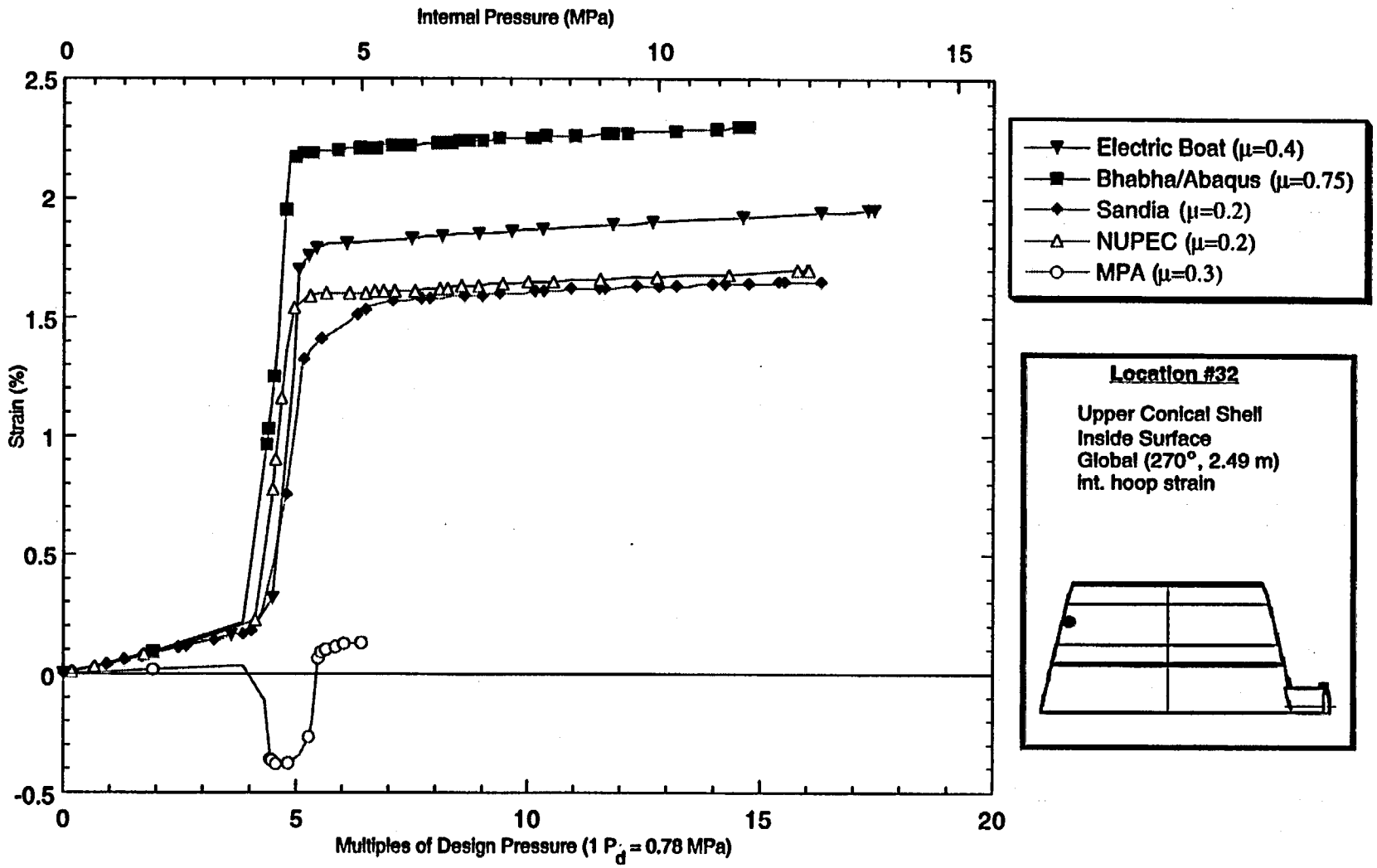

Figure D-64. Standard Output Location #32 (nonzero friction case)

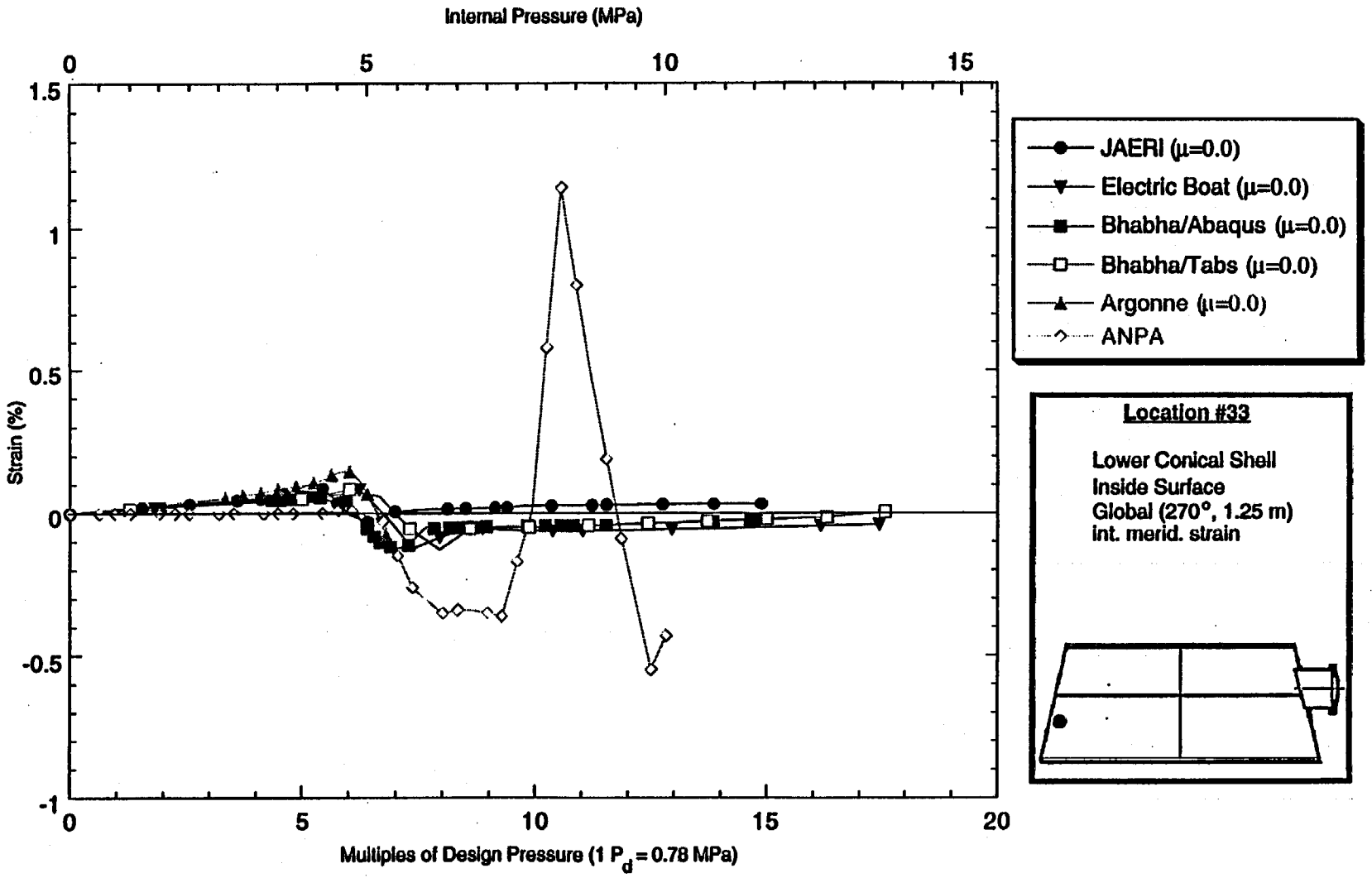

Figure D-65. Standard Output Location #33 (zero friction case)

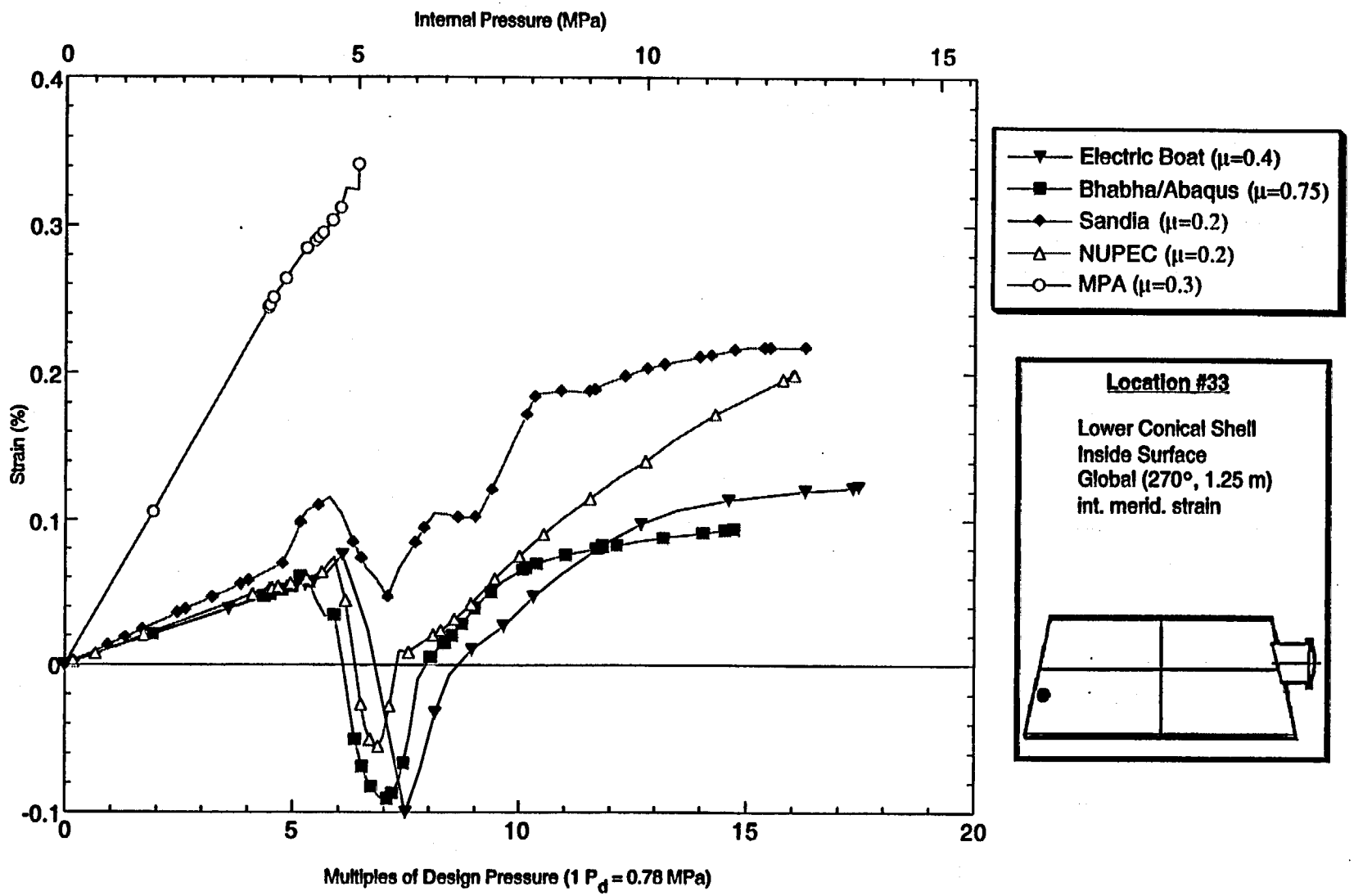

Figure D-66. Standard Output Location #33 (nonzero friction case)

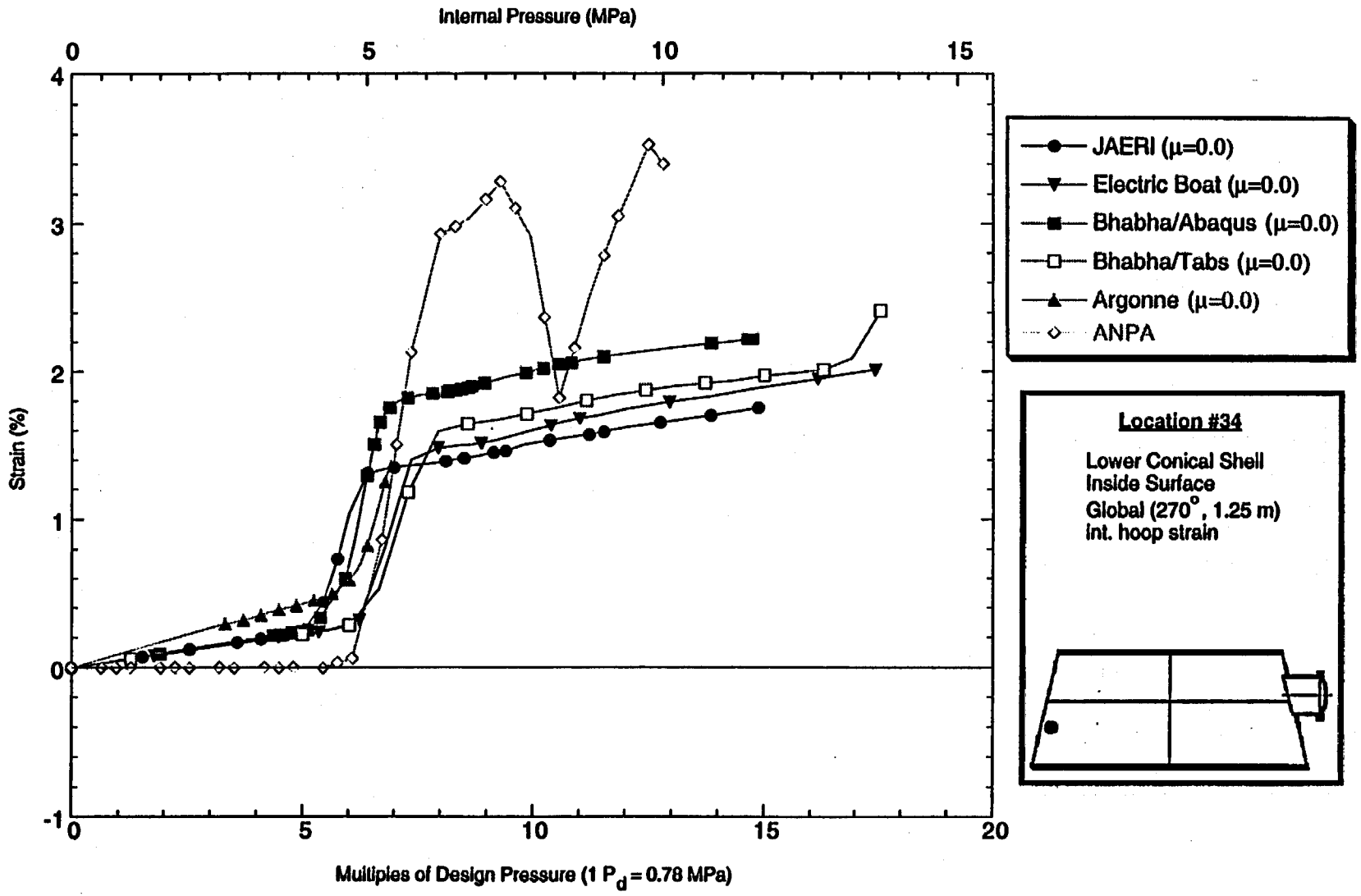

Figure D-67. Standard Output Location #34 (zero friction case)

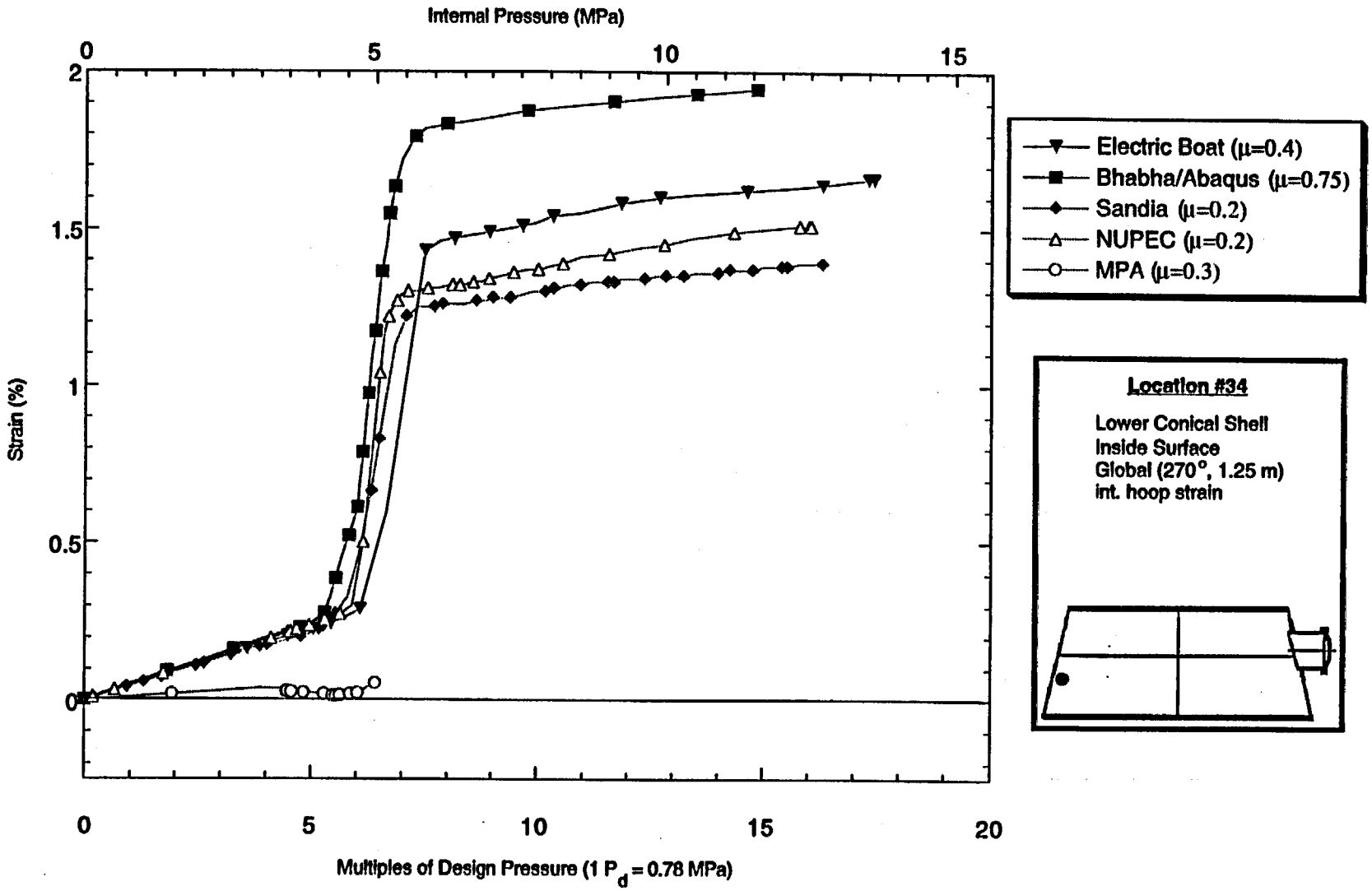

6

Figure D-68. Standard Output Location #34 (nonzero friction case)

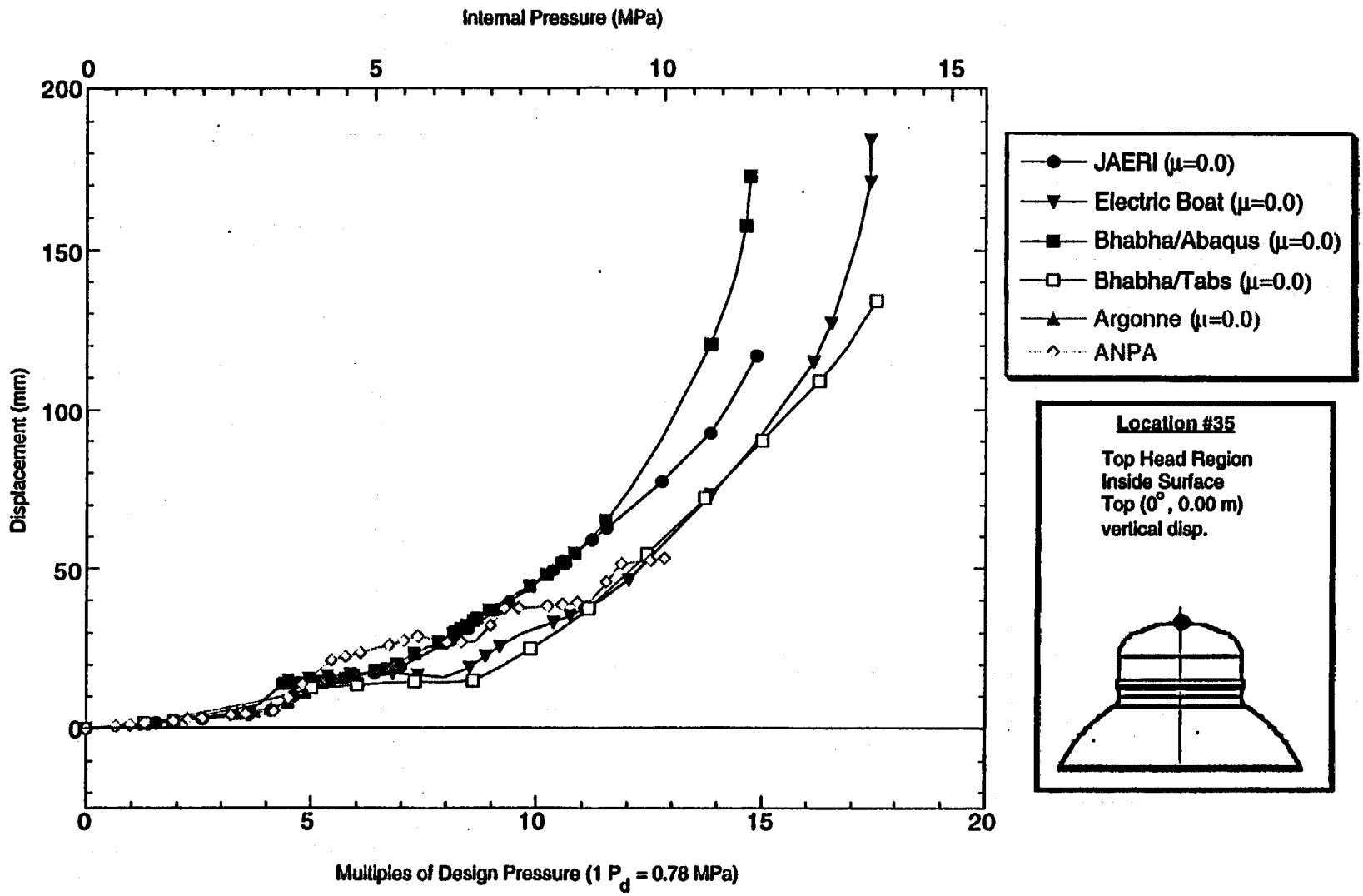

Figure D-69. Standard Output Location #35 (zero friction case)

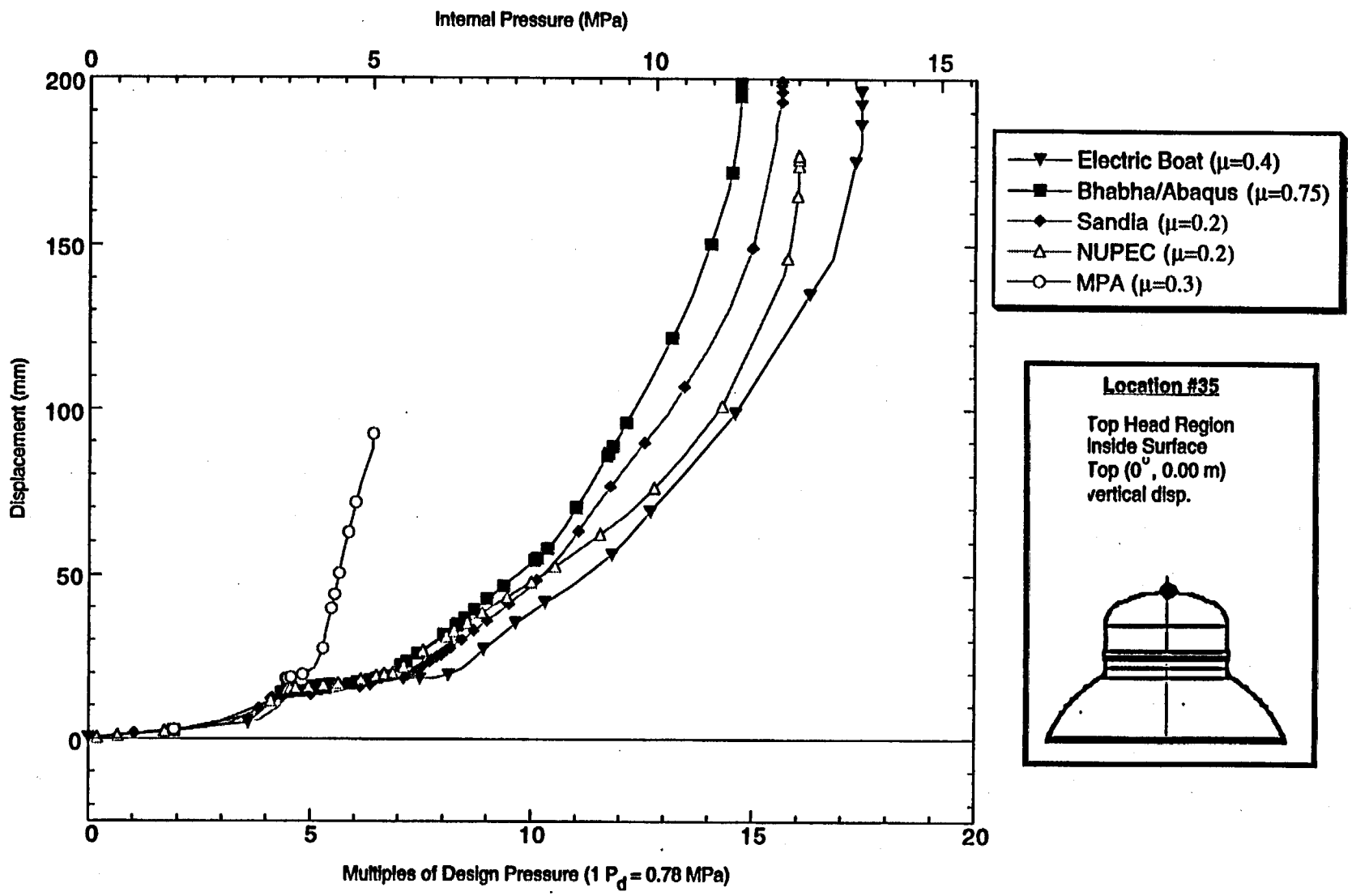

Figure D-70. Standard Output Location #35 (nonzero friction case)

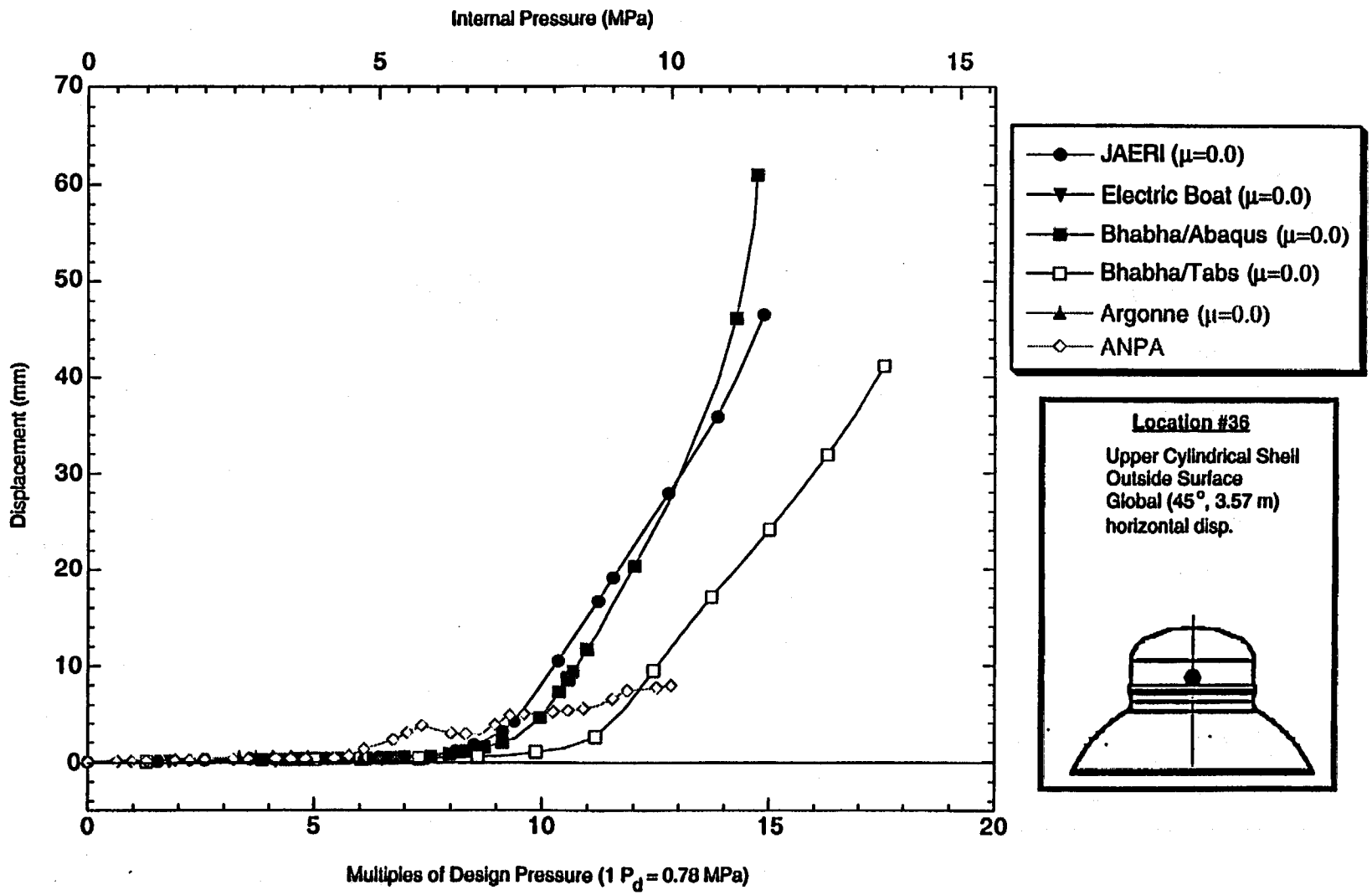

Figure D-71. Standard Output Location #36-outside (zero friction case)

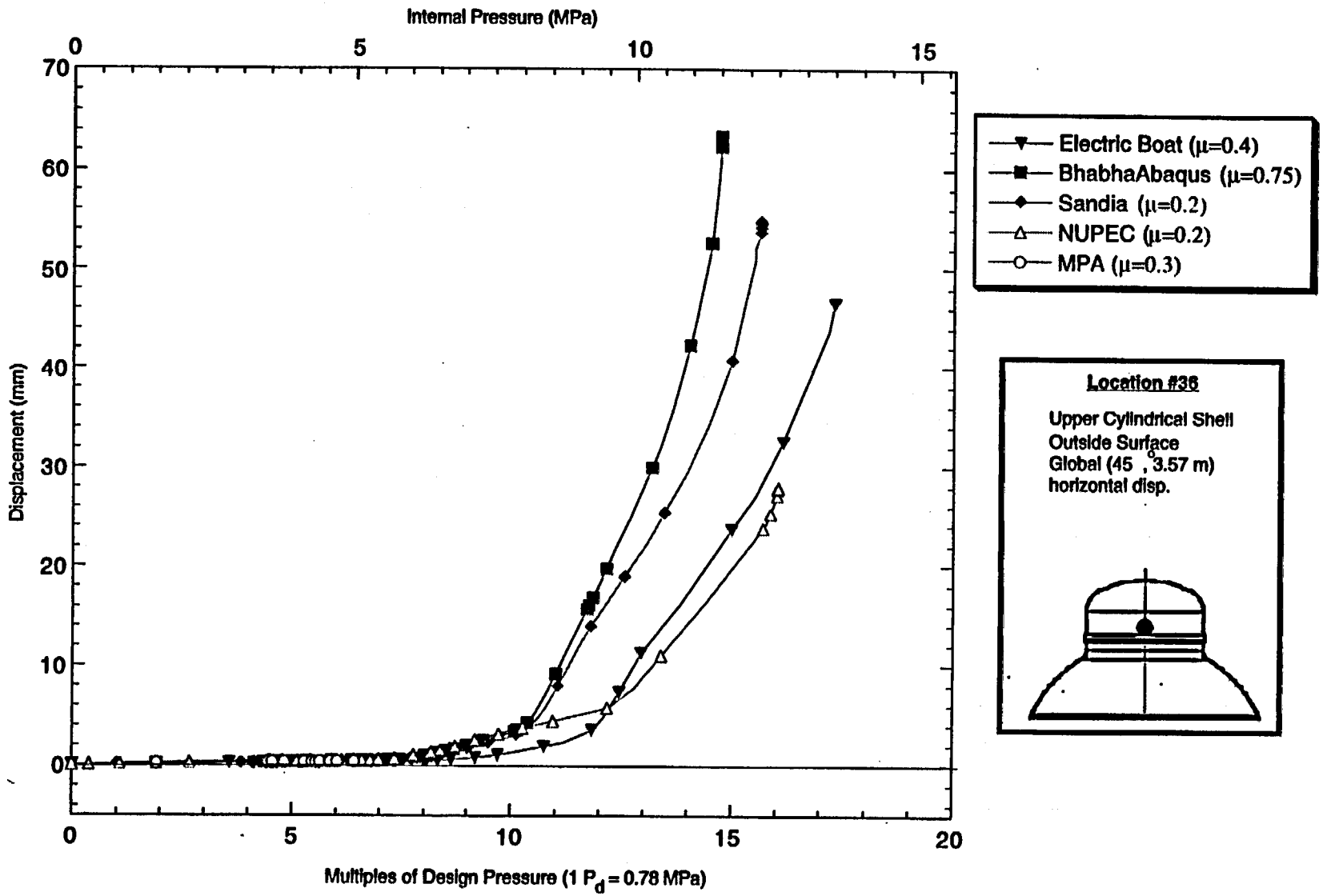

Figure D-72. Standard Output Location #36-outside (nonzero friction case)

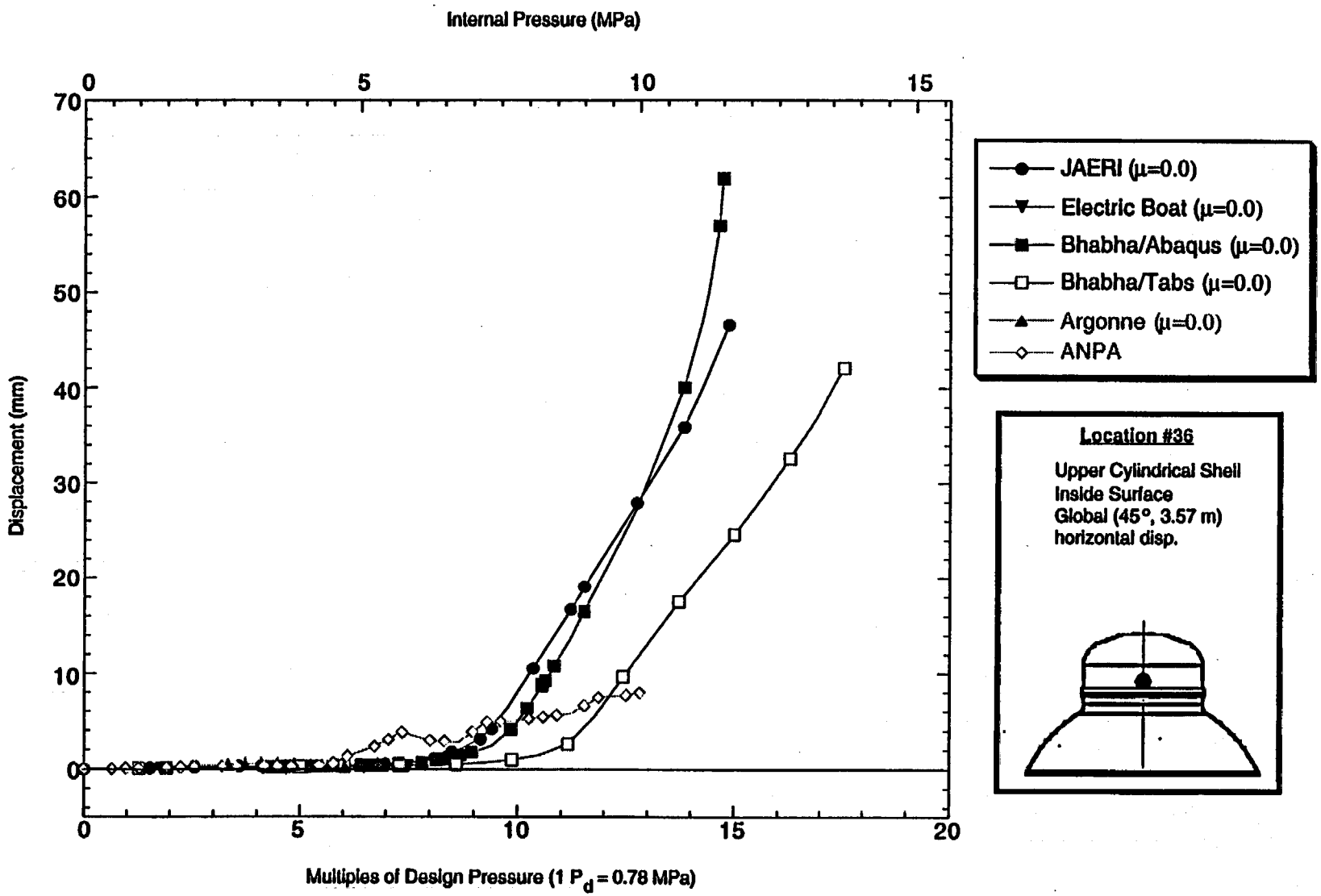

Figure D-73. Standard Output Location #36-inside (zero friction case)

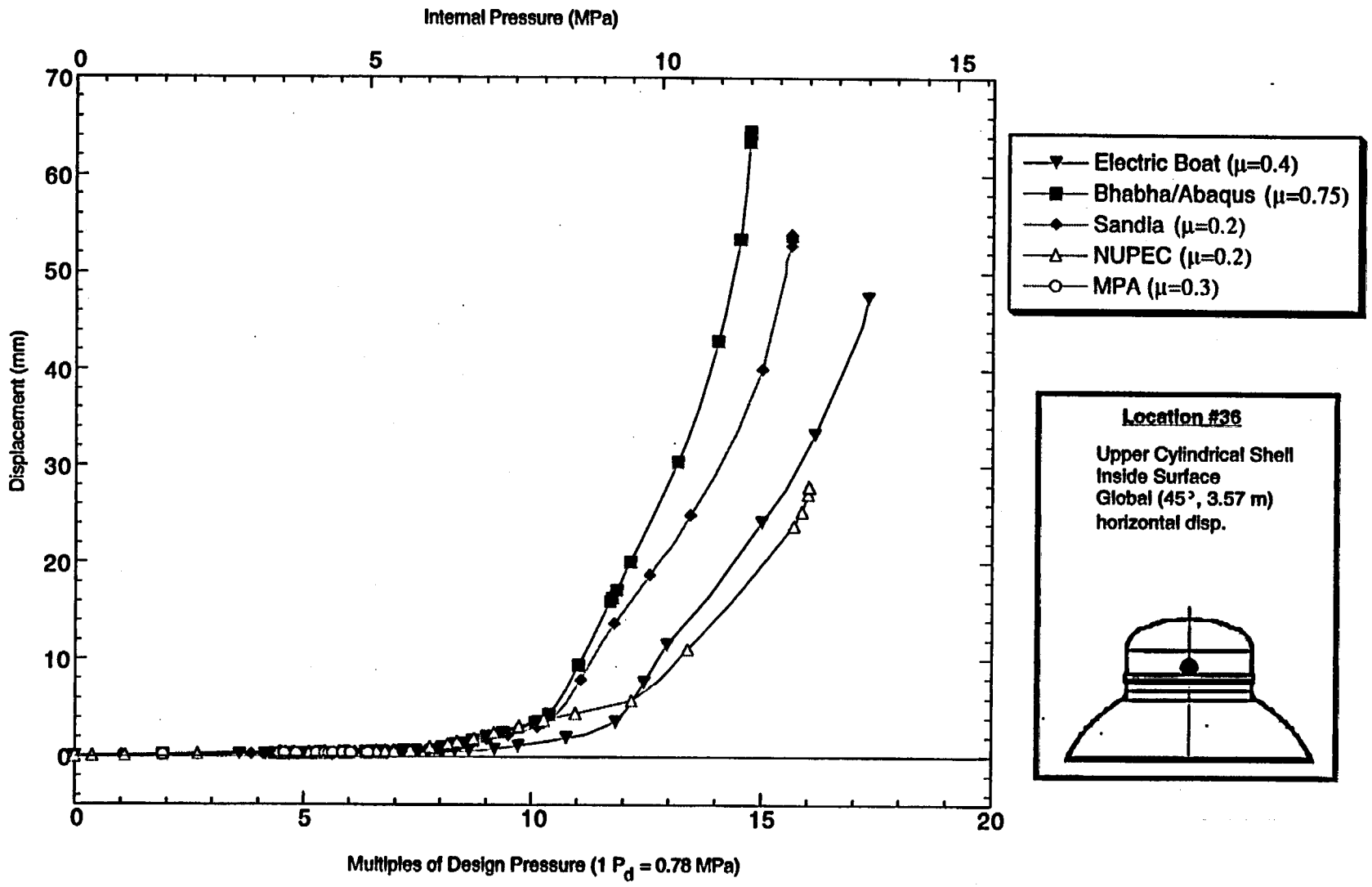

Figure D-74. Standard Output Location #36-inside (nonzero friction case)

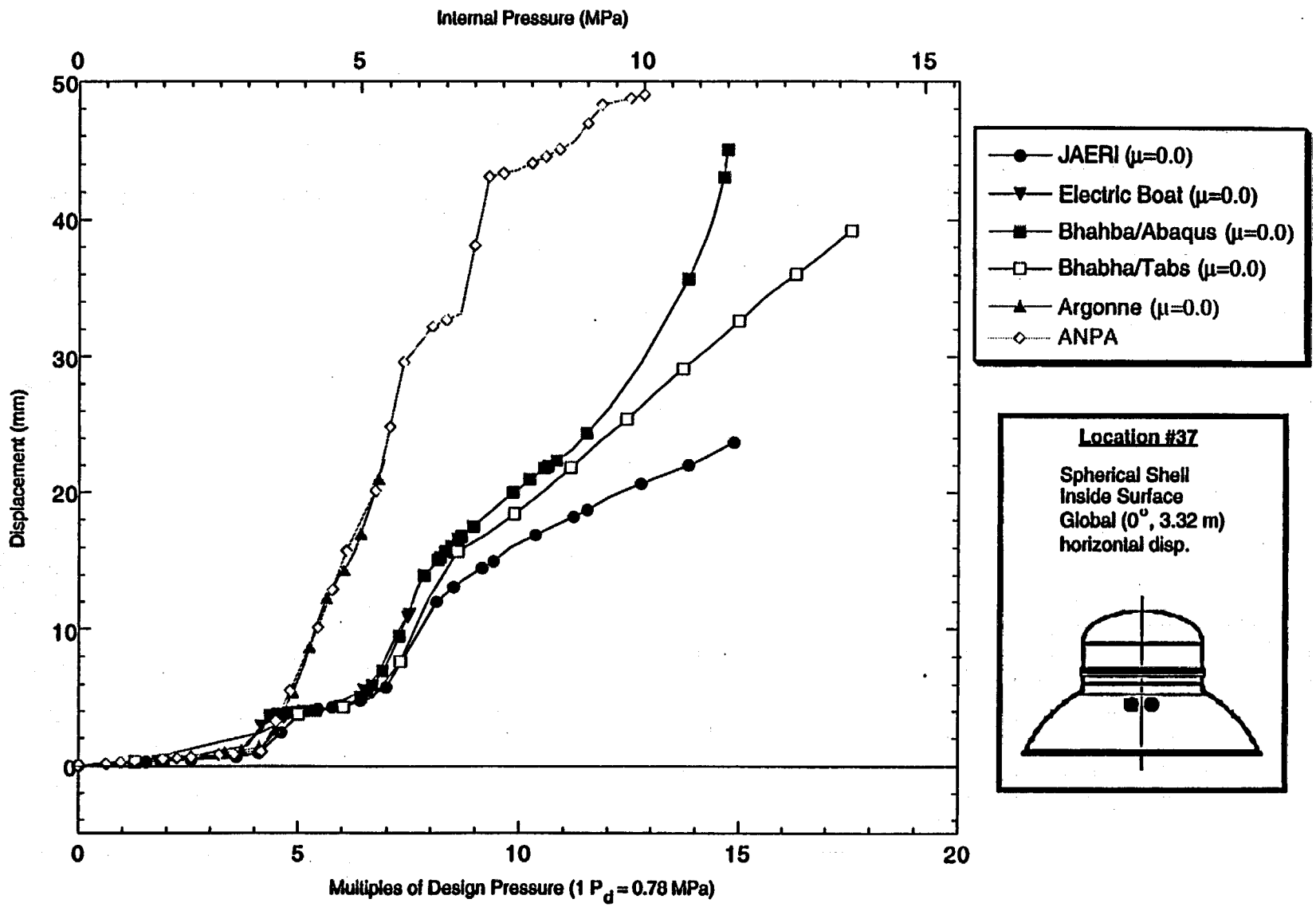

Figure D-75. Standard Output Location #37 (zero friction case)

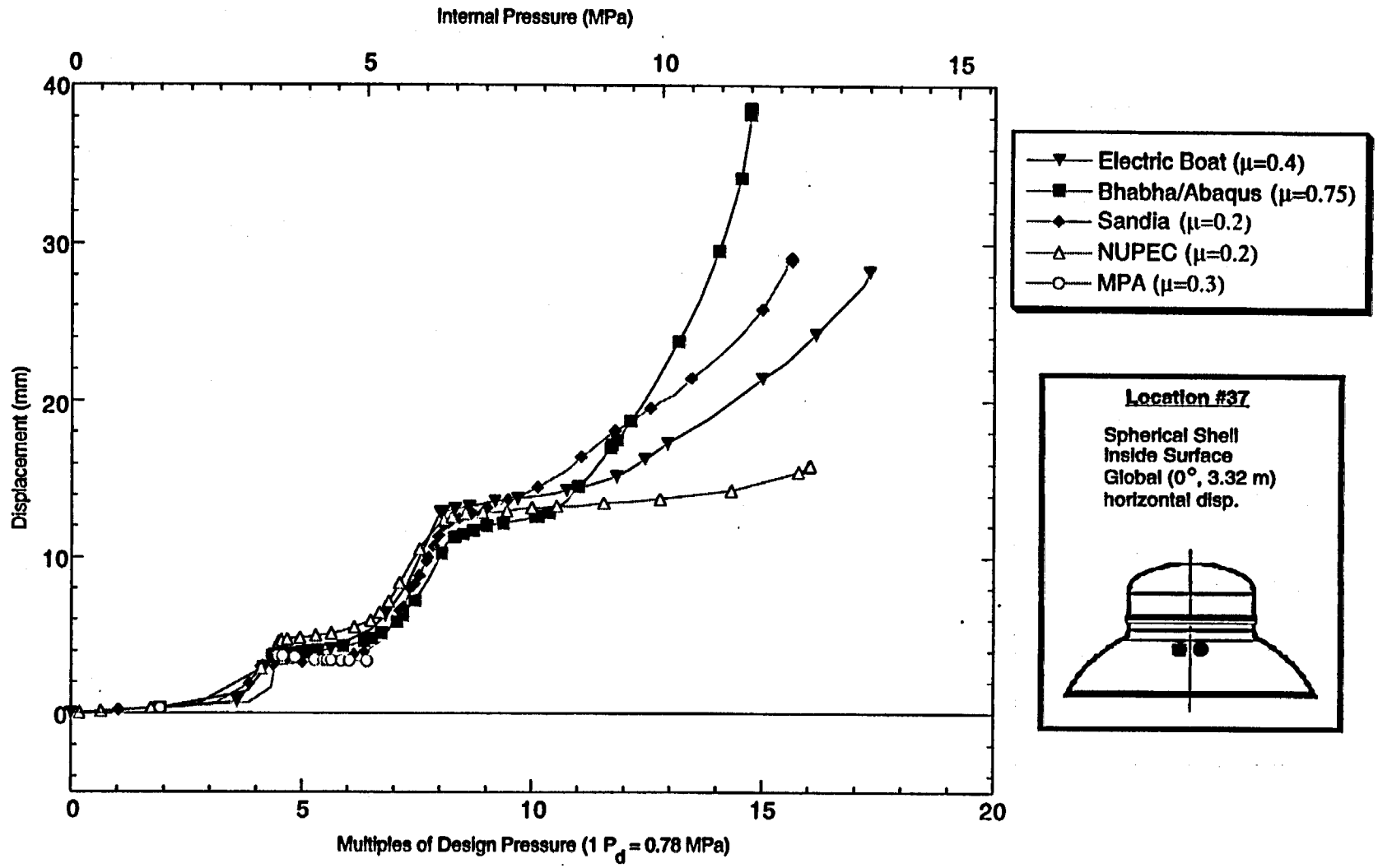

Figure D-76. Standard Output Location #37 (nonzero friction case)

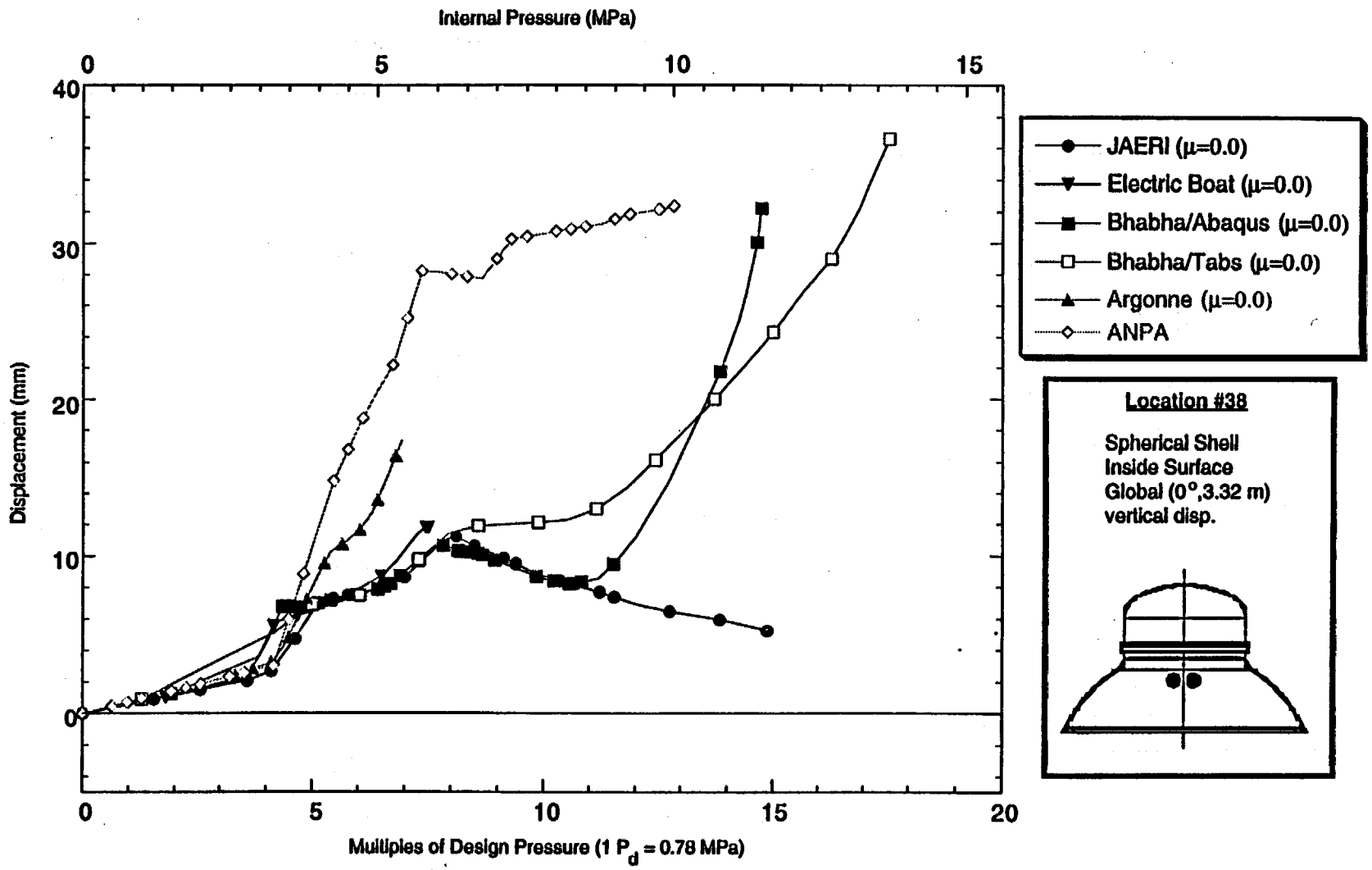

Figure D-77. Standard Output Location #38 (zero friction case)

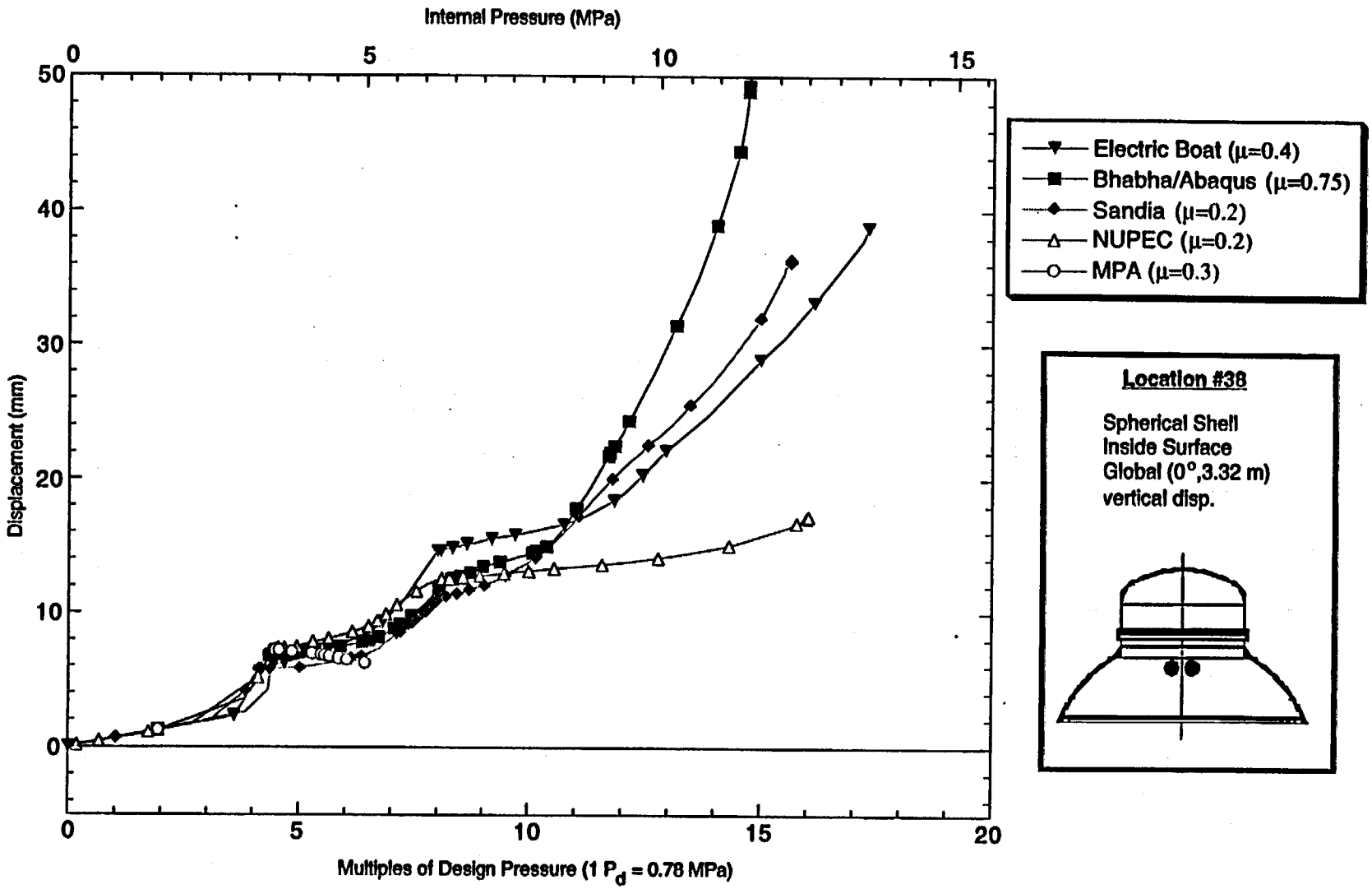

Figure D-78. Standard Output Location #38 (nonzero friction case)

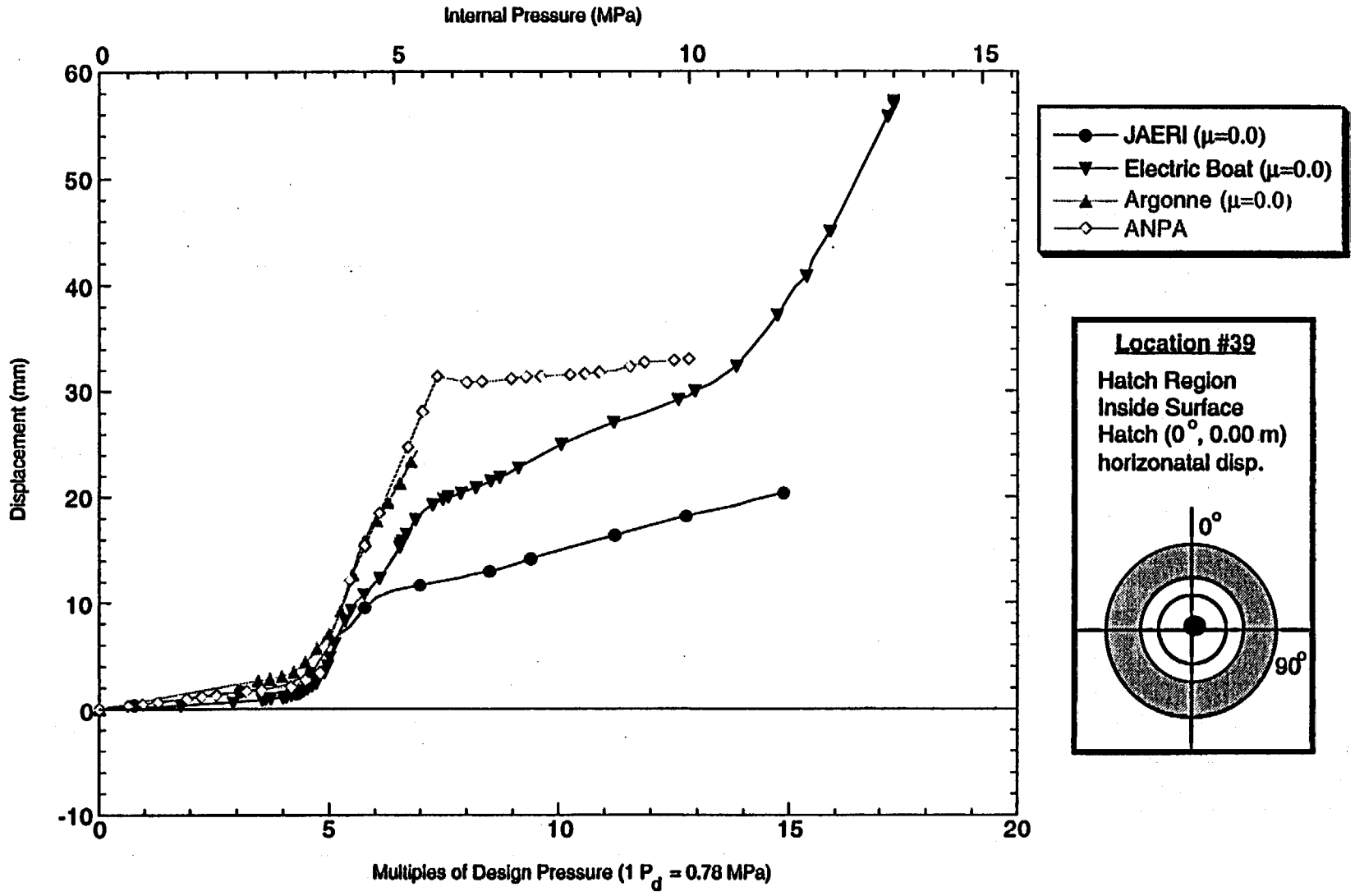

Figure D-79. Standard Output Location #39 (zero friction case)

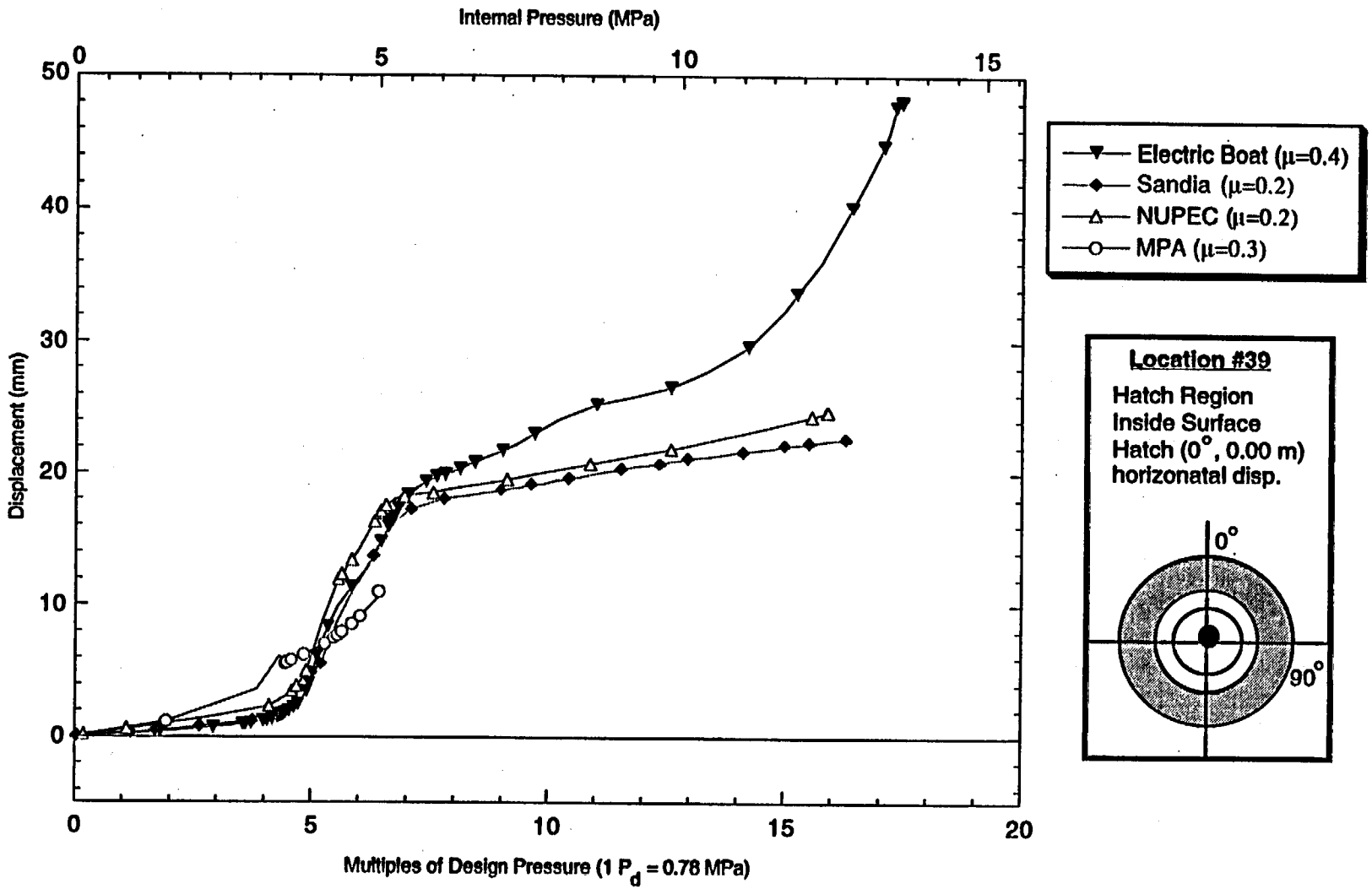

Figure D-80. Standard Output Location #39 (nonzero friction case)

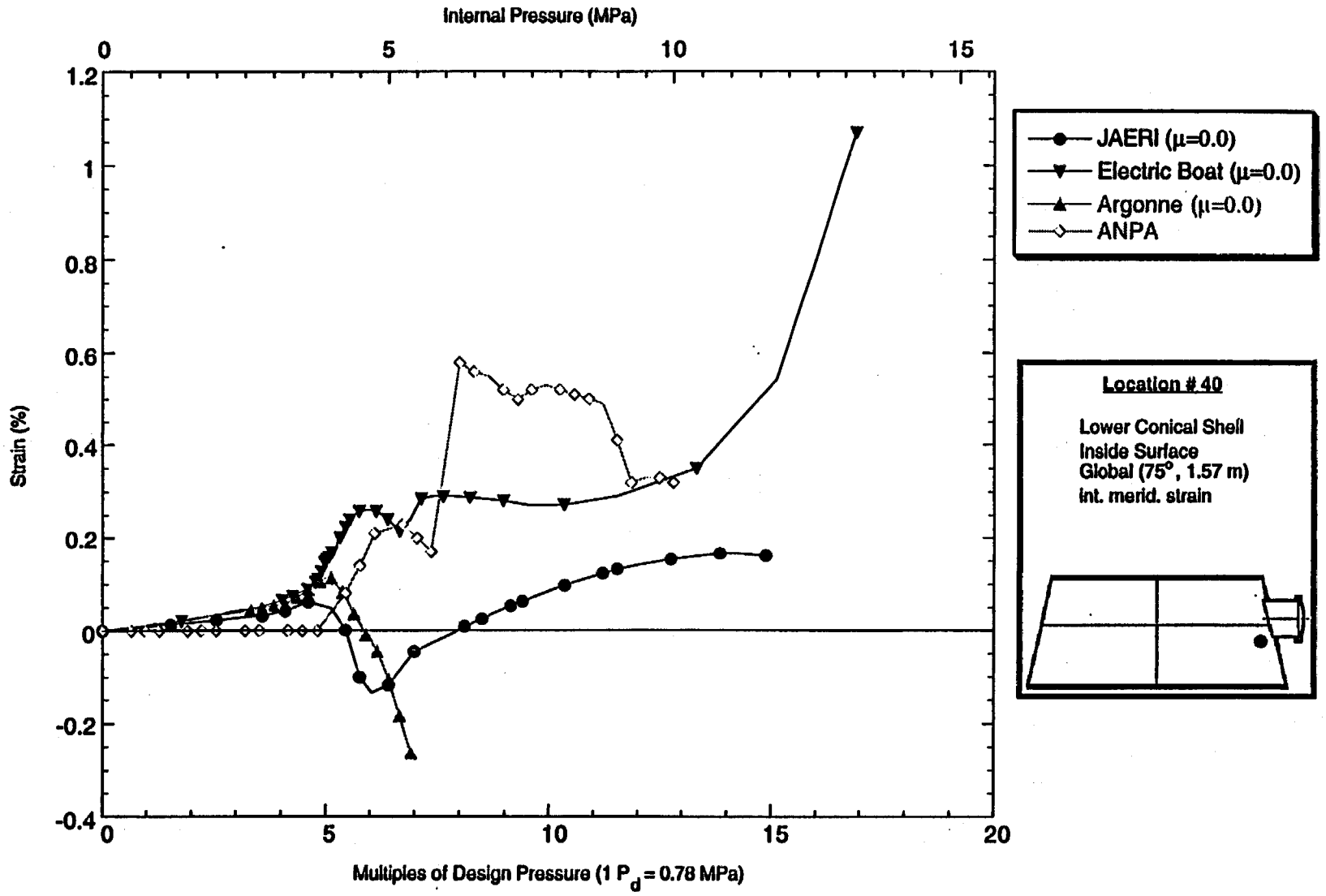

Figure D-81. Standard Output Location #40 (zero friction case)

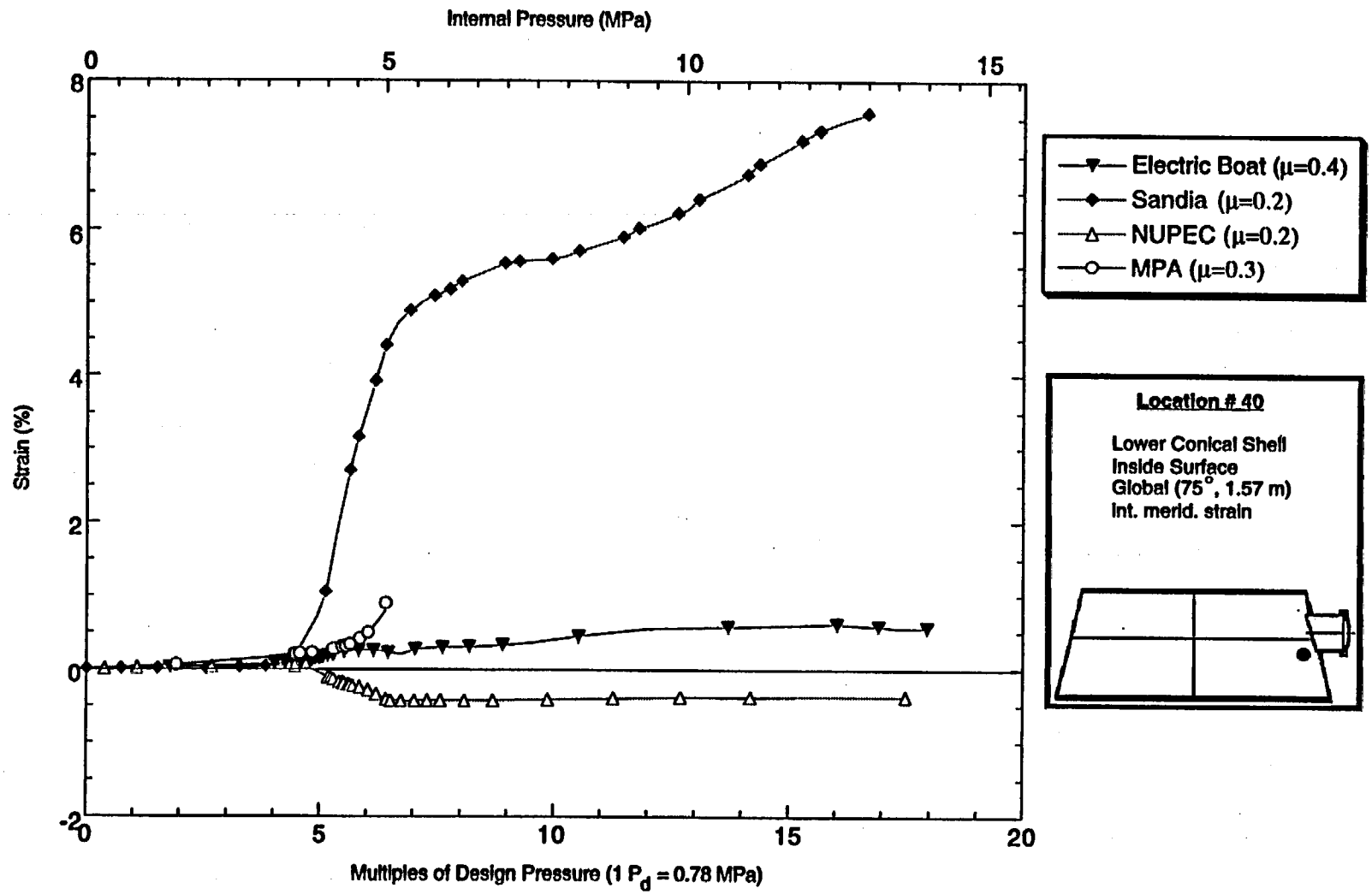

Figure D-82. Standard Output Location #40 (nonzero friction case)

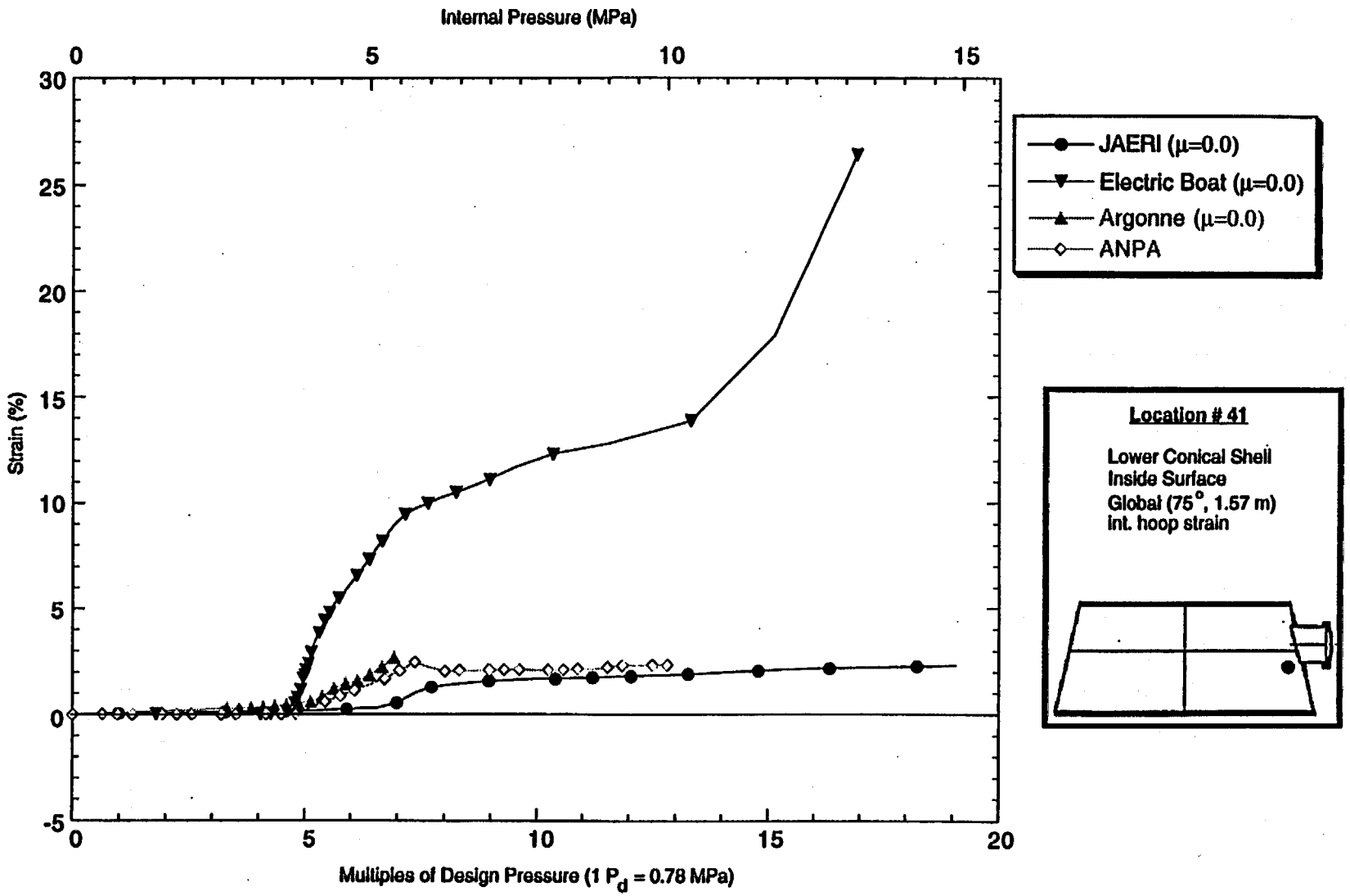

Figure D-83. Standard Output Location #41 (zero friction case)

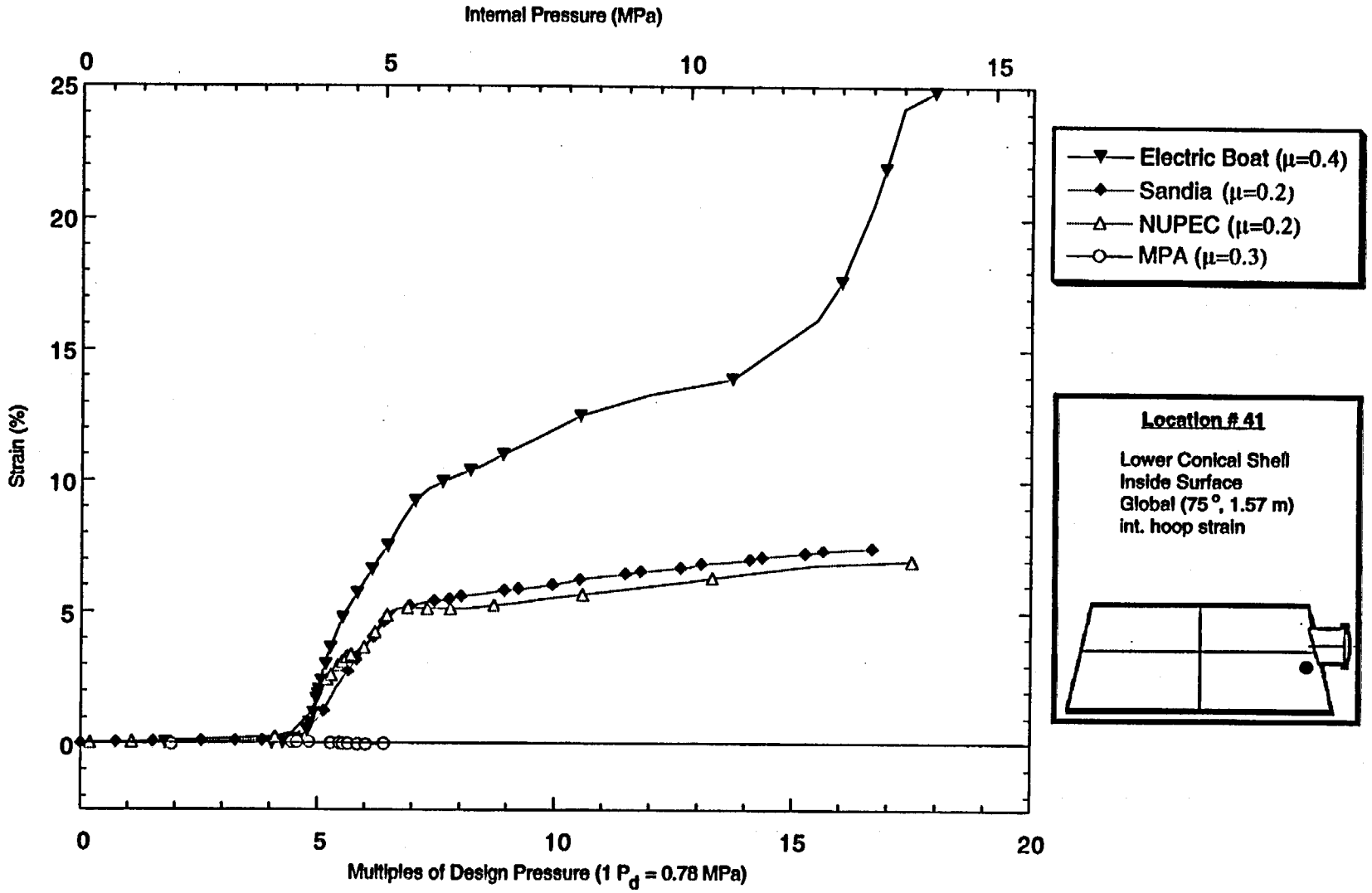

Figure D-84. Standard Output Location #41 (nonzero friction case)

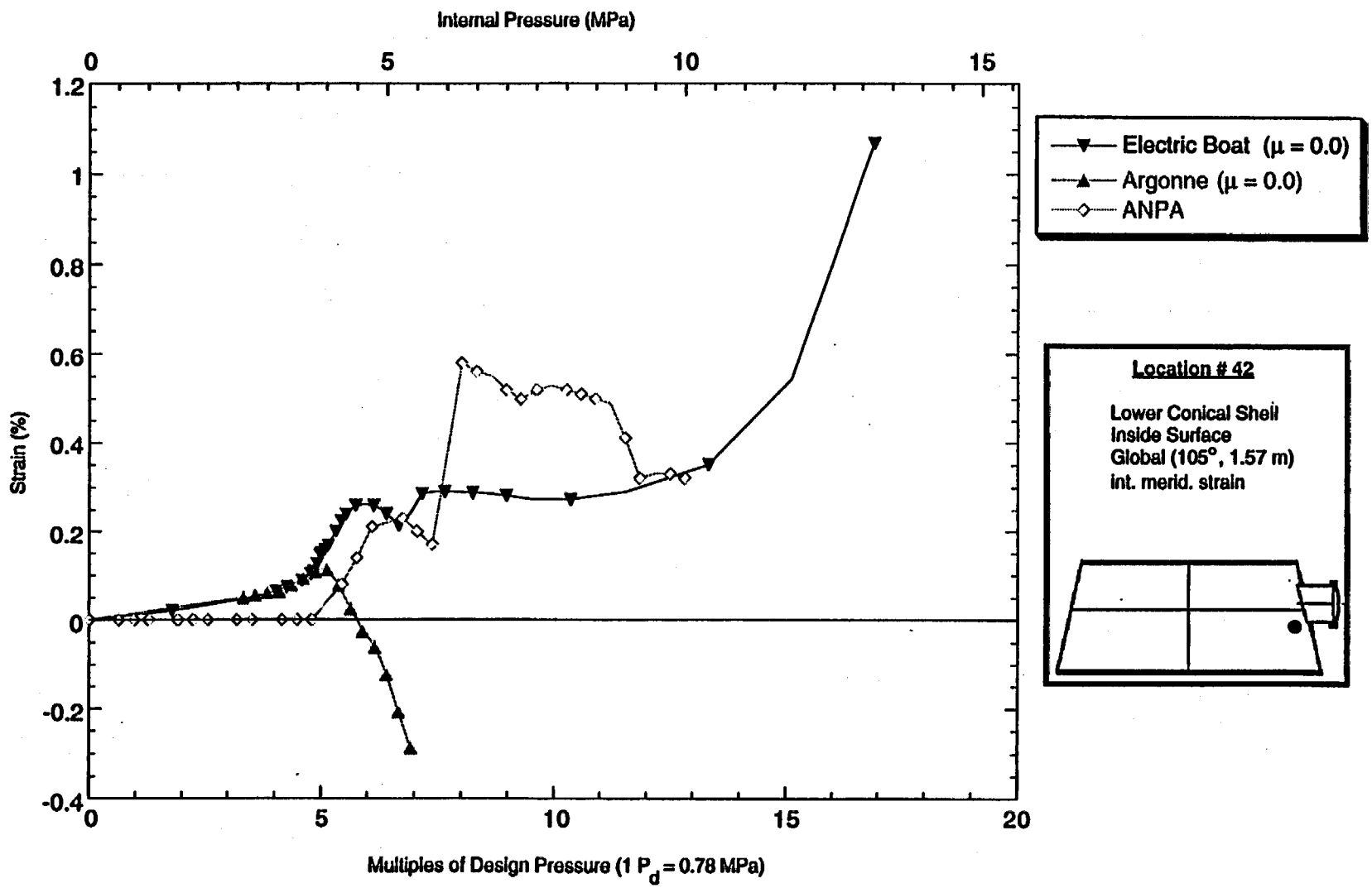

Figure D-85. Standard Output Location #42 (zero friction case)

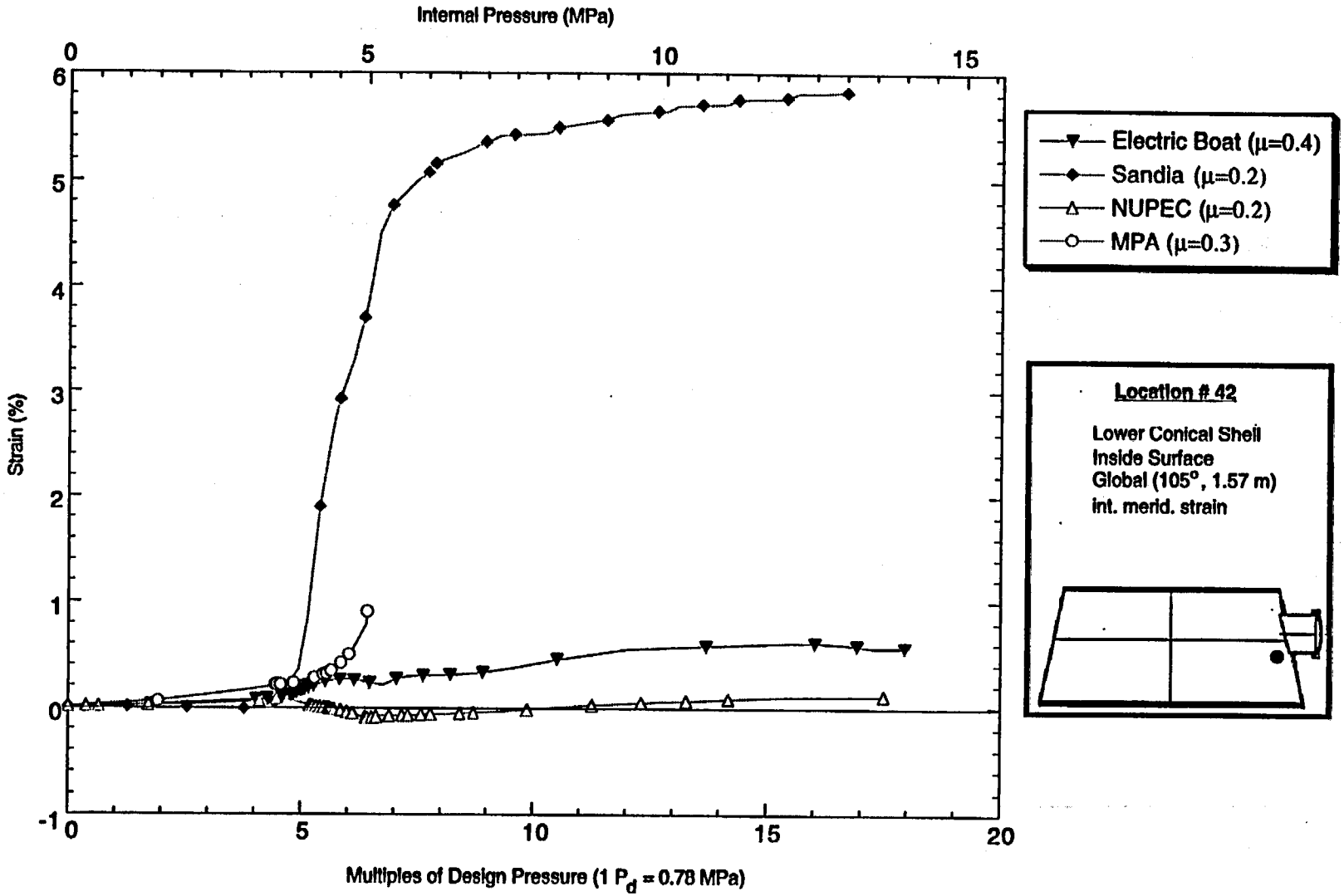

Figure D-86. Standard Output Location #42 (nonzero friction case)

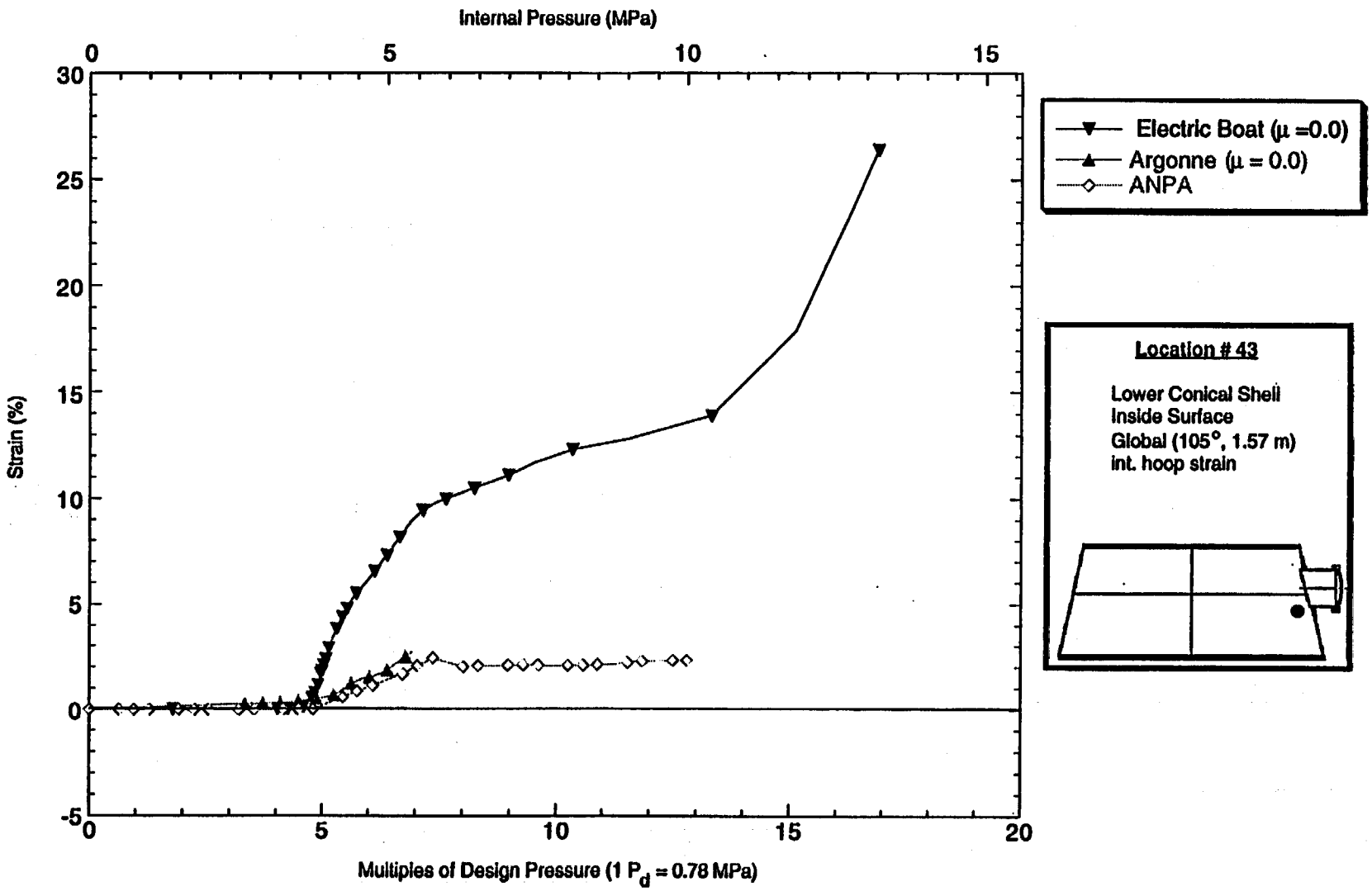

Figure D-87. Standard Output Location #43 (zero friction case)

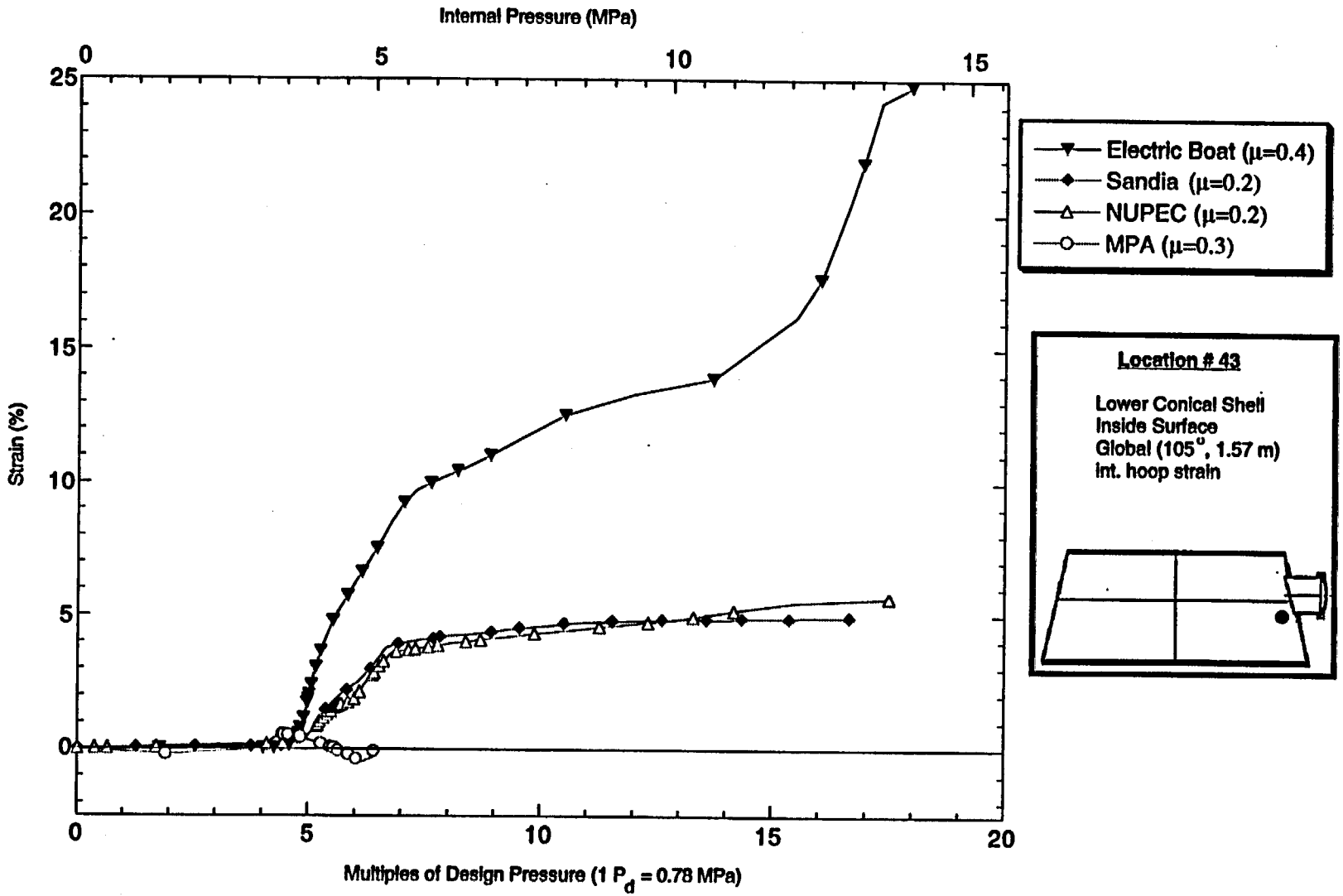

Figure D-88. Standard Output Location #43 (nonzero friction case)

Round Robin Participants' Analysis Reports and Results

Appendix E-1

Argonne National Laboratory

U.S.

Argonne National Laboratory
Round-Robin Pretest Analyses of a 1:10-Scale Steel Containment Vessel

by:

P. A. Pfeiffer, R. F. Kulak
Reactor Engineering Division, Argonne National Laboratory

F. I. Saral
IAEA Fellow, Turkey

and

J. Bonnet
INPG-INSTN Student, France

4.1 INTRODUCTION

Pretest predictions were made by the Reactor Engineering Division of Argonne National Laboratory (ANL) for the response of the 1:10 scale Steel Containment Vessel (SCV) to be tested by Sandia National Laboratories (SNL). The SCV model is scaled 1:10 in overall geometry and a 1:4 scale is used for the thickness from a prototype BWR Mark-II containment. The pretest predictions were made with a full three-dimensional model using the NEPTUNE finite element code. The NEPTUNE [4.1, 4.2 and 4.3] code was primarily intended for 3-D fluid structure interaction problems, however additions [4.4] to the code were made to incorporate simulation of pressurized vessel analyses.

NEPTUNE is a three-dimensional finite element program that was developed to simulate the response of reactor components in 3-D space to design and beyond-design-basis loads. The code has evolved over the years to address safety issues. Since the code was developed to solve a variety of problems, the current version is a general purpose 3-D finite element code primarily suited for nonlinear problems. An important feature of NEPTUNE is its ability to handle nonlinear problems, which often occur during beyond-design basis loads. The element formulations can properly treat large deformations (i.e. geometric nonlinearities), and the rate-type material models can handle large material strains (i.e. material nonlinearities). A Von Mises elastic-plastic constitutive material law is utilized for yielding and post yielding of material. The failure model used is based on a Davis triaxial factor for multiaxial state of stress in combination with Von Mises elastic-plastic constitutive law. Explicit solution algorithms are used to economically solve short duration transient problems, and a dynamic relaxation (DR) method is utilized to simulate quasi-static problems.

The explicit time integration scheme is used in the NEPTUNE code. The numerical algorithm for the explicit time integration is based on the solution of the following equation of motion

$$m_{iI}\ddot{u}_{iI} + f_{iI}^{int} = f_{iI}^{ext}, \text{ (no sum)} \tag{4.1}$$

where m_{iI} is a diagonal mass matrix, u_{iI} is a nodal displacement, f_{iI}^{int} and f_{iI}^{ext} are the internal and external nodal forces, respectively, of node I in the ith direction. Superscript dots are used to denote temporal derivatives. The equations of motion are solved using the central difference formulas. For static analysis the equilibrium equations are given by

$$f_{iI}^{int} = f_{iI}^{ext} \tag{4.2}$$

There are various methods available for obtaining static solutions, NEPTUNE uses the dynamic relaxation (DR) method. Details are provided in Ref. [4.4] on the numerical algorithm utilized for the DR method. The main problem associated with the DR algorithm, as well as other iterative techniques, is whether the current solution vector is close enough to the true solution so that the iteration process can be terminated. Premature termination will result in an incorrect solution, whereas excessive iterations will increase the time of the solution. An effective and efficient way to determine when the iteration process should cease is utilized in the code. The dual criteria used are

$$\frac{\left\| f_{iI}^{ext,n} - f_{iI}^{int,n} \right\|_2}{\left\| f_{iI}^{ext,n} \right\|_2} x100 \le \varepsilon_f \tag{4.3}$$

$$\frac{\left\| \dot{u}_{iI}^{n+1/2} \Delta t \right\|_2}{\left\| u_{iI}^{n+1} \right\|_2} x100 \le \varepsilon_u \tag{4.4}$$

where $\| \quad \|_2$ indicates the Euclidean norm. Accurate results without excessive computations are usually obtained with $\varepsilon_f = 1.0$ and $\varepsilon_u = 0.1$ in Eqs. (4.3) and (4.4). Once these equations are satisfied, the iteration process is terminated, a load increment is applied, and the iteration process is restarted. The DR method does not change the basic architecture of the central difference scheme, but enhances it so that static problems can be solved.

4.2 MODEL DESCRIPTION

The finite element model is depicted in Figs. 4.1 and 4.2. Figure 4.1 is the SCV solid model and Fig. 4.2 is the Contact Structure (CS) solid model. The overall model contains 27538 nodes (3 degrees of freedom) and 18001 elements. The SCV consists of 9734 quadrilateral plate elements for the steel shell and 400 bar elements for the 5 stiffeners (i.e. 80 bar elements for each stiffener). The CS consists of 3888 quadrilateral plate elements

for the steel shell and 3979 contact elements are located between the CS and the SCV. The model contains 9790 translational nodes and 9790 rotational nodes in the SCV and 3979 translational nodes and 3979 rotational nodes in the CS.

The model is subjected to a fixed boundary condition (no translation or rotation allowed) at the 0.000 m elevation for the SCV and CS, and at the -0.400 m elevation of the SCV. These are the upper and lower elevation of the ring support girder. It was assumed that the support girder was rigid, and thus, a fixed boundary condition was used.

4.3 MATERIAL DATA

The material test data that was provided by SNL was used to obtain material property values for input to the constitutive model for metals. The true stress - true strain data was analyzed by a best fit least square algorithm. The data was split into two portions, elastic and elastic-plastic, with each portion fit to a line equation. The bi-linear stress-strain data is used as input for the material law in NEPTUNE. The fits are shown in Figs. 4.3 through 4.14. Figure 4.3 indicates a Young's modulus of 2.09×10^{11} Pa, yield stress of 416.8 MPa, plastic modulus of 1.4×10^{9} Pa, ultimate stress of 694 MPa and an ultimate failure strain of 20%. The coefficient of correlation, r, for the plastic region of the data fits varies from 0.941 to 0.986 with most of data fits around r = 0.97, which indicates a very good fit of the all the test data provided. When no test data was available for a material with a certain thickness in the finite element model, the closest thickness for the material was used for material properties. Poisson's ratio was assumes to be 0.33 for all materials. The CS was assumed to have ASTM-A36 steel properties as given by SNL.

4.4 FAILURE MODEL

An elastic-plastic analysis was performed and failure is assumed to occur when the effective plastic strain reaches the ultimate strain. When an elastic-plastic analysis is utilized, the effect of multiaxial stress needs to be accounted for in the analysis. Manjoine [4.5] discusses the effect of multiaxial stress on the uniaxial stress-strain behavior. Reference [4.6] also discusses the effect of multiaxial stress on failure. Essentially, the ductility of a material can vary under a multiaxial state of stress, which in turn may reduce the plastic strain at which the material will fail. Manjoine proposed a formulation for the ductility ratio based on the Davis triaxial factor. The Davis triaxiality factor, TF_D, is equal to the sum of the principal stresses divided by the octahedral shearing stress and normalized to unity for plane stress or uniaxial tension. Thus,

$$TF_D = \frac{\sigma_1 + \sigma_2 + \sigma_3}{\frac{1}{\sqrt{2}}\left[(\sigma_1 - \sigma_2)^2 + (\sigma_2 - \sigma_3)^2 + (\sigma_3 - \sigma_1)^2\right]^{1/2}} \tag{4.5}$$

where σ_1, σ_2 and σ_3 are the principal stresses. The ductility ratio is defined as

$$c = \frac{\text{effective von mises strain}}{\text{tensile elongation}} \tag{4.6}$$

and the ductility ratio can be described by the triaxiality factor as

$$c = 2^{(1-TF_D)}, c_{max} \leq 2.0 \tag{4.7}$$

Therefore, under multiaxial stress states the equivalent uniaxial strain is

$$\varepsilon_u = \frac{\varepsilon_{eff}}{c} \tag{4.8}$$

where ε_{eff} is the calculated effective Von Mises strain and ε_u is the strain to be compared with, i.e. uniaxial or tensile elongation data. The value of TF_D under uniaxial stress is 0 and thus c = 1.0, and the value of TF_D under a biaxial state of stress ($\sigma_1 = \sigma_2$) is 2.0, and thus, c = 0.5. Therefore under a biaxial state of stress ($\sigma_1 = \sigma_2$), the strain to failure is reduced by 50%. This is important when the strain to failure is the dominating failure mode under multiaxial stresses.

4.5 CONTACT ELEMENT

The contact element utilized in this analysis was a line interface contact element that consists of two nodes connected by a spring type element. This element is based upon a penalty formulation that allows compression only, i.e. no tension. Thus, when contact is made a compressive force develops, and when the nodes separate a zero tension force develops, which allows the two nodes to act independently. Reference [4.7] provides the details for the contact element formulation used in NEPTUNE, Ref. [4.8] addresses the critical time step concerns with this type of element, and Ref. [4.4] provides an overview of the contact elements.

The contact element requires the initial gap distance, between the two contact nodes, for input to determine when contact will occur. The actual measured gap distances were used in the model for the elevations and angles provided by SNL. A double interpolation was done with the gap data to provide an approximate gap distance for the contact element locations that were in-between the measured locations.

4.6 VESSEL RESPONSE DUE TO PRESSURIZATION

The load is a pressure incrementally applied to the inside surface of the SCV. Initially the vessel model was run elasticity to determine when the yield stress will be reached under internal pressure. That value is approximately 2.6 MPa internal pressure with yielding near the bottom connection of the equipment hatch and the vessel. The vessel model was then analyzed for an elastic-plastic response. A pressure of 2.6 MPa is applied in the first load step, and 0.1 MPa increments are used thereafter for each load step. The model was

pressurized incrementally up to failure, which occurred at 5.5 MPa. At each load step, static equilibrium was checked with Eqs. 4.3 and 4.4 using $\varepsilon_f = 1.5$ and $\varepsilon_u = 0.1$ for the convergence check. Static equilibrium was obtained for load steps 1 through 29 (i.e. internal pressure = 5.4 MPa).

Yielding of the vessel occurred first at the bottom of the equipment hatch sleeve and the vessel reinforcing plate ($\theta_H = 180^o$, $R_H = 200$ mm in the hatch coordinate system) for a pressure of 2.6 MPa. At a pressure of 2.8 MPa yielding occurs all around (360°) the knuckle at the top (elev. 3.431 m) and the bottom (elev. 3.354 m). Contact between the CS and SCV occurs at 4.4 MPa at an elevation of 2.402 m. The vessel model fails at a pressure of 5.5 MPa at the location just above the knuckle in the 6 mm thick upper cylindrical shell. The failure plastic strain is reduced to 9.9% strain because of the biaxial state of stress in the shell, the value of c in Eqs. 4.7 and 4.8 is approximately 0.5.

Displacements and strains for the model are given in Figs. 4.15 through 4.34, the displacements are shown in Figs. 4.15 through 4.19 and the strains are depicted in Figs. 4.20 through 4.34. The locations are the same as the standard PLOT ID requested by SNL, the PLOT ID numbers are given in the ordinate label of the figures. However, the displacement plots (Figs. 4.15 through 4.19) are for the nodes in the finite element model which are the centerline deflections of the plate elements, i.e. approximately the average of the inside and outside deflections of the plate. Thus, for PLOT ID #36 in Fig. 4.16, the deflection shown is the average of the inside and outside deflection. In Figs. 4.15, 4.17, 4.18 and 4.19 the centerline deflections are very close to the inside deflections requested, because of the deflection shape at these locations in the vessel. The figures indicate the elastic and elastic-plastic response of the SCV to internal pressure.

4.7 BUCKLING EFFECTS IN TOP HEAD

No buckling occurred during the internal pressurization of the SCV model. The DR method employed is capable of capturing buckling behavior, but none was observed.

4.8 FRICTION EFFECTS BETWEEN SCV AND THE CS

The contact element that was used in the analysis does not include friction effects, thus no transverse force develops when the CS and SCV contact. This preliminary analysis indicates that when two nodes contact, very little transverse motion occurs after contact. Thus, if friction were included it would be of a secondary effect and should not be a major concern by our estimation.

4.9 INITIAL YIELD AND CONTACT

Yielding of the vessel occurred at the bottom of the equipment hatch sleeve and the vessel reinforcing plate ($\theta_H = 180^o$, $R_H = 200$ mm in the hatch coordinate system) at a pressure of 2.6 MPa. Initial contact between the CS and SCV occurred at 4.4 MPa at an elevation

of 2.402 m and locally at $\theta_G = 0^o$, 90°, 180° and 270° as indicated in Fig. 4.35. The dark lines on the vessel surface indicate initial contact locations between the CS and SCV.

4.10 CONTACT RESPONSE

The contact response is depicted in Figs. 4.35 through 4.40 for increasing pressures. Contact initially occurs at 4.4 MPa and is maintained up until the failure pressure of 5.5 MPa. Contact is indicated by the short black lines shown on the surface of the SCV. The figures indicate how the contact region grows as the pressure increases. Contact is predicted to be confined between elevations of 1.656 m to 2.548 m as shown in Fig. 4.40.

4.11 FAILURE PRESSURE

The vessel model fails at an internal pressure of 5.5 MPa at the location just above the knuckle in the 6 mm thick upper cylindrical shell. The uniaxial ultimate strain (plastic failure strain) is reduced to 9.9% strain because of the biaxial state of stress in the shell; the value of c in Eqs. 4.7 and 4.8 is approximately 0.5. Once the 6 mm shell fails, the failure could propagate around the circumference and the top head and upper cylindrical shell will exit (fly off) the SCV.

4.12 SUMMARY

The predicted failure of the steel containment vessel is at an internal pressure of 5.5 MPa. The location of the failure is just above the knuckle, and could occur at any point along the circumference in the upper cylindrical shell. Therefore, a maximum pressure of 5.4 MPa is estimated before a failure will occur. The maximum pressure with high confidence (>95%) that there is a low probability of failure (<1%) of the model would be about 90 % of this value, i.e. maximum internal pressure of 4.9 MPa. The 90% factor is based on the uncertainties in modeling, code calculation, material property response, and residual stresses due to welding and manufacturing.

The vessel will remain elastic until an internal pressure of 2.6 MPa is reached. The vessel wall is predicted to impact the contact structure at an internal pressure of 4.4 MPa.

4.13 ACKNOWLEDGMENT

This work was performed under the auspices of the U.S. Department of Energy, Technology Support Programs, under Contract W-31-109-Eng-38.

6.0 REFERENCES

[4.1] R. F. Kulak, "A Finite Element Formulation for Fluid-Structure Interaction in Three-Dimensional Space", J. of Pressure Vessel Technology, Vol. 103, No. 2, 1981, pp. 183-190.

[4.2] R. F. Kulak, "A Finite element Quasi-Eulerian Method for Three-Dimensional Fluid-Structure Interactions", Computers and Structures, Vol. 18, No. 2, 1984, pp. 319-332.

[4.3] R. F. Kulak, "Three-Dimensional Fluid-Structure Coupling in Transient Analysis", Computers and Structures, Vol. 21, No. 3, 1985, pp. 529-542.

[4.4] R. F. Kulak and C. Fiala, "NEPTUNE: A System of Finite Element Programs for Three-Dimensional Nonlinear Analysis," Nuclear Engineering and Design, Vol. 106, 1988, pp. 47-68.

[4.5] M. J. Manjoine, "Creep-Rupture Behavior of Weldments," Welding Journal, Proceedings of American Welding Society, Vol. 49, 1982, pp. 505-575.

[4.6] R. A. Dameron, R. S. Dunham, Y. R. Rashid and H. T. Tang, "Conclusions of the EPRI Concrete Containment Research Program," Nuclear Engineering and Design, Vol. 125, 1991, pp. 41-55.

[4.7] R. F. Kulak, "Adaptive Contact Elements for Three-Dimensional Explicit Transient Analysis," Computer Methods in Appl. Mechanics and Eng., Vol. 72, 1989, pp. 121-151.

[4.8] R. F. Kulak, "Critical Time Step Estimation for Three-Dimensional Explicit Impact Analysis," Structures Under Shock and Impact, Proc of the 1st Int. Conf., Cambridge, MA, July 1989, pp. 156-163.

LIST OF FIGURES

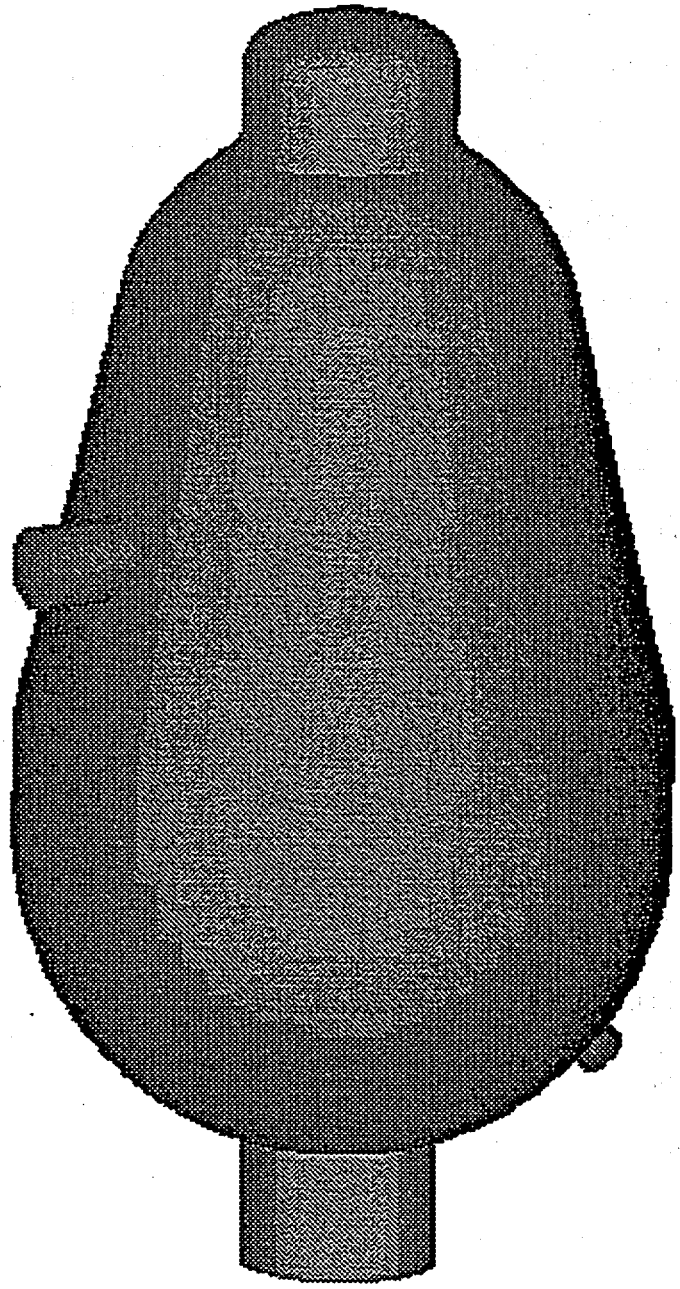

Figure 4.1 Solid Finite Element Model of SCV

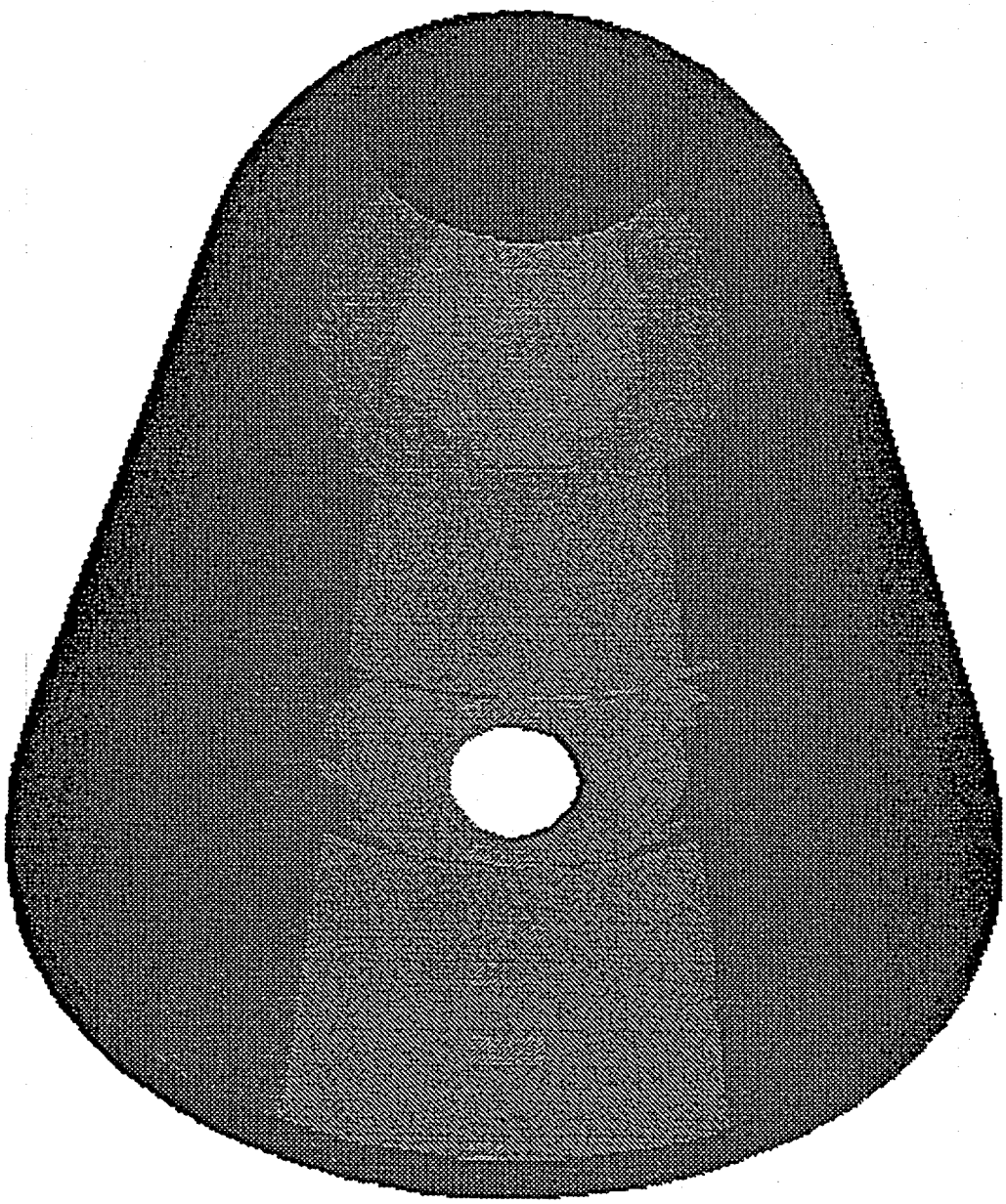

Figure 4.2 Solid Finite Element Model of CS

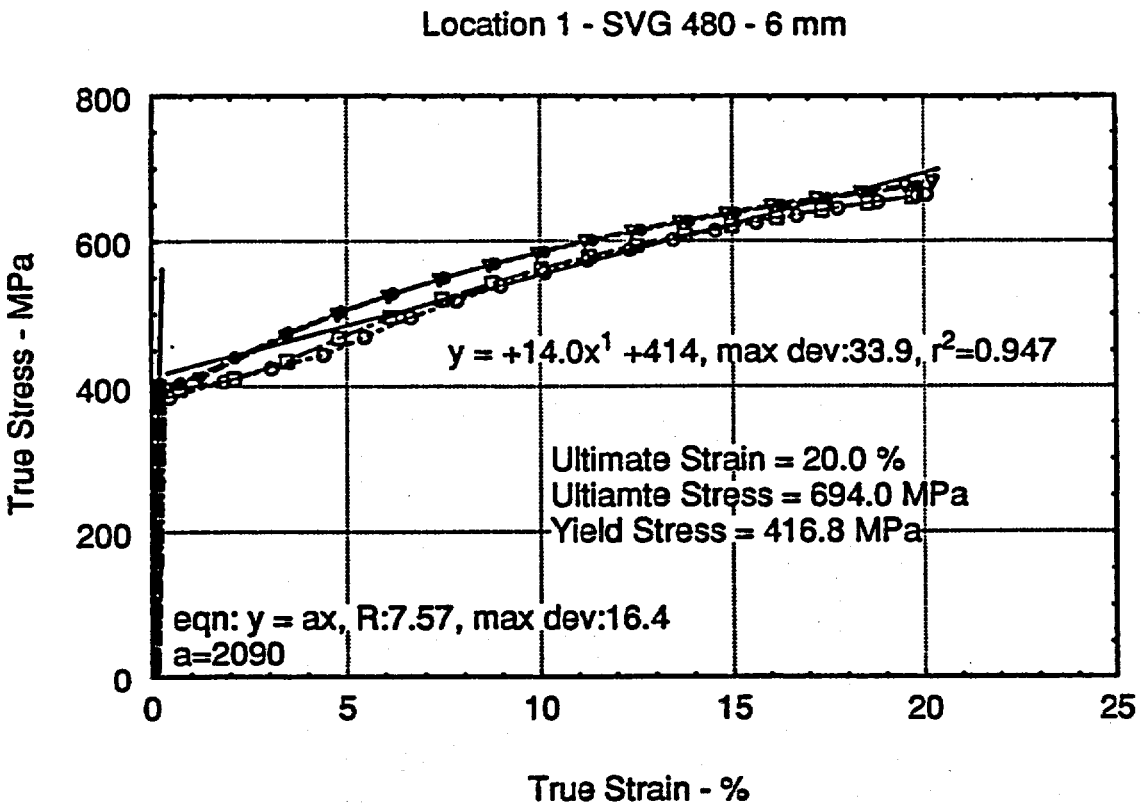

Figure 4.3 Material Property Fit at Test Location 1

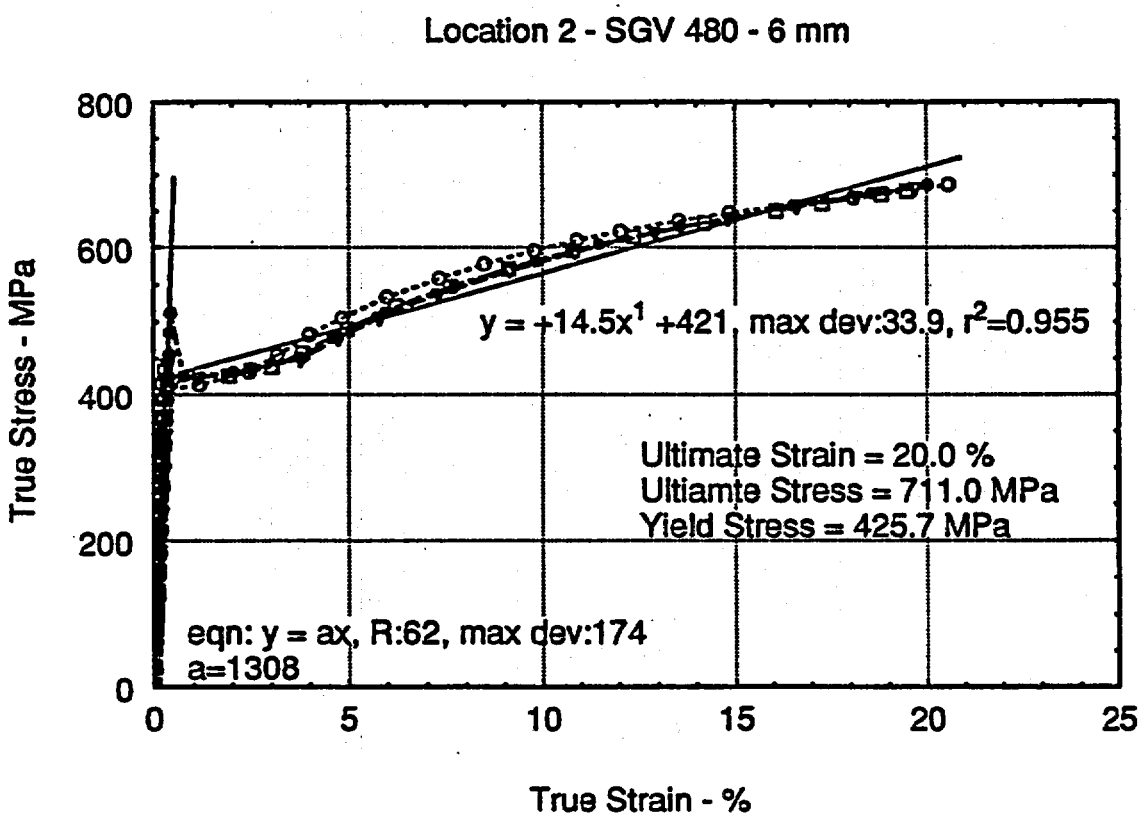

Figure 4.4 Material Property Fit at Test Location 2

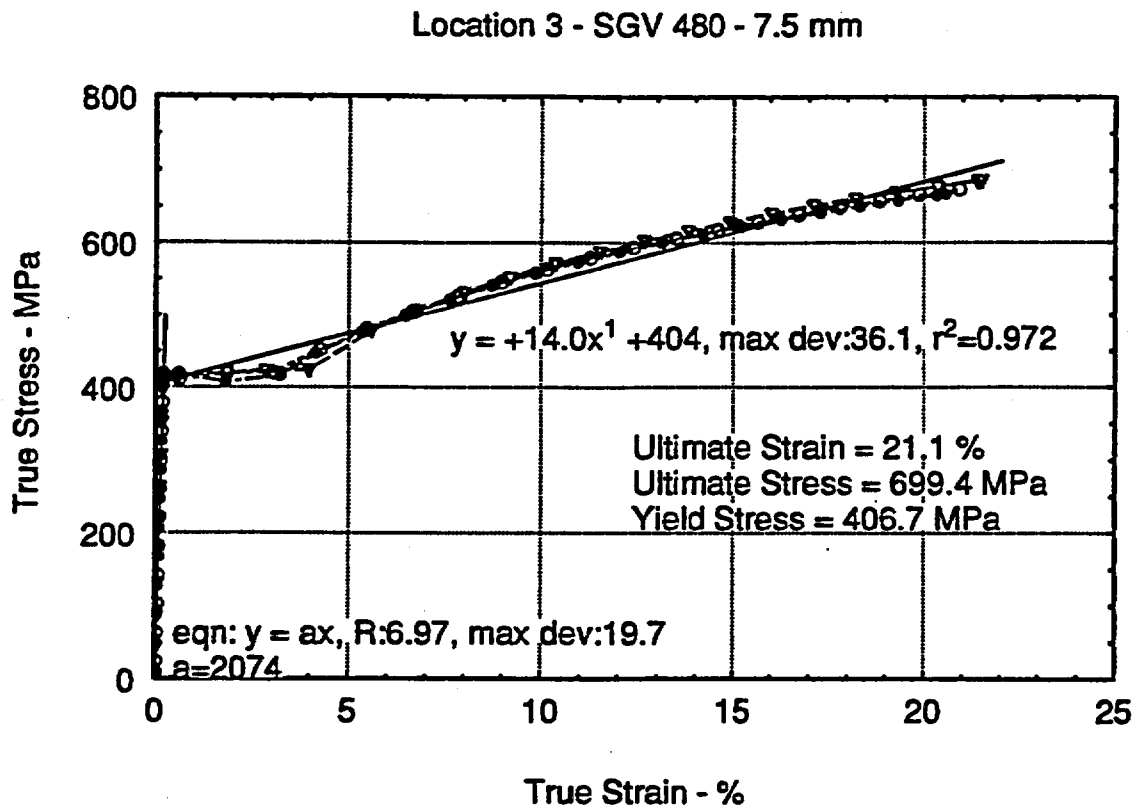

Figure 4.5 Material Property Fit at Test Location 3

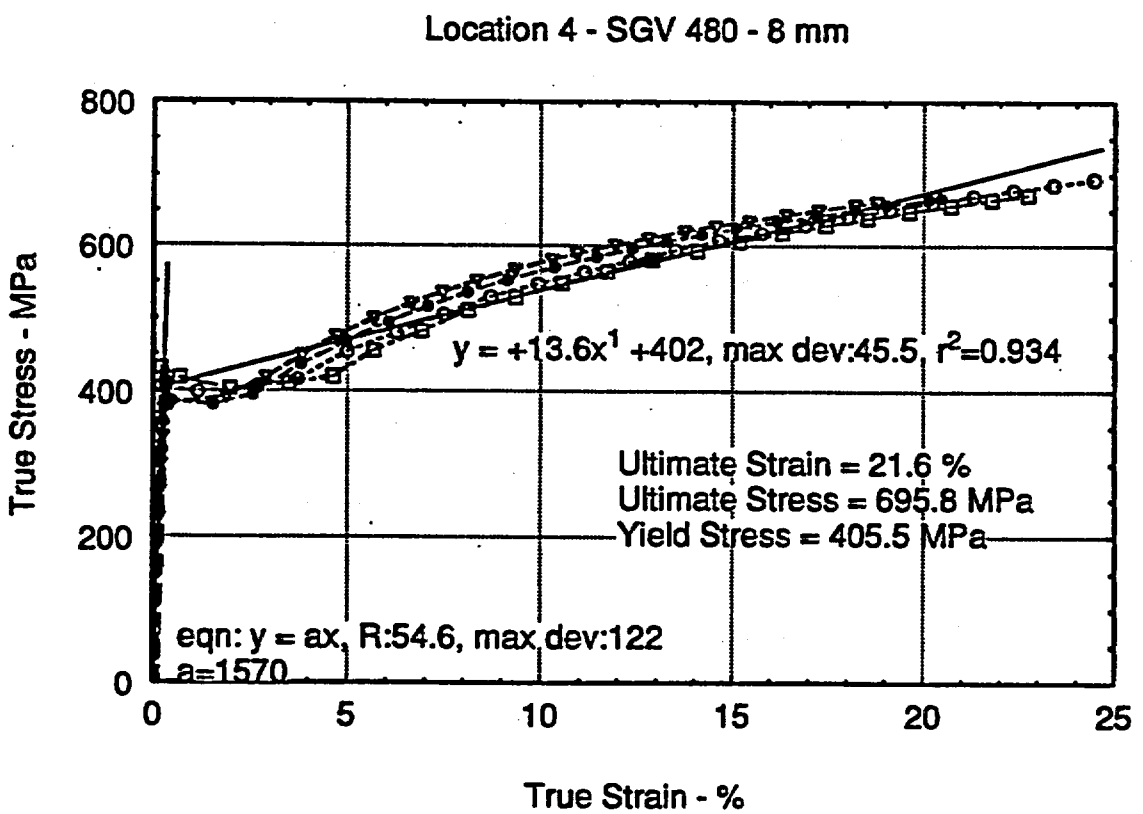

Figure 4.6 Material Property Fit at Test Location 4

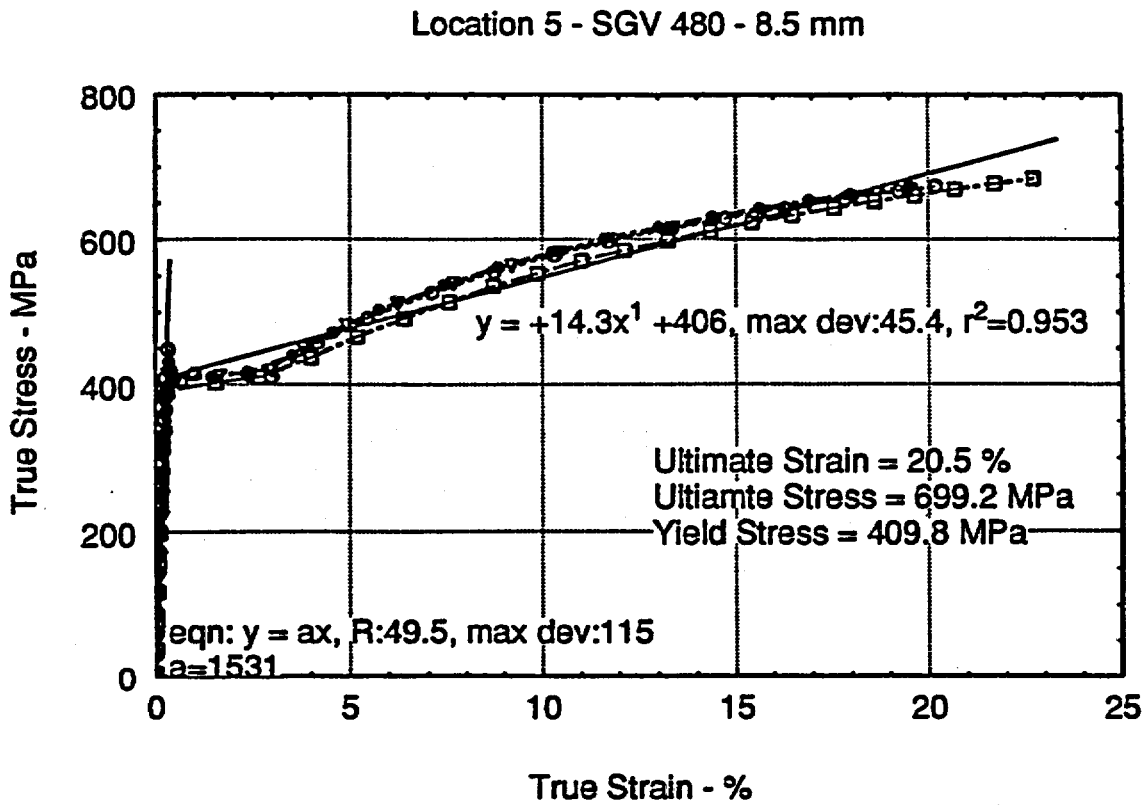

Figure 4.7 Material Property Fit at Test Location 5

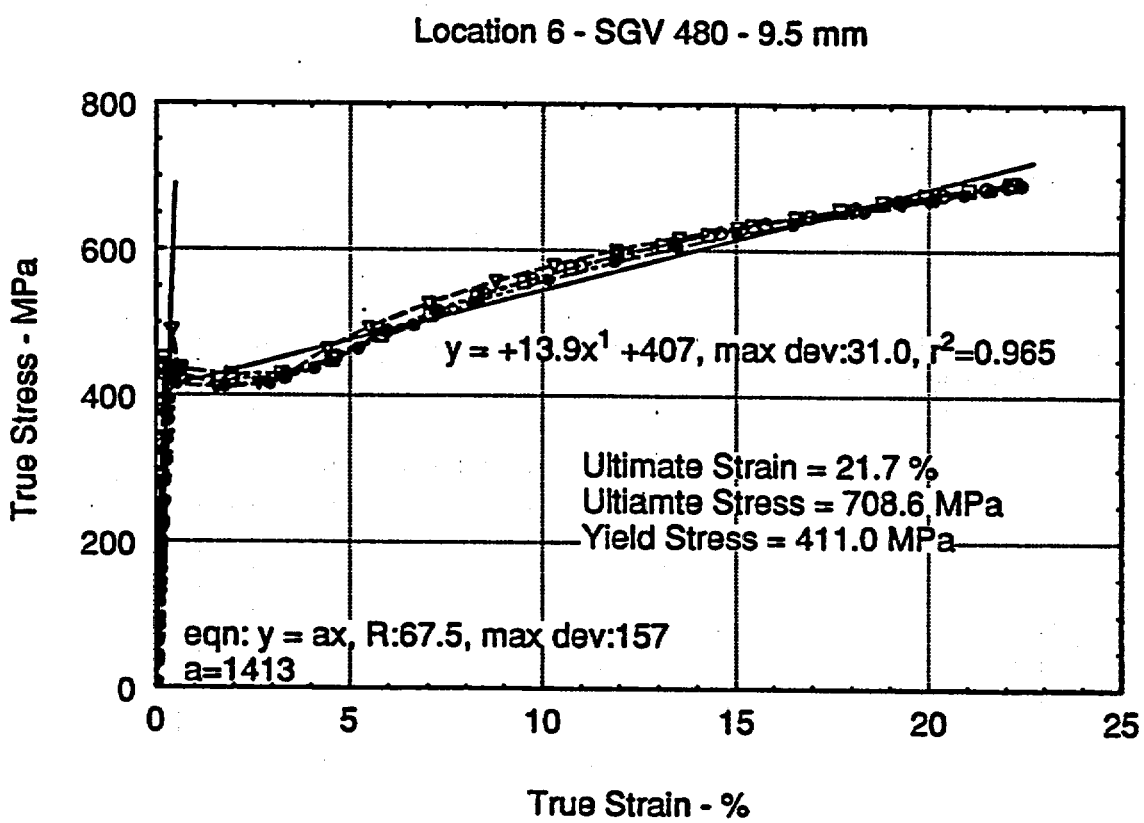

Figure 4.8 Material Property Fit at Test Location 6

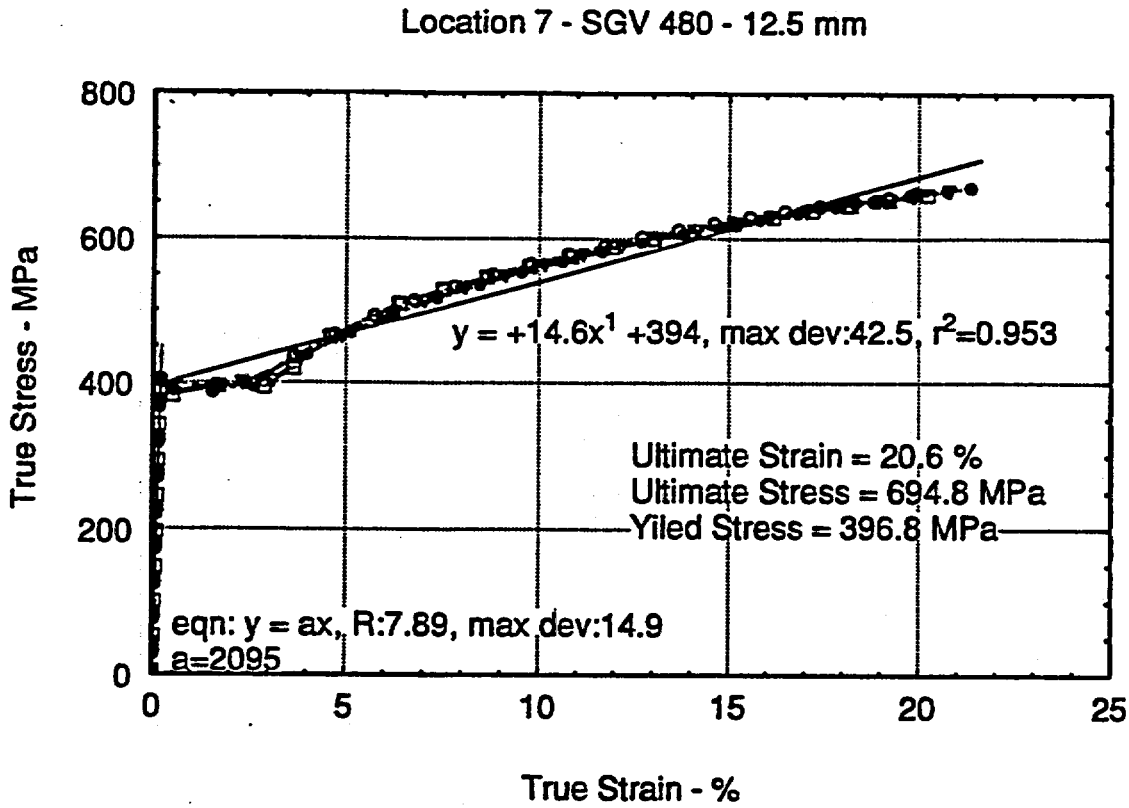

Figure 4.9 Material Property Fit at Test Location 7

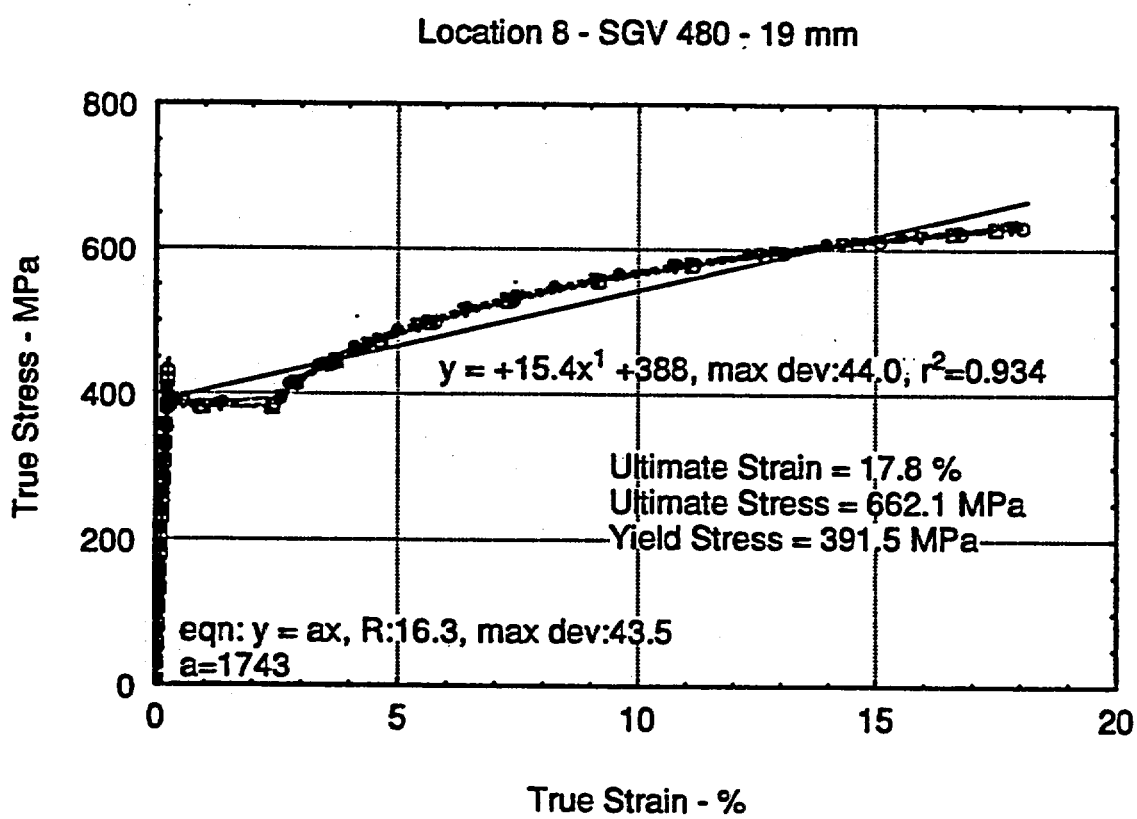

Figure 4.10 Material Property Fit at Test Location 8

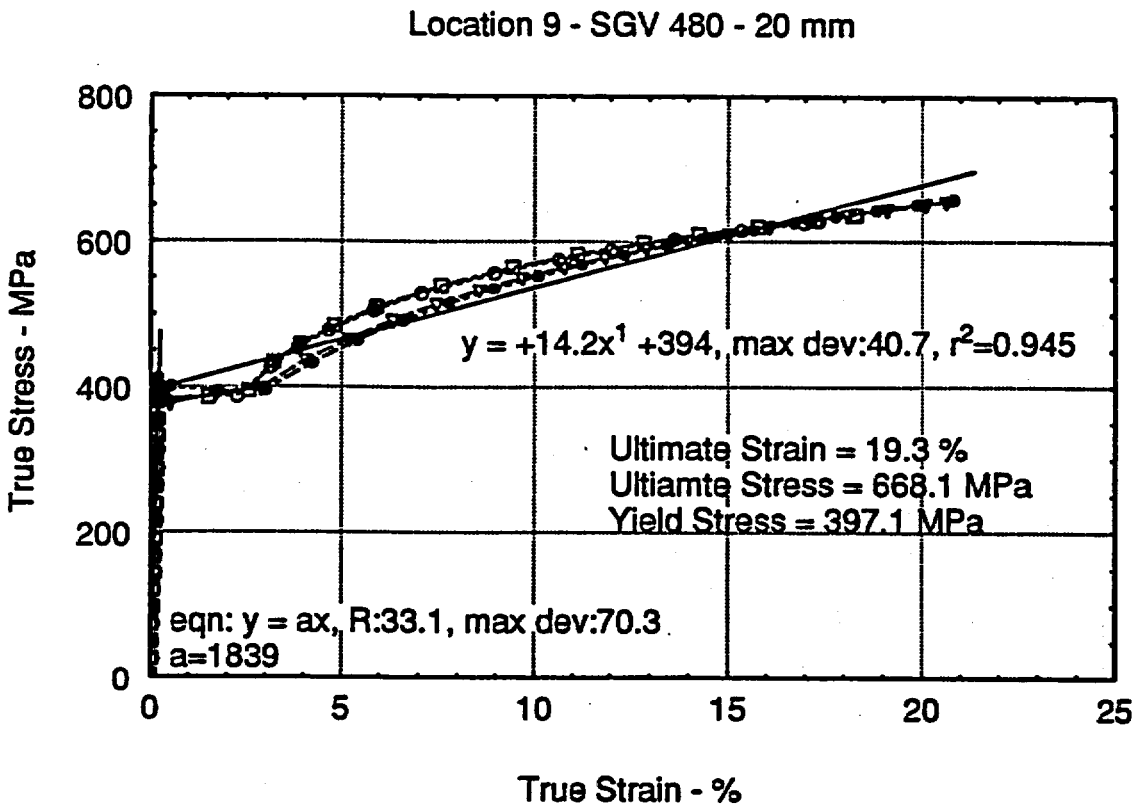

Figure 4.11 Material Property Fit at Test Location 9

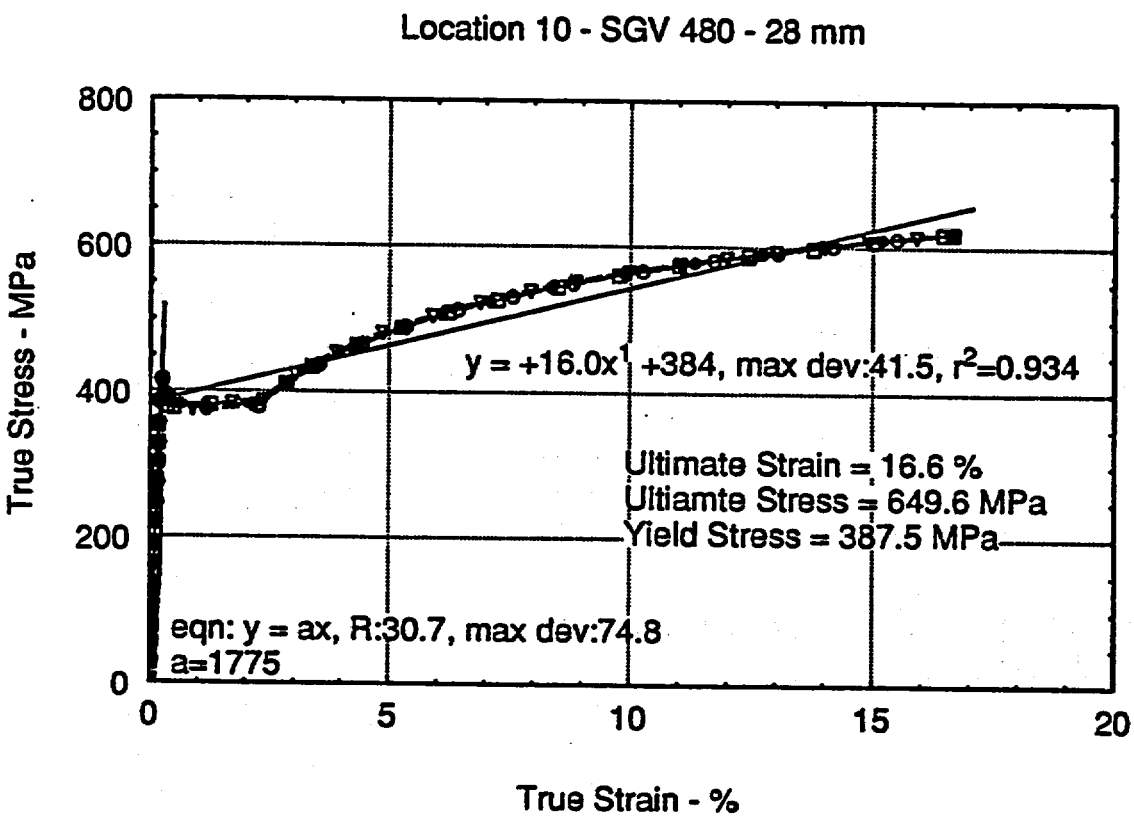

Figure 4.12 Material Property Fit at Test Location 10

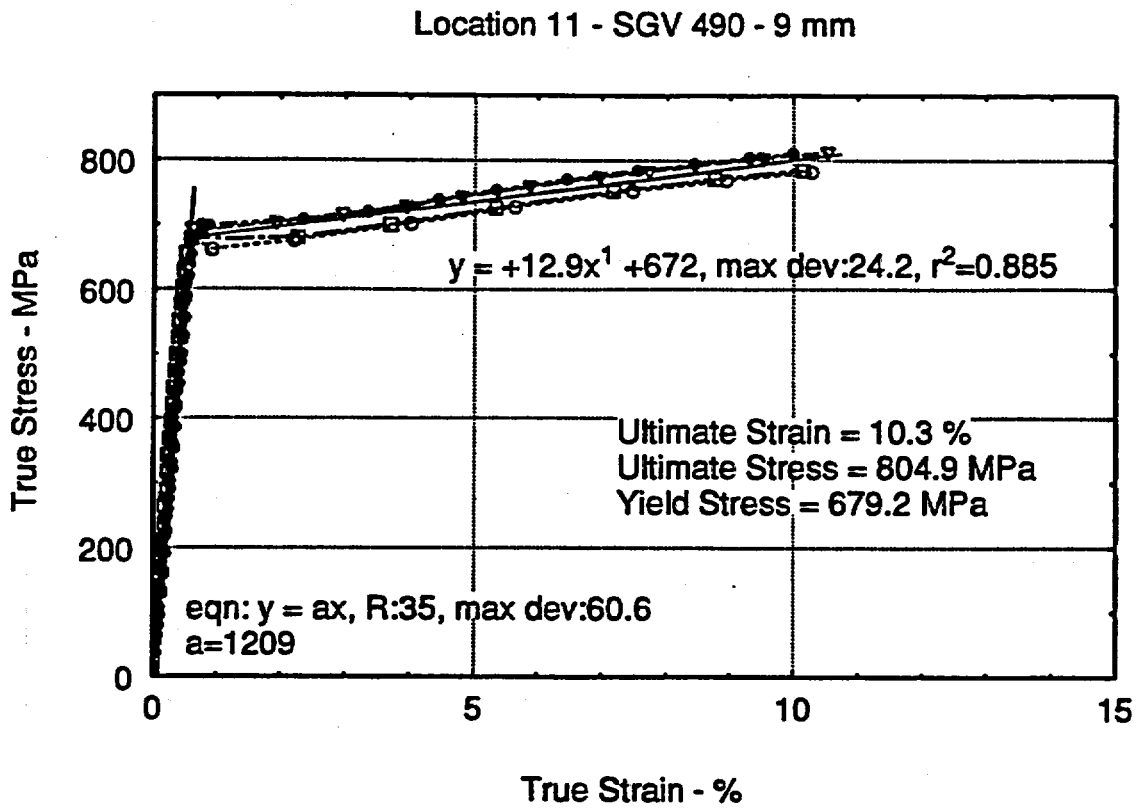

Figure 4.13 Material Property Fit at Test Location 11

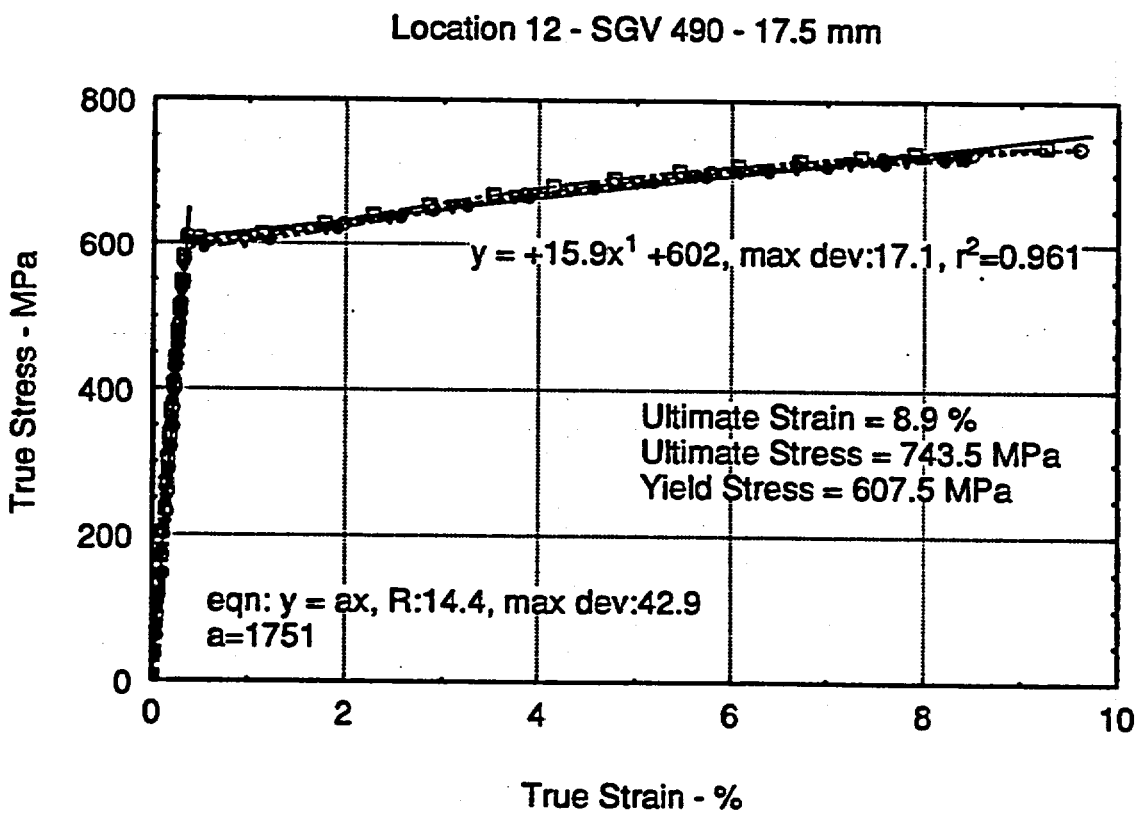

Figure 4.14 Material Property Fit at Test Location 12

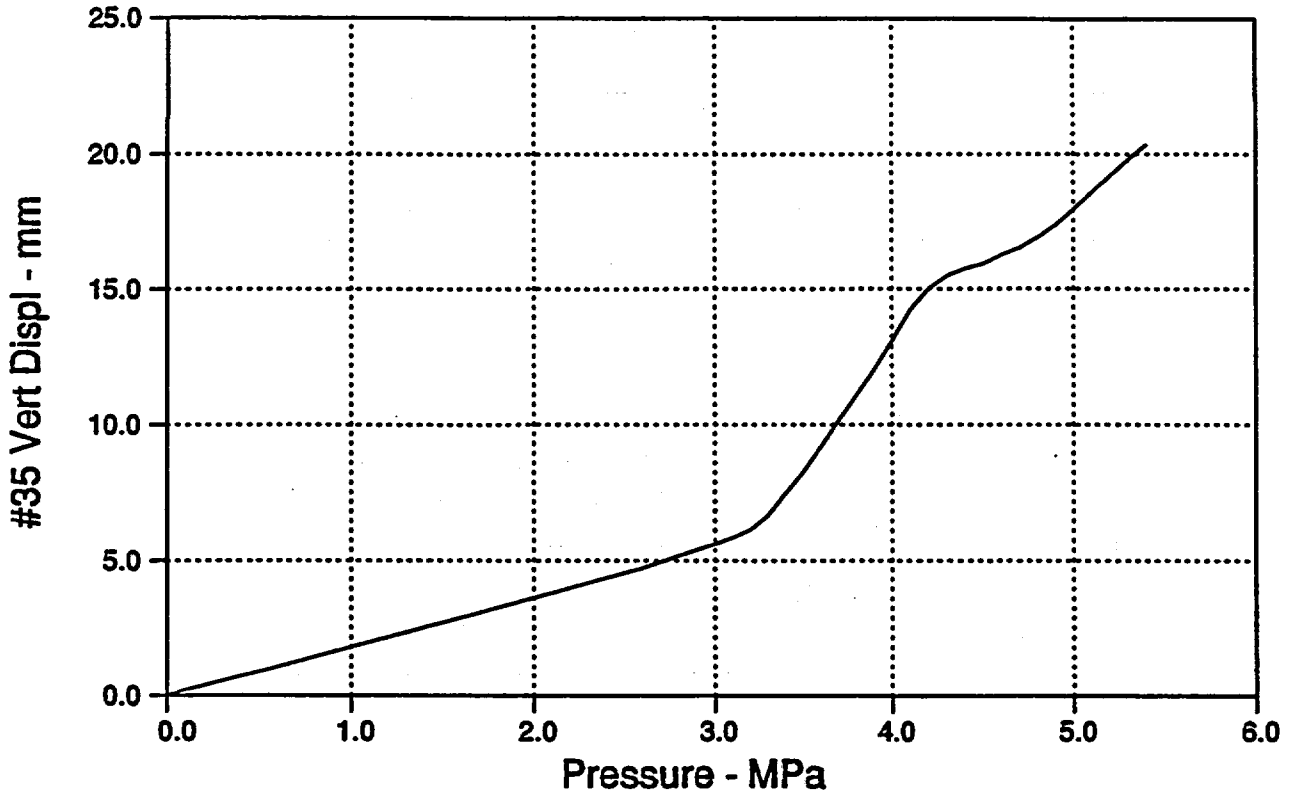

Figure 4.15 Vertical Displacement at Apex of Top Head

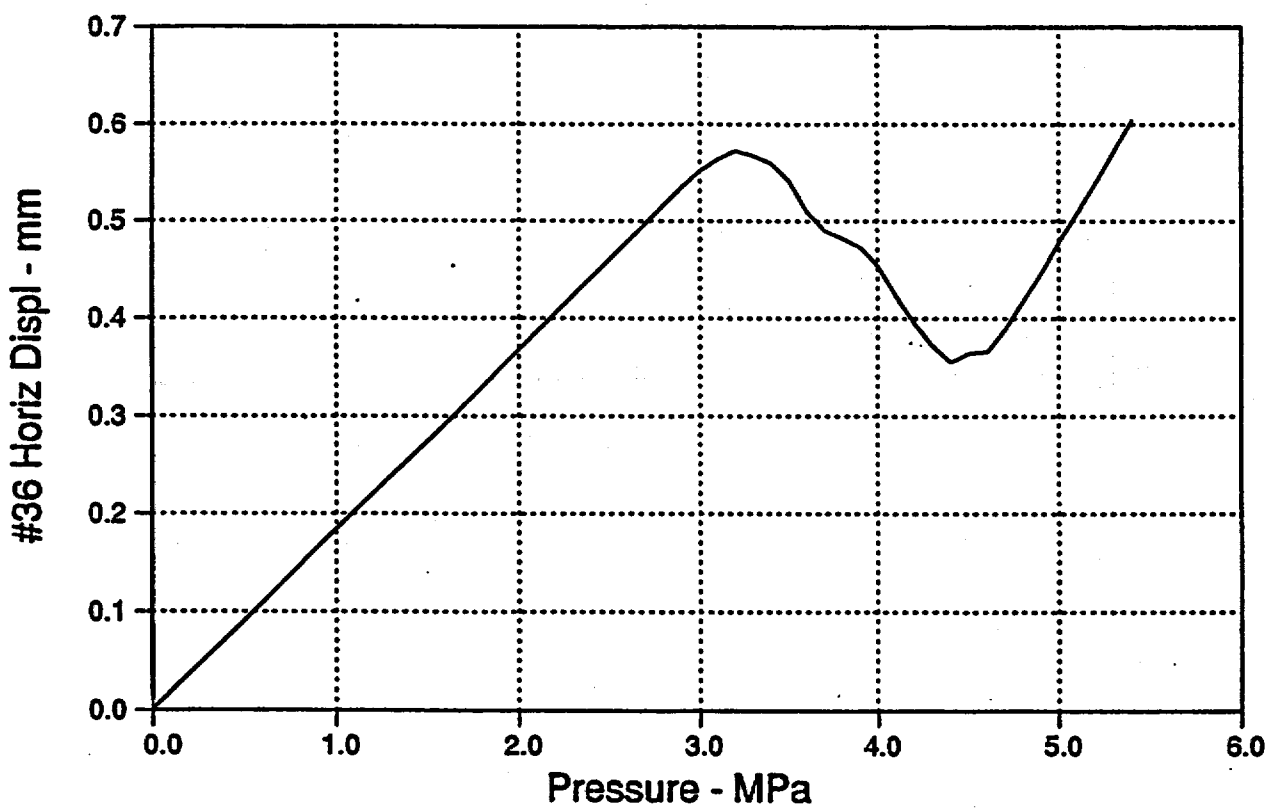

Figure 4.16 Horizontal Displacement at $\theta_G = 45^o$ and $Z_G = 3.5$ m

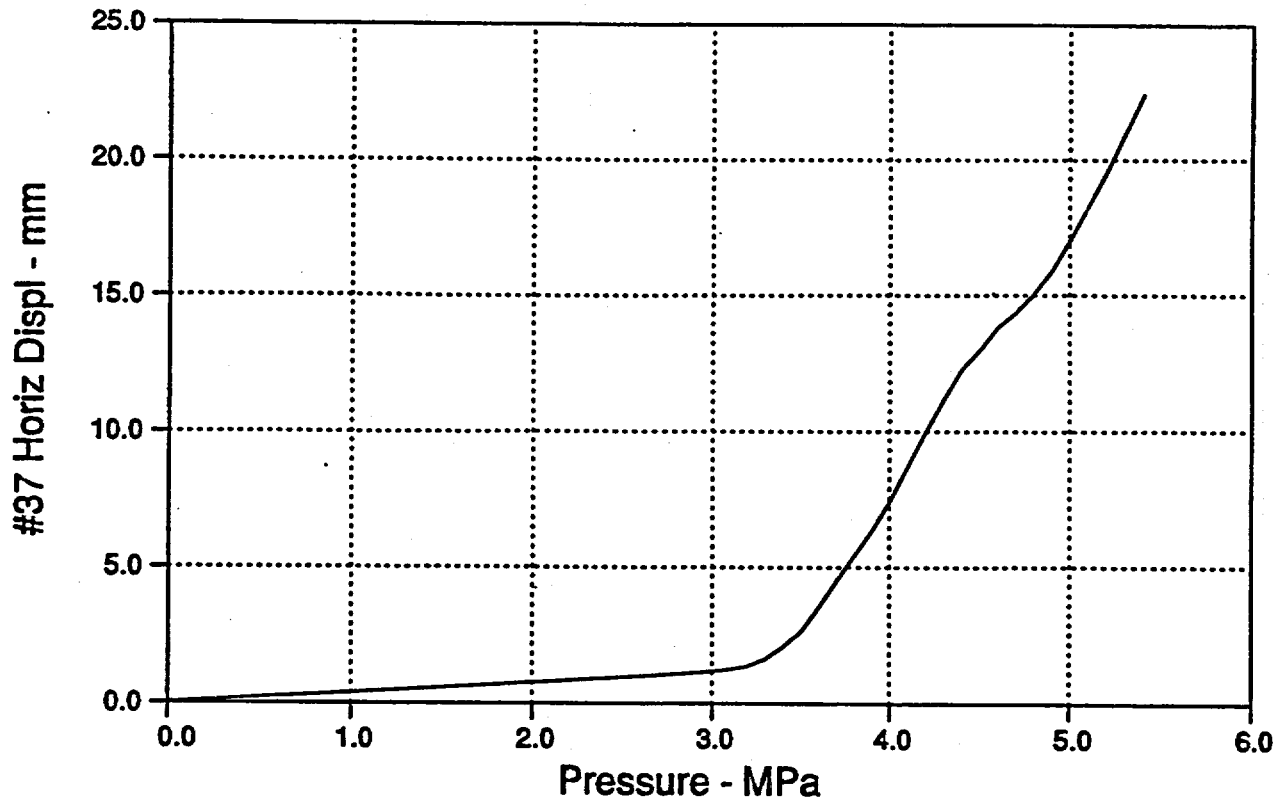

Figure 4.17 Horizontal Displacement at $\theta_G = 0^o$ and $Z_G = 3.32$ m

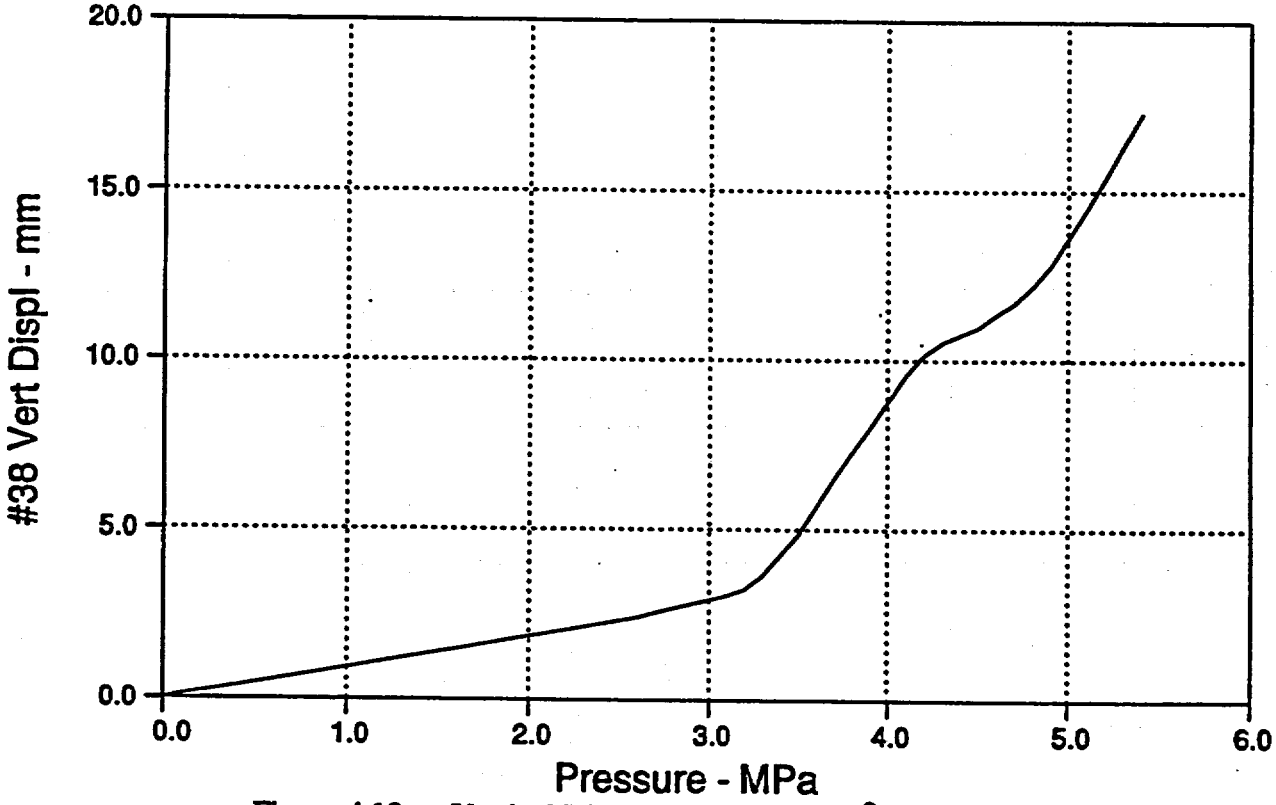

Figure 4.18 Vertical Displacement at $\theta_G = 0^o$ and $Z_G = 3.32$ m

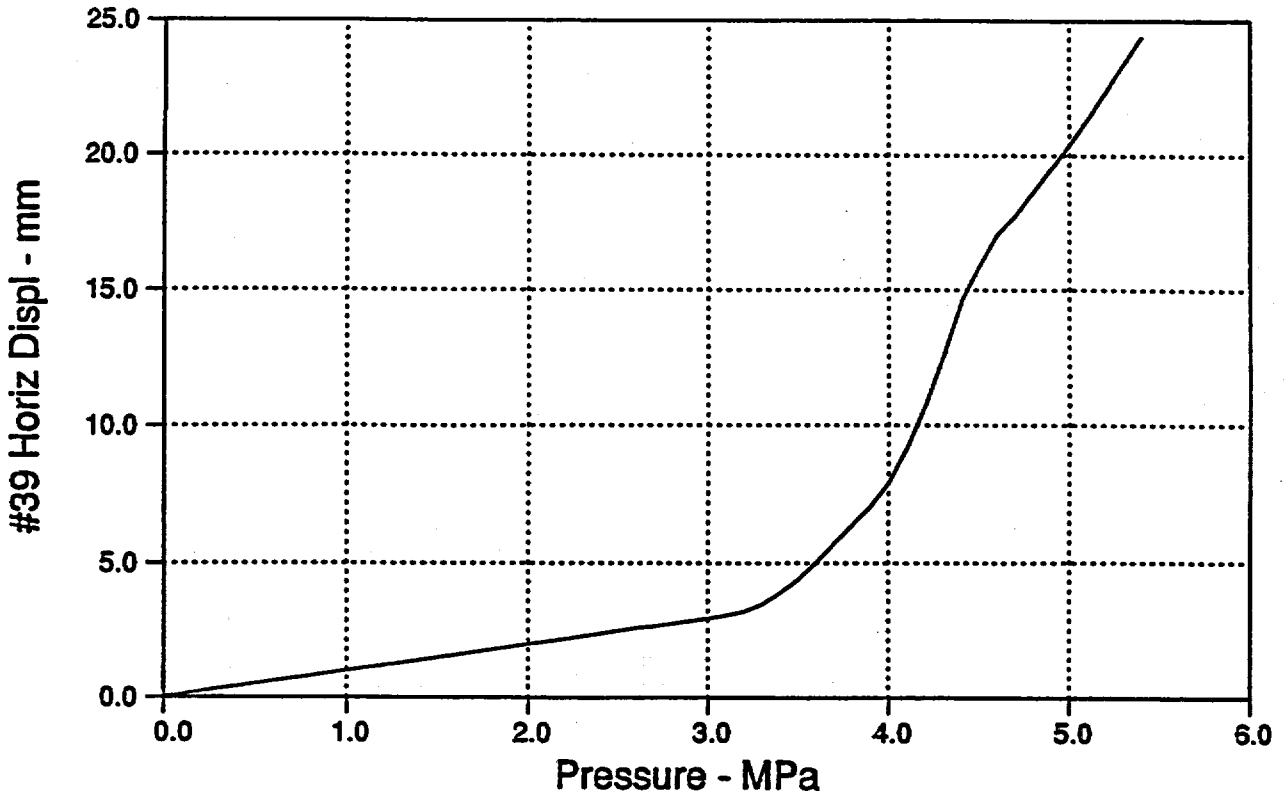

Figure 4.19 Horizontal Displacement at Center of Equipment Hatch Cover

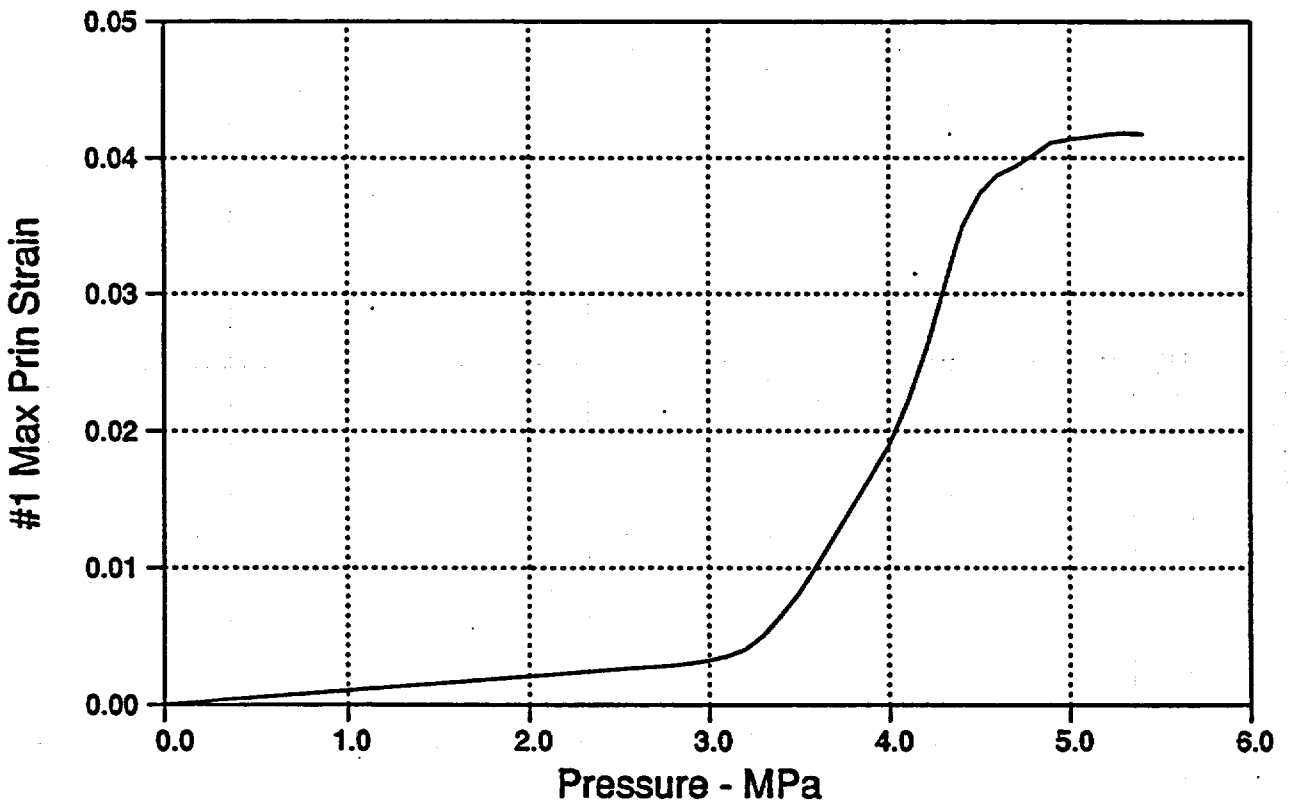

Figure 4.20 Maximum Principal Strain at $\theta_H = 67.5^o$ and $R_H = 0.36$ m

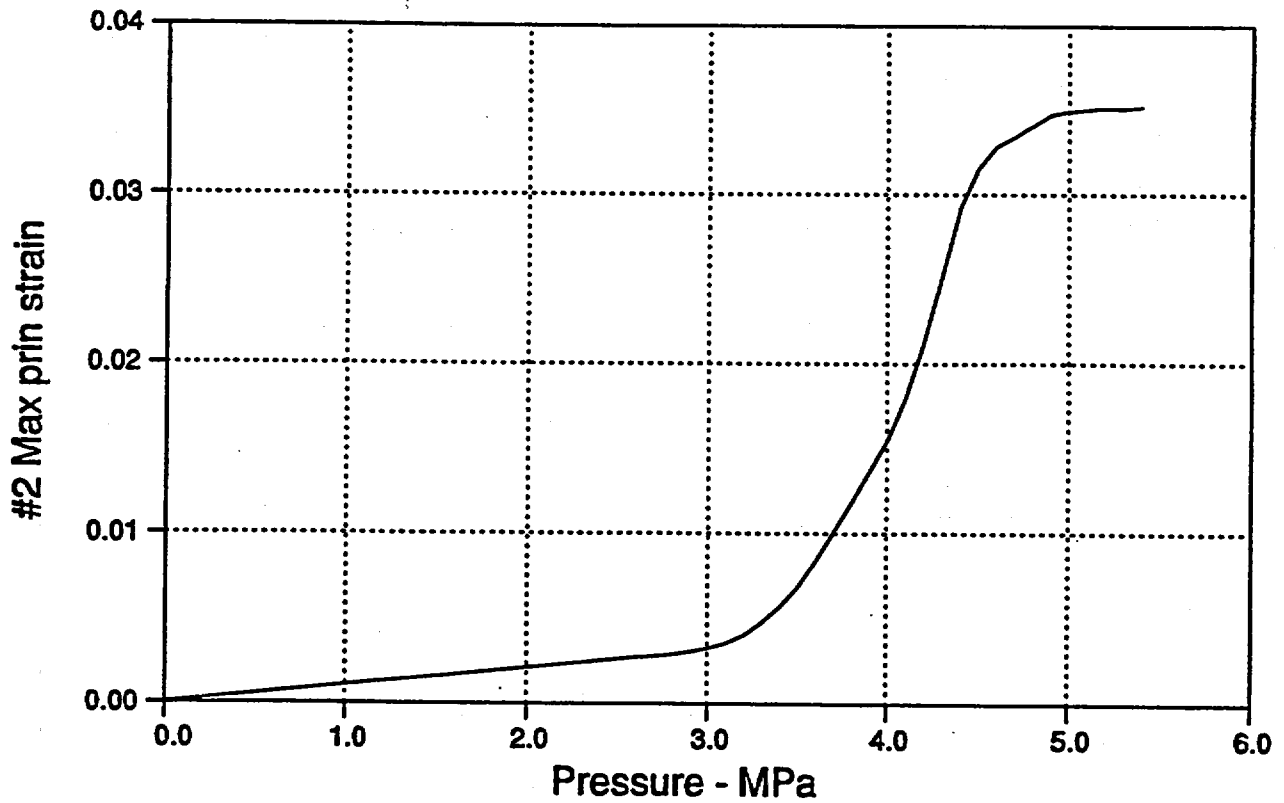

Figure 4.21 Maximum Principal Strain at $\theta_H = 45^o$ and $R_H = 0.36$ m

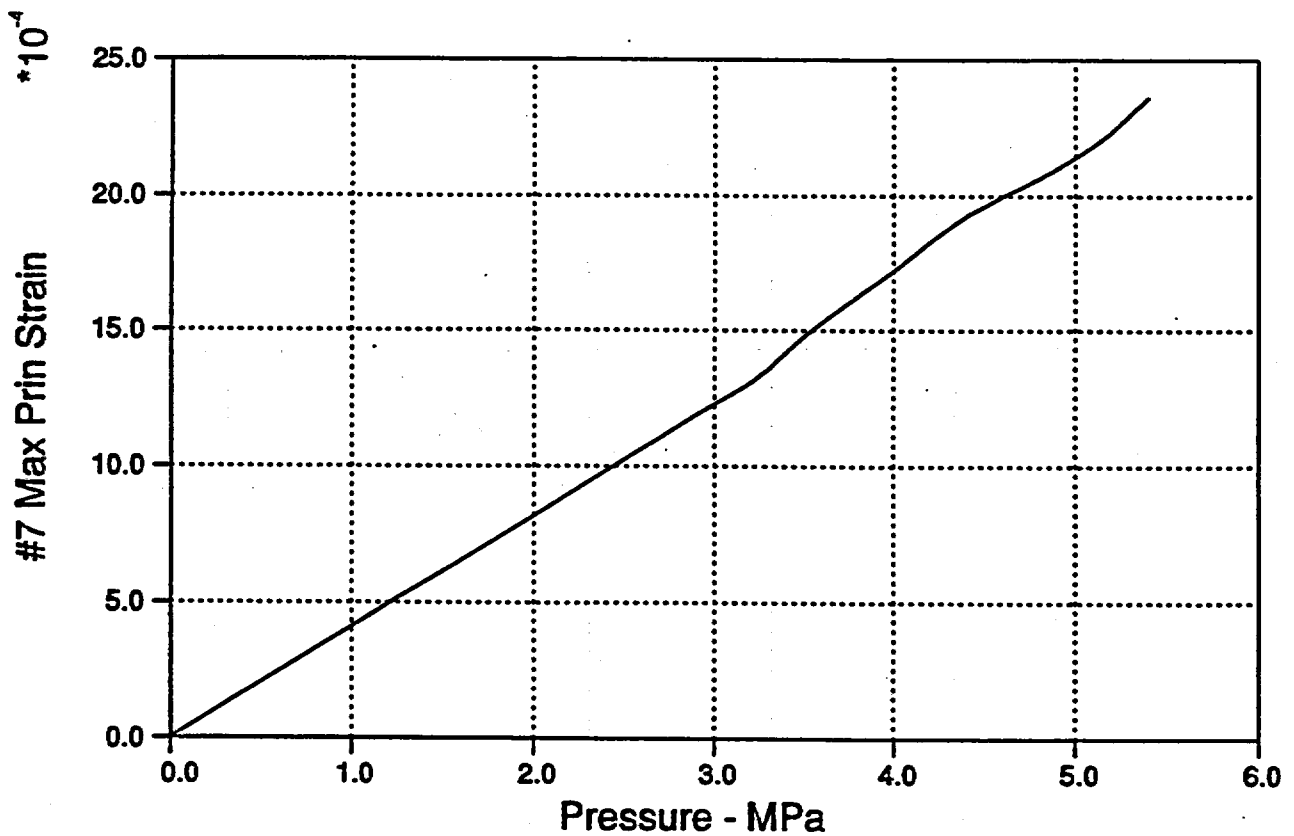

Figure 4.22 Maximum Principal Strain at Apex of Top Head

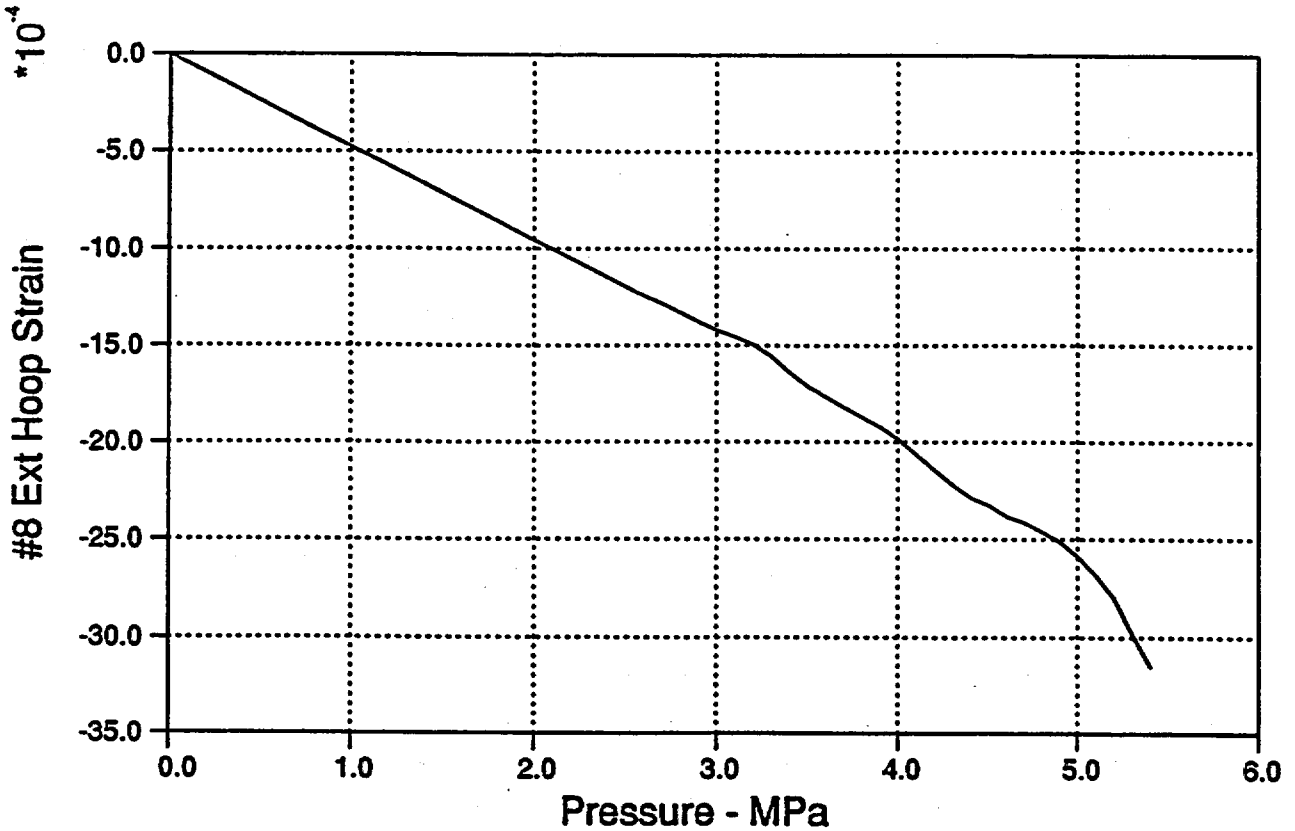

Figure 4.23 Exterior Hoop Strain at $\theta_T = 270^o$ and $R_T = 0.48$ m

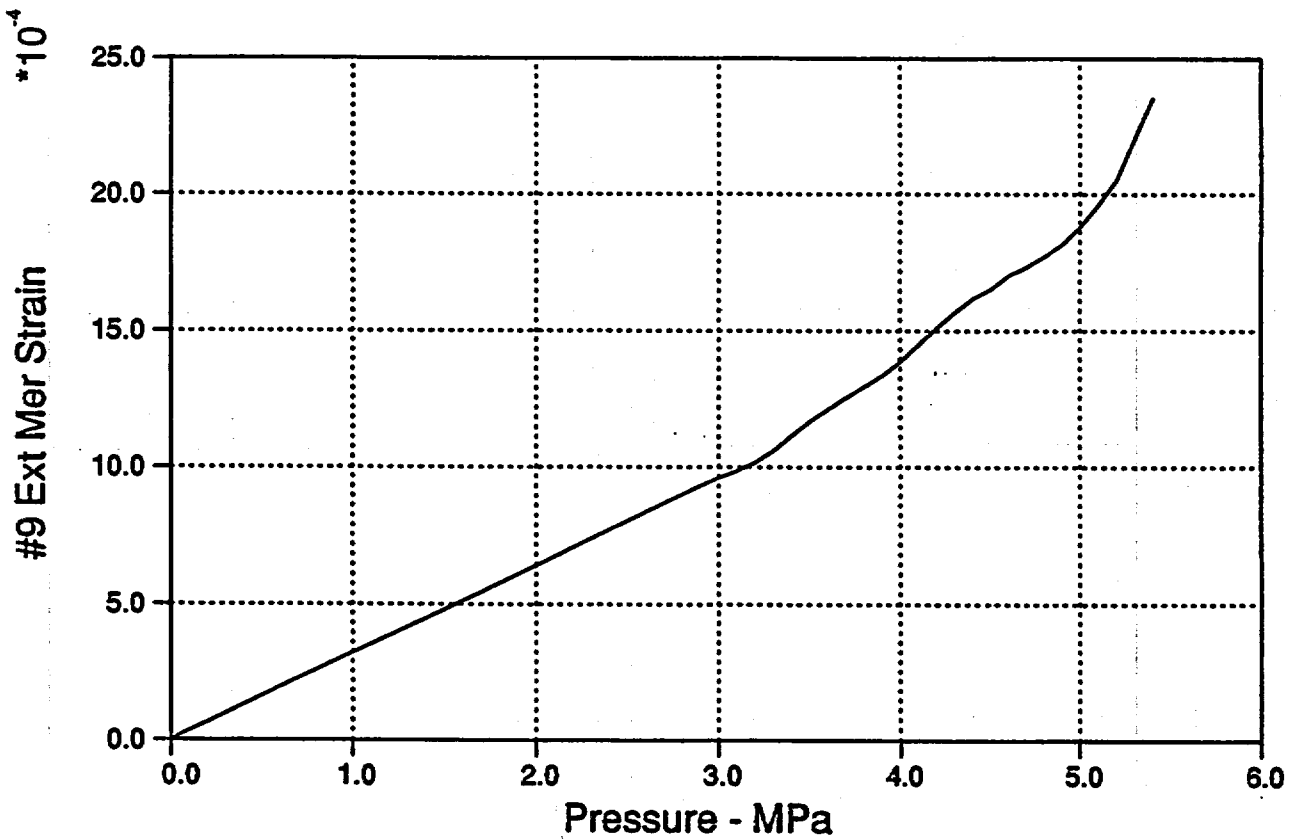

Figure 4.24 Exterior Meridional Strain at $\theta_T = 270^o$ and $R_T = 0.48$ m

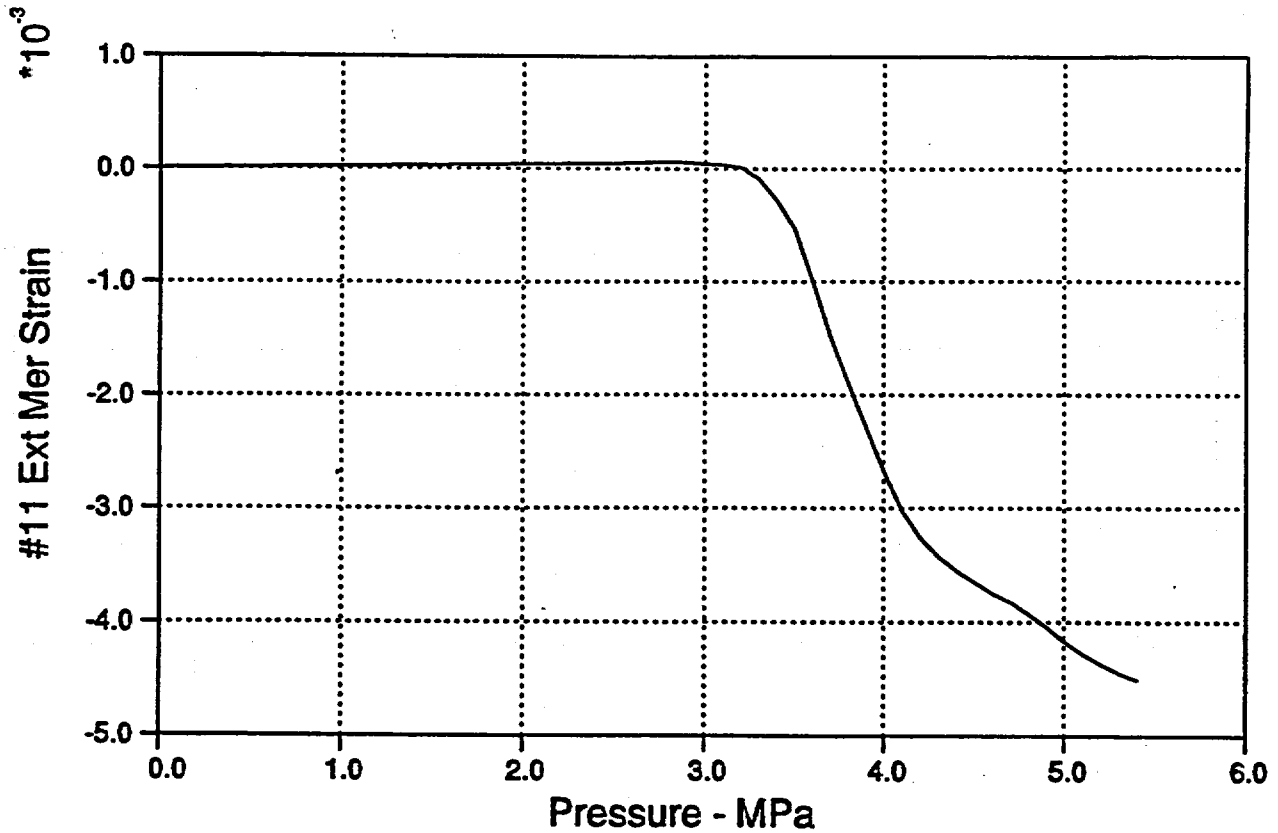

Figure 4.25 Exterior Meridional Strain at $\theta_G = 0^o$ and $Z_G = 3.47$ m

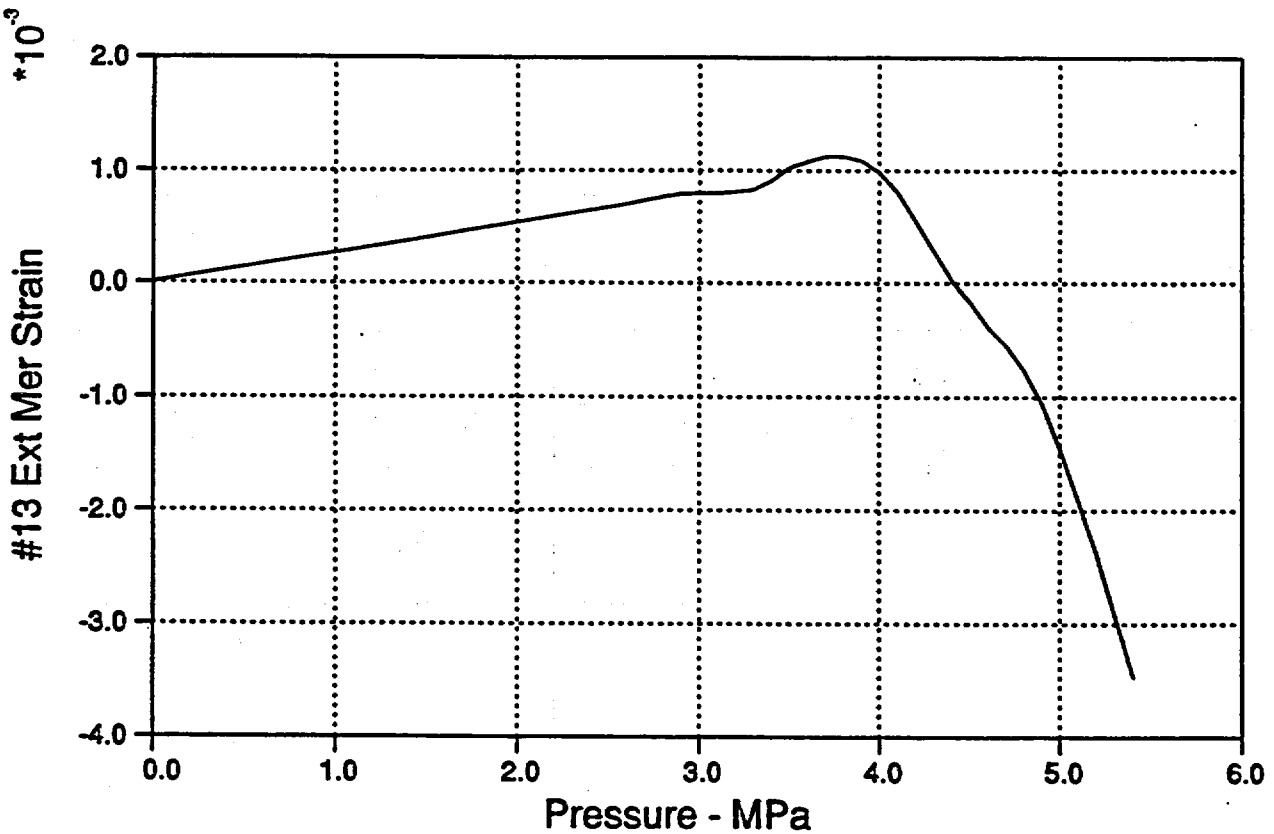

Figure 4.26 Exterior Meridional Strain at $\theta_G = 0^o$ and $Z_G = 3.32$ m

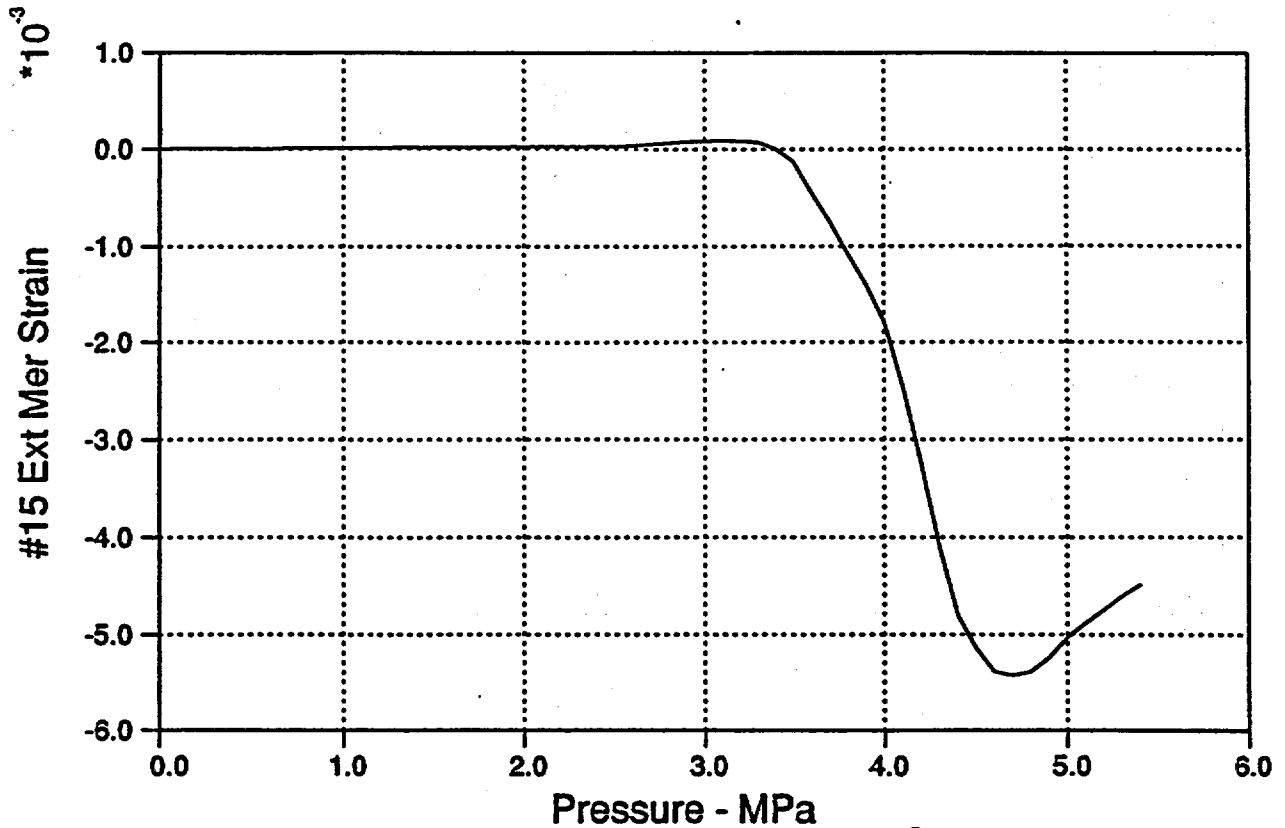

Figure 4.27 Exterior Meridional Strain at $\theta_G = 0^o$ and $Z_G = 2.10$ m

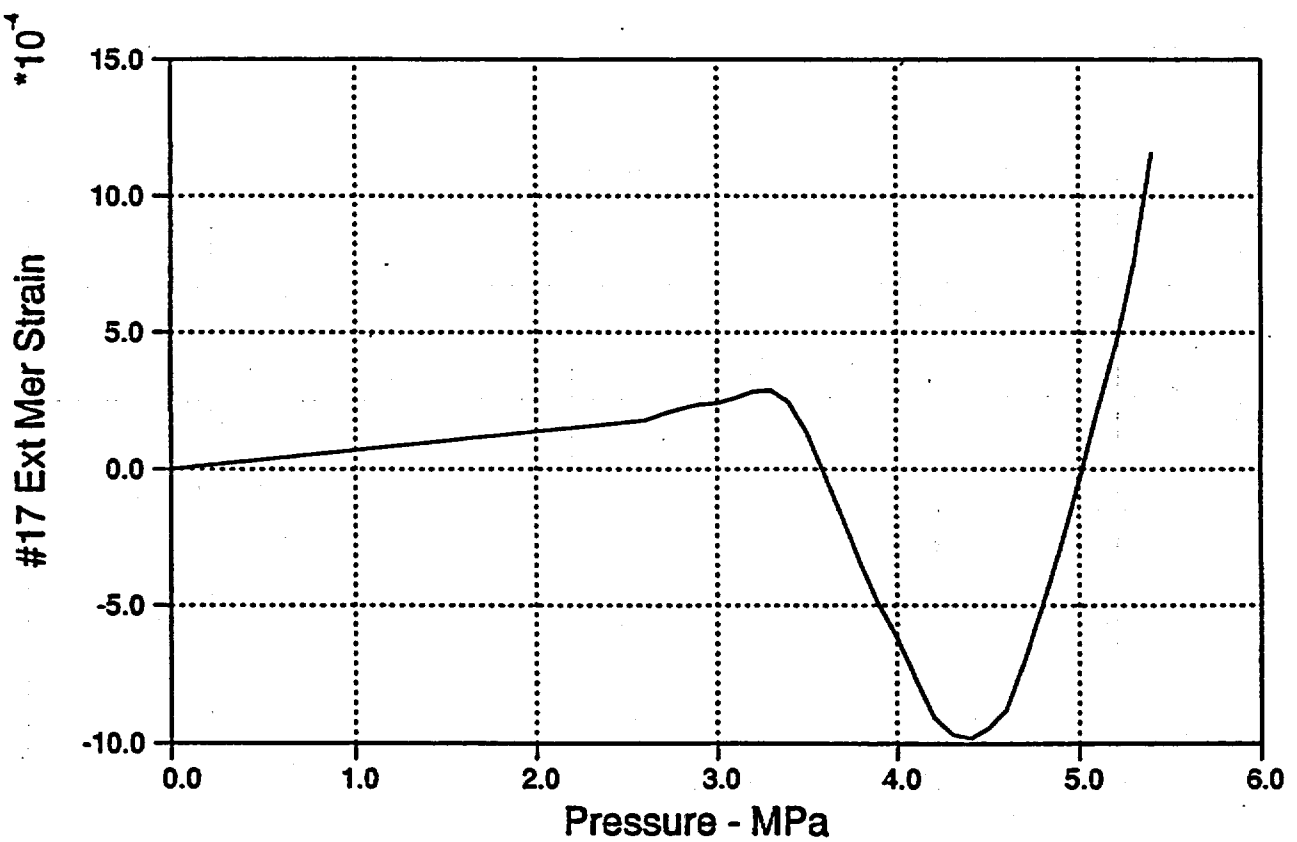

Figure 4.28 Exterior Meridional Strain at $\theta_G = 0^o$ and $Z_G = 1.60$ m

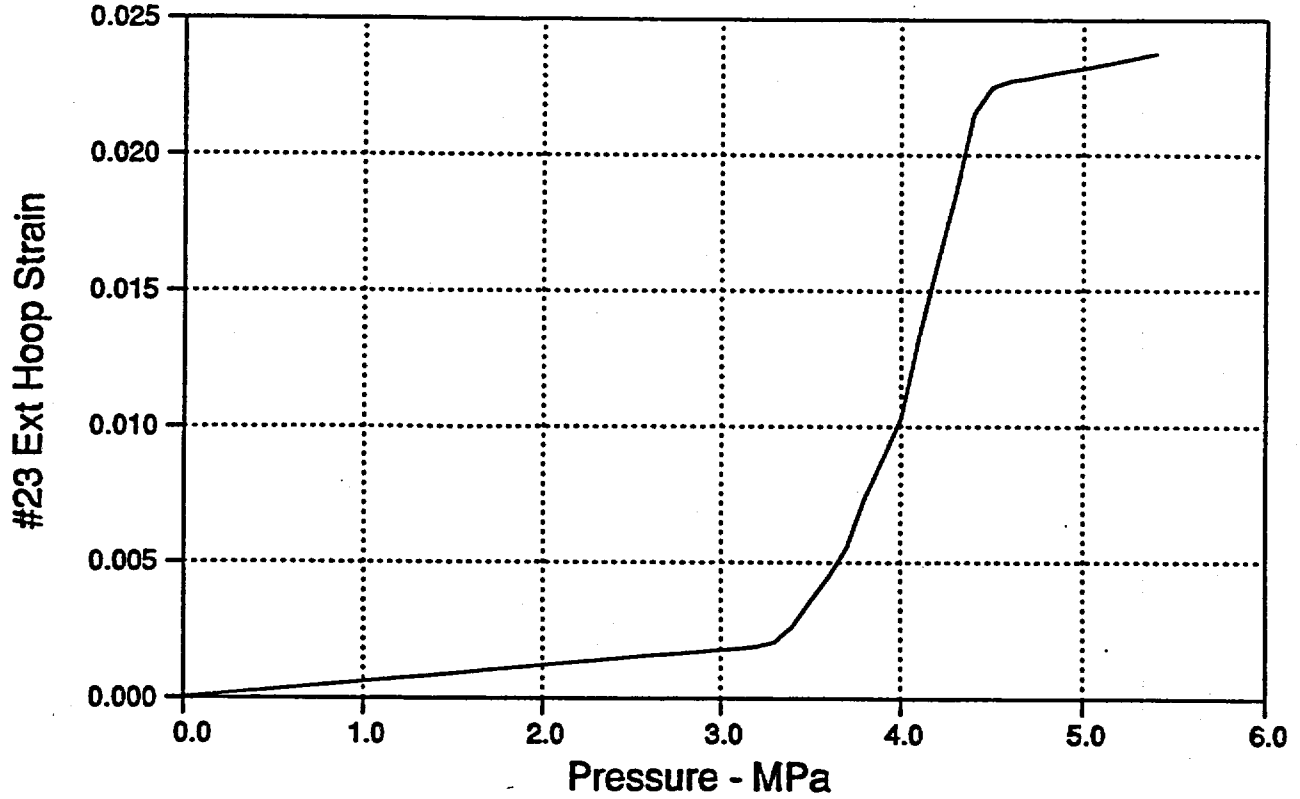

Figure 4.29 Exterior Hoop Strain at $\theta_G = 45^o$ and $Z_G = 2.49$ m

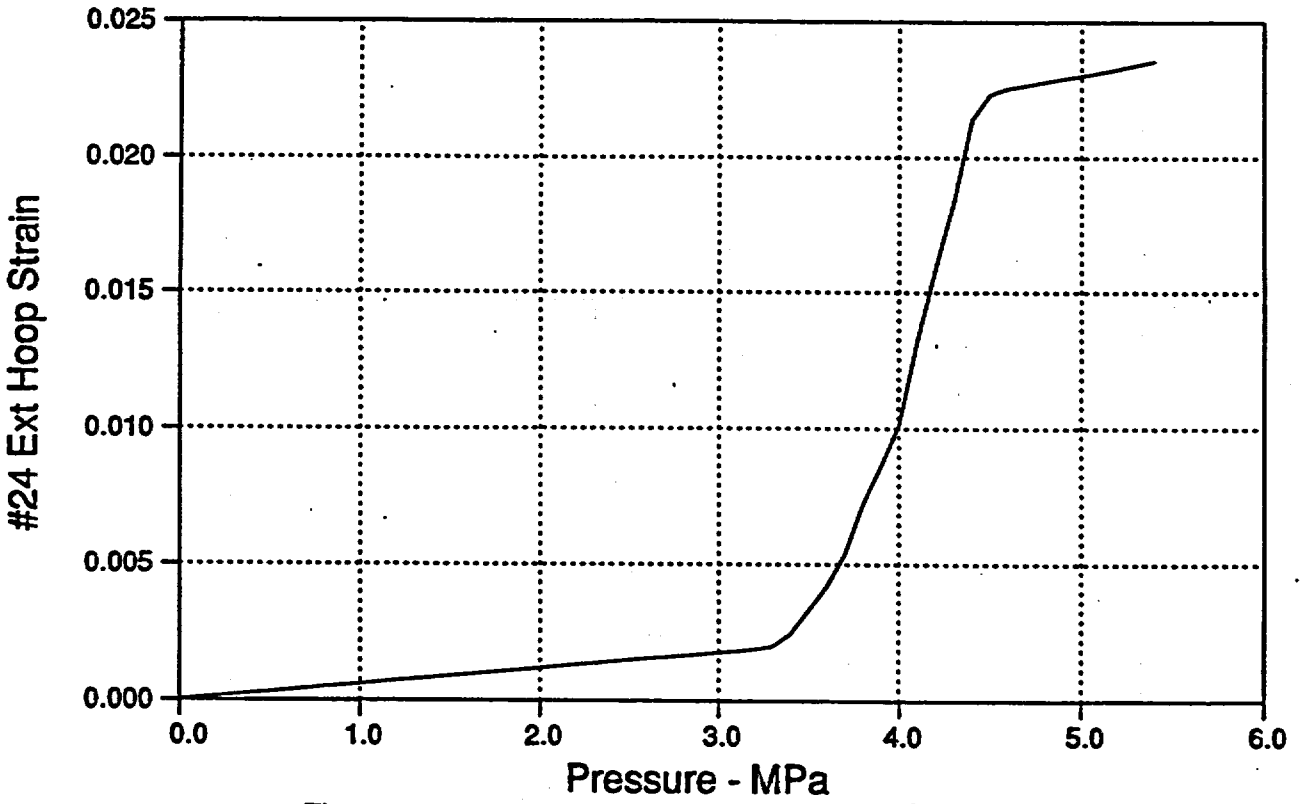

Figure 4.30 Interior Hoop Strain at $\theta_G = 45^o$ and $Z_G = 2.49$ m

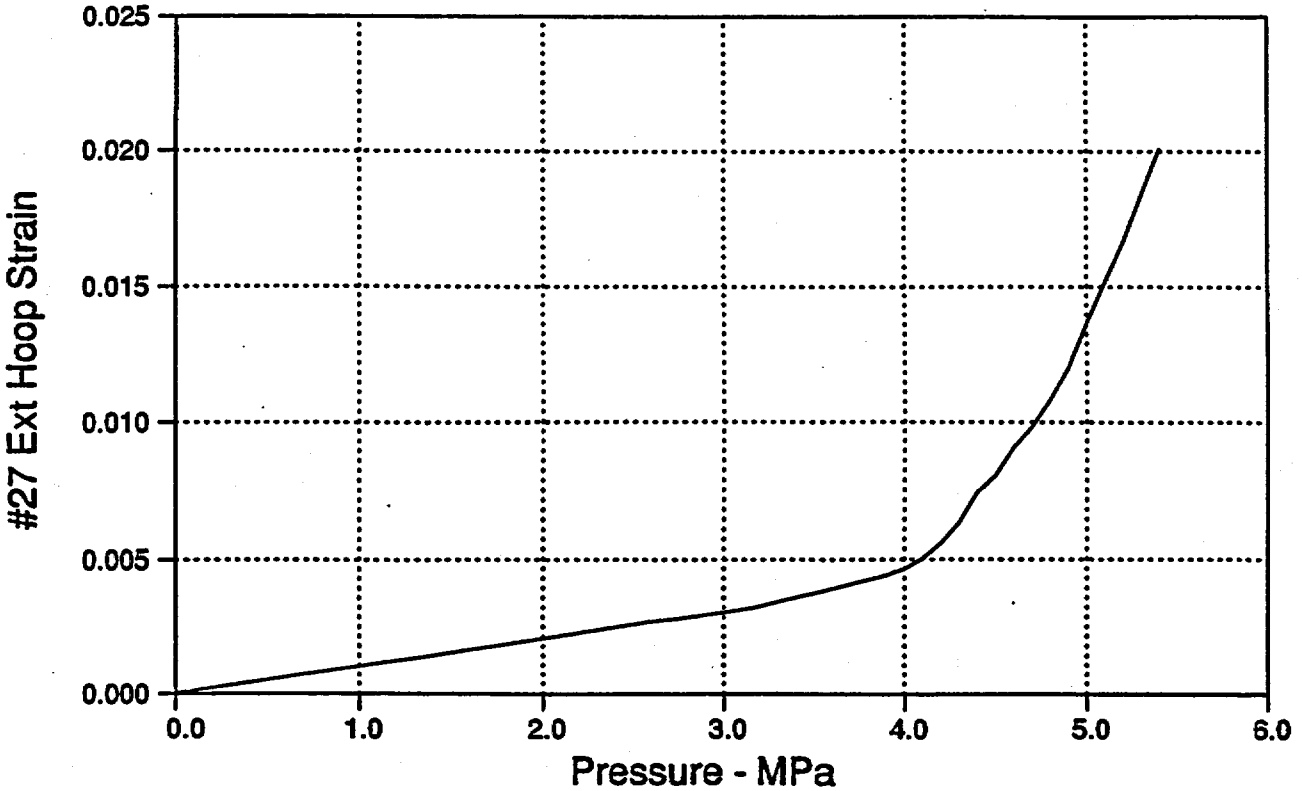

Figure 4.31 Exterior Hoop Strain at $\theta_G = 45^o$ and $Z_G = 1.45$ m

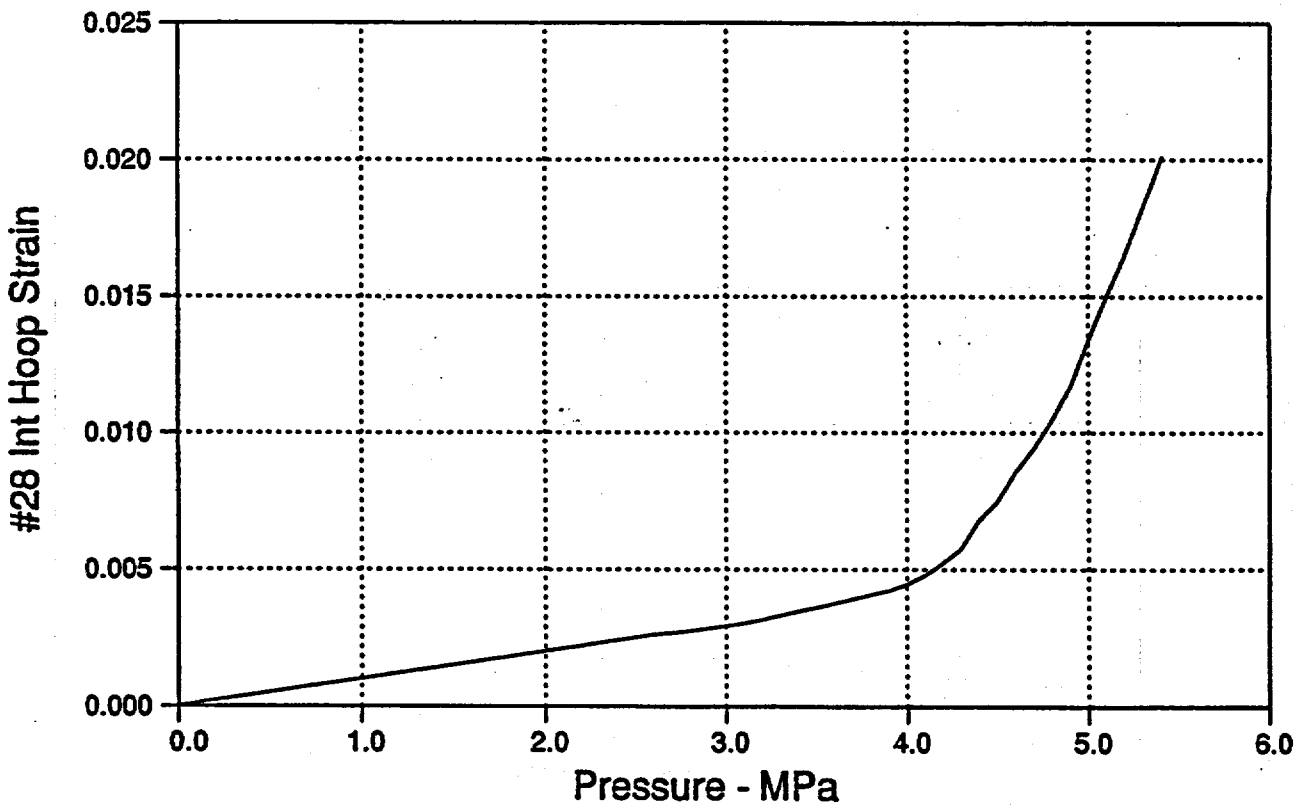

Figure 4.32 Interior Hoop Strain at $\theta_G = 45^o$ and $Z_G = 1.45$ m

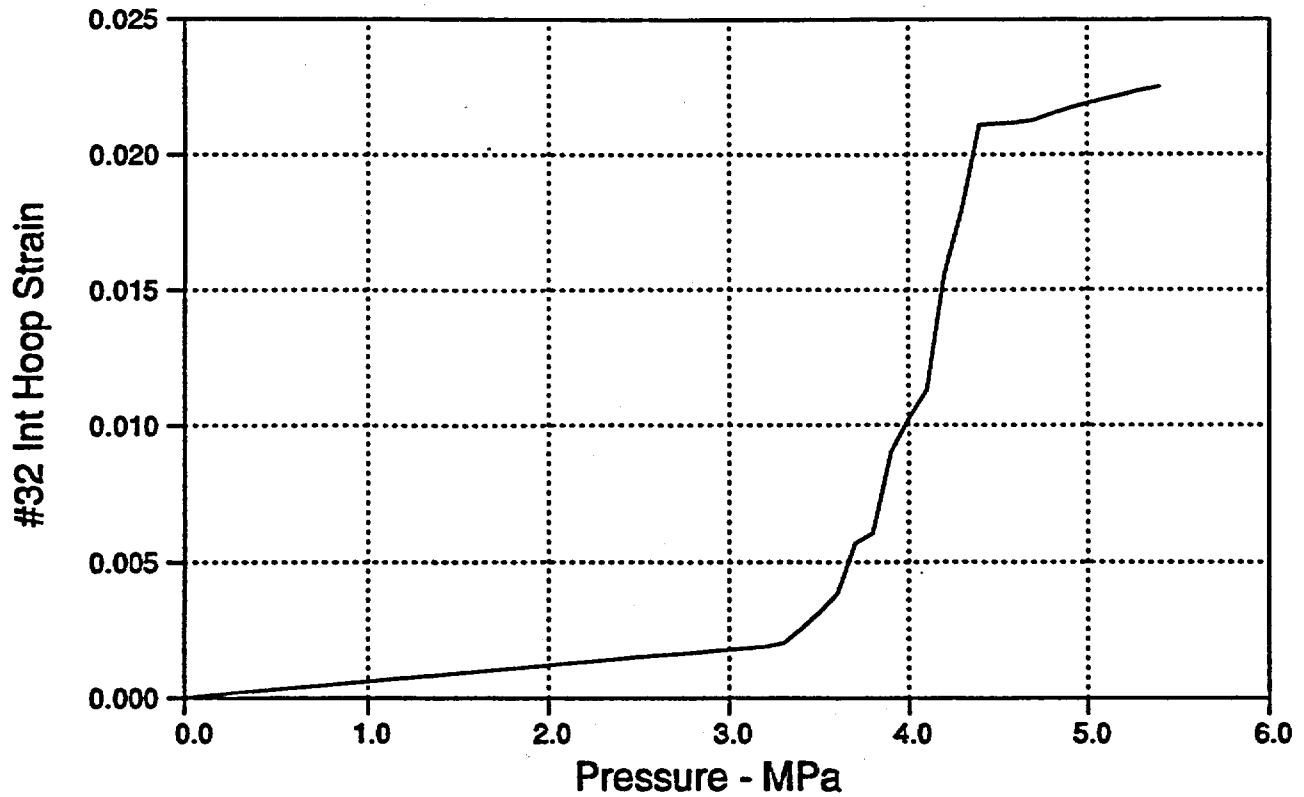

Figure 4.33 Interior Hoop Strain at $\theta_G = 270^o$ and $Z_G = 2.49$ m

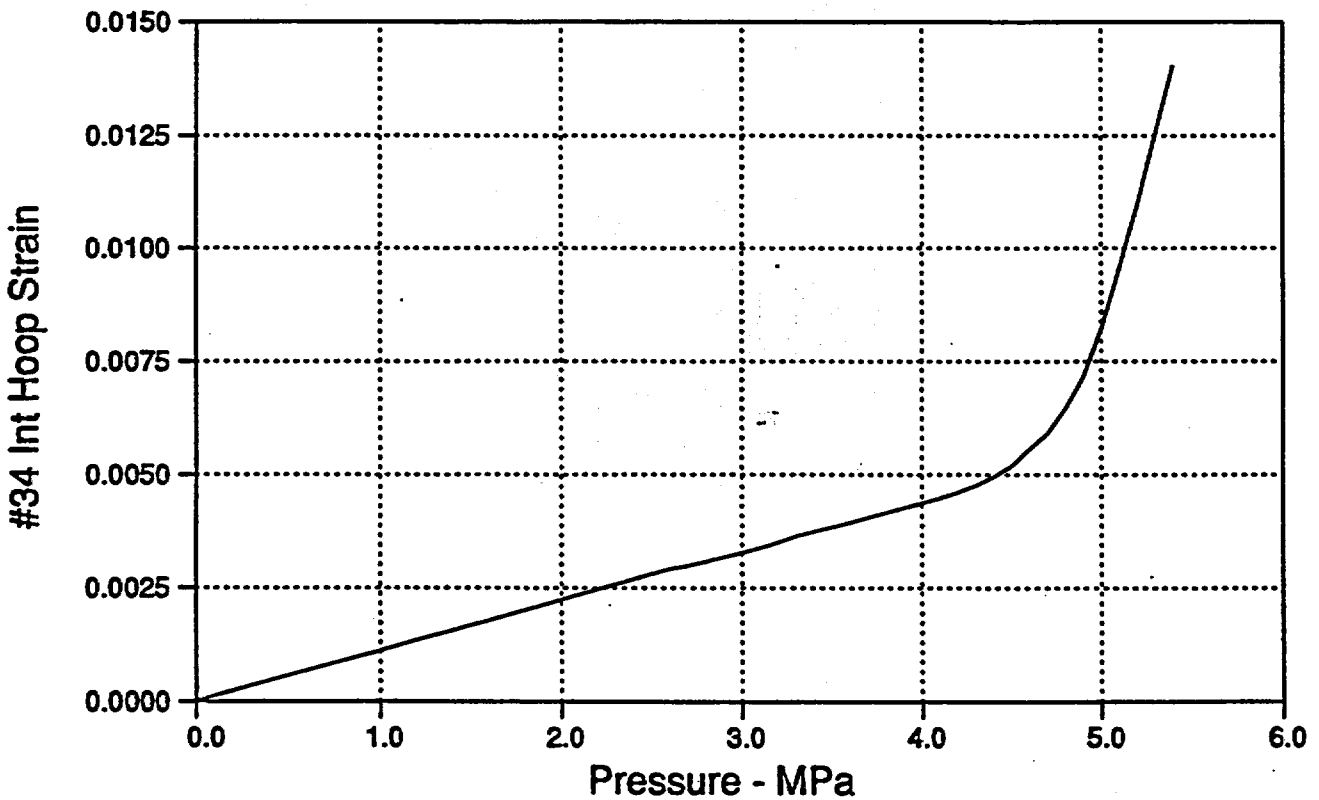

Figure 4.34 Interior Hoop Strain at $\theta_G = 270^o$ and $Z_G = 1.25$ m

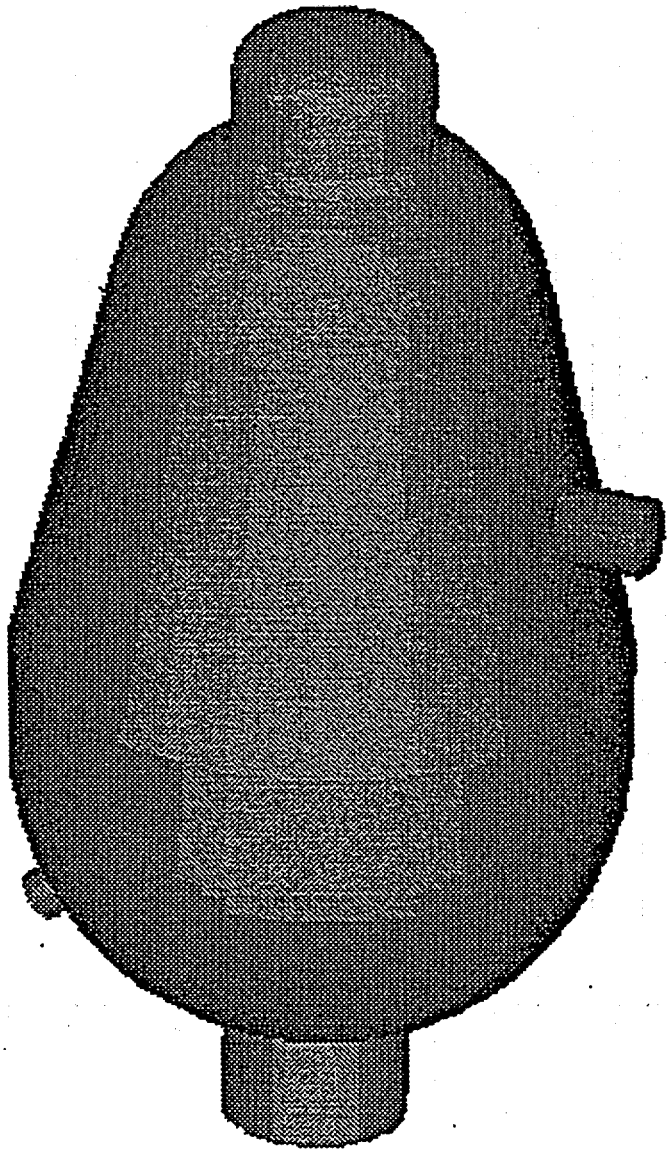

Figure 4.35 Contact Configuration at 4.4 MPa Internal Pressure

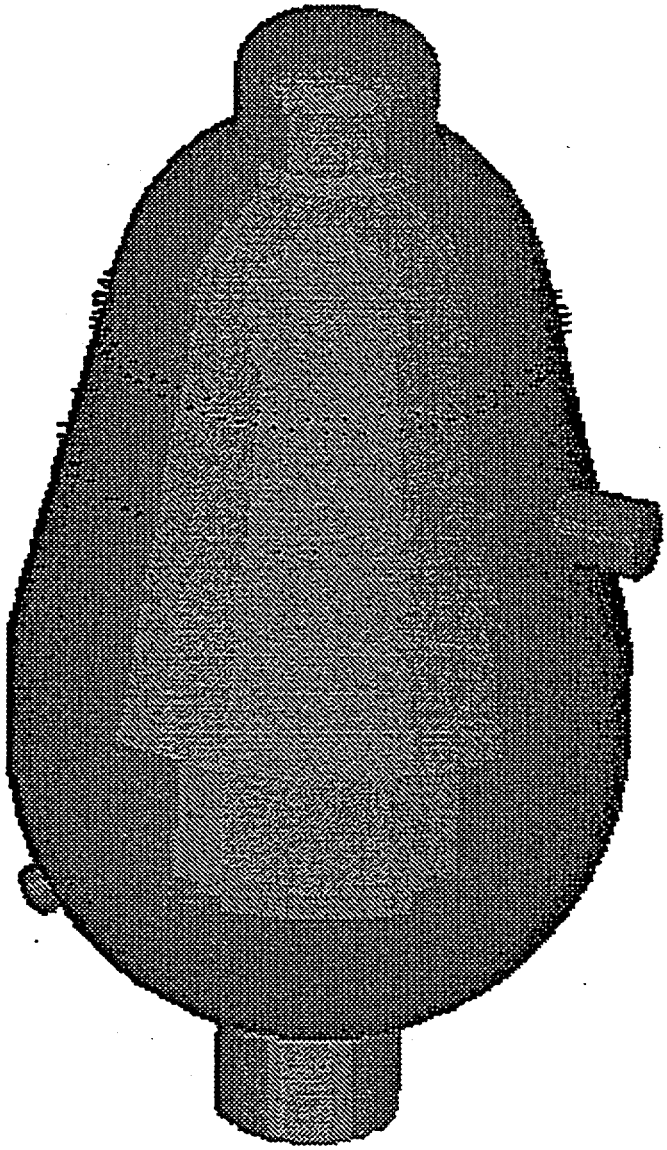

Figure 4.36 Contact Configuration at 4.6 MPa Internal Pressure

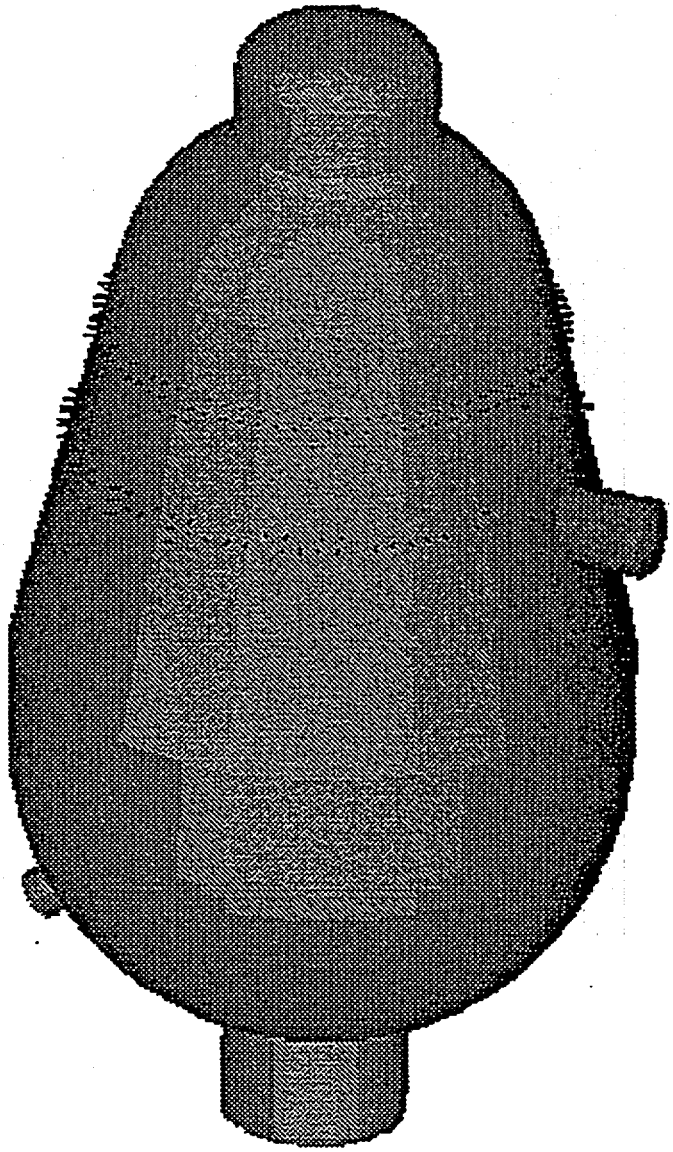

Figure 4.37 Contact Configuration at 4.8 MPa Internal Pressure

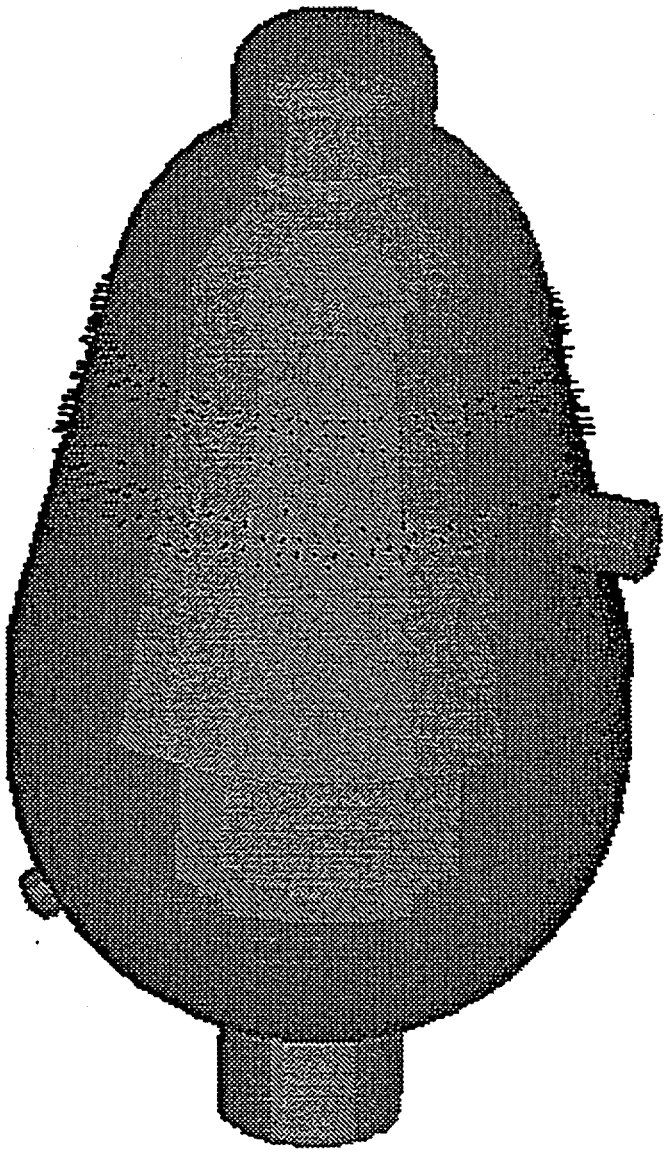

Figure 4.38 Contact Configuration at 5.0 MPa Internal Pressure

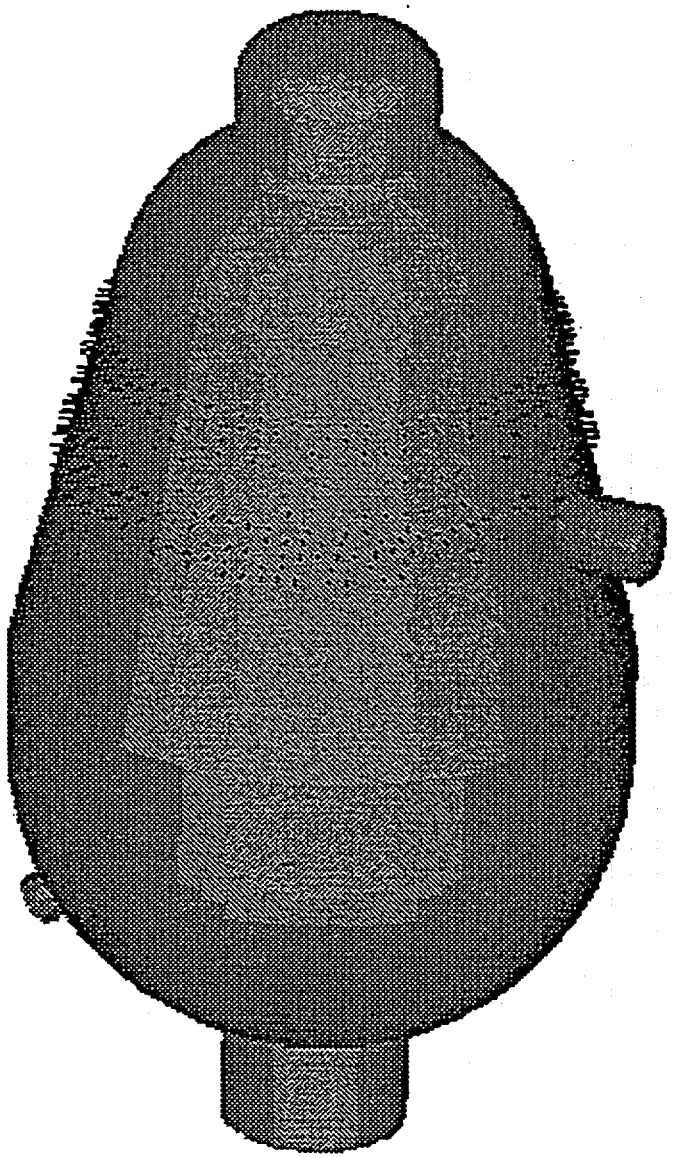

Figure 4.39 Contact Configuration at 5.2 MPa Internal Pressure

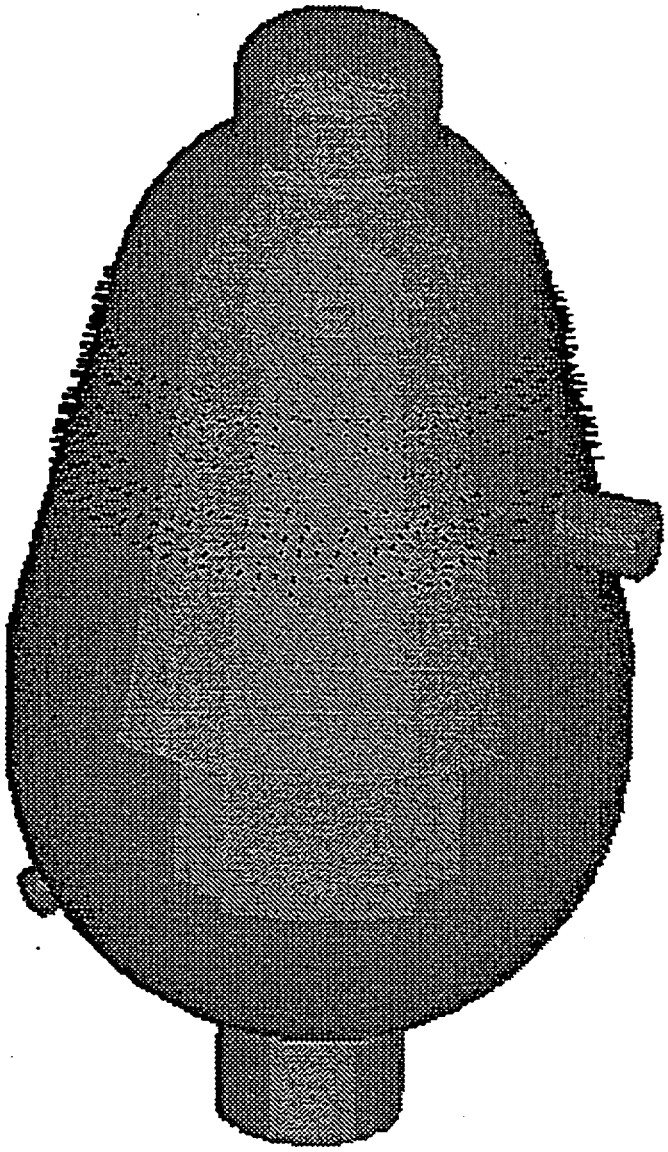

Figure 4.40 Contact Configuration at 5.4 MPa Internal Pressure

Appendix E-2

Agenzia Nazionale per la Protezione dell Ambienti

Italy

PRE-TEST VESSEL ANALYSIS
(In absence of the Contact Structure)

Giuseppe Maresca - Giovanni Pino

ANPA
Agenzia Nazionale per la Protezione dell'Ambiente
Via Brancati 48 - 00144 Rome - ITALY

-July 96-

INTRODUCTION

Elastic-plastic computations have been performed on a 3-D shell model, representing a quarter of the vessel. To this purpose the MARC computer code has been used. This code allows for finite element modelling of shell structures. The element type 75 (thick shell) of the MARC library has been chosen. This is a four nodes element with a bilinear shape function formulation. Contact problems have been managed using the contact option of the MARC code.

Prototypic structure is the BWR vessel. The design pressure is 0.31 Mpa. Thickness is reproduced according to a scale 1:4 while the scale 1:10 helds for the overall geometry.

VESSEL GEOMETRY

The geometry of the vessel under analysis is defined by the vessel outline provided in tab. 1. In the table the location of each relevant point on a meridian of the vessel inner surface is reported. Location on the outer surface are also determined taking into account the local thickness. Note that in the modelling only the inner surface has been considered to locate the shell elements, the outer surface being defined by the shell thickness. When available data were redundant to completely define the geometry only a selected set of independent data has been considered, being the other data obtained by geometric conditions. This is to assure congruence between data and geometric assumptions. By this reason small discrepancies whith the provided data can arise.
Stiffeners data are reported in Tab.2. A negative value for the stiffener wideness means it is internal with respect to the vessel surface.
All the shell elements of the model have been distributed in different sets which differ with regard to the shell thickness or to the material data. In Tab. 3 the extension of each set is reported together with the corresponding thickness and material identification number.
Two views of the model are shown in Figs. 1 and 2.

TAB. 1
VESSEL OUTLINE
(Reference: July 10, 95 - Fig. 1)

Item	Location	X (m)	Ro	Ri
Origin	A	0.000	1.4670	1.4290
Bottom Head-Lower Cylindrical Shell Transition	B	0.250	1.4590	1.4500
Lower Cylindrical -Lower Conical Shell Transition	C	0.750	1.4590	1.4500
First Lower Stiffener	D1	0.816	1.4444	1.4352
"	Dm	0.822	1.4430	1.4338
"	D2	0.828	1.4417	1.4325
Second Lower Stiffener	E1	0.916	1.4219	1.4127
"	Em	0.921	1.4208	1.4116
"	E2	0.926	1.4197	1.4105
Material Change Interface	F	1.579	1.2731	1.2639
Middle Stiffener	G1	2.070	1.1623	1.1536
"	Gm	2.0795	1.602	1.1515
"	G2	2.089	1.1580	1.1493
Weld Line at 2.275 m	H	2.275	1.1163	1.1076
Weld Line at 2.694 m - Conical to Sherical Transition	I	2.694	1.0212	1.0135
Upper Stiffener	J1	2.884		
"	Jm	2.8935		
"	J2	2.903		
Sherical Shell- Knuckle Transition	K	3.359		0.5246
Knuckle -Upper Cylindrical Shell Transition	L	3.432	0.4885	0.4825
Top Flange	M1	3.512	0.4885	0.4825
"	Mm	3.522	0.4885	0.4825
"	M2	3.532	0.4885	0.4825
Upper Cylindrical Shell - Top Head Transition	N	3.746	0.4885	0.4825
Curvature Change	O	3.892		0.3963
Top Head Apex	P	3.994		0.0

Spherical Shell Geometry

1. (sphere)
XO1=2.461 ; YO1=0 ; R=1.040
XE1=2.694 ; YE1=1.0135
XE2=3.359 ; YE2=0.5246

2. (knuckle)
XO2=3.432 ; YO2=0.567 ; R=0.0849
XE1=3.359 ; YE1=0.5246
XE2= 3.432 ; YE2=0.4825

3. (torospherical head)
XO3=3.746 ;YO3=0.3158 ; R=0.1667
XE1=3.746 ; YE1=0.4825
XE2=3.892 ; YE2=0.3963

XO4=3.173 ; YO4= 0 ; R=0.8207
XE1=3.892 ; YE1=0.3963
XE2=3.994 ; YE2=0

Equipment Hatch Sleeve Geometry

axis level=1.633 (corresponding inner radius=1.2517)
inner radius=0.180 ; outer radius 0.200
plate radius= 0.332

TAB. 2
Stiffeners data

Stiffener	Wideness (m)	Location	Thickness (m)	Level (m)
STIFF1	-0.090	Dm	0.0125	0.822
STIFF2	-0.020	Em	0.095	0.921
STIFF3	-0.0613	Gm	0.019	2.0795
STIFF4	-0.0562	Jm	0.019	2.8935
STIFF5A	+0.0175	Mm	0.020	3.522
STIFF5B	-0.0415	Mm	0.020	"

TAB. 3
Shell thickness and related material

Zone	From	To	Thickness (m)	Material
1	A	B	0.038	12
2	B	C	0.009	11
3	C	Dm	0.009	11
4	Dm	Em	0.009	11
5	Em	F	0.009	11
6	F	Gm	0.0085	5
7	Gm	H	0.0085	5
8	H	I	0.0075	3
9	I	Jm	0.008	4
10	Jm	K	0.008	4
11	K	L	0.0165	10
12	L	Mm	0.006	1
13	Mm	N	0.006	1
14	N	O	0.006	2
15	O	P	0.006	2
Plate			0.0175	12
Hatch			0.020	9
Stiff1	Dm	Dm	0.0125	7
Stiff2	Em	Em	0.0095	6
Stiff3	Gm	Gm	0.019	8
Stiff4	Jm	Jm	0.019	8
Stiff5	Mm	Mm	0.020	9

a

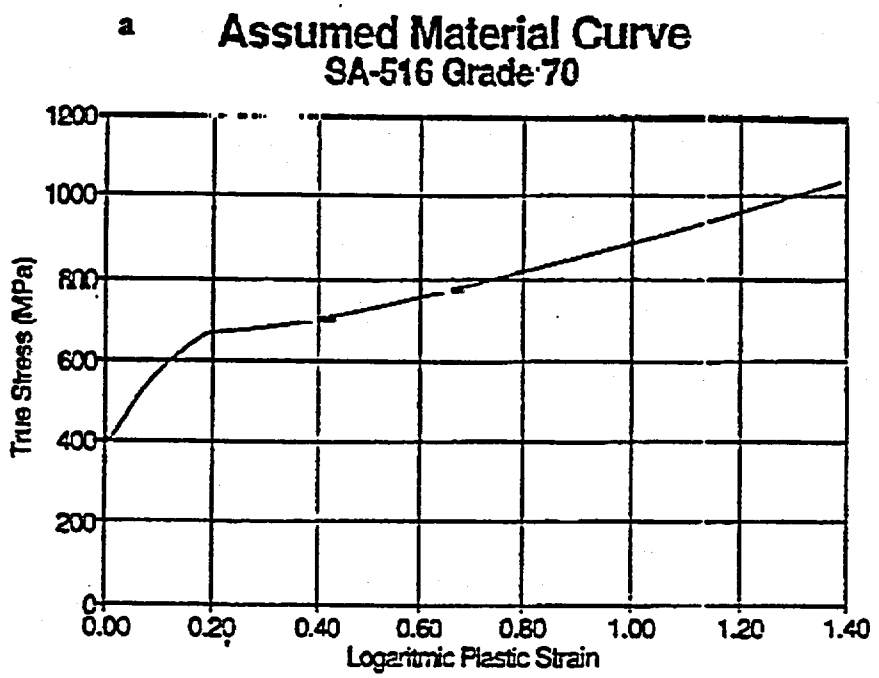

b

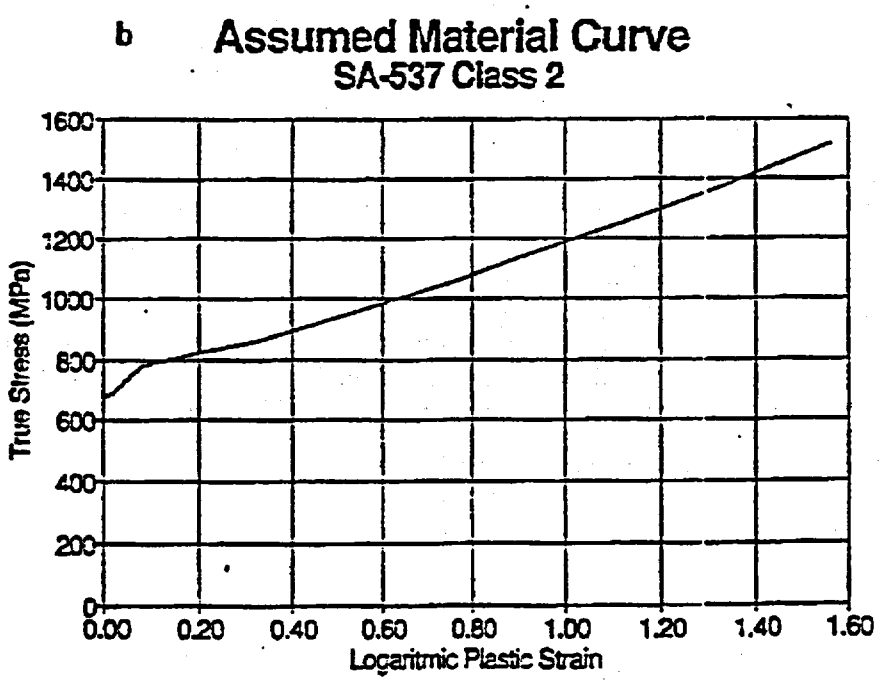

- Material data assumed in the analysis. The true stress versus the logarithmic plastic strain is reported. Curves begin at the yield stress. a) SA-516 Grade 70 - b) SA-537 Class 2.

MATERIAL DATA

Material data as provided by SNL have been treated to obtain data suitable for MARC code application.
Plastic analysis is performed by the code according to the Prandtl-Reuss model of incremental plasticity and a true stress-natural plastic strain curve is required to define the material behaviour in the plastic range.
Test data have been provided by SNL for twelve different locations. For each location four tensile tests have been performed, two for the roll direction of the shell and two for the transverse direction.
The steps of the data treatment are listed below.

1. To each quadruple of data a yield stress has been associated as the average of the experimental (lower) yield stresses.
2. From each single true stress-true (total)strain curve a true stress-true plastic strain curve has been obtained by subtracting the term $\sigma(\varepsilon)/E$ from the total strain.
3. By interpolation data on each single curve have been computed for a same set of strains
4. For each location an average curve has been obtained by averaging the stress values related to the same natural plastic strain.

The above steps provide suitable curves up to the ultimate stress. After this point necking occurs and strains are no more uniform in the specimen. Experimental strains provided by test reports are averaged on the initial gauge lenght of the specimen. Obviously a local stress-strain correlation needs to perform accurate plastic calculations in the post necking region. To obtain this it has been assumed, according to Mc Gregor and Davidenkov, that a linear relation exists between the average stress and the local natural strain in the after-necking region. Therefore, from the knowledge of the average stress at rupture local data can be computed inside the necked region. This can be made using the Bridgmann formula. However, to this purpose, a value of the curvature radius at the neck must be provided. This value should be obtained from the experimental tests. More precisely a complete characterization of the material behaviour in the after necking region would require an experimental diagram relating the curvature in the neck to the area reduction as it increases from the beginning of the instability to the rupture. In the absence of experimental data an hypothesis on the shape of the neck must be made. In the present analysis proportionality between the curvature radius at the neck and the local natural strain has been assumed. The curvature radius has been assumed to be zero at the beginning of the necking phase. At rupture a value of 0.75 for the ratio between the curvature radius and the reduced radius of the specimen because of neck has been assumed, on the basis of experimental data on carbon steel available at ANPA.
In any case the postnecking region of the material behaviour cannot be reached in the present analysis because of the primary load nature of pressure. In fact plastic instability should occur under increasing pressure at a strain value lesser than the maximum uniform strain.

See page 5a for assumed material curves for SA-516 and SA-537.

FAILURE CRITERIA

Two modes of failure have been considered. The first one is plastic instability which can be reached locally as soon as an increase in pressure cannot be balanced any more increasing the strain. This condition appears in the computation as a numerical instability stopping the calculation.

The second one is local ductility reduction because of triaxiality effects and it can be relevant in the neighborough of penetrations and stiffeners. This is considered computing the ductility reduction according to the formula:

$$\frac{\varepsilon_r}{e_r} = 2^{(1-TFD)}$$

with

ε_r=equivalent strain
e_r=elongation at rupture by the uniaxial test

and

$$TFD = \frac{\sqrt{2}\cdot(\sigma_1+\sigma_2+\sigma_3)}{\sqrt{(\sigma_1-\sigma_2)^2+(\sigma_2-\sigma_3)^2+(\sigma_3-\sigma_1)^2}}$$

The shell elements used in the model are based on a plane stress formulation and therefore they are not suitable to provide local triaxiality factors. However an approximate evaluation can be performed. If a triaxial condition exists deviatoric stresses and plastic strains are reduced. Supposing to have an imposed total strain in the direction normal to the shell surface and given stresses in the shell plane, the local out of plane strress can be determined according to the Prandtl-Reuss model.

Finally it must be observed that buckling at the torospherical head is also possible. If buckling occurs local rupture by bending stress in the meridional direction can follow. To take into account this latest possibility the buckling load for the torospherical head has been computed according to the Galletly simplified formula:

$$P_b = 260\cdot\sigma_{yp}\cdot\left(\frac{r}{L}\right)\cdot\left(\frac{D}{t}\right)^{-1.5}$$

The computation provides a buckling pressure of 10.87 MPa.

SIMPLIFIED ANALYSIS

Some evaluations have been performed by simplified analysis to provide a first picture of the results to be expected.
First of all the pressure corresponding to the contact between the vessel and the CS structure has been evaluated . A pressure equal to 3.5 MPa has been obtained. This pressure is below the limit values obtained from the analysis of the vessel in the absence of the CS structure. Therefore no rupture should occur before the contact. After the contact stress redistribution occurs. As a possible mode of failure local bending near changes in thickness has been considered. For example the reinforcement plate around the hatch has a thickness of 0.0175 m while the surrounding shell at the same level has a thickness of 0.008 m. As the plate touches the CS structure the surrounding shell remains at 0.0095 m from the CS. Increasing the pressure also the surrounding shell goes into contact but locally, near the thickness change a bending occurs. To evaluate this effect the following formulas have been used:

$$l = \sqrt[4]{\frac{72 \cdot \delta \cdot E_r \cdot t^3}{12 \cdot P}}$$

$$E_r = \frac{4 \cdot E \cdot E_t}{\left(\sqrt{E} + \sqrt{E_t}\right)^2}$$

$$\Delta\varepsilon^+ = \frac{2 \cdot E_r \cdot t^3 \cdot h^+}{12 \cdot P \cdot l^2}$$

$$\Delta\varepsilon^- = \frac{2 \cdot E_r \cdot t^3 \cdot h^-}{12 \cdot P \cdot l^2}$$

$$h^+ = \frac{t}{1 + \sqrt{\frac{E_t}{E}}}$$

$$h^- = \frac{t}{1 + \sqrt{\frac{E}{E_t}}}$$

At a pressure of 4 Mpa, which is beyond the value related to the first contact with the CS the following data are obtained:

$$l = 0.068m$$

$$\Delta\varepsilon^+ = 1.18 \cdot 10^{-4}$$

showing that the considered effect is negligible.

RESULTS

Plastic deformations, total strains and displacements at the required locations are reported in figs. 3-23.
Note that only plastic strains are reported. So they are zero in each location untill yielding occurs.
Conventional time is reported on the abscissa. To get the corresponding pressure value in MPa the time value must be multiplied by 0.05.
The output variables which are reported in the figures can be identiffied according to the list reported below.

plmax1:	maximum principal strain inside	
plmax5:	maximum principal strain outside	
epln11:	meridional strain inside	
epln12:	circumferential strain inside	
epln51:	meridional strain outside	
epln52:	circumferential strain outside	
displacement x:	horizzontal displacement (90° direction)	(m)
displacement y:	vertical displacement	(m)
displacement z:	horiizzontal displacement (180° direction)	(m)

The correspondence between the nodes which are representative of the required locations and the plot identification numbers is reported in Tab. 4.

TAB. 4
Correspondence betweeen gauge locations,
representative nodes in the model and figures.

Plot Id.	Node	Fig.	Plot Id.	Node	Fig.	Plot Id.	Node	Fig.	Plot Id.	Node	Fig.
1	186	3	12	1490	9	23	240	14	34	716	18
2	948	4	13	1258	10	24	240	14	35	1846	19
3	195	5	14	1258	10	25	128	15	36	1548	20
4	195	5	15	157	11	26	128	15	37	1258	21
5	942	6	16	157	11	27	128	15	38	1258	21
6	942	6	17	104	12	28	128	15	39	2154	22
7	1846	7	18	104	12	29	1314	16	40	831	23
8	419	8	19	78	13	30	1314	16	41	831	23
9	419	8	20	78	13	31	220	17	42	831	23
10	419	8	21	240	14	32	220	17	43	831	23
11	1490	9	22	240	14	33	716	18	-	-	-

Note that in the absence of the CS the plastic instability occurs at the pressure 0.05*121 MPa. When the CS is considered this value can be passed because of stress redistribution after contact. Limit pressures in the absence of the CS are reported in Tab. 5.

Tab. 5
Limit Pressure MPa

Failure mode	Without CS	With CS
Plastic instability	6.05	-
Local ductility reduction	(1)	-
Local buckling of the torospherical head	10.87	10.87
Plastic instability in the upper cylinder (2)	> 6.98	> 6.98
Plastic instability in the lower cylinder (2)	> 4.78	> 4.78

Notes:

1. By dimplified methods a triaxiality factor equal to 2.05 has been obtained near the penetration at a pressure of 3.5 Mpa, just before the contact of the vessel with the CS. The local equivalent strain is equal to 0.0023. According to the above criterion no rupture because of local ductility should occur before the contact.
2. Plastic instability in these regions has been evaluated by the Cooper's formula for thin cylinders. Therefore the values for the limit pressure are underestimated because of differences between the cylindrical shape and the local deformed shape due to the effect of the stiffeners.

CONCLUSIONS

According to the performed analysis no rupture should occur before the contact of th the CS. After the contact the value of the limit pressure computed for different modes the absence of the CS could be passed and further analyses are required to evaluate the in this latest case.

Fig. 1 - Vessel Model - x view.

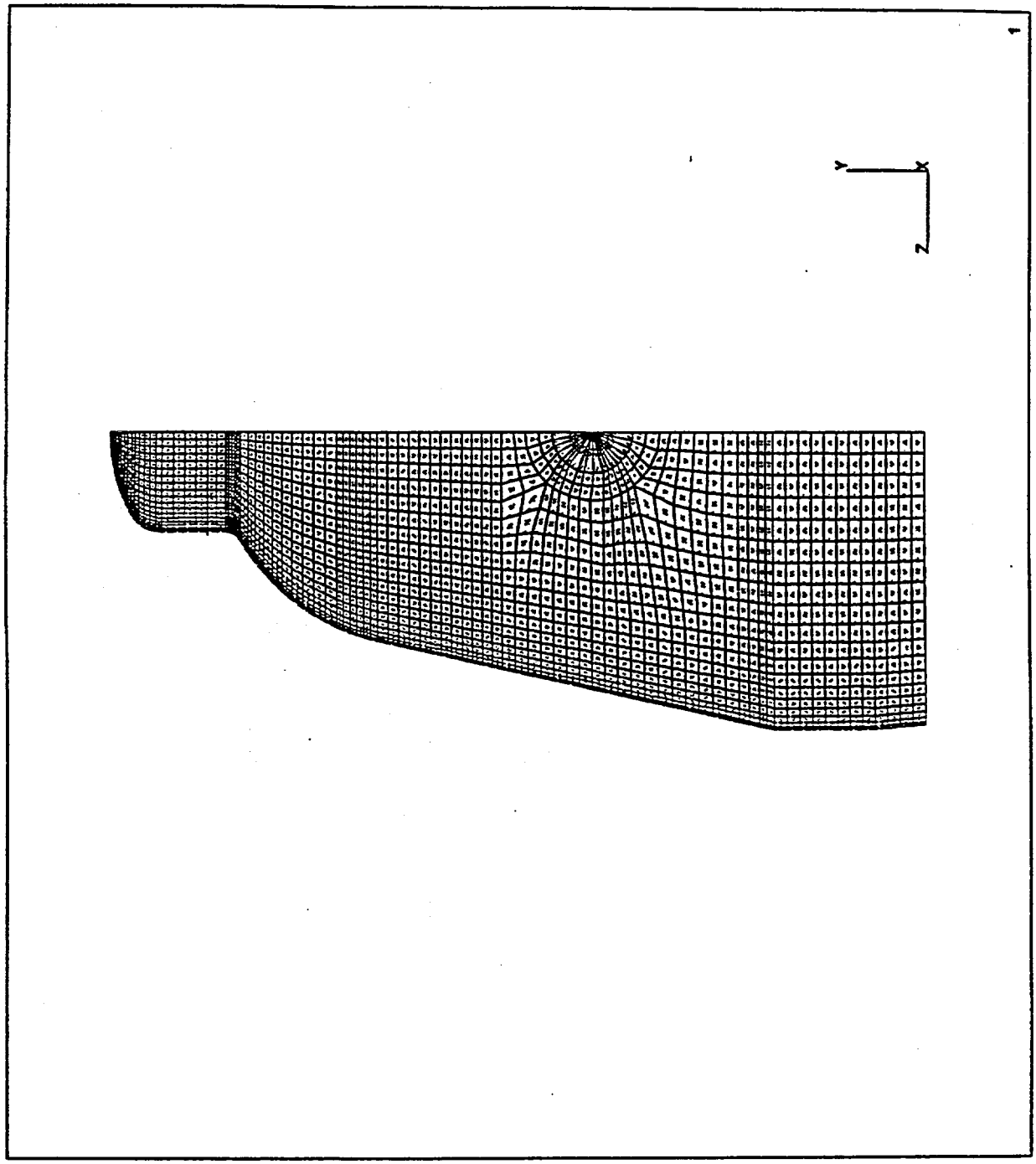

Fig. 2 - Vessel Model - z view.

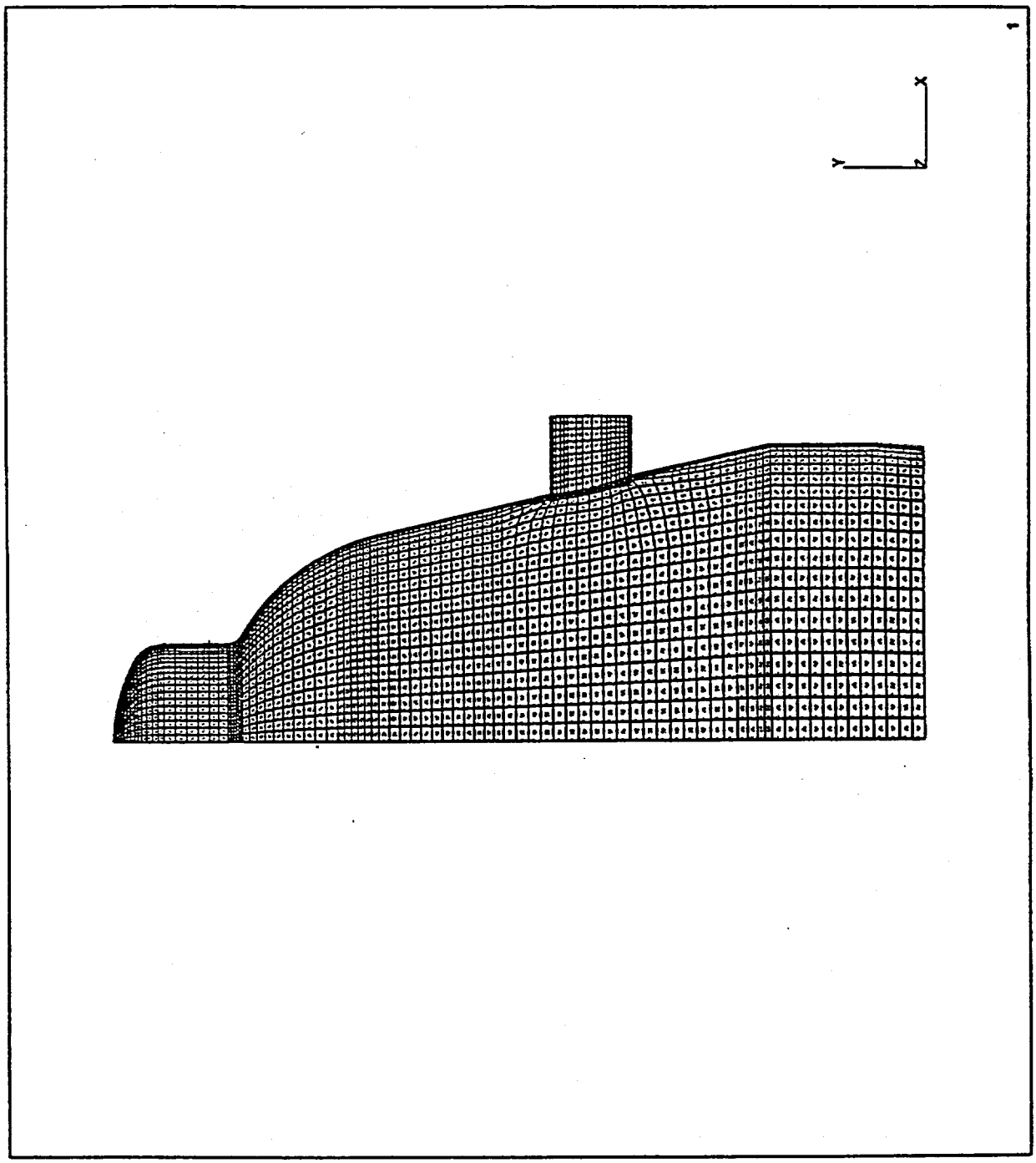

Fig. 3 - Plot 1.

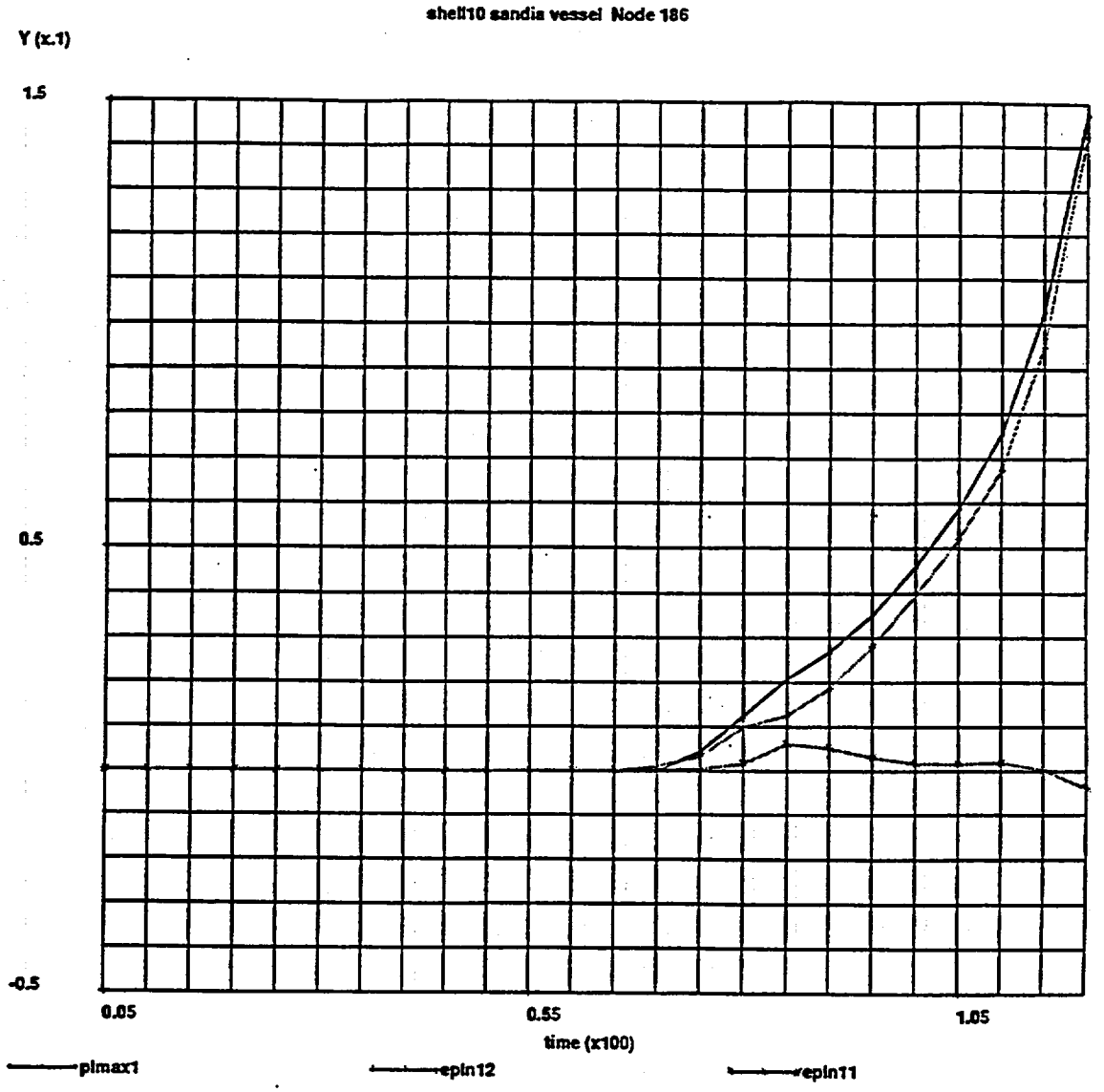
shell10 sandia vessel Node 186
Y (x.1)
1.5
0.5
-0.5
0.05
0.55
1.05
time (x100)
plmax1
epln12
epln11

Fig. 4 - Plot2.

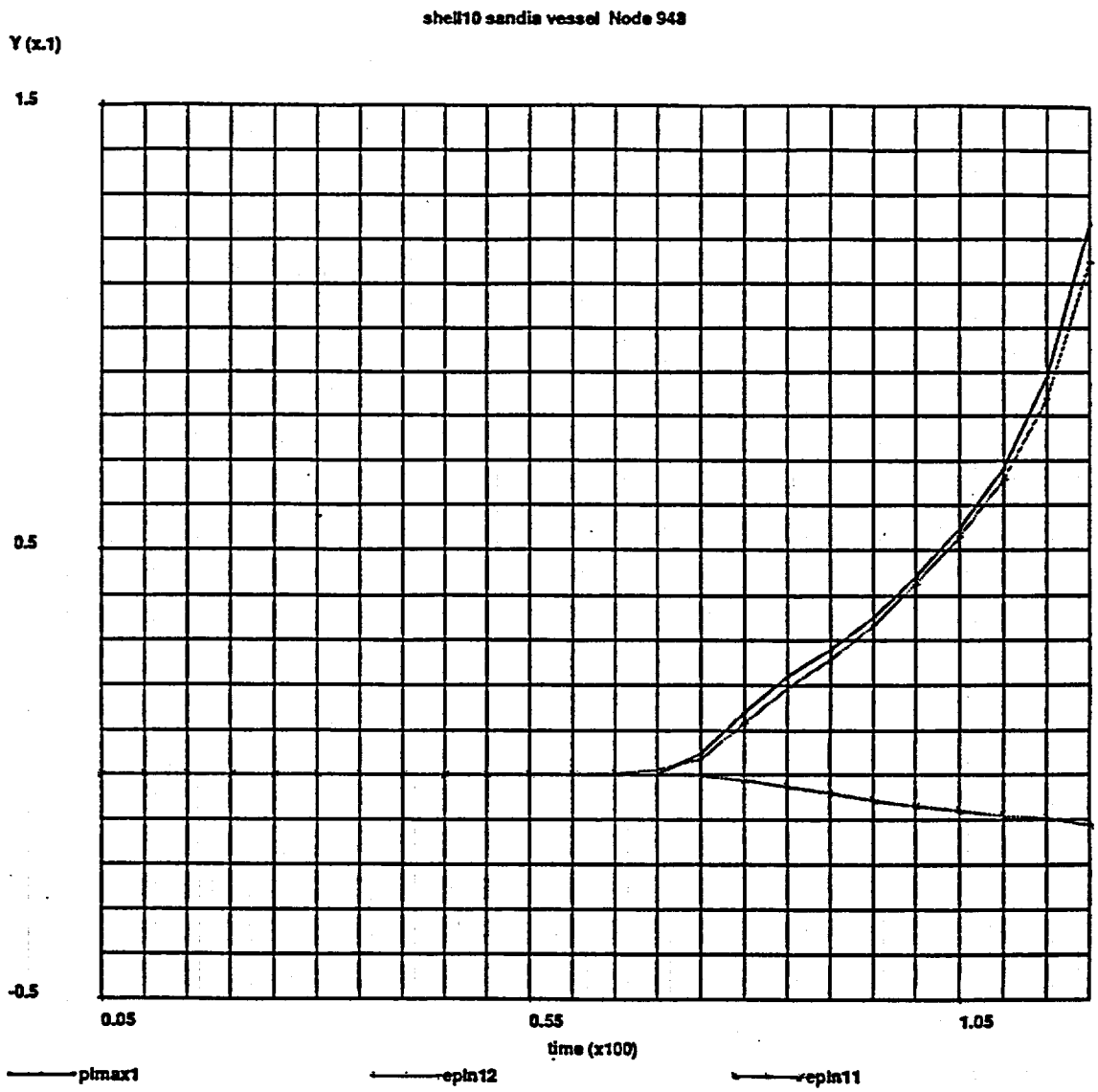
shell10 sandia vessel Node 948
Y (x.1)
1.5
0.5
-0.5
0.05
0.55
1.05
time (x100)
plmax1
epln12
epln11

Fig. 5 - Plots 3, 4.

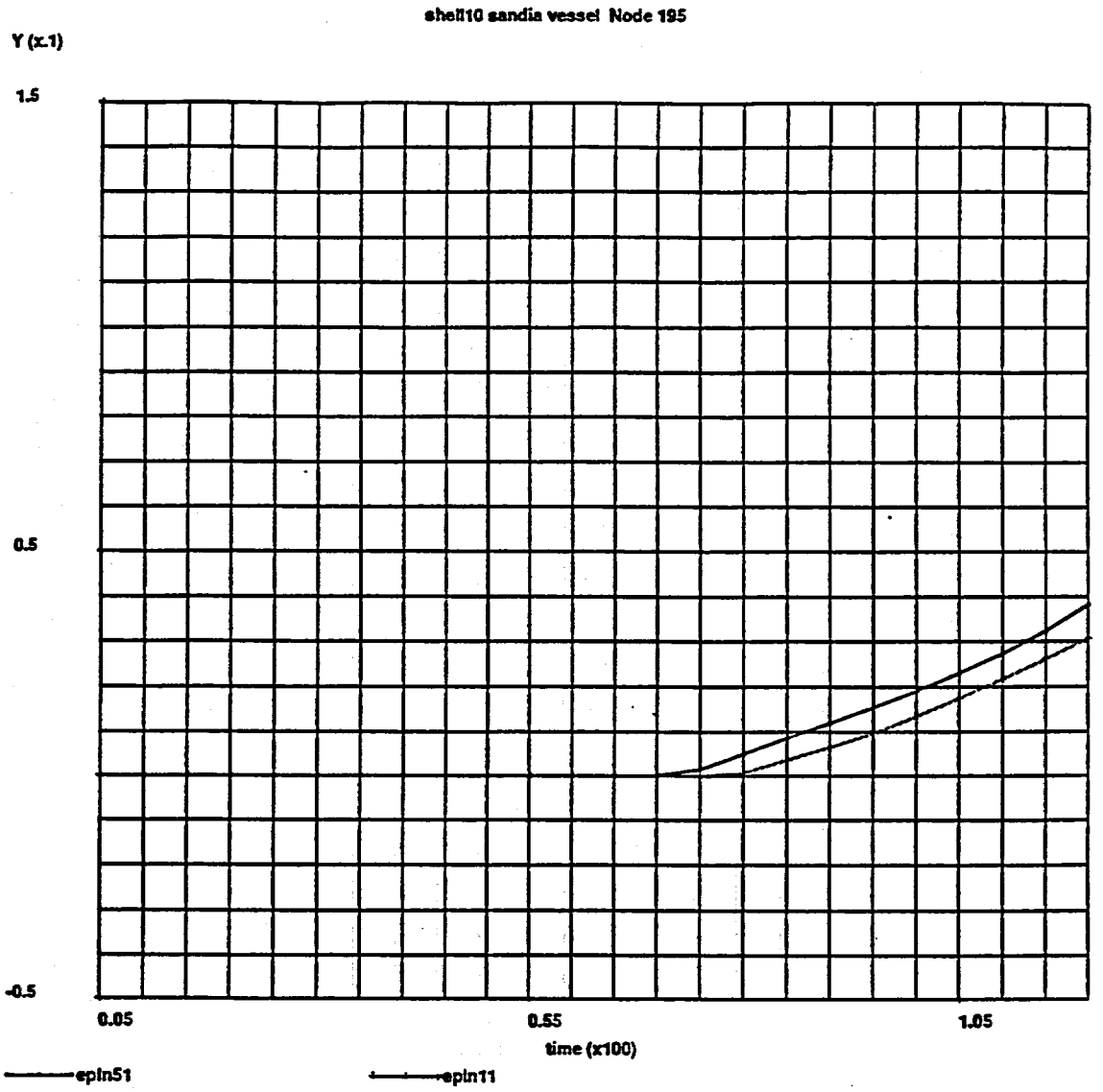

Fig. 6 - Plots 5, 6.

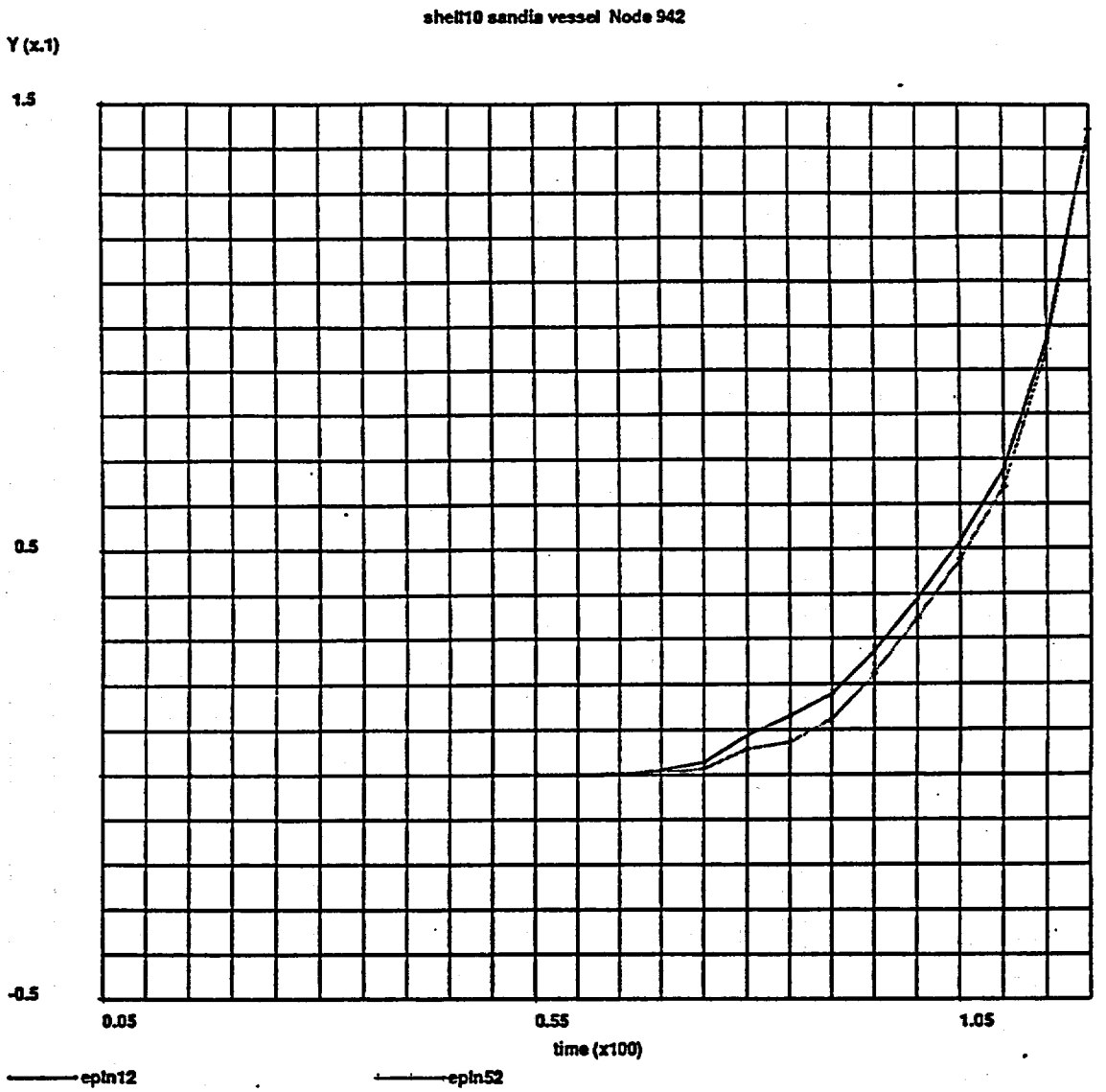

Fig. 7 - Plot 7.
(Zero plastic strain is obtained because the yielding point is never passed.)

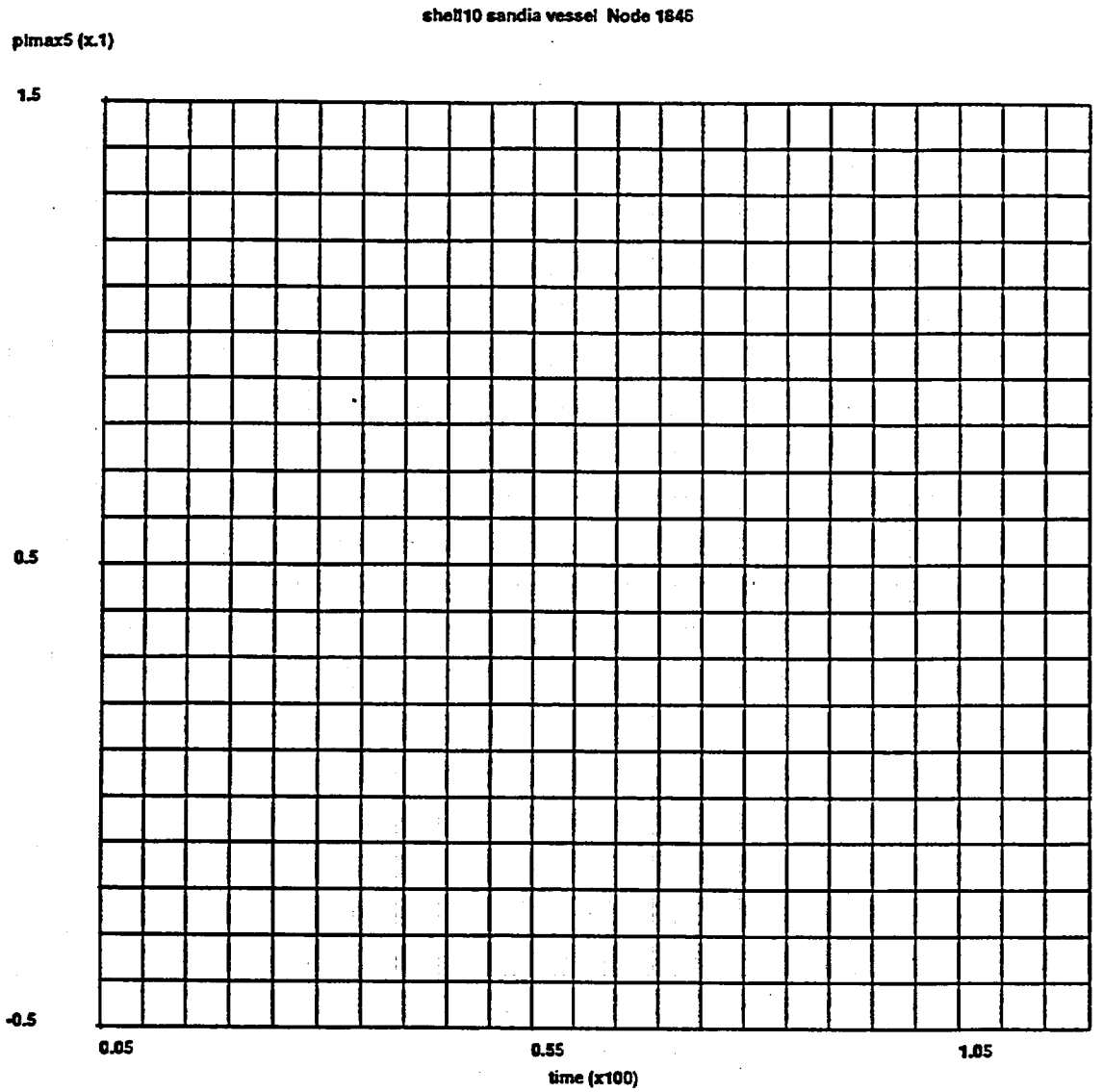

Fig. 8 - Plots 8, 9,10.

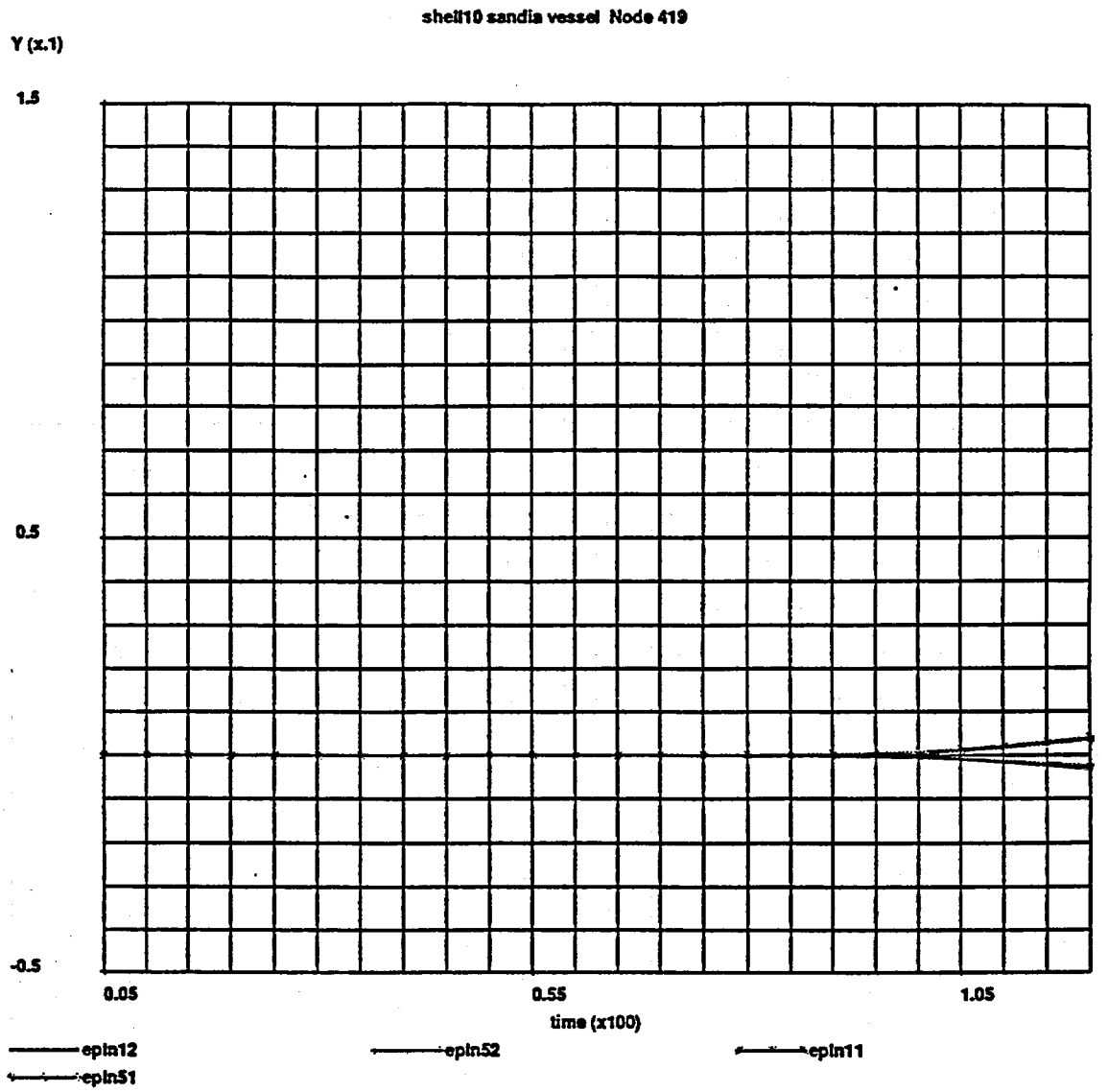

Fig. 9 - Plots 11, 12.

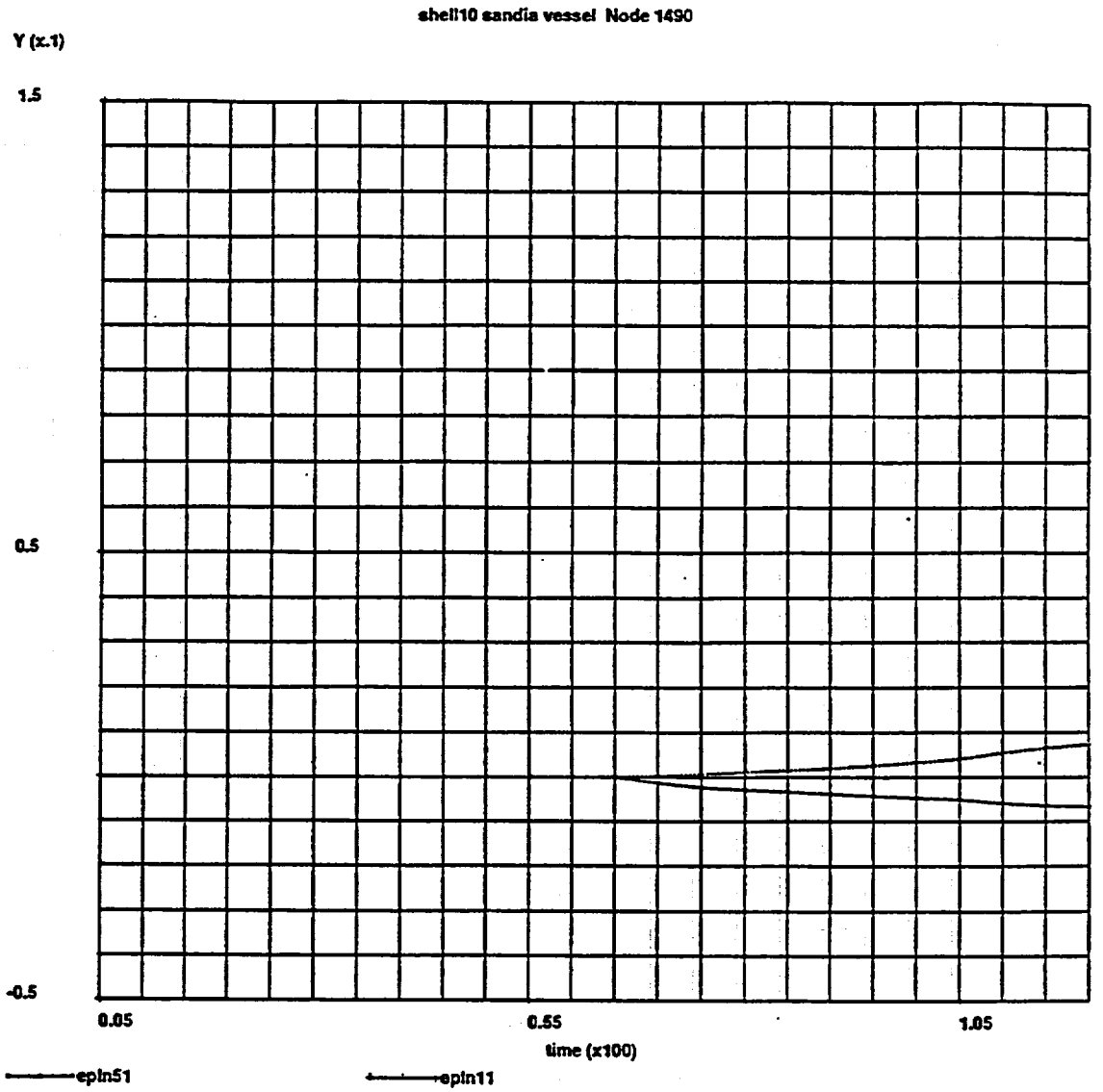

Fig. 10 - Plots 13, 14.

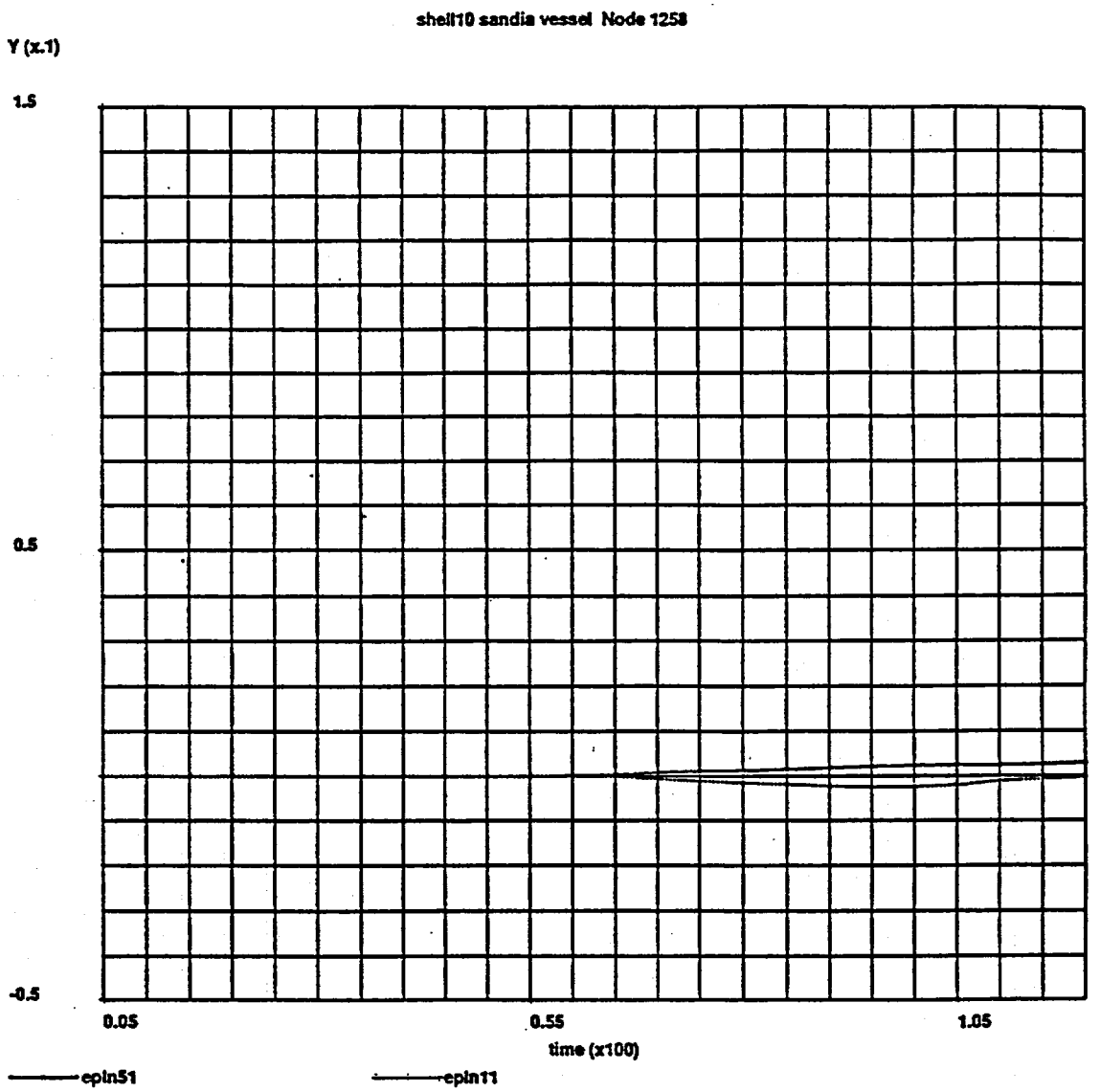

Fig. 11- Plots 15, 16.

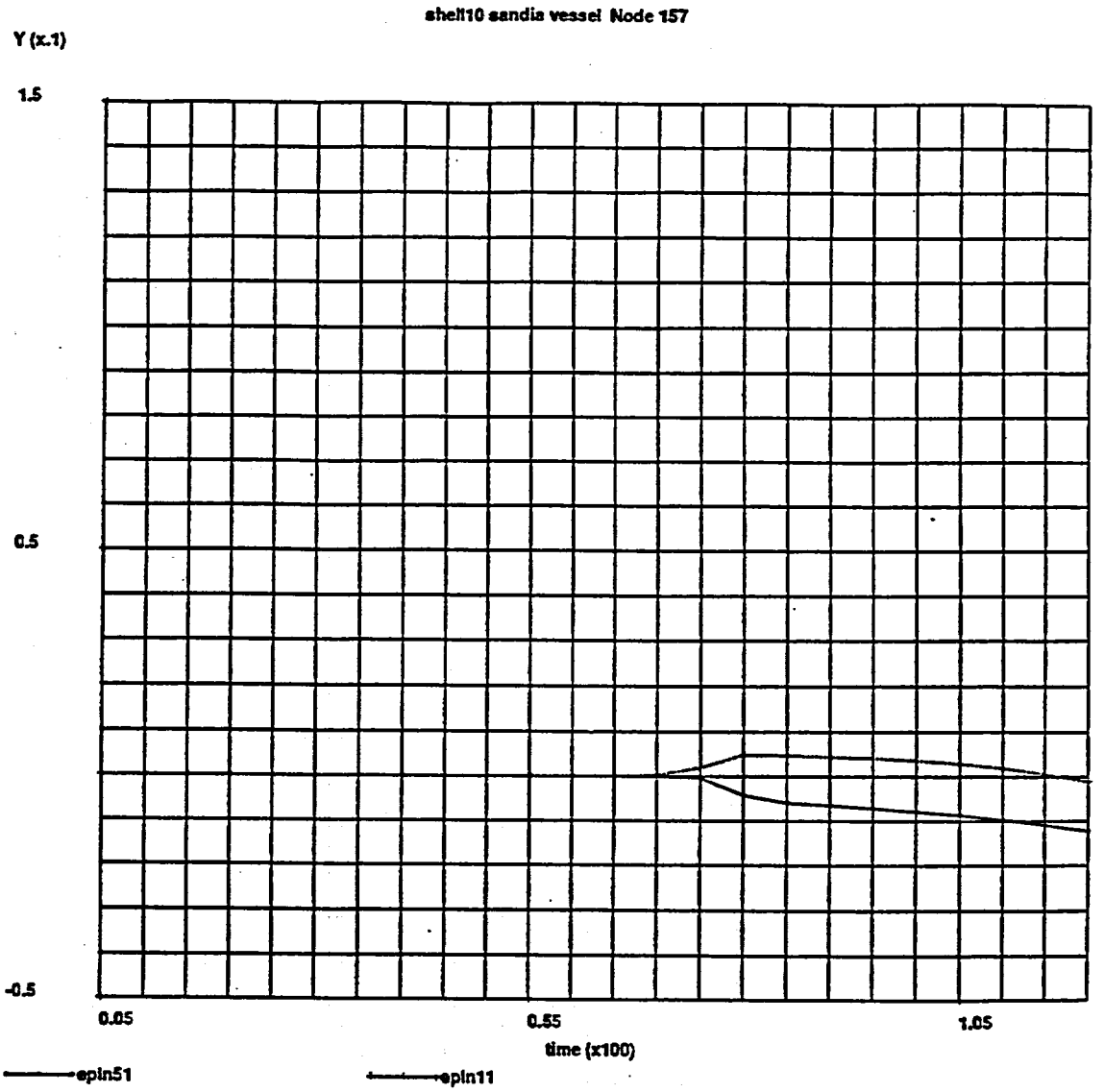

Fig. 12 - Plots 17, 18.

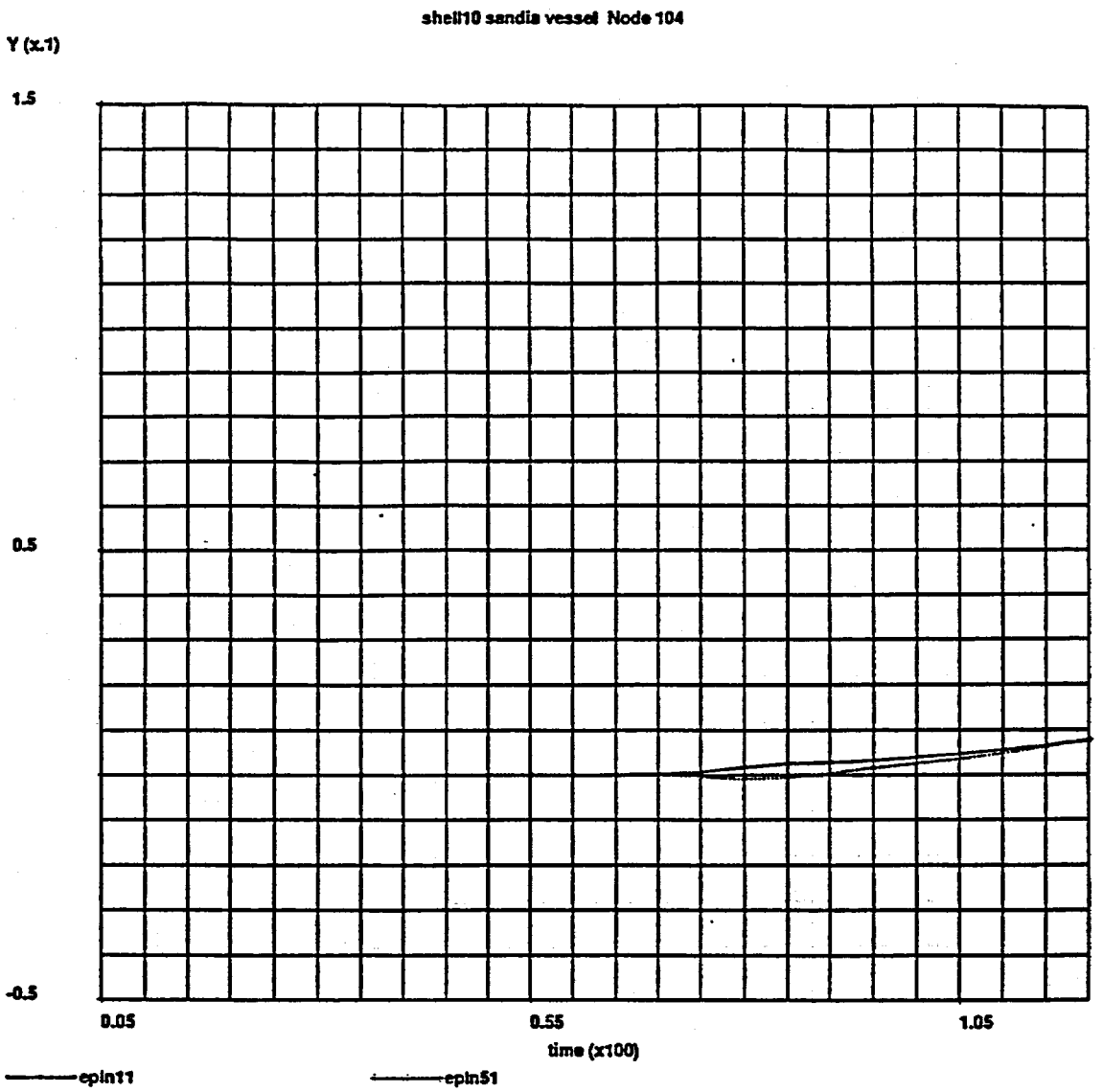

Fig. 13 - Plots 19, 20.

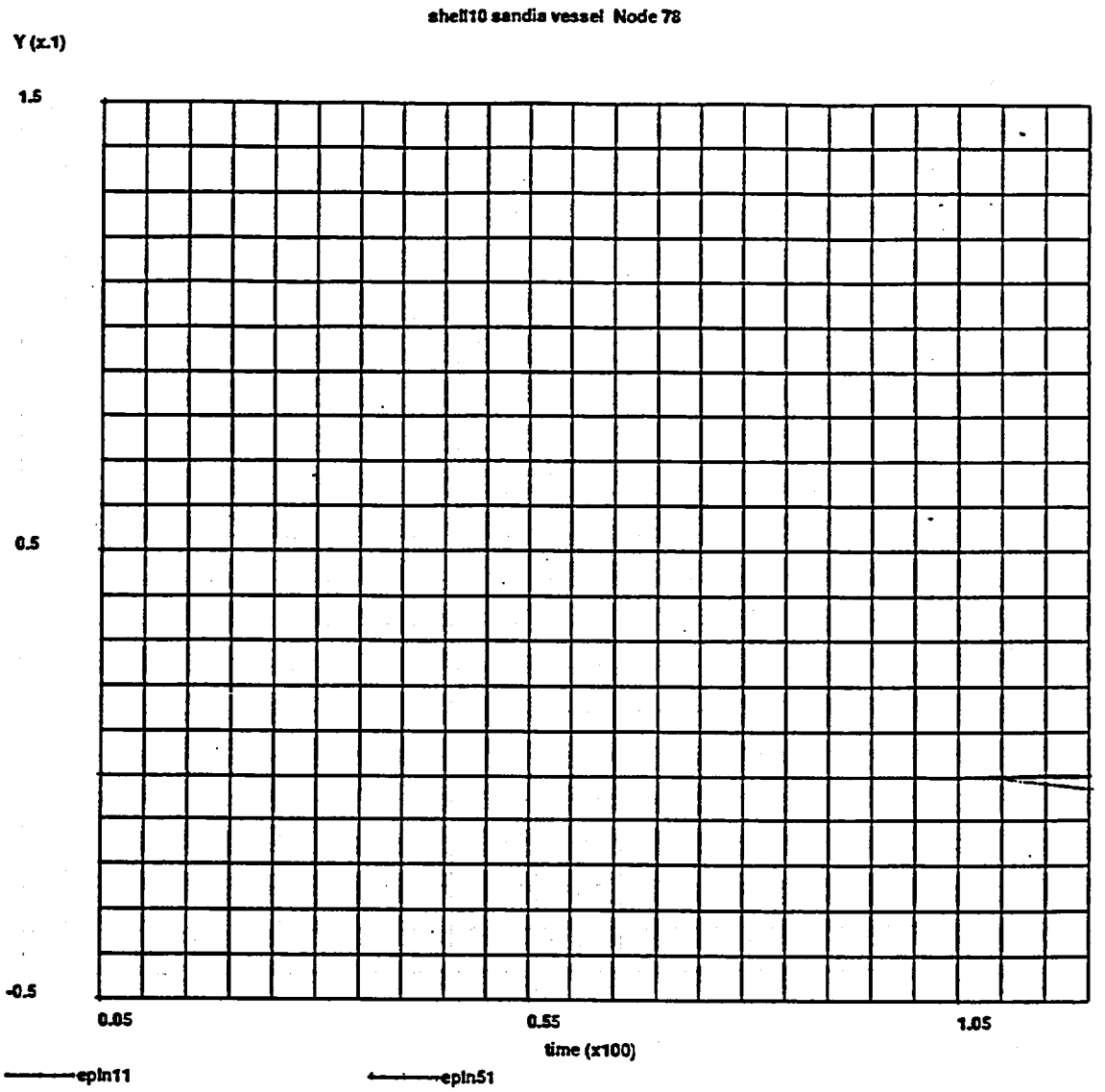

Fig. 14 - Plots 21, 22, 23, 24.

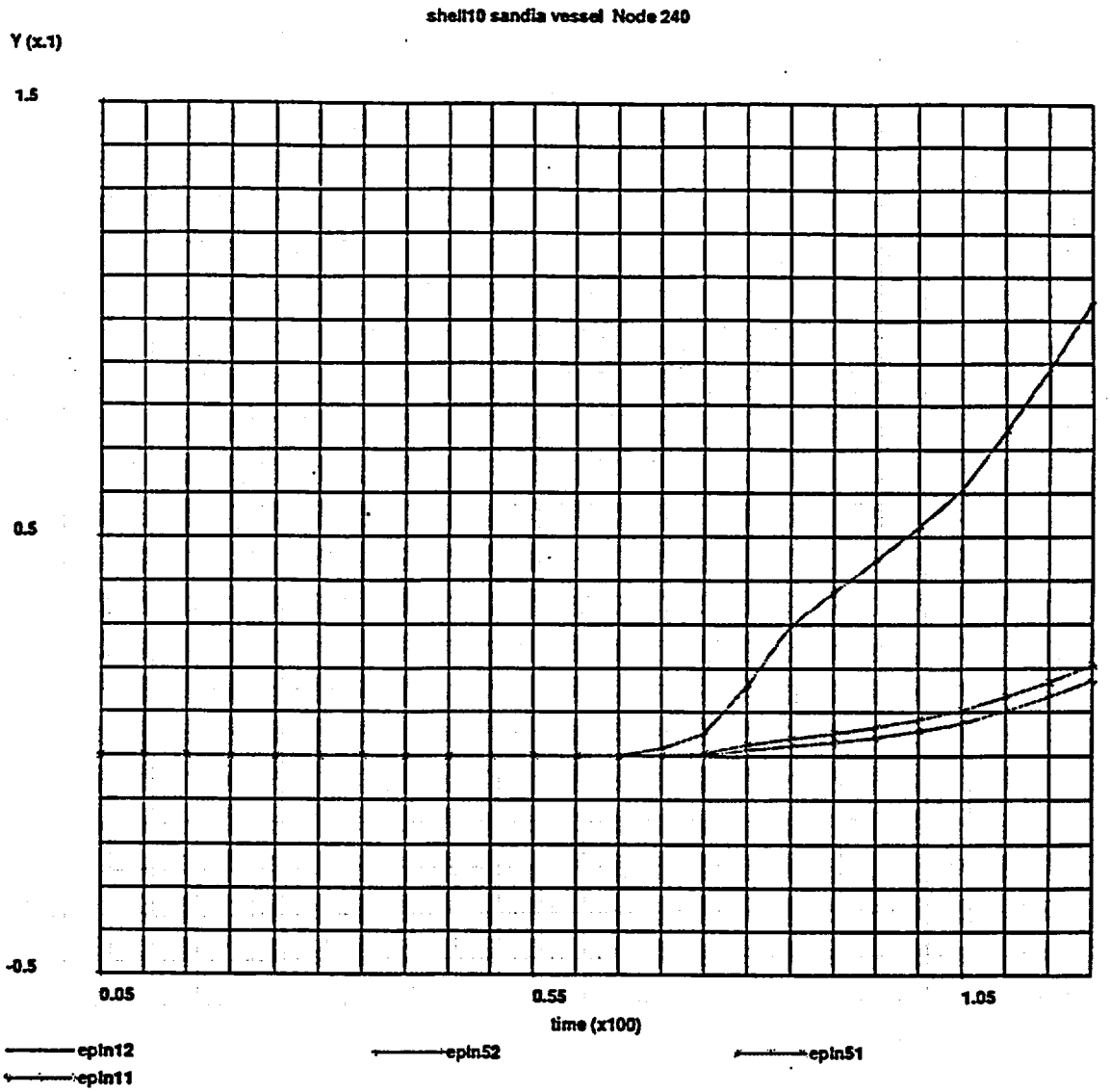

Fig. 15 - Plots 25, 26, 27, 28.

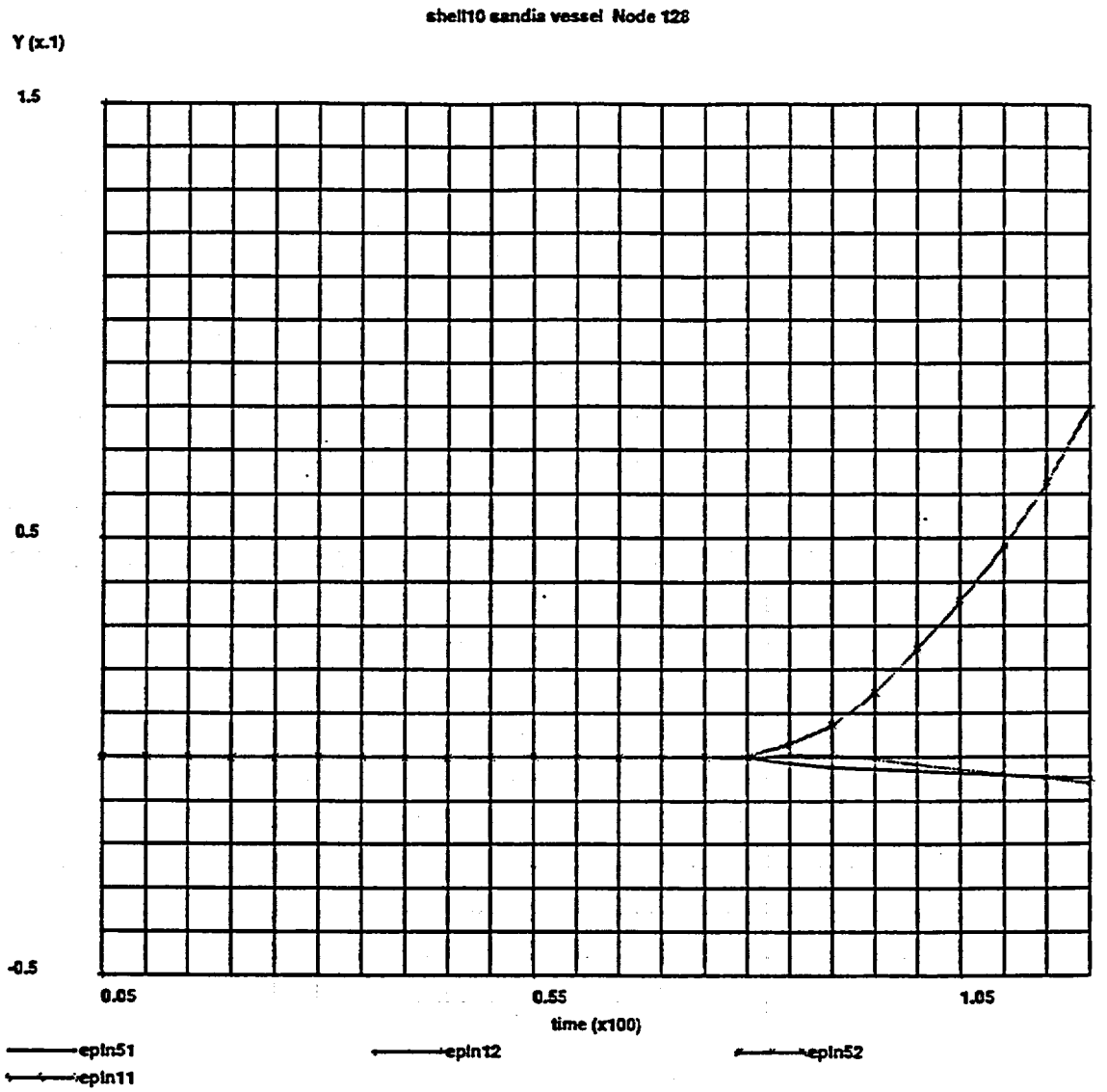

Fig. 16 - Plots 29, 30.

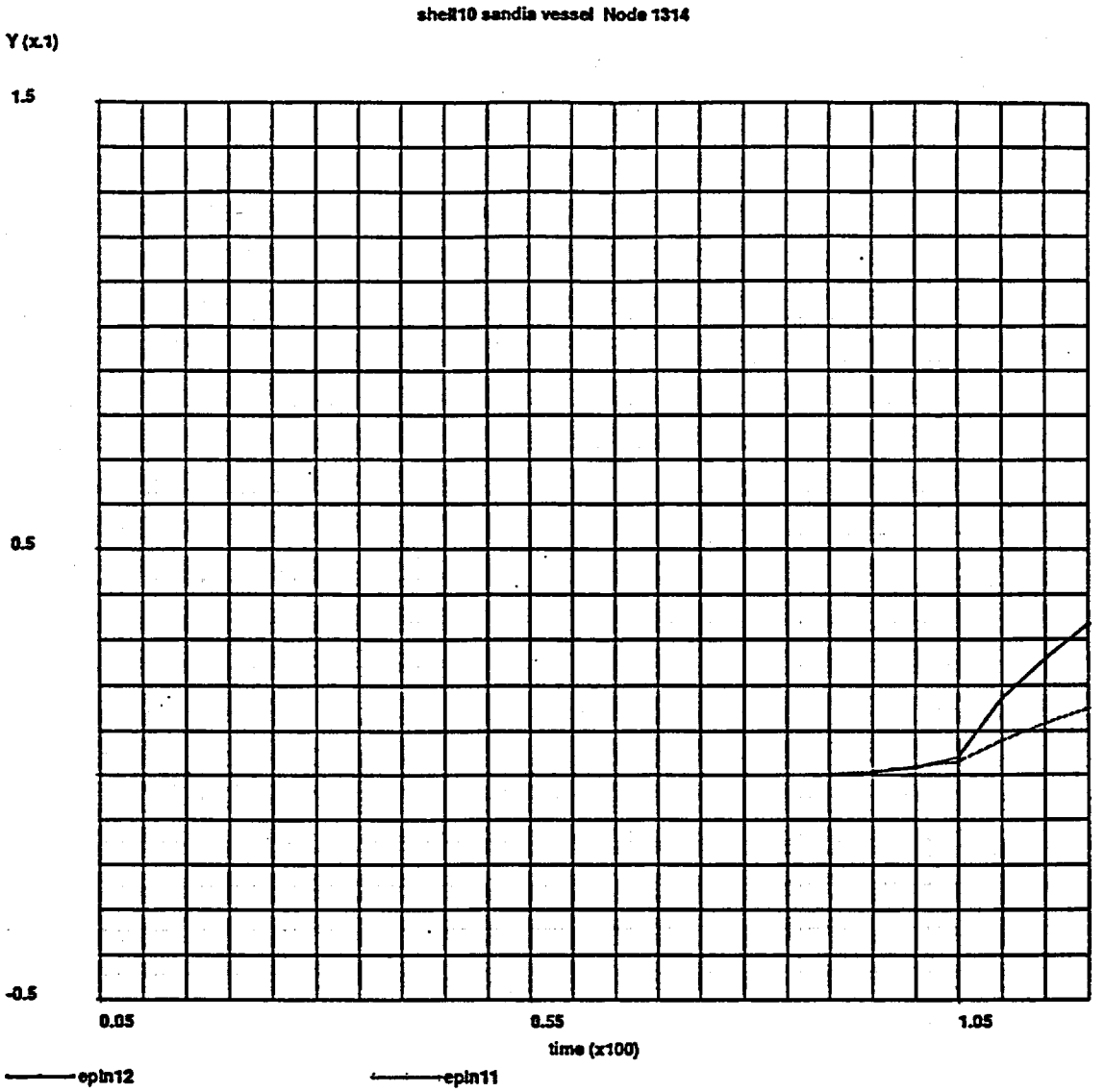

Fig. 17 - Plots 31, 32.

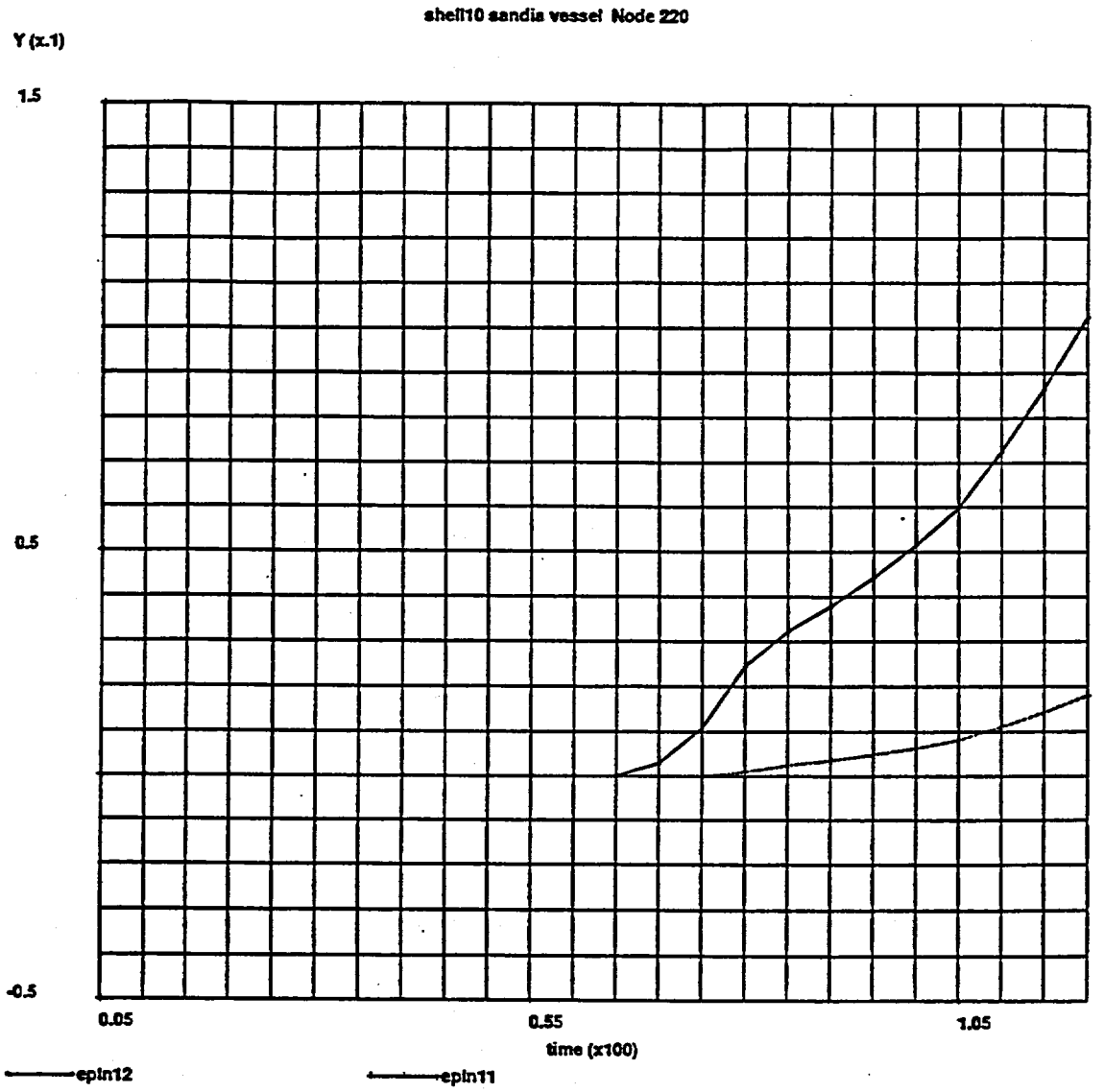

Fig. 18 - Plots 33, 34.

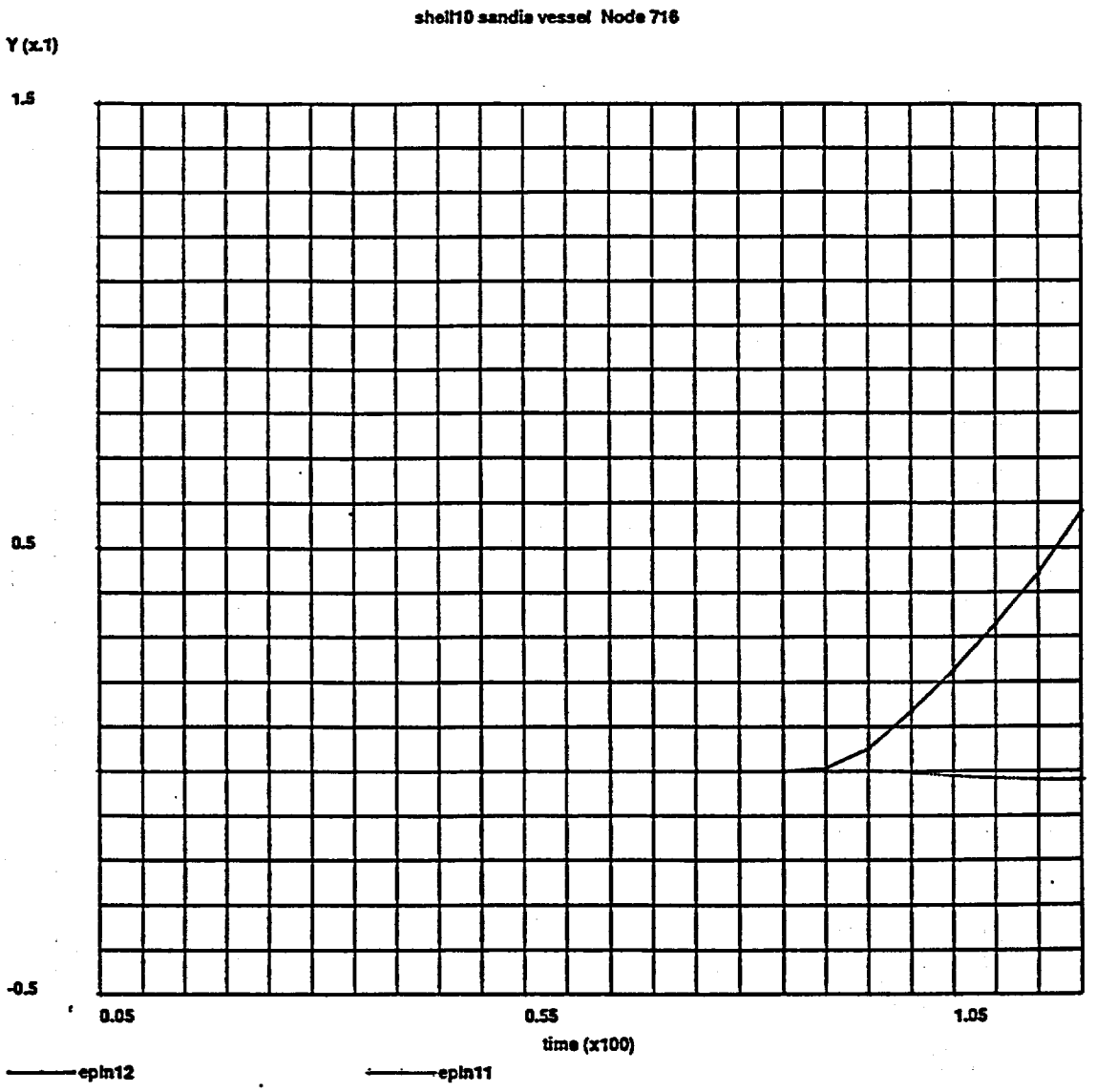

Fig. 19 - Plot 35.

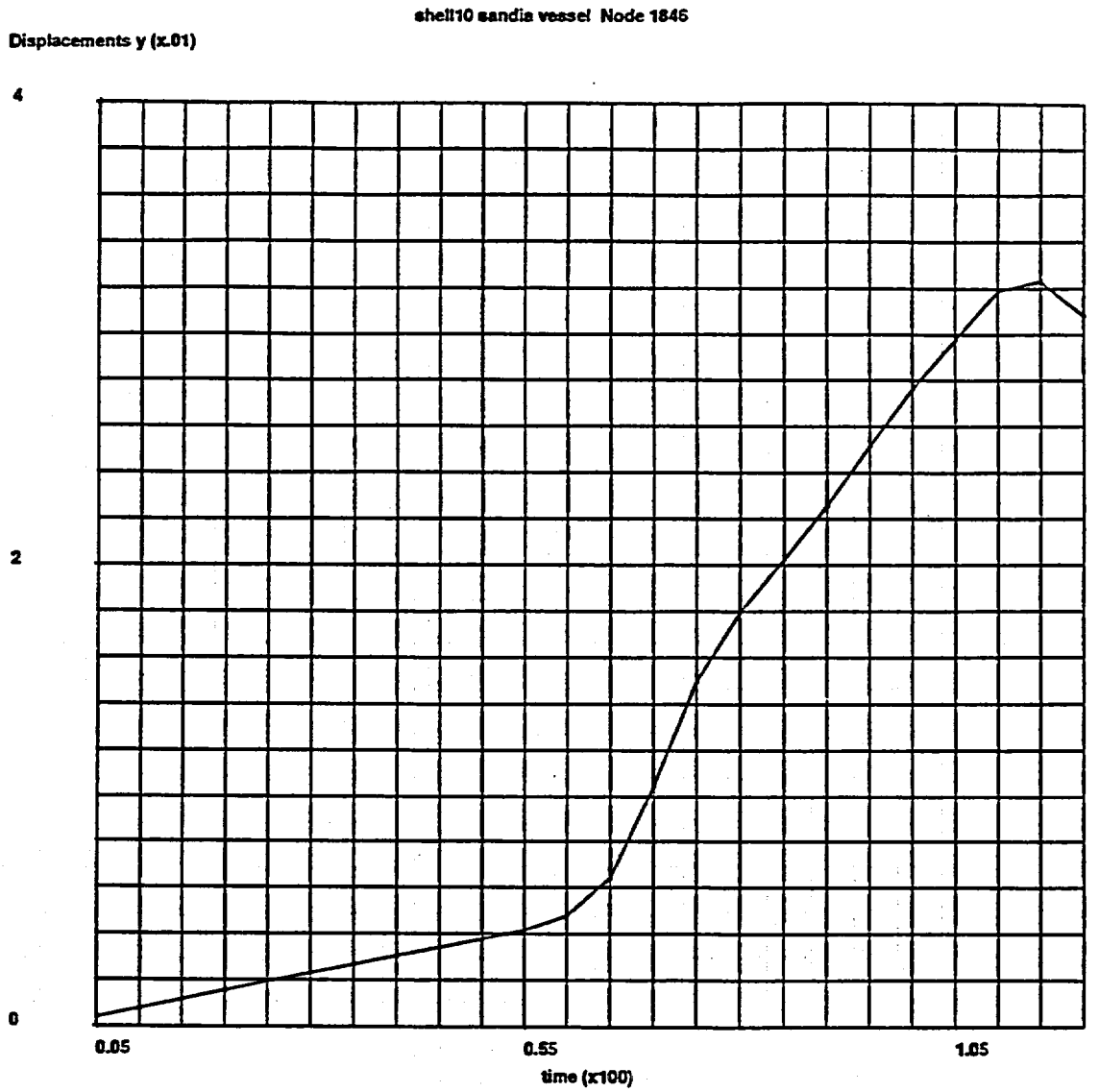

Fig. 20 - Plot 36.

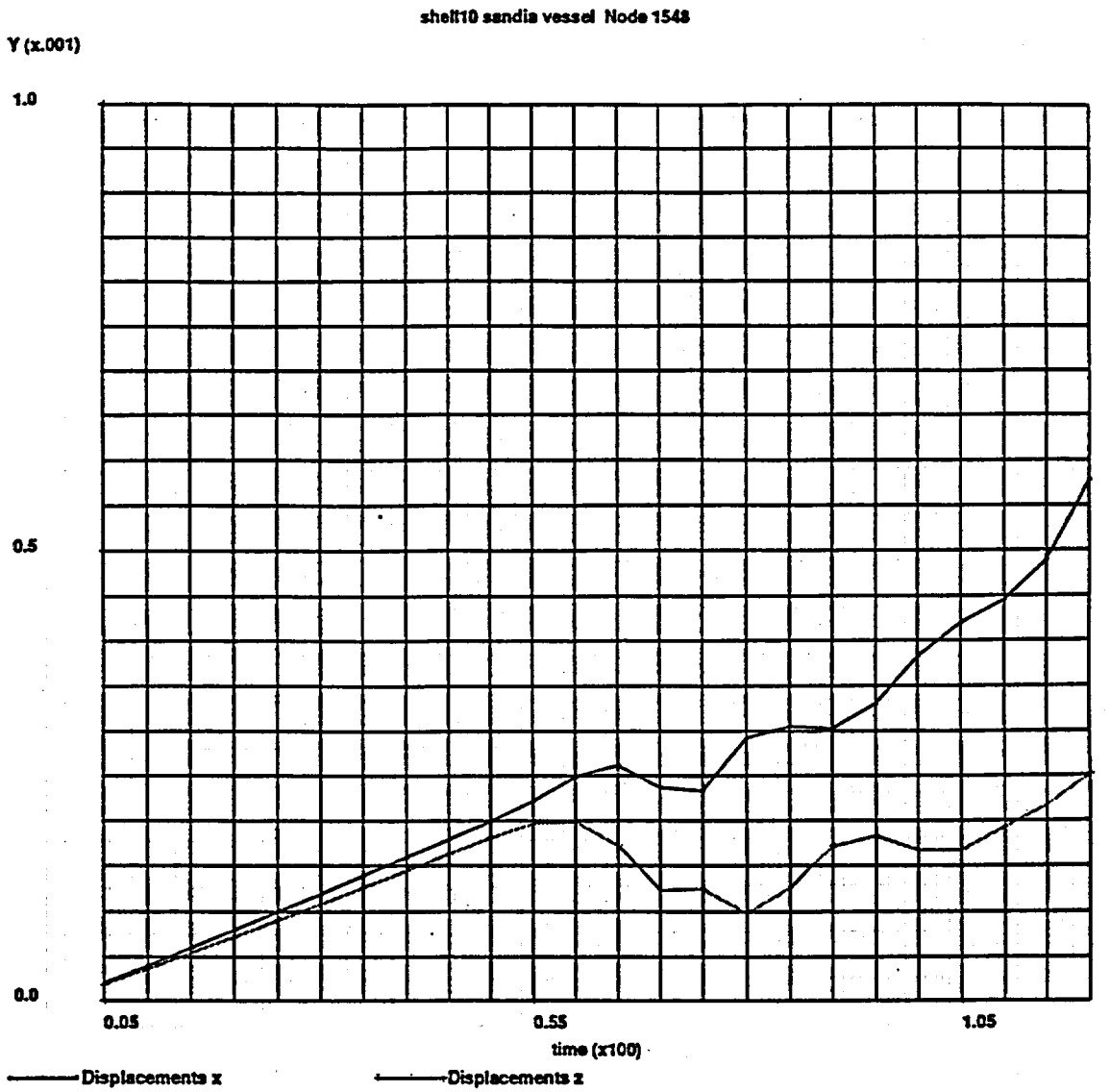

Fig. 21 - Plots 37, 38.

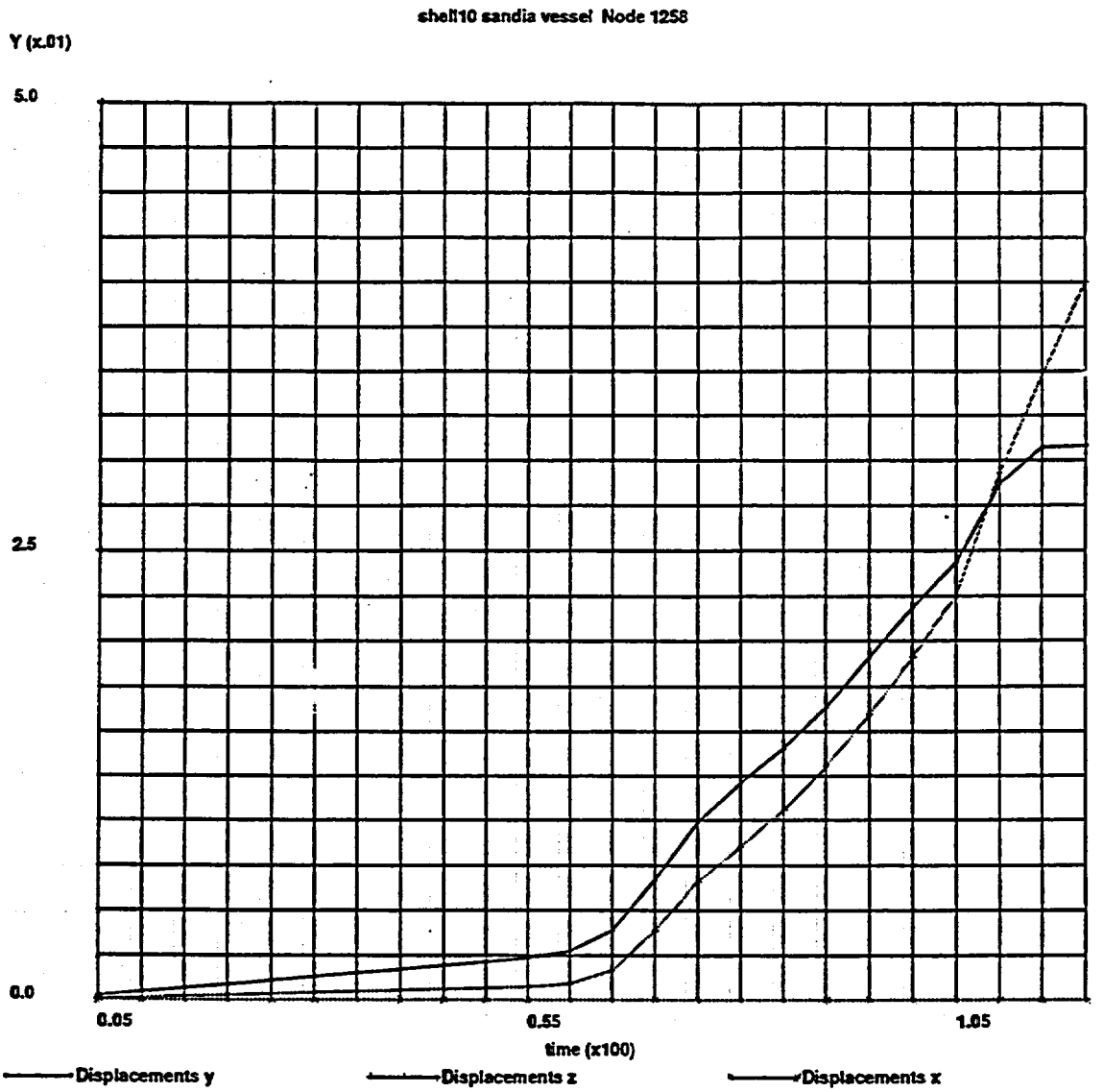

Fig. 22 - Plot 39.

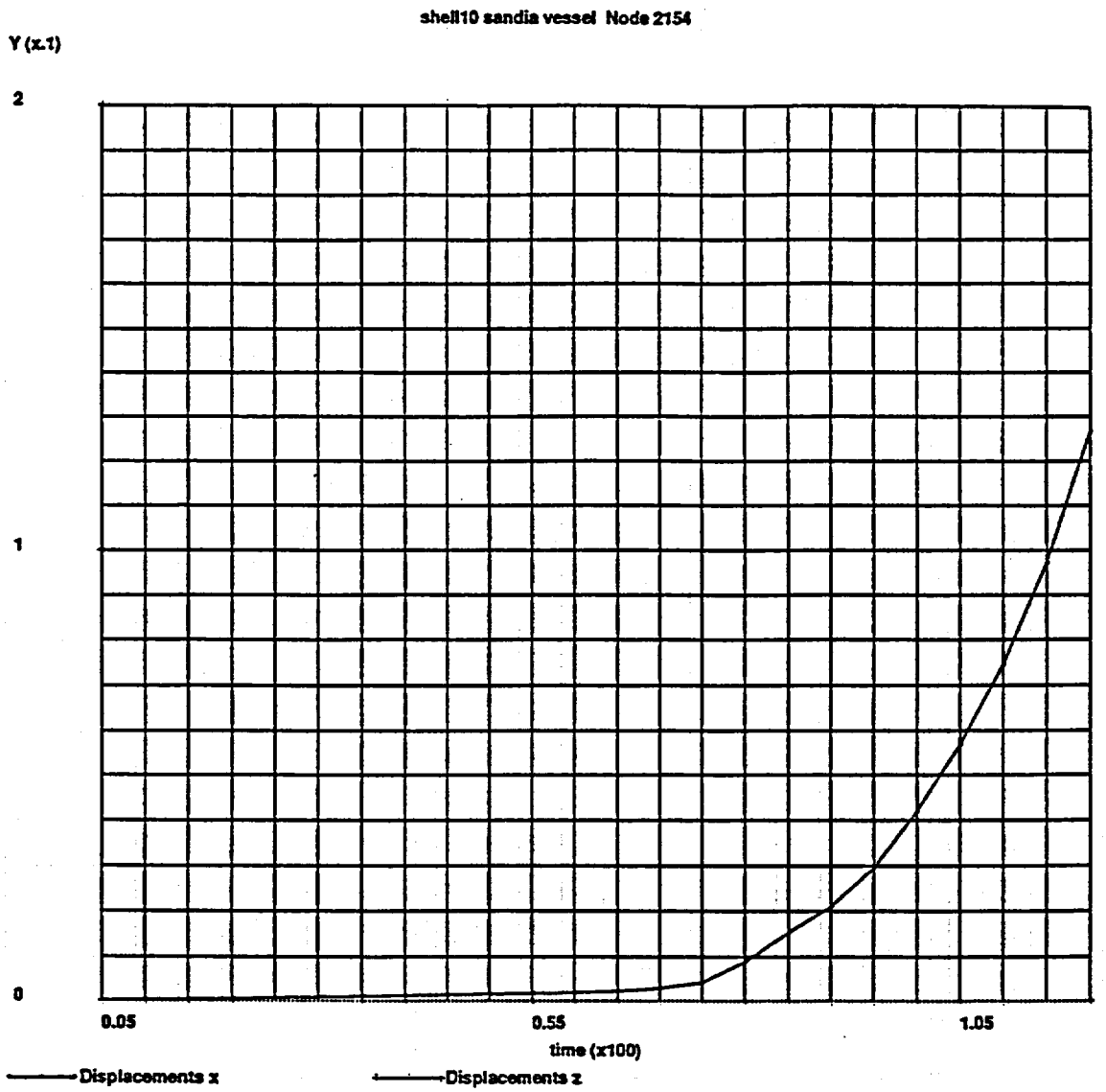

Fig. 23 - Plots 40, 41, 42, 43.

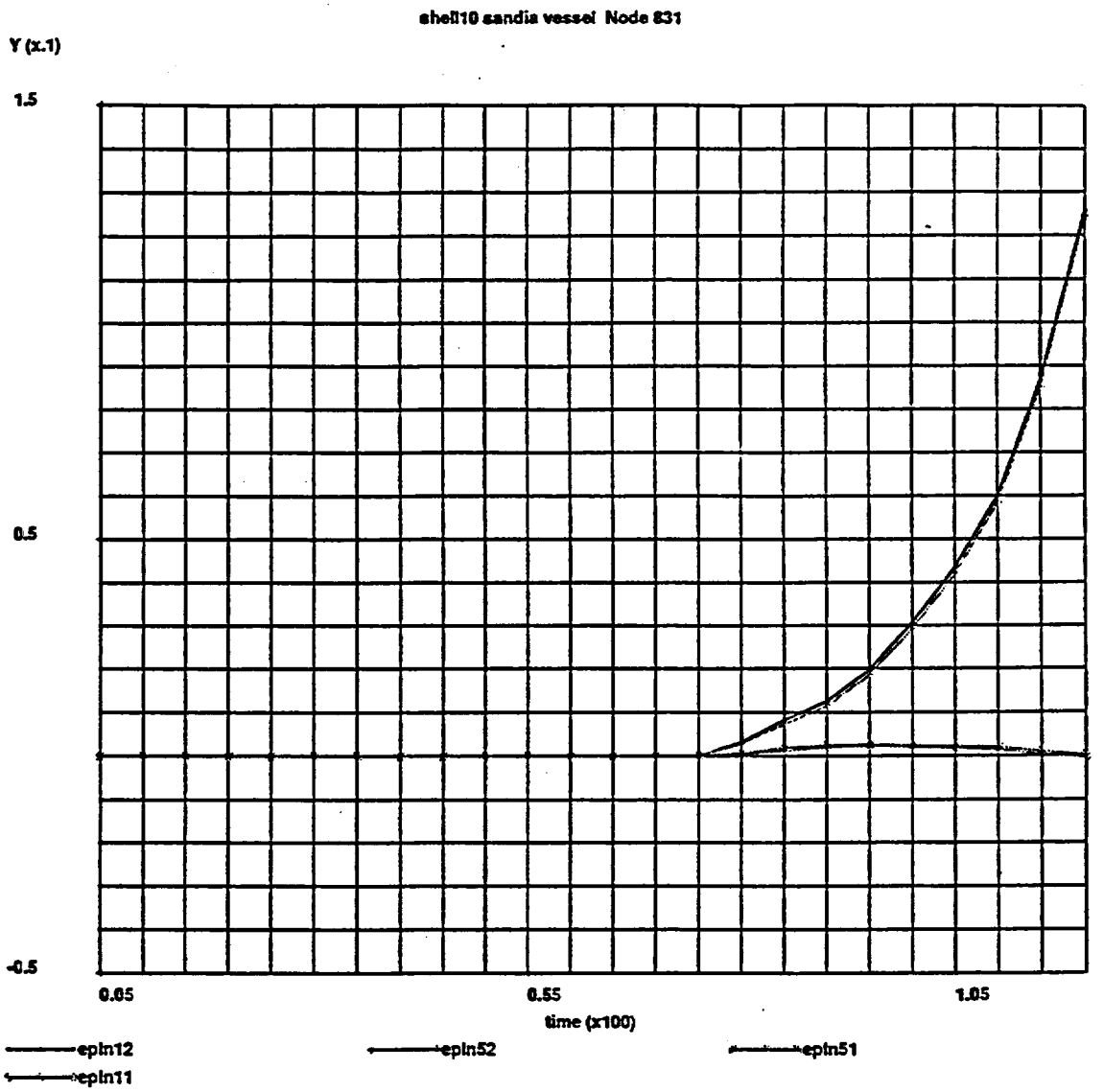

PRE-TEST VESSEL ANALYSIS
(Contact Structure Included)

Giuseppe Maresca - Giovanni Pino

ANPA
Agenzia Nazionale per la Protezione dell'Ambiente
Via Brancati 48 - 00144 Rome - ITALY

-August 96-

INTRODUCTION

A 3-D analysis of the Vessel to be tested, but with no Contact Structure (CS) is reported in (1). In the present note the same model is considered but the CS is now represented. To this purpose the contact option of the MARC code has been used. The CS has been simulated by a set of rigid surfaces, limiting the displacements of the Vessel shell. In the model the CS structure is axisymmetric but the axis of simmetry has been displaced with respect to the Vessel axis in order to make the related gaps partially consistent with the measured data. A maximum pressure of 10 MPa has been reached in the calculation.

VESSEL GEOMETRY AND MATERIAL DATA

The geometry of the vessel under analysis is the same defined in (1). As far as it concerns material data they are also reported, for the vessel in (1).

CONTACT SURFACE

The CS structure has been introduced in the model as a rigid surface which limits the deformation of the vessel shell. A tronco-conic surface, defined by the data listed below, has been considered.

Level of the upper base: 2.6972 m
Upper base radius: 1.0729 m
Level of the lower base: 0.2245 m (0.7000 m in the model to limit the contact controls)
Lower base radius: 1.6193 m (1.5142 m in the model to limit the contact controls)

A spherical surface has also been added, in order to represent the upper region of the CS. Data defining this region are listed below.

Level of the center of the sphere: 2.4601 m
Level of the starting point on the surface: 2.6972 m
Radius of the starting point on the surface: 1.0729
Level of the ending point on the surface: 3.4260 m
Radius of the ending point on the surafce: 0.5239 m

Finally the vertical axis of the CS has been displaced, towards the 180° direction, by 0.02468 m with respect to the vertical axis of the vessel, to get a gap of 0.02939 m at the location 9 as measured.

Contact controls have not been applied on the hatch nodes and on the vessel nodes located under the hatch. This to the purpose of simulating the opening in the CS.

FAILURE CRITERIA

The same failure criteria as in (1) have been considered. Because of the Contact Structure the occurrence of the the plastic instability is displaced towards an higher pressure. Really the analysis has been performed up to a maximum pressure of 10 MPa with no appearance of plastic instability.

As far as it concerns local ductility reduction because of triaxiality effects only some rough extimation have been performed. They do not indicate any local rupture before 10 Mpa. However a more detailled analysis regarding this failure mode is now in progress.
As reported in (1) buckling of the torospherical head is expected at 10.87 MPa.

RESULTS

Plastic deformations, total strains and displacements at the required locations are reported in figs. 3-23.
Note that only plastic strains are reported. So they are zero in each location untill yielding occurs.
Conventional time is reported on the abscissa. To get the corresponding pressure value in MPa the time value must be multiplied by 0.05.
The output variables which are reported in the figures can be identified according to the list reported below.

plmax1:	maximum principal strain inside	
plmax5:	maximum principal strain outside	
epln11:	meridional strain inside	
epln12:	circumferential strain inside	
epln51:	meridional strain outside	
epln52:	circumferential strain outside	
displacement x:	horizzontal displacement (90° direction)	(m)
displacement y:	vertical displacement	(m)
displacement z:	horizzontal displacement (180° direction)	(m)

The correspondence between the nodes which are representative of the required locations and the plot identification numbers is reported in Tab. 1.

TAB. 1
Correspondence betweeen gauge locations,
representative nodes in the model and figures.

Plot Id.	Node	Fig.	Plot Id.	Node	Fig.	Plot Id.	Node	Fig.	Plot Id.	Node	Fig.
1	186	3	12	1490	9	23	240	14	34	716	18
2	948	4	13	1258	10	24	240	14	35	1846	19
3	195	5	14	1258	10	25	128	15	36	1548	20
4	195	5	15	157	11	26	128	15	37	1258	21
5	942	6	16	157	11	27	128	15	38	1258	21
6	942	6	17	104	12	28	128	15	39	2154	22
7	1846	7	18	104	12	29	1314	16	40	831	23
8	419	8	19	78	13	30	1314	16	41	831	23
9	419	8	20	78	13	31	220	17	42	831	23
10	419	8	21	240	14	32	220	17	43	831	23
11	1490	9	22	240	14	33	716	18	-	-	-

Note that in the absence of the CS the plastic instability occurs at the pressure 0.05*121 MPa. When the CS is considered this value can be passed because of stress redistribution after contact. Limit pressures in the absence of the CS as well as in the case of CS included are reported in Tab. 2.

Tab. 2
Limit Pressure MPa

Failure mode	Without CS	With CS
Plastic instability	6.05	>10
Local ductility reduction	(1)	(3)
Local buckling of the torospherical head	10.87	10.87
Plastic instability in the upper cylinder (2)	> 6.98	> 6.98
Plastic instability in the lower cylinder (2)	> 4.78	> 4.78

Notes:

1. By simplified methods a triaxiality factor equal to 2.05 has been obtained near the penetration at a pressure of 3.5 Mpa, just before the contact of the vessel with the CS. The local equivalent strain is equal to 0.0023. According to the above criterion no rupture because of local ductility should occur before the contact.
2. Plastic instability in these regions has been evaluated by the Cooper's formula for thin cylinders. Therefore the values for the limit pressure are underestimated because of differences between the cylindrical shape and the local deformed shape due to the effect of the stiffeners.
3. Triaxiality effects are comparable with the CS missing case.

CONCLUSIONS

In the present analysis a maximum pressure of 10 MPa has been reached without any occurrence of plastic instability. This result should be compared with the plastic instability pressure of 6.05 MPa obtained in absence of the Contact Structure. Anyway, buckling of the torospherical head is expected at a pressure of 10.87 MPa. Triaxiality effects have also been considered in a simplified manner. No rupture according to this mode of failure has been found up to the maximum pressure of 10 MPa. However the performed anlysis is thought to be not sufficient to provide a reliable result with respect to this latest mode of failure.

REFERENCES

1. Giuseppe Maresca, Giovanni Pino "Pre-Test Vessel Analysis (In absence of the Contact Structure)" . ANPA document, July 96.

Fig. 1 - CS Model.

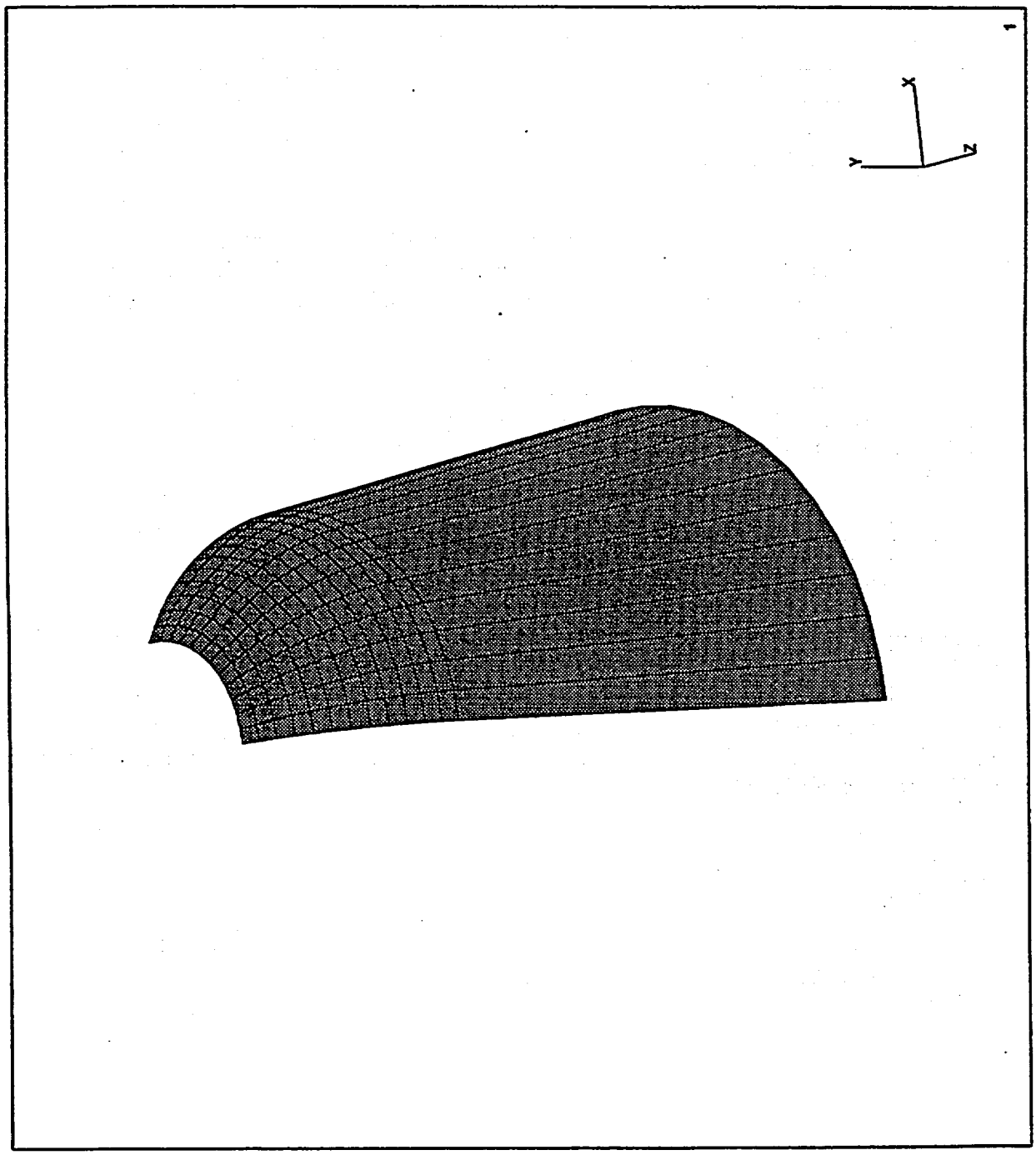

Fig. 2 - Vessel and CS together.

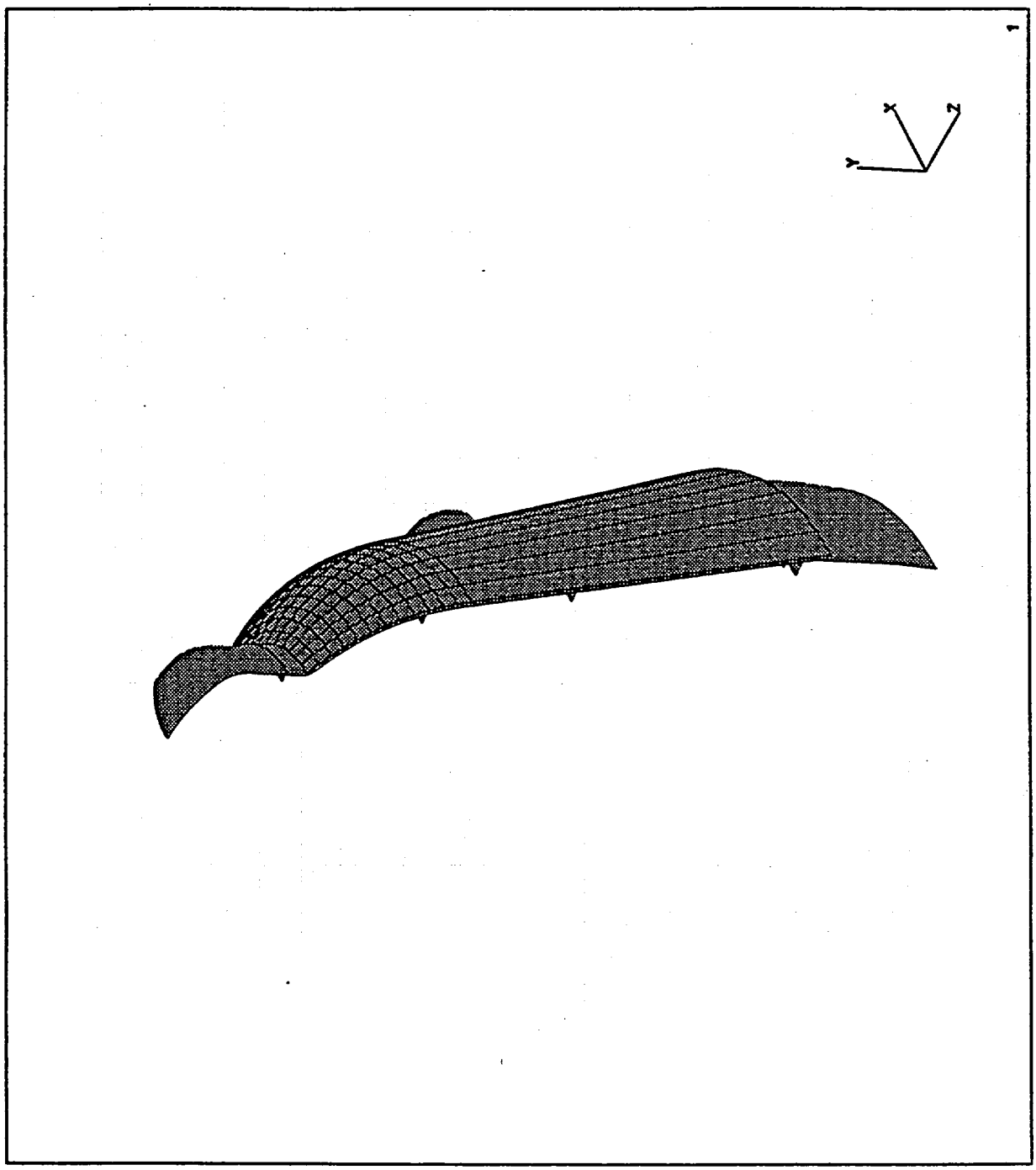

Fig. 3 - Plot 1.

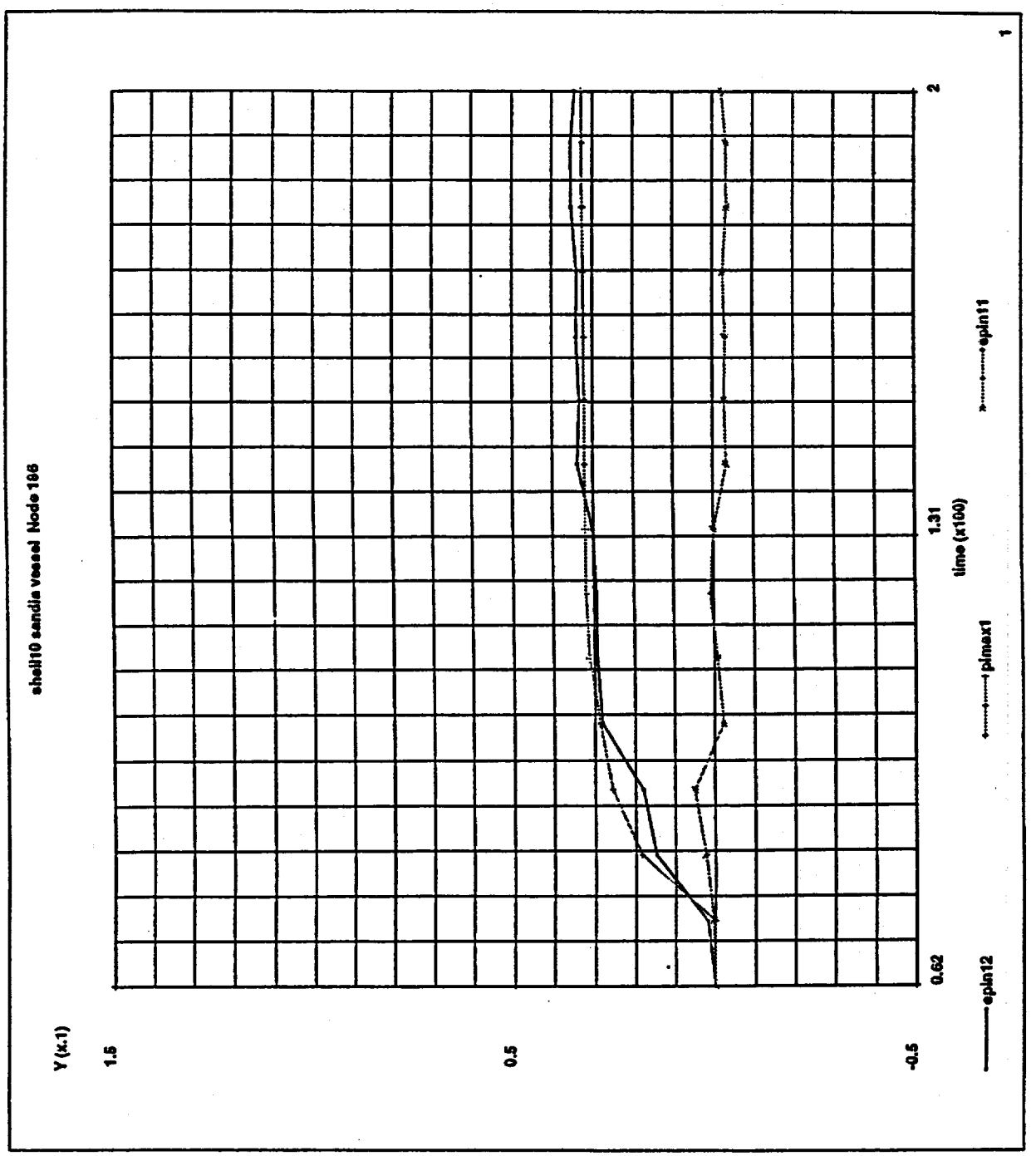
shell10 sandia vessel Node 166
Y (x.1)
1.5
0.5
-0.5
0.62
1.31
2
time (x100)
epln12
plmax1
epln11
1

Fig. 4 - Plot2.

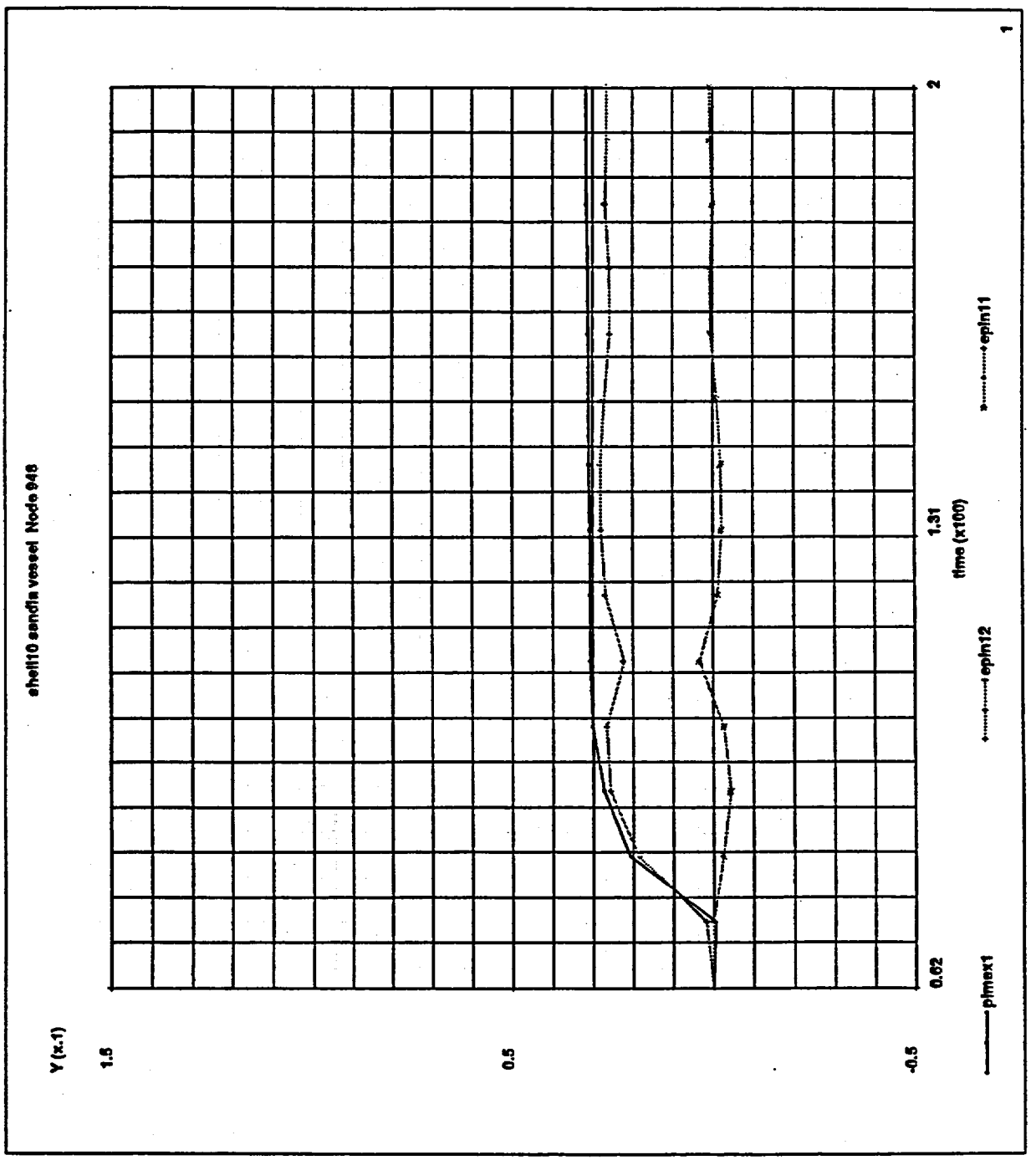
shell10 sandia vessel Node 948
Y (x.1)
1.5
0.5
-0.5
0.02
1.31
2
time (x100)
plmax1
epln12
epln11
1

Fig. 5 - Plots 3, 4.

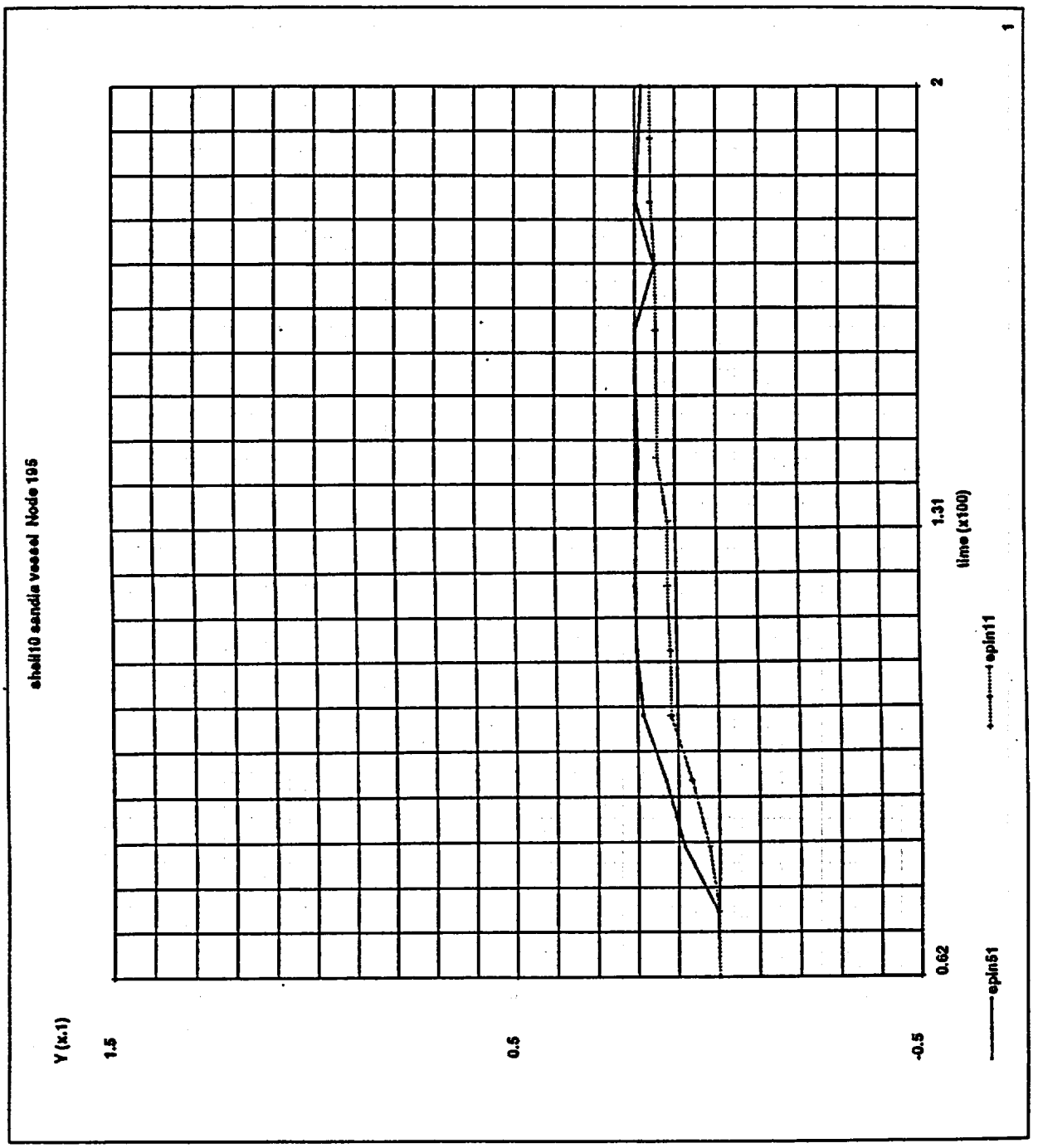

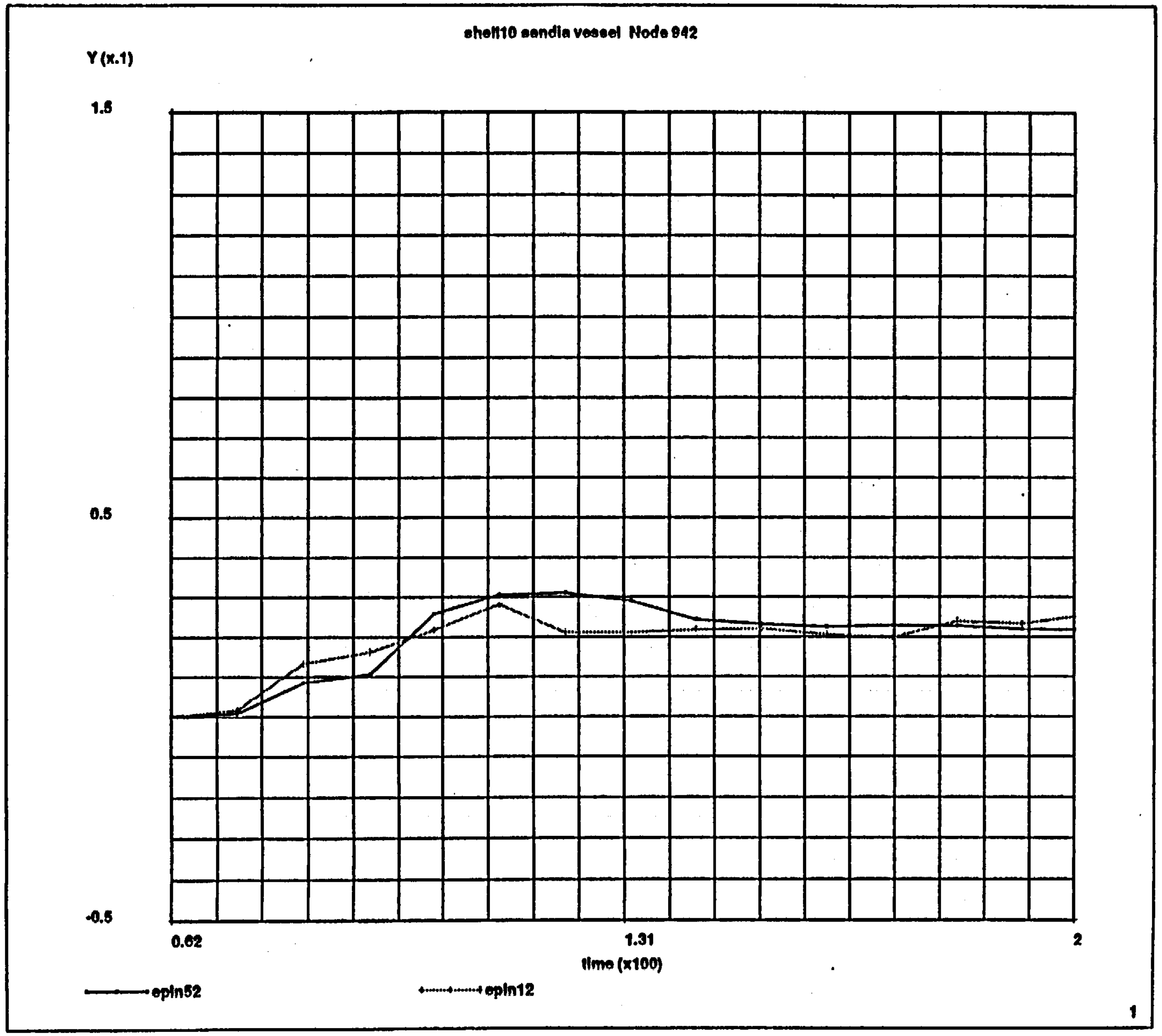

Fig. 6 - Plots 5, 6.

Fig. 7 - Plot 7.

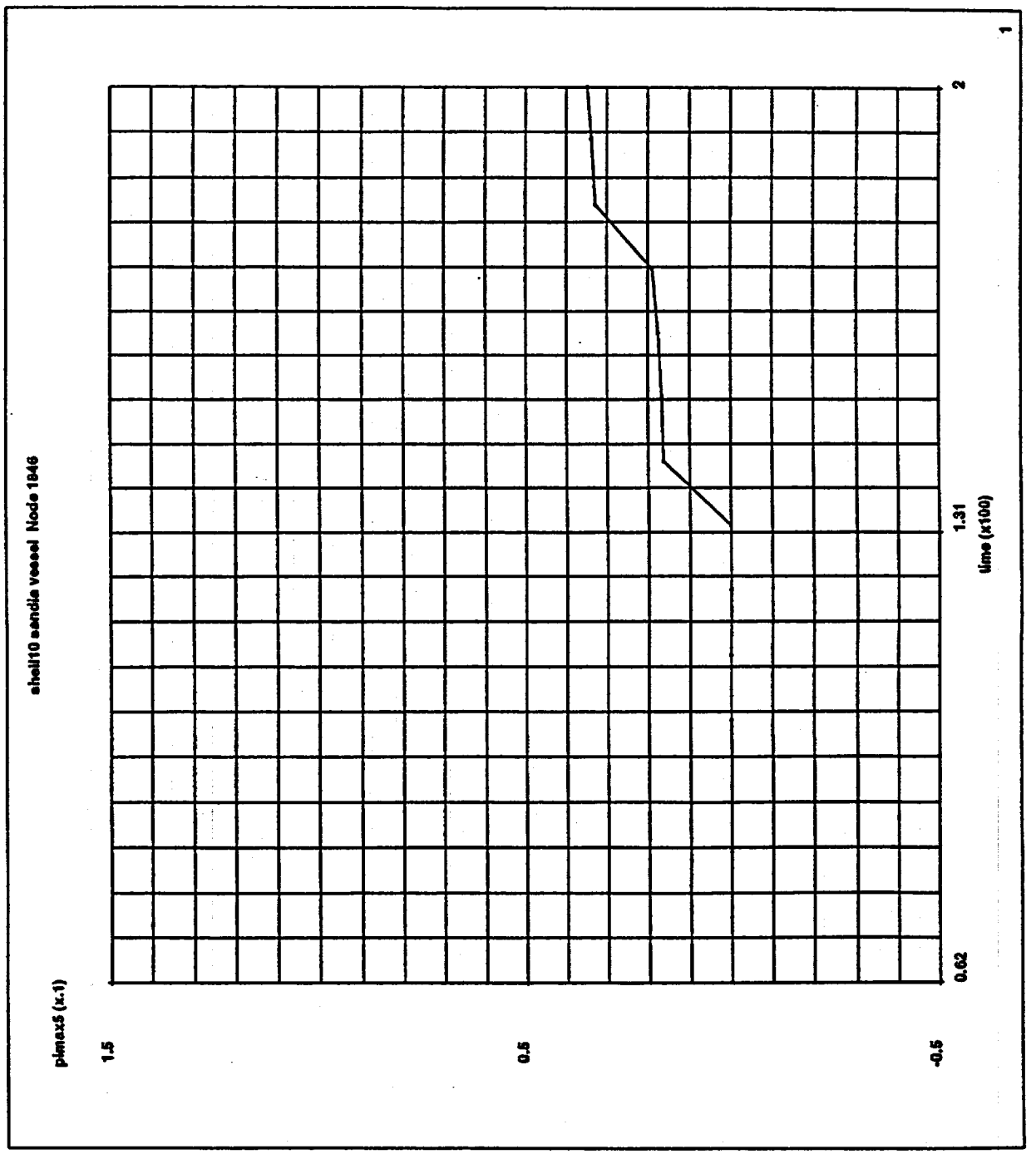
shell10 sandia vessel Node 1846
pimax5 (x.1)
1.5
0.5
-0.5
0.62
1.31
2
time (x100)
1

Fig. 8 - Plots 8, 9,10.

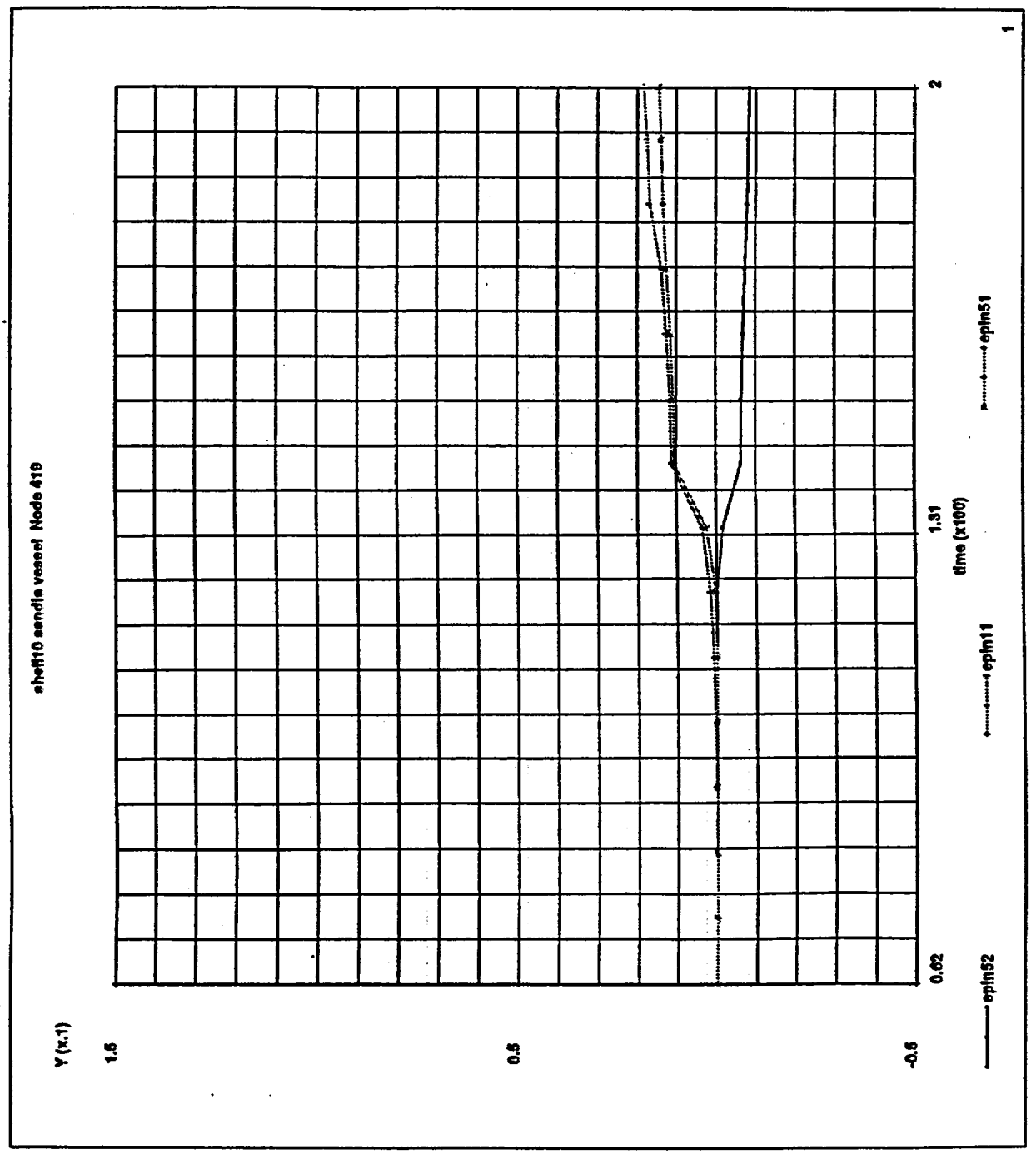

Fig. 9 - Plots 11, 12.

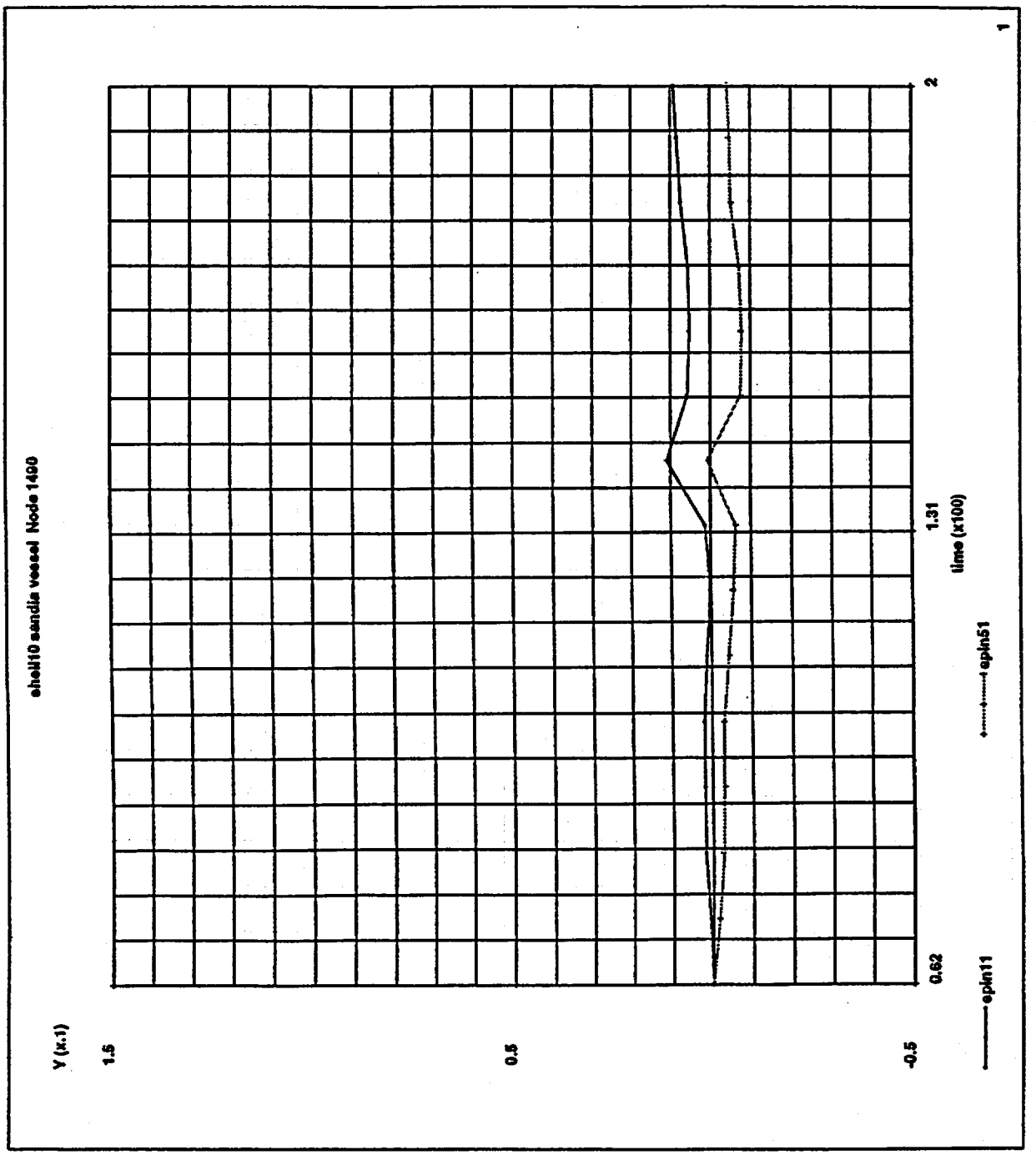

Fig. 10 - Plots 13, 14.

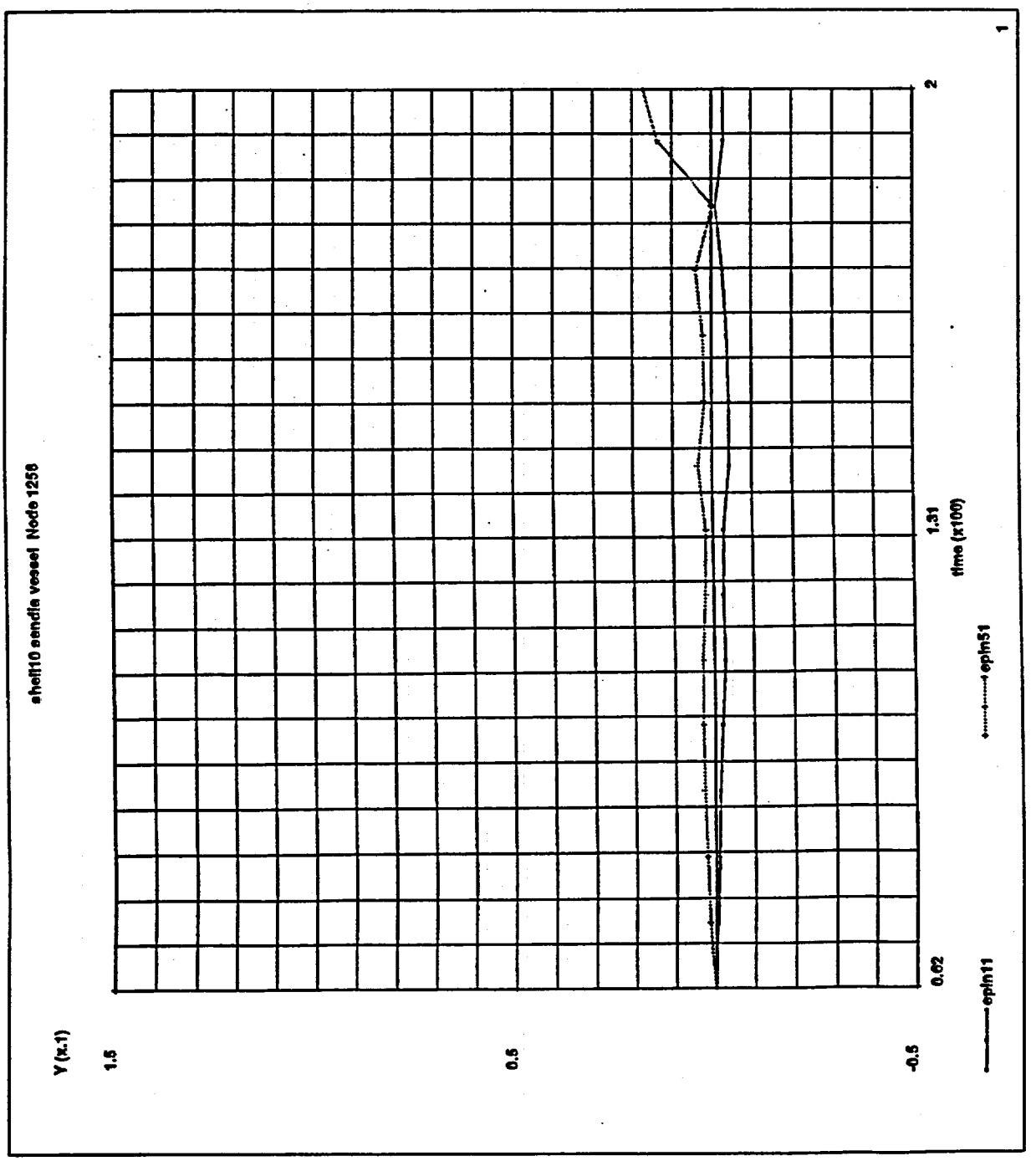

Fig. 11- Plots 15, 16.

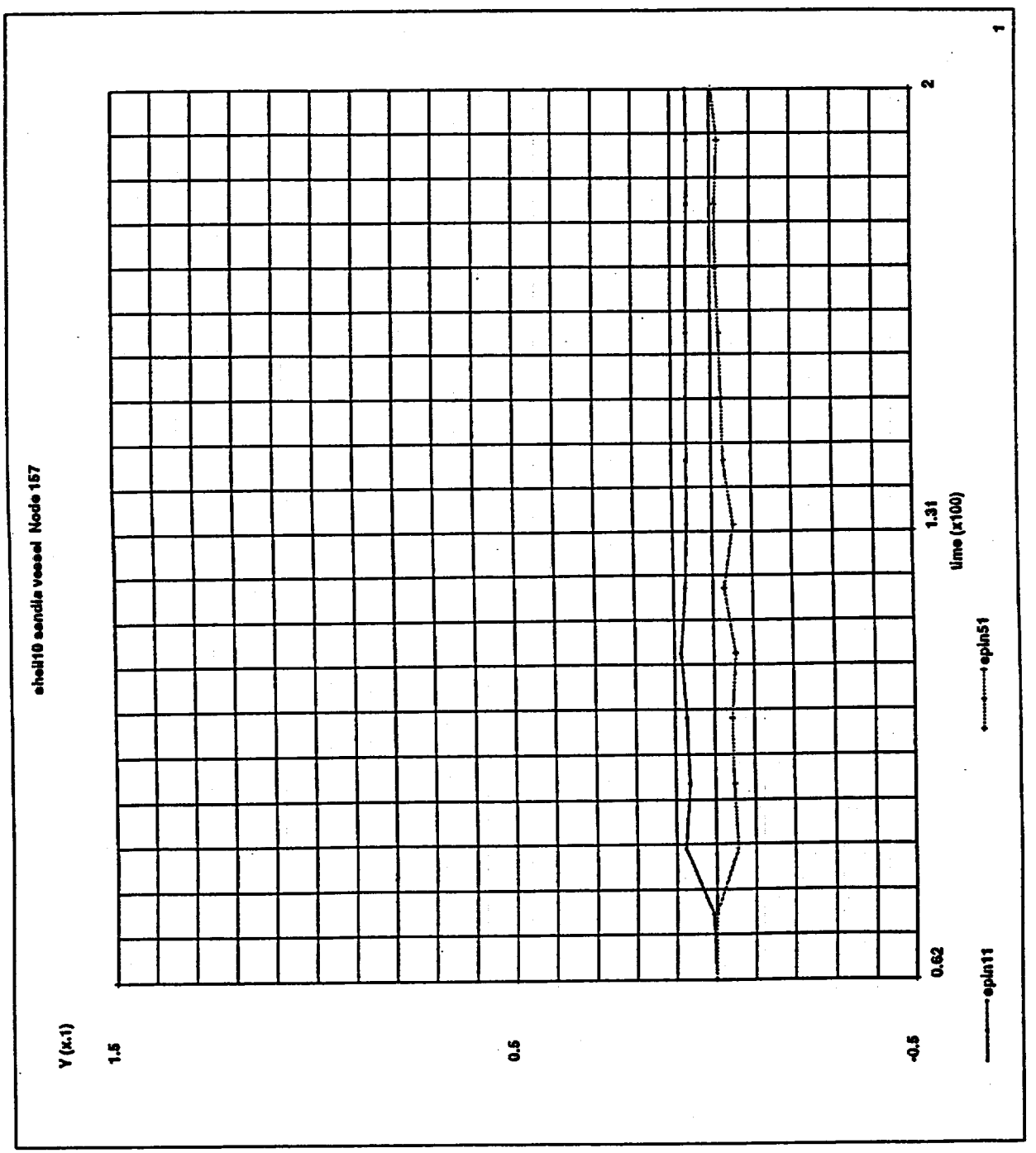

Fig. 12 - Plots 17, 18.

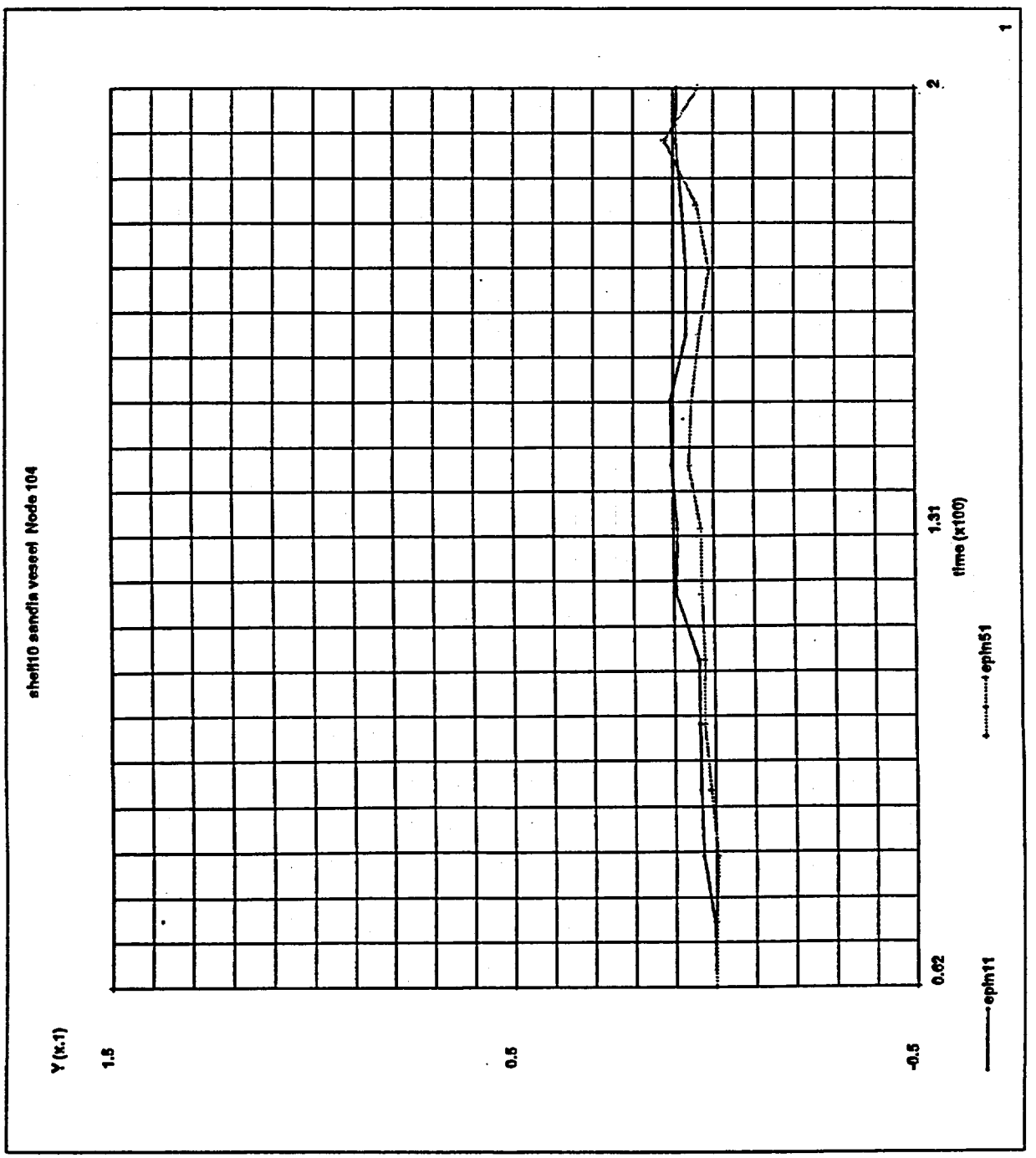

Fig. 13 - Plots 19, 20.

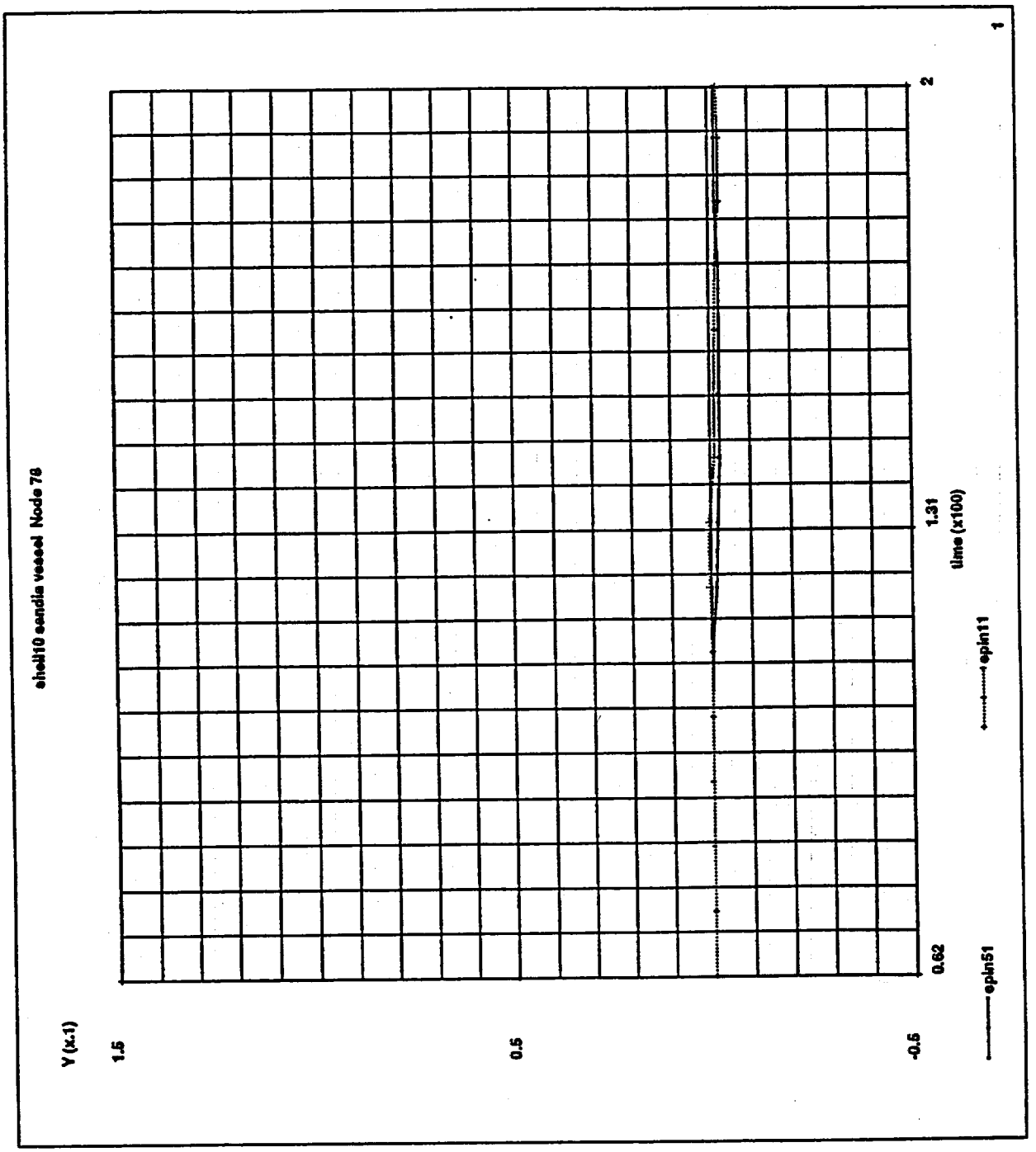

Fig. 14 - Plots 21, 22, 23, 24.

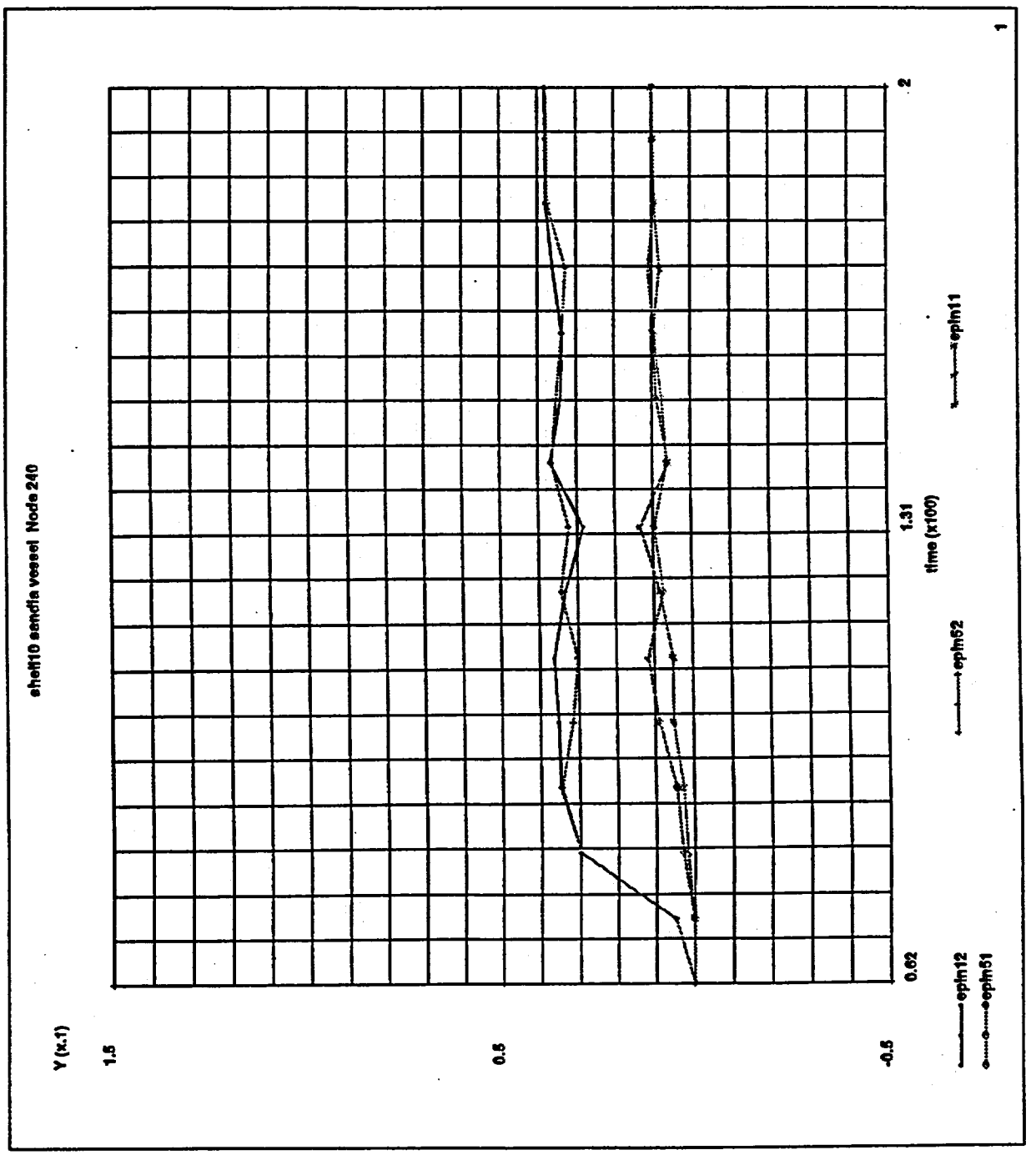

Fig. 15 - Plots 25, 26, 27, 28.

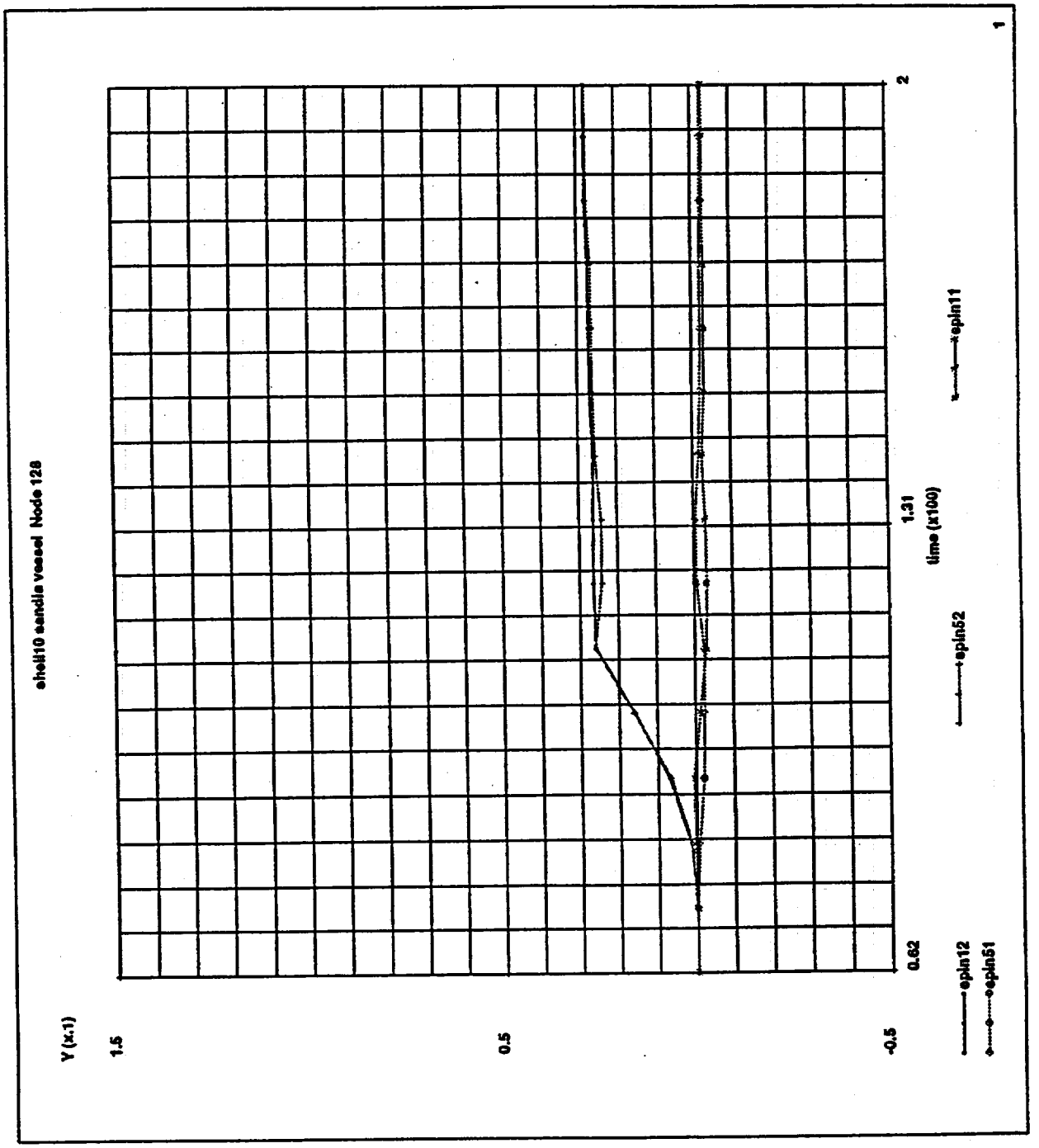

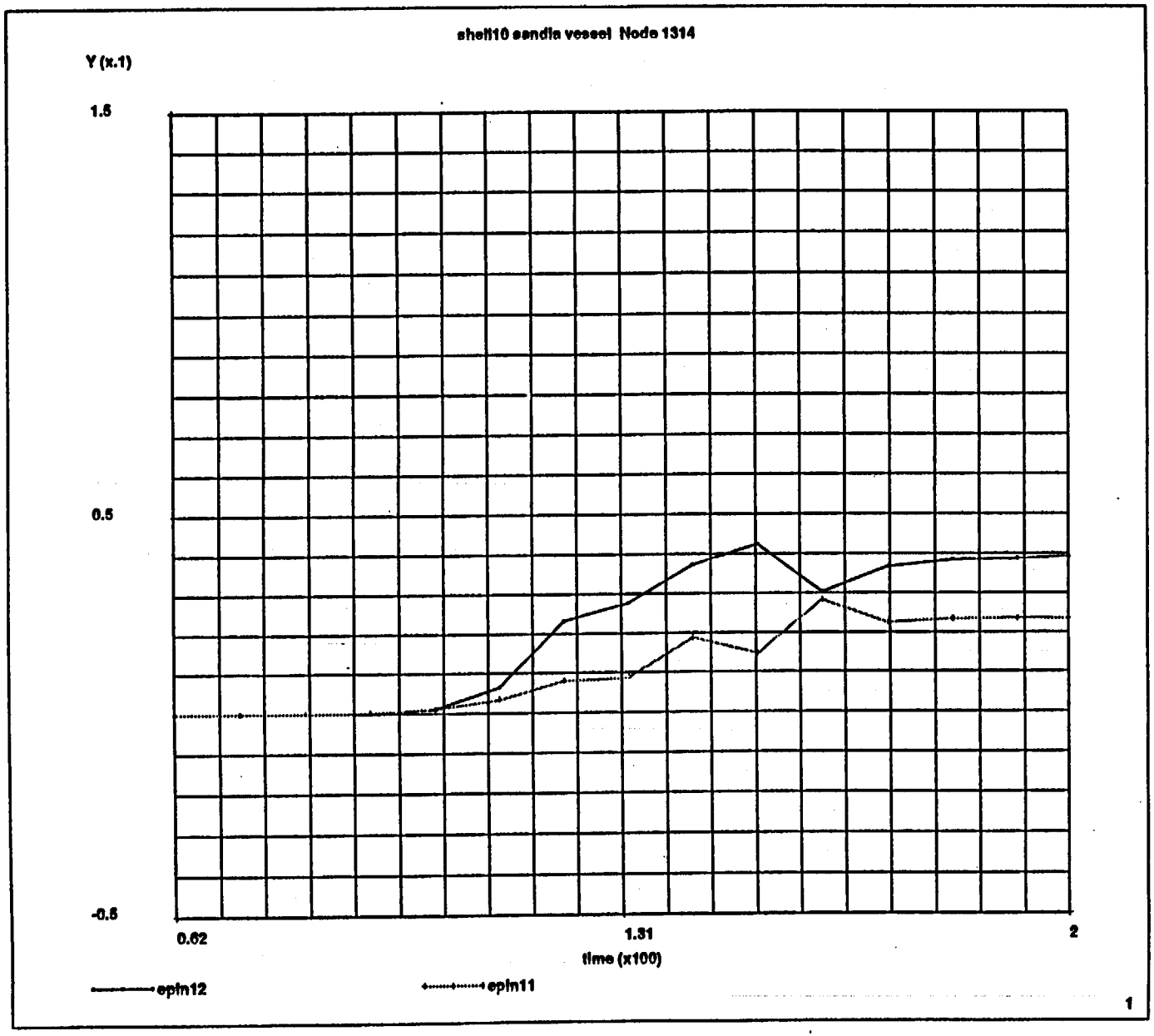

Fig. 16 - Plots 29, 30.

Fig. 17 - Plots 31, 32.

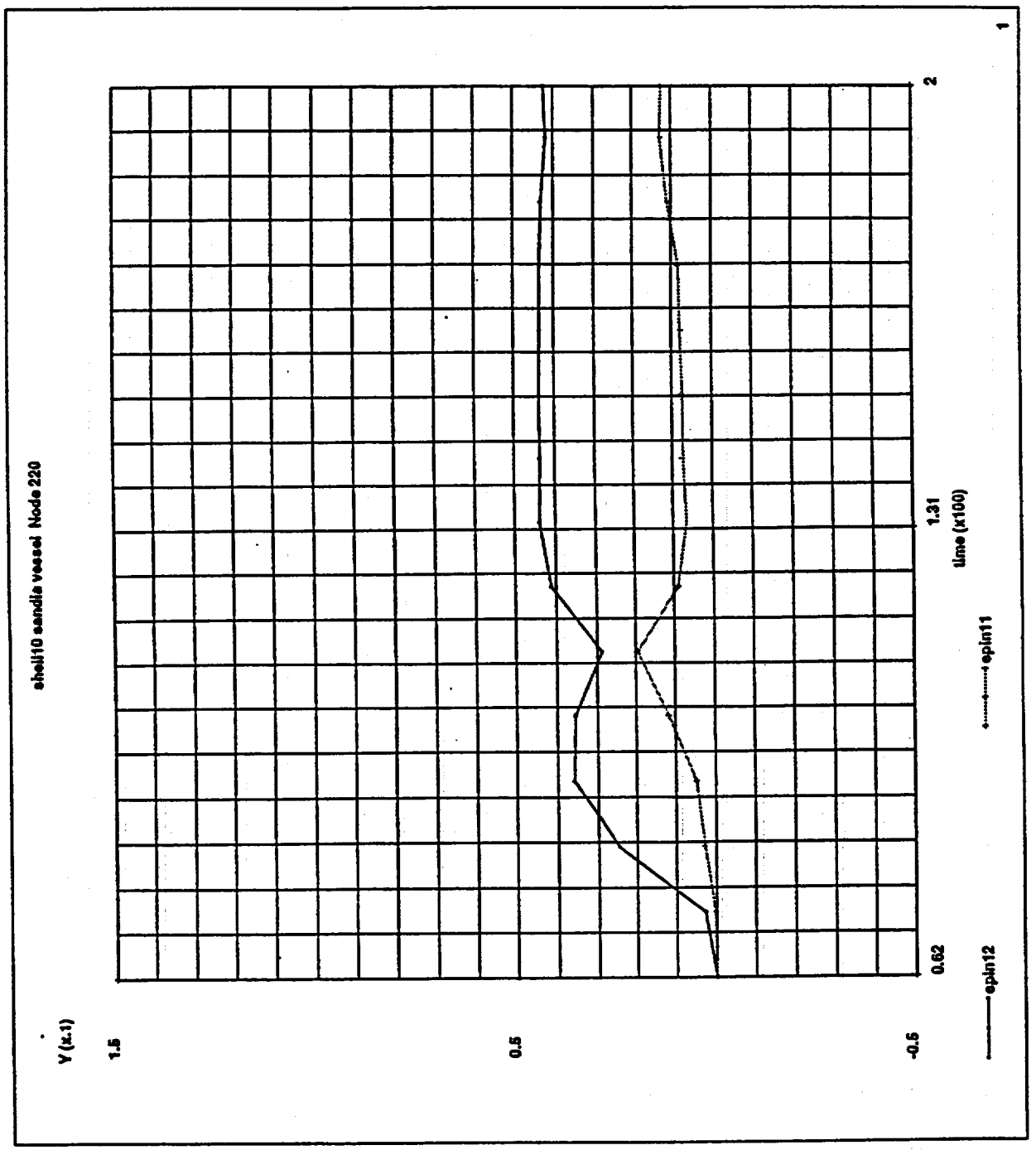

Fig. 18 - Plots 33, 34.

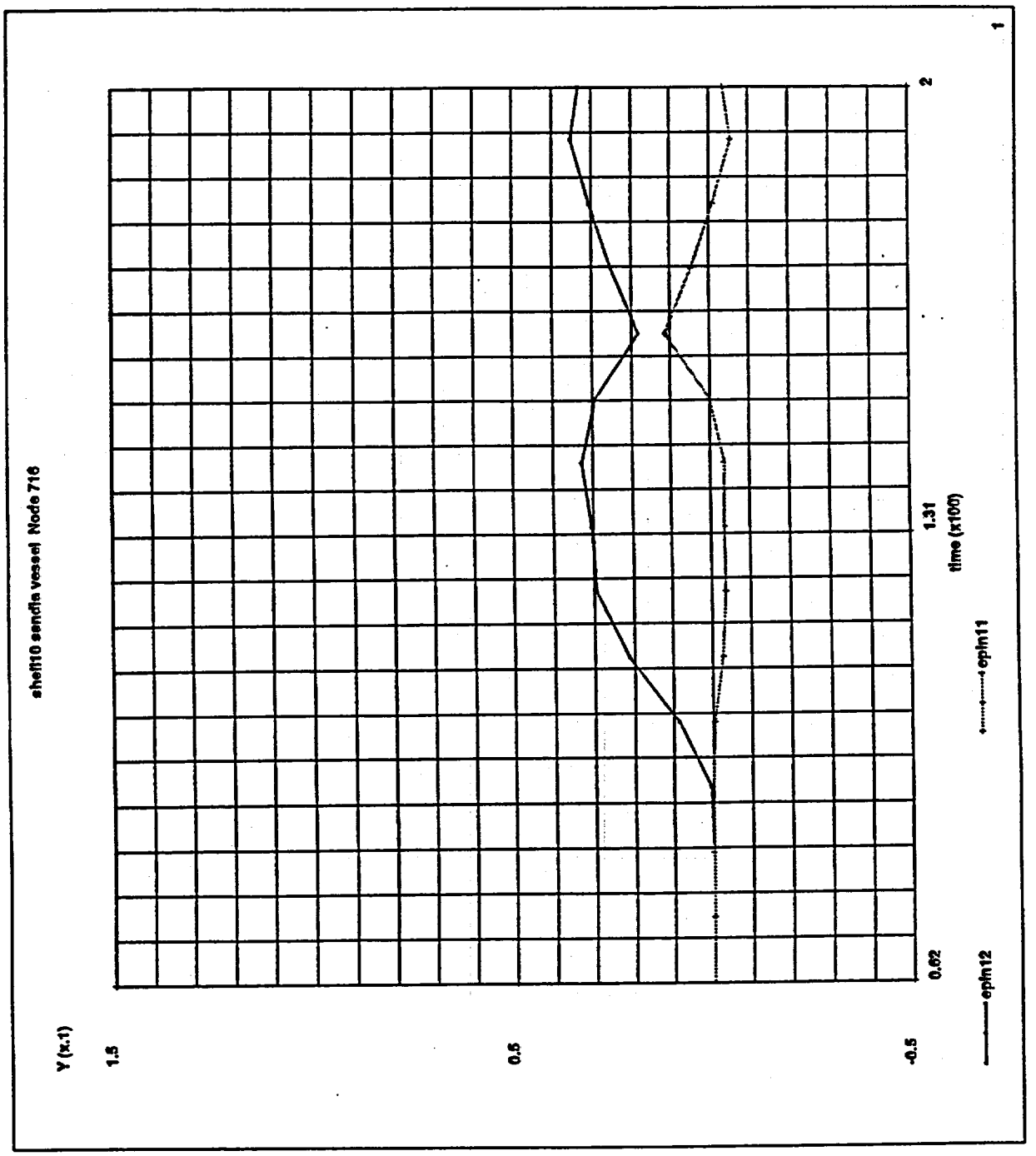

Fig. 19 - Plot 35.

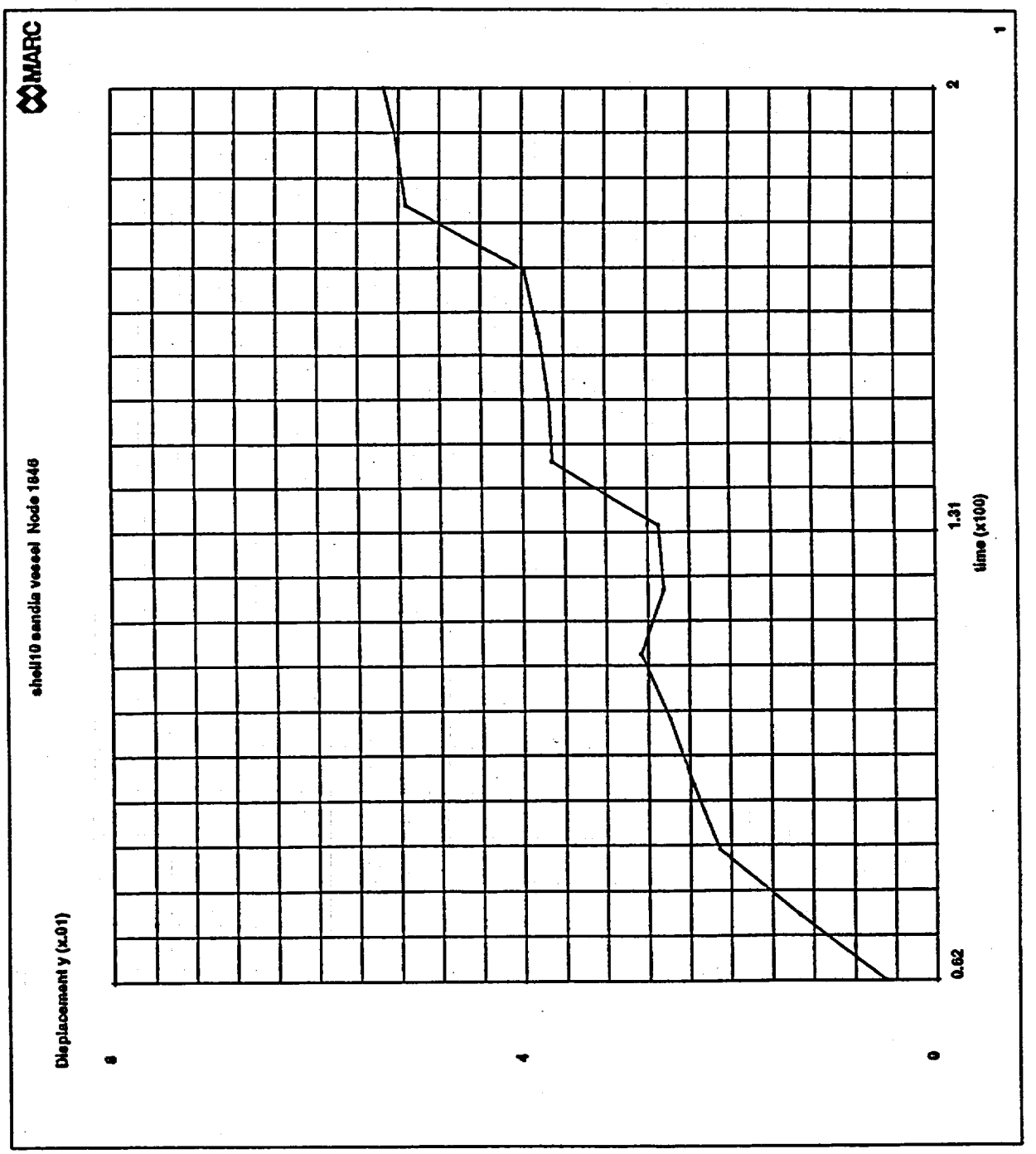

Fig. 20 - Plot 36.

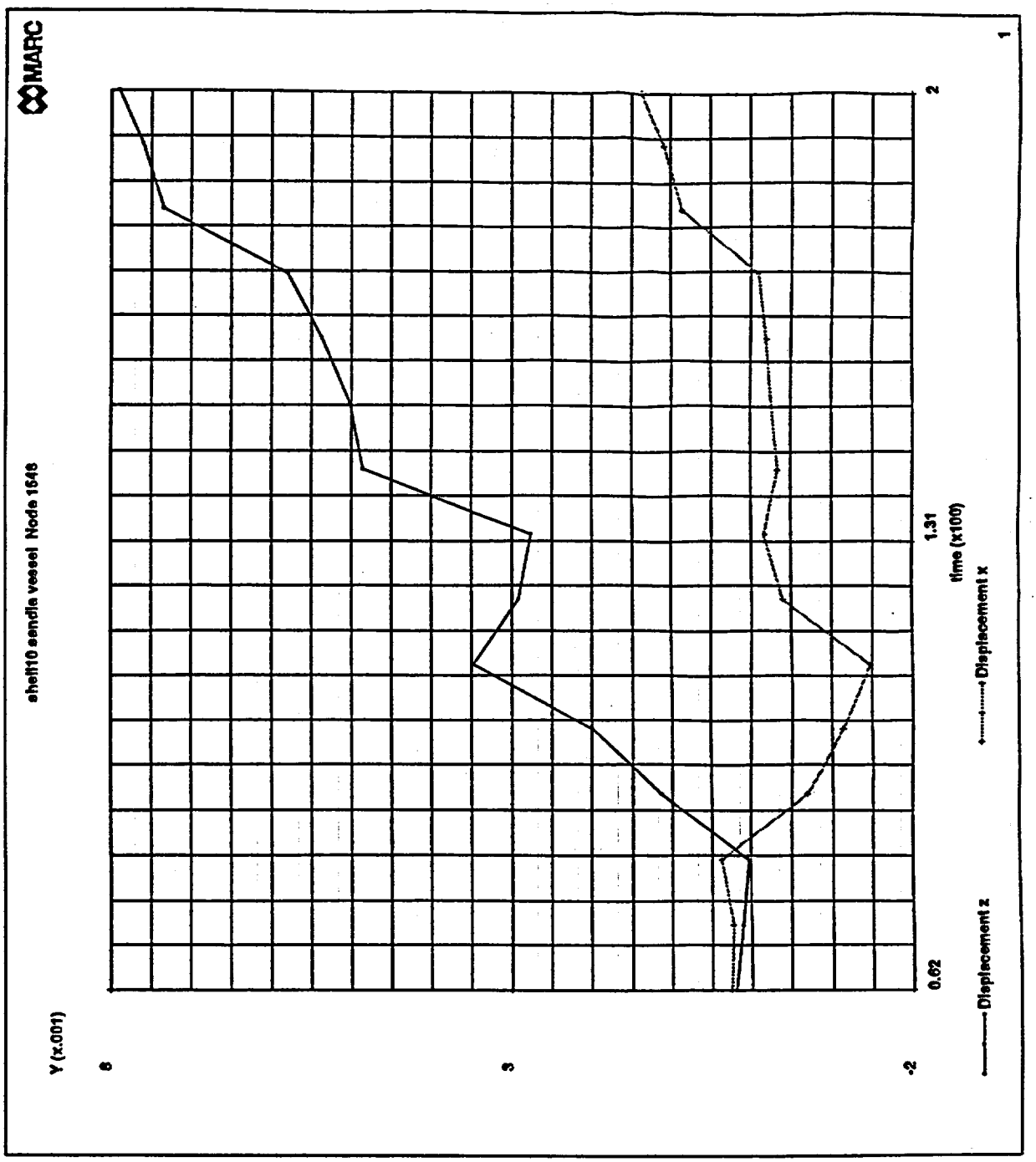

Fig. 21 - Plots 37, 38.

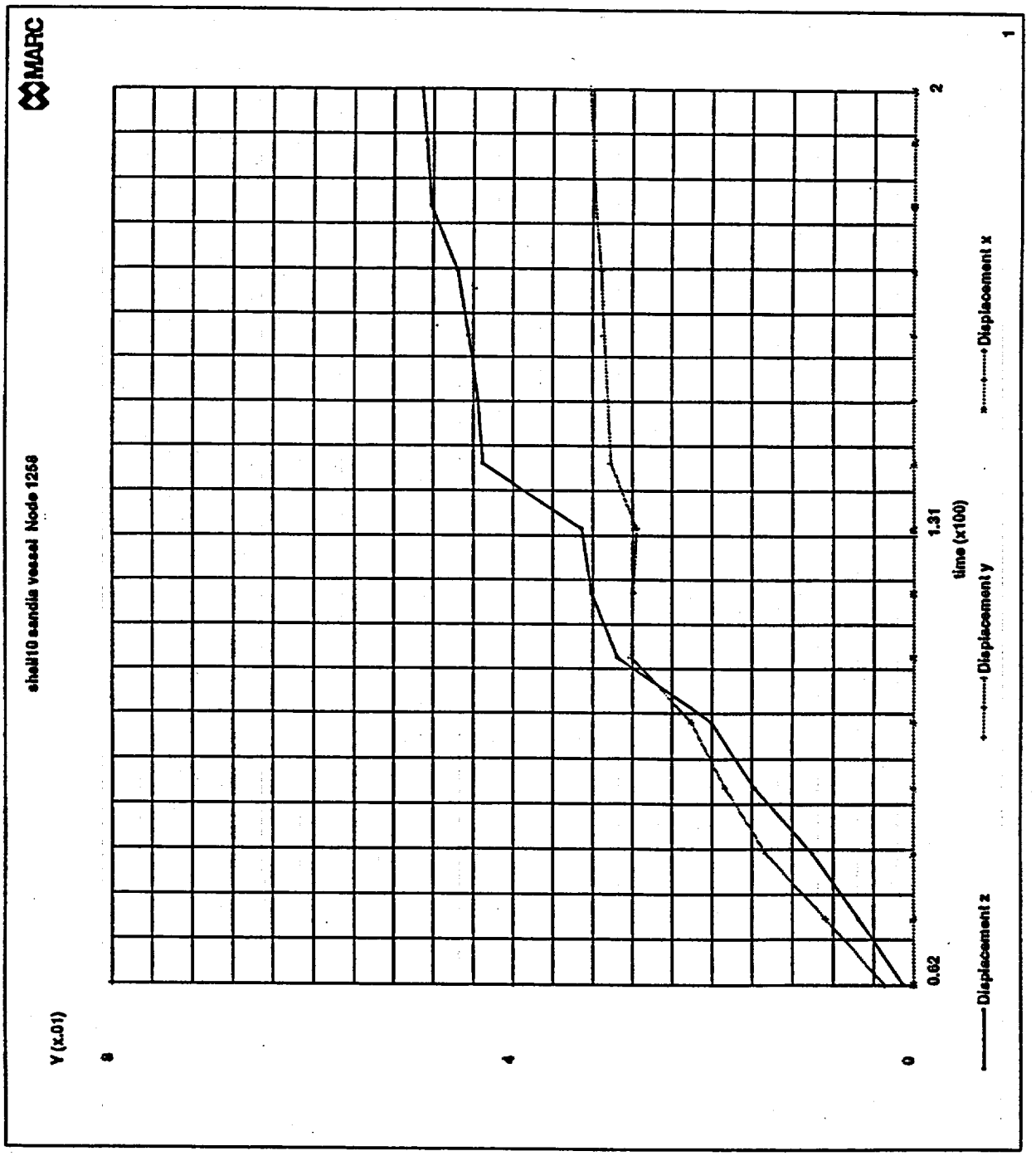

Fig. 22 - Plot 39.

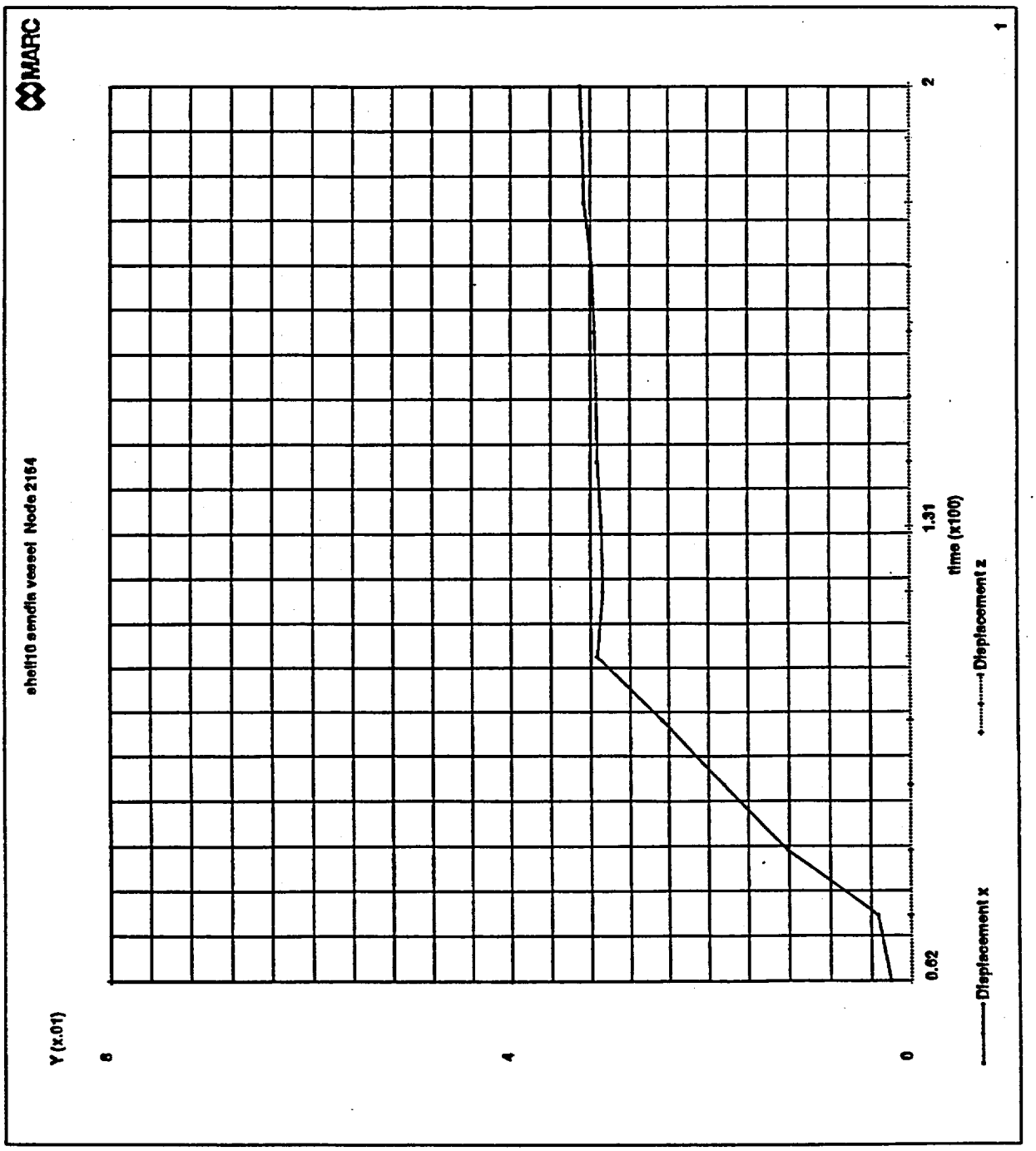

Fig. 23 - Plots 40, 41, 42, 43.

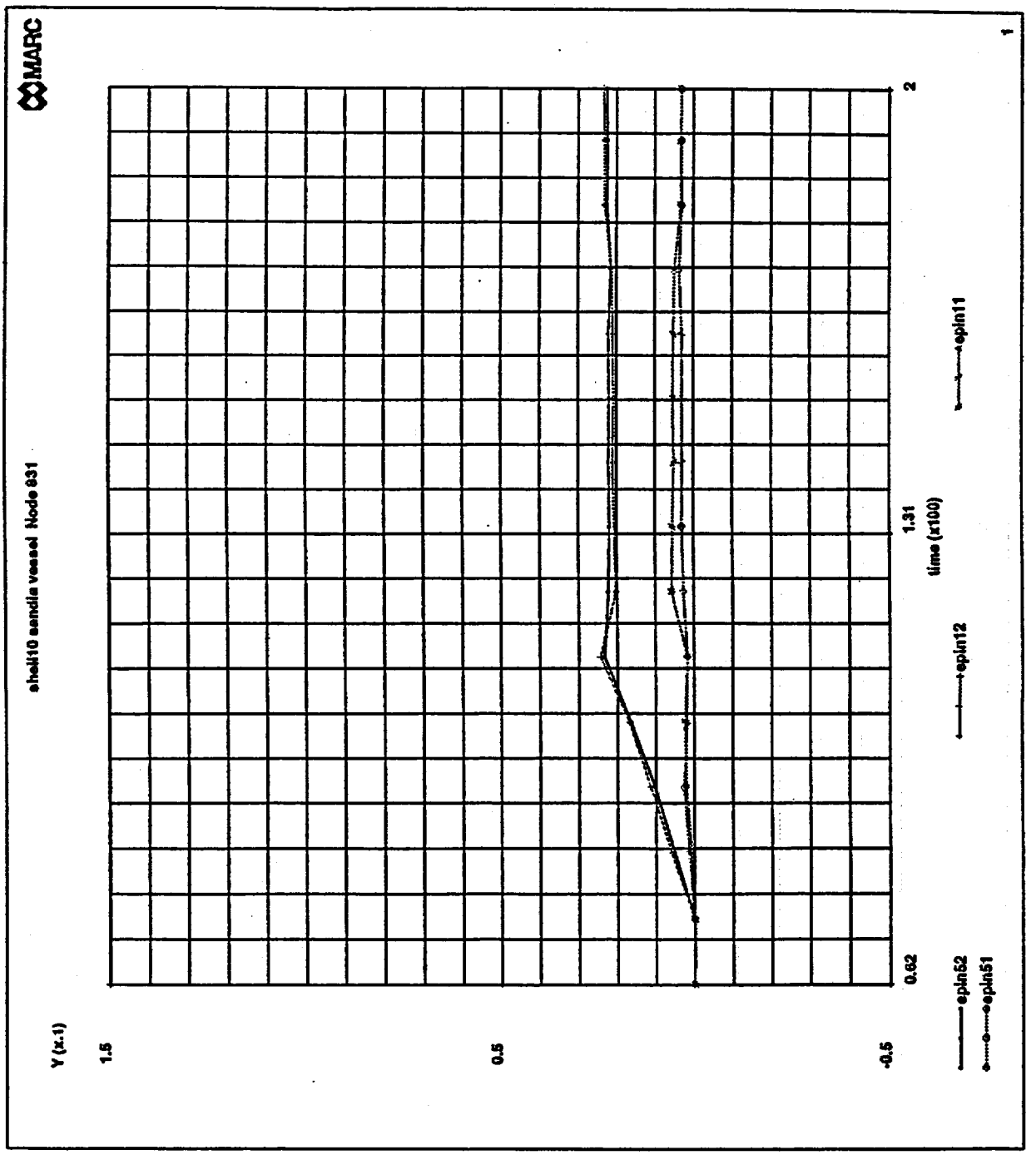

Appendix E-3.1

Bhabha Atomic Research Centre

India

PRETEST ANALYSIS REPORT FOR STEEL CONTAINMENT VESSEL ROUND ROBIN EXERCISE

SURESH KRISHNAN, VIVEK BHASIN, H.S. KUSHWAHA

REACTOR DESIGN AND DEVELOPMENT GROUP
BHABHA ATOMIC RESEARCH CENTRE
TROMBAY, BOMBAY-400 085
INDIA

Introduction

Analytical studies of Steel Containment Vessel (SCV) model, were done as a part of Round Robin Analysis Activity for the Cooperative Containment Model Programme. This programme is being coordinated by Sandia National Laboratories (SNL), [1]. This cooperative programme involves analytical studies followed by experimental studies (to be done by SNL) on SCV model. This is a pretest analysis report.

The SCV model is scaled from a prototype BWR Mark-II containment, [1] & [2]. The SCV model is fabricated by welding rolled steel plates of different thickness. The model has equipment hatch opening with thickened reinforcement plate. The SCV model consists of different sections and has several stiffeners. In this report the different sections will be referred to as "spherical shell", "upper conical shell", "lower conical shell", "knuckle", "top head", "top head knuckle" etc. The complete outline of the model along with the names of different sections and stiffeners is shown in Fig.1.

The SCV model is coaxially located within the Contact Structure (CS) fabricated out of 38 mm thick steel plate. The CS extends upto the knuckle region of SCV model. Except in the lower cylindrical shell region, the gap between the SCV and CS is almost constant.

The SCV model is made up of two materials. The upper portion is made up of SGV-480 (SA-516 Grade 70 steel) while the lower portion of SPV-490 (SA-537 Class 2 steel). The CS is made up of SA516-70 steel, [1].

The SCV model was subjected to increasing internal pressure. The analysis was done using Finite Element Method (FEM). Two different models namely, 3-Dimensional (3D) Shell Model and Axisymmetric Model were employed. The results, discussed in this report and submitted in the form of plots, pertain to axisymmetric model only. Finite element computer code "ABAQUS" Ver. 5.3, [3], was used for the analysis.

1.0 Finite Element Model

Initially it was planned to analyse a 3D half symmetric (180 degree) finite element model of the SCV along with the CS. Some preliminary studies were done using this model. The results showed that the deflection pattern, stress & strain distribution is axisymmetric about the vertical axis, except in the region around the equipment hatch opening.

This observation led to the conclusion that in a gross sense, an axisymmetric model will correctly predict, the deformation of the SCV and its contact pattern, except in the region near hatch opening.

Both 3D shell and axisymmetric models are described in the following sections. The models are as per the original dimensions given in SCV design package, [1]. The as measured dimensions given in reference [2], have not been used for the analysis.

1.1 Axisymmetric Model

SCV and CS were modelled using 8 noded axisymmetric solid elements with reduced integration option ("CAX8R" elements of ABAQUS, [3]). The gap between them was maintained as per the design drawings, [1]. The gap monitoring and post contact behaviour was modelled using 3-Noded axisymmetric interface contact elements ("ISL22A" of ABAQUS).

All the sections of SCV and the corresponding thickness changes at interfaces, have been modelled. The model was fixed at the base. The base of the model is the top flange of the ring support girder. The model is subjected to internal pressure.

The stiffeners and the top flange were also modelled using 8 noded axisymmetric solid elements with reduced integration option ("CAX8R"). The model uses 770 "CAX8R" elements in the containment vessel, 20 "CAX8R" elements in the contact structure and 236 "ISL22A" contact elements. The total number of nodes, in F.E. model, are 3159.

The axisymmetric model is shown in Fig.2 through Fig.4.

1.2 Shell Model

The 3D half symmetric (180 degree) finite element model of SCV is shown in Fig.5 through Fig.7. The model also includes contact structure and equipment hatch with its cover. 4 noded shell elements with reduced integration option (designated as "S4R5"), were used to discretize the structure. The gap monitoring and post contact behaviour was modelled using slideline interface contact elements (designated as "ISL31A") There are 3744 "S4R5" elements in the containment structure, 132 "S4R5" elements in the contact structure and 307 "ISL31A" contact elements. There are 4007 nodes in F.E. model.

2.0 Use of NUPEC Tensile Test Data

The true stress - true strain curves were used in the analysis. One representative stress-strain curve is used in the analysis for each of the two materials. For the material SGV-480, the data for specimen R1, given in Table 6 of the design specification, [1], was used. The material stress-strain curve is also shown in Fig.8. The specimen R1, is of thickness of 6 mm. The Top Head is not shielded by contact structure and is the least thickness region of SCV. Its thickness is 6 mm. This region is likely to fail under large internal pressure. Therefore, the stress-strain material data from this region of SCV, is used to represent the material SGV-480.

For the material SPV 490, the data for specimen R21, given in Table 14 of the design specification, [1], was used. The material stress-strain curve is also shown in Fig.9. The specimen R21, is 9 mm thick.

The value of modulus of elasticity (E) used in analysis, is for the roll direction, since the material stress-strain data used, corresponds to the roll direction. The E value considered for both the materials, is 216,700 MPa. The Poisson's ratio for both the materials is taken as 0.3.

3.0 Analytical Models

In this analysis both material and geometric nonlinearity have been considered. The von mises isotropic yield criteria is used. The analysis employs a large strain, large displacement, updated lagrangian formulation to account for the geometric nonlinearity. The applied load adapts itself to shape changes in the structure as the analysis progresses. Reduction in shell thickness, as a result of deformation, has been accounted for.

4.0 Steel Containment Vessel / Contact Structure Interaction

The magnitude of gap between SCV and CS, is taken, as given in the original design drawings, [1]. The interaction between SCV and CS was modelled using 3-Noded axisymmetric contact elements. During analysis gap is monitored all along the CS, at each integration point of contact element. Some of the details of modelling of these contact elements are listed below:

(a) When contact occurs, the SCV loads CS and CS inturn exerts reaction unto SCV. After contact CS also shares the load.

(b) The opening of contact is allowed. The contact opens if the reaction force on SCV becomes tensile or zero.

(c) Sliding of SCV on CS is permitted.

(d) Coefficient of friction (μ) is used to characterize the sliding friction effect. The value of μ used, corresponds to static & dry friction conditions. The standard design handbooks, [4] & [5], suggest that for clean steel plates, the value of μ lies between 0.7 and 0.8. Therefore, for this analysis, a mean value of 0.75 was used.

(e) When any point on SCV comes into contact with CS, then its meridional movement is constrained until it overcomes the frictional resistance. In absence of friction, free sliding is permitted.

5.0 Analysis Procedure and Results

The analysis was done by increasing the load in steps with auto load stepping procedure. The maximum load step was 1.5 MPa and the minimum was 0.00015 MPa. The convergence in each load step was set in terms of ratio of the residual force to the average force (= 5.0E-3) and the ratio of displacement correction to the incremental displacement, of that load step (=1.0E-2).

Two cases were studied. In one of the case, coefficient of friction (μ) was taken as 0.75 and in another case the friction effects were neglected (μ = 0.0). The results of both these cases are submitted. For both the cases the maximum pressure, upto which analysis could proceed was 11.49 MPa. At this pressure, the strain induced in "top head crown" approaches the true ultimate strain of SGV-480 material.

The detailed results of deflection v/s pressure and strain v/s pressure are given in the form of plots, at different locations. These locations are defined in the SCV design package, [1], in the form of Plot ID numbers. These plots are given in Appendix. Since, submitted results pertain to axisymmetric model only, hence, plots of strain v/s load near equipment hatch opening are not included. These plots correspond to Plot ID 1-6 and Plot ID 39. The computer programme yields strain output in global coordinate system. These strains were transformed in local directions, in order to evaluate strain in meridional direction.

Some of the results are included in this report also. These are given in the form of plots. The vertical deflection v/s load, at apex of "top head crown", is shown in Fig.10, for the cases with and without friction effects. It is observed that the vertical deflection at apex is not significantly affected by friction. The horizontal deflection v/s load, in the knuckle region of top head ("top head knuckle") is shown in Fig.11 and Fig.12. These figures are for two different locations in "top head knuckle". The observations from Fig.11 and Fig.12, are discussed in art.6.0.

6.0 Potential of Buckling of SCV model in the Head Region.

Fig.11 shows a plot of the horizontal displacement at node no 1646 which lies in "top head knuckle". From this figure it is seen that at a pressure of 10.0 MPa reversal of direction of horizontal displacement takes place. Upto this pressure the horizontal displacement is negative (i.e. "top head knuckle" deform inwards). After about 10.0 MPa the deformation suddenly shoots up in positive direction (i.e. "top head knuckle" starts deforming outwards). This is the clear indication that the tendency towards buckling exists. Upto 10 MPa pressure the stresses are compressive. However, with the increasing load these stresses becomes tensile. It is observed, from the graph, that for the same value of horizontal displacement there are two different values of internal pressure. Similar behaviour is noticed in Fig.12, for node 1654. This node also lies in "top head knuckle".

7.0 Effect of Friction on the Interaction of SCV and CS

The presence of friction forces (or surface tractions) along contact interface, affects the post contact interaction of SCV and CS. This effect was studied based on the results of analyses done for $\mu = 0.75$ and $\mu = 0.0$. The important observations at each Plot ID location are listed below. For reference, see plots of strain v/s pressure and deflection v/s pressure, at these locations.

For Plot ID 8,9,10 the strains for the two cases (with friction and without friction) match with each other. This is true for meridional and hoop strain.

For Plot ID 11,12 the strains, with friction, are higher than the strains without friction.

For Plot ID 13, the maximum positive strain, in the case of friction, is about 5 times that without friction. Also, the negative strain with friction (at maximum load) is about 2 times that without friction.

For Plot ID 14, the strain v/s pressure behaviour, with and without friction, is quite different.

For Plot ID 15,16,17,18 strains, with friction, are lower than the strains without friction case.

For Plot ID 19,20, the strain v/s pressure behaviour, with and without friction, is quite different.

For Plot ID 21,22 meridional strains are considerably lower with friction than the meridional strains without friction.

For Plot ID 23,24 hoop strains, with friction, are slightly lower than the hoop strains without friction.

For Plot ID 25,26 meridional strains, with and without friction, match with each other upto a pressure of 5.0 MPa. At higher pressure the strains with friction are lower.

For Plot ID 27,28 hoop strains, with friction, are slightly lower than the hoop strain without friction.

For Plot ID 29,30 meridional strains, with friction, are slightly higher than the meridional strains without friction.

For Plot ID 33 meridional strains, with friction, are higher than the meridional strains without friction.

For Plot ID 34 hoop strains, with friction, are slightly lower than the hoop strain without friction.

For Plot ID 36, the displacements with and without friction are almost matching.

For Plot ID 37, horizontal displacements, with friction, are slightly lower.

For Plot ID 38, after about a pressure of 6 MPa, the vertical displacements, with friction, are much higher.

The presence of friction increases the constraint of the structure. The contact structure restricts the movement of SCV in normal direction. The presence of friction restricts the movement in meridional direction also, to the extent that meridional force is unable to overcome the frictional resistance of the contact. The increase in constraint, leads to lower strains in the free field regions. The free field regions are away from discontinuities. Whereas, increase in constraint leads to higher strains in the region of discontinuities such as regions near flanges, spherical to knuckle junction etc. Some of the free field regions (like mid height of spherical shell) also experience slightly higher strains due to presence of friction. This could be due to its proximity to discontinuity or due to secondary bending caused by localised shape changes after contact.

The strains at locations, away from contact structures (like top head crown), are not affected significantly, by presence or absence of friction. The load and location, of first yield and first contact are not effected by the presence of friction. The magnitude of maximum pressure is, also, not effected by the presence of friction.

8.0 Pressure and Location of First Yield and First Contact

The first yield occurs at a pressure of 1.78 MPa just below the knuckle, at the intersection with the spherical shell. The material at this location is SGV-480. The first contact occurs at a pressure of 3.42 MPa at the knuckle.

9.0 Expected Pattern of Contact Propagation

The expected pattern of contact propagation, with increase in internal pressure, is discussed briefly in Table 1. At internal pressure values of 4.605, 6.480, 8.400 and 11.490 MPa, the contact pattern is also shown in the form of deformed plots (see Fig.13 through Fig.24). Table 1 pertains to the analysis case in which coefficient of friction was taken as 0.75. Frictional effect does not cause a major change in the pattern of contact at any given pressure.

Table 1 : Expected Contact Propagation with increase in internal pressure

Internal Pressure (in MPa)	Expected Contact Location and propagation
3.420	contact occurs at knuckle
3.780	contact initiates in upper conical shell with 7.5 mm thickness (just above 2.275 m elevation weld line)
3.780 to 3.945	the contact zone initiated at 3.78 MPa pressure (i.e. in upper conical shell) , spreads in upwards direction
3.990	contact initiates in middle conical shell with 8.5 mm thickness (between middle stiffener and material change interface)
4.000 to 4.600	(a) contact zone initiated at 3.78 MPa (in upper conical shell), spreads further in upward direction (b) contact zone initiated at 3.99 MPa (in middle conical shell), spreads in upwards and downwards direction
4.605	**the deformed plot of SCV and CS, depicting contact pattern, is shown in Fig.13 through Fig.16.**
4.605 to 4.75	contact zones spread further in a manner, as discussed for 4.0 to 4.6 MPa pressure
4.750 to 5.049	(a) contact zone initiated at 3.78 MPa (in upper conical shell), spreads further upwards and also starts spreading in downwards direction (b) contact zone initiated at 3.99 MPa, spreads further in upper and lower direction
5.050	(a) contact initiates in lower conical shell (just near the material interface) (b) contact zones initiated at 3.78 MPa and 3.99 MPa, spread further in upper and lower direction

Table 1 (Continued) : Expected Contact Propagation

5.055 to 6.000	contact zones initiated at 3.78 MPa, 3.99 MPa and 5.050 MPa, spread further in upper and lower direction
6.105	(a) contact zone initiates in spherical shell portion (near mid-height of spherical portion) (b) contact zone initiated at 3.78 MPa, 3.99 MPa and 5.055 MPa, spread further in upper and lower direction
6.110 to 6.470	(a) contact zone initiated at 6.105 MPa (at mid height of spherical shell), spreads in upward direction towards knuckle (b) contact zones initiated at 3.78 MPa, 3.99 MPa and 5.050 MPa, spread further in upper and lower direction
6.480	**the deformed plot of SCV & CS, depicting contact pattern, is shown in Fig.17 through Fig.18 .**
6.480 to 7.755	(a) contact zone initiated at 3.78 MPa (in upper conical shell), spreads further and approaches near upper stiffener and middle stiffener (b) contact zone initiated at 3.99 MPa (in middle conical shell), spreads further and approaches near middle stiffener and material change interface (c) contact zone initiated at 5.05 MPa (in lower conical shell), spreads further and approaches near lower stiffeners and material change interface (d) contact zone initiated at 6.105 MPa (at mid height of spherical shell), spreads further in upper and lower direction
7.760 to 8.230	(a) the upper one, of the two lower stiffeners, comes into contact (b) contact zone spreads in between the two lower stiffeners (c) contact zone initiated at 6.105 MPa (at mid height of spherical shell), spreads further in upper and lower direction
8.235	contact initiates in lower cylindrical shell (just below the lower stiffeners)

Table 1 (continued) :Expected Contact Propagation

8.235 to 8.390	(a) contact zone initiated at 6.105 MPa (at mid height of spherical shell), spreads further in upper and lower direction
8.400	**the deformed plot of SCV & CS, depicting contact pattern, is shown in Fig. 19.**
8.400 to 11.480	(a) most of the portion of spherical shell comes into contact (b) contact zone initiated at 8.235 MPa (in lower cylindrical shell - just below the lower stiffeners), starts spreading downwards
11.490	**(a) the deformed plot of SCV & CS, depicting contact pattern, is shown in Fig.20 to Fig.24.** **(b) this is the maximum pressure achieved**

10.0 Concluding Remarks

Finite element nonlinear analyses were done for SCV model subjected to internal pressure. The analyses were done for two cases viz. with friction and without friction. Based on these studies it was concluded that :

(1) The top head region, of the SCV, is the critical region. At a pressure of 11.49 MPa the strain value in crown approaches true ultimate strain. This leads to collapse of SCV. The magnitude of this pressure is independent of friction effects.

(2) The region just below the knuckle yield first, at a pressure of 1.78 MPa. The first contact occurs at 3.42 MPa, at the knuckle.

(3) At a pressure of about 10 MPa, there is a sudden change in the deflection pattern of "top head knuckle". Below 10 MPa it deforms inwards, whereas above 10 MPa it deforms outwards.

(4) The presence of friction affects the post contact interaction between SCV and CS, due to increase in constraint. However, the magnitude of maximum pressure is not affected..

(5) The presence of "equipment hatch opening" demands rigorous 3D analysis. Preliminary studies on 3D shell model indicate that the effect of opening is localised in nature. Therefore, axisymmetric model will yield realistic results, except around the equipment hatch. The possibility of failure near equipment hatch opening is less since, it is reinforced by thick plate and is shielded by CS. The gap between SCV and CS, near the equipment hatch opening is lesser than the other regions. After contact it will experience a rigid support.

11.0 References

[1] Steel Containment Vessel Design Package (July 10, 1995) and Supplement No.1 of Steel Containment Design Package (September 21, 1995), Sandia National Laboratories, Albuquerque, New Mexico, USA.

[2] Letter No. SO-95-099 (dated December 1, 1995) "regarding as measured data of SCV and CS", Sandia National Laboratories, Albuquerque, New Mexico, USA.

[3] ABAQUS Ver.5.3-1, "Finite Element Computer Code", HKS Inc., Rhode Islands, USA.

[4] Baumeister, T., Avallone, E.A., Baumeister III, T., "Marks's Standard Handbook for Mechanical Engineers", 8th edition, McGraw Hill Book Company.

[5] Green, R.E. (editor) et al, "Machinery's Handbook", 24th edition, Industrial Press Inc., New York, 1992.

Figure 1.

Steel Containment Vessel

(all elevations in meters)

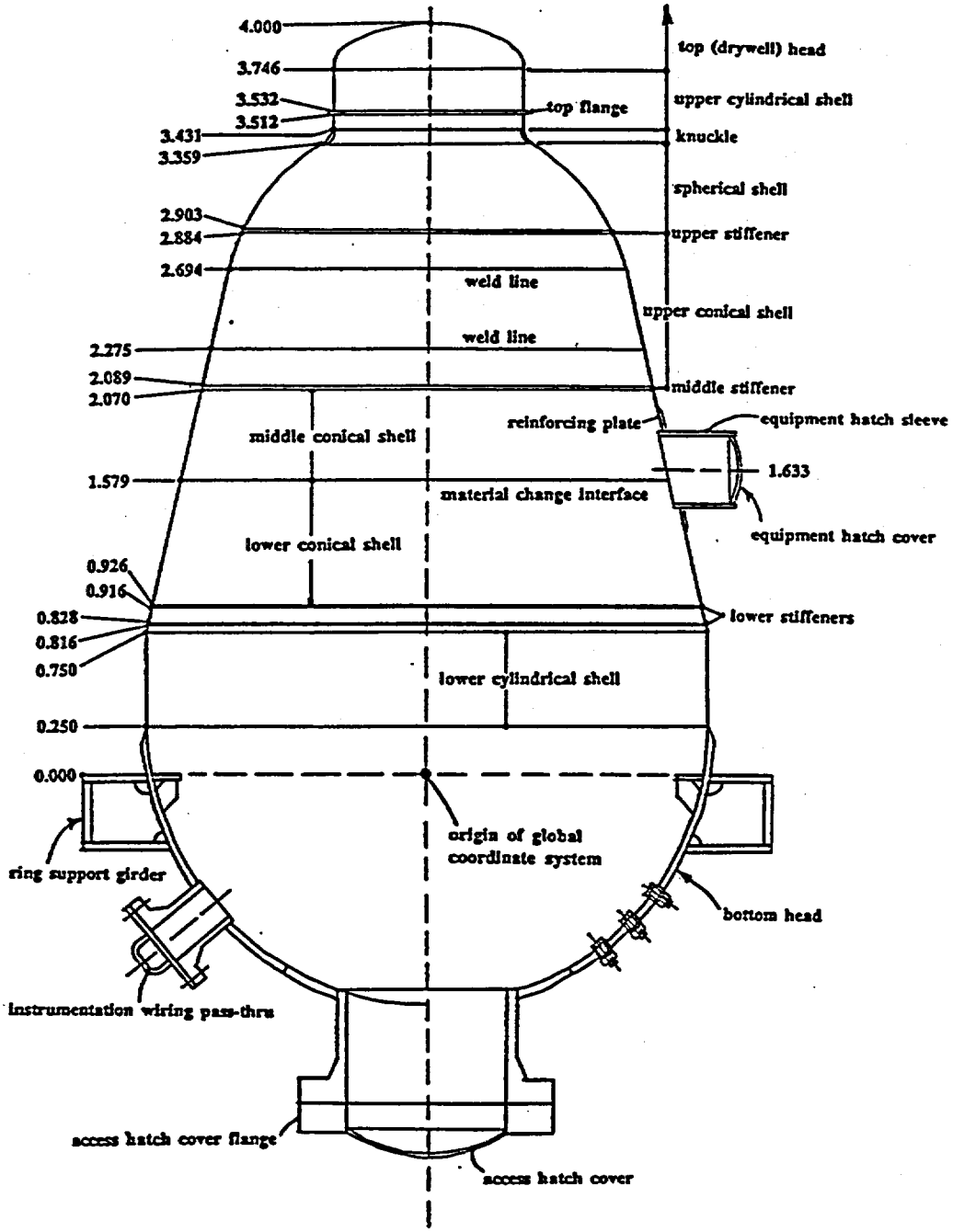

Fig. 1 Outline of Steel Containment Vessel Test Model

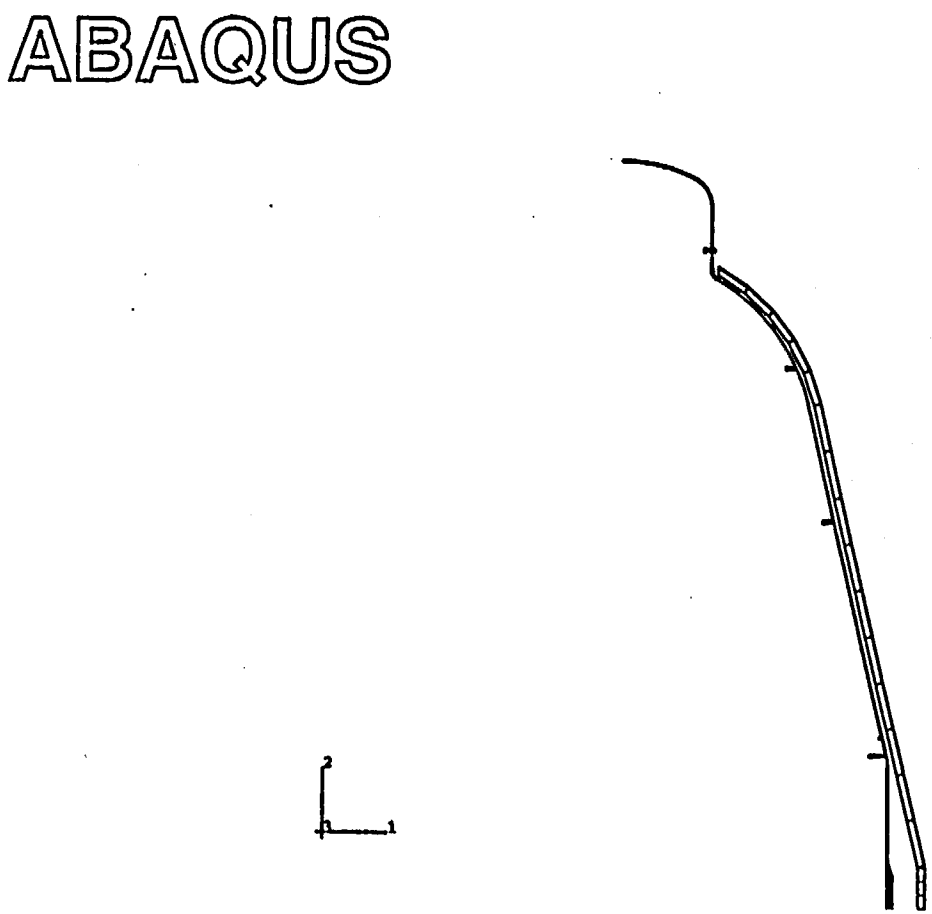

Fig.2 Finite Element Mesh of Axisymmetric Model

ABAQUS

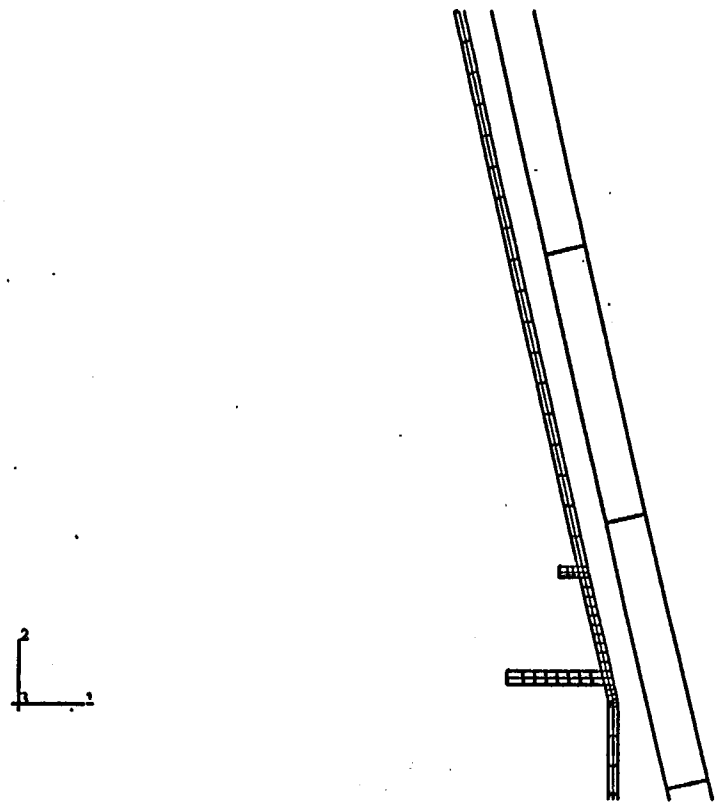

Fig.3 View of Axisymmetric F.E.Model near Lower Stiffners

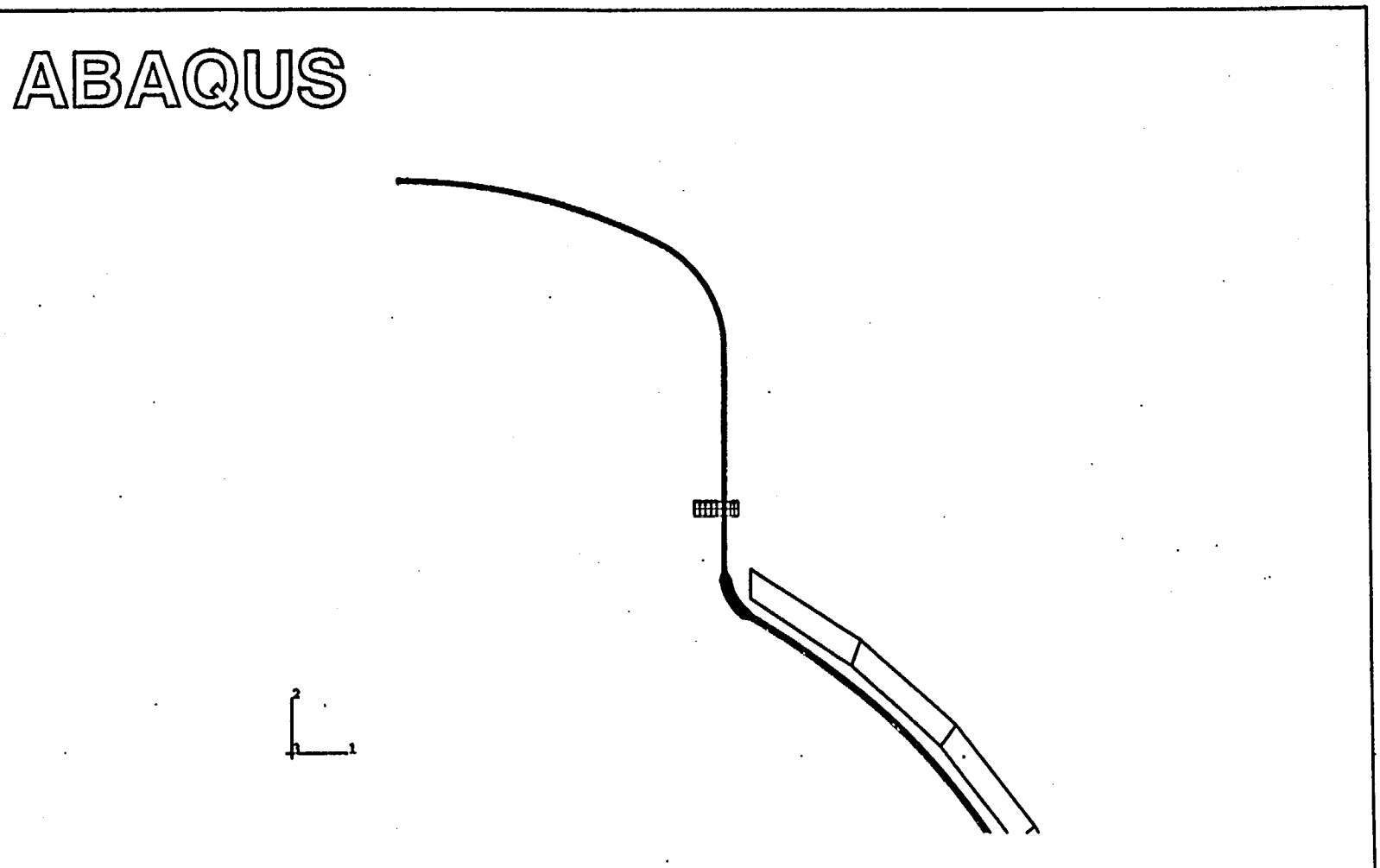

Fig. 4. View of Axisymmetric F.E.Model in Top Head Region

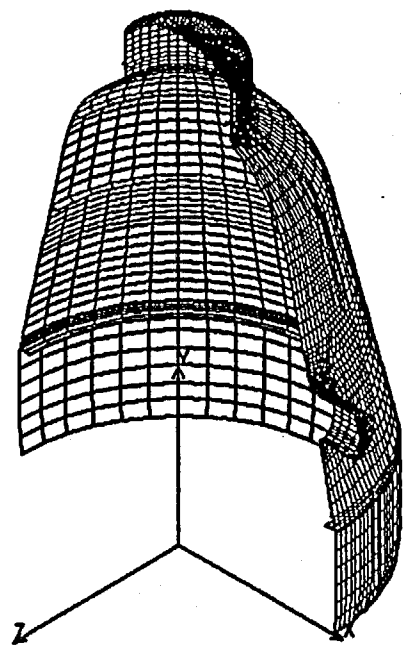

Fig. 5 Half Symmetric (180 degree) Shell Model of SCV

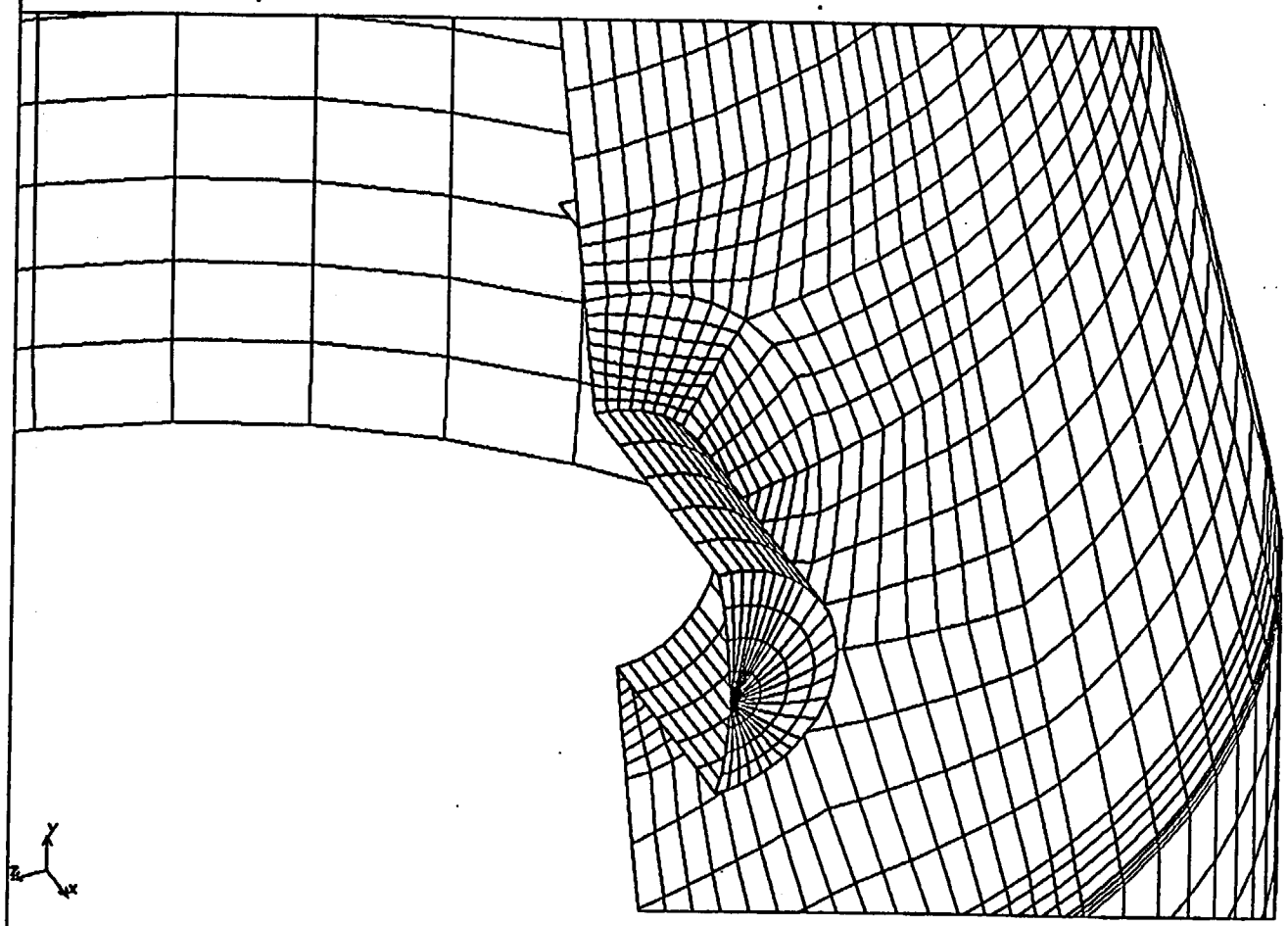

Fig. 6 Details of Shell Model near the Equipment Hatch

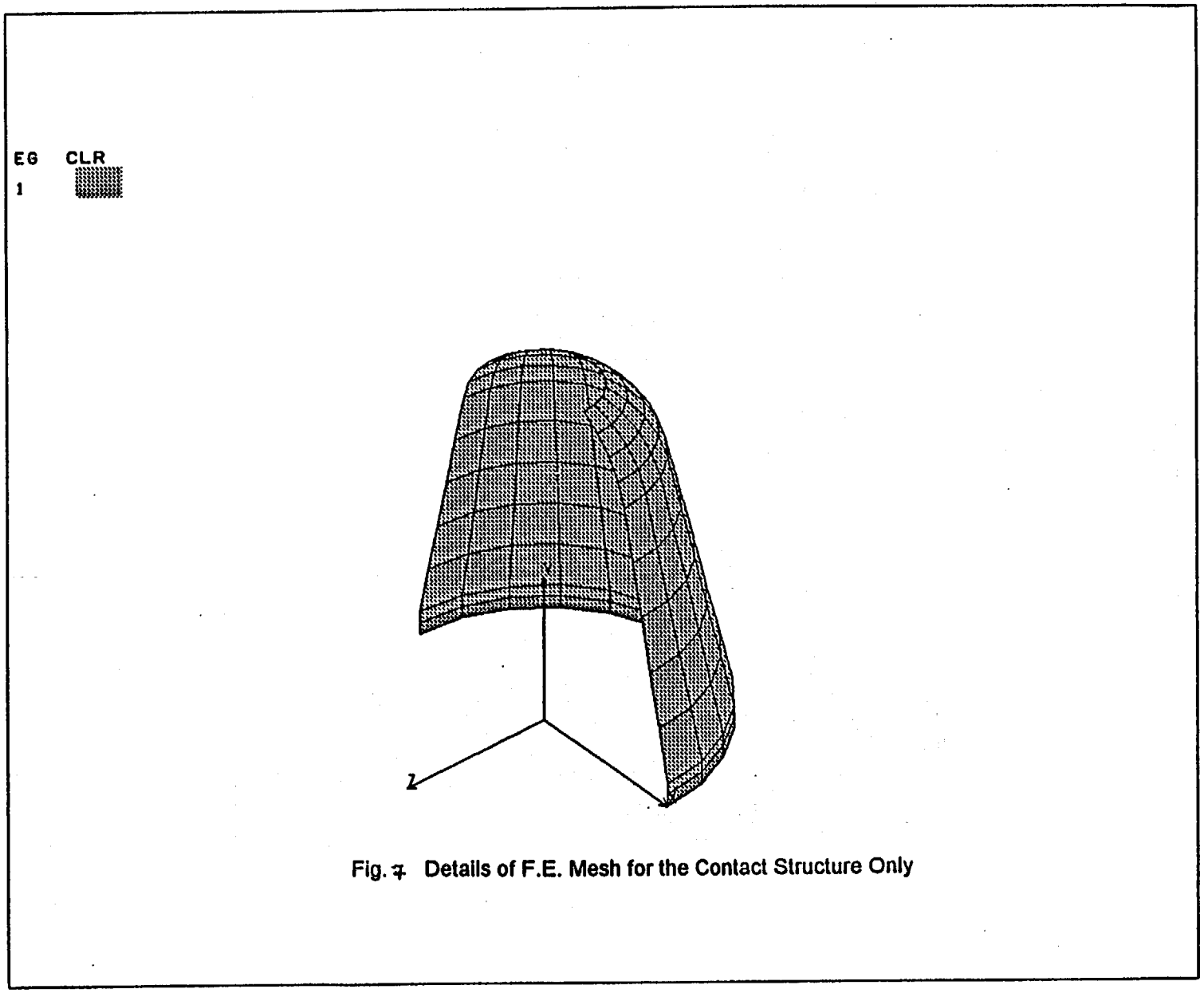

Fig. 7 Details of F.E. Mesh for the Contact Structure Only

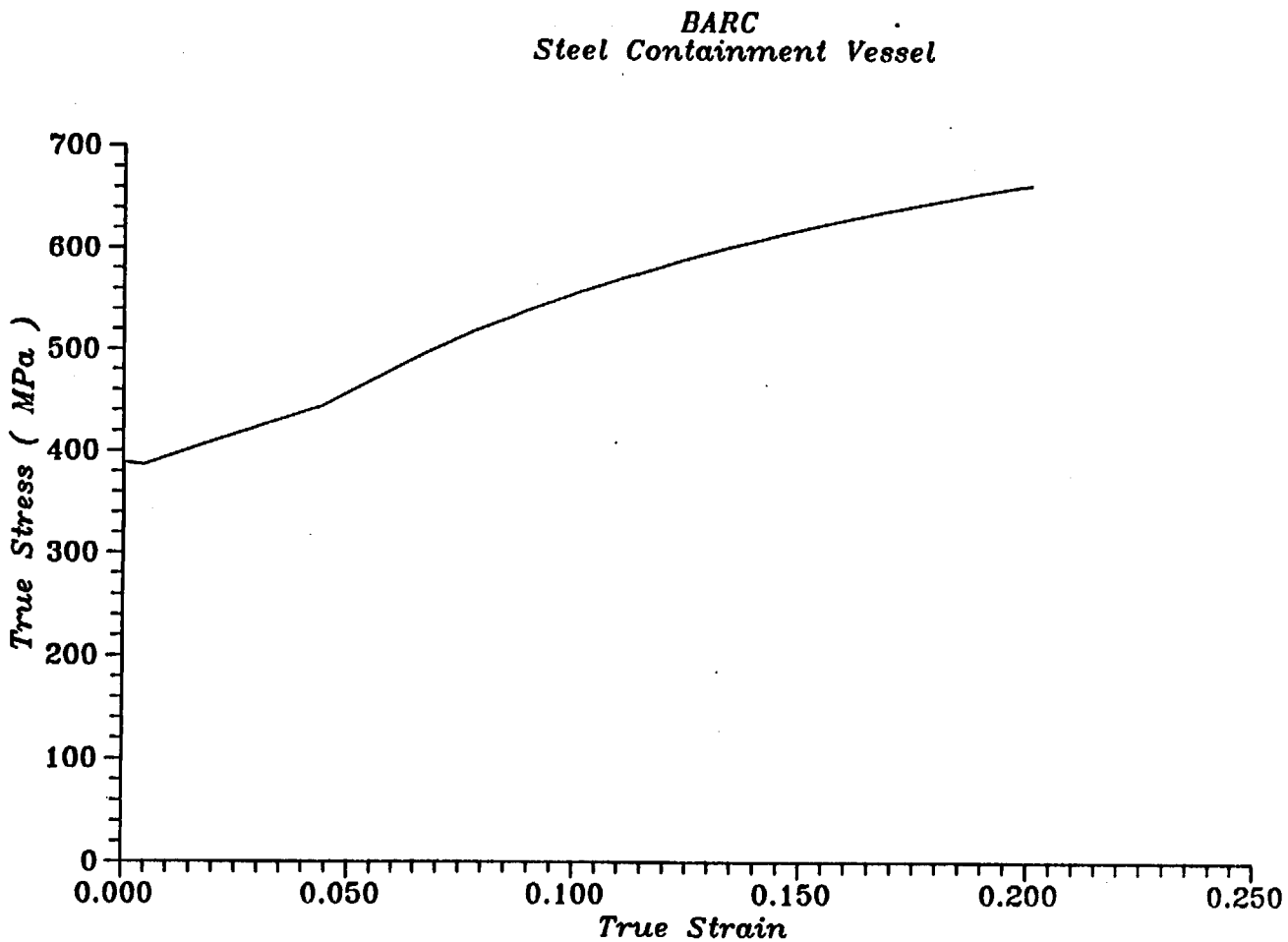

Fig.No.8 Plot of True Stress v/s. True Strain for SGV 480
(As used in our Analysis)

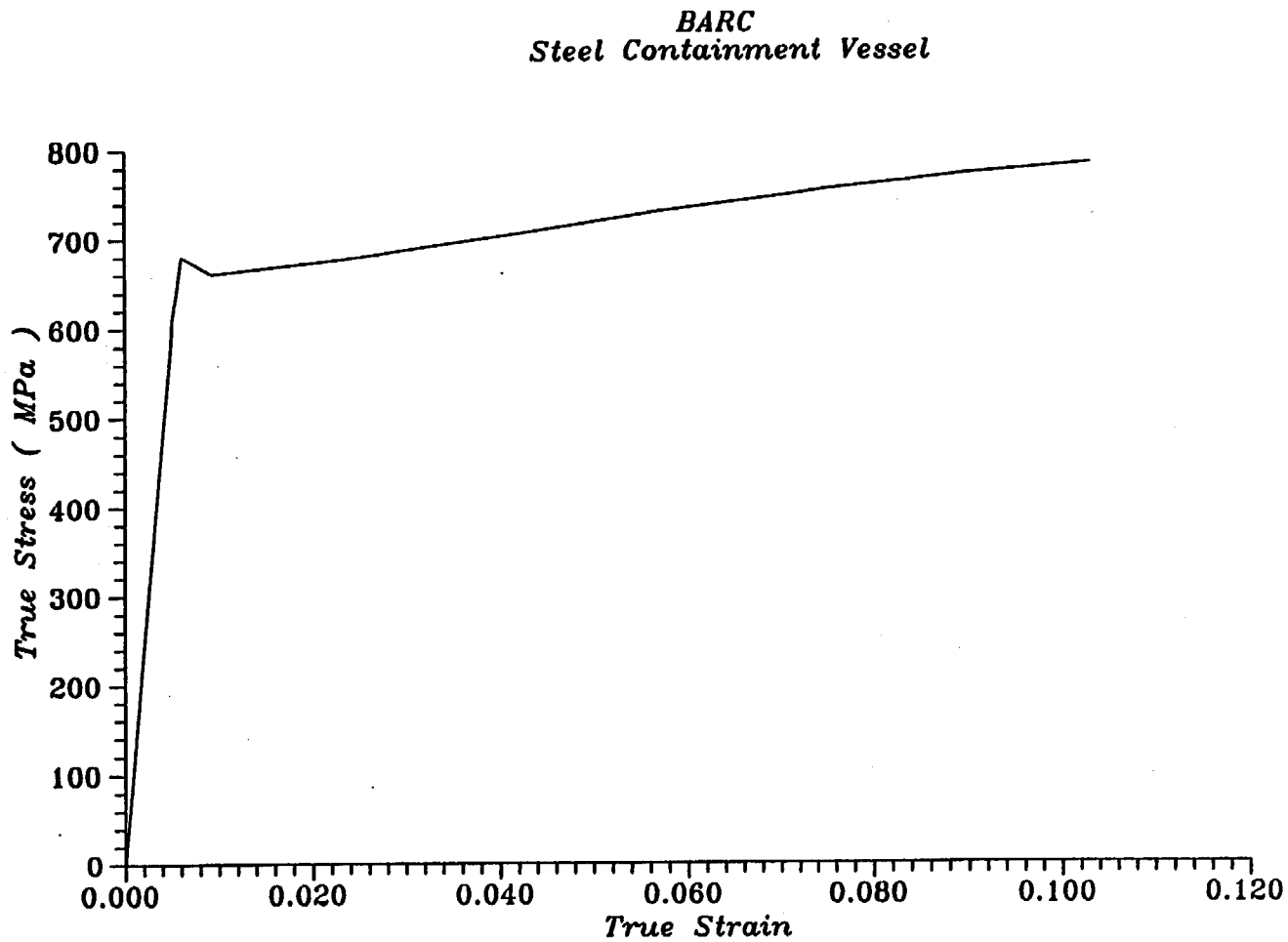

Fig.No.9 Plot of True Stress v/s. True Strain for SPV 490
(As used in our Analysis)

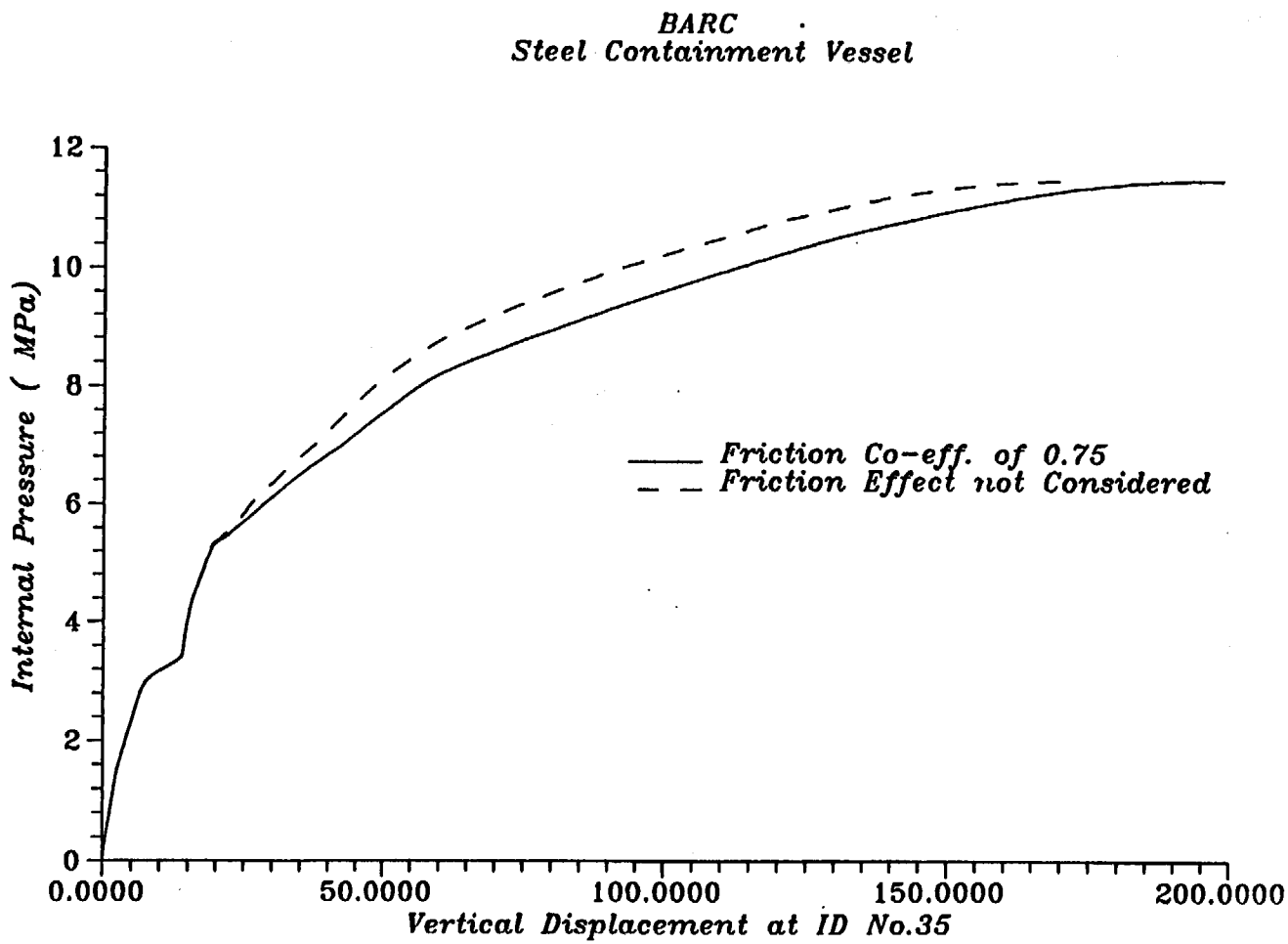

Fig.No.10 Plot of Load v/s. Displacement at ID No.35
(Comparison of Displacements for the Two Cases)

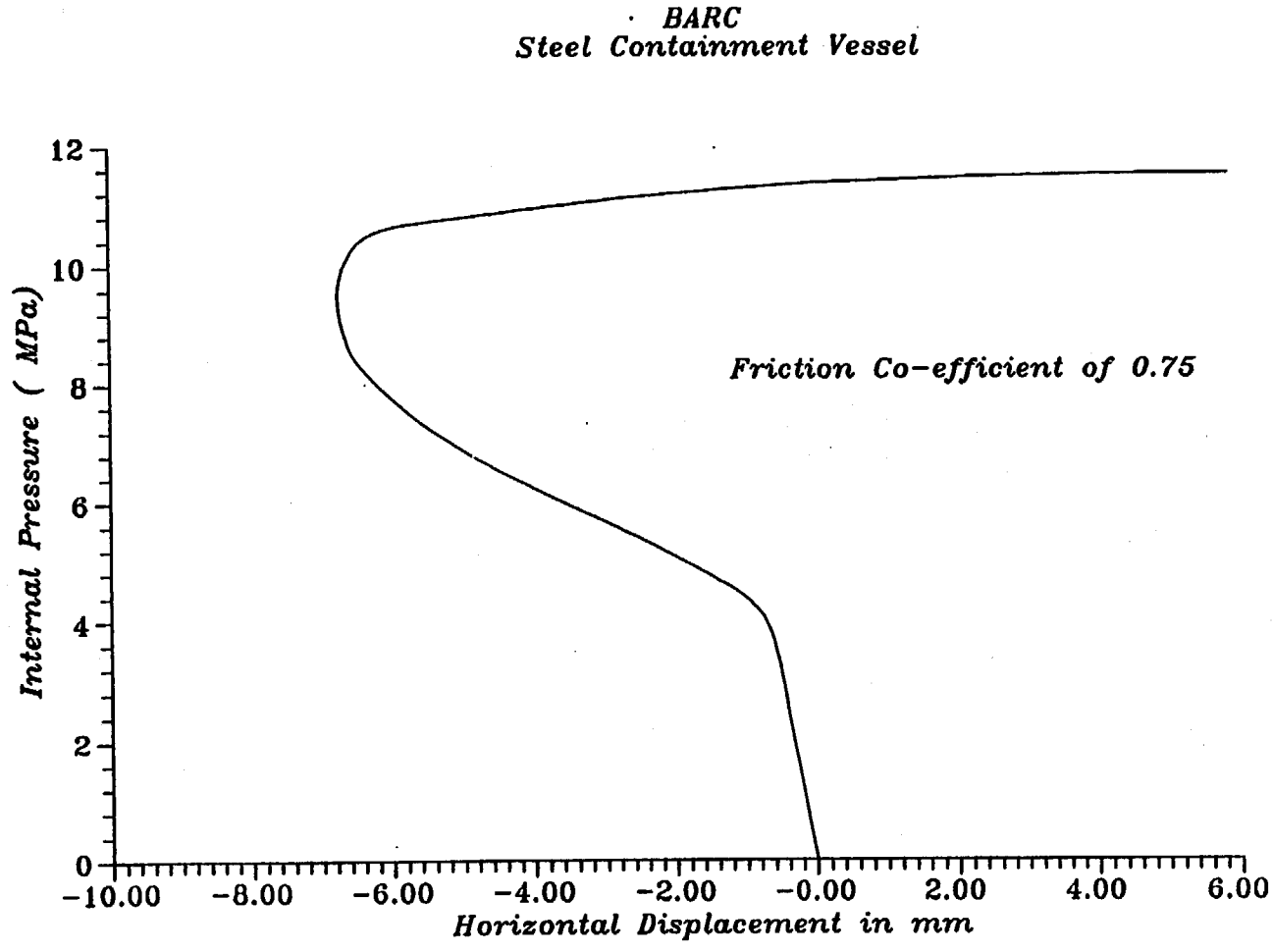

Fig.No.11 Plot of Load v/s. Displacement node 1646 (TPKNU)

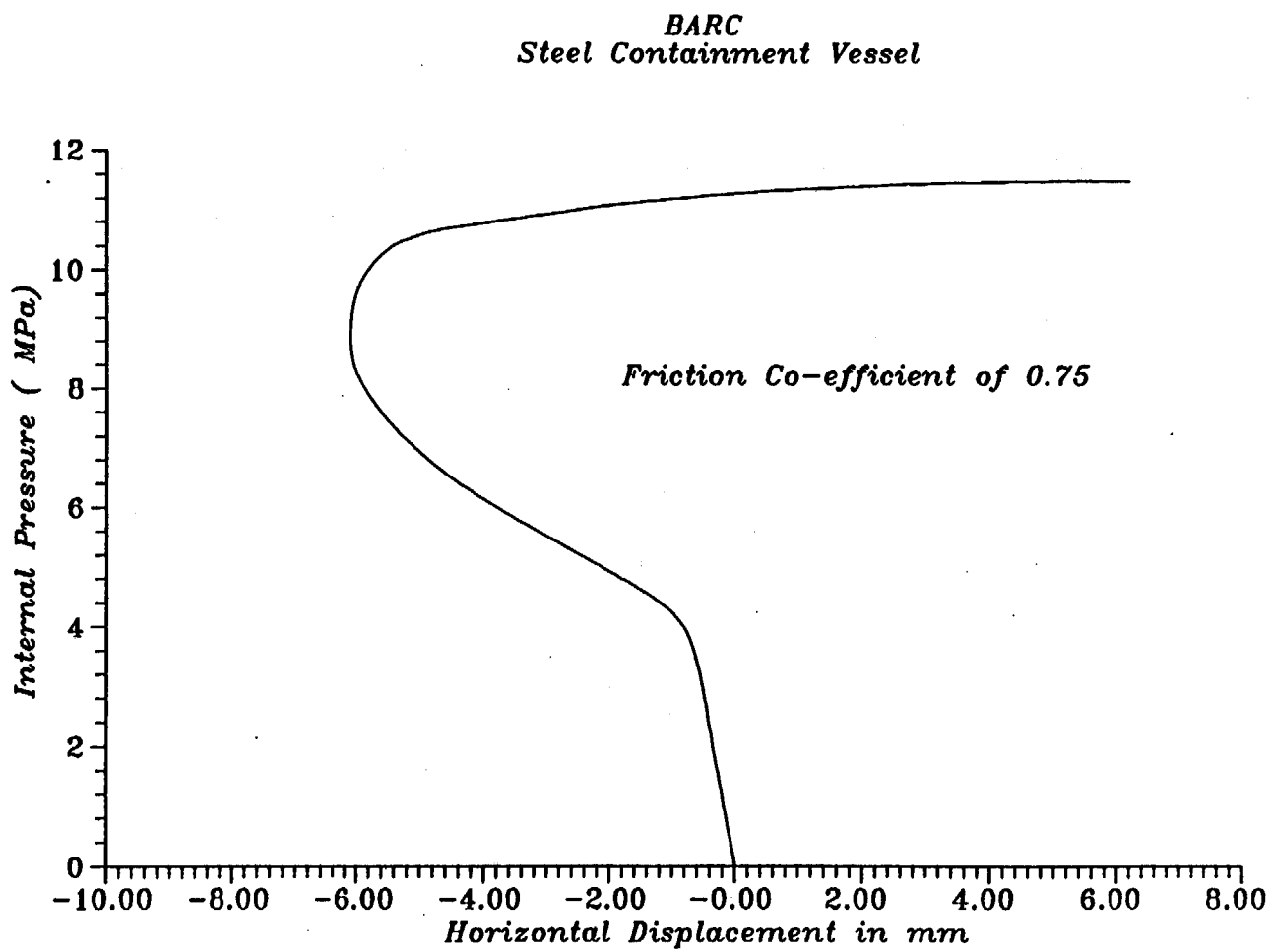

Fig.No.12 Plot of Load v/s. Displacement node 1654 (TPKNU)

ABAQUS

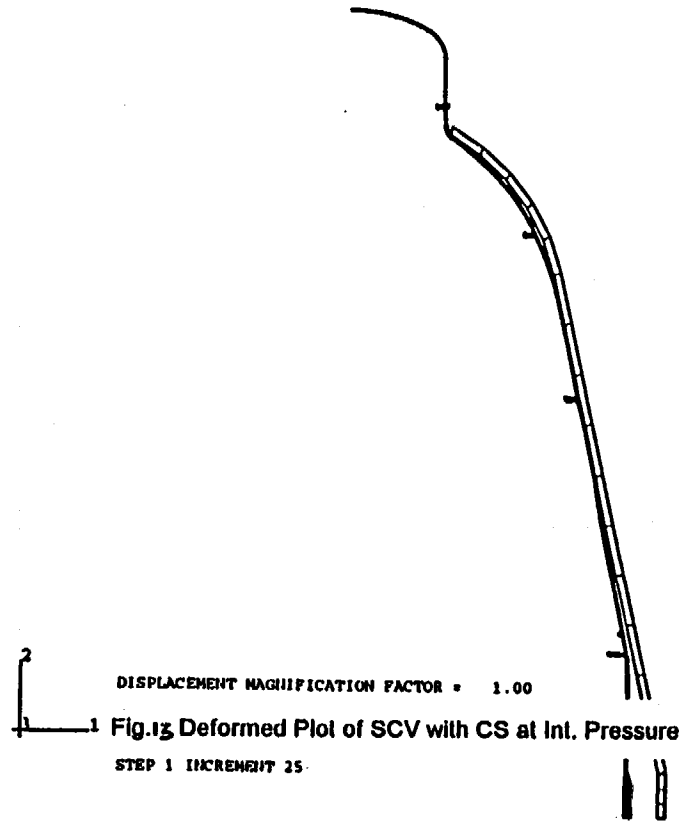

Fig.13 Deformed Plot of SCV with CS at Int. Pressure of 4.605 MPa showing Contact Pattern.

ABAQUS

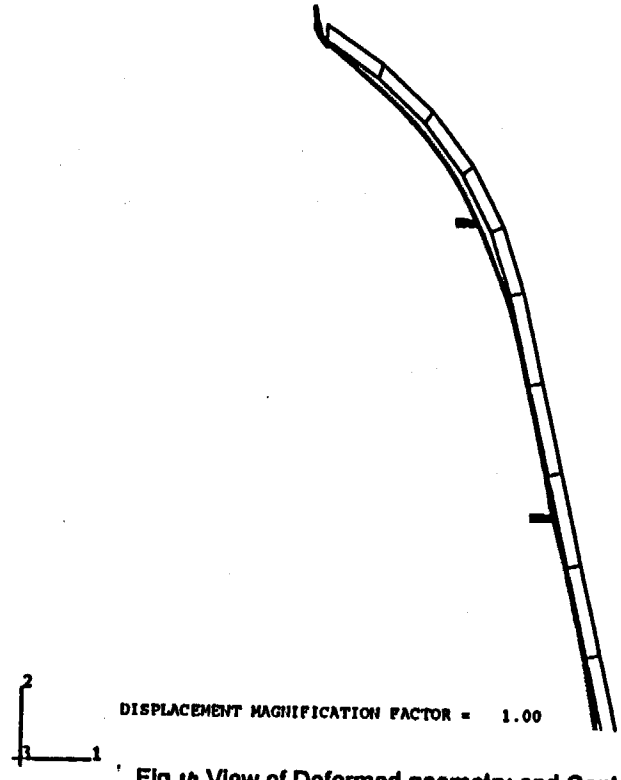

Fig.14 View of Deformed geometry and Contact Pattern at 4.605 MPa
(Details of Spherical Shell & Conical Shell)

ABAQUS

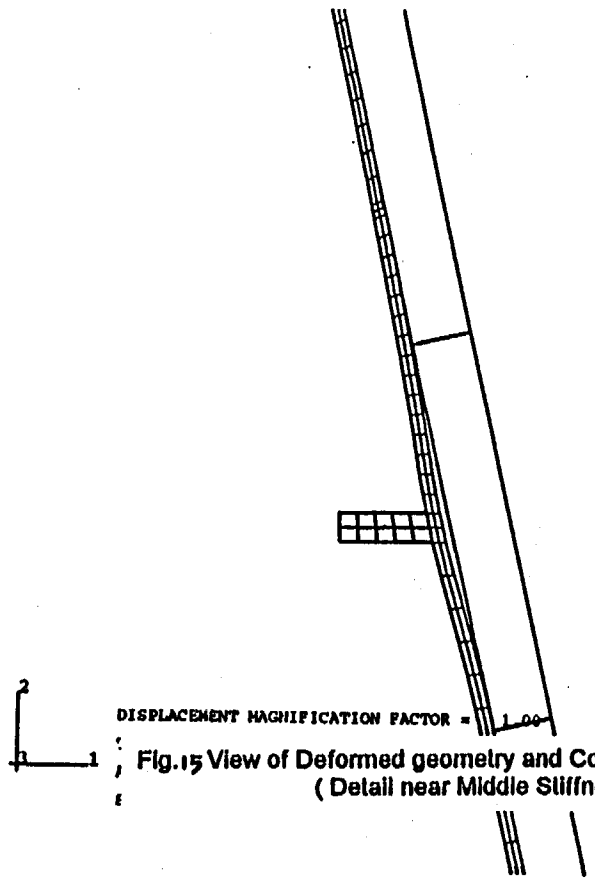

Fig.15 View of Deformed geometry and Contact Pattern at 4.605 MPa
(Detail near Middle Stiffner)

ABAQUS

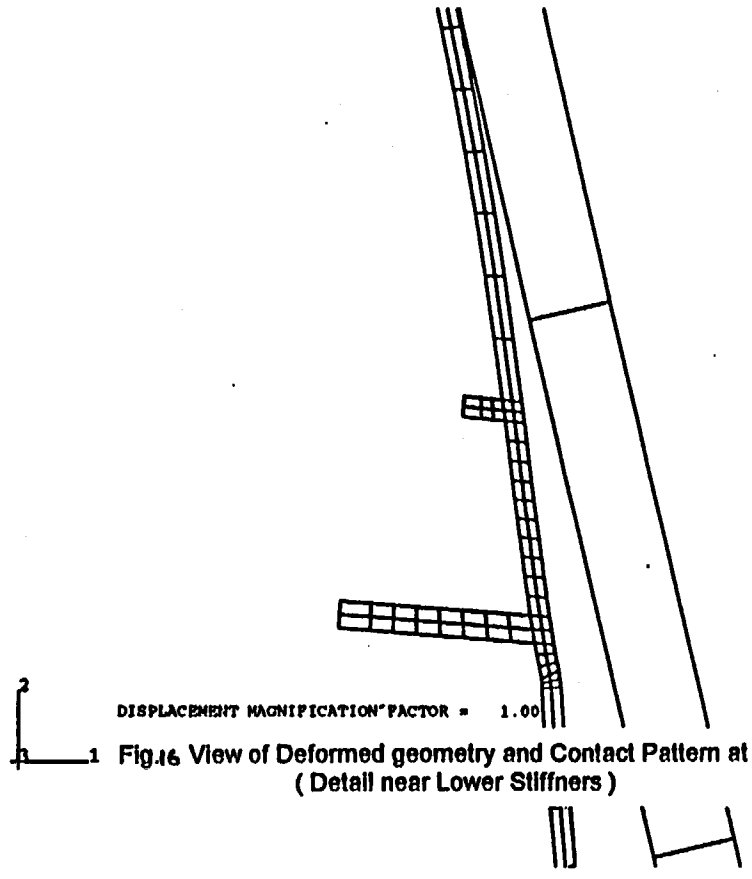

Fig.16 View of Deformed geometry and Contact Pattern at 4.605 MPa
(Detail near Lower Stiffners)

ABAQUS

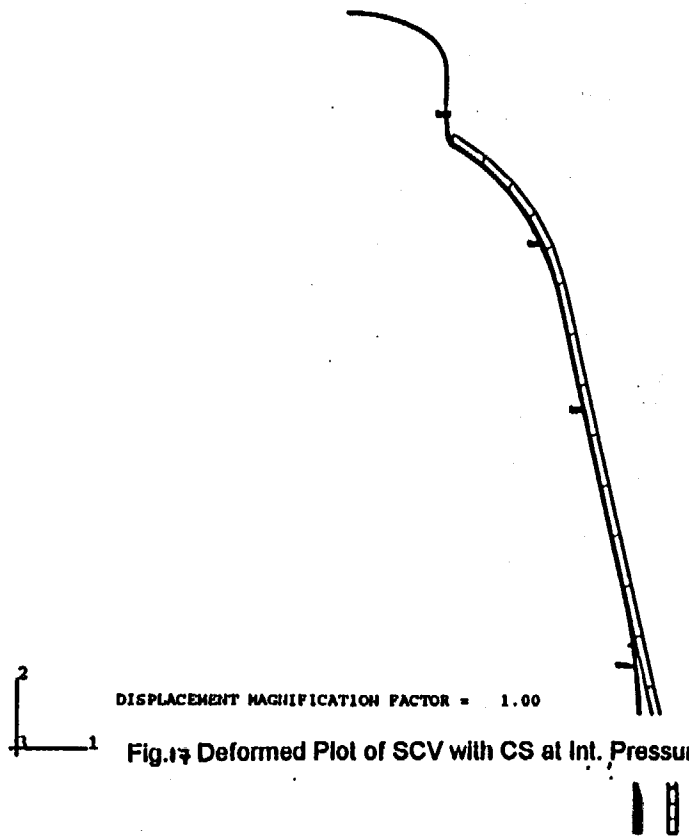

Fig.17 Deformed Plot of SCV with CS at Int. Pressure of 6.480 MPa showing Contact Pattern.

ABAQUS

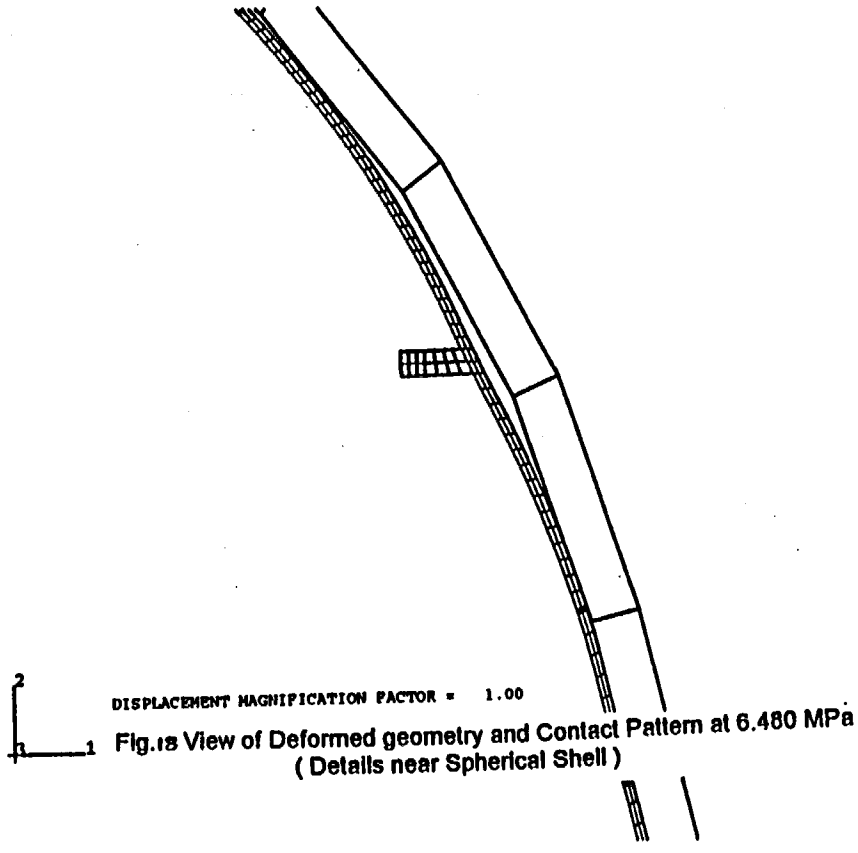

Fig.18 View of Deformed geometry and Contact Pattern at 6.480 MPa
(Details near Spherical Shell)

ABAQUS

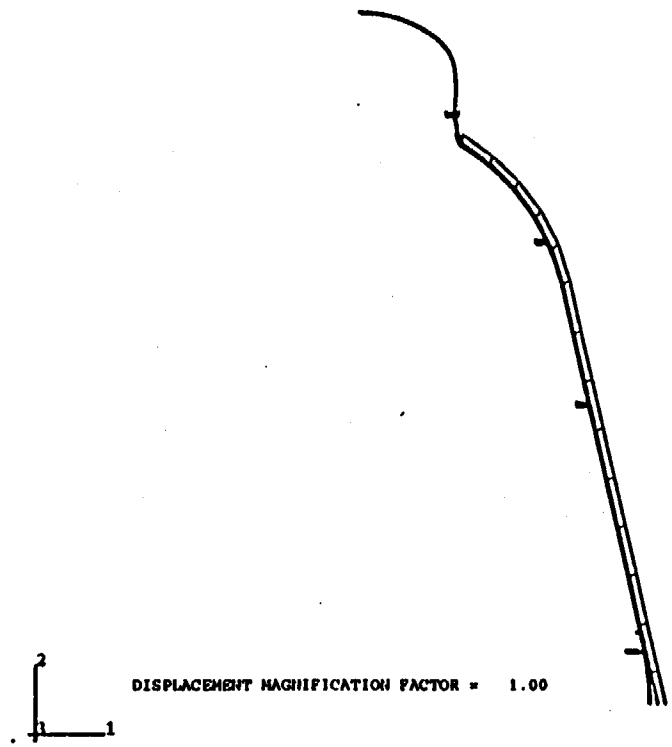

Fig.19 Deformed Plot of SCV with CS at Int. Pressure of 8.400 MPa showing Contact Pattern.

ABAQUS

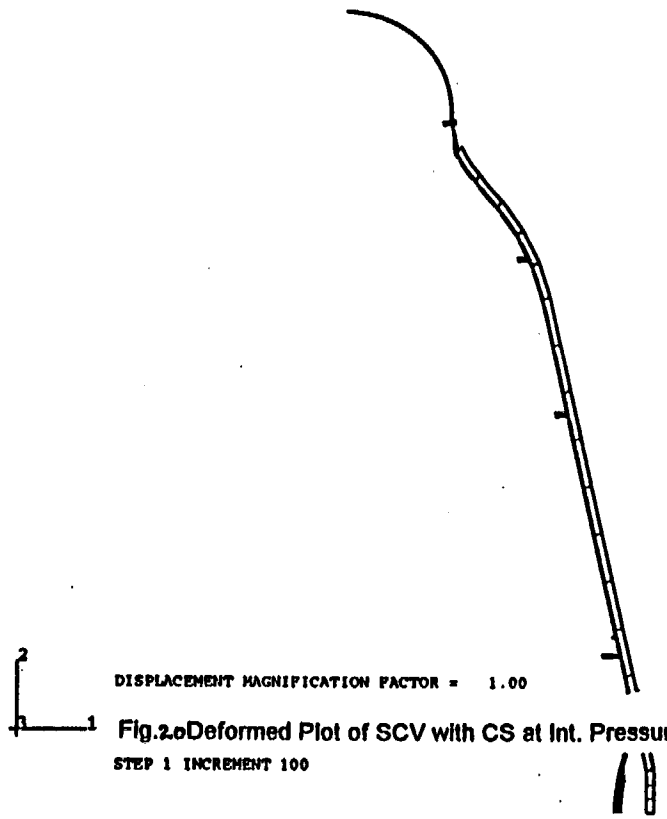

Fig.2.oDeformed Plot of SCV with CS at Int. Pressure of 11.49 MPa showing Contact Pattern.

ABAQUS

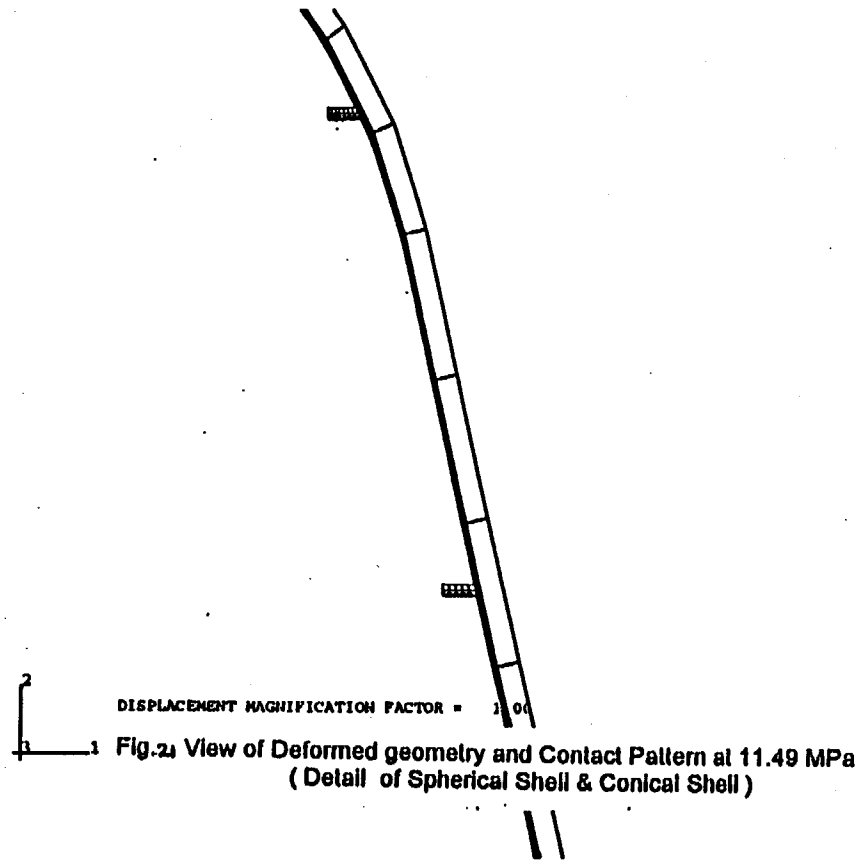

Fig.24 View of Deformed geometry and Contact Pattern at 11.49 MPa
(Detail of Spherical Shell & Conical Shell)

ABAQUS

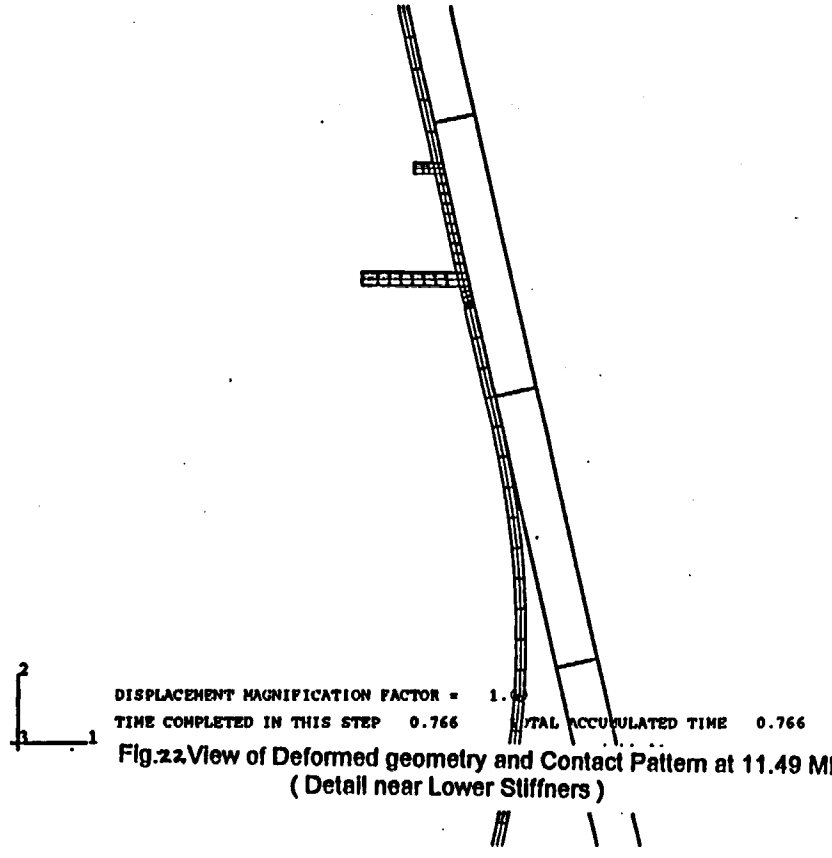

Fig.22 View of Deformed geometry and Contact Pattern at 11.49 MPa
(Detail near Lower Stiffners)

ABAQUS

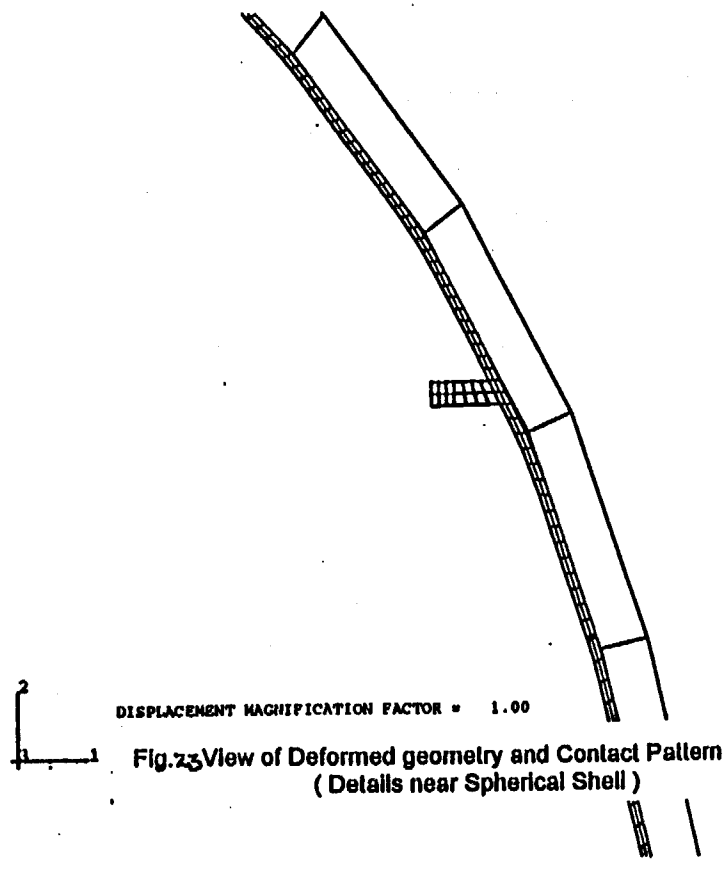

Fig.23 View of Deformed geometry and Contact Pattern at 11.49 MPa
(Details near Spherical Shell)

ABAQUS

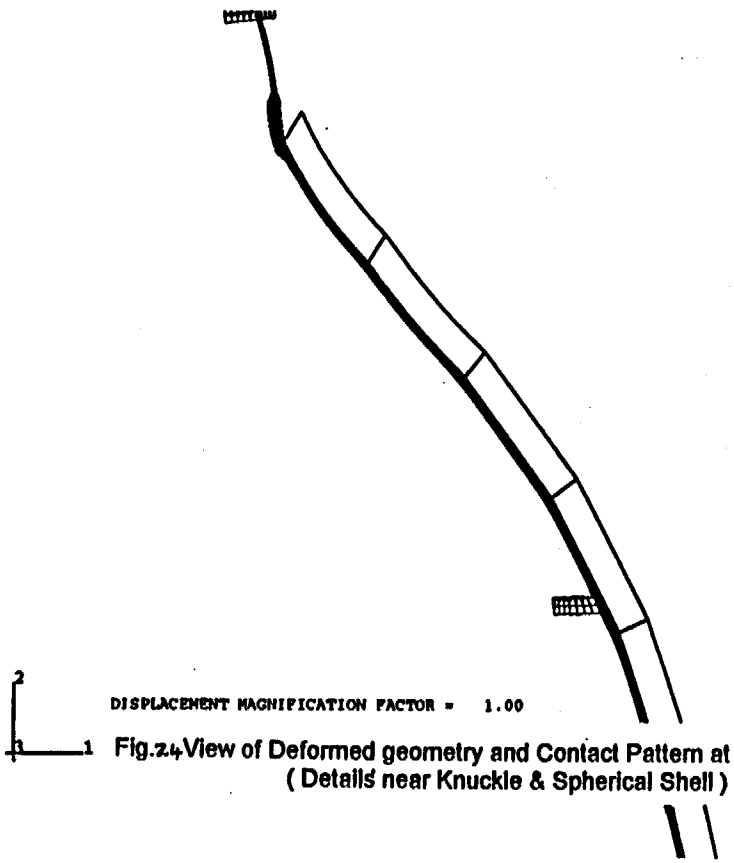

Fig.24 View of Deformed geometry and Contact Pattern at 11.49 MPa
(Details near Knuckle & Spherical Shell)

APPENDIX A

STRAIN V/S PRESSURE AND DEFLECTION V/S PRESSURE PLOTS IN THE FORM OF DIGITAL DATA

The digital data of strain v/s pressure and deflection v/s pressure plots, is given in the floppy diskettes, enclosed along with the pretest report.

The Diskette marked **A**, containing files plot7.dat to plot38.dat, is for the analysis, in which coefficient of friction =0.75. One additional file plot7e.dat contains the plot data for the minimum principal strain (but maximum in magnitude) at ID7.

The Diskette marked **B**, containing files p7.dat to p38.dat, is for the analysis, in which coefficient of friction =0.0. One additional file p7e.dat contains the plot data for the minimum principal strain (but maximum in magnitude) at ID7.

Since the submitted results pertain to axisymmetric model, hence plot data corresponding to locations, near equipment hatch opening (plot1.dat to plot6.dat and plot39.dat), are not included.

APPENDIX B

STRAIN V/S PRESSURE AND DEFLECTION V/S PRESSURE PLOTS IN THE FORM OF HARDCOPIES

The strain v/s pressure and deflection v/s pressure plots are enclosed. The plots at different locations can be identified by Plot ID number indicated on them. These Plot ID numbers are corresponding to those mentioned in SCV design package. Since the submitted results pertain to axisymmetric model, hence plots at locations near equipment hatch opening are not included. These correspond to Plot ID no. 1-6 and 39.

Fig.25 to Fig.58, are plots of strain v/s pressure and deflection v/s pressure, for the case in which coefficient of friction (μ) =0.75.

Fig.59 to Fig.92, are plots of strain v/s pressure and deflection v/s pressure, for the case in which coefficient of friction (μ) =0.0

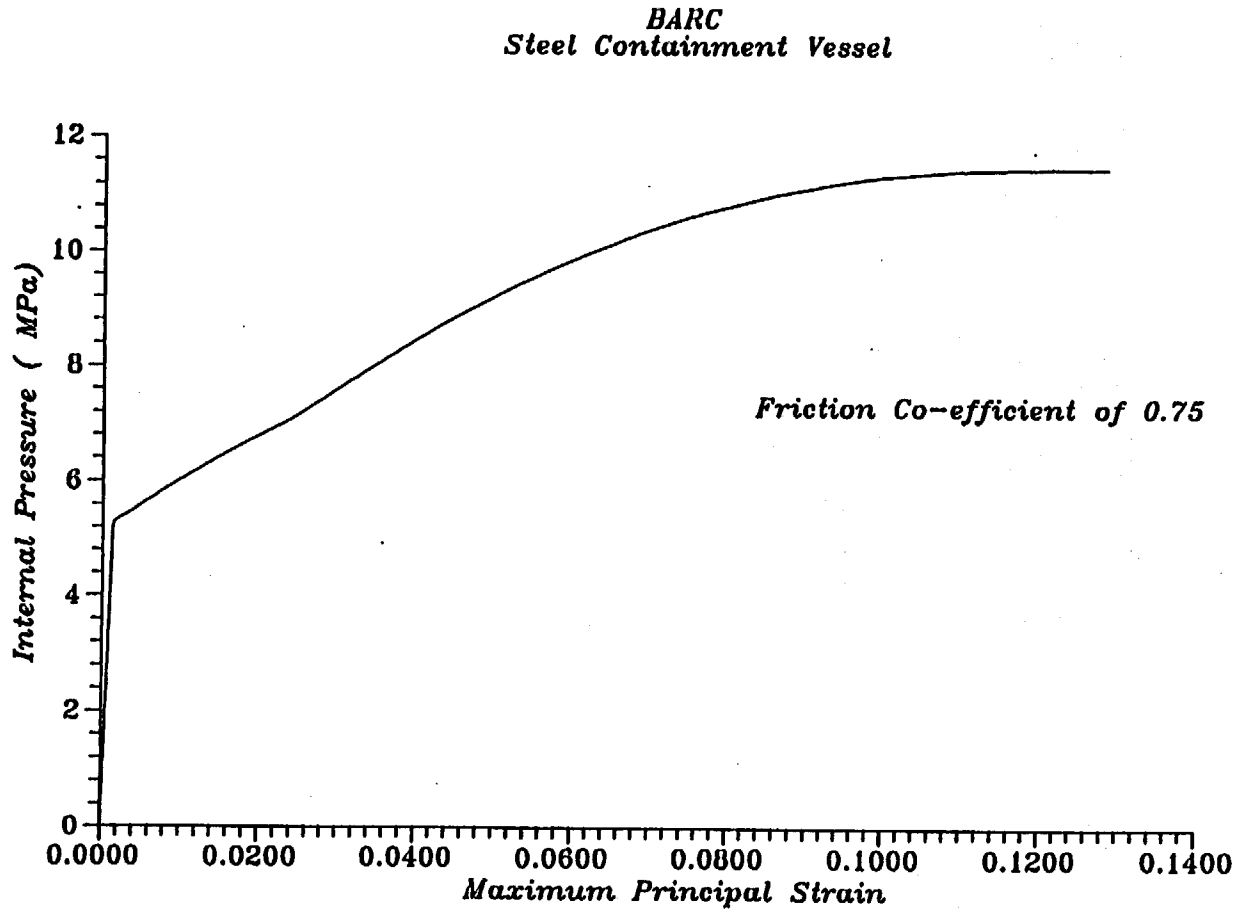

Fig.No.25 Plot of Load v/s. Strain at ID No.7

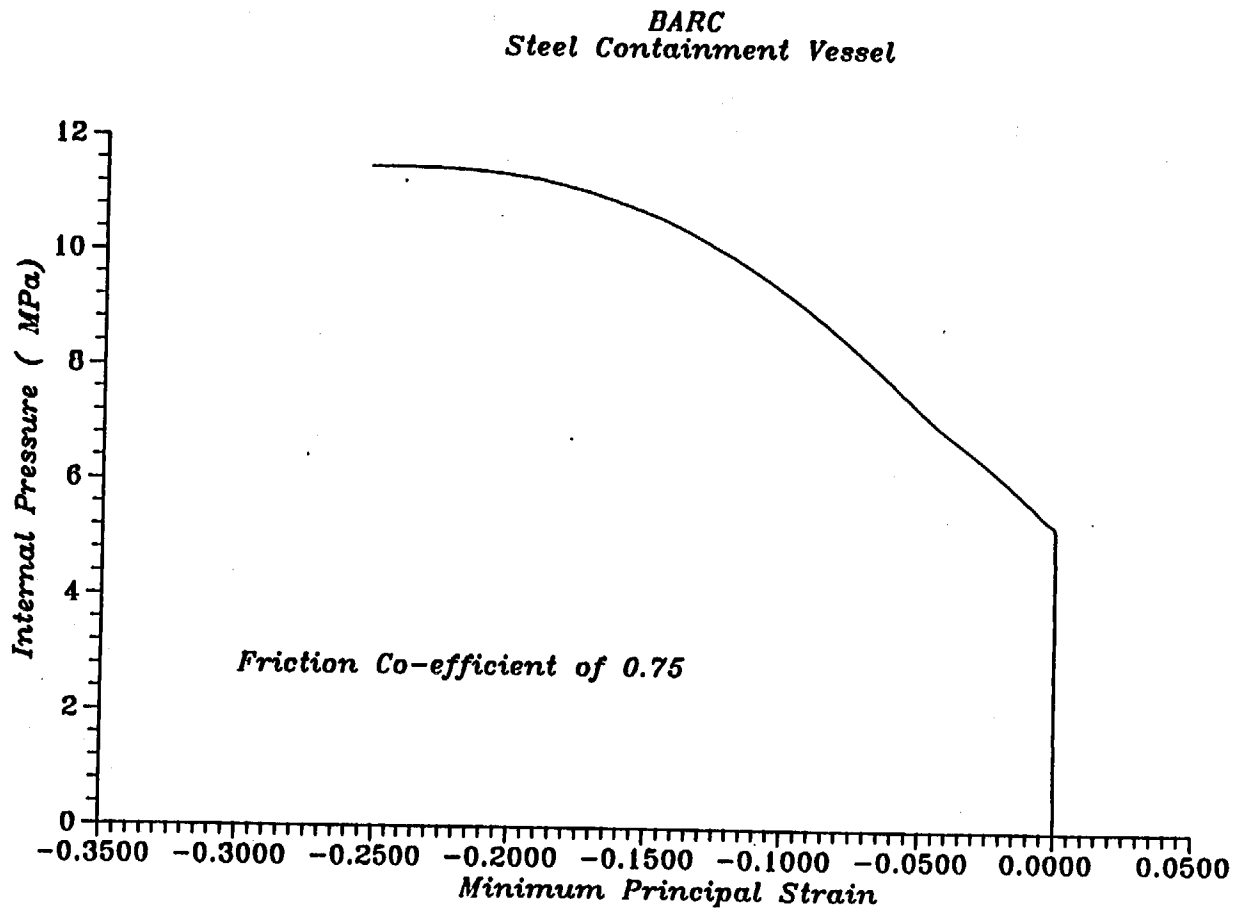

Fig.No.26 Plot of Load v/s. Strain at ID No.7

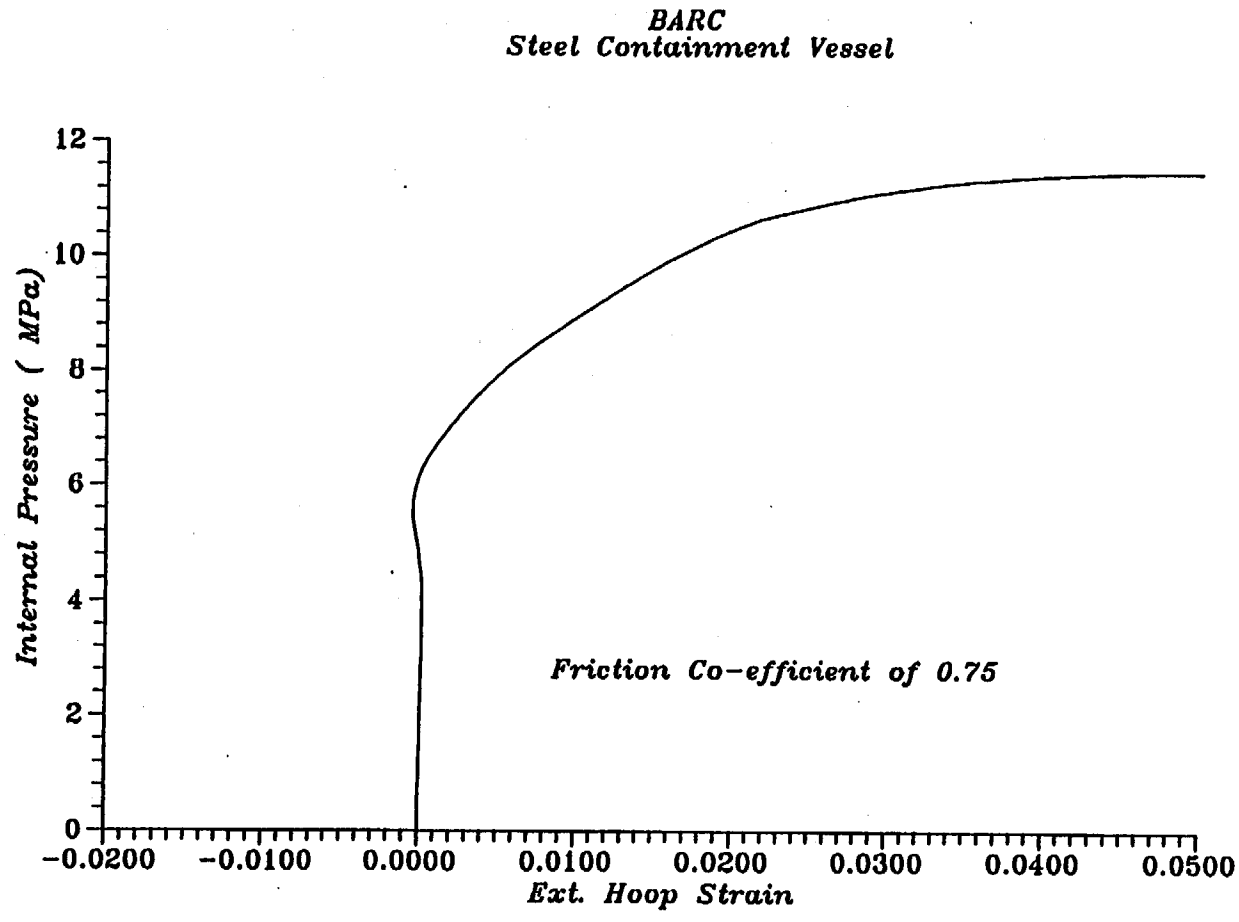

Fig.No.27 Plot of Load v/s. Strain at ID No.8

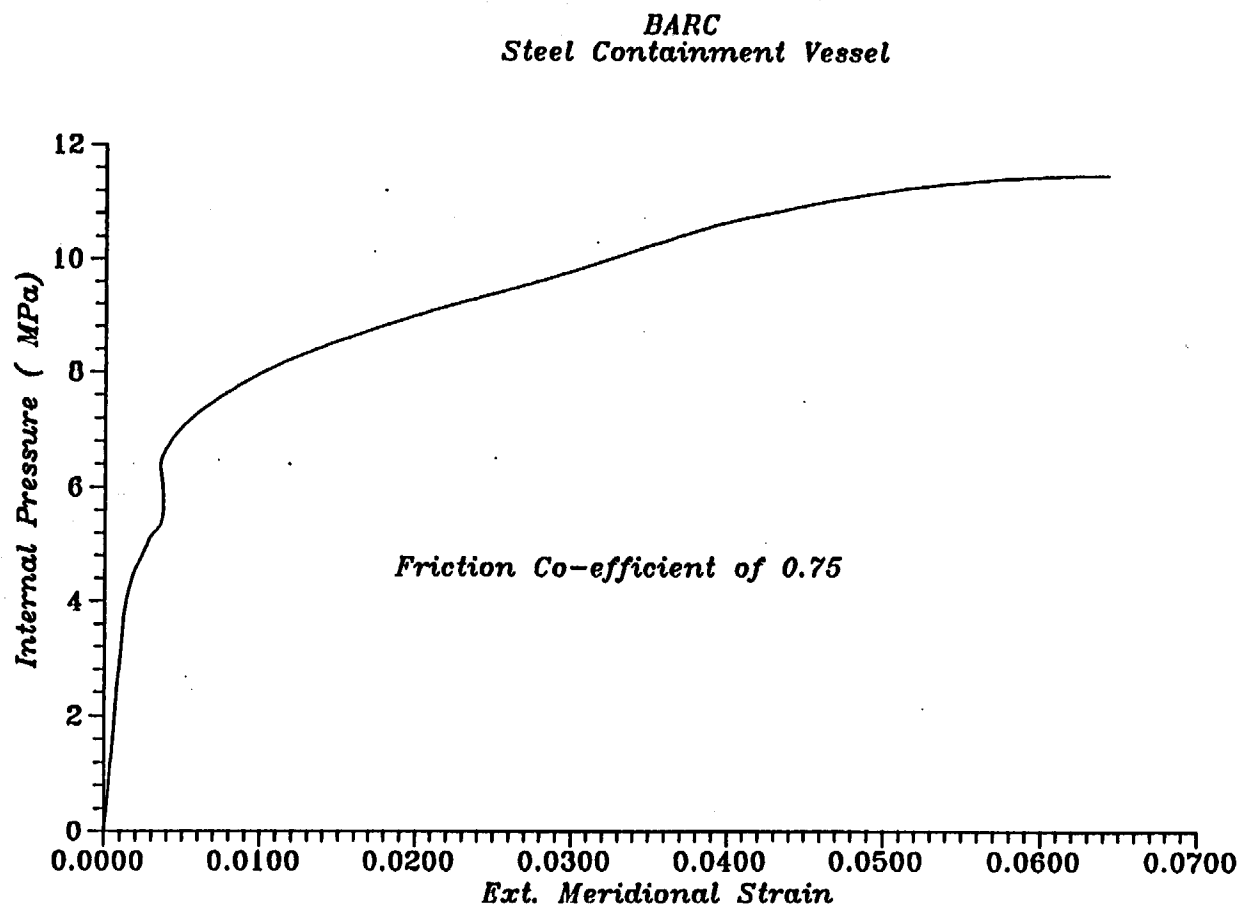

Fig.No.28 Plot of Load v/s. Strain at ID No.9

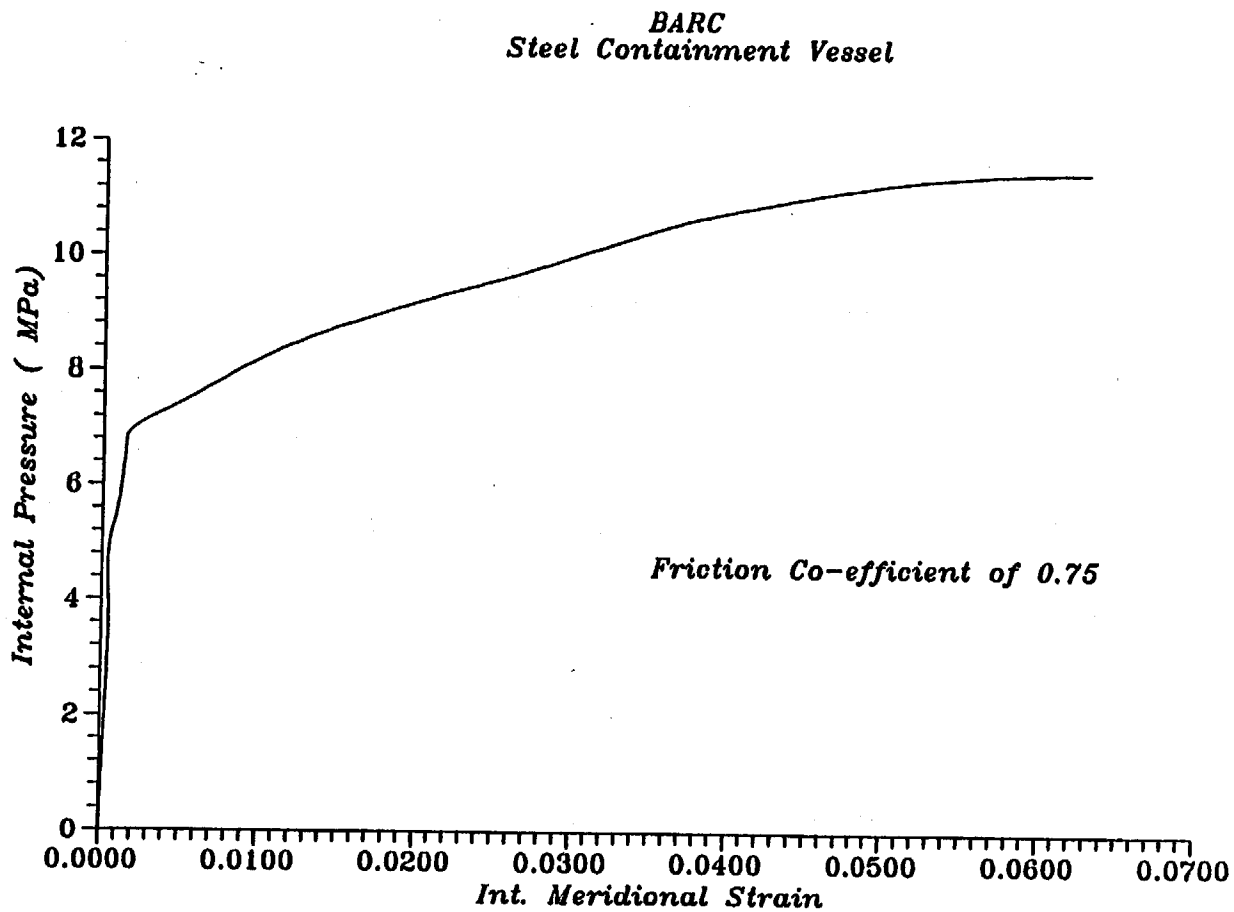

Fig.No.29 Plot of Load v/s. Strain at ID No.10

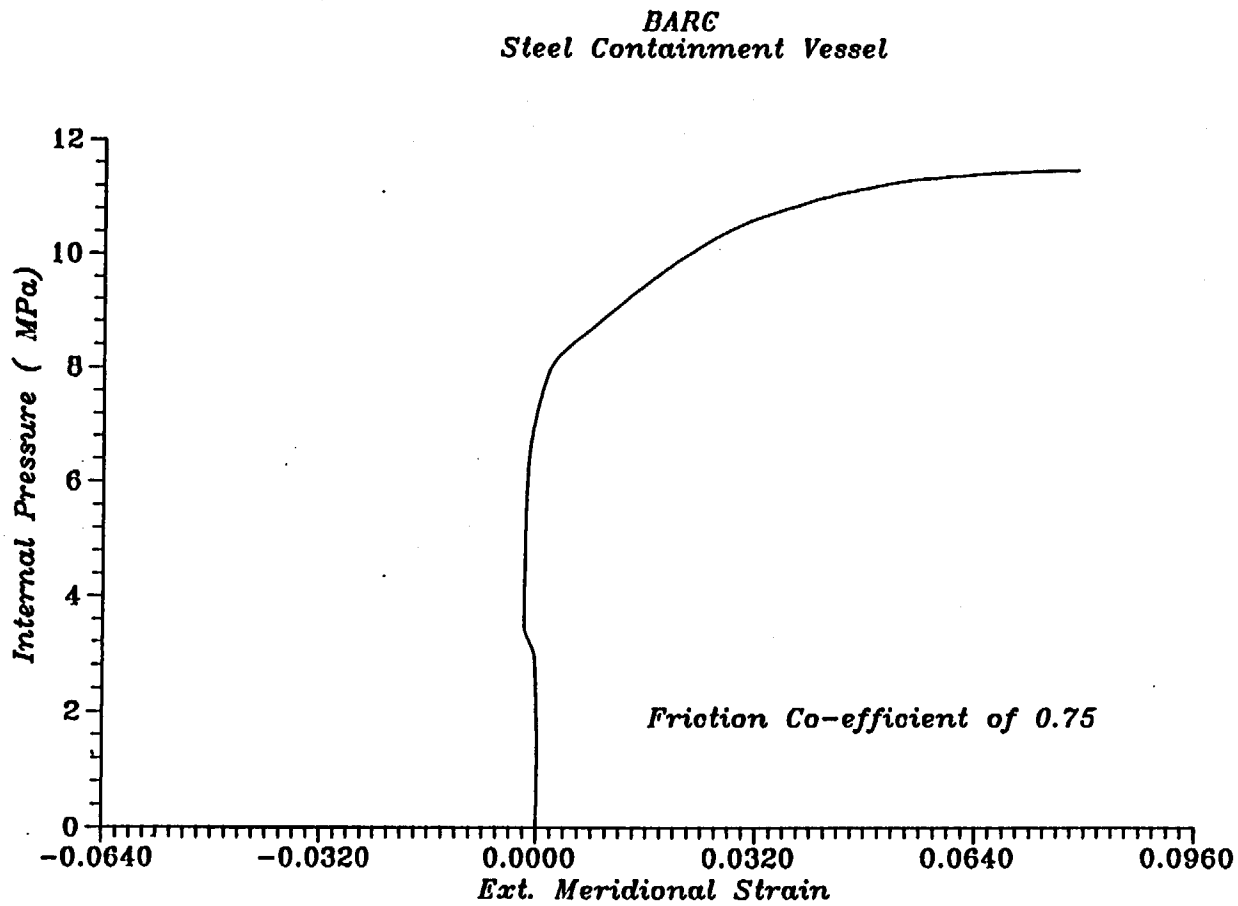

Fig.No.30 Plot of Load v/s. Strain at ID No.11

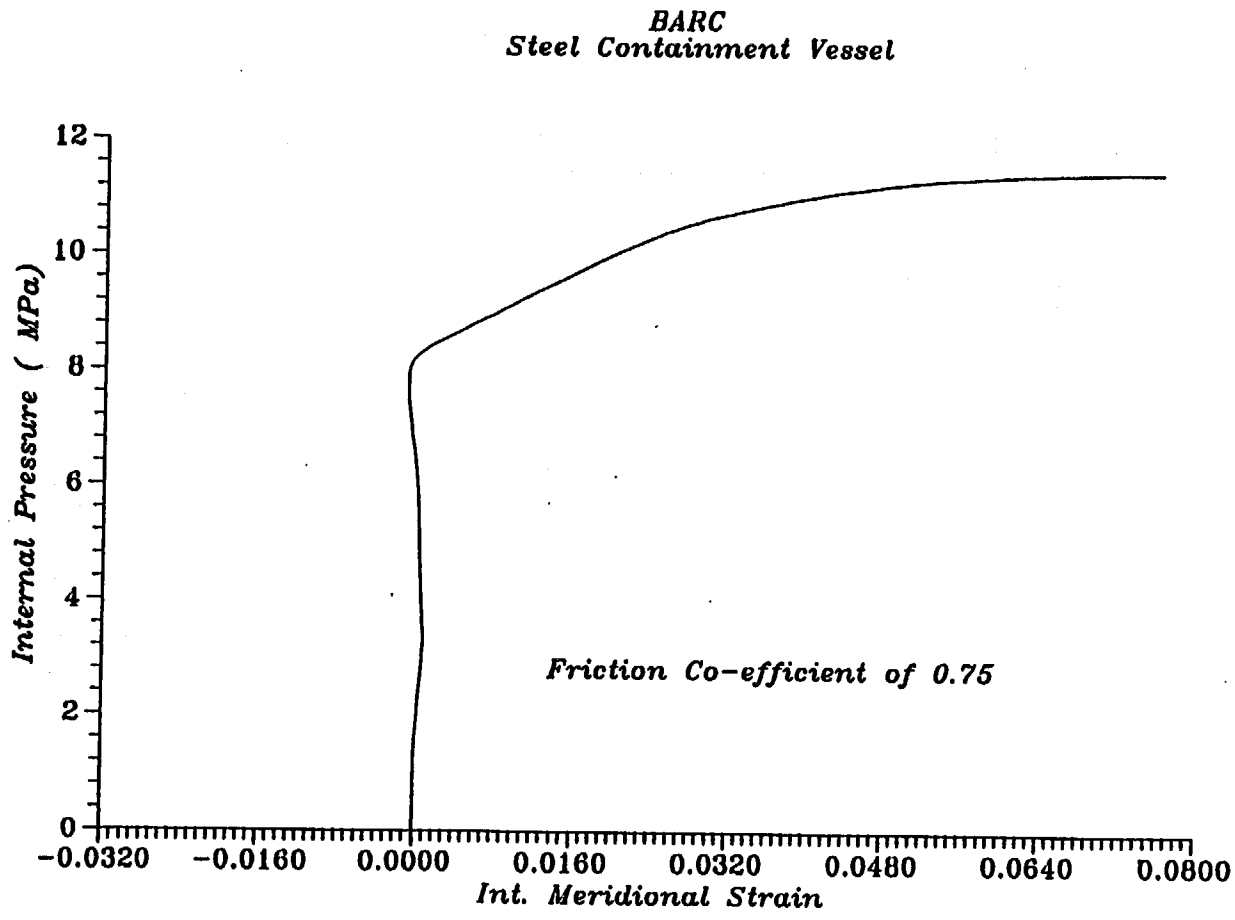

Fig.No.31 Plot of Load v/s. Strain at ID No.12

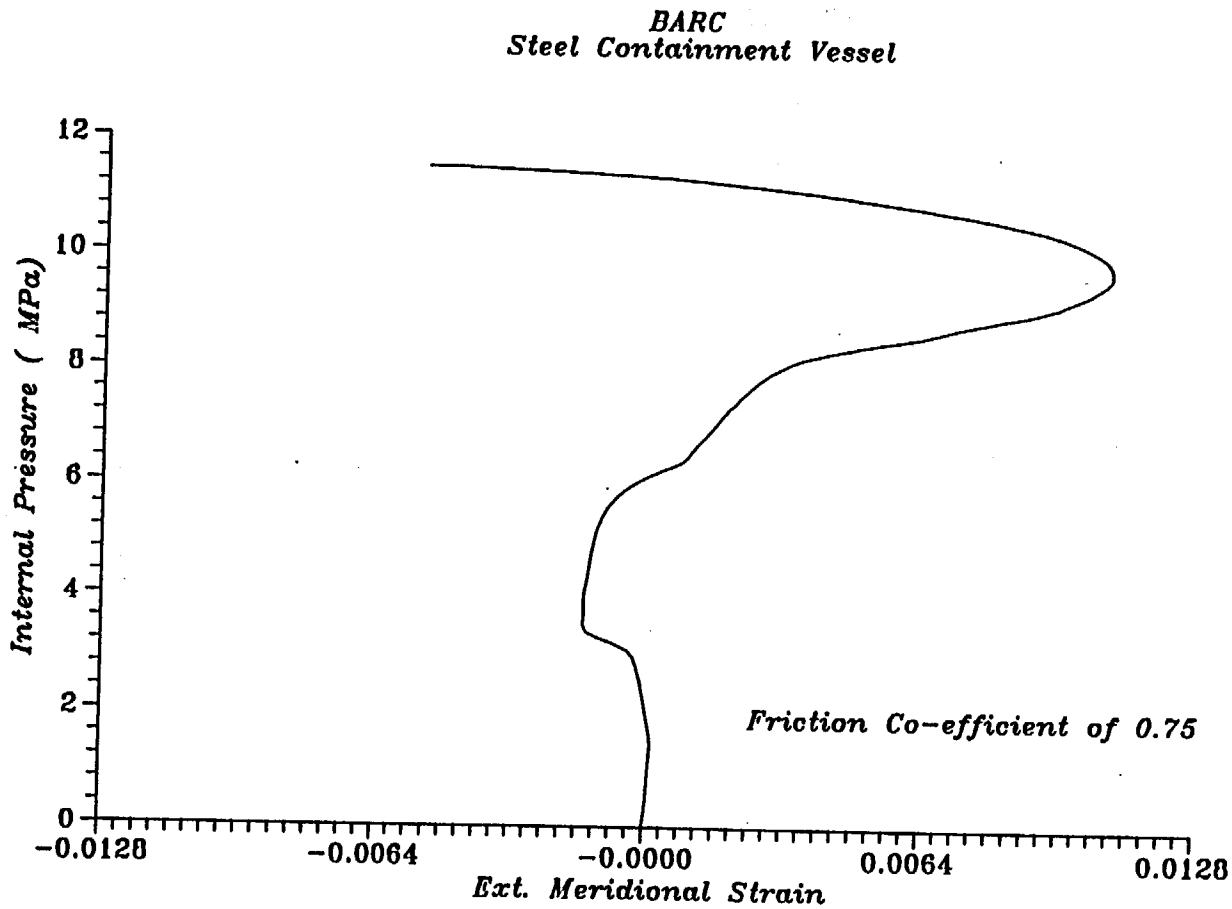

Fig.No.32 Plot of Load v/s. Strain at ID No.13

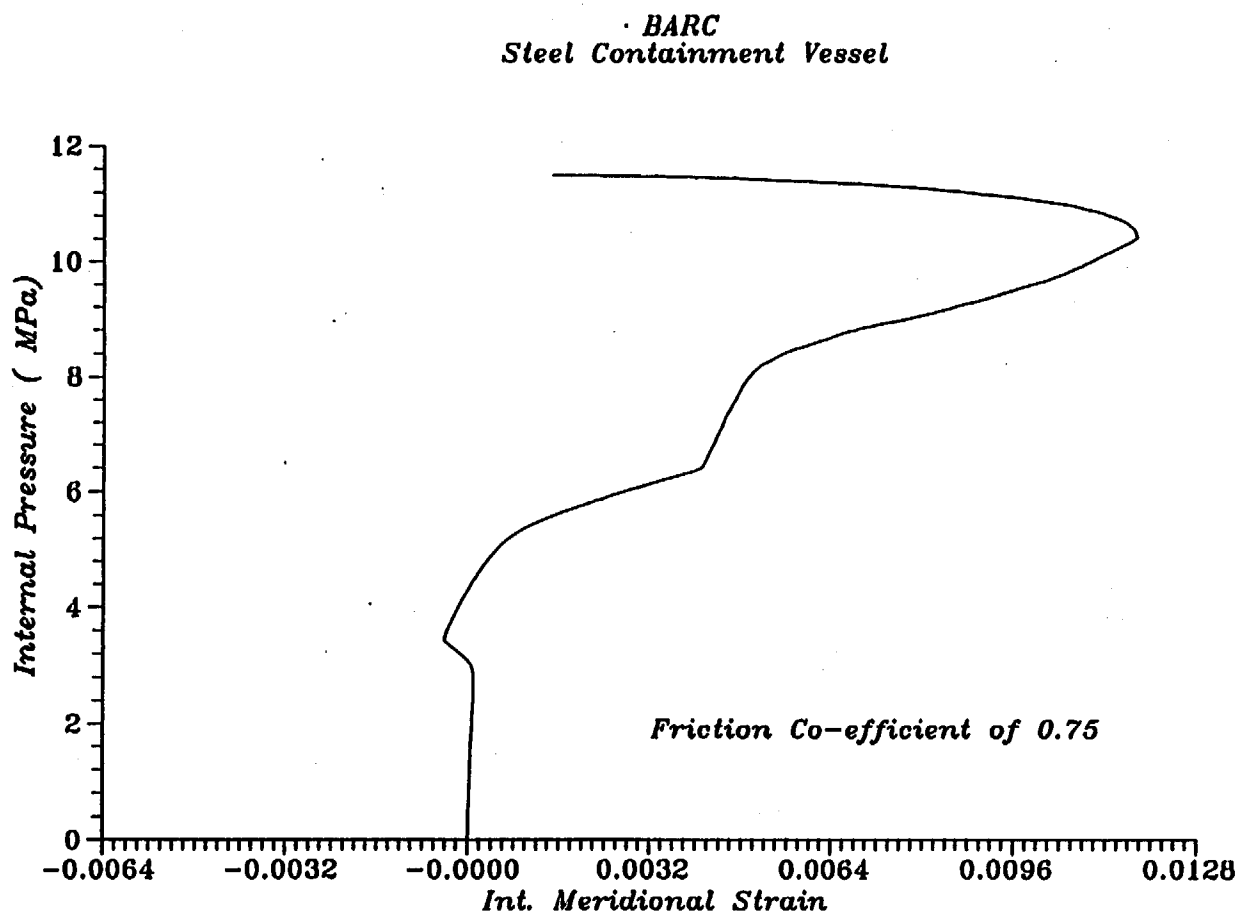

Fig.No.33 Plot of Load v/s. Strain at ID No.14

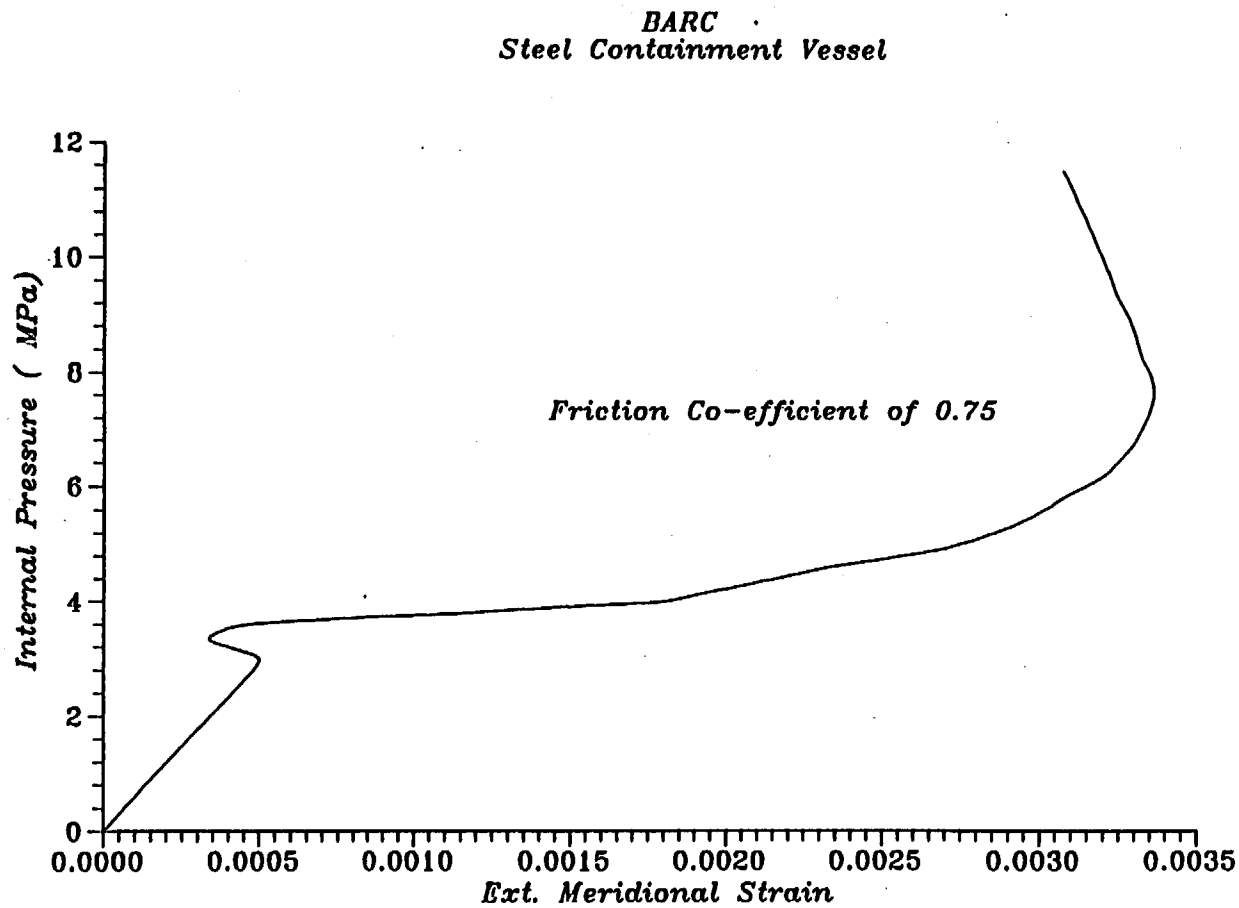

Fig.No.34 Plot of Load v/s. Strain at ID No.15

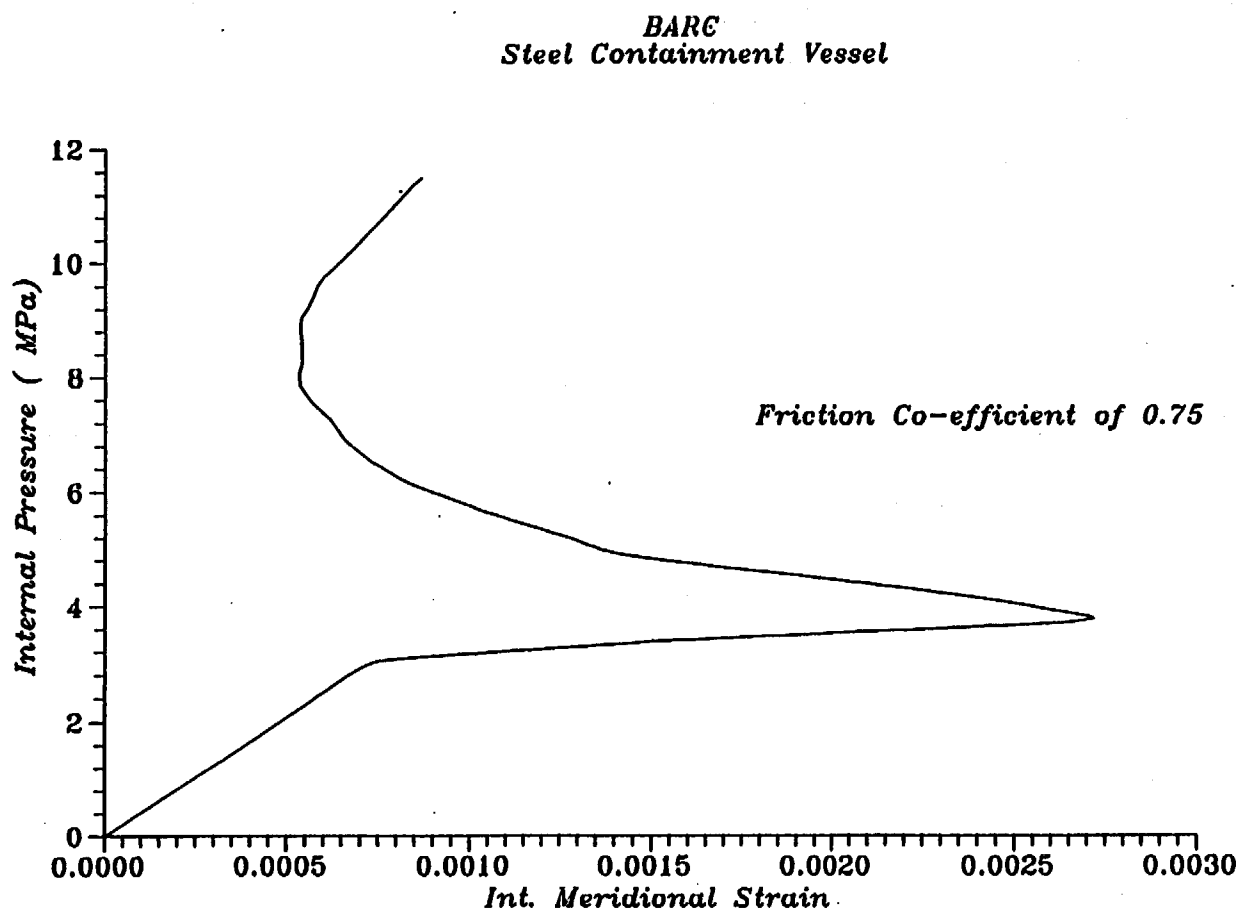

Fig.No.35 Plot of Load v/s. Strain at ID No.16

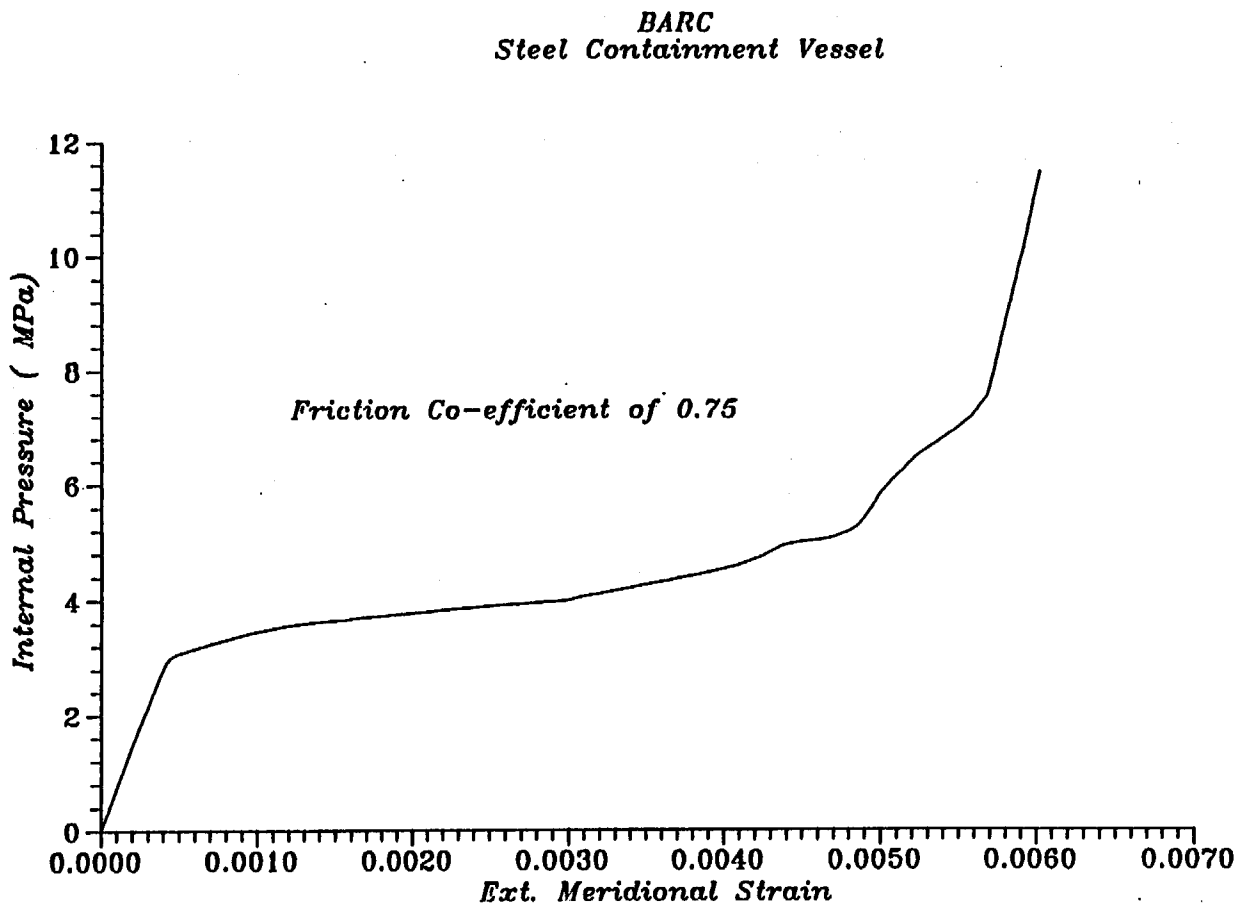

Fig.No.36Plot of Load v/s. Strain at ID No.17

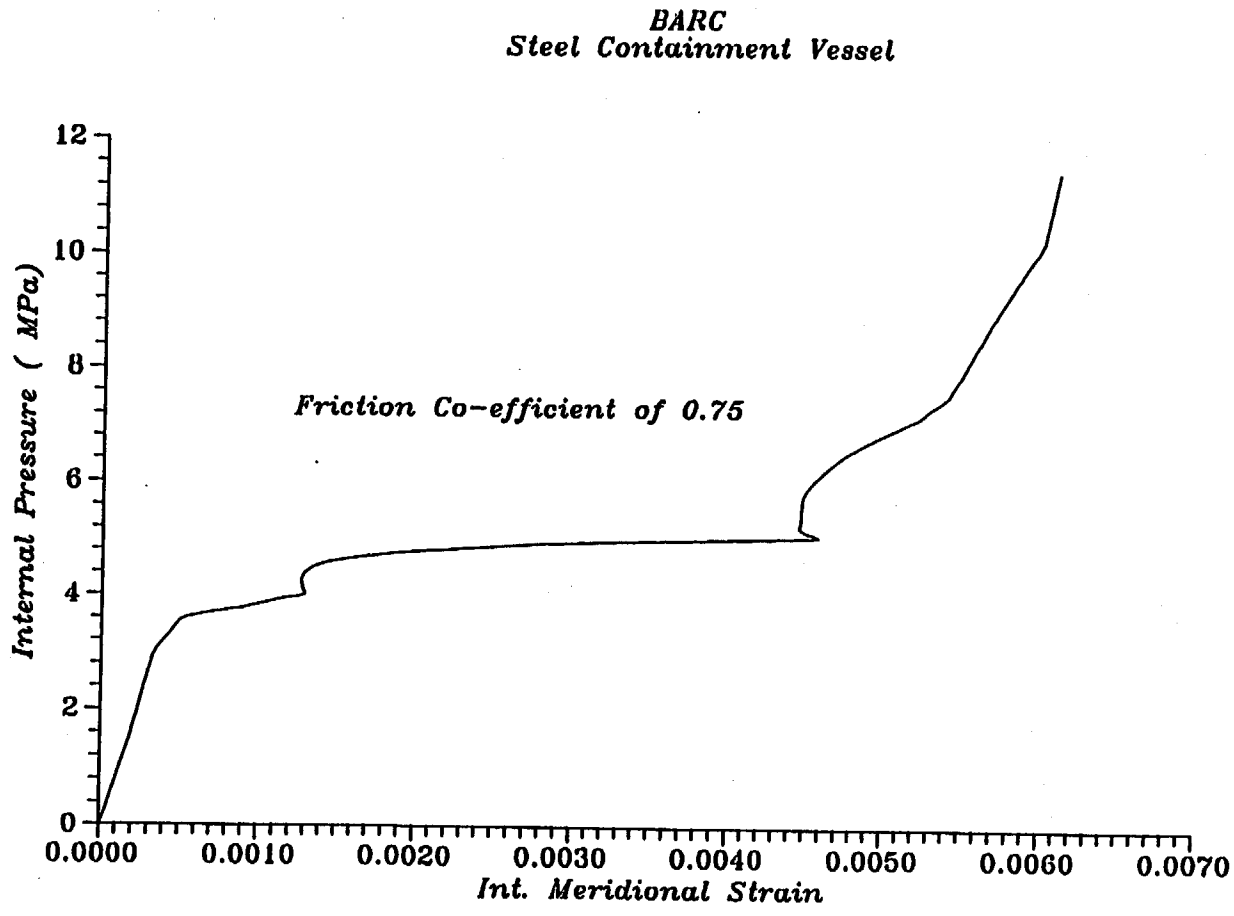

Fig.No.57 Plot of Load v/s. Strain at ID No.18

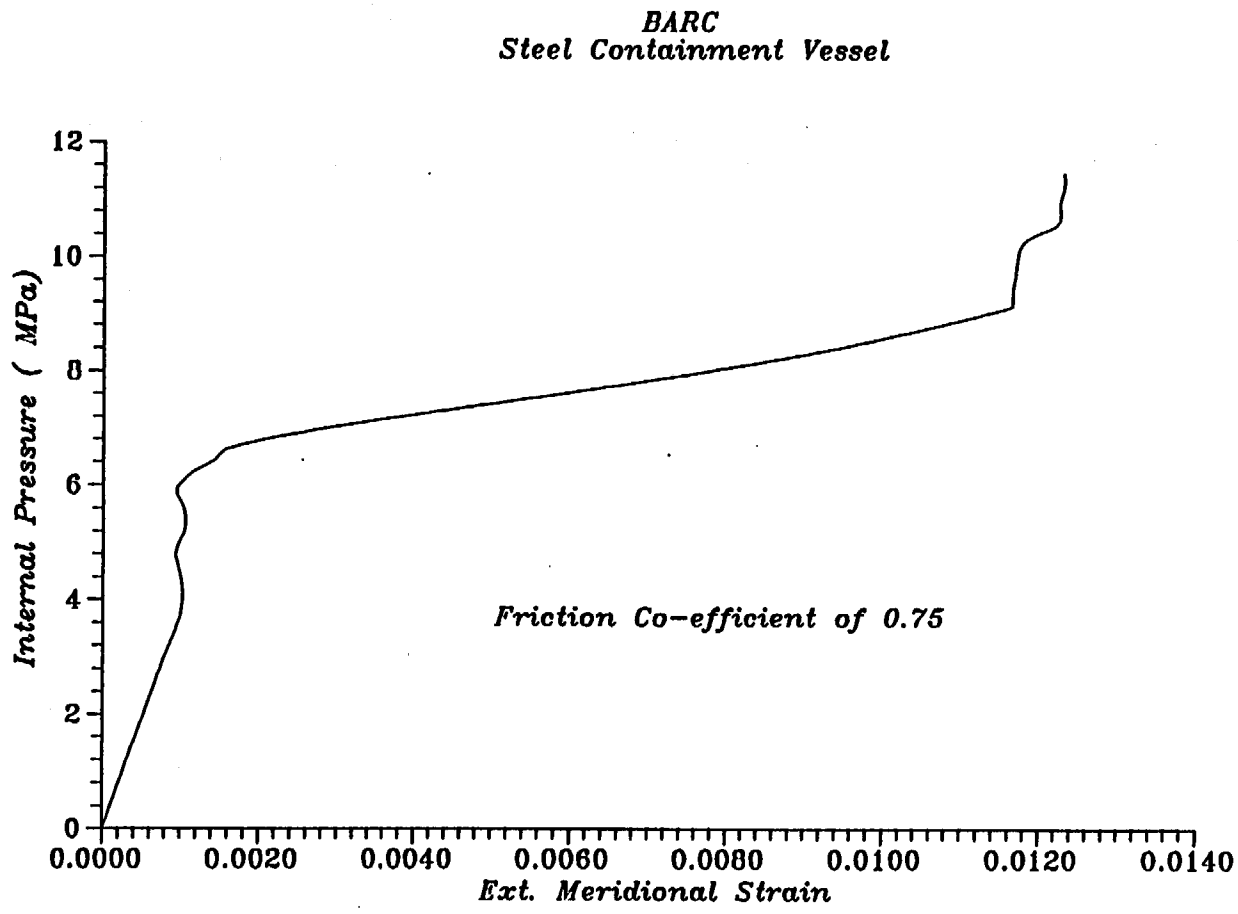

Fig.No.38 Plot of Load v/s. Strain at ID No.19

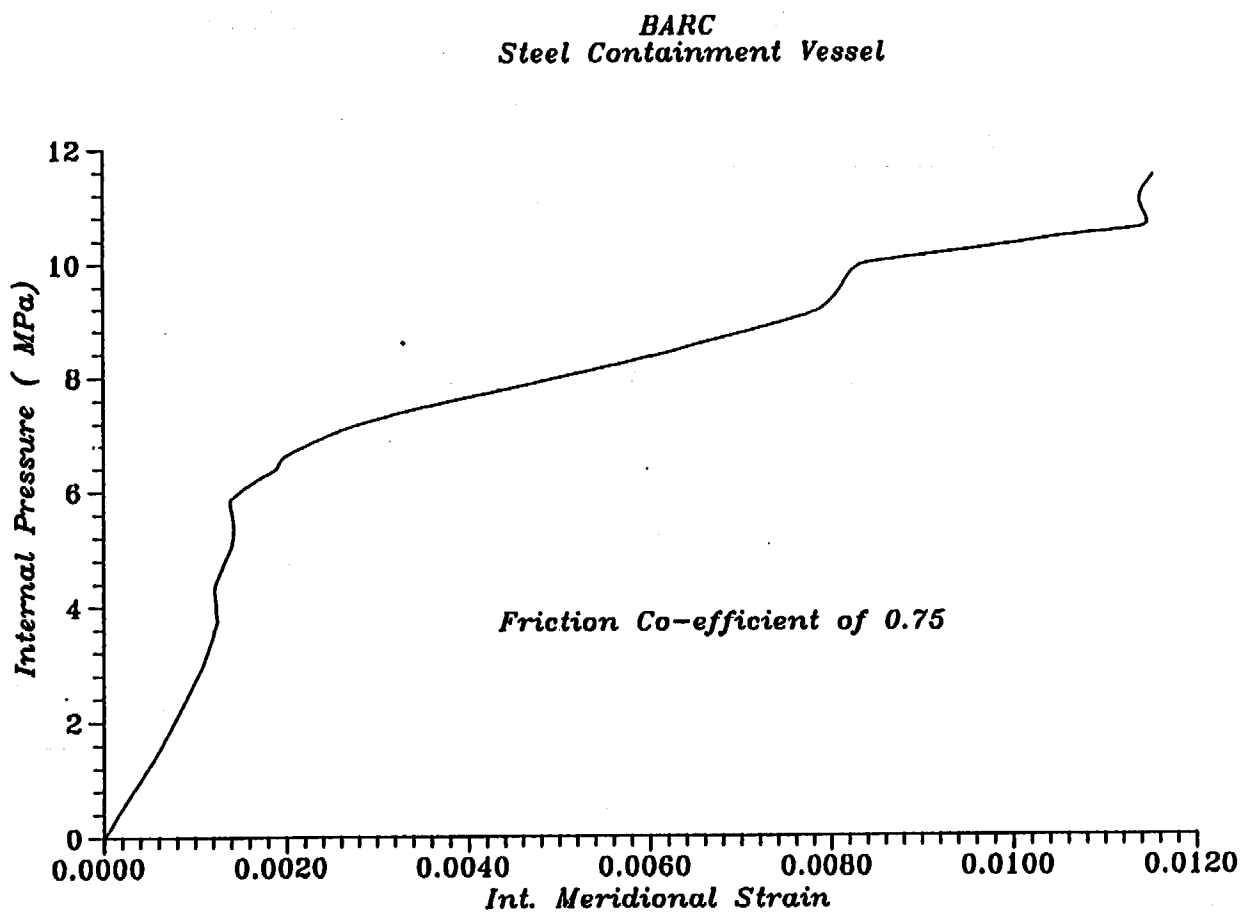

Fig.No.39 Plot of Load v/s. Strain at ID No.20

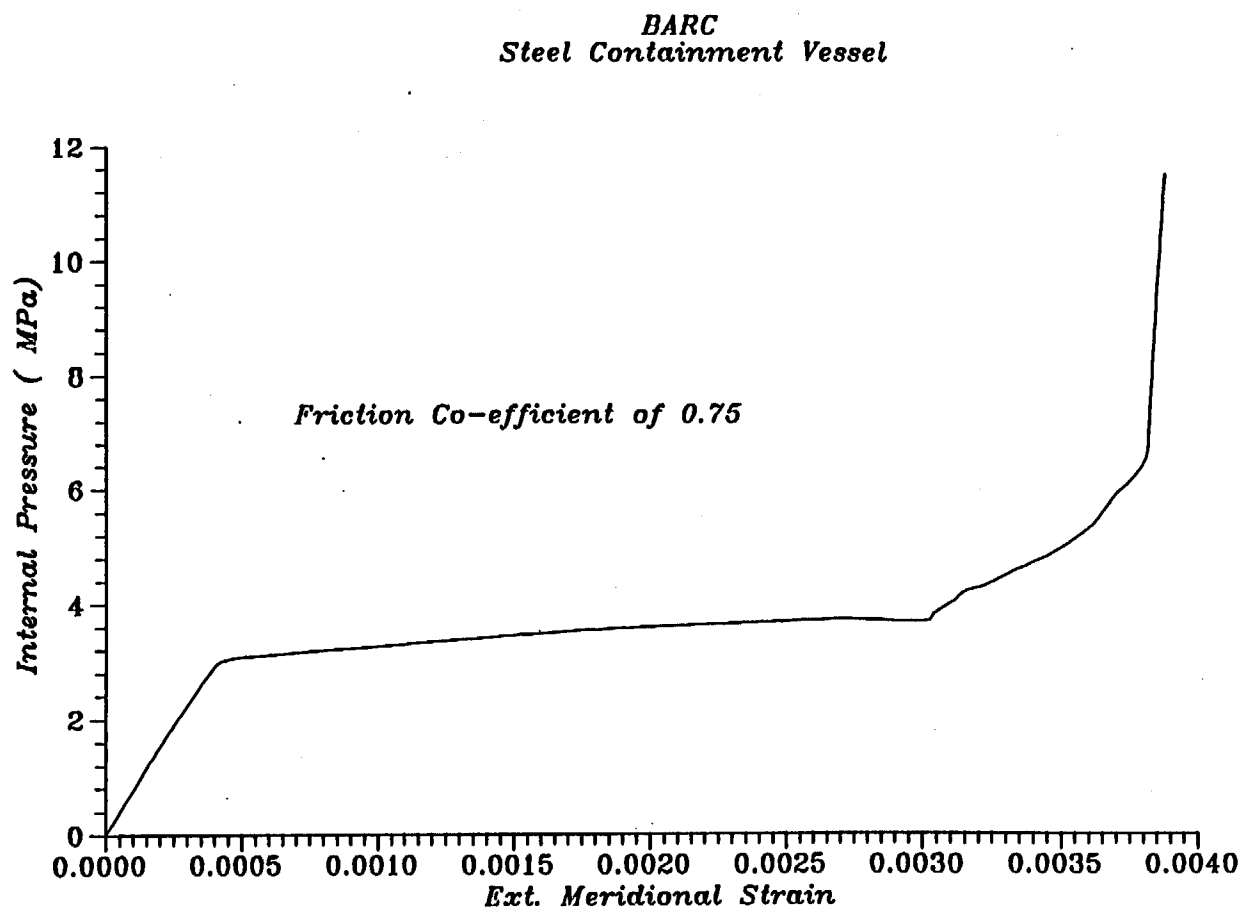

Fig.No.40 Plot of Load v/s. Strain at ID No.21

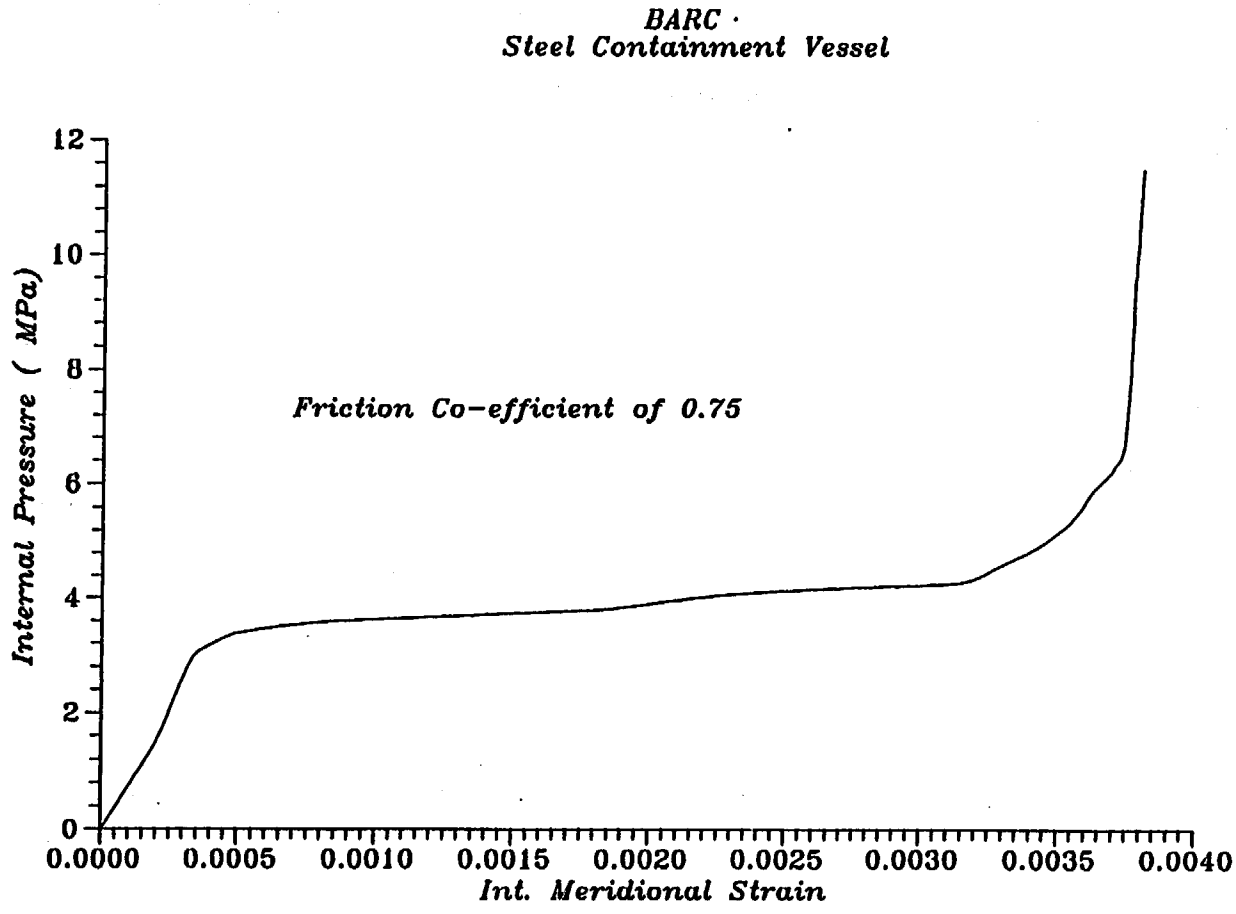

Fig.No41 Plot of Load v/s. Strain at ID No.22

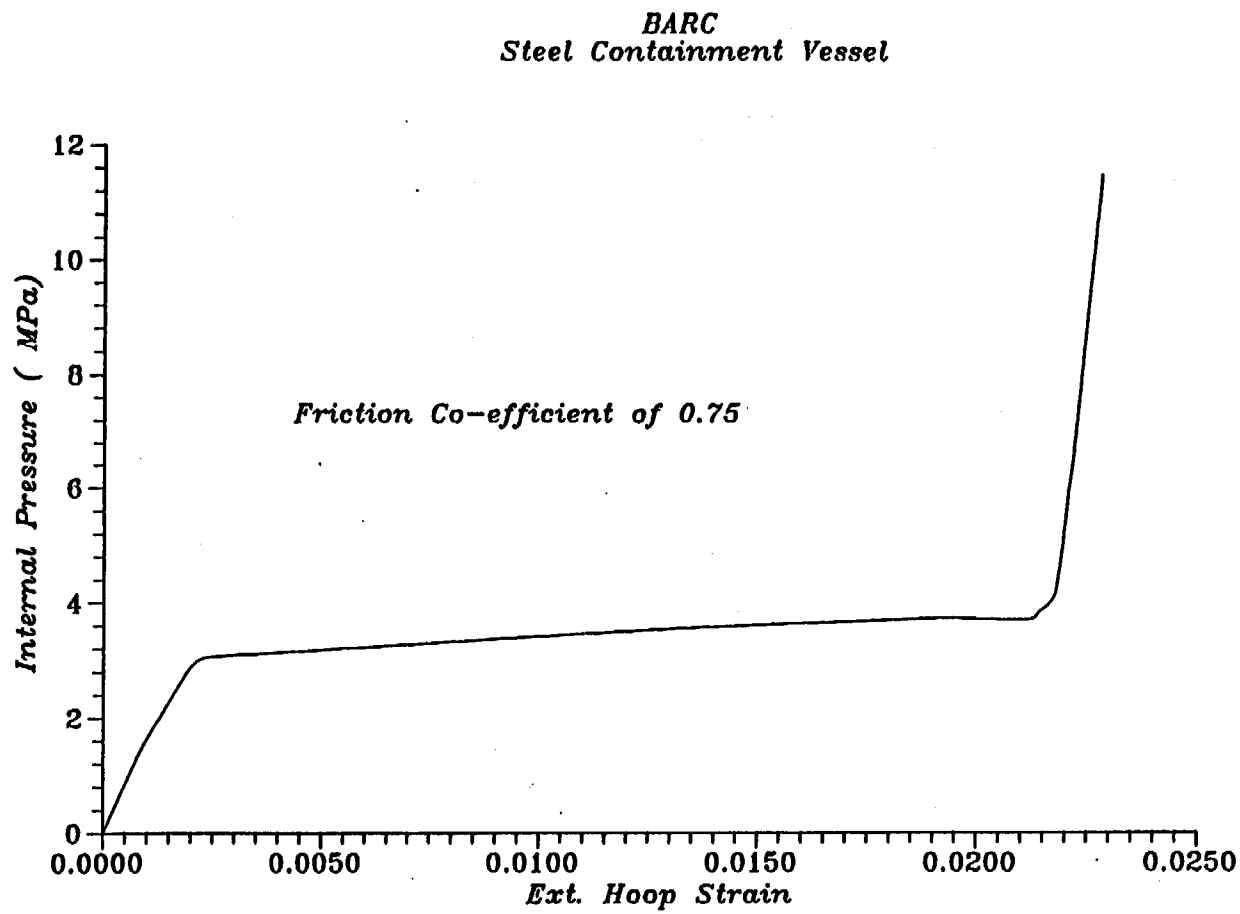

Fig.No.42 Plot of Load v/s. Strain at ID No.23

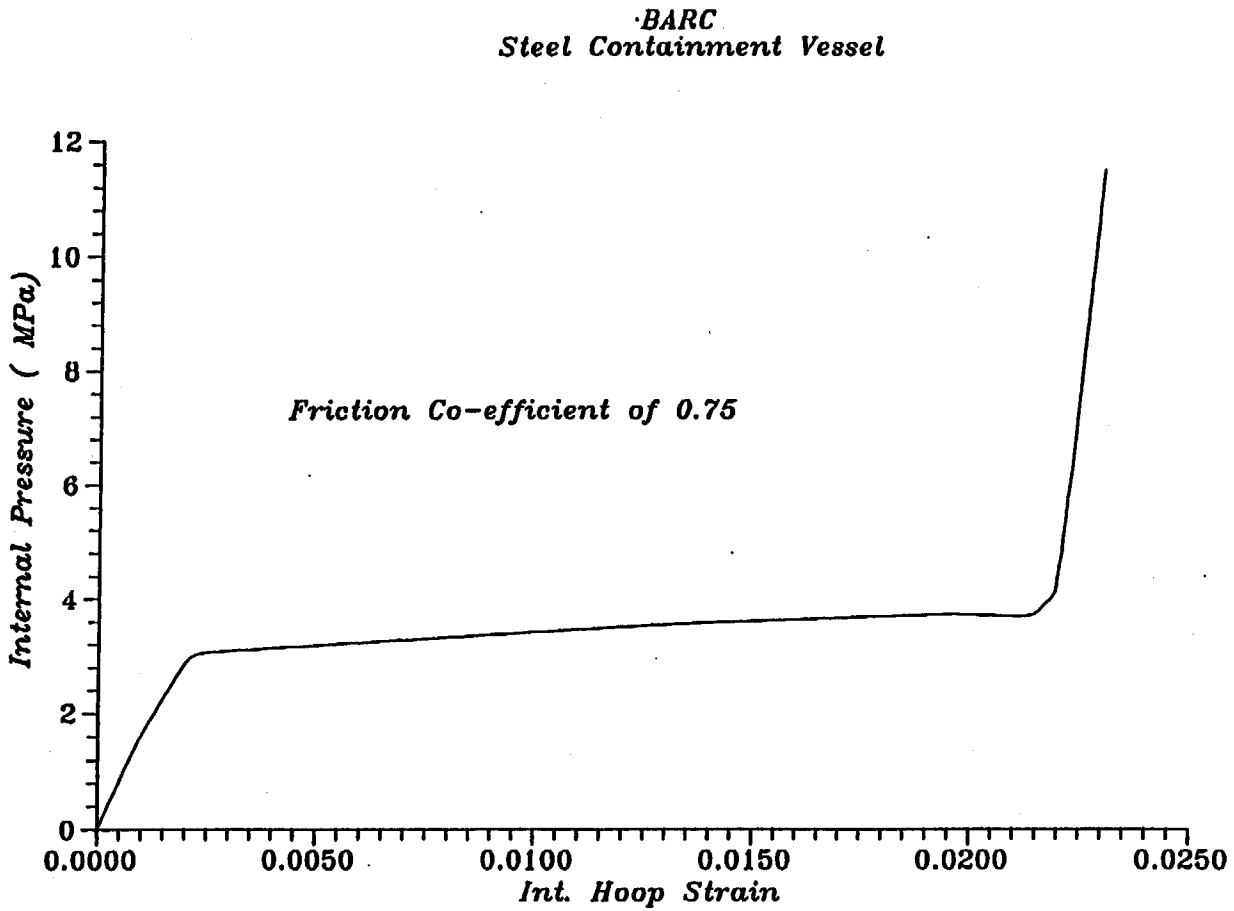

Fig.No.43 Plot of Load v/s. Strain at ID No.24

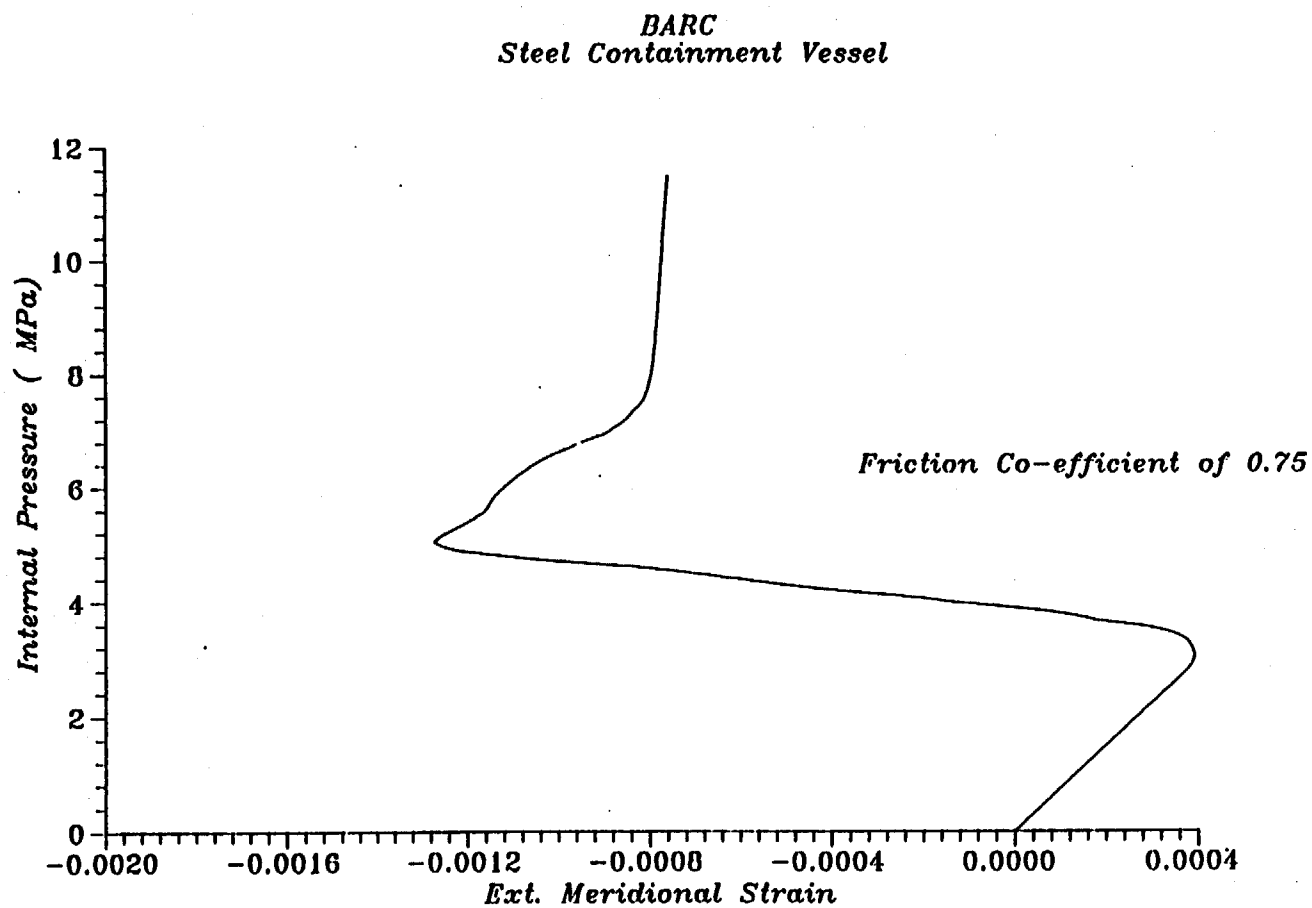

Fig.No.44 Plot of Load v/s. Strain at ID No.25

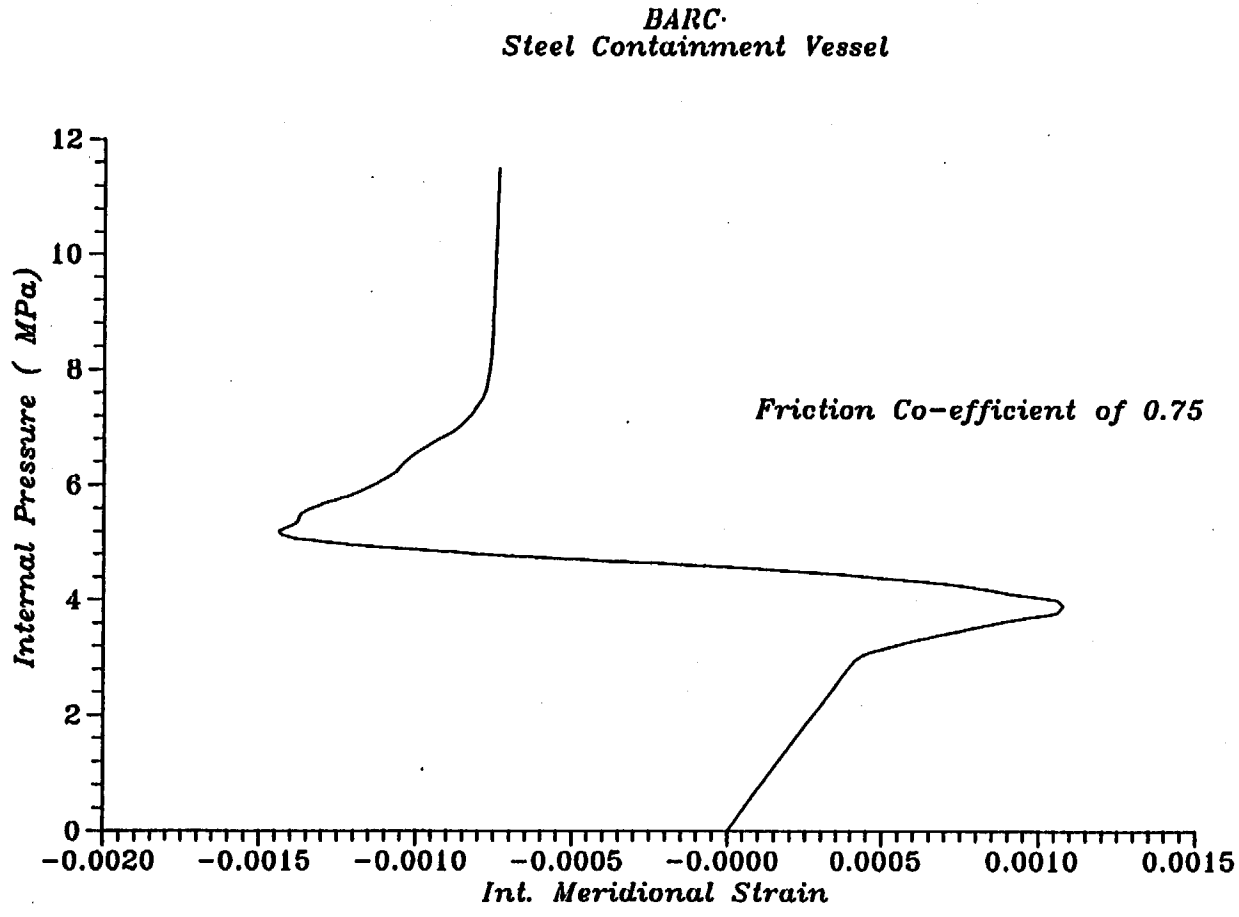

Fig.No45 Plot of Load v/s. Strain at ID No.26

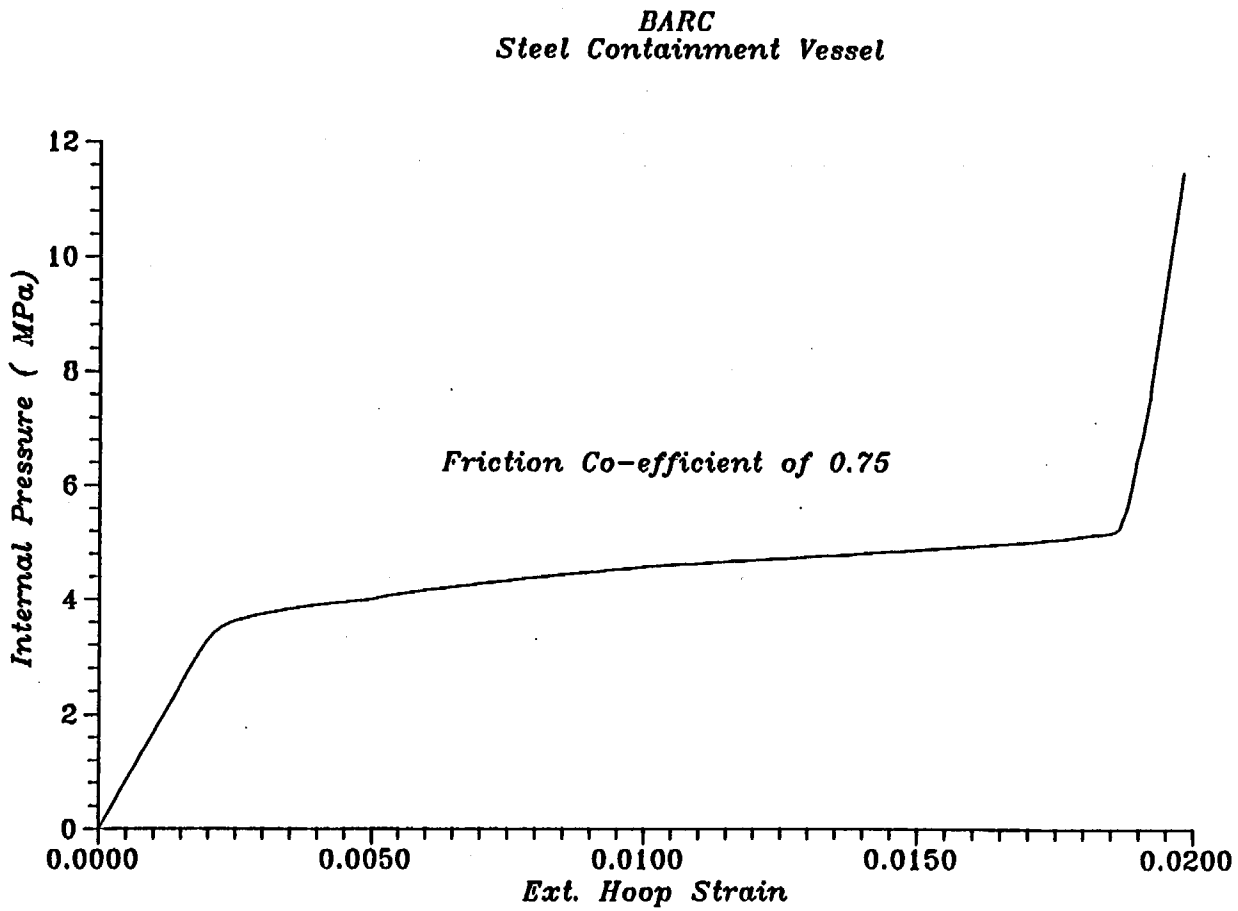

Fig.No.46 Plot of Load v/s. Strain at ID No.27

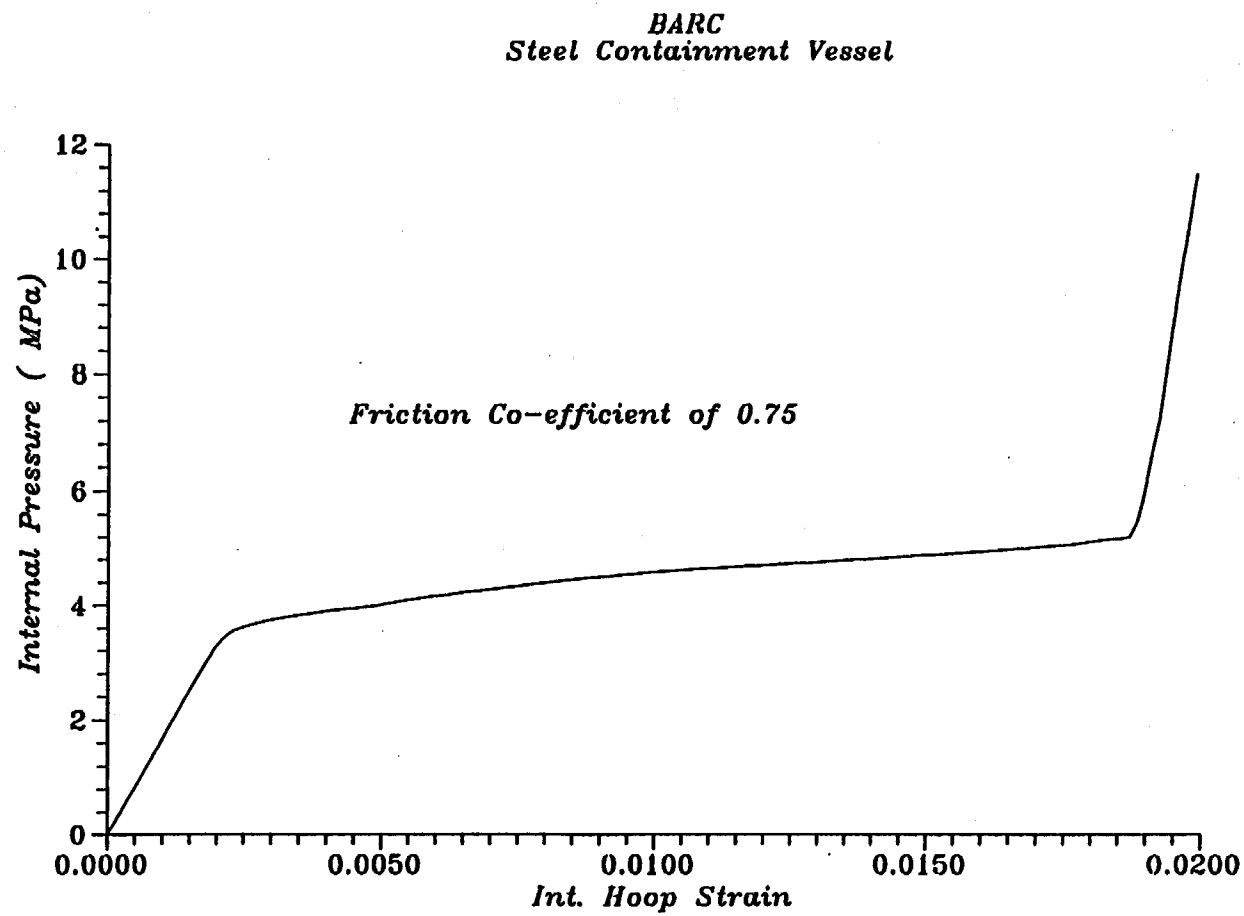

Fig.No47 Plot of Load v/s. Strain at ID No.28

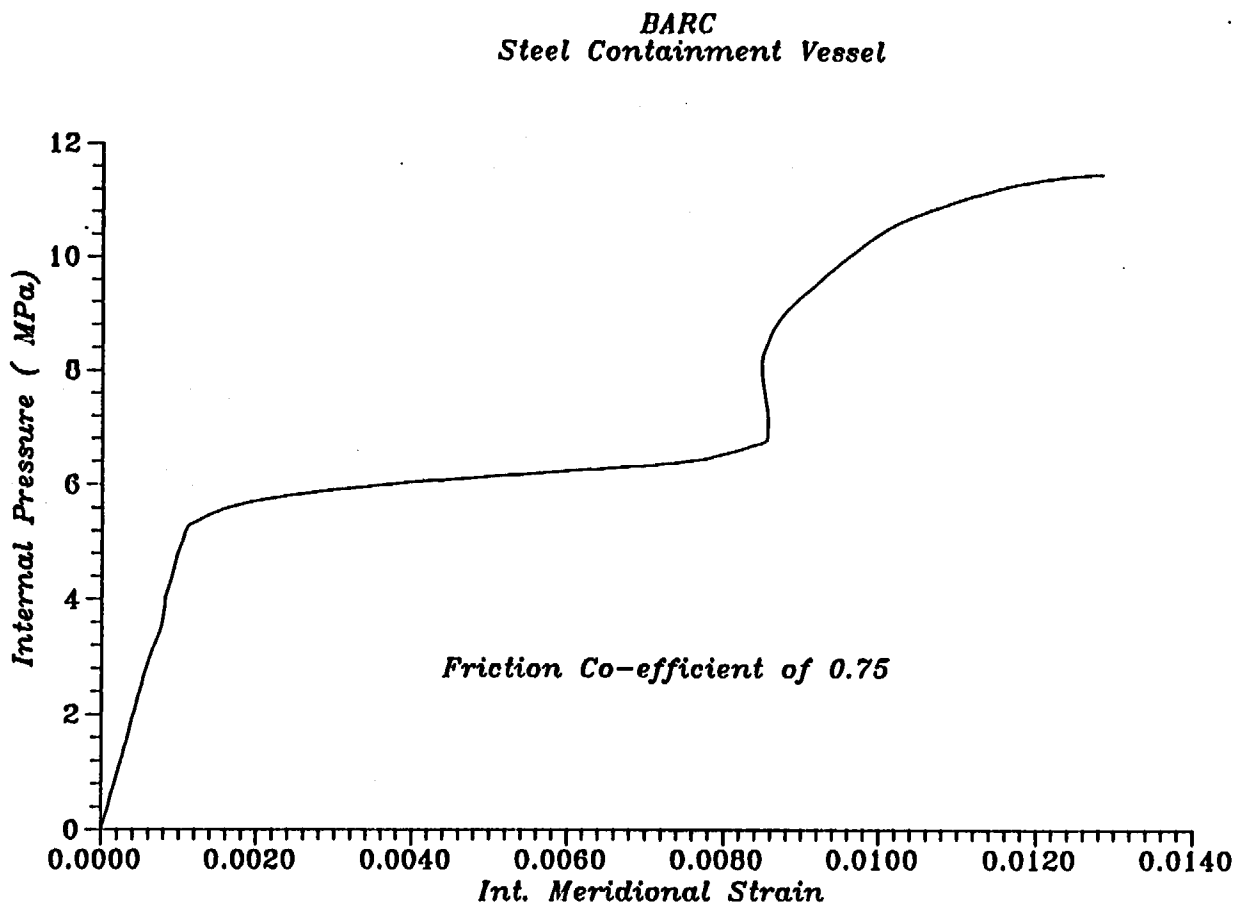

Fig.No48 Plot of Load v/s. Strain at ID No.29

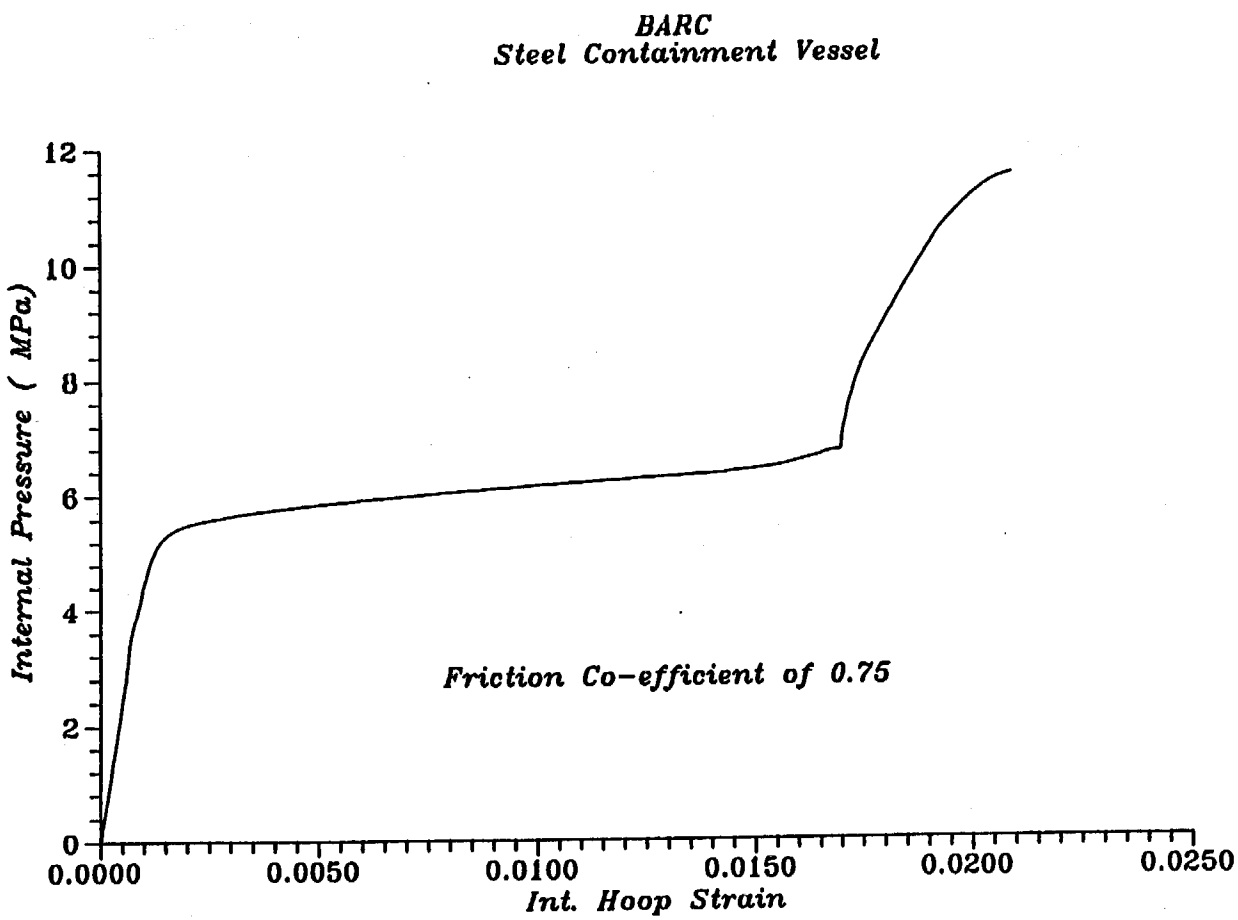

Fig.No49 Plot of Load v/s. Strain at ID No.30

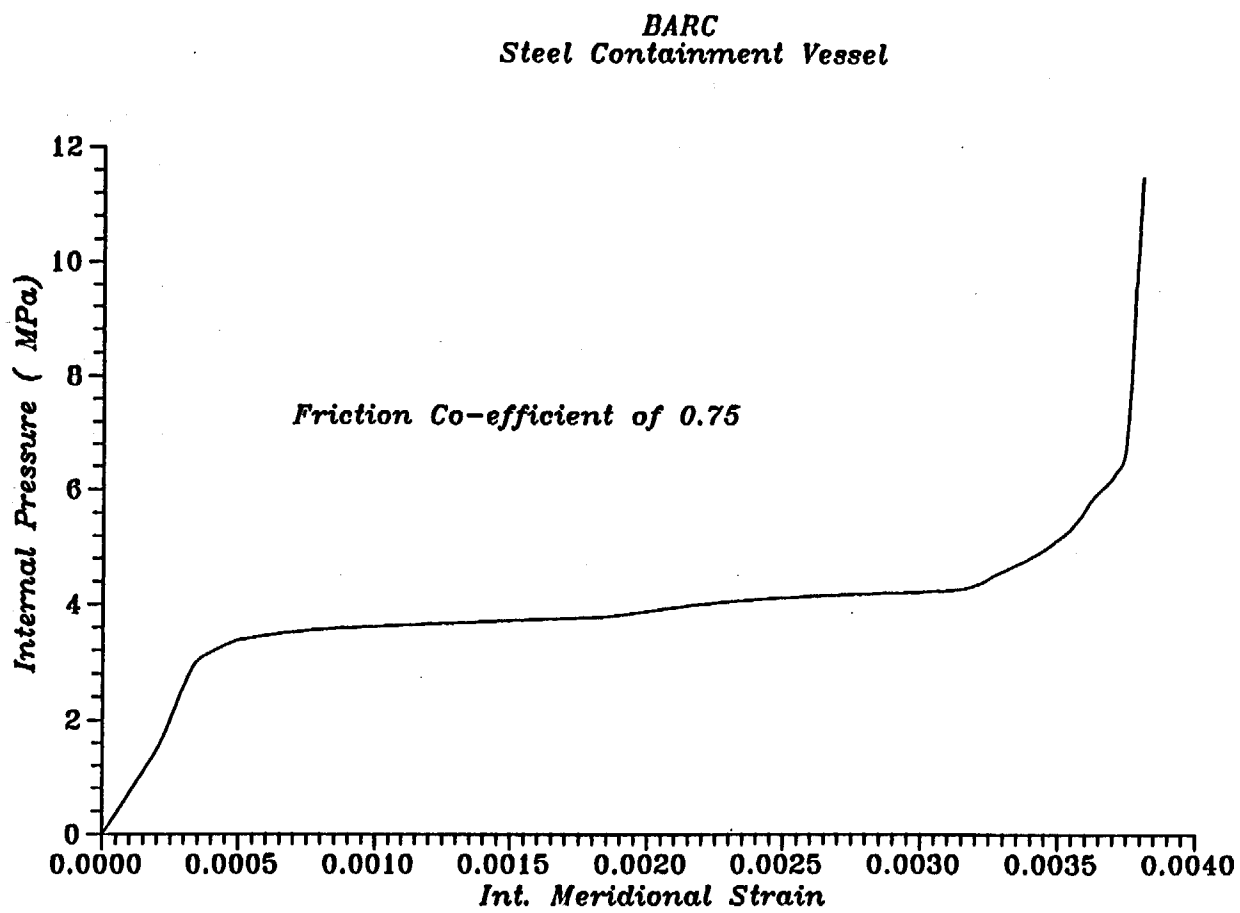

Fig.No50 Plot of Load v/s. Strain at ID No.31

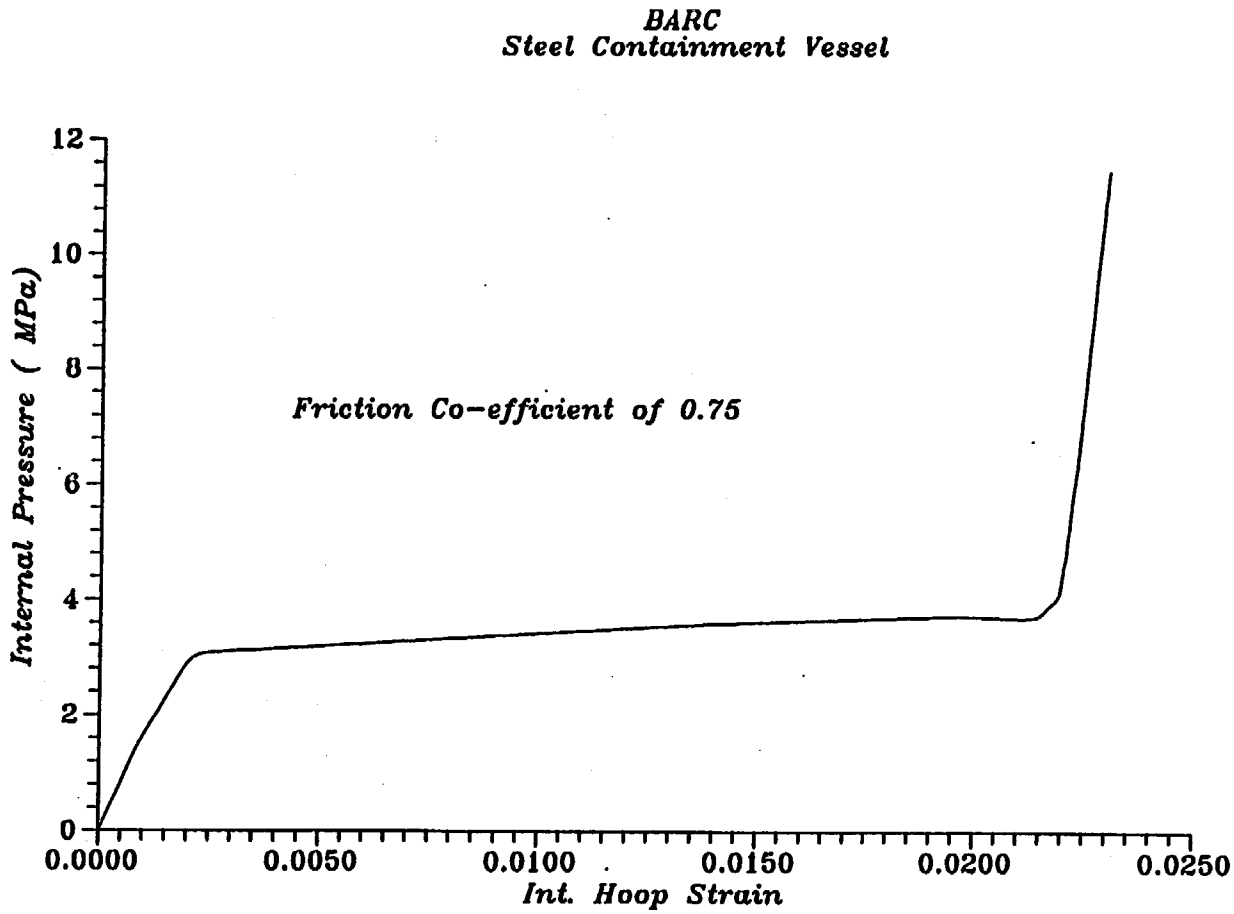

Fig.No51 Plot of Load v/s. Strain at ID No.32

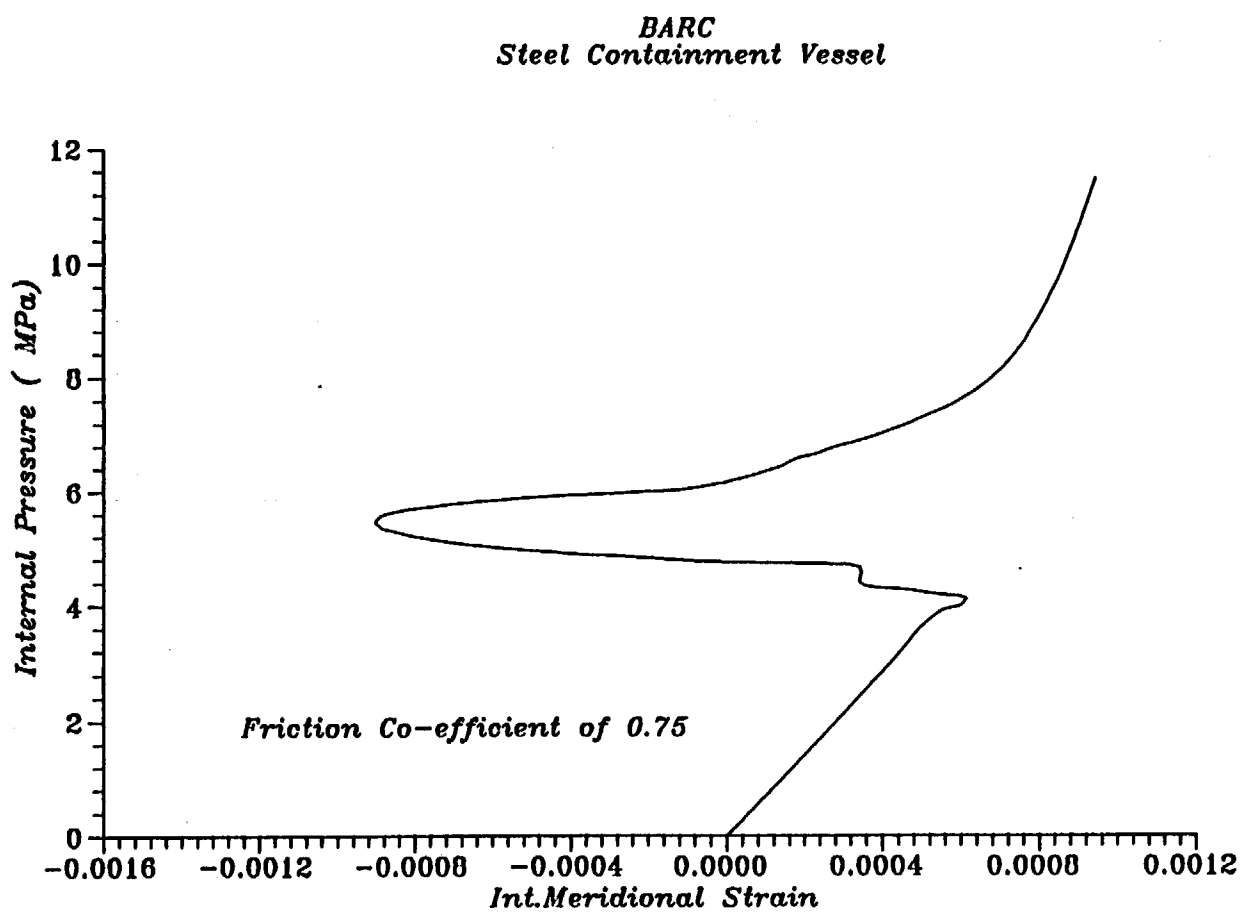

Fig.No.52 Plot of Load v/s. Strain at ID No.33

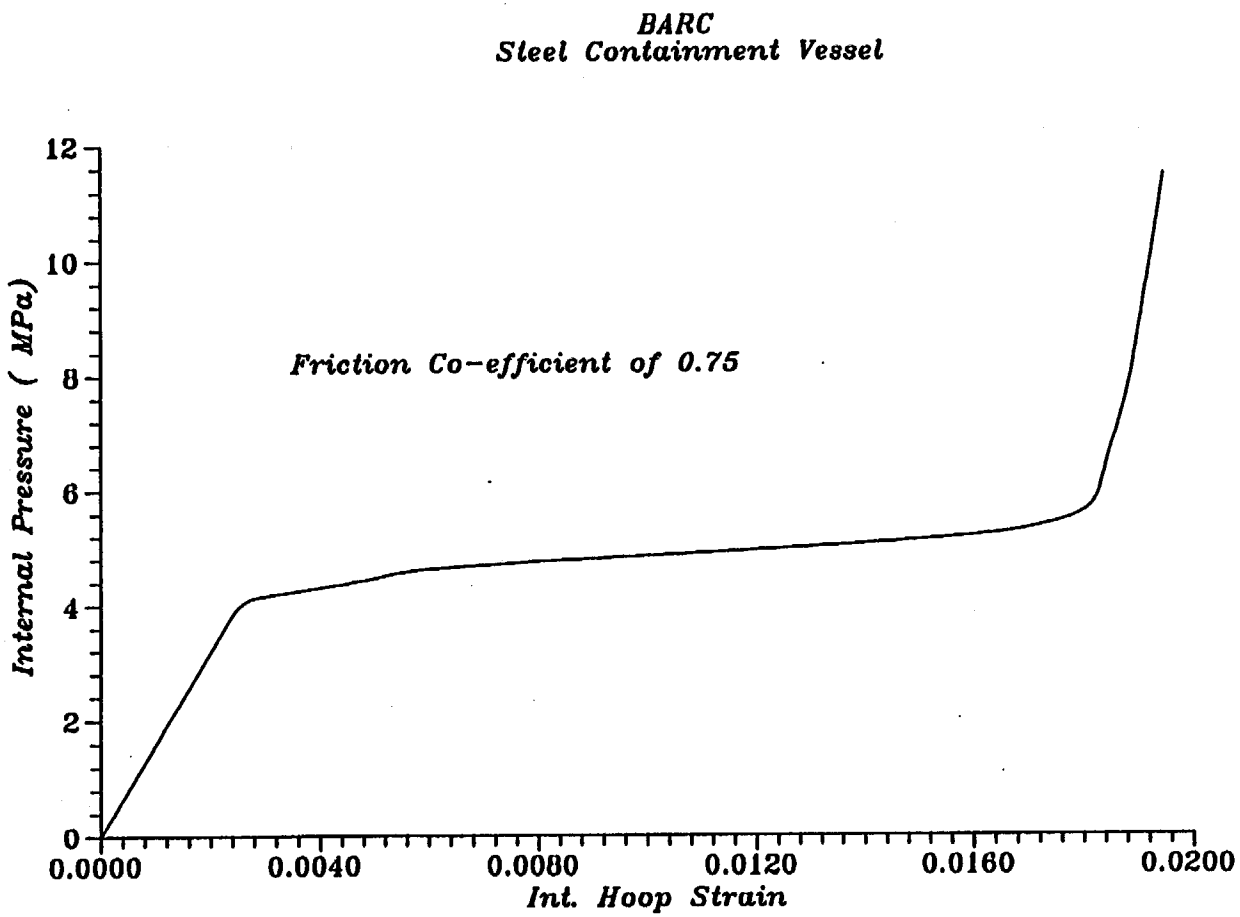

Fig.No53 Plot of Load v/s. Strain at ID No.34

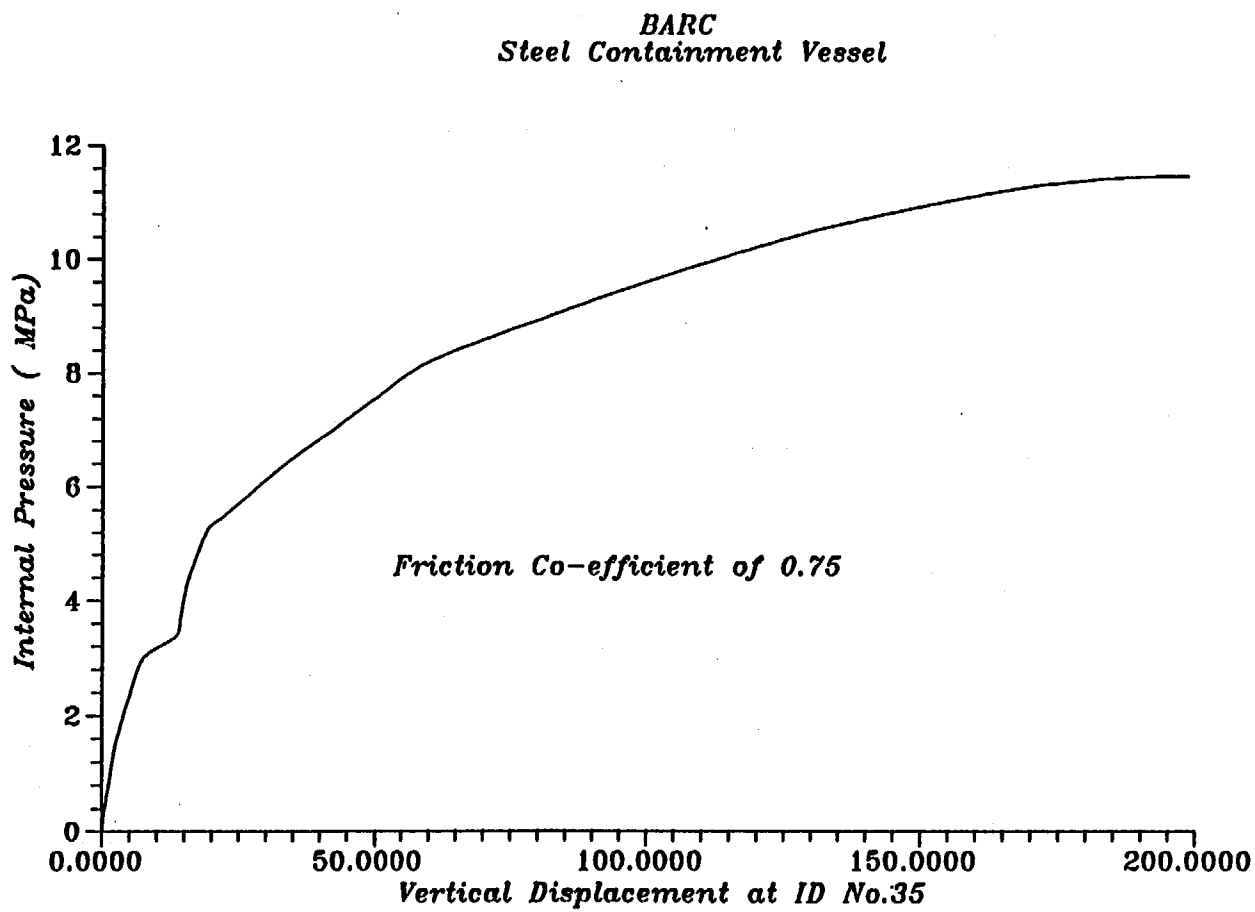

Fig.No54 Plot of Load v/s. Displacement at ID No.35

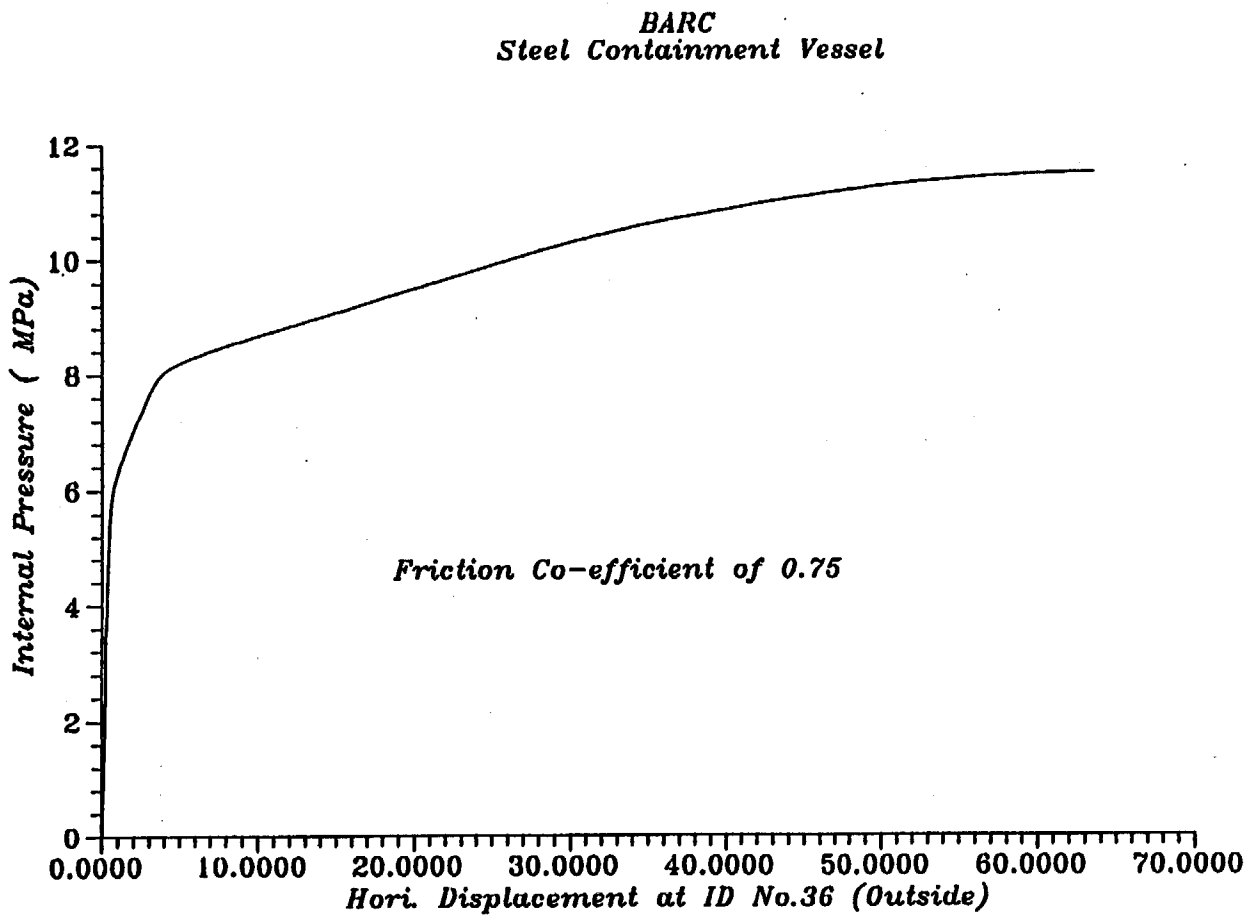

Fig.No55 Plot of Load v/s. Displacement at ID No.36

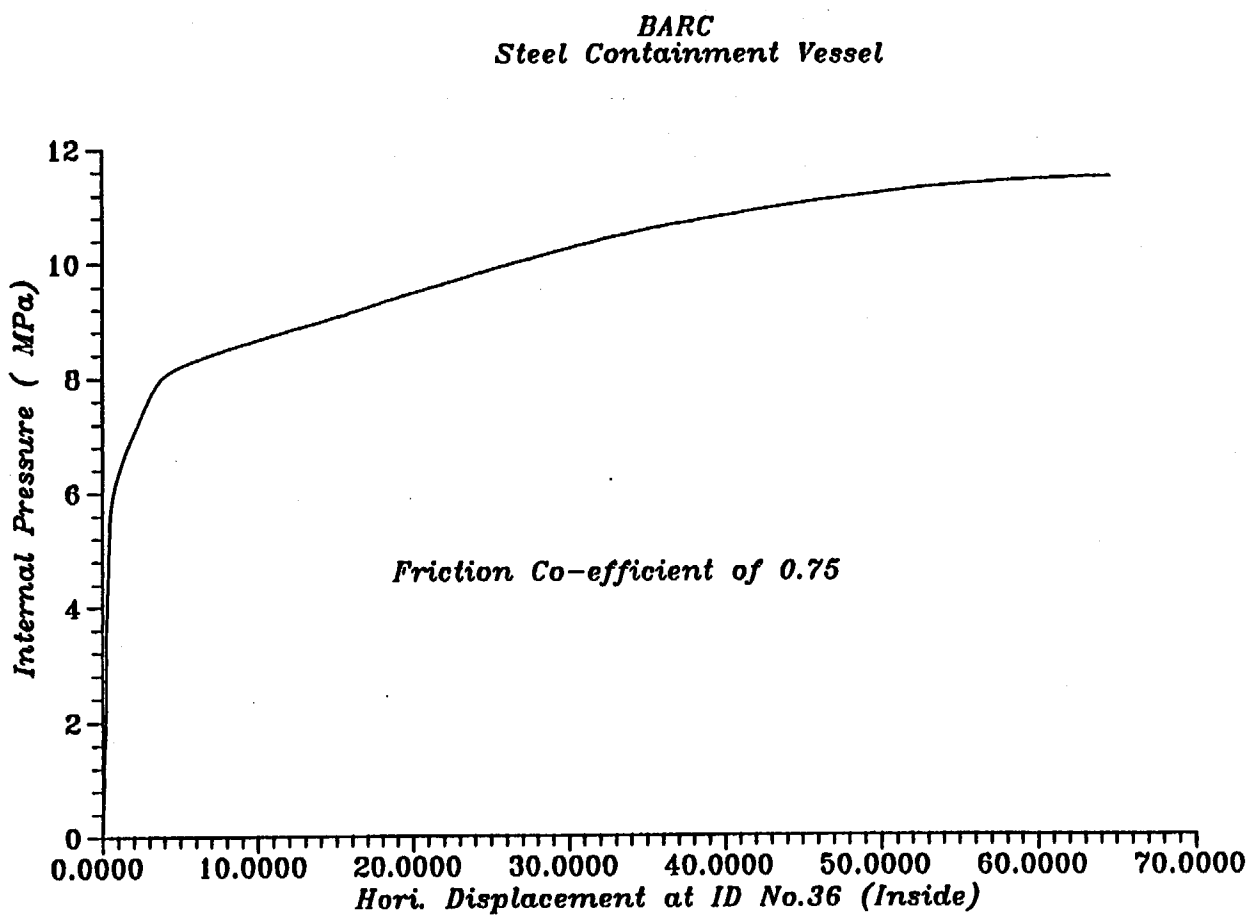

Fig.No56 Plot of Load v/s. Displacement at ID No.36

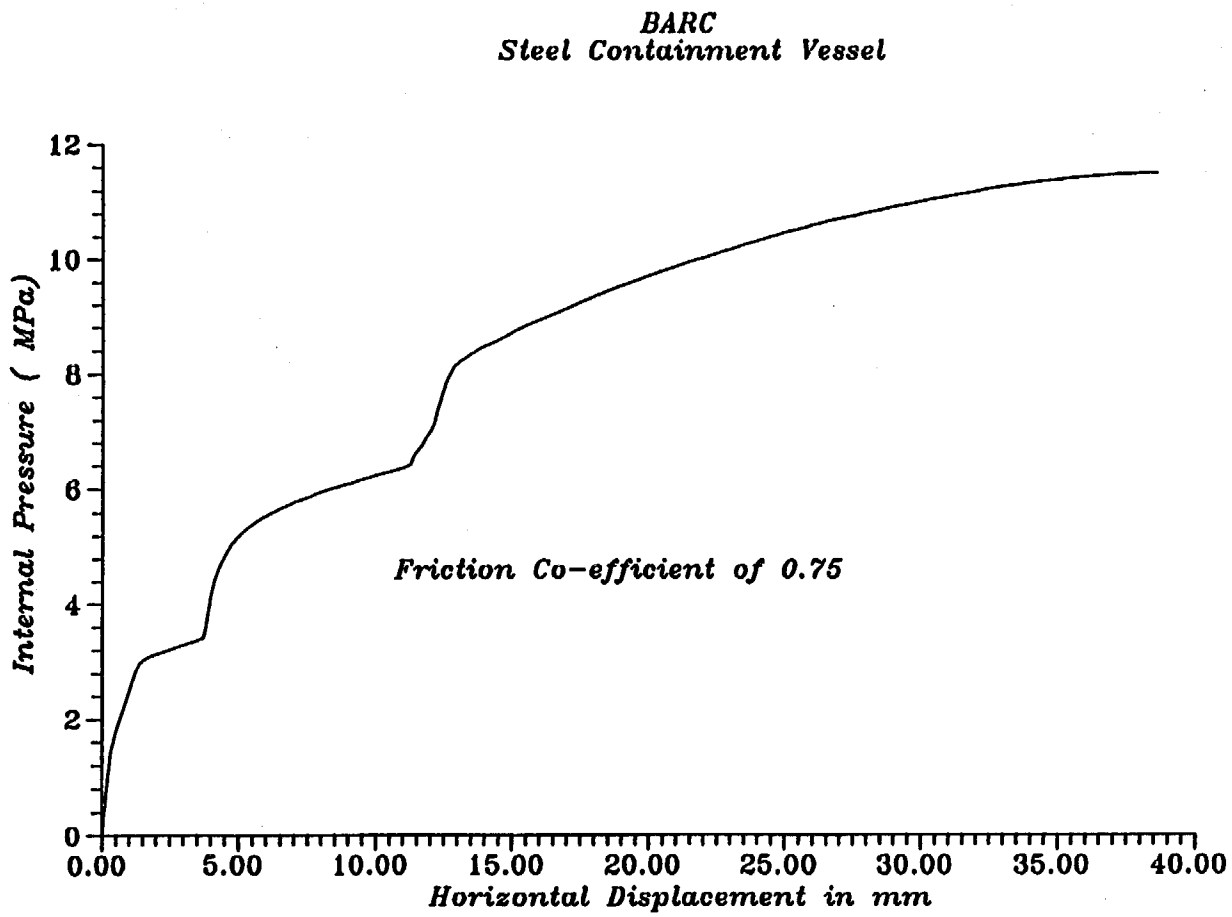

Fig.No57 Plot of Load v/s. Displacement at ID No.37

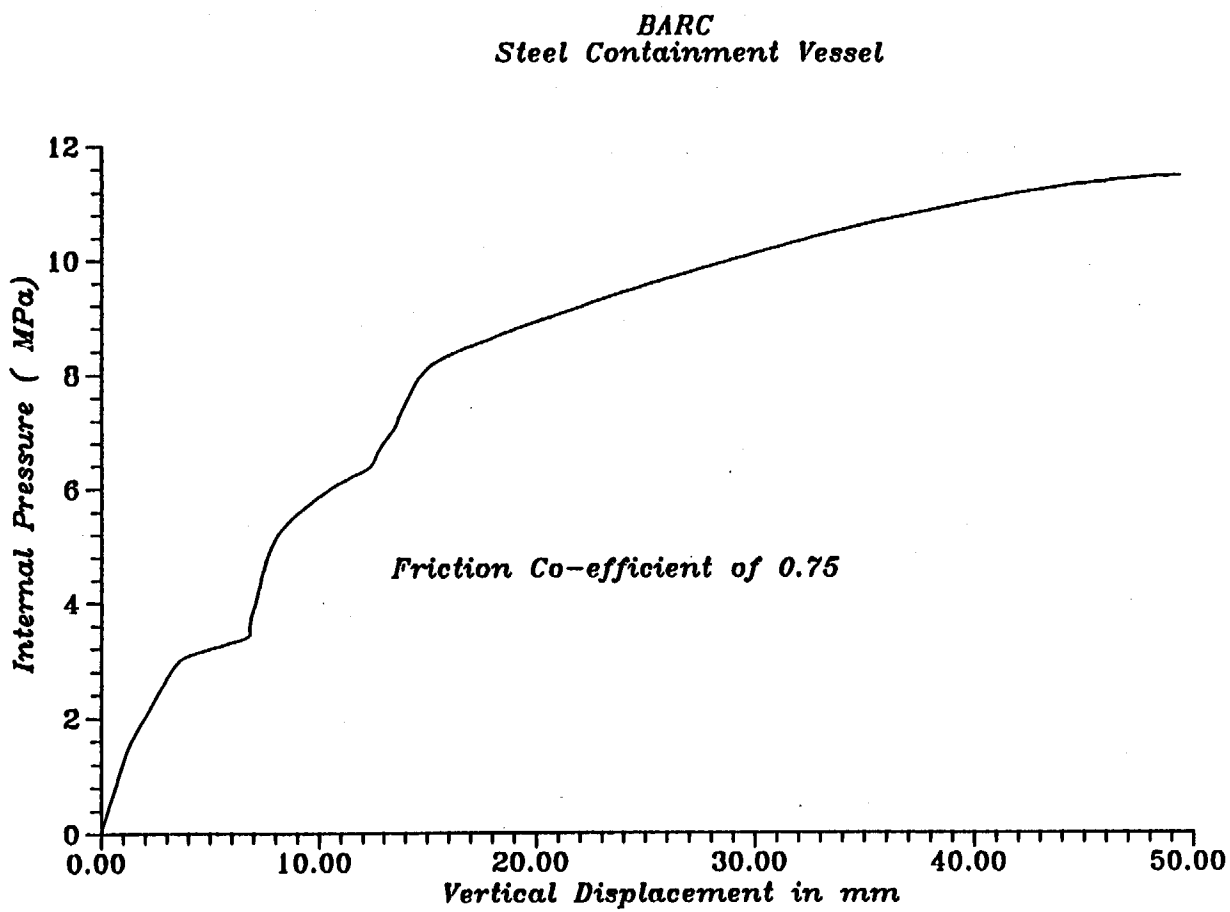

Fig.No.58 Plot of Load v/s. Displacement at ID No.38

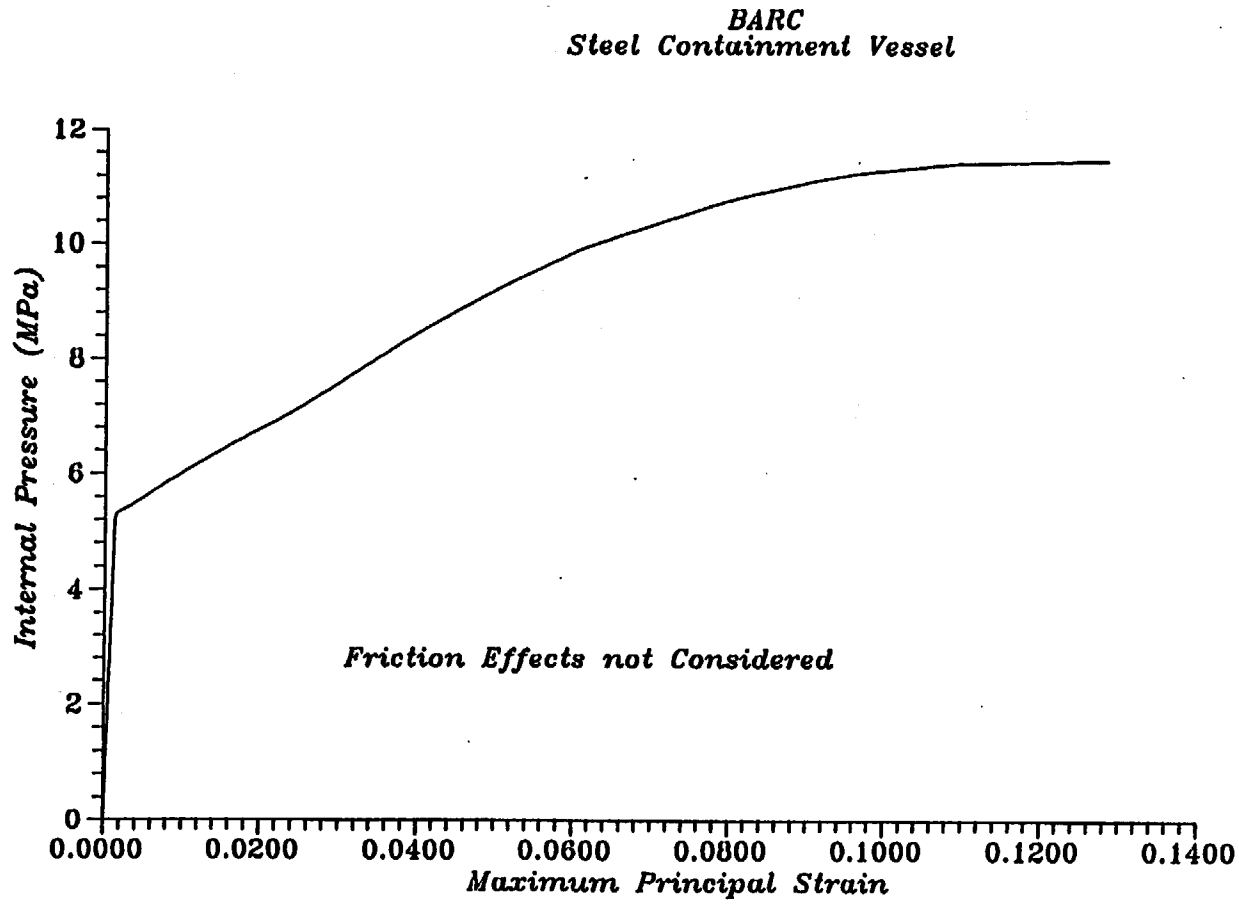

Fig.No.59 Plot of Load v/s. Strain at ID No.7

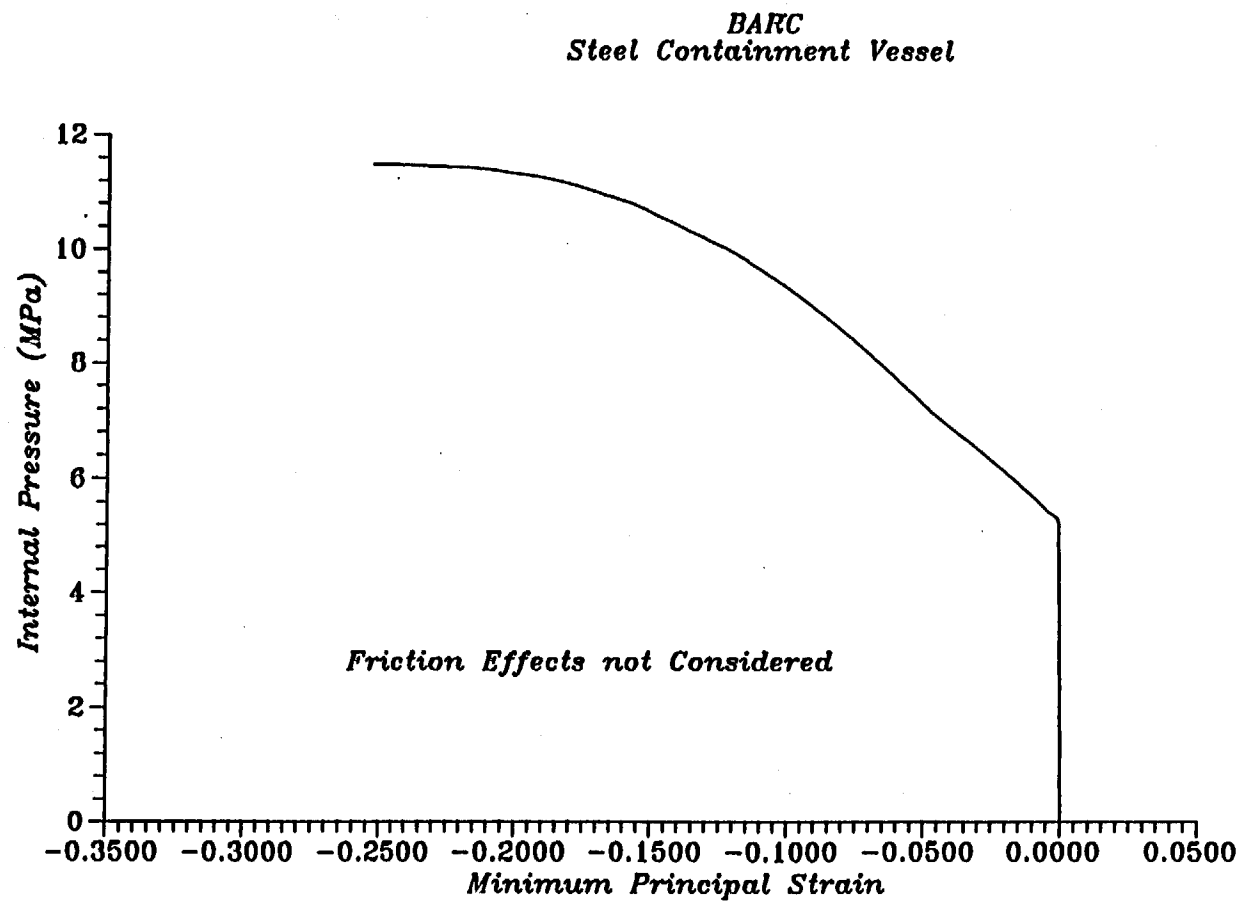

Fig.No.60 Plot of Load v/s. Strain at ID No.7

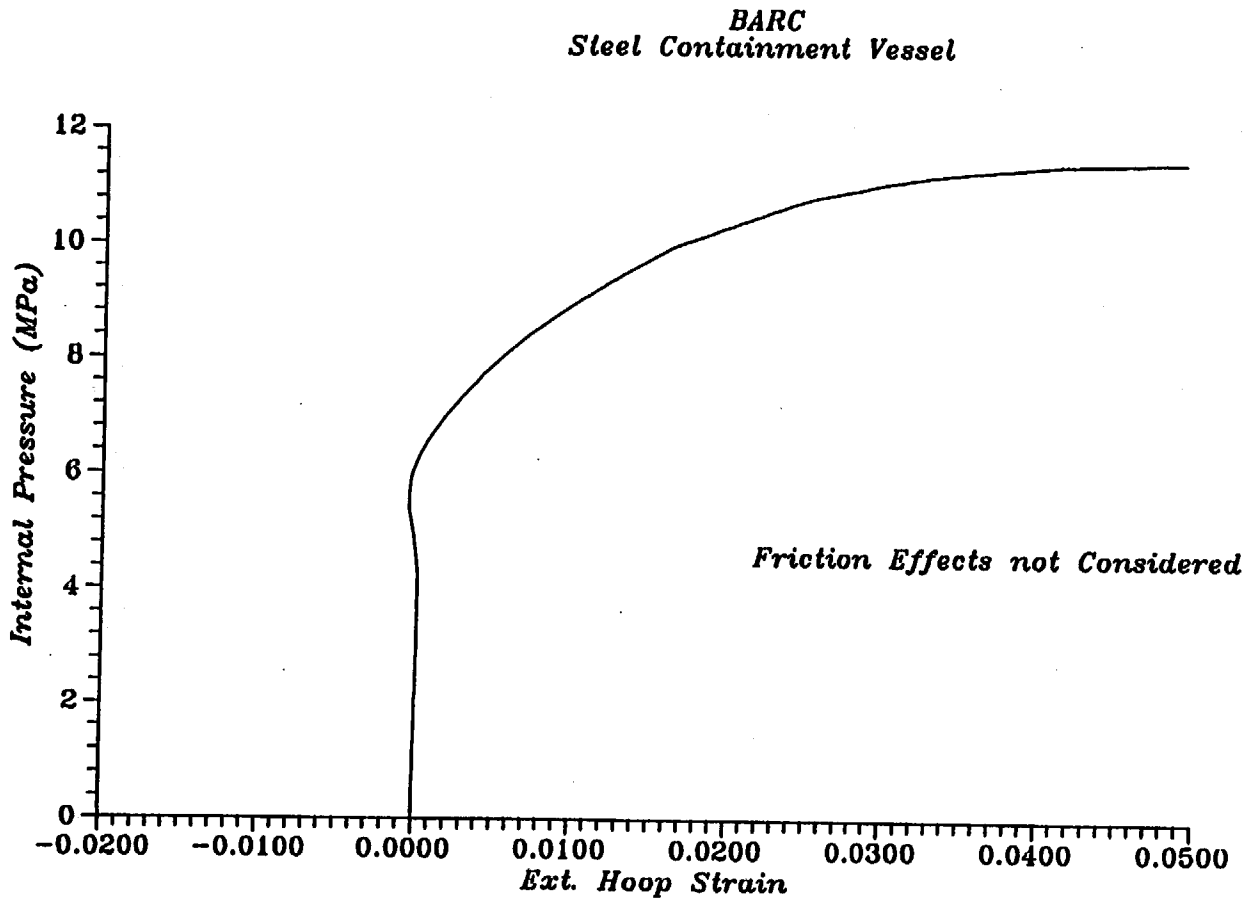

Fig.No.61 Plot of Load v/s. Strain at ID No.8

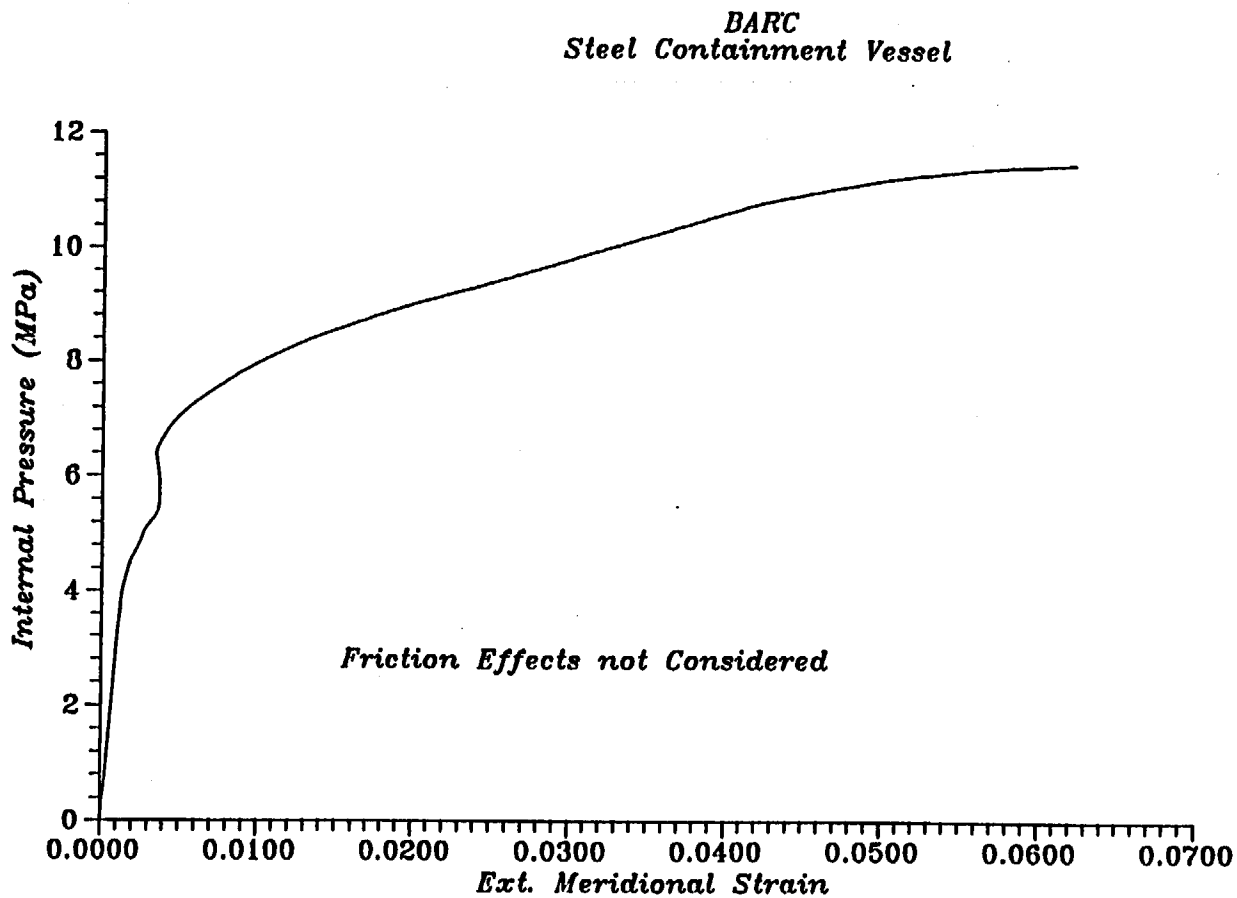

Fig.No.62 Plot of Load v/s. Strain at ID No.9

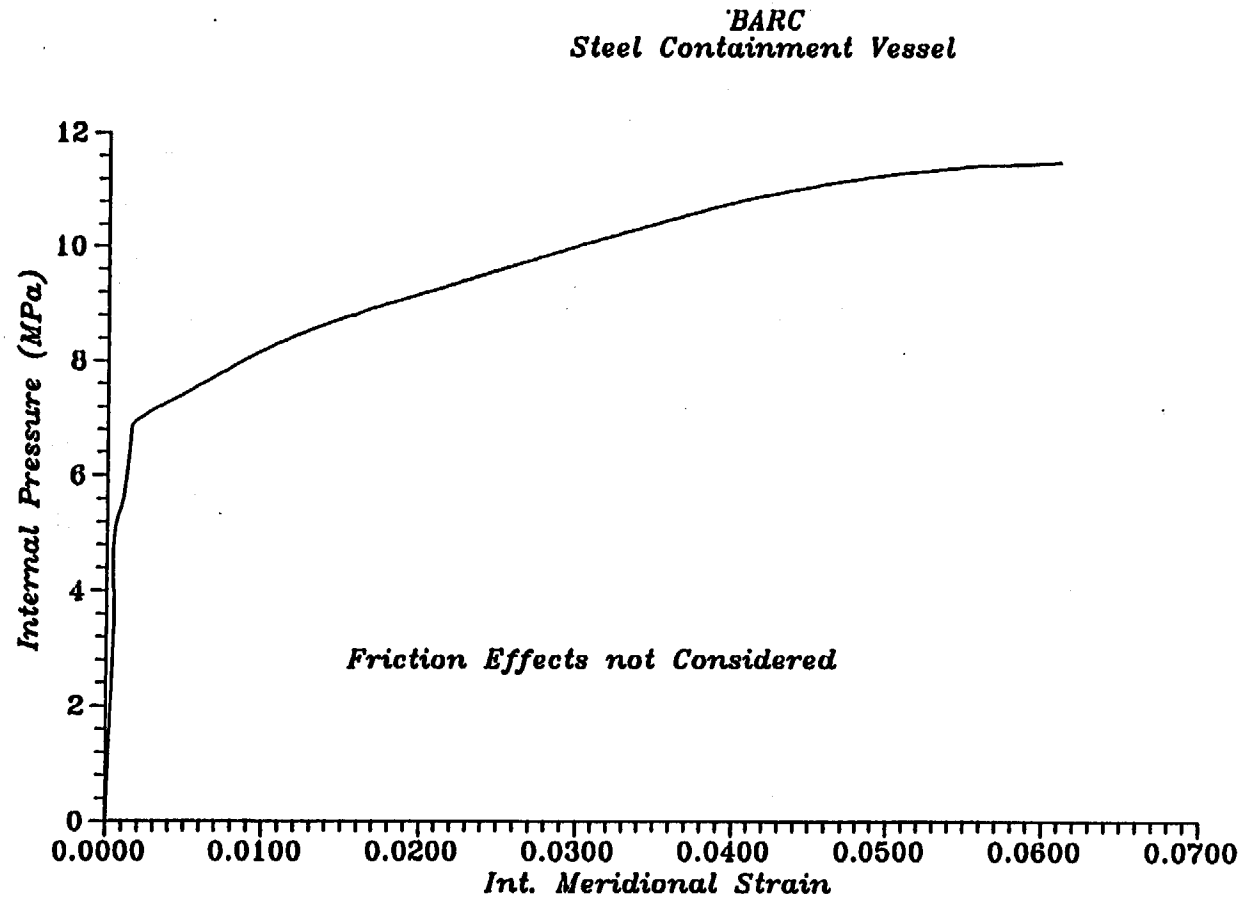

Fig.No.63 Plot of Load v/s. Strain at ID No.10

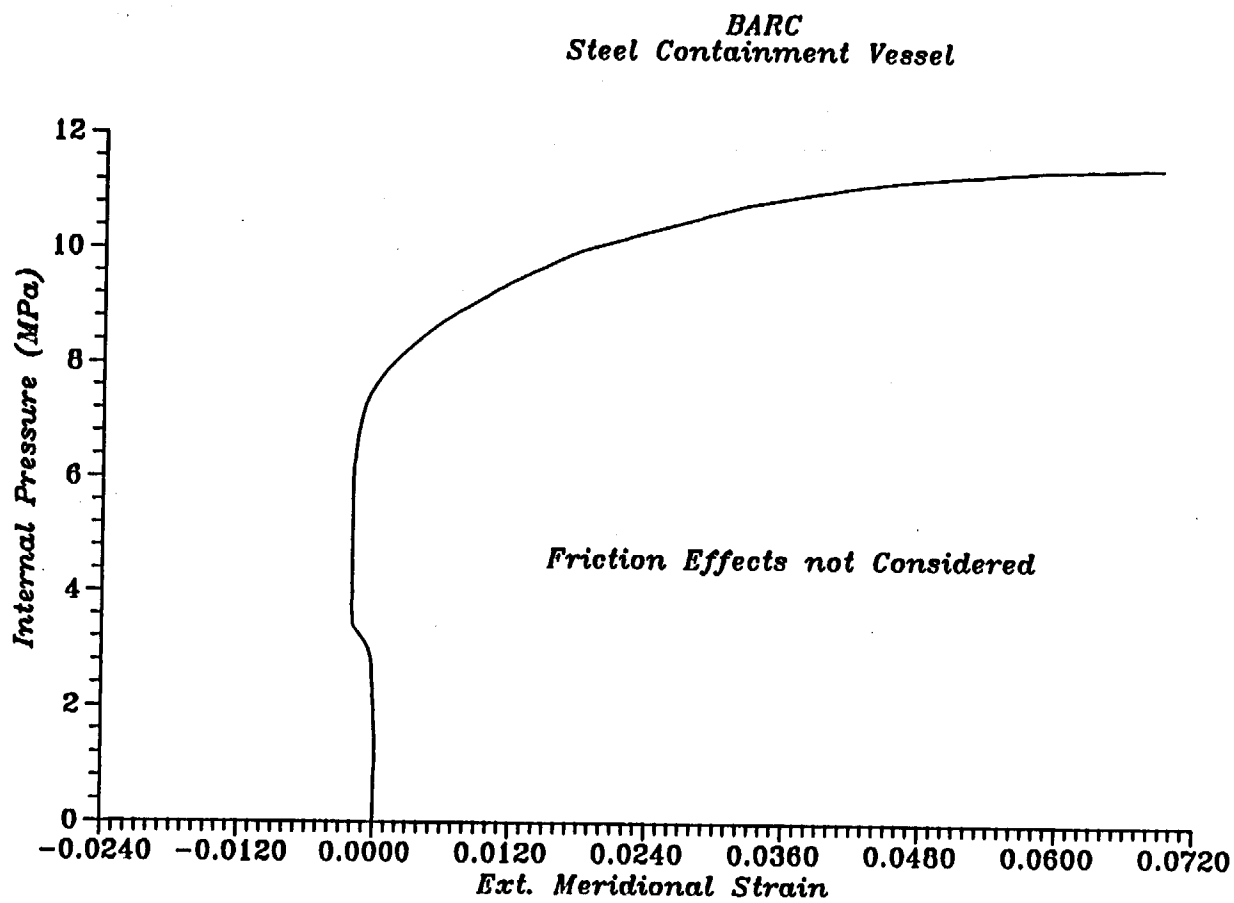

Fig.No.64 Plot of Load v/s. Strain at ID No.11

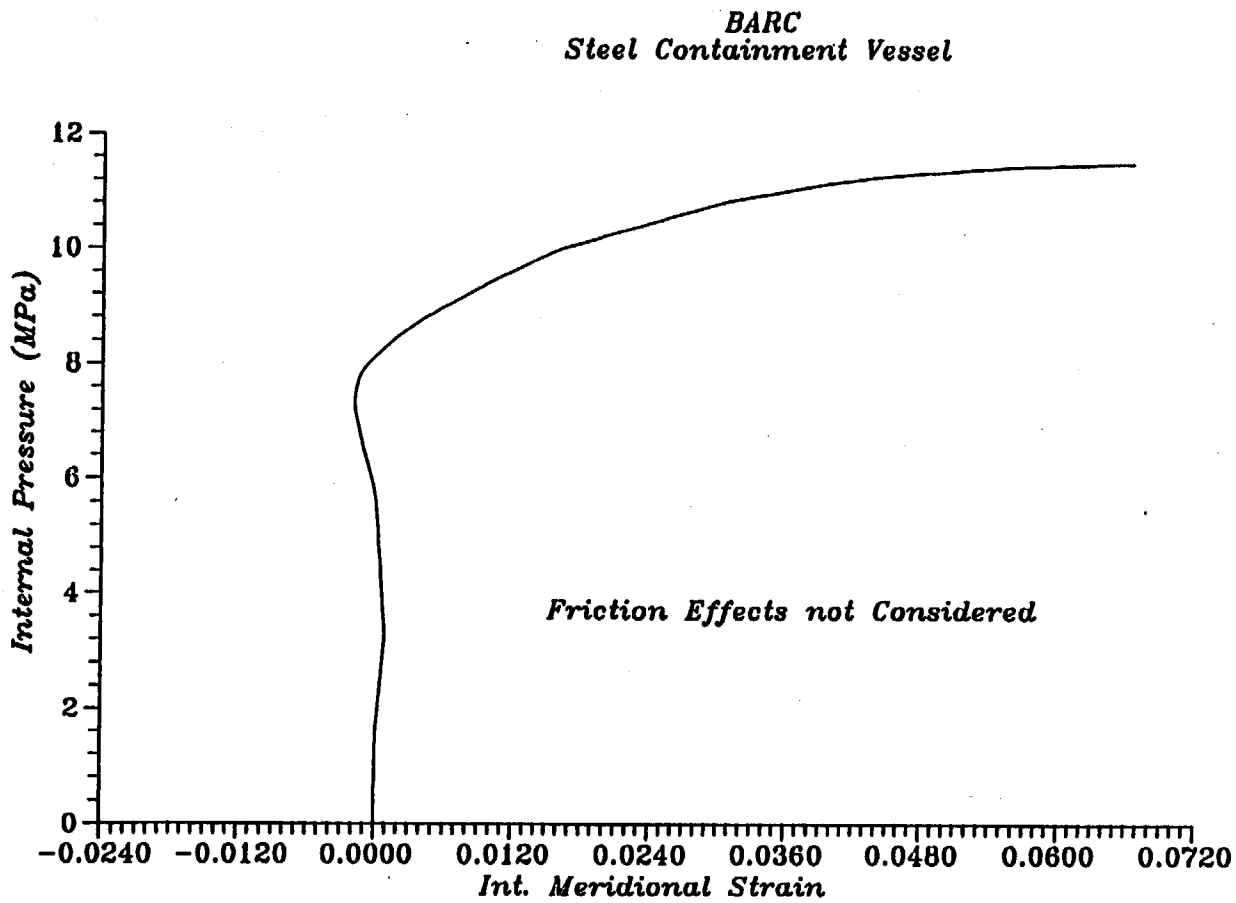

Fig.No.65 Plot of Load v/s. Strain at ID No.12

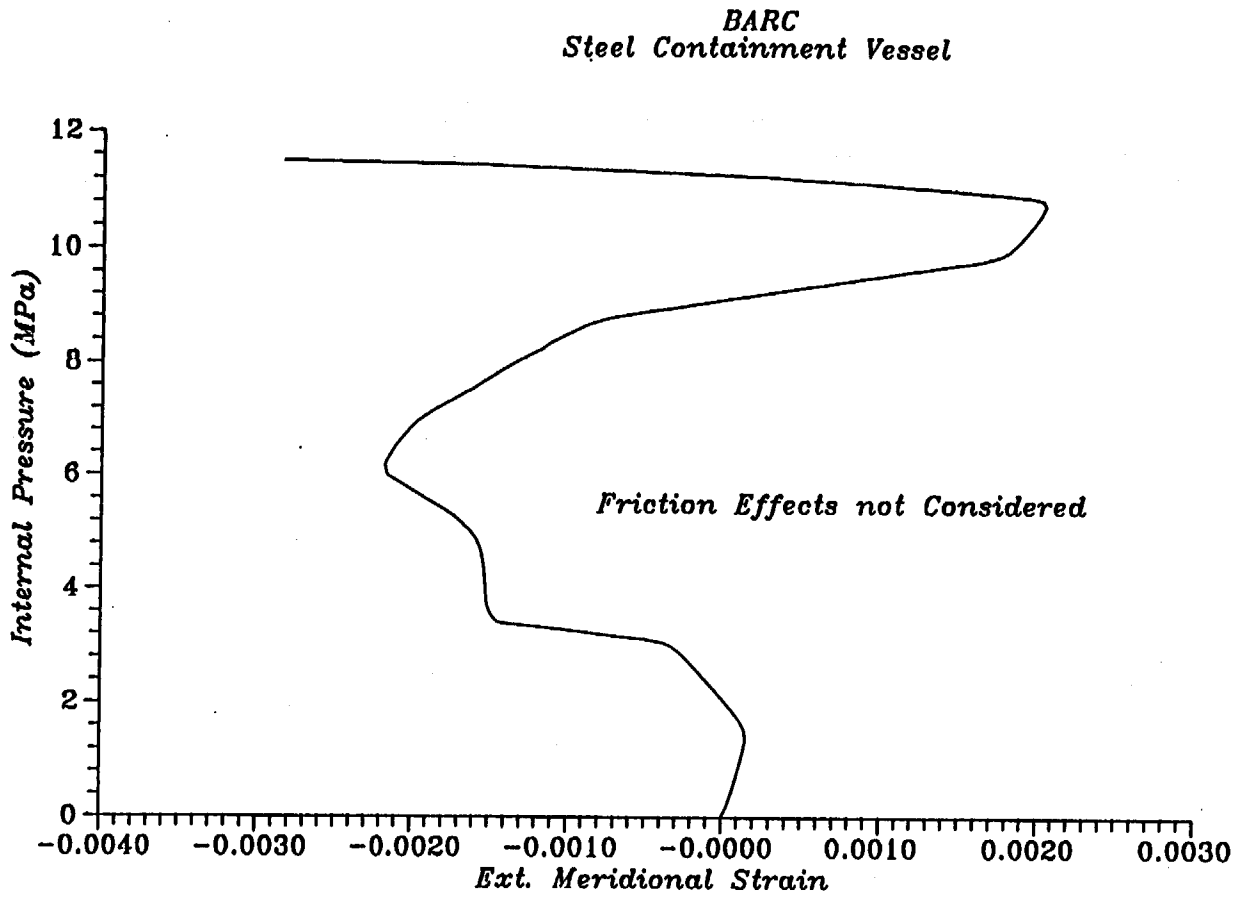

Fig.No.66 Plot of Load v/s. Strain at ID No.13

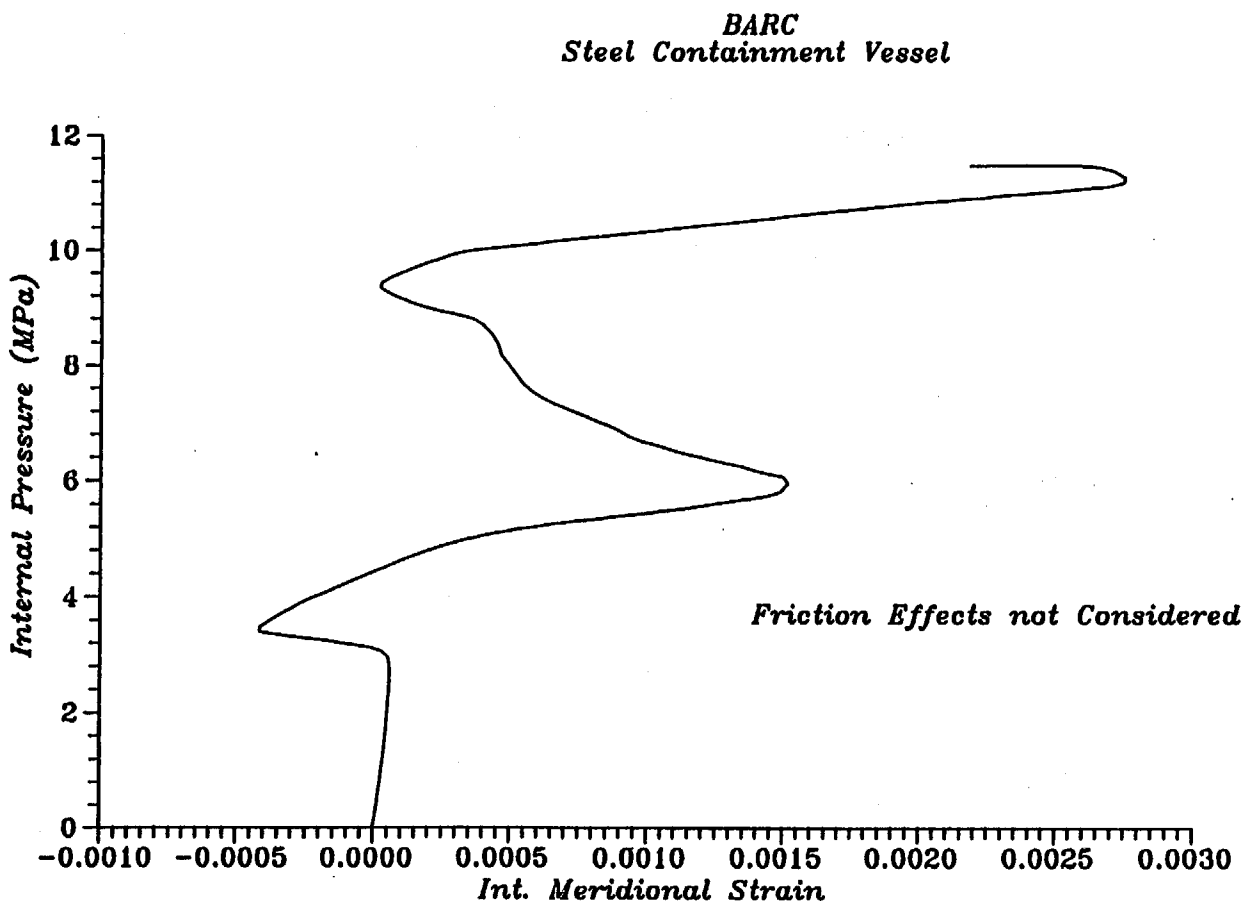

Fig.No.6+ Plot of Load v/s. Strain at ID No.14

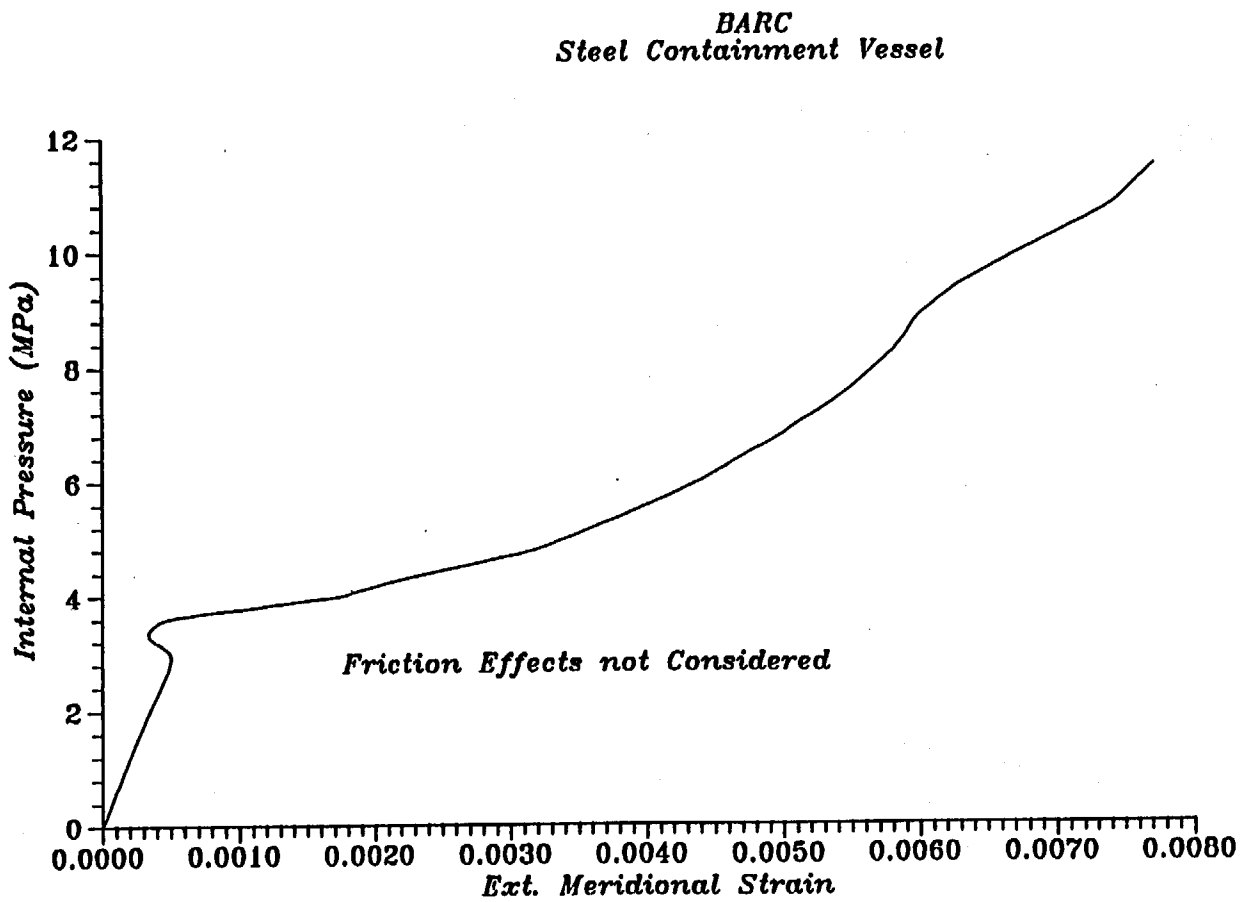

Fig.No.68 Plot of Load v/s. Strain at ID No.15

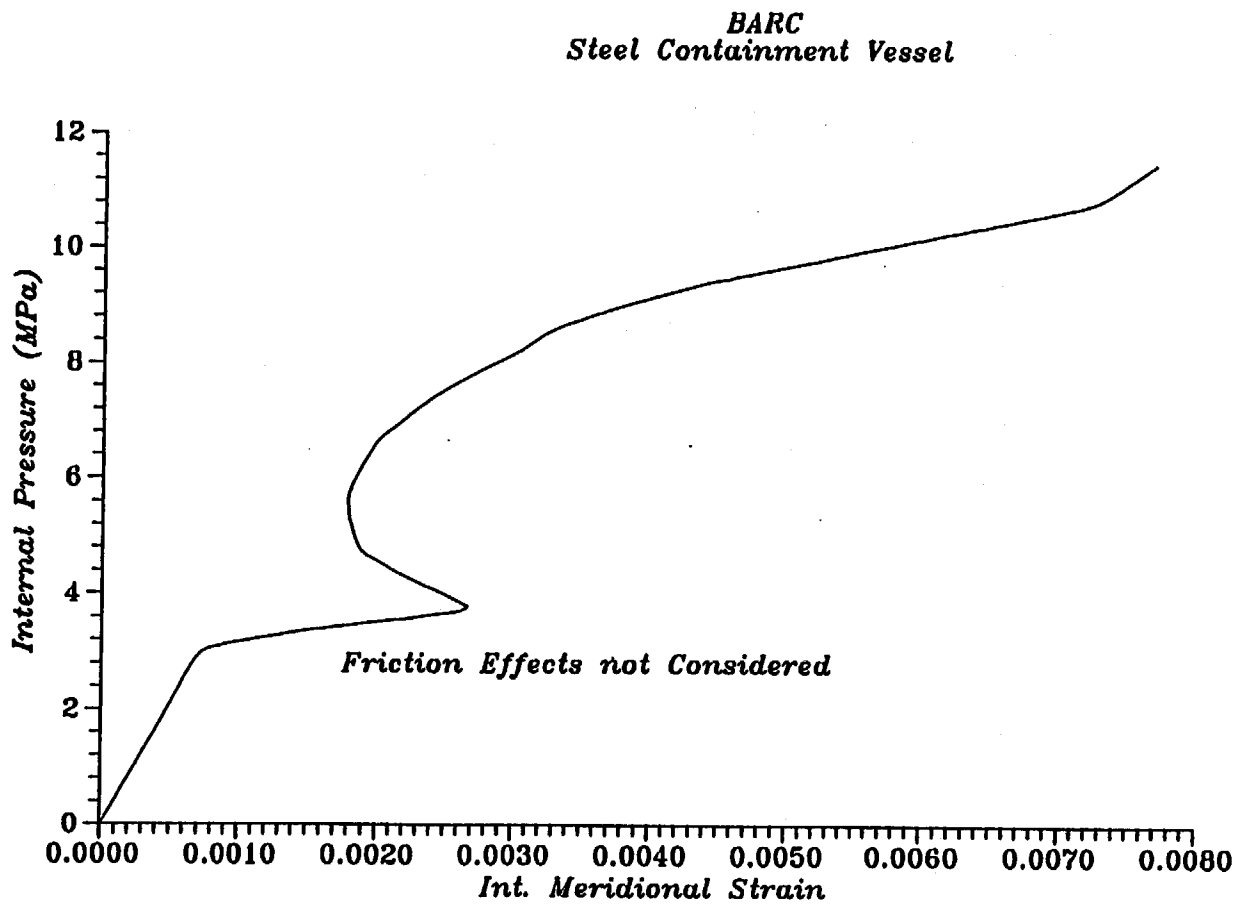

Fig.No.69 Plot of Load v/s. Strain at ID No.16

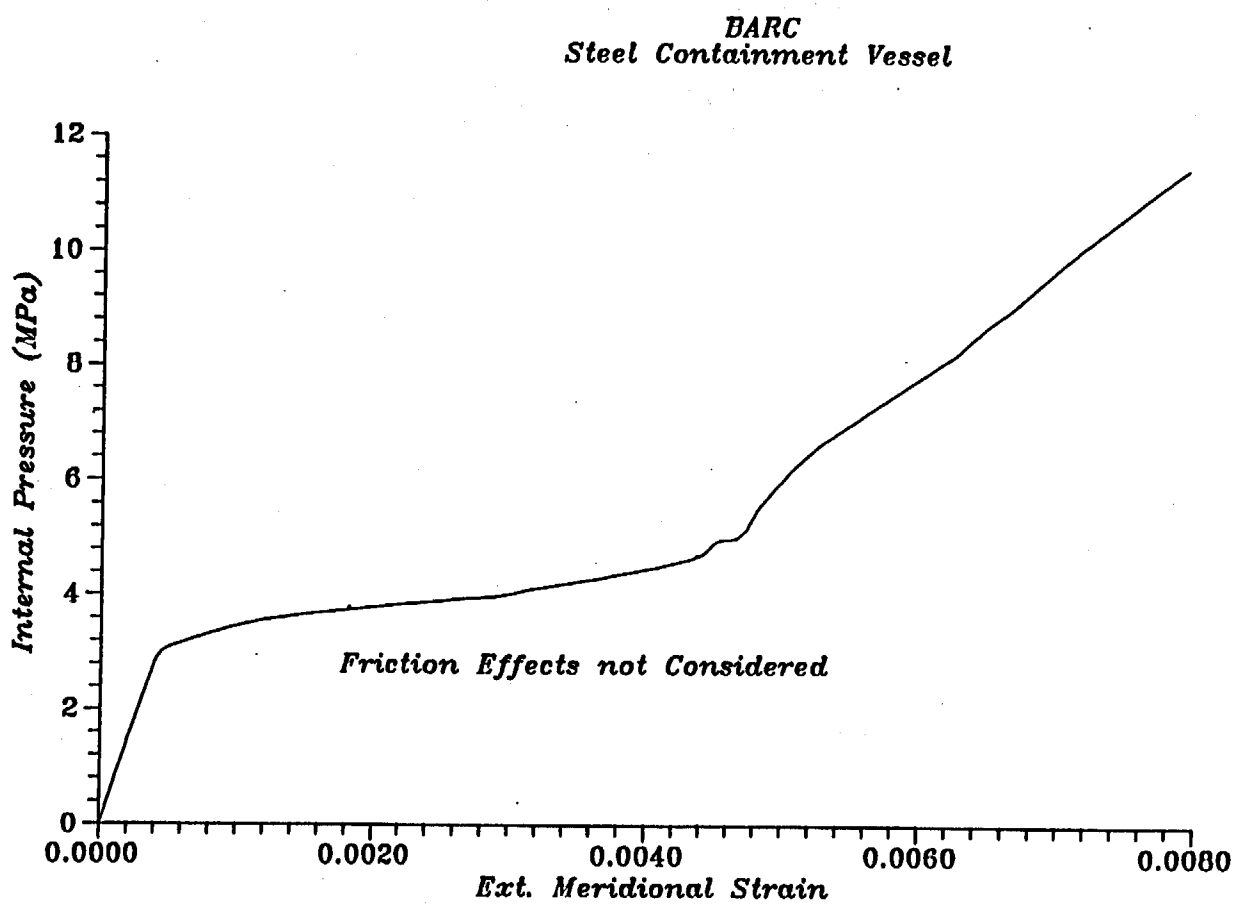

Fig.No.70 Plot of Load v/s. Strain at ID No.17

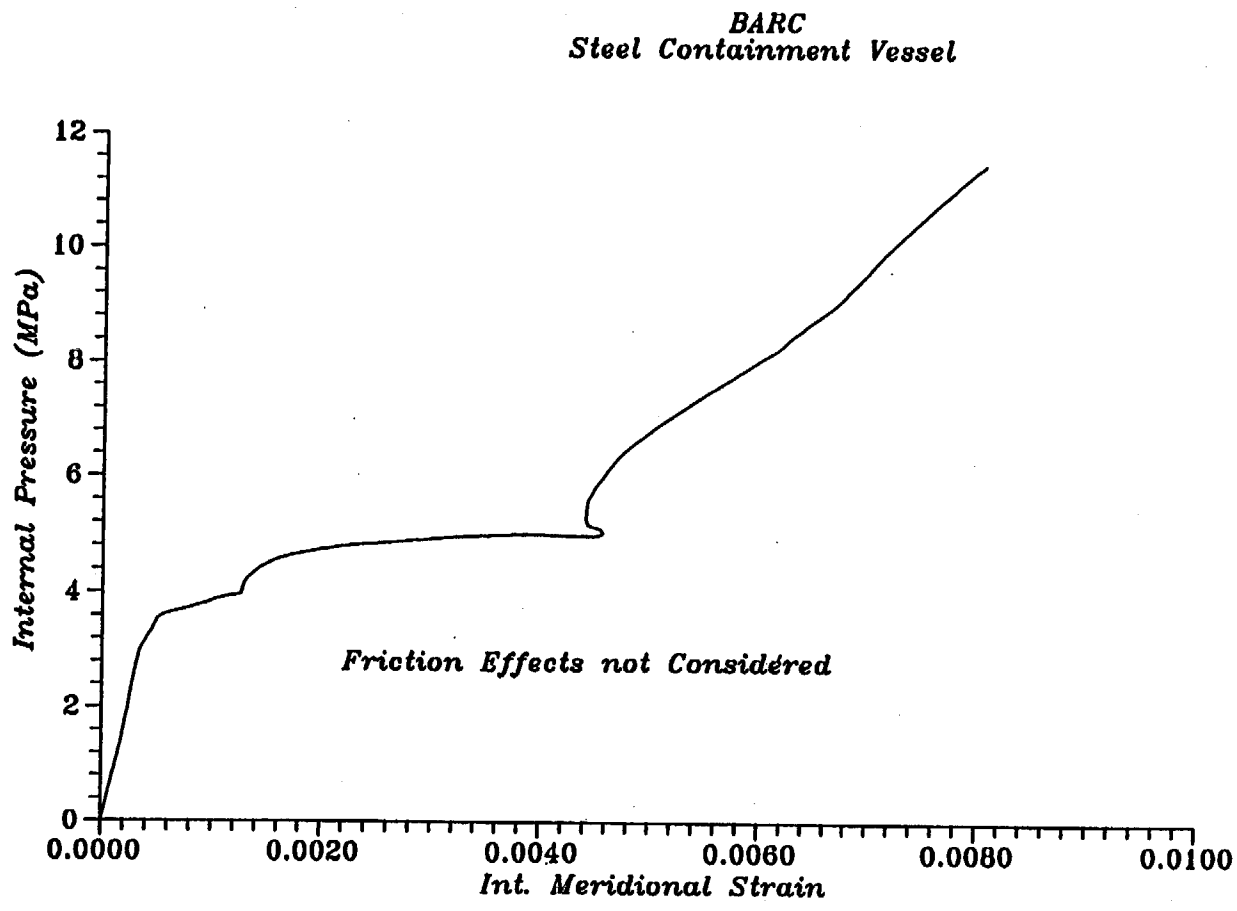

Fig.No.74 Plot of Load v/s. Strain at ID No.18

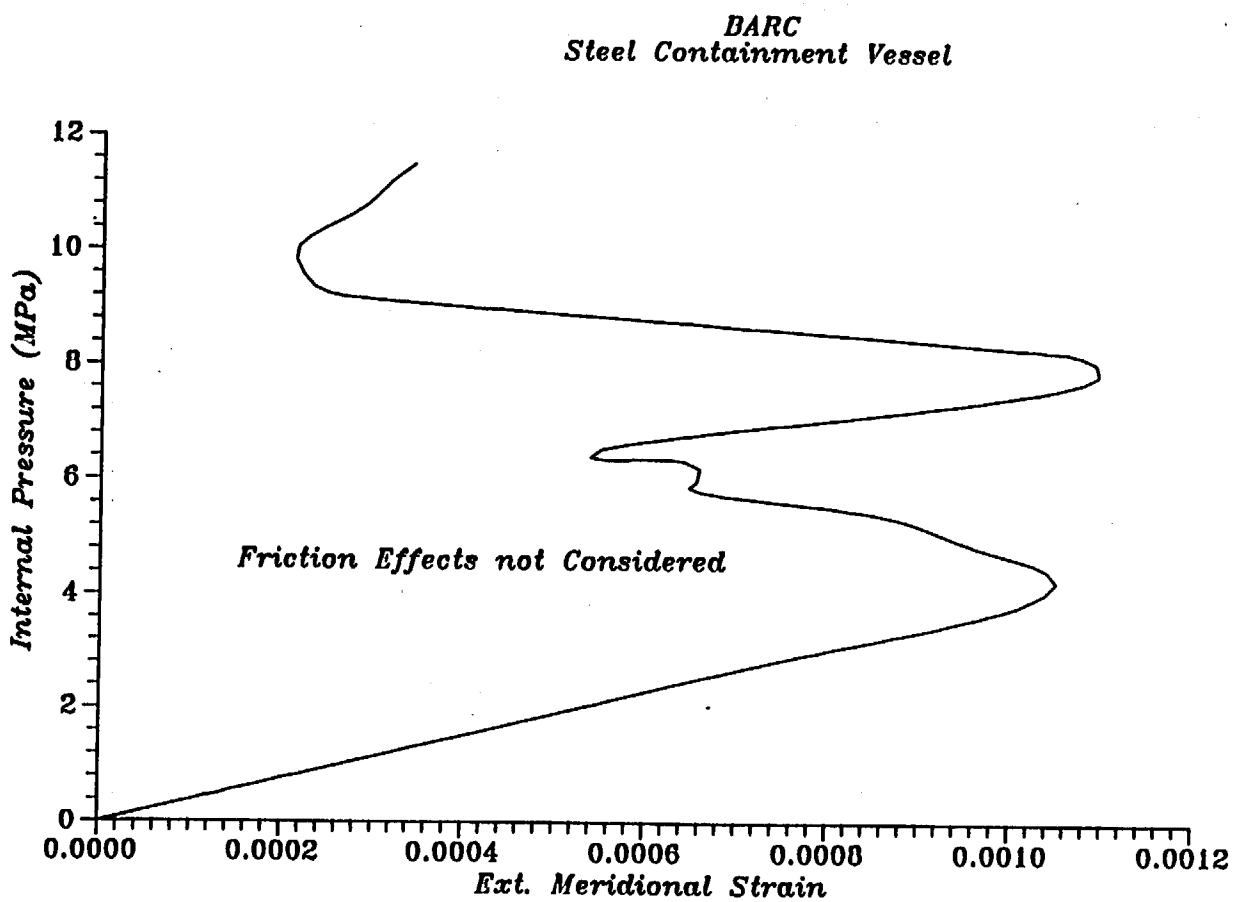

Fig.No.72 Plot of Load v/s. Strain at ID No.19

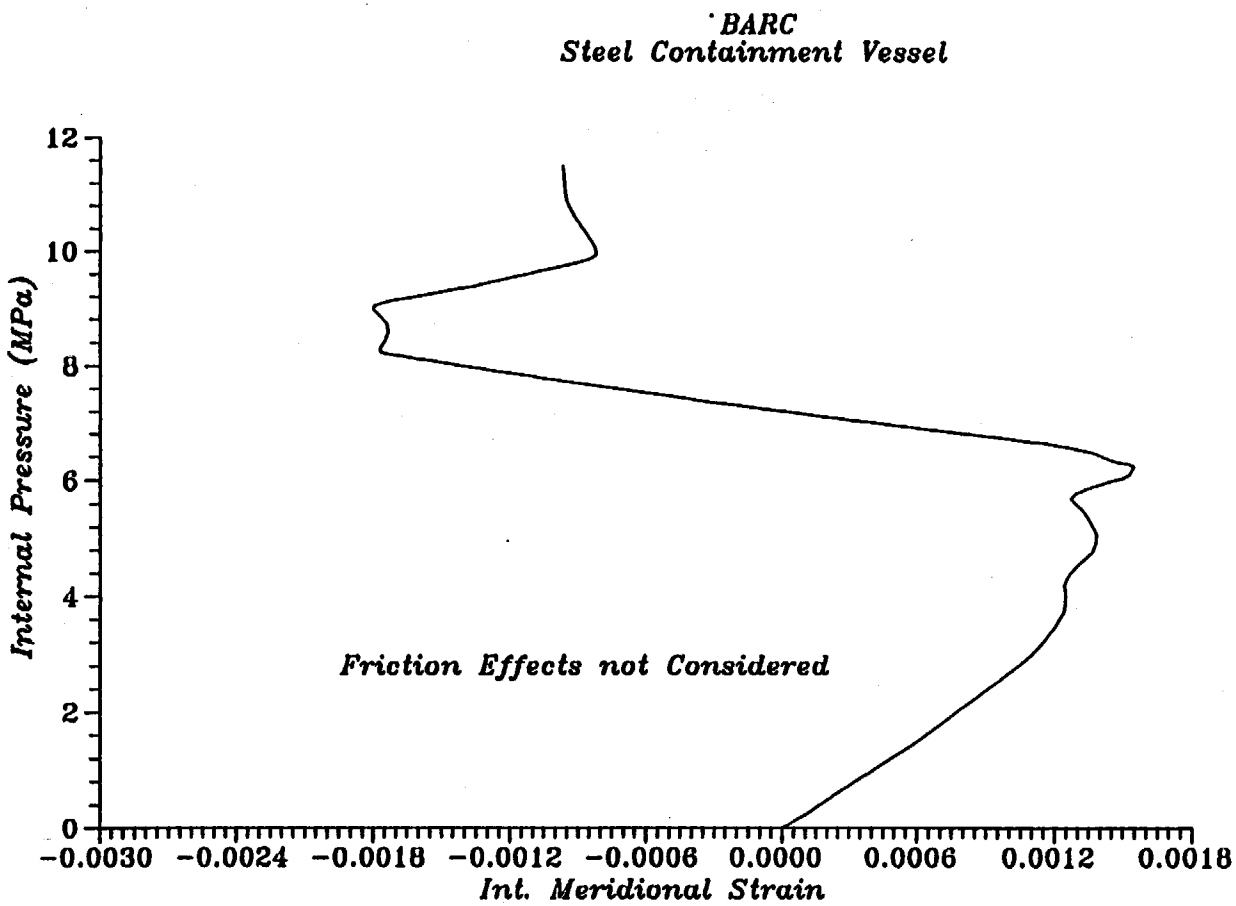

Fig.No.73 Plot of Load v/s. Strain at ID No.20

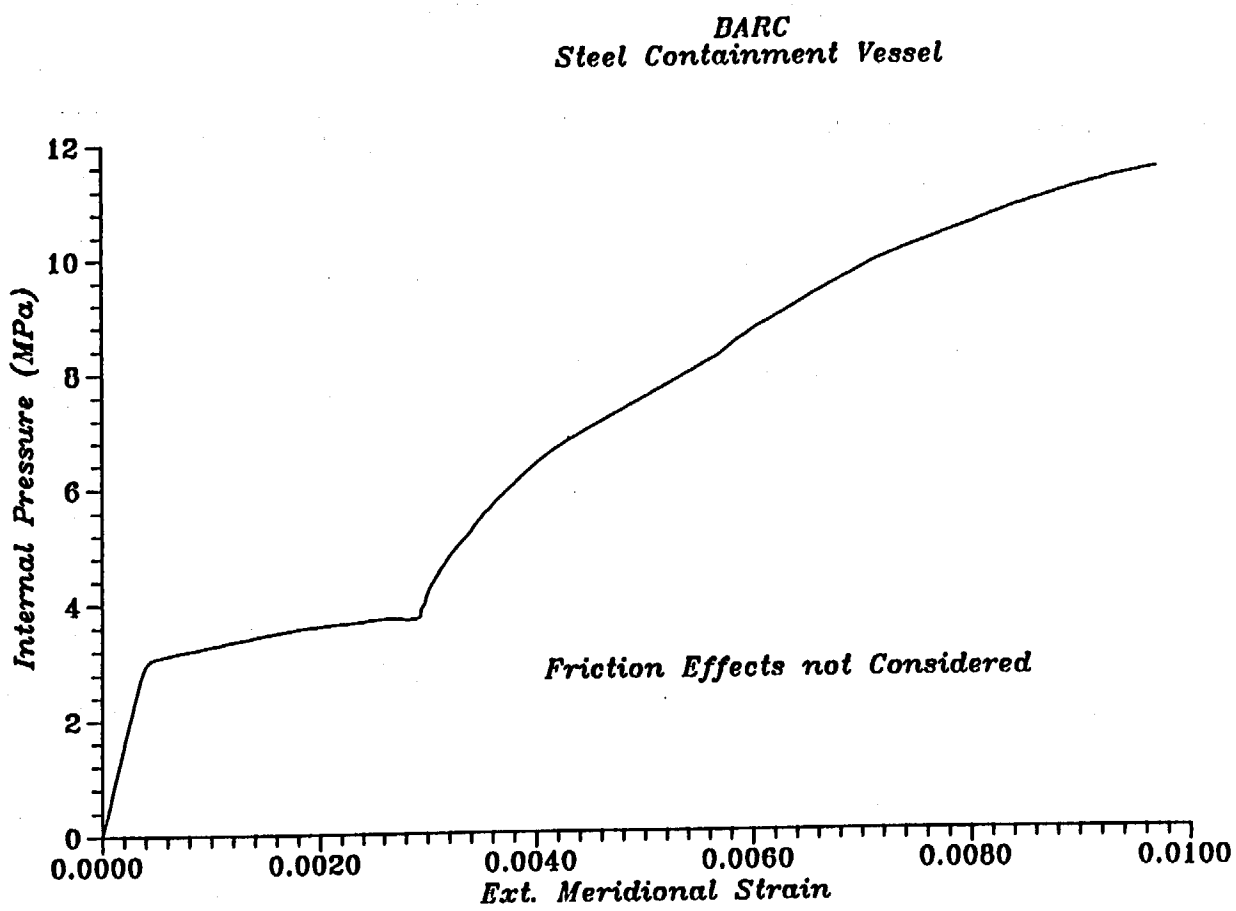

Fig.No.74 Plot of Load v/s. Strain at ID No.21

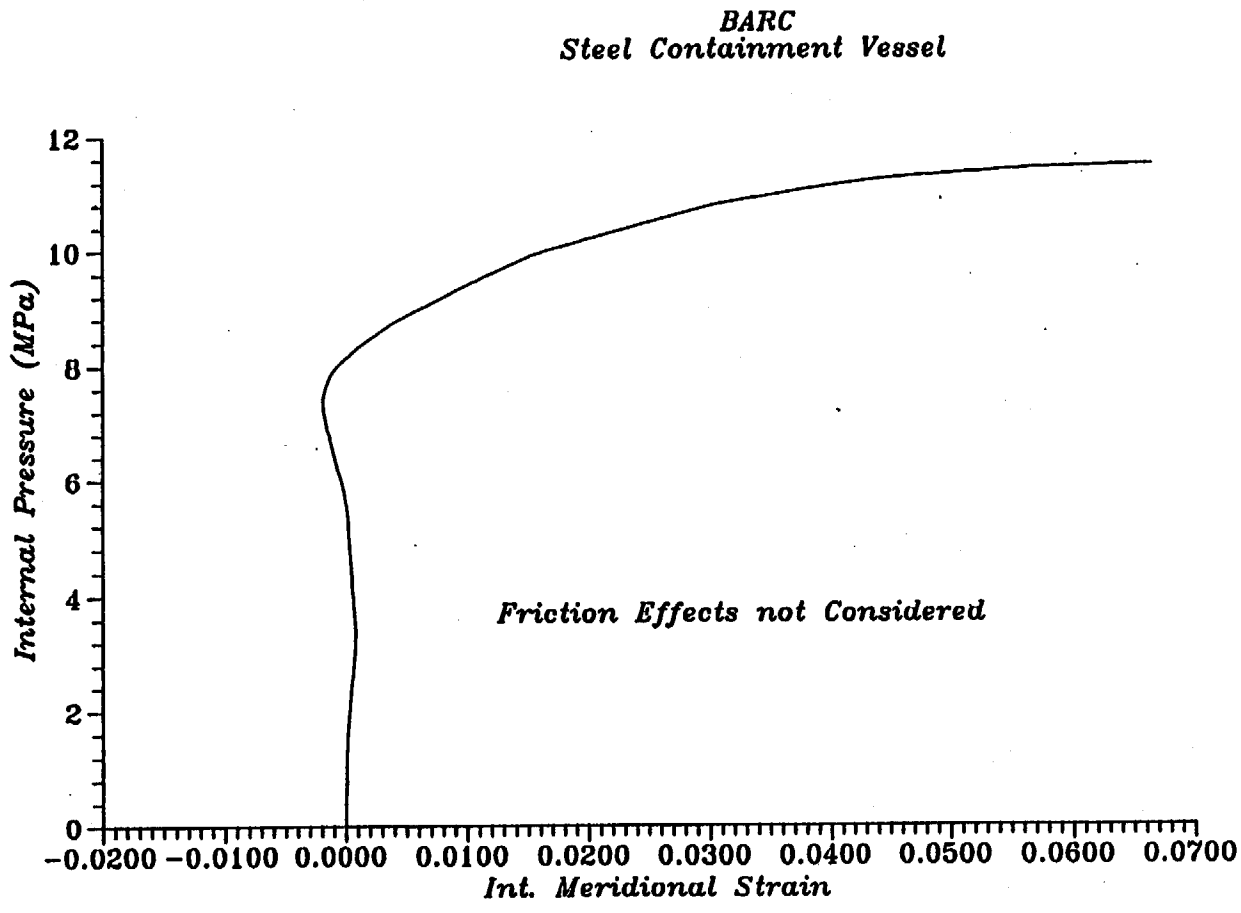

Fig.No.75 Plot of Load v/s. Strain at ID No.22

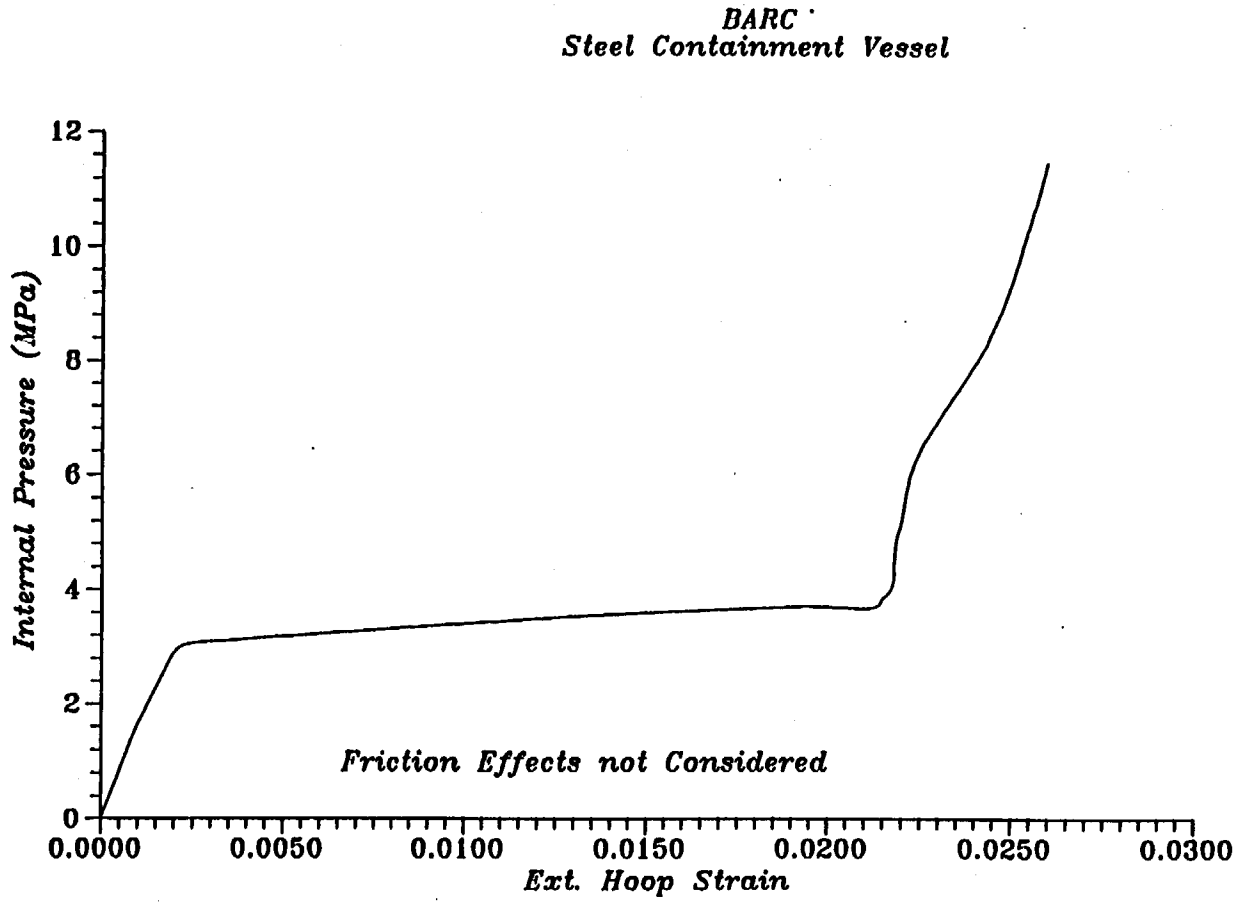

Fig.No.76 Plot of Load v/s. Strain at ID No.23

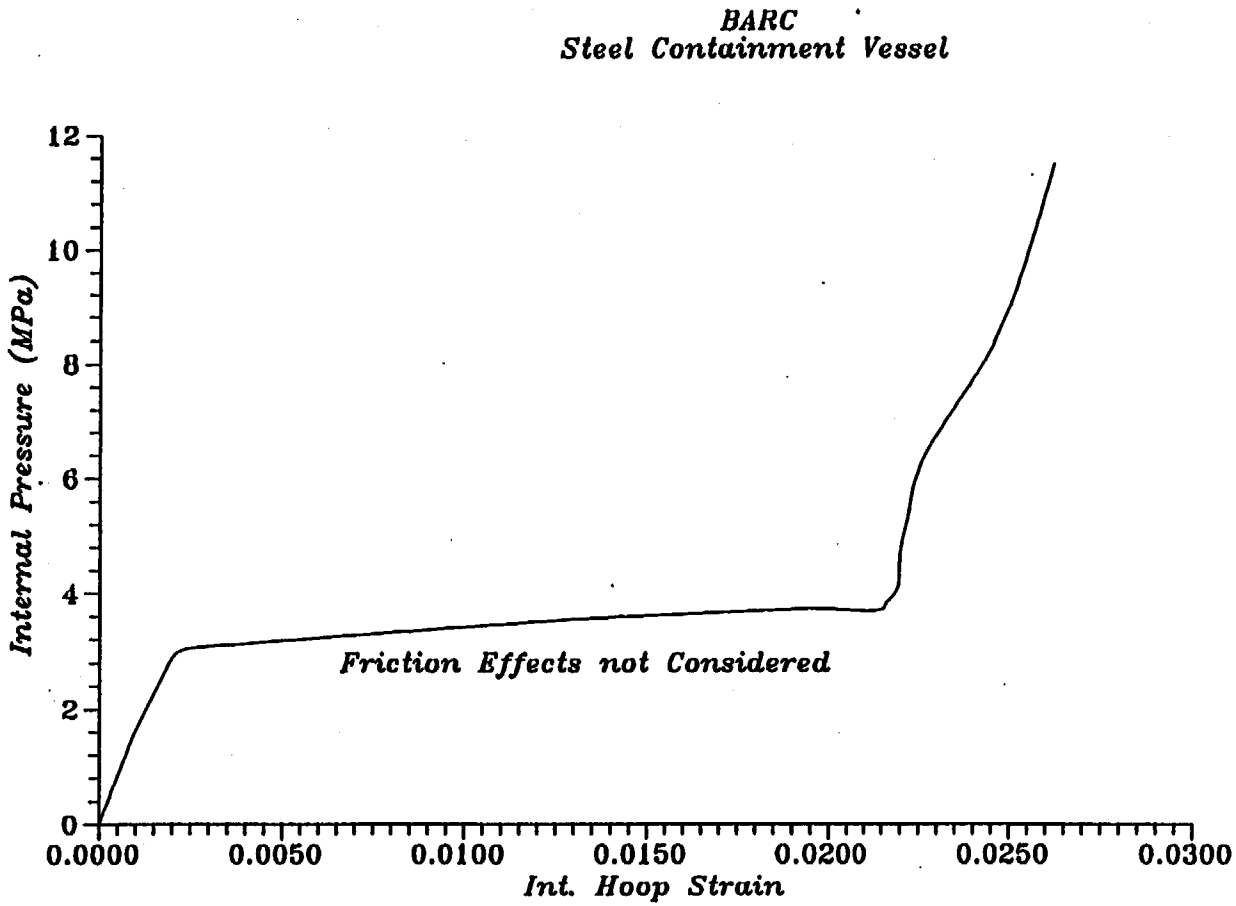

Fig.No.77 Plot of Load v/s. Strain at ID No.24

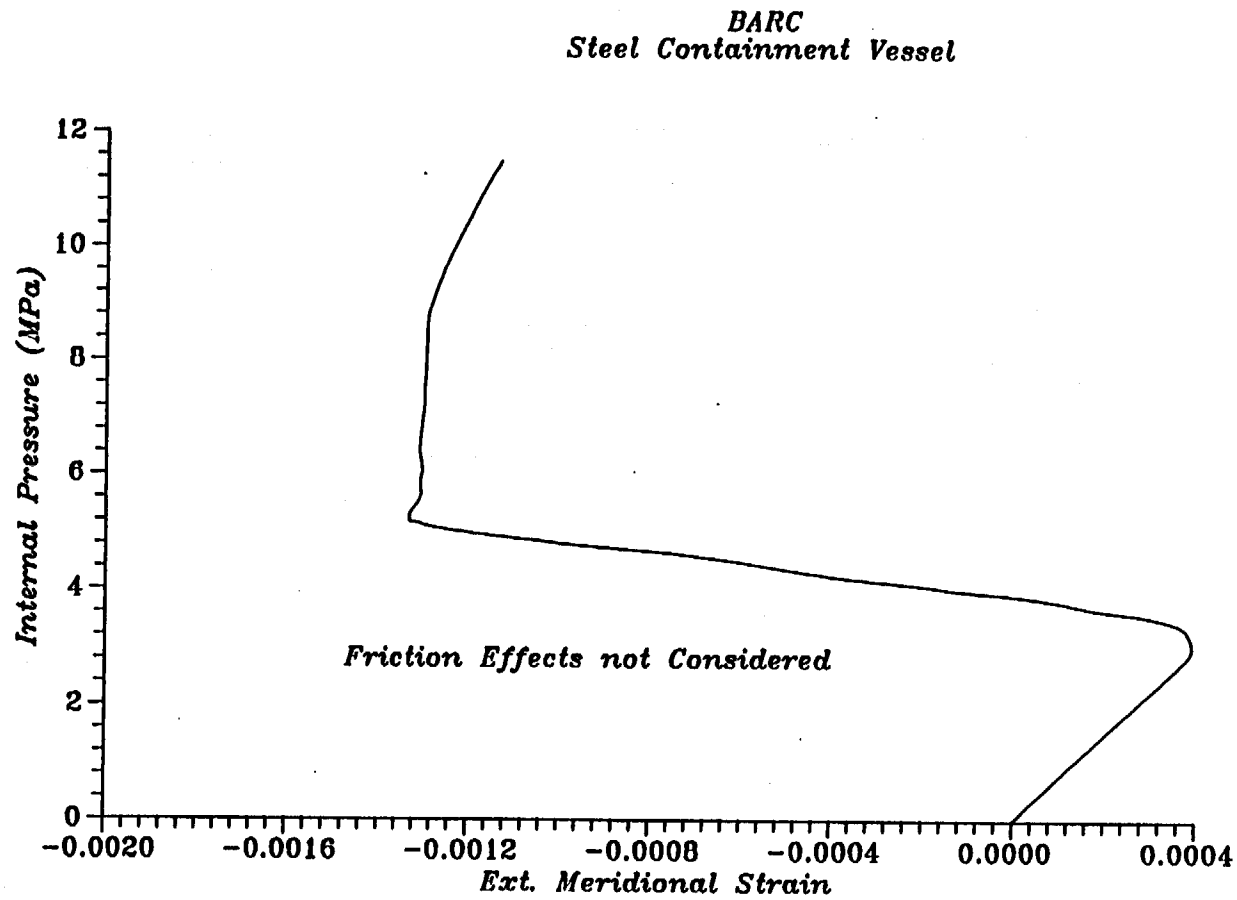

Fig.No.78 Plot of Load v/s. Strain at ID No.25

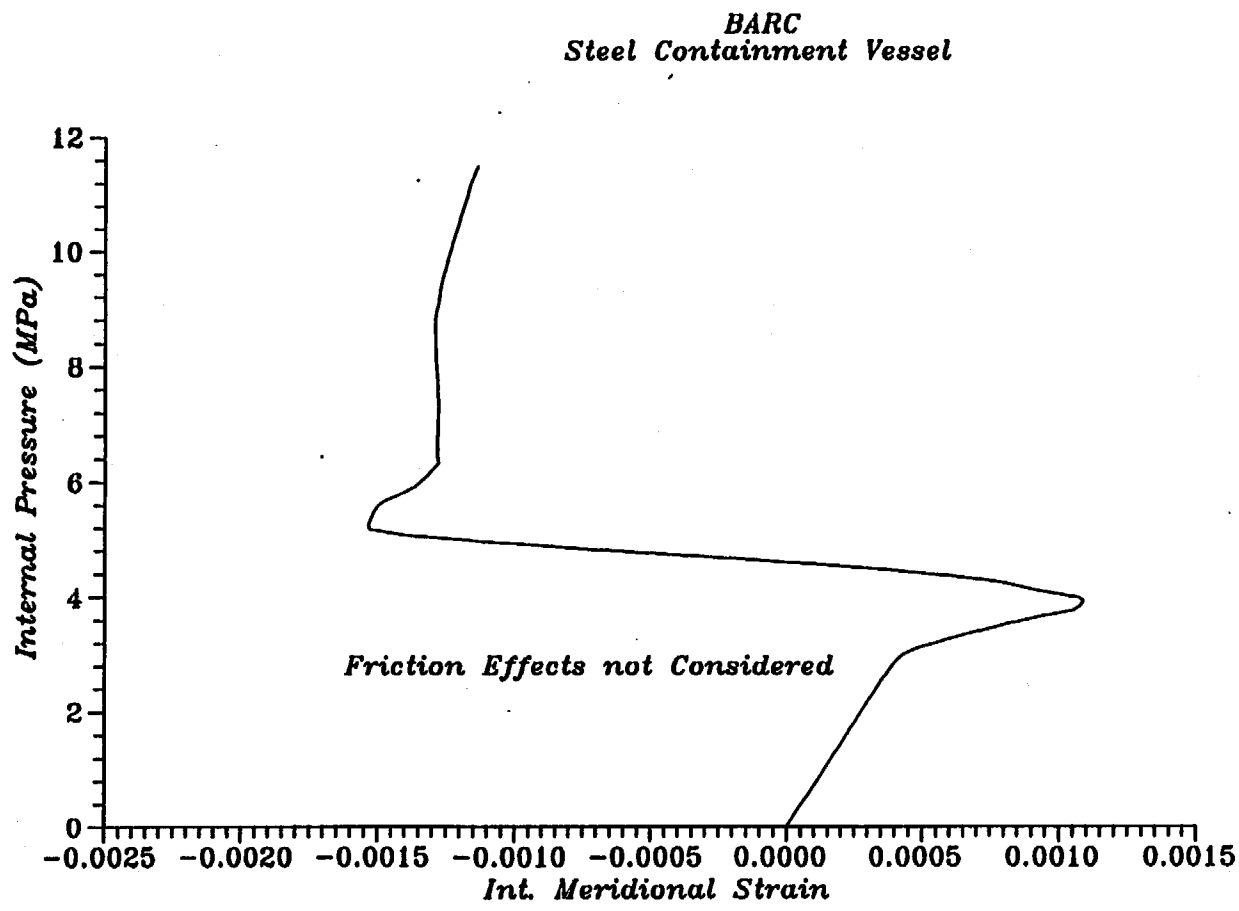

Fig.No.79 Plot of Load v/s. Strain at ID No.26

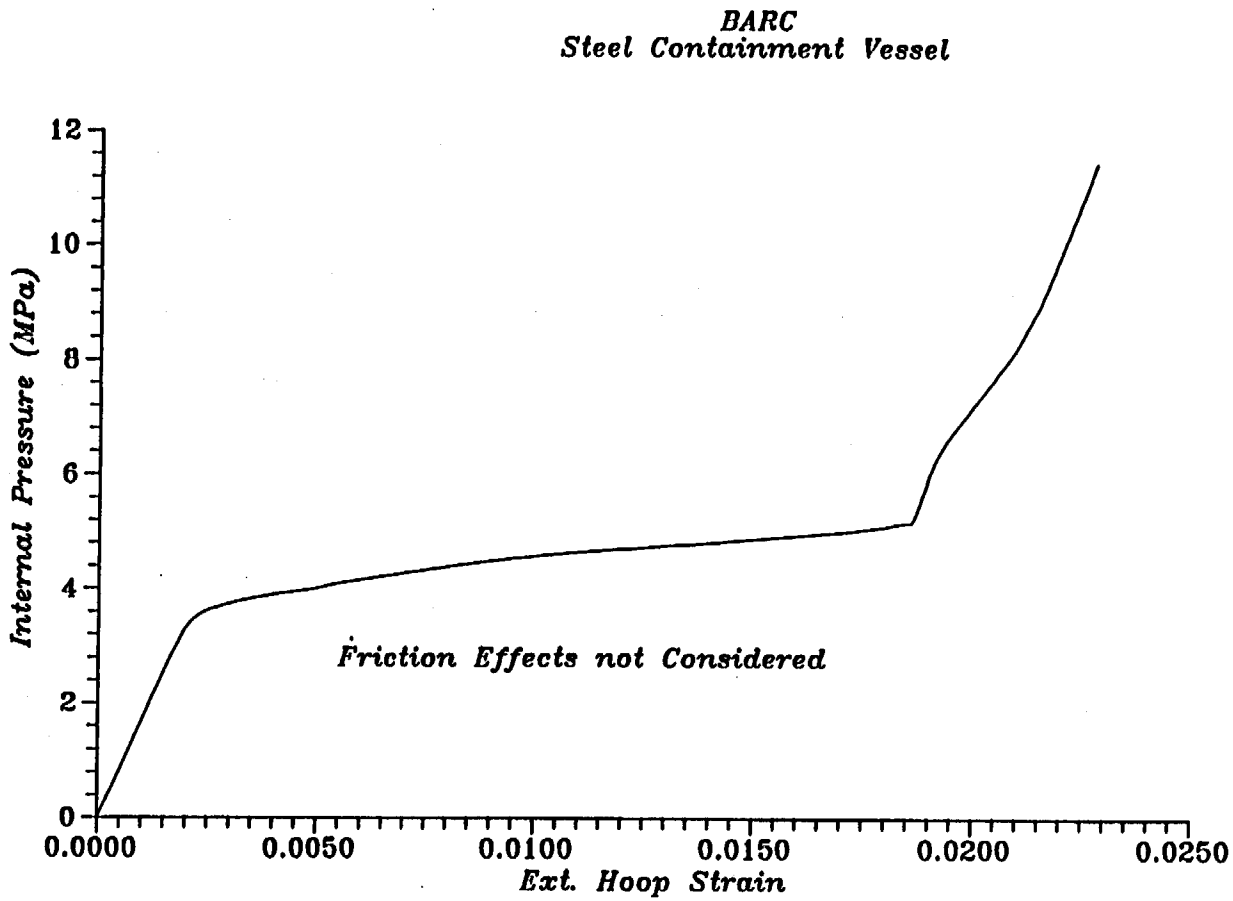

Fig.No.80 Plot of Load v/s. Strain at ID No.27

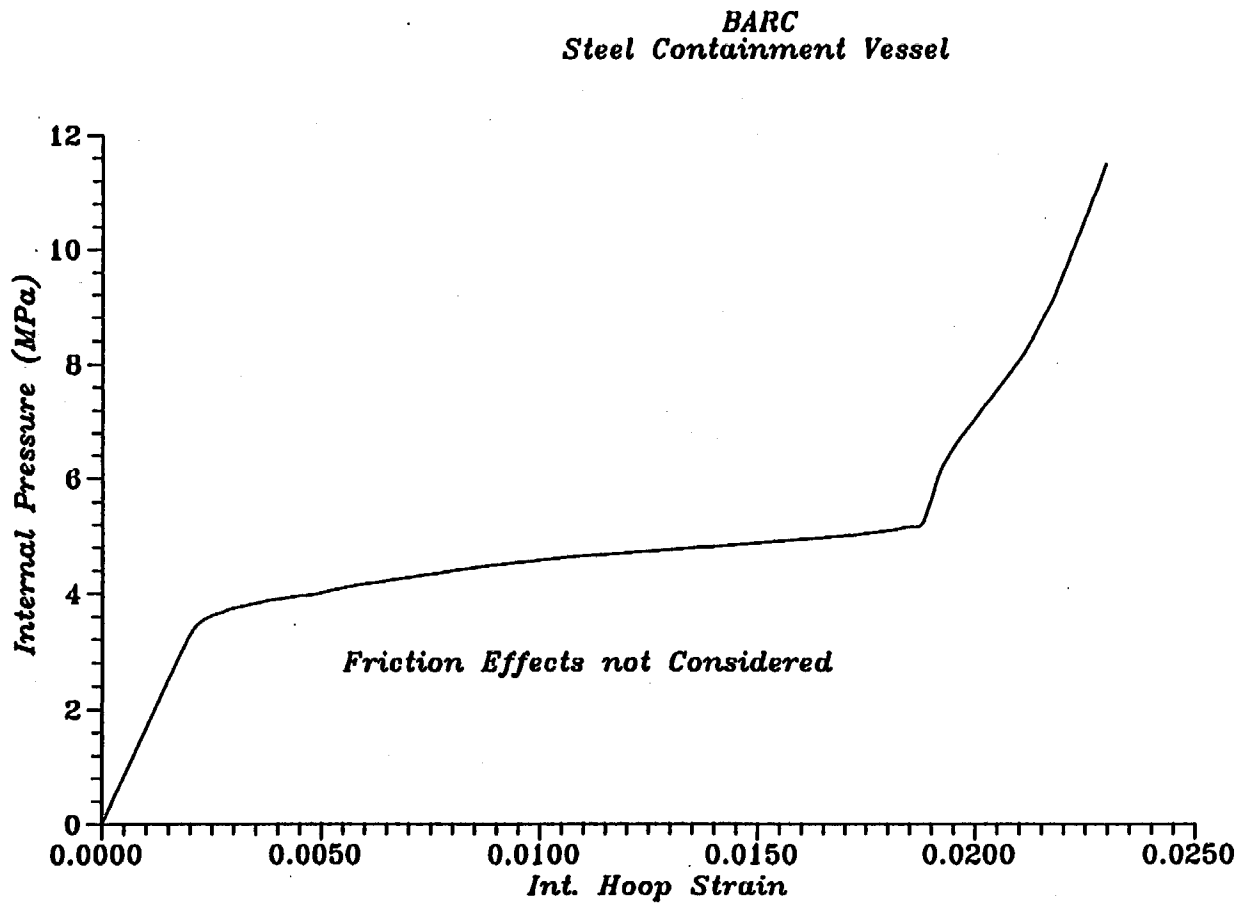

Fig.No.31 Plot of Load v/s. Strain at ID No.28

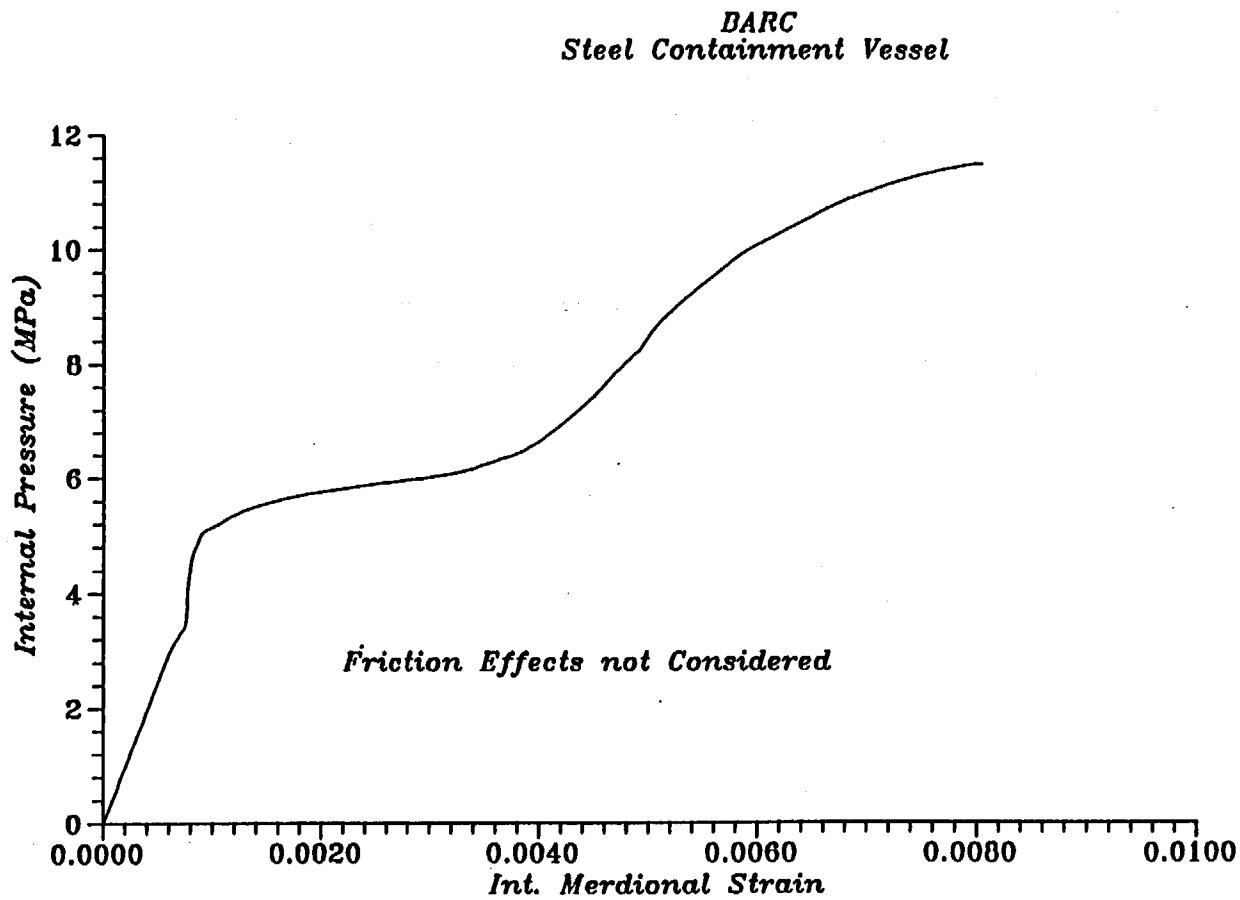

Fig.No.82 Plot of Load v/s. Strain at ID No.29

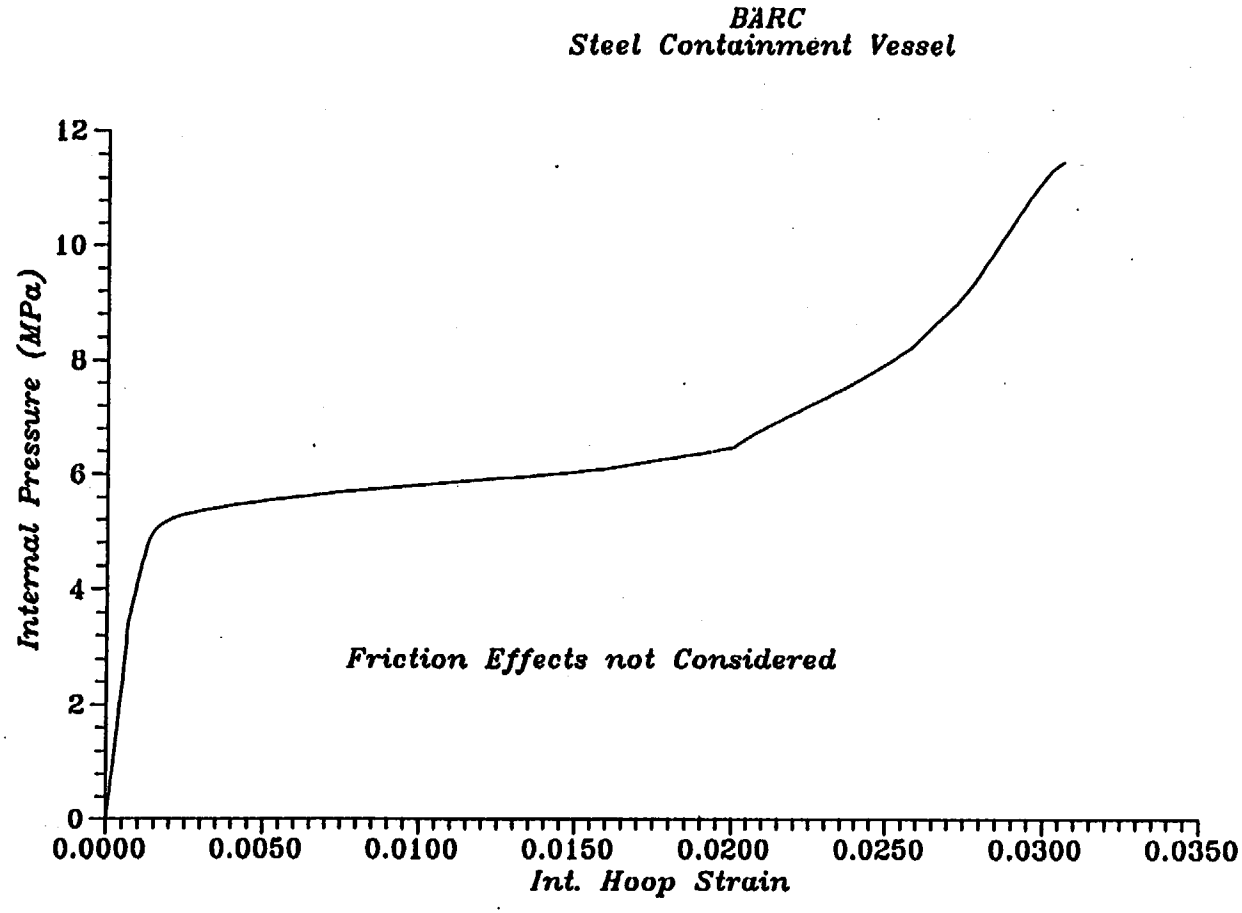

Fig.No.35 Plot of Load v/s. Strain at ID No.30

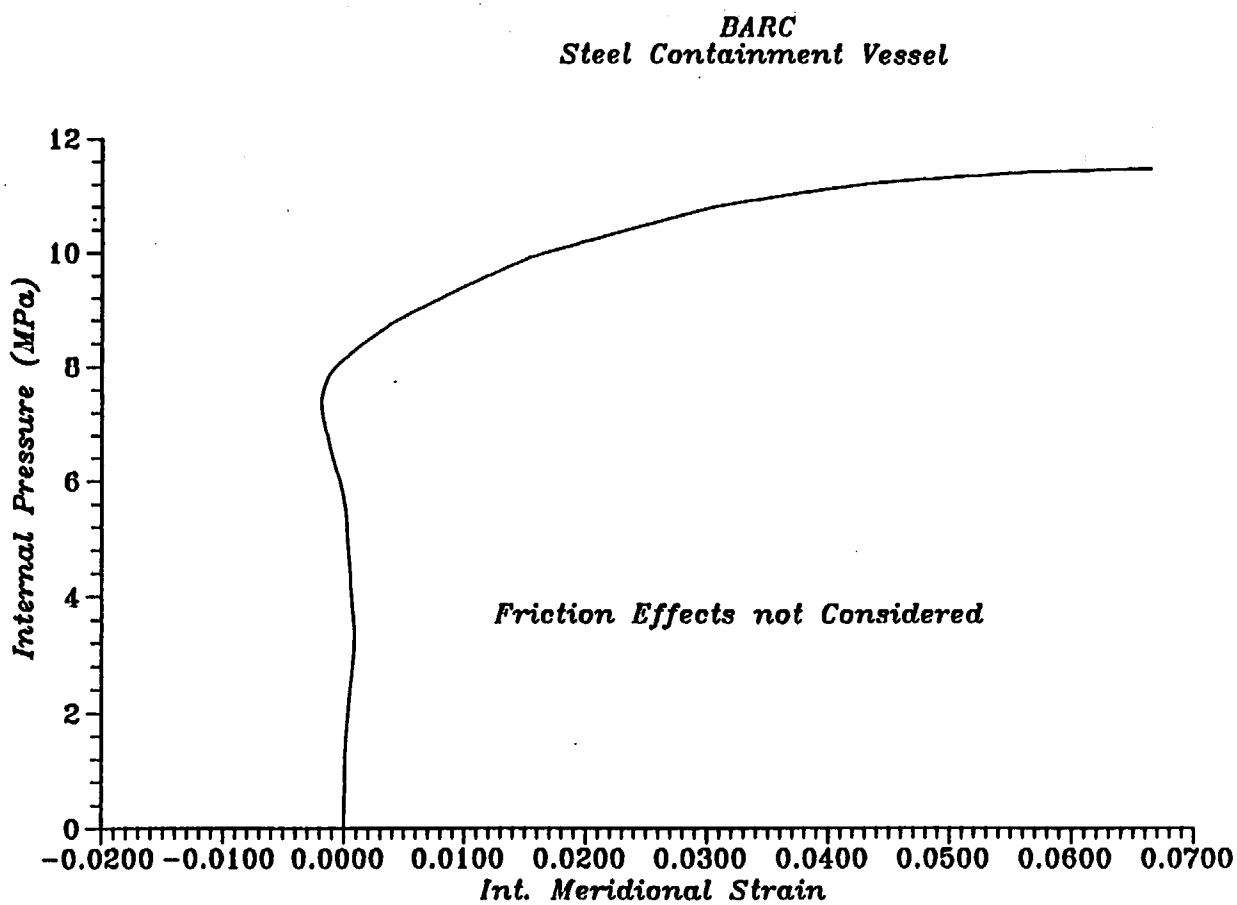

Fig.No.24 Plot of Load v/s. Strain at ID No.31

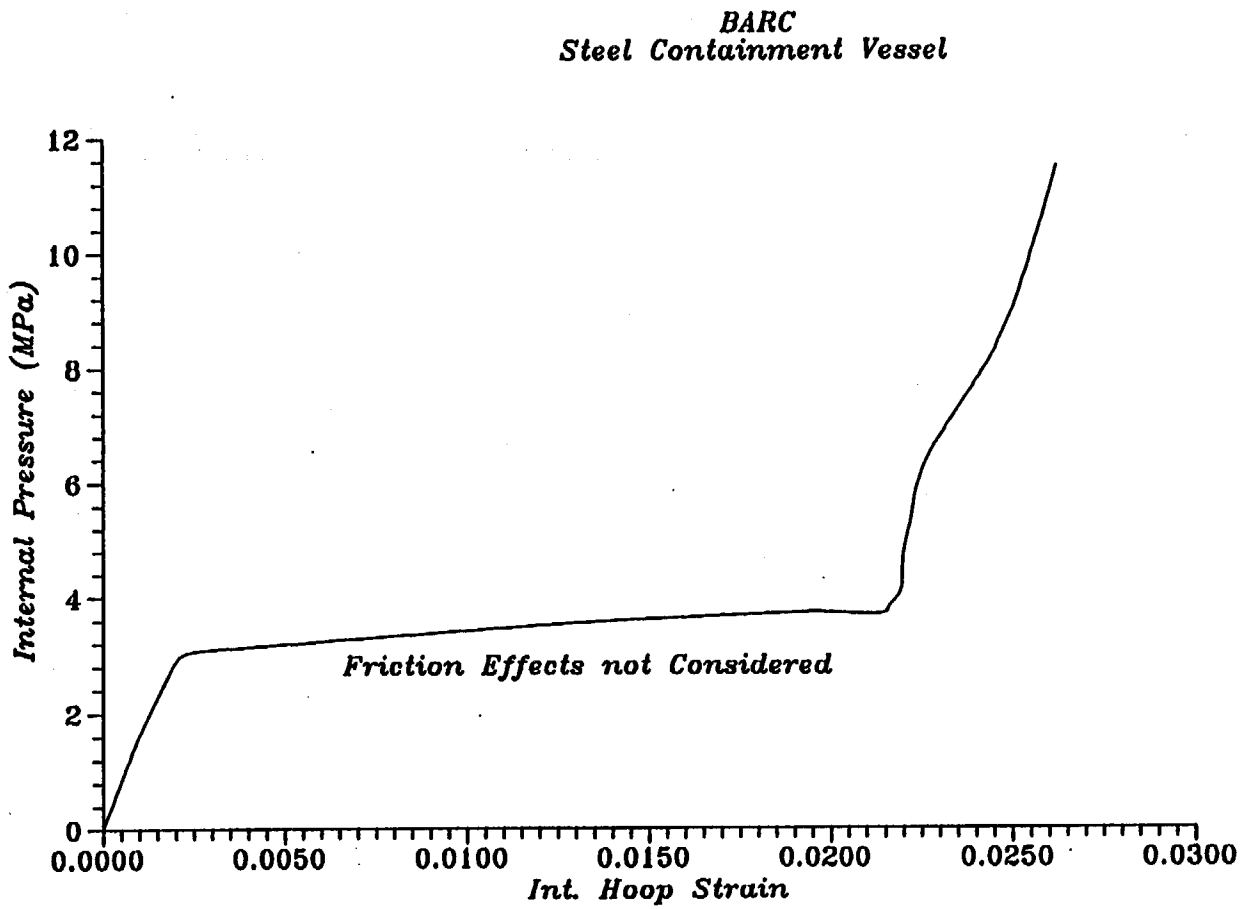

Fig.No.85 Plot of Load v/s. Strain at ID No.32

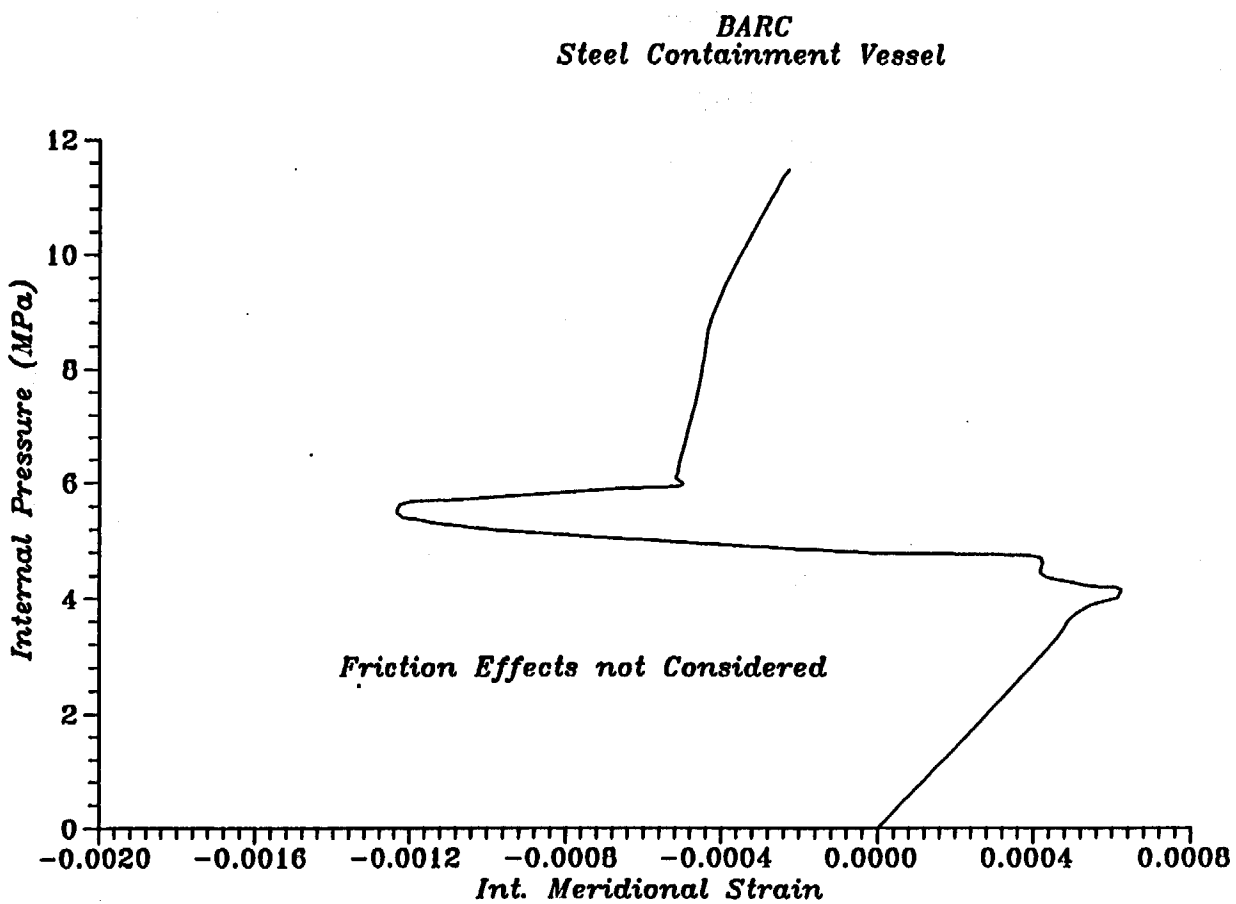

Fig.No.86 Plot of Load v/s. Strain at ID No.33

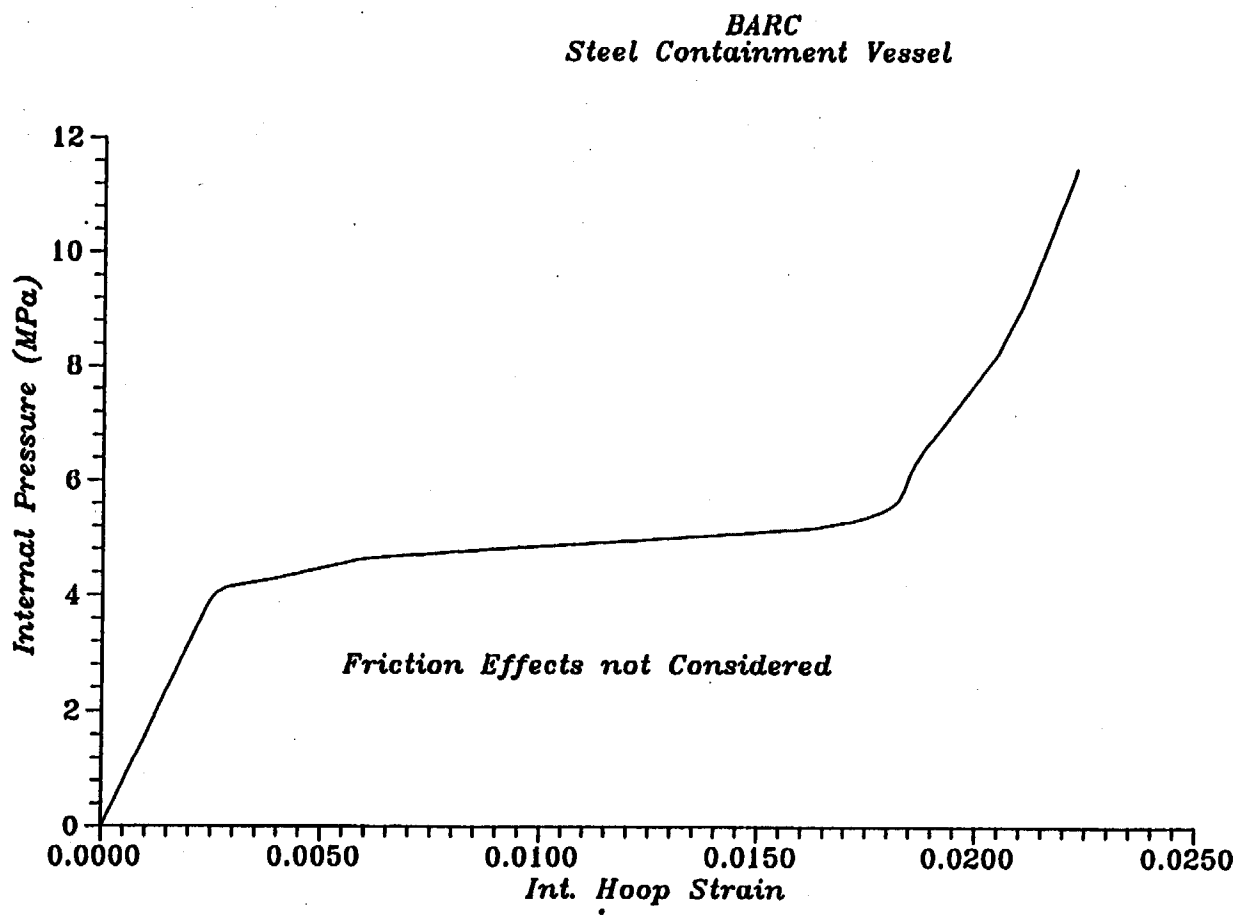

Fig.No.87 Plot of Load v/s. Strain at ID No.34